

TECHNISCHE UNIVERSITÄT MÜNCHEN
Lehrstuhl für Entwicklungsgenetik

Establishment of combinatorial genetics in zebrafish for analyzing
cellular mechanisms of hindbrain development

Martin Distel

Vollständiger Abdruck der von der Fakultät Wissenschaftszentrum Weihenstephan für Ernährung, Landnutzung und Umwelt der Technischen Universität München zur Erlangung des akademischen Grades eines

Doktors der Naturwissenschaften

genehmigten Dissertation.

Vorsitzender: Univ.-Prof. Dr. S. Scherer

Prüfer der Dissertation: 1. Univ.-Prof. Dr. W. Wurst

2. Univ.-Prof. Dr. A. Gierl

3. Univ.-Prof. A. Schnieke, Ph. D.

Die Dissertation wurde am 14.12.2009 bei der Technischen Universität München eingereicht und durch die Fakultät Wissenschaftszentrum Weihenstephan für Ernährung, Landnutzung und Umwelt am 16.02.2010 angenommen.

Establishment of combinatorial genetics in zebrafish for analyzing
cellular mechanisms of hindbrain development

Kumulative Arbeit

Martin Distel

Abstract

Zebrafish embryos have become a popular model system for the study of developmental biology, mainly because of their transparency and external development, which allow for *in vivo* investigations and easy manipulation. However, some methods are not well developed for zebrafish. In my PhD project, I have thus addressed the need for combinatorial genetics, imaging of opaque adult fish and cell type-specific subcellular imaging.

The Gal4-UAS combinatorial genetic system provides spatial and temporal control over gene expression and thus enables one to perform sophisticated genetic studies. I adapted the Gal4-UAS system to zebrafish by creating optimized Gal4 activators and UAS effector constructs, which show good bio-tolerance and non-mosaic transactivation. My quantification of the expression activity of these activator/effector combinations provides a rational basis for the prediction of expression levels and thus allows to model concentration dependent effects. Subsequently, I generated 60 tissue specific transgenic Gal4 activator strains in a self-reporting enhancer trap approach biased for the central nervous system. As these strains express a red fluorescent protein in Gal4 expressing cells, embryos of these strains can be readily used to study the development of the respective tissues *in vivo* by time-lapse microscopy. Furthermore, these strains reliably transactivate any UAS-dependent transgene and thus represent a valuable resource for reverse genetic studies. To be able to plan and to analyse Gal4 mediated transgene expression experiments, I analysed the transactivation kinetics of an enhancer trap strain expressing optimized Gal4 (KalTA4) in rhombomeres 3 and 5 (r3/5). KalTA4 expression was found to be present transiently at early embryonic stages and was restricted to r3/5. In order to follow the fate of r3/5, I generated an effector strain, Kaloop, which is capable of prolonging reporter gene expression in r3/5 until adulthood in a KalTA4 mediated self-maintaining feedback loop. Using this Kaloop strain, I showed that the rhombomeric organisation of the zebrafish hindbrain persists until adult stages, similar to frog or chick. Furthermore, I found that the secondary octaval nucleus (SON) is derived from *egr2b* expressing cells of r5. This demonstrates that the Kaloop effector strain can be used in combination with tissue specific Gal4 activator strains to explore the relationship between embryonic and adult structures. As the established Gal4 strains are capable of transgene activation they can be used to study gene functions in a tissue specific manner in both gain and loss of function experiments. In a collaborative effort the r3/5 specific enhancer trap strain was used to rescue the phenotype of *lunatic fringe* morphants, which showed increased neurogenesis, specifically in r3/5. This experiment confirmed the hypothesis that Lunatic

Fringe is required to maintain cells in a progenitor state in the zebrafish hindbrain. Additionally, Gal4 strains were successfully used to generate tumor models. By tissue specific overexpression of human oncogenic *HRAS-G12V* we generated a glioma model with fast onset of tumorigenesis, as well as a melanoma model strongly resembling human melanoma based on its morphological, molecular, genetic and epigenetic properties. These models will be used for screens for compounds effective against cancer and for mechanistic *in vivo* studies of tumorigenesis and disease progression.

Ideally, the progression of tumors in such models would be followed in a live animal. In contrast to optical methods, which suffer from light scattering, photoacoustic imaging can visualize structures deep within highly scattering tissue. Photoacoustic imaging is based on the conversion of absorbed light into ultrasound, which can be detected outside the tissue. However, this technique had not previously been applied to visualize fluorescently labelled structures. In collaboration with the Institute of Biological and Medical Imaging at the Helmholtz Center Munich, we established multispectral opto-acoustic tomography (MSOT), a variation of photoacoustic imaging, in order to visualize fluorescent protein expressing cells. Using MSOT, we could resolve the fluorescently labelled vertebral column and the crista cerebellaris of adult transgenic Gal4 fish *in vivo*. Together with Gal4-UAS genetics this technique allows one to investigate and manipulate processes like tumorigenesis, adult neurogenesis or regeneration in the living organism.

Finally, the Gal4-UAS system can also be used to study a biological process at the subcellular level. Here, I established a Gal4 based subcellular labelling system for the *in vivo* characterization of migration of tegmental hindbrain nuclei (THN) neurons. Multiple subcellularly targeted fluorescent proteins simultaneously expressed under UAS control were used to observe the dynamics of cell organelles in migrating cells within live zebrafish embryos. My subcellular analysis of THN neuron migration revealed that, in contrast to the classic model of neuronal migration, the centrosome is not permanently positioned ahead of the nucleus, but instead is overtaken by the nucleus in a saltatory manner during tangential migration. Furthermore, the position of the centrosome does not determine the site of axon outgrowth in THN neurons *in vivo* as previously observed in cultured hippocampal neurons. Gal4 mediated subcellular labelling can be readily combined with Gal4 mediated overexpression of dominant-negative variants of proteins, which in the future will allow for functional studies into the roles of candidate proteins in migration and axonogenesis with a direct *in vivo* read-out. Thus Gal4 mediated subcellular labelling promises to merge the fields of developmental biology and cell biology into a new field of *in vivo* cell biology.

Zusammenfassung

Der embryonale Zebrafisch ist aufgrund seiner Transparenz und externen Entwicklung, die einfache genetische Manipulationen und *in vivo* Untersuchungen erlauben, ein beliebter Modellorganismus für entwicklungsbiologische Studien geworden. Dennoch wurden einige Methoden bisher nicht ausreichend für eine Anwendung im Zebrafisch entwickelt. In dieser Arbeit habe ich ein System für kombinatorische Genetik für die Anwendung im Zebrafisch und Methoden, sowohl zur Untersuchung von fluoreszenzmarkierten Geweben im lebenden adulten, als auch der Dynamik von Zellorganellen im lebenden embryonalen Zebrafisch etabliert.

Kombinatorische genetische Systeme, wie etwa das Gal4-UAS System, haben sich als wertvolle Werkzeuge für genetische Studien in *Drosophila* erwiesen. Das Gal4-UAS System erlaubt räumliche und zeitliche Kontrolle über die Expression von Transgenen und ermöglicht somit komplexe genetische Experimente. Ich habe das Gal4-UAS System für seine Anwendung im Zebrafisch adaptiert und optimierte Gal4 Aktivatoren und Effektorstrukturen generiert, deren Expression im Zebrafisch keinen schädlichen Einfluss auf seine Entwicklung hat und die nicht-mosaik Transaktivierung zeigen. Die Quantifizierung der Expressionsstärken verschiedener Aktivator/Effektor Kombinationen ermöglicht zudem die Planung und Durchführung von Experimenten, bei denen unterschiedliche Mengen eines Transgens exprimiert werden sollen, um konzentrationsabhängige Effekte zu studieren.

Mit diesem optimierten Gal4 System habe ich durch einen „Screen“ nach regulatorischen Elementen 60 gewebsspezifische transgene Gal4 Aktivator Linien erzeugt, von denen die Mehrzahl Gal4 in Geweben des zentralen Nervensystems exprimiert. Gal4 exprimierende Zellen sind in diesen Linien durch die Expression eines roten Fluoreszenzproteins erkennbar. Daher können diese Linien benutzt werden, um die Entwicklung eines Gewebes anhand seiner fluoreszierenden Zellen im lebenden Zebrafisch mittels konfokaler Mikroskopie zu verfolgen. Da man in diesen Linien jedes beliebige Transgen unter regulatorischer Kontrolle von Gal4 gewebsspezifisch exprimieren kann, sind diese Gal4 Linien eine wertvolle Ressource für reverse genetische Studien. Um Gal4 Expressionsexperimente zu planen und richtig zu interpretieren, habe ich die Transaktivierungskinetik einer Enhancer Trap Linie, die Gal4 in den Rhombomeren 3 und 5 (R3/5) exprimiert, im Detail analysiert. Gal4 wurde für einen kurzen Zeitraum, früh in der Embryonalentwicklung spezifisch in R3/5 exprimiert. Um der Entwicklung dieser Rhombomere folgen zu können, habe ich eine Effektorlinie generiert

(Kaloop), die die Reporterexpression in den Rhombomeren bis in adulte Stadien verlängert. Mittels dieser „Kaloop“ Linie konnte ich zeigen, dass wie im Frosch oder im Huhn, die embryonale Organisation in Rhombomere im Zebrafisch bis in adulte Stadien besteht und dass der Sekundäre Oktavuskern aus Rhombomer 5 stammt. Dies demonstriert die Fähigkeit der „Kaloop“ Linie, in Kombination mit gewebsspezifischen Gal4 Aktivator Linien die Herkunft von Strukturen im adulten Zebrafisch zu bestimmen.

Da die generierten Gal4 Linien die Expression von Transgenen aktivieren können, stellen sie ein hilfreiches Werkzeug dar, um Genfunktionen zu untersuchen. In einer Kollaboration haben wir die Funktion von Lunatic Fringe während der Entwicklung des Hinterhirns des Zebrafisches untersucht. Zebrafische, bei denen die Translation von *lunatic fringe* inhibiert wurde, zeigten erhöhte Neurogenese. Gal4 vermittelte Überexpression von *lunatic fringe* in Rhombomeren 3 und 5 konnte diesen Phänotyp umkehren, was die Hypothese bekräftigte, dass Lunatic Fringe notwendig ist, um undifferenzierte Vorläuferzellen im Hinterhirn des Zebrafisches zu erhalten.

Meine Gal4 Linien wurden außerdem erfolgreich genutzt, um Tumormodelle im Zebrafisch zu generieren. Durch gewebsspezifische Überexpression des humanen Onkogens *HRAS-G12V* konnte ein Glioma und ein Melanoma Modell im Zebrafisch etabliert werden. Diese Modelle werden in Zukunft zur Untersuchung der Tumorentstehung und Entwicklung im lebenden Organismus und für „Wirkstoff-Screens“ verwendet werden.

Um die Tumorentwicklung im lebenden adulten Zebrafisch beobachten zu können, wird eine Methode benötigt, die fluoreszierende Zellen im streuenden Gewebe sichtbar machen kann. Aufgrund der starken Streuung sind optische Methoden für solche Untersuchungen nicht geeignet, allerdings konnten bereits mittels photo-akustischer Techniken Strukturen innerhalb stark streuenden Gewebes dargestellt werden. Photo-akustische Verfahren basieren auf der Konvertierung von Licht in Ultraschall, der außerhalb des Gewebes detektiert werden kann. Solche Verfahren wurden allerdings bisher noch nicht angewendet, um Fluoreszenzproteine sichtbar zu machen. In Kollaboration mit dem Institut für Biologische und Medizinische Bildgebung am Helmholtz Zentrum München etablierten wir multispektrale opto-akustische Tomographie (MSOT). Mit diesem Verfahren konnten wir Gewebe im adulten Zebrafisch sichtbar machen, welche Fluoreszenzproteine exprimieren. Zusammen mit den Gal4 basierten genetischen Möglichkeiten verspricht dieses Bildgebungsverfahren, Prozesse wie Tumorentwicklung oder Regeneration im lebenden Organismus untersuchen zu können. Solche Untersuchungen werden zum Verständnis dieser Prozesse beitragen.

Zur Charakterisierung der neuronalen Migration tegmentaler Hinterhirnkerne (THK), habe ich mein bestehendes Gal4-UAS System zur Visualisierung von Zellorganellen erweitert. Dieses System kann nun benutzt werden, um mehrere Fluoreszenzproteine zu exprimieren, die Zellorganellen markieren, um somit die Dynamik dieser Zellorganellen mittels konfokaler Zeitraffermikroskopie im lebenden Zebrafisch sichtbar zu machen. Meine subzelluläre Charakterisierung der Wanderung von THK Neuronen zeigte, dass im Gegensatz zum klassischen Modell der neuronalen Wanderung das Zentrosom nicht immer vor dem Zellkern zu finden ist, sondern stattdessen in einer sprunghaften Bewegung vom Zellkern überholt wird. Die bisherigen mechanistischen Modelle zur neuronalen Zellwanderung werden mit dieser Beobachtung in Frage gestellt. Außerdem bestimmt die Position des Zentrosoms in THK Neuronen im lebenden Zebrafisch nicht die Stelle, von der das Axon hervorgeht, wie dies bei hippocampalen Neuronen in Zellkultur der Fall ist. Diese klaren Unterschiede der Axonogenese *in vivo* und *in vitro* verlangen nach weiteren mechanistischen *in vivo* Studien. Das Gal4-UAS System erlaubt die gleichzeitige Expression von dominant-negativen Proteinvarianten zusammen mit subzellulär lokalisierten Fluoreszenzproteinen. Dies ermöglicht funktionelle Studien spezifischer Kandidatenproteine in der Zellwanderung. Mittels konfokaler Zeitraffermikroskopie können Effekte auf die Zellkomponenten und deren Zusammenspiel direkt im lebenden Zebrafisch untersucht werden. Diese Möglichkeit könnte dazu beitragen, die bisher getrennten Felder der Entwicklungsbiologie und der Zellbiologie in einem neuen Feld der *in vivo* Zellbiologie zu vereinen.

Index:

Abstract	I
Zusammenfassung	III
Index:	1
1. Introduction	4
1.1. The hindbrain	5
1.2. Development of the hindbrain.....	6
1.2.1. Morphogenesis of the neural tube in zebrafish	6
1.2.2. Induction of the neural plate	11
1.2.3. Anterior-posterior patterning of the central nervous system	12
1.2.4. Proliferation and neuronal migration in the developing hindbrain	17
1.3. The role of cellular organelles during neuronal differentiation	19
1.3.1. Interkinetic nuclear migration	19
1.3.2. The centrosome in neuronal differentiation	23
1.3.3. Molecular mechanisms in neuronal migration	25
1.4. The Gal4-UAS system	28
1.4.1. Gal4 in yeast – Composition and Function	28
1.4.2. Gal4-based technologies	29
1.4.3. Gal4-UAS mediated gene expression – a versatile tool in Drosophila research	31
1.4.4. Adaptation of the Gal4-UAS system in zebrafish	36
1.5. <i>In vivo</i> time-lapse microscopy	41
1.6. Photoacoustic tomography	42
1.7. Aims and achievements.....	44
1.7.1. Adaptation of the Gal4-UAS system for zebrafish	44
1.7.2. Generation of hindbrain specific Gal4 activator strains by enhancer trapping	44
1.7.3. Investigation of rhombomere fate	45
1.7.4. Opto-acoustic tomography of adult zebrafish	45
1.7.5. <i>In vivo</i> cell biology of tegmental hindbrain nuclei (THN) neurons	46
2. Materials & Methods	48
2.1. Materials.....	48
2.1.1. Bacteria	48
2.1.2. Cell lines	48
2.1.3. Chemicals	48
2.1.4. Devices	49
2.1.5. Equipment	49
2.1.6. Solutions	52
2.1.7. Antibodies	54
2.1.8. Enzymes and Kits	54
2.1.9. DNA	55
2.1.10. Vectors	55

2.1.11.	Zebrafish strains	59
2.2.	Methods	60
2.3.	Molecular biological methods	60
2.3.1.	Restriction digest of plasmid-DNA	60
2.3.2.	Blunting 5'-DNA overhangs	60
2.3.3.	Dephosphorylation of DNA	60
2.3.4.	DNA-Ligation	61
2.3.5.	Production of CaCl ₂ competent cells	61
2.3.6.	Transformation of bacteria	61
2.3.7.	TA-Cloning	62
2.3.8.	DNA-preparations	63
2.3.9.	Determination of nucleic acid concentration	66
2.3.10.	Separation of DNA in an agarose gel	66
2.3.11.	Amplification of DNA sequences via PCR (polymerase chain reaction)	67
2.3.12.	DNA Extraction and Inverse Nested PCR	68
2.3.13.	Synthesis of mRNA	68
2.3.14.	Separation of RNA in an agarose gel	69
2.3.15.	RNA-cytoplasmic injection	70
2.3.16.	DNA-cytoplasmic injection	70
2.3.17.	Whole-mount in-situ-hybridisation (ISH)	70
2.3.18.	Immunohistochemistry	75
2.3.19.	Rhodamine Dextran Retrograde Labelling	75
2.3.20.	Cell culture	75
2.3.21.	Culturing zebrafish pac2 embryonic fibroblasts	76
2.3.22.	Determining cell numbers	76
2.3.23.	Transfection	76
2.3.24.	Quantitation of the Gal4 – mediated expression system	77
2.3.25.	Luciferase assays	77
2.3.26.	Bodipy Ceramide staining	79
2.3.27.	Embedding Embryos for microscopic investigations	79
3. Results	81
3.1.	Adaptation of the Gal4-UAS system for zebrafish.....	81
3.1.1.	Generation of transgenic Gal4 zebrafish	81
3.2.	Generation of hindbrain specific Gal4 activator strains	84
3.3.	Investigating rhombomere fate.....	94
3.4.	Further applications of Gal4 enhancer trap strains.....	98
3.4.1.	Elucidating the role of Lunatic Fringe in hindbrain development	98
3.4.2.	Gal4 mediated tumor models	101
3.5.	Photoacoustic imaging of fluorescent proteins in adult zebrafish.....	104
3.6.	<i>In vivo</i> cell biology of tegmental hindbrain nuclei	109
3.6.1.	Subcellular intravital labelling in zebrafish cells using fluorescent fusion proteins	110
3.6.2.	Simultaneous multicolour labelling	111
3.6.3.	Generation of a rhombic lip specific KalTA4 activator strain	114
3.6.4.	Subcellular analysis of THN neuronal progenitor behaviour	116

3.6.5.	Axonogenesis in THN neurons is not induced by proximity of the centrosome	119
4.	Discussion	124
4.1.	Adaptation of the Gal4-UAS System for zebrafish	124
4.1.1.	Self-reporting Gal4 enhancer trapping	124
4.1.2.	Prolonging reporter gene expression until adulthood by a Gal4 dependent feedback loop	127
4.1.3.	Further applications of Gal4 enhancer trap strains	129
4.2.	Photoacoustic imaging of fluorescent proteins in adult zebrafish	130
4.3.	<i>In vivo</i> cell biology	131
4.3.1.	Gal4 mediated subcellular labelling	132
4.3.2.	Investigating THN precursor behaviour on a subcellular level	132
4.3.3.	The centrosome does not precede nuclear movement during ventral migration	133
4.3.4.	The centrosome position does not determine the site of axon outgrowth <i>in vivo</i>	134
5.	Movie legends	137
6.	Abbreviations	140
7.	Literature	143
8.	Appendices	155
9.	Acknowledgements	
10.	Publications	

1. Introduction

“The human brain, then, is the most complicated organization of matter that we know.”
-Isaac Asimov- (1920-1992)

In order to establish the human central nervous system (CNS) 10^{11} cells must be positioned correctly and 10^{15} connections between them need to be established to form functional neural circuits (Kandel et al., 2000). For more than one hundred years, since Ramón y Cajal's (1852-1934) pioneering investigations into the structure of the brain, elucidating the mechanisms underlying the development of this organ has been a major challenge.

During CNS development the behaviour and the fate of a cell is determined by interactions with other cells. For example, migrating cells or axons are guided to their destination by secreted factors or direct interactions with surrounding cells. Thus, the development of the central nervous system is ideally studied in a living organism, where all natural interactions between cells are present.

Among vertebrate model organisms, zebrafish (*Danio rerio*) with its external development and its transparency during embryonic stages offers the unique opportunity to study developmental processes in their natural environment. *In vivo* imaging using zebrafish as a model system is a powerful approach to unravel some of the mechanisms underlying the development of the central nervous system.

Therefore, in my PhD project I was using intravital imaging approaches ranging from confocal time-lapse microscopy to novel multispectral optoacoustic tomography to contribute to our understanding of the mechanisms underlying hindbrain development in zebrafish.

Although zebrafish is a well established model organism, until recently a conditional genetic system like the Gal4-UAS system in *Drosophila* or the Cre-lox system in mouse was not available. The first part of my PhD work was therefore dedicated to adapt the Gal4-UAS system for zebrafish, thus generating a versatile tool for combinatorial genetics (described in 3.1 and **Appendix 1**).

To take advantage of the genetic opportunities offered by the optimized Gal4-UAS system in studying hindbrain development, I performed a Gal4 enhancer trap screen to obtain hindbrain specific Gal4 strains (described in 3.2 and **Appendix 1**). I then used one of these strains to

follow the fate of distinct rhombomeres and their derivatives from embryonic to adult stages in a Gal4 mediated fate-mapping approach (described in 3.3 and **Appendix 1**).

Next, I generated a Gal4 based subcellular labelling system to answer the question how cellular components and in particular the centrosome, are involved in interkinetic nuclear movements, migration and axonogenesis. Applying this system to visualize cellular components of tegmental hindbrain nuclei (THN) precursors, I elucidated the dynamics of the centrosome during different differentiation stages by time-lapse microscopy (described in 3.6).

In my introduction, I will give a short overview about the development of the central nervous system, in particular the hindbrain in zebrafish. I will briefly discuss what is known about the underlying events and factors involved in hindbrain development. Next, I will summarize current knowledge about the role of the centrosome in neural migration and axonogenesis. Concluding my introduction, I will give a detailed description of the Gal4-UAS system and its versatile use in *Drosophila* research, as the adaptation and modification of the Gal4-UAS system was a major part of my PhD work.

1.1. The hindbrain

The hindbrain or rhombencephalon is the evolutionarily most ancient part of the vertebrate brain (Jackman et al., 2000) and its organization is therefore similar across vertebrate species. In the adult human and the adult zebrafish, the hindbrain is composed of the posteriorly located medulla oblongata, the ventro-anterior pons and the dorso-anterior cerebellum (Fig.1). The medulla and pons together with the midbrain are often referred to as the “brainstem”. Neuronal groups in the medulla oblongata participate in regulating blood pressure and respiration. The medulla oblongata also contains neuronal cell groups involved in taste, hearing, maintenance of balance and control of neck and facial muscles (Kandel et al., 2000). The pons lies rostral to the medulla and protrudes from the ventral surface of the brainstem. The ventral portion of the pons contains a large number of neuronal clusters, the pontine nuclei, that relay information about movement and sensation from the cerebral cortex to the cerebellum. The dorsal portion of the pons contains structures involved in respiration, taste and sleep (Kandel et al., 2000).

The cerebellum receives somatosensory input from the spinal cord, motor information from the cerebral cortex and input about balance from the vestibular organs of the inner ear. The main functions of the cerebellum are the control of balance, coordination of head and eye

movements and fine tuning of muscle movements. It is also involved in learning motor skills and, as suggested by functional imaging studies may even have a role in language and other cognitive functions in humans (Kandel et al., 2000).

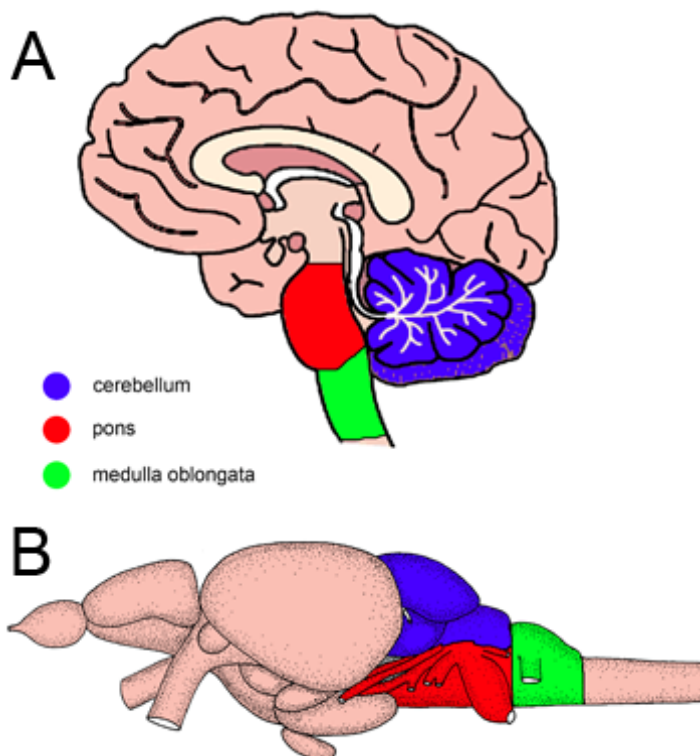


Fig. 1: Comparison of a human and a zebrafish brain

A) Schematic drawing of a human brain. B) Schematic drawing of a zebrafish brain. The cerebellum is depicted in blue, the pons in red and the medulla oblongata in green. Adapted from (Wullmann et al., 1996)

1.2. Development of the hindbrain

1.2.1. Morphogenesis of the neural tube in zebrafish

Compared to the human embryo, zebrafish embryonic development is extremely fast. Within 72 hours all major organs are established (Movie 1). In comparison, the human zygote only undergoes three cleavages within the same time (Nilsson and Hamberger, 1990).

During gastrulation stages, the germ layers of the developing zebrafish are established: the ectoderm, which gives rise to the nervous system and the skin, and the mesendoderm, splitting up into endoderm, which gives rise to tissues like the gut, the liver and the pancreas and the mesoderm, which develops into the muscles, kidneys, skeleton, heart and blood.

The beginning of involution of future mesendodermal cells defines the onset of gastrulation in zebrafish. As a consequence, a thickened marginal ring, termed the germ ring, appears. The

germ ring plays an important role in conferring posterior CNS identity as will be discussed in 1.2.3.

Fate-mapping studies revealed that already at this early stage, at the beginning of gastrulation (6 hpf), cells of the presumptive neuroectoderm are arranged in largely non-overlapping regions that are destined to give rise to distinct anterior posterior identities of the future CNS (telencephalon, diencephalon, mesencephalon, rhombencephalon) (Fig.2) (Woo et al., 1995).

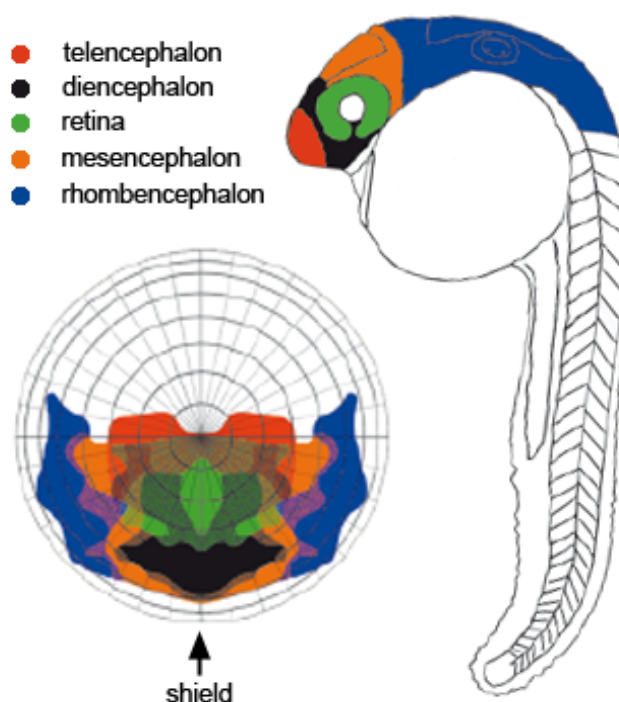


Fig. 2: Fate-map of the early zebrafish gastrula

Fate-map of the neural region at 6 hpf (shield stage - left) and zebrafish embryo at 24 hpf (right). Domains, which give rise to the telencephalon (red), diencephalon (black), retina (green), mesencephalon (orange) and rhombencephalon (blue) are depicted. Adapted from (Woo et al., 1995) and (Moens and Prince, 2002)

After involution convergence movements produce a local accumulation of cells at one position along the germ ring, the so-called embryonic shield, which functions as an organizer to induce neuroectoderm (see 1.2.2) (Kimmel et al., 1995).

In addition, the primary body axis is formed by cells converging towards the midline and the body axis is expanded along the anterior posterior axis by intercalation of cells.

Around tailbud stages at the end of gastrulation, a thickening of the dorsal epiblast appears, the first morphological sign of the development of the CNS rudiment, the neural plate

(Fig.3A). Between the stages of 6-10 somites, the neural plate condenses to form the neural keel (Fig.3B). At 15 somite stage the neural keel has transformed into the cylindrically shaped neural rod, which has detached from adjacent skin ectoderm and starts to be covered with epidermis (Fig.3C). Lateral positioned cells are rearranged to dorsal positions and will give rise to neural crest cells by delamination (red cells in Fig.3). In a secondary cavitation process beginning at 17 somite stage, a neural lumen forms and the neural tube is established (Fig.3D) (Kimmel et al., 1995).

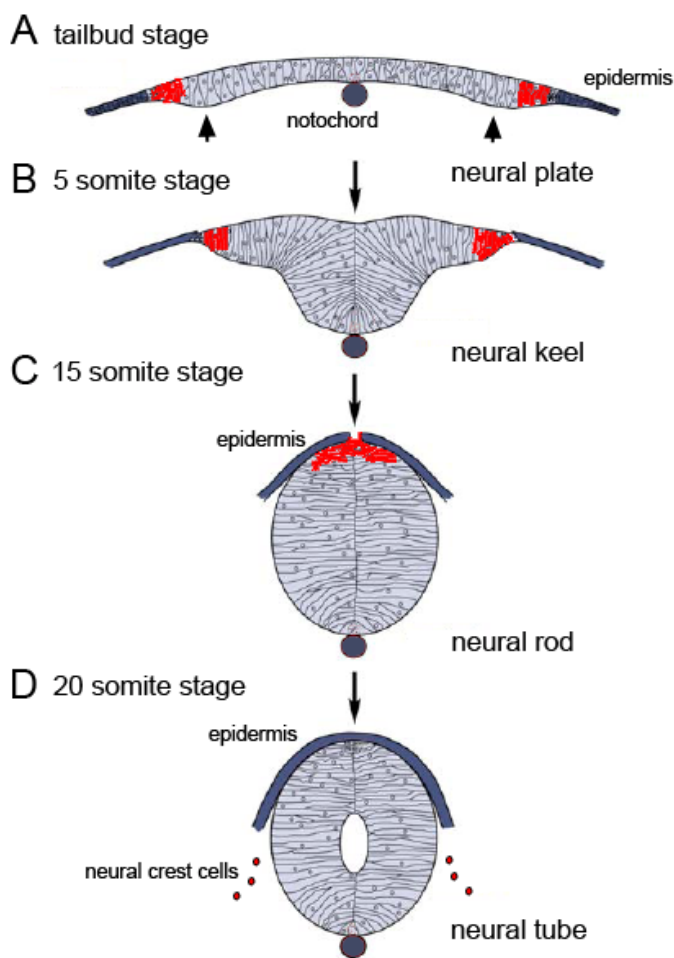


Fig. 3: Stages of zebrafish neurulation

Schematic drawings of cross sections through the early zebrafish embryo at different stages. Neural crest cells and their precursors are depicted in red. During the process of neurulation initially medially located cells of the neural plate will be positioned ventrally in the neural tube and lateral positioned cells of the neural plate will end up dorsally in the neural tube. A) At the tailbud stage the neural plate is a pseudostratified epithelium with two lateral bulges (arrows). B) At the 5 somite stage convergent movements towards the midline have formed the neural keel. C) At the 15 somite stage the neural rod is established. The neural rod has detached from adjacent epidermis, which starts to cover the neural rod D) In a secondary cavitation process a neural lumen has formed at the 20 somite stage and the CNS anlage is now termed neural tube. Adapted from (Geldmacher-Voss et al., 2003)

Around the same time as neurulation, segmentation of the nervous system begins along the anterior-posterior axis. Constrictions divide the neural tube into so called neuromeres. The so-called midbrain-hindbrain boundary (MHB) is a characteristic and important constriction that can be observed separating the midbrain from the hindbrain. At the 18 somite stage 10 neuromeres are visible, the telencephalon, the diencephalon, the mesencephalon and seven neuromeres in the rhombencephalon, termed rhombomeres (r1-7) (Fig.4) (Kimmel et al., 1995).

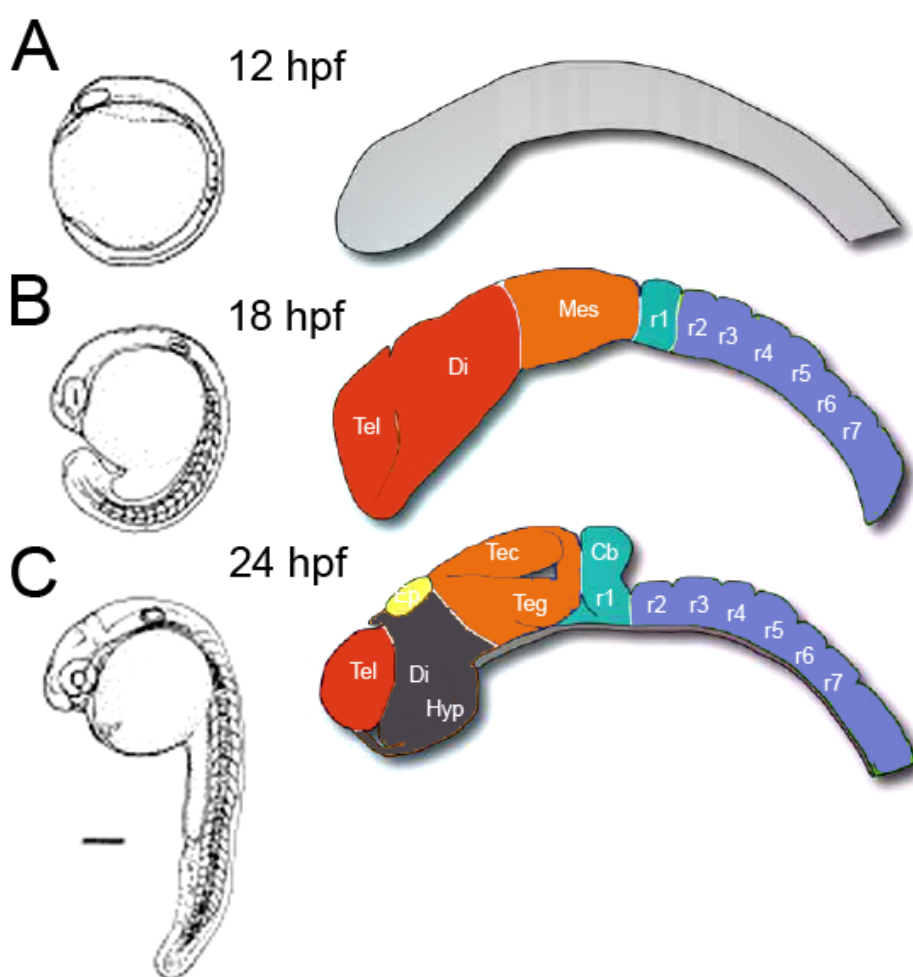


Fig. 4: Segmentation of the central nervous system in zebrafish

Schematic drawings of the entire zebrafish embryo are shown on the left with accompanying schematic drawings of the brain rudiment at the respective stage on the right. A) At 12 hpf no segmentation of the brain rudiment is visible. B) At 18 hpf 10 neuromeres have developed, the telencephalon (Tel), the diencephalon (Di), the mesencephalon (Mes) and the 7 neuromeres of the rhombencephalon (r1-7). C) At 24 hpf brain morphogenesis has advanced and several structures like the hypothalamus (Hyp), the epiphyses (Ep), the tectum (Tec) and tegmentum (Teg) can be recognized. The cerebellar anlage (Cb) is evident in the dorsal region of rhombomere 1. Abbreviations: Tel: Telencephalon, Di: Diencephalon, Hyp: Hypothalamus, Ep: Epiphyse, Tec: Tectum, Teg: Tegmentum, Mes: Mesencephalon, Cb: Cerebellar anlage, r1-7: Rhombomeres 1-7. Scale bar 200µm. Adapted from (Kimmel et al., 1995)

Segmentation of the hindbrain into rhombomeres is a strategy to specify compartments with distinct identities and future functions, e.g. control of distinct facial muscles by different cranial nerves. The mechanisms and molecular players that are involved in the process of segmentation will be discussed in 1.2.3. Rhombomeres are true segments as proliferation, neurogenesis and axonal projections are arranged in a reiterative fashion in successive rhombomeres (Kiecker and Lumsden, 2005). Rhombomeres are further separated by cell lineage restriction boundaries, being established by the interaction of Eph and Ephrins as will be described in 1.2.3.3 (Kiecker and Lumsden, 2005).

Pharyngeal arches lie ventral to the head and like the hindbrain show a segmental organization. Neural crest cells, which give rise to bones, cartilages and connective tissue of the pharyngeal arches arise from the dorsal part of the neural tube from different rhombomeres (Fig.3). The segmentation and patterning of the hindbrain and the pharyngeal arches are intimately linked by these neural crest cells (Lumsden et al., 1991). For example, zebrafish neural crest cells that arise from r1-3 migrate into the first pharyngeal arch to form jaw structures (Schilling and Kimmel, 1994). The hindbrain also gives rise to cranial nerves V-XII in a rhombomere dependent organization. Cranial nerves can have both motor and sensory components and hindbrain cranial nerves are involved in taste, hearing, balance, mastication, facial expressions and eye movements. Like neural crest cells, hindbrain derived cranial nerves innervate pharyngeal arches in a segment-dependent manner. For example, the first pharyngeal arch is innervated by the trigeminal branchiomotor nerve, which has its cell bodies in r1-3.

The reticulospinal neurons of the hindbrain, which provide the major route through which the brain communicates with the spinal cord to control locomotion are also arranged in a rhombomere dependent manner (Moens and Prince, 2002).

All these examples show the close link between morphological organisation and later function of neuronal clusters in the hindbrain and of cells derived from it.

The morphological appearance of rhombomeres as bulges is only transient (see Fig.4). The same holds true for the expression of genes, characteristic for distinct rhombomeres, like *krox20* (*egr2b* in zebrafish) in r3/5 (Oxtoby and Jowett, 1993). The question then arises as to whether the segmental hindbrain organisation is maintained up to adult stages. By orthotopically transplanting quail cells from r3/5 into chicken embryos (both E2) Wingate and Lumsden could show that rhombomeres in chicken are maintained at least up to E10 (Wingate and Lumsden, 1996). Experiments at later stages were not performed.

I therefore use a Gal4 mediated fate-mapping approach to ask, whether segmental hindbrain organisation is still maintained up to adult stages in zebrafish (see 3.3).

1.2.2. Induction of the neural plate

Cell dissociation experiments using *Xenopus* gastrula-stage animal caps suggested that ectodermal cells have an innate tendency to differentiate into neural tissue, if they receive no signal at all (Born et al., 1989; Godsave and Slack, 1989; Grunz and Tacke, 1989). In contrast, “Bone Morphogenic Protein” (BMP) in particular BMP4 signalling via Smad1 induces them to become epidermis (Stern, 2005).

In their famous experiment in 1924 Spemann and Mangold identified an organizing region (later called the Spemann-organizer), the most dorsal-lip of the amphibian blastopore destined to form the dorsal mesoderm, which when transplanted to the ventral side of another embryo induced ectodermal cells to acquire a neural fate and led to the formation of a secondary body axis including a complete second nervous system (Spemann and Mangold, 1924). This ability of the Spemann-organizer to specify neural tissue is termed neural induction. The equivalent structures in other species, Hensen’s node in avians, the node in mammals and the embryonic shield in teleosts, were found to have similar inductive properties (Beddington, 1994; Shih and Fraser, 1996; Waddington, 1932).

Later on the molecular mechanisms underlying neural induction were discovered and it could be shown that the Spemann-organizer expresses BMP antagonists like Chordin (Sasai et al., 1994), Noggin (Smith and Harland, 1992) and Follistatin (Hemmati-Brivanlou et al., 1994) during gastrulation in *Xenopus*, which inhibit BMP signalling and thus induce the neural plate. However, more recent findings in *Xenopus* and chick suggest that the actual mechanism underlying neural induction is more complex than proposed in this simple “default model” and that additional factors, e.g. FGFs (Furthauer et al., 1997), IGFs (Pera et al., 2001) and Wnts (Baker et al., 1999) play important roles as well. In fact, inhibiting FGF-signalling in *Xenopus* or chick completely blocked neural induction (Stern, 2005). However, BMP and FGF show different importance for neural induction in different species. For example in ascidians, which are basal chordates, FGF activity rather than BMP inhibition, is the endogenous factor responsible for generating the nervous system (Inazawa and Kitakaze, 1998). Interestingly FGF, IGF and BMP pathways were found to converge at the level of BMP downstream targets, reconciling the default model with the new findings implicating FGFs and IGFs in neural induction. It has been shown that FGF or IGF activate MAP kinase

(MAPK), which inhibits the BMP effector Smad1 by phosphorylation, hereby inducing a neural fate (Pera et al., 2003; Wilson and Edlund, 2001). In zebrafish, it has been proposed that both BMP inhibition and FGF signalling can act as direct neural inducers, with BMP antagonists functioning to induce the anterior CNS, while FGFs induce posterior neural plate; the combination of both specifies intermediate regions (Furthauer et al., 1997; Furthauer et al., 2004; Kudoh et al., 2004).

1.2.3. Anterior-posterior patterning of the central nervous system

After ectodermal cells have been induced to follow a neuroectodermal fate their position along the anterior-posterior axis of the later nervous system needs to be specified.

In the classical two step “activation-transformation” model for neural patterning (Nieuwkoop, 1952) it was hypothesized that during gastrulation all neural tissue newly induced by an organizer (activation step) is initially of anterior (forebrain) character and that a second posteriorizing signal (transformation step) modifies this character in a graded manner to give rise to more posterior structures like the hindbrain and the spinal cord (Sasai and De Robertis, 1997).

In agreement with this model zebrafish cells expressing a forebrain marker (*otx2*) at early gastrula stage were found to downregulate it by mid-gastrula stages and express mid- and hindbrain markers instead (Erter et al., 2001).

The posteriorizing signal was found to originate from the germ ring as transplanted mesodermal tissue from the ventral or lateral germring was able to induce expression of hindbrain specific genes in the forebrain of host embryos (Woo and Fraser, 1997).

1.2.3.1. Wnt and Retinoic Acid in anterior posterior patterning

Retinoic acid (RA) and Wnt signalling appear to be the major pathways specifying the hindbrain territory. Wnt8 and Retinaldehyde Dehydrogenase 2 (Raldh2), the ultimate enzyme in the retinoic acid biosynthetic pathway are both expressed in the germring at the onset of gastrulation (Begemann et al., 2001; Erter et al., 2001).

Blocking Wnt8 function causes expansion of the forebrain and loss of zebrafish hindbrain markers. In contrast, the absence of Wnt inhibitors like Masterblind/Axin, which antagonizes Wnt signalling through phosphorylation of β -Catenin, causes loss of the anterior forebrain

(Heisenberg et al., 2001).

Thus, posteriorizing signals seem to be required to inhibit anterior identities, but these signals must in turn be antagonized anteriorly to limit the spread of posterior identities (Moens and Prince, 2002).

The boundary between the midbrain and the hindbrain is defined by the two homeobox genes *otx2* and *gbx2* (*gbx1* in zebrafish), which are expressed in a non-overlapping manner in the anterior and posterior neural plate, respectively at the end of gastrulation. The junction between *Otx2* and *Gbx2* defines the position of the MHB (Wurst and Bally-Cuif, 2001).

Posterior to the MHB retinoic acid directly regulates Hox gene expression, to confer segment identity to regions of the hindbrain, as the enhancers of several *Hox* genes contain retinoic acid response elements (RARE) (Gavalas and Krumlauf, 2000).

Further, reduction of retinoic acid signalling results in hindbrain patterning defects ranging from partial transformations of hindbrain rhombomere identities to severe loss of posterior hindbrain and anterior spinal cord tissues, depending on the degree of interference.

The zebrafish mutant *neckless*, which carries a mutation in *Raldh2*, has delayed and abnormal *Hox* gene expression and shows a truncated hindbrain posterior to rhombomere 6 (Begemann et al., 2001). This and other studies suggest that more posterior territories are specified by high levels of retinoic acid (Gavalas, 2002).

Shortly after gastrulation at around 10hpf the future zebrafish hindbrain is already subdivided into areas that have distinct molecular identities and will give rise to the rhombomeres. Expression of specific rhombomere markers like *krox20* in rhombomere 3 and 5 (see **Appendix 1**) and *valentino/mafB* in rhombomeres 5 and 6 can already be observed. Valentino and Krox20 act upstream of *Hox* genes. Valentino has been shown to regulate the expression of *hoxb3* in both the mouse (Manzanares et al., 1997) and the zebrafish (Prince et al., 1998). Valentino is required autonomously for cells to acquire rhombomere 5 and 6 identity as cells lacking *valentino/mafB* are excluded from rhombomere 5/6 of a wildtype host embryo (Moens et al., 1998; Moens et al., 1996).

The zebrafish mutant *valentino/mafB* lacks rhombomeres 5 and 6, and instead possesses a region one rhombomere in length and of mixed identity, termed rX, that lies between (but does not form morphological boundaries with) r4 and r7 (Moens et al., 1996).

1.2.3.2. Hox genes in anterior posterior patterning

Hox genes are expressed in an ordered and nested manner in the hindbrain and their borders of expression coincide with rhombomere boundaries (Wilkinson et al., 1989).

Interestingly, hindbrain architecture bears a striking resemblance to the *Drosophila* embryo body plan, which is established through a cascade of genes that drive progressive antero-posterior subregionalization to produce a segmented larva in which every segment will give rise to a specific part of the adult fly. As in the vertebrate hindbrain the positional identity of each segment in *Drosophila* is defined by the combinatorial expression of Homeotic Selector genes such as the *Hox* genes (Kiecker and Lumsden, 2005).

The function of *Hox* genes in hindbrain segmentation has been extensively studied in mice, where many of the genes have been mutated by homologous recombination (Lumsden and Krumlauf, 1996). The classical phenotype associated with *Hox* mutations is a transformation to a more anterior segment identity. For example, *Hoxb1a* is uniquely expressed in r4. This rhombomere shows characteristics of r2 in *Hoxb1a* deficient mice and zebrafish. Facial motor neurons born in r4 fail to migrate to r6 and vestibular-acoustic neurons fail to migrate to the contro-lateral side of r4. Instead, both types of neurons follow a dorso-lateral migration resembling r2-specific trigeminal neurons (McClintock et al., 2002; Studer et al., 1996).

All vertebrates have multiple clusters of *Hox* genes, which are believed to reflect ancient genome duplications (Sidow, 1996). Mouse and human have four *Hox* clusters (A-D), each lying on a different chromosome. The genes fall into 13 paralogous groups, but due to multiple gene losses no individual cluster has all 13 paralogs. The teleost fishes have undergone another major genome duplication event, which has resulted in a seven *Hox* cluster arrangement in zebrafish. Although there are a larger number of *Hox* genes in zebrafish (48 compared to 39 in mouse), overall they show a similar expression pattern to their murine homologs (McClintock et al., 2001) (Fig.5) and also exert similar functions (McClintock et al., 2002). The particular combinations of expressed *Hox* genes give identity to the different hindbrain rhombomeres. Thus, in vertebrates, as in flies, the role of *Hox* genes is to confer positional identity on individual elements of a meristic series (Bell et al., 1999).

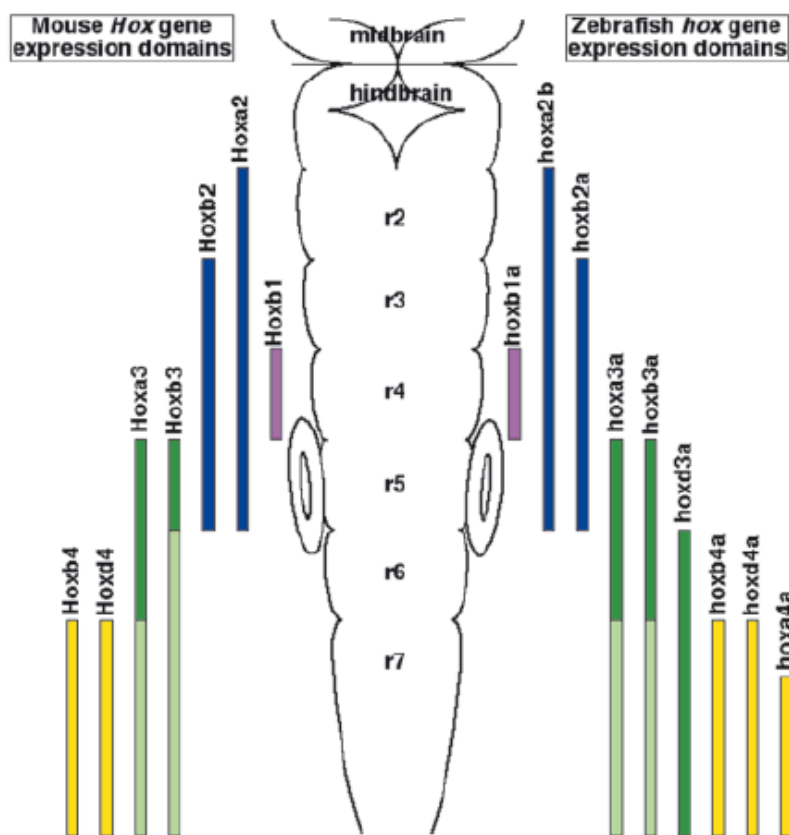


Fig. 5: Expression domains of *Hox* genes mouse and zebrafish

Schematic drawing comparing the expression domains of *Hox* genes in the hindbrain in mouse (left) and in zebrafish (right). Anterior is to the top. Paralogous groups are colour coded. From (Moens and Prince, 2002)

1.2.3.3. The role of Eph receptors and Ephrins in establishing rhombomere boundaries

To maintain organized patterns of segmental identity, such as the rhombomeres, the cell mixing between distinct domains must be inhibited by the formation of boundaries.

Eph receptor tyrosine kinases and their ligands, the Ephrins play a major role in setting up rhombomere boundaries and in maintaining them by mediating repulsion between cells of different rhombomere identity, and also by mediating adhesion between cells within a rhombomere.

The Eph family of receptors and their ligands, the Ephrins, are both divided into two classes, A and B according to their binding properties (Flanagan and Vanderhaeghen, 1998; Holder and Klein, 1999). As a general scheme, Ephrins from class A bind to EphA receptors and Ephrins from class B bind to EphB receptors. EphA4 is the only receptor shown to bind Ephrins of both classes A and B (Gale et al., 1996). Eph and Ephrins are both membrane-bound and following their interaction each can transduce signals that regulate cell responses.

In the zebrafish hindbrain, interacting Ephs and Ephrins are expressed in complementary, rhombomere-restricted domains such that each rhombomere boundary forms at an interface between the expression domains of one or more receptor ligand pairs (Fig.6). The expression of Eph receptors and Ephrins is regulated by segmentally expressed transcription factors. For example, Valentino and Krox20, besides regulating *Hox* gene expression, also control *eph* expression. The transcription of *epha4* in r3 and r5 is under direct control of Krox20. Valentino positively regulates *ephb4a* and negatively regulates *ephrinB2a* expression in r5/6. Eliminating EphA4 in r3/5 in zebrafish embryos by morpholino injection results in improper cell sorting and disorganized rhombomeres. In addition, in mosaic embryos EphA4 expressing and non-expressing cells sort from one another within r5, indicating an EphA4 dependent adhesion within rhombomeres (Fig.7) (Cooke et al., 2005). The repulsion mediated by Eph-Ephrin pairs at rhombomere boundaries is initiated by endocytosis of interacting Eph-Ephrin pairs, which induces cytoskeletal collapse and leads to the disengagement of cells (Poliakov et al., 2004).

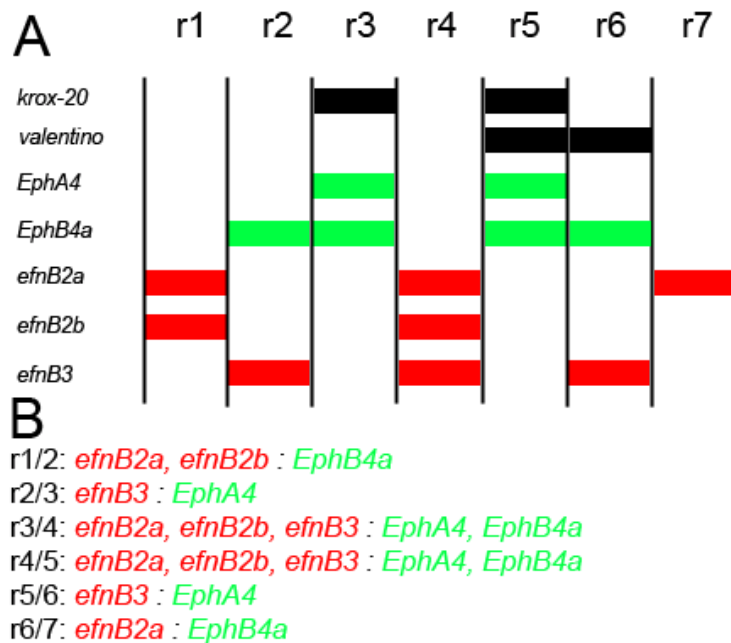


Fig. 6: Expression of Eph receptors and Ephrins in the hindbrain

A) Schematic drawing of expression domains of Eph receptors (green) EphA4 and EphB4a, Ephrins (red) ephrinB2a (*efnB2a*), ephrinB2b (*efnB2b*) and ephrinB3 (*efnB3*) and upstream regulatory genes (black) *krox20* and *valentino* in the zebrafish hindbrain. B) Boundaries between rhombomeres (e.g. r1/2) are established by interaction of the depicted Ephrin and Eph receptor pairs (e.g. *efnB2a*, *efnB2b* and *EphB4a* in the case of r1/2). Adapted from (Cooke et al., 2005).

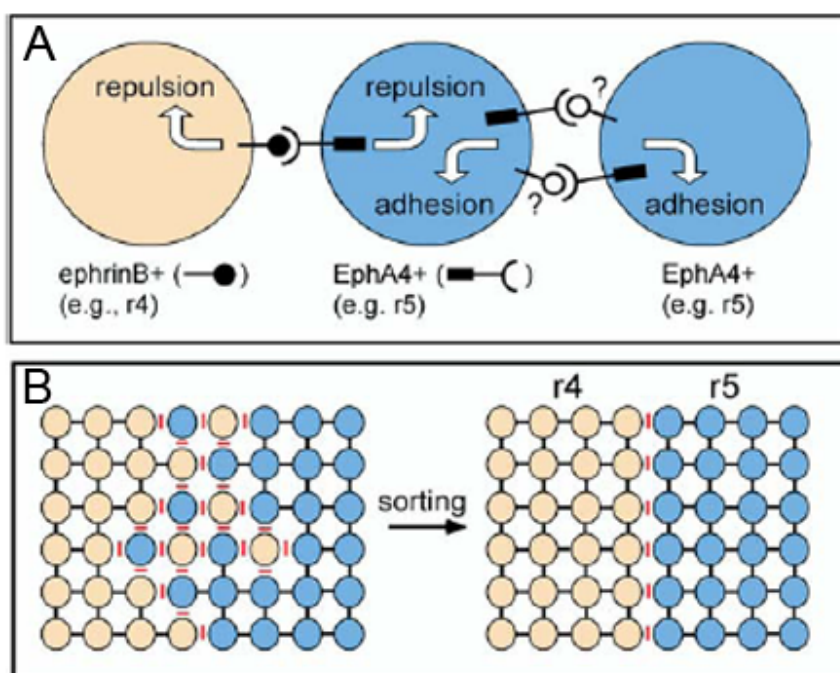


Fig. 7: Eph receptors and Ephrins in rhombomere boundary formation

A) At the forming boundary, where *ephA4* expressing cells (blue) from r5 are intermingled with *ephrinB* expressing cells (pink) from r4, contact between EphA4 and ephrinB cells leads to repulsion. At the same time, contact between *ephA4* expressing cells within r5 leads to an adhesive response. Currently the ligand for EphA4 within r3/5 is unknown, as indicated by a question mark. B) Cell sorting at the r4/5 boundary involving both repulsion between unlike and adhesion between like cells is thermodynamically more stable, because it minimizes repulsive interactions (red bars) and maximizes adhesive interactions (black joiners). From (Cooke et al., 2005)

1.2.4. Proliferation and neuronal migration in the developing hindbrain

The rhombic lip is the proliferative zone lining the 4th ventricle in the dorsal hindbrain (Fig.8). It is subdivided into an anterior part in r1, the upper rhombic lip (URL), which continues along the ventricle and is then termed lower rhombic lip (LRL) in its posterior part. Molecularly, neural progenitors in the rhombic lip are characterized by the expression of the bHLH transcription factor *Atonal1* (Wingate 2005).

The URL produces different neuronal cell types, which migrate out of the proliferation zone in a temporal sequence. The generation of different neuronal cell populations by the URL seems to be conserved among vertebrates. In the developing mouse, progenitors of the parabrachial, the parabigeminal and the laterodorsal-pedunculopontine tegmental hindbrain nuclei migrate first out of the URL, followed by neurons of the deep cerebellar nuclei and finally cerebellar granule cells (Machold and Fishell, 2005); (Wang et al., 2005). In zebrafish, progenitors of tegmental hindbrain nuclei, namely of the secondary gustatory nucleus, the secondary viscerosensory nucleus, the nucleus isthmi and the superior reticular nucleus are generated first by the URL between 16hpf and 48hpf (Volkman et al. 2009 under review),

followed by granule cell progenitors (Volkman et al., 2008). The homologues of deep cerebellar nuclei, the Eurydendroid cells arise from a different proliferation zone ventral to the upper rhombic lip, the ventricular zone (Bae et al., 2009).

In vivo studies characterized the migration and later axonogenesis of tegmental hindbrain nuclei precursors (THN) on a cellular level at stages when the cerebellum consists of a primitive neuroepithelium (about 28hpf) (Köster and Fraser, 2001a). At these stages THN precursor cells span the entire width of the neuroepithelium with connections to the basal side at the MHB and the apical side at the 4th ventricle. Time-lapse movies of zebrafish embryos expressing cytosolic GFP suggested a two step migration. In a first step, THN precursors migrate anteriorly out of the URL towards the MHB. During this phase cells show a leading process in the direction of migration and also maintain a long process still connecting them to their place of origin. At the MHB precursor cells change their polarity from bipolar to unipolar by retracting their trailing process, establish a presumptive axon from the leading process and change the direction of migration. In this second step, these neurons migrate ventrally to settle in ventral brainstem regions (Köster and Fraser, 2001a) (Fig.8).

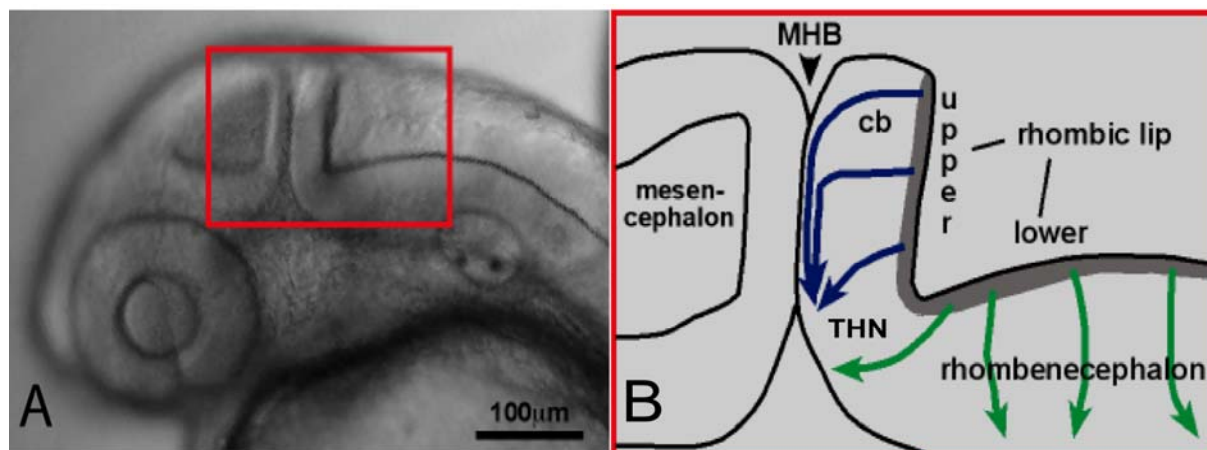


Fig. 8: Migratory pathways of rhombic lip descendents in zebrafish embryos

A) Embryonic zebrafish brain at 28hpf, the boxed area shows the enlarged region in B. B) Migratory pathways of upper rhombic lip descendents obtained from time-lapse recordings (Köster and Fraser, 2001a). Most rhombic lip descendents migrate rostrally towards the midbrain-hindbrain boundary (MHB). This is followed by ventral migration along the MHB. Adapted from (Köster and Fraser, 2001a).

Abbreviations: cerebellum (cb), mid-hindbrain boundary (MHB), tegmental hindbrain nuclei (THN)

1.3. The role of cellular organelles during neuronal differentiation

The compartmentalization of the hindbrain is important to confer positional identity on neurons, which is intimately linked with their later functions.

In addition, neuronal precursors have to undergo a variety of developmental steps themselves in order to establish functional neuronal networks. After proliferation, they have to migrate, terminally differentiate, generate axons and dendrites and finally undergo synaptogenesis to connect to their functional partners. These dynamic cell behaviours have to be coordinated by cellular organelle dynamics within the developing neuron.

1.3.1. Interkinetic nuclear migration

Neurons arise during development from a pseudostratified columnar epithelium composed of mitotically active neuroepithelial cells. These cells have an elongated shape, with cytoplasmic connections to both, the apical (ventricular) and basal surfaces. Their nuclei undergo characteristic apical-basal movements so-called interkinetic nuclear migration or interkinetic nuclear movements (INM), occupying different levels within the epithelium depending on the phase of the cell cycle. Mitotic (M phase) nuclei are located in close proximity to the apical surface, while nuclei undergoing DNA synthesis (S phase) are displaced more basally (Fig.9) (Frade, 2002).

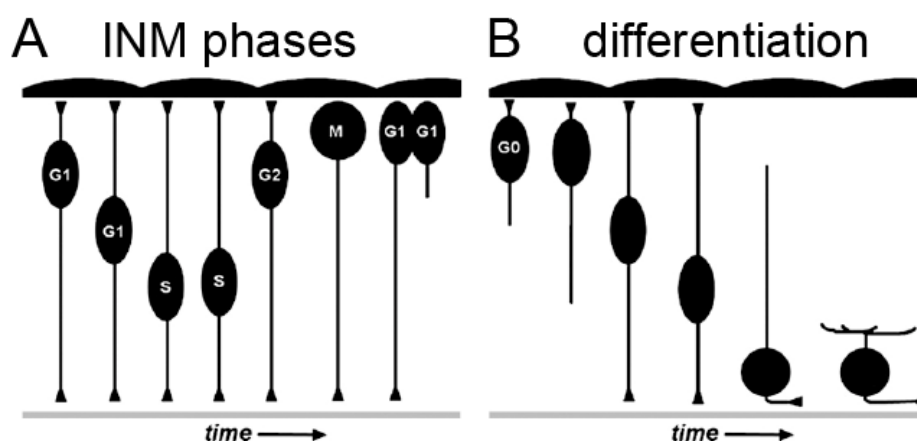


Fig. 9: Neuronal differentiation

A) Neuronal precursors in a proliferative neuroepithelium undergo interkinetic nuclear migration (INM). Their nuclei move from apical to basal and then from basal to apical in phase with the cell cycle. Mitotic cleavages are restricted to the apical side. During INM, cells keep both, apical and basal processes. B) Following cell cycle exit, progenitors migrate via nuclear translocation, start to differentiate and send out axons and dendrites. Apical is up and basal is down. Adapted from (Baye and Link, 2008).

Most studies on INM have been carried out in the retina and recently the dynamics of INM have been shown to correlate with neurogenic cell divisions, such that cells in which the nucleus migrates further basally are biased to become postmitotic neurons (Baye and Link, 2007). A possible mechanism was suggested by Del Bene et al. (2008), who discovered a Notch gradient in the zebrafish retina with high levels of Notch in the apical domain and high levels of Delta in the basal domain. In *Drosophila* Notch signalling was shown to inhibit neuronal differentiation by “lateral inhibition” (Chitnis, 1995) (Fig.10). Notch is a transmembrane receptor. Upon binding to its ligands Delta or Serrate (Jagged in mammals), which are expressed on neighbouring cells, the Notch intracellular domain (NICD) is released through cleavage by ADAM proteases and γ -secretase. NICD activates the expression of Hes factors (Her factors in zebrafish), which inhibit proneural genes, keeping the cell in a progenitor state (Bertrand et al., 2002). Initially neighboring cells show only small differences in Delta and Notch levels. In cells experiencing less Notch signalling, proneural genes like neurogenin will be expressed and a positive feedback loop will lead to higher amounts of Delta on the cell surface. Such a cell will undergo neuronal differentiation. Thus, by the process of lateral inhibition differences in Delta and Notch expression are amplified in neighboring cells so that only a subset of progenitors are selected to undergo neuronal differentiation. This mechanism seems to be conserved in the vertebrate retina (Jadhav et al., 2006; Nelson et al., 2006; Perron and Harris, 2000).

The purpose of INM, besides ensuring enough space for cells undergoing mitosis (Baye and Link, 2008) seems to be to regulate the duration and level of exposure of progenitor nuclei to neurogenic signals (Delta), ensuring the correct number of cells in a differentiated state and in a progenitor state (Fig.11) (Del Bene et al., 2008).

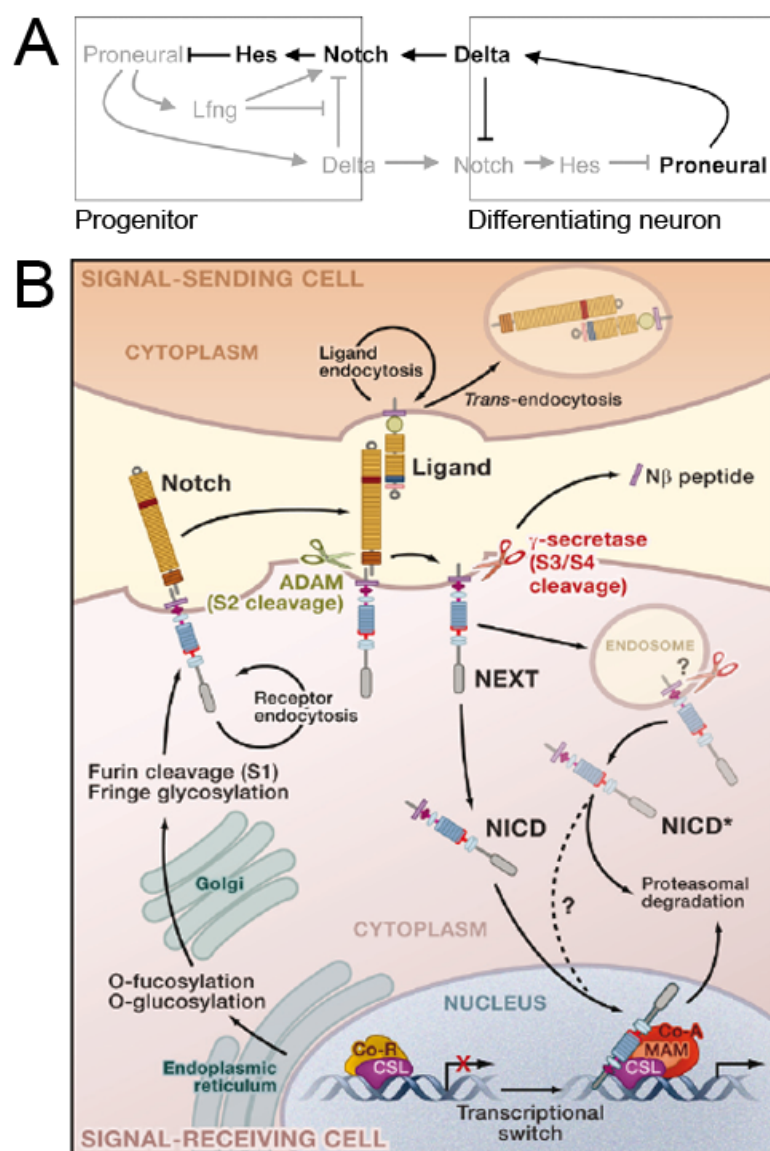


Fig. 10: Notch signalling in “Lateral inhibition”

A) Model of lateral inhibition: Notch signalling mediated by Delta binding to the Notch receptor leads to the upregulation of *Hes* genes, which in turn inhibit proneural genes in the Notch expressing cell. As Delta is positively regulated by proneural genes, strong Notch signalling leads to low levels of Delta. Low levels of Delta in turn, lead to low levels of Notch signalling in the neighboring cell, resulting in expression of proneural genes and Delta. By this means, a cell expressing high levels of Notch is kept in a progenitor state, whereas the proneural gene expression drives the neighboring cell to differentiate. The sensitivity of Notch towards its ligands can be regulated by glycosylation of Notch by Fringes like Lunatic Fringe (Lfng). B) Mechanism of Notch signalling. Binding of Notch ligands to the Notch receptor lead to cleavage of the Notch receptor by ADAM metalloprotease and γ -secretase, thereby releasing the Notch intracellular domain (NICD). NICD then enters the nucleus where it associates with the DNA-binding protein CSL. The transcriptional co-activator Mastermind (MAM) then recognizes the NICD/CSL interface and this triprotein complex recruits additional co-activators (CoA) to initiate transcription. Adapted from (Kopan and Ilagan, 2009) and (Nikolaou et al., 2009)

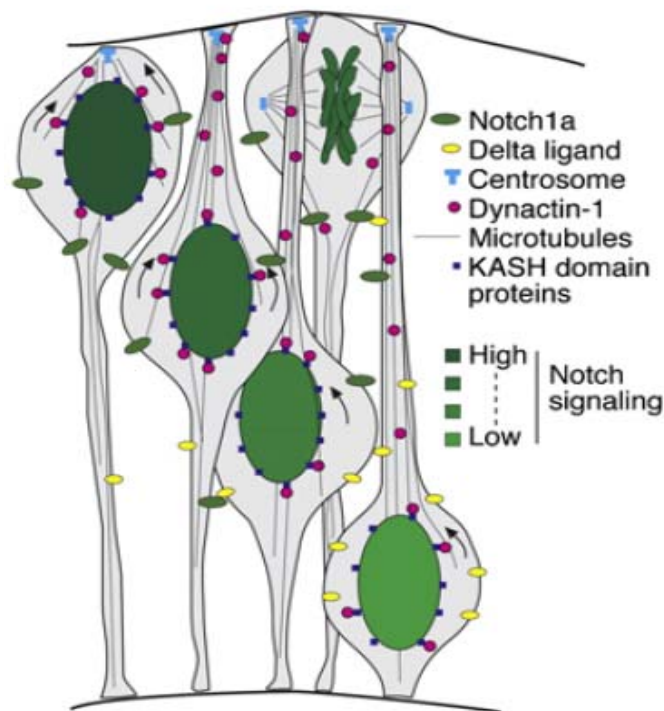


Fig. 11: Model of the Mechanism that couples INM with graded Notch activation

A) A gradient of Notch along the apico-basal axis of the neuroepithelium is likely to play a key role in neurogenesis. Notch mRNA is increased on the apical side, whereas Delta mRNA and protein are enriched basally. High concentrations of NICD can be found in the apical domains and increased *her4* expression in cells whose nuclei move into the high-Notch environment. Between mitoses, a progenitor nucleus moves twice through a Notch spatial gradient. If the nucleus stays close to the apical side, it will encounter high Notch levels throughout the cell cycle, and both of its daughters are likely to remain proliferative. On the other hand, if the nucleus is translocated more basally, Notch activity is reduced, predisposing the progenitor to produce one or two daughter neurons during its subsequent mitosis. From (Del Bene et al., 2008)

In good agreement with this model, in zebrafish *mikre oko* (*mok*) mutants retinal progenitors exit the cell cycle prematurely due to defects in INM, resulting in an overproduction of retinal ganglion cells (RGCs) and a severe reduction in the numbers of bipolar and Müller glia cells (Del Bene et al., 2008). *Mok* mutants are deficient in the motor protein Dynactin-1. Dynactin mediates the interaction of the microtubule minus end directed motor dynein with many cargoes and is required for correct nuclear migration (Fan and Ready, 1997; Whited et al., 2004). As the apical translocation of the nucleus via dynactin/dynein is disturbed in these mutants, retina progenitor cells are not kept in a proliferative state by Notch signalling, which is confined to the apical part of the neuroepithelium. Instead these progenitors exit the cell cycle prematurely (Del Bene et al., 2008). Additional experiments disrupting the coupling between nucleus and dynactin/dynein motor by morpholino knock down of the KASH domain containing anchor protein *Syne2a* showed the same phenotyp, thereby supporting this model (Del Bene et al., 2008).

Establishment of intrinsic cell polarity is an important prerequisite for the apico-basal Notch gradient. Thus, not surprisingly, the zebrafish mutant *heart and soul* (*has*), which is deficient in the atypical protein kinase λ (aPKC λ) shows defects in correct cell cycle exit in retinal ganglion cells (Zolessi et al., 2006). aPKC λ is part of the Par3/Par6/aPKC signalling complex associated with tight junctions and it is an important factor in establishing apico-basal polarity. Therefore aPKC λ deficiency leads to a variety of apico-basal phenotypes in retinal progenitors including basal localized mitosis, altered division plane orientation, postmitotic positioning defects and a reduced number of neurons (Baye and Link, 2007; Cui et al., 2007; Horne-Badovinac et al., 2001; Zolessi et al., 2006).

Establishment of polarity is also an important process during migration and axonogenesis. One of the key markers for cell polarity is the centrosome, also known as microtubule organizing center (MTOC). The position of the centrosome seems to be precisely regulated during neurogenesis, migration and differentiation to ensure the correct segregation of cell fate factors, efficient nucleokinesis and directed neurite outgrowth (Higginbotham and Gleeson, 2007).

1.3.2. The centrosome in neuronal differentiation

1.3.2.1. Centrosome dynamics during INM

In an electron microscopic analysis of proliferating neuroepithelial cells of the cerebral vesicle in mouse (Hinds and Ruffett, 1971) and in an immunohistochemical analysis of neuroepithelial cells of the cortical ventricular zone in ferret (Chenn et al., 1998) centrosomes were found to strictly localize to the apical (ventricular) side to maintain apico-basal polarity. During INM in the zebrafish retina the centrosomes were also found at the apical side. Centrosomes were only observed to leave this position, when cells detached their apical process to undergo differentiation (Del Bene et al., 2008; Zolessi et al., 2006). If these centrosome dynamics are a general scheme for developing brain compartments is poorly understood so far.

As retinal ganglion cells (RGCs) do not undergo extensive migration, knowledge about centrosome dynamics mainly originates from experiments on migrating cortical and cerebellar granule neurons in culture.

1.3.2.2. Centrosome dynamics during migration

Initial *in vitro* observations of the centrosome in these migrating cells have revealed that typically the centrosome is located ahead of the nucleus in the direction of migration (Gregory et al., 1988; Rakic, 1972). Subsequent time-lapse experiments of granule cells in cerebellum slice cultures have shown that neuronal migration occurs as a stepwise process. In a first step the migrating cell establishes a leading process. In a second step the centrosome moves into this process, hereby elongating the centrosome-nucleus distance. This is followed by a saltatory translocation of the nucleus in the direction of migration towards the centrosome. In a last step the trailing membrane is retracted. The shortened leading process subsequently elongates and the cycle repeats (Bellion et al., 2005; Higginbotham et al., 2006; Solecki et al., 2004; Tsai and Gleeson, 2005). This distinct type of neuronal migration is termed nucleokinesis (Tsai and Gleeson, 2005) (Fig.12).

In neuronal migration via nucleokinesis, the centrosome is always positioned ahead of the nucleus at the hub of the microtubule network termed the perinuclear cage, which was observed to surround the nucleus of mouse cerebellar granule cells *in vitro* (Tanaka et al., 2004) and *in vivo* in cerebellum slice culture (Solecki et al., 2004). It was thus postulated that the nucleus is being pulled forward by this microtubule network and that the centrosome acts as a link to relay the pulling forces generated in the leading process to the nucleus (Higginbotham and Gleeson, 2007). Interference with functions of proteins involved in stabilizing microtubules of the perinuclear cage like doublecortin (DCX) (Moores et al., 2006) or in coupling of the centrosome and the nucleus with the perinuclear cage like Lis1 (also known as PAFAH1b1) and the microtubule minus end directed motor protein dynein each leads to an impairment of nuclear translocation (Tanaka et al., 2004; Tsai et al., 2007).

In addition, actomyosin contraction at the rear of the cell likely also plays a prominent role to drive translocation of the nucleus and inhibiting non muscle myosin II by blebbistatin blocks the movement of the nucleus (Bellion et al., 2005; Tsai et al., 2007).

However, the molecular mechanisms underlying nucleokinesis are still under debate as the experimental data, especially on the role of the centrosome, is somewhat contradictory. For example, Umeshima et al. (2007) observed in their time-lapse imaging studies of radially migrating granule cells in mouse cerebellar slices that the movements of the nucleus and centrosome appeared to occur independently of each other. The nucleus often migrated ahead of the centrosome during its saltatory movement, negating the supposed role of the centrosome in pulling the nucleus. Furthermore, the nucleus was associated with dynamic

microtubules enveloping the entire nucleus and stable microtubules extending from the leading process to the anterior part of the nucleus. Neither of these perinuclear microtubules converged at the centrosome (Umeshima et al., 2007).

Additional experiments are therefore needed to unravel the dynamics of neuronal migration. Up to now, studies in living animals investigating neuronal migration over longer time-periods have not been carried out. Ideally, future studies will use subcellular time-lapse microscopy to address the dynamics and interactions of cell organelles over long time periods during neuronal migration in the living animal.

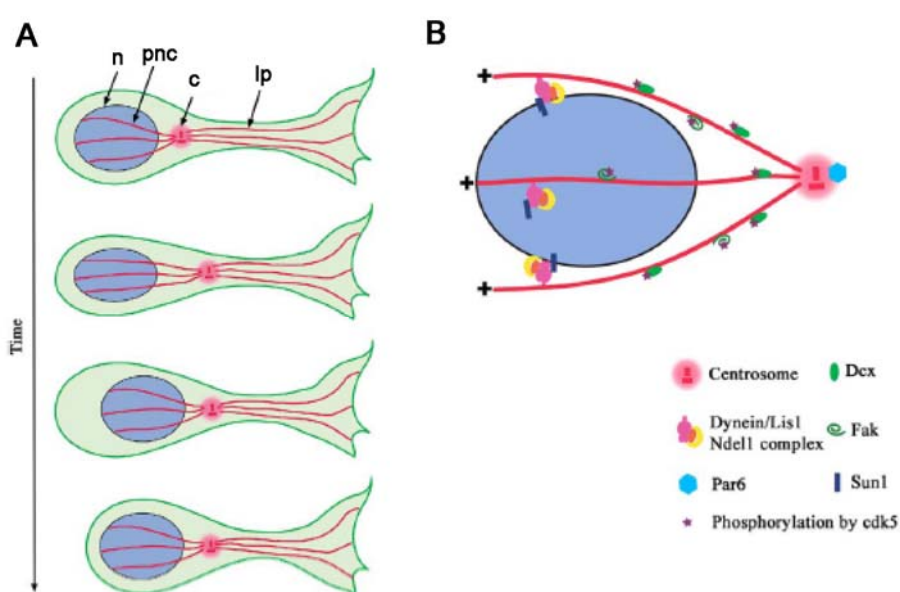


Fig. 12: Schematic representation of nucleokinesis

A) Schematic representation of the characteristic steps of nucleokinesis. Creation of a leading process (lp) filled with microtubule fibres initiates the movement. This is followed by the movement of the centrosome (c) into the leading process. The nucleus (n) is translocated, putatively by the microtubule network of the perinuclear cage (pnc), in the same direction, leaving a cytoplasm filled trailing process behind. The last cellular component to follow the previous movements is this trailing cytoplasm. B) Proteins involved in connecting the microtubule network to the nucleus (Dynein, Lis1, Ndel1 and Par6) or stabilizing the microtubules (Dcx and Fak). From (Tsai and Gleeson, 2005)

Abbreviations: leading process (lp), centrosome (c), perinuclear cage (pnc), nucleus (n)

1.3.3. Molecular mechanisms in neuronal migration

To switch from INM to migration via nucleokinesis the centrosome has to be relocated from the apical side of the cell in front of the nucleus. The question as to which factors play a role in positioning the centrosome within the leading process has mainly been addressed in primary rat astrocyte “scratch wound” assays. The reorientation of the centrosome in front of

the nucleus in the direction of the “wound” was found to be dependent on integrin stimulated activity of the Rho-GTPase CDC42, which regulates signalling from cell surface receptors to the actin-microtubule cytoskeleton (Etienne-Manneville and Hall, 2001) (Raftopoulou and Hall, 2004). CDC42 activity at the leading edge recruits and activates mPar6-aPKC ζ a regulator of polarity, which in turn inactivates Glycogen Synthetase Kinase 3 β (GSK-3 β).

Active GSK-3 β normally interferes with the binding of adenomatous polyposis coli (APC) to microtubule plus-ends (Etienne-Manneville and Hall, 2001; Zumbunn et al., 2001), but upon GSK-3 β inactivation, APC binds to microtubule ends and stabilizes them. APC binding facilitates microtubule capture at the leading edge by dynein, a microtubule motor required for centrosome positioning in many cell types (Etienne-Manneville and Hall, 2001; Palazzo et al., 2001). The microtubule minus-end motor activity of dynein pulls captured microtubules toward the leading edge and orients the centrosome within the protrusion towards the wound (Fig.13).

1.3.3.1. Centrosome dynamics in axonogenesis

Another important question that arises with respect to centrosome function during neuronal migration is its role in initiating and determining axon formation.

Real-time experiments using hippocampal neurons in culture suggested that the centrosome position determines the site of axon outgrowth (de Anda et al., 2005). De Anda and co-workers further showed that the generation of two centrosomes through blocking the cytokinesis with cytochalasin D led to the formation of neurons with two long axon-like neurites. Conversely, laser inactivation of the centrosome in *Drosophila melanogaster* neurons impaired axon formation (de Anda et al., 2005). Also, centrosomes could be found to localize to the site of newly emerging axons in cultured cerebellar granule cells (Zmuda and Rivas, 1998) and of pioneering neurons of the grasshopper (Lefcort and Bentley, 1989).

Intriguingly however, *DSas-4* mutant flies, which are unable to replicate centrioles and therefore lack functional centrosomes by the third instar larval stage have a morphologically normal CNS. Axon outgrowth is unaffected in these mutants questioning the importance of the centrosome in axonogenesis (Basto et al., 2006).

Elegant *in vivo* time-lapse studies in zebrafish have further shown that the centrosome does not localize to the site of axon outgrowth in retinal ganglion cells (Zolessi et al., 2006).

At the moment it remains elusive as to whether this discrepancy in the role of centrosome localization is due to differences between the *in vitro* and *in vivo* situation.

Additional studies are therefore needed to address this question in the living organism.

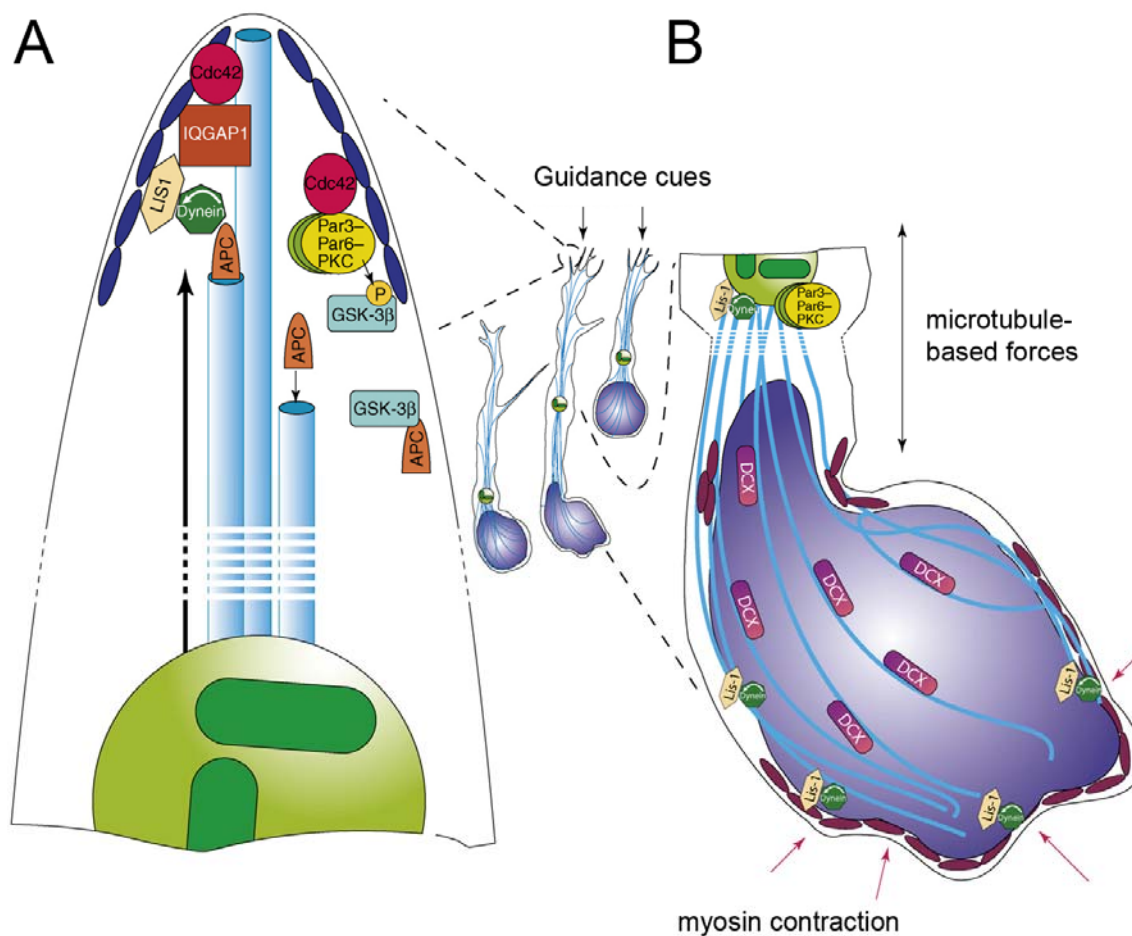


Fig. 13: Model of centrosomal positioning and mechanism of nuclear translocation during migration

A) Proposed mechanism of centrosomal positioning within the leading process during neuronal migration. Extracellular guidance cues stimulate Cdc42 mediated actin polymerization in the leading process. Cdc42 targets the Par complex to the leading edge, where it inactivates GSK-3 β , enabling microtubule plus end protein APC to bind to microtubules ends to stabilize them. IQGAP1 provides a link between actin and plus end microtubule tip proteins like APC. Lis1 and dynein provide pulling forces on microtubules that orients the centrosome within the leading process. B) Proposed mechanism of nuclear translocation. Lis1, dynein and Par6 α couple the centrosome and nucleus during nuclear translocation. Dynein motor movement generates forces on microtubules, whereas Doublecortin (DCX) stabilizes the microtubules of the perinuclear cage. Extension of the leading process generates tension between the centrosome and nucleus, pulling it forward (black arrows). Myosin (red ovals) constriction at the trailing edge squeezes the nucleus forward into the leading process (red arrows). From (Higginbotham and Gleeson, 2007).

Because of their accessibility for *in vivo* studies and well characterized behaviour on a cellular level, neurons derived from the zebrafish upper rhombic lip offer the opportunity to address the role of the centrosome in migration and axonogenesis in the living zebrafish embryo by time-lapse microscopy. Still, a subcellular labelling system to simultaneously label cellular components of URL derived progenitors is necessary for such studies. The Gal4-UAS system fulfils the requirements for such a system.

1.4. The Gal4-UAS system

The ability to regulate gene expression in a celltype-specific and temporally restricted manner provides a powerful means to monitor subcellular structures, label subsets of cells for developmental studies, but also to test gene function, bypass the action of lethal genes and target tissues for selective ablation or physiological analyses. Different methods for conditional genetics have been developed like the Gal4-UAS, Cre/loxP, Flp/FRT, Tet ON/OFF or the lexA system. In recent years, the adaptation of the Gal4-UAS system for zebrafish has received most attention.

1.4.1. Gal4 in yeast – Composition and Function

The Gal4-UAS system is originally derived from *Saccharomyces cerevisiae*.

The *GAL* gene family is required for the growth of yeast on galactose and is comprised of structural (*GAL1*, *GAL10*, *GAL2* and *GAL7*) and regulatory (*GAL4*, *GAL80* and *GAL3*) genes. The transcriptional regulatory protein Gal4 activates transcription of *GAL* genes in the presence of galactose by binding to defined DNA sequences upstream of target genes, the so-called upstream activating sequences (UAS), analogous to an enhancer element defined in multicellular eukaryotes (Guarente et al., 1982). The consensus UAS is a 17mer of the sequence 5' -CGG- N₁₁ -CCG- 3' (Giniger et al., 1985). The number of UAS sites and their relative affinity for Gal4 vary among the *GAL* genes and this leads to differential activation (Lohr et al., 1995) (Fig.14).

Gal4 is a modular 881-amino-acid protein with a Zn–Cys binuclear clustertype DNA-binding domain (DBD), a linker domain, a dimerization domain and two acidic activation domains (ADI and ADII) (Johnston, 1987; Lohr et al., 1995).

The crystal structure of the minimal DNA-binding domain (amino acids 1–65) in complex with a consensus UAS shows that Gal4 binds as a dimer (Marmorstein et al., 1992). The Gal4 Zn–Cys domains contact the CGG elements directly, whereas the linker and dimerization domains interact with the phosphate backbone of the spacer residues in the 17mer. The CGG

residues and the exact length of the spacer region are crucial for Gal4 binding (Liang et al., 1996). Domain-swap experiments with activators of the same family (Gal4, Put3 and Ppr1) showed that DNA-binding specificity is a function of a 19-amino-acid region C-terminal to the Zn–Cys cluster and not of the Zn–Cys cluster itself (Reece and Ptashne, 1993). Gal4 binding to multiple UAS elements is cooperative *in vitro* and leads to synergistic activation of transcription *in vivo* (Giniger and Ptashne, 1987; Giniger and Ptashne, 1988; Giniger et al., 1985; Kang et al., 1993).

Gal4 activates transcription by recruiting coactivators and the general transcription machinery to promoter regions through its activation domain. Proteins of the transcription machinery that have been shown to interact specifically with the Gal4 activation domain include TBP, TFIIB and SAGA (Bhaumik et al., 2004; Melcher and Johnston, 1995; Wu et al., 1996).

In the absence of galactose, Gal4 is inactive because of the repressor protein Gal80, which binds to the Gal4 activation domain and thereby inhibits its interaction with the transcriptional machinery, e.g. with the TATA-binding protein (TBP) or TFIIB (Johnston et al., 1987; Ma and Ptashne, 1987; Wu et al., 1996).

In the presence of galactose Gal3 binds to Gal80 hereby releasing it from Gal4 so that the Gal4 activation domain can interact with transcription factors to initiate transcription of target genes downstream of UAS sites. (Zenke et al., 1996) (Fig.15).

1.4.2. Gal4-based technologies

Two major technologies based on the transcriptional properties of Gal4 have been developed: the “yeast two-hybrid” system for screening protein-protein interactions and the Gal4-UAS system for tissue specific gene expression.

The “yeast two-hybrid” system is based on the findings of Fields and Song, who determined that the two separate and independent Gal4 DNA binding and transactivation domains, which lack function alone, could be synthesized as chimeric proteins with each Gal4 domain fused to one protein of interacting partner proteins (X and Y). Successful binding of partner proteins (X and Y) to each other brings the activation domain into close proximity to the DNA binding domain, thereby reconstituting the function of the Gal4 transcription activator protein and driving expression of a downstream reporter gene (Fields and Song, 1989). This technology is often applied by using the protein of interest fused to the DBD as a “bait” and screening libraries of proteins fused to the AD as “prey” for potential binding partners.

Many sophisticated variants on the “yeast two-hybrid” theme have been developed. For example, “one-hybrid” systems are used to identify proteins that recognize a specific DNA sequence. Here the DNA sequence is cloned upstream of a reporter gene and libraries of proteins fused to the Gal4 AD are then screened for their ability to activate the reporter gene (Li and Herskowitz, 1993).

“Three-hybrid” systems are being applied to investigate protein-RNA interactions. Here a hybrid RNA molecule is used as a linker for two RNA binding proteins, or domains, each generated as one half of the two-hybrid system (SenGupta et al., 1996).

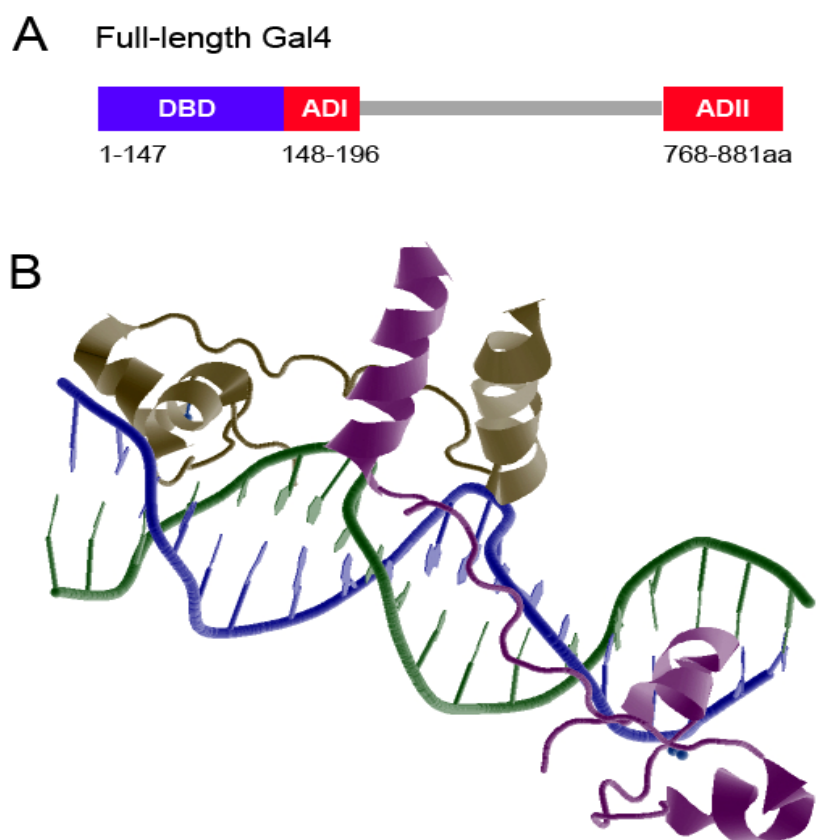


Fig. 14: Gal4

A) Schematic scheme of the Gal4 activator protein, highlighting the DNA binding domain (DBD) comprised of amino acids 1-147 in blue and the activation domains ADI from amino acid 148-196 and ADII from 768-881 in red.

B) X-ray crystallographic structure of 65-residue N-terminal fragment of Gal4 bound to DNA at a resolution of 2.7 Angström. The protein binds as a dimer to a symmetrical 17-base-pair sequence. A small, Zn (2+)-containing domain recognizes a conserved CCG triplet at each end of the site through direct contacts with the major groove. Adapted from (Asakawa and Kawakami, 2008) and (Marmorstein et al., 1992).

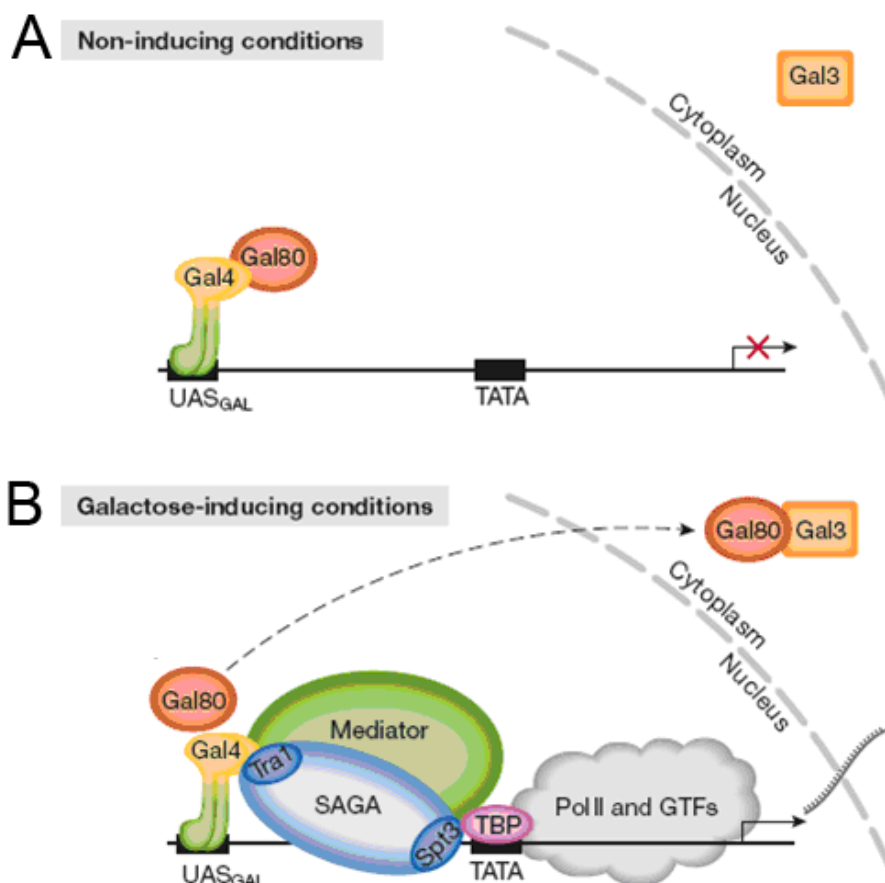


Fig. 15: Transcriptional activation by Gal4 in yeast

A) Under non-inducing conditions Gal4 activity is inhibited by the interaction of the Gal80 repressor with the Gal4 activation domain. B) Upon Galactose induction, Gal80 is removed by interaction with Gal3 from the Gal4 activation domain, which is then able to recruit the transcriptional machinery to initiate transcription. Adapted from (Traven et al., 2006)

Abbreviations: GTFs: general transcription factors, Pol II: RNA Polymerase II, SAGA: Spt-Ada-Gcn5 acetyltransferase, TBP: TATA-binding protein

Ever since the first description of the Gal4-UAS interaction in yeast, the potential of this binary system to manipulate gene expression *in vivo* has been well appreciated. Importantly, Gal4 and its DNA binding motif (UAS) is absent from higher eukaryotes. However, the mechanism for transcriptional activation is conserved throughout eukaryotes, which has enabled variations on the Gal4-UAS approach to be applied in a wide range of organisms.

1.4.3. Gal4-UAS mediated gene expression – a versatile tool in *Drosophila* research

In 1988, Fischer et al. first demonstrated that yeast Gal4-dependent transcriptional activation functions effectively in *Drosophila* (Fischer et al., 1988).

A major advance of the Gal4-UAS system in *Drosophila* research was its implementation in large-scale enhancer or gene trap screens, which was made possible by the controlled mobilization of transposable elements. Enhancer trapping in *Drosophila* traditionally involved incorporation of a β -galactosidase (*lacZ*) reporter into P-element vectors containing a minimal promoter element, so that *lacZ* is expressed upon insertion nearby an endogenous enhancer (O'Kane and Gehring, 1987). Taking advantage of P-element transposition, Brand and Perrimon were the first to design enhancer trap vectors to integrate the *gal4* gene randomly into the fly genome so that adjacent, endogenous regulatory regions would control its transcription (Brand and Perrimon, 1993). Spatially restricted Gal4 expression domains were revealed through the activation of UAS-regulated “reporter” genes such as *lacZ*. Once generated, a transgenic enhancer trap strain expressing Gal4 in a particular cell type or tissue-specific manner can be crossed to any UAS line and can be used as a general resource to drive gene expression in the same spatially restricted manner (Fig.16). Close to 10,000 transgenic “activator” strains that confer specific patterns of Gal4 activity are currently available to *Drosophila* researchers, and other large-scale efforts are underway to create many more. In addition, more than 1000 transgenic *Drosophila* “effector” strains bearing transgenes under UAS control have been generated using transposition technology (<http://flymap.lab.nig.ac.jp/getdb.html>; <http://flystocks.bio.indiana.edu> and <http://www.dgrc.kit.ac.jp/en/index.html>).

Furthermore, a misexpression screen relying on random P-element mediated integration of a construct harbouring 14 repeats of UAS sites, that promoted transcription, when juxtaposed to an endogenous gene, yielded many more UAS “effector” strains (Rorth, 1996). In this method, ectopic activation of gene expression by virtue of an adjacent UAS insertion is limited to cells of interest by employing the respective tissue specific Gal4 “activator” strains. Researchers using this modular misexpression approach mapped nearly 3000 independent insertions of the multicopy UAS element and characterized the phenotypes produced by ectopic expression of each targeted “effector” gene with tissue-specific Gal4 drivers (Rorth, 1996). As with Gal4 transgenic strains, the panel of UAS strains driving misexpression of endogenous genes has served as a general resource for *Drosophila* researchers.

A further powerful application of the modular misexpression approach was the identification of genes that when overexpressed, can suppress or enhance a mutant phenotype, thereby revealing new components of a genetic pathway.

The bipartite approach, in which the two components of the system, the activator and effector, are maintained as separate parental strains, has numerous strengths. The combinatorial nature of the system allows one to study either the effect of expression of one transgene in different tissues or the effect of expression of different transgenes in the same tissue, simply by mating the respective Gal4 activator and UAS effector strains (Fig.16).

Furthermore, the transcriptional inactivity of the parental effector line allows one to generate transgenic effector strains for gene products that are toxic, lethal or cause reduced viability, like oncogenes when expressed. When mated to a specific Gal4 activator line, tissue specific induction of such genes can be used to ablate specific cell types. For example, Zhou et al. (1997) studied the effects of induced ectopic midline cell death by tissue specific Gal4 mediated expression of two genes, *reaper* and *head involution defective*, which trigger programmed cell death (Zhou et al., 1997). Such experiments allow one to dissect the contribution of a certain celltype to the development and function of the organism.

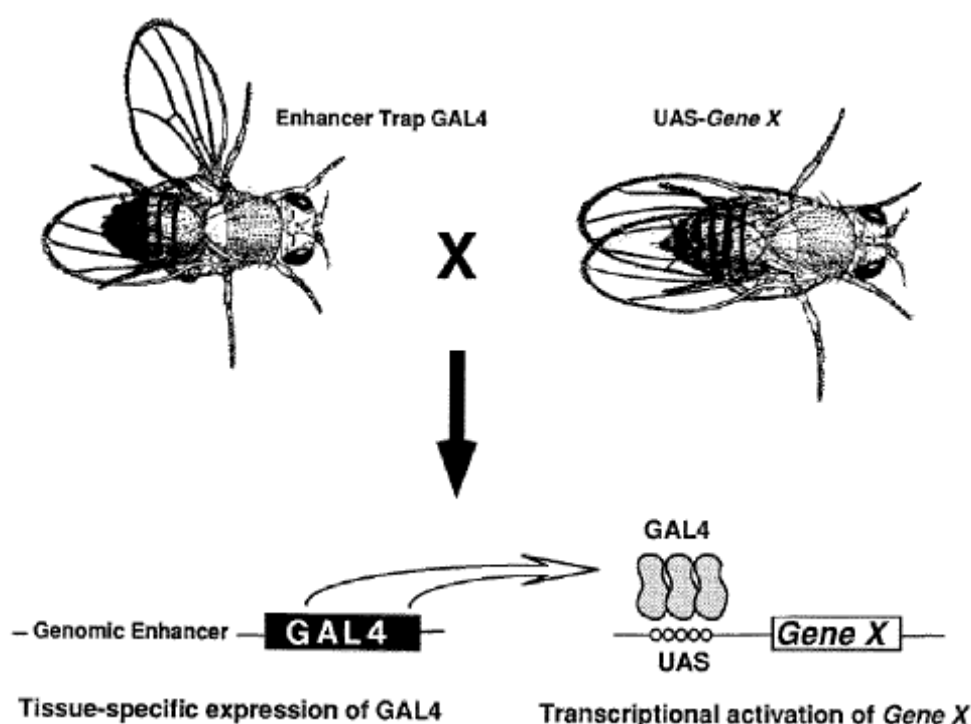


Fig. 16: Gal4-mediated gene expression in *Drosophila*

To obtain tissue specific Gal4 activator strains, the *gal4* gene was inserted randomly into the genome by an enhancer trap approach (left). Effector strains harbouring Gal4-dependent genes of interest were constructed by subcloning these genes under control of UAS sites (right). The transgene is not expressed in the effector line due to the absence of Gal4. Only when the effector strain is mated to a Gal4 activator strain is the transgene expressed in the same tissue specific manner as Gal4. By this means it is possible to observe the effect on development of this directed mis- or overexpression in the progeny of the cross. From (Brand and Perrimon, 1993).

Modifications of the Gal4-UAS system in *Drosophila* have become increasingly sophisticated, and have been applied to study all stages of development, as well as adult physiology and behaviour.

Due to the modular structure of Gal4, its functional domains can be modified easily for different purposes. Wu et al. generated a truncated “mini-Gal4”, consisting of the Gal4 DNA binding domain joined by a seven amino acid linker to residues 840-881 of the acidic C-terminal transactivation domain (Wu et al., 1996). This compact Gal4 activator is sufficient to drive transcription in both yeast and *Drosophila* and still contains the activity of full-length Gal4 (Chakshusmathi et al., 2004; Mondal et al., 2007).

Another valuable Gal4 variant is the Gal4 DNA binding domain fused to the herpes simplex virus VP16 activating region (Gal4-VP16), resulting in a significantly more potent hybrid transcriptional activator (Sadowski et al., 1988). Gal4-VP16 has been widely used to express exogenous and endogenous genes at high levels in animal and plant systems (Engineer et al., 2005; Grabher and Wittbrodt, 2004; Köster and Fraser, 2001b; Xu et al., 1993).

In order to gain temporal in addition to spatial control over Gal4 expression a multitude of inducible methods have been established. These methods could be subdivided into a) the use of chemically inducible Gal4 chimeras, b) the use of temperature sensitive Gal4 variants and c) combinations of Gal4-UAS with other systems for conditional genetics.

1.4.3.1. Chemically inducible Gal4 chimeras

Hormone receptors are known for their ligand induced regulation of gene expression. By fusing a mutated human progesterone receptor ligand binding domain (PRLBD-delta) to the Gal4 DNA binding domain (DBD) and the HSV VP16 transcriptional activation domain a hormone inducible Gal4 chimera (GeneSwitch) was generated (Burcin et al., 1998) . Importantly, GeneSwitch is activated by RU486 (mifepristone) but not by progesterone or other endogenous progestins.

Taking advantage of this inducible Gal4 activator, Osterwalder and colleagues generated a *Drosophila* GeneSwitch line (ELAV-GeneSwitch) adding temporal to the spatial control. By mating this GeneSwitch line to a UAS:GFP effector line they found that in the absence of RU486 GeneSwitch accumulated in the nuclei in its transcriptionally inactive state. Upon systemic administration of RU486 Gal4 dependent transcription of GFP was induced. GeneSwitch also displayed a robust control over the level of gene expression by varying the concentration of RU486. In addition, when mothers were fed RU486, embryos and newly

hatched larvae expressed GFP, indicating that RU486 is transferred from mothers to the embryo, where it can activate GeneSwitch (Osterwalder et al., 2001).

By enhancer trapping using the P[Switch] element many more inducible GeneSwitch activator strains in *Drosophila* were generated (Roman et al., 2001).

Webster et al. (1988) constructed inducible Gal4 chimeras, GAL-ER and GAL-GR, consisting of the DNA-binding domain of the yeast transcription factor GAL4 joined to the C-terminal region containing the hormone-binding domain of either the human estrogen (hER) or human glucocorticoid (hGR) receptor. Here Gal4 dependent transcription could be induced by administration of the respective hormone, estradiol or dexamethasone (Webster et al., 1988). Han et al. successfully applied Gal4-ER in *Drosophila* to investigate the function of follicular subpopulations during *Drosophila* oogenesis, by expressing a modified form of the diphtheria toxin that causes cell death under control of Gal4-ER (Han et al., 2000).

1.4.3.2. Temperature sensitive Gal4 variants

Recently, Mondal et al. (2007) succeeded in isolating Gal4 variants harbouring mutations in their DNA binding domain, which confer temperature sensitivity (TS) to the Gal4 protein (Mondal et al., 2007). Four amino acid residues that contact critical nucleotide repeats within the UAS were identified from the analysis of the crystal structure of Gal4 bound to DNA (Marmorstein et al., 1992) and randomly mutated by PCR. Gal4 variants were tested in a yeast viability assay that relied on Gal4 induction of an essential UAS-regulated gene. Several temperature sensitive Gal4 mutants (Gal4TS) were found to restore viability at low temperatures (21°C), but not when shifted to higher ones (30°C or 37°C). Remarkably, the two Gal4TS mutants that were the most susceptible to temperature regulation in yeast also showed a strong temperature-dependent response in transgenic flies (Mondal et al., 2007).

1.4.3.3. Combinations with other systems for conditional genetics

Gal4-UAS can also be used in conjunction with other well-established conditional genetic systems such as Tet or FLP/FRT to achieve spatial and temporal control.

Stebbins et al. (2001) combined a modified version of an inducible tetracycline responsive transactivator (rtTA-M2-alt) with the Gal4 system by placing the inducible transactivator under UAS control (UAS-rtTA-M2-alt). In this tripartite system the gene of interest is placed under control of Tet operator sequences (TetO). rtTA-M2-alt expression is mediated by Gal4

and is thus spatially controlled. Temporal control is added by the inducibility of rtTA-M2-alt. In the absence of tetracycline (tet) or its analog doxycycline (dox) rtTA-M2-alt is unable to bind to TetO sequences and activate transcription. Addition of tet or dox results in induction of rtTA-M2-alt activity and expression of the gene of interest (Stebbins et al., 2001).

In contrast to this positively-inducible TetOn system a TetOff system, in which transcription is negatively regulated by applying tet or dox has also been combined with the Gal4-UAS system (Stebbins and Yin, 2001).

In addition to the Gal4-UAS/Tet system another tripartite approach to increase the resolution of Gal4-UAS inducibility has been undertaken using the yeast FLP recombinase.

Here, an FRT flanked terminator is either placed between Gal4 and its regulatory elements or between the UAS elements and the transgene (Ito et al., 1997; Nellen et al., 1996; Pignoni and Zipursky, 1997; Zecca et al., 1996). In either case, expression of the transgene in response to Gal4 is dependent on the additional presence of FLP to mediate removal of the intervening terminator cassette. Thus, an added level of temporal control can be achieved with a heat-shock inducible FLP line. For further spatial regulation strains in which FLP is expressed under the control of tissue-specific regulatory elements can be used.

Another level of regulatory finesse is brought to transcriptional activation in the fly by the split Gal4 technique (Luan and White, 2007). In this technique, transcription is restricted to the intersection of expression from two different promoters, with one regulating the Gal4 DNA binding domain fused with a synthetic leucine zipper and the other regulating a complementary leucine zipper fused to the activation domain of Gal4. When both components are coexpressed with spatial and temporal overlap, they heterodimerize, reconstituting transcriptional activity and expression of UAS regulated genes.

1.4.4. Adaptation of the Gal4-UAS system in zebrafish

Although Gal4-UAS has proven an immensely valuable tool in *Drosophila* its application in zebrafish research progressed rather slowly. Scheer and Campos-Ortega (1999) pioneered the use of Gal4 in zebrafish (Scheer and Campos-Ortega, 1999). Using full-length yeast Gal4 downstream of ubiquitous promoters, such as SV40/thymidine kinase or carp β -actin they produced first stable transgenic activator strains. As UAS effector, a line harbouring a constitutively active form of the Notch receptor downstream of 5xUAS was

created (UAS:myc-notch1a-intra). Although they could demonstrate Gal4-dependent transcriptional activation, the levels of gene expression were low and not sufficient for routine combinatorial genetics.

Addressing this concern, the Gal4-UAS system was further modified for zebrafish by Köster and Fraser (2001) by using the strong activator Gal4-VP16 instead of yeast Gal4 (Köster and Fraser, 2001b). The vectors used for injection at the one-cell stage included the Gal4-VP16 activator and GFP under control of the 14xUAS repeats produced for ectopic misexpression in the fly either on one or on separate constructs for transient transgenesis. In transient assays high levels of reporter gene expression were observed in injected embryos. However, stable transgenic strains could not be established likely due to negative effects of high levels of Gal4-VP16 and/or GFP on embryonic development.

Indeed studies on the Gal4 system showed that the expression of a Gal4 DNA-binding domain fused to strong transcriptional activators causes inhibition of transcription of genes, which are not under control of UAS sites, a phenomenon referred to as “sqelching” (Gill and Ptashne, 1988). The suggested mechanism behind “sqelching” is titration of transcription factors (likely a TATA binding protein) essential for transcription. “Sqelching” strongly correlates with cell growth arrest, which indicates that toxicity through sqelching is a quantitative problem where the intracellular concentration and the strength of the activation domains are crucial parameters (Gilbert et al., 1993).

Nevertheless, Gal4-VP16 and 14xUAS constructs became the standard tools for activating transgenes of interest in zebrafish.

Other efforts for increasing Gal4 activity in zebrafish have involved expressing the *gal4* gene under the control of an inducible zebrafish heat shock promoter (*hsp70:Gal4*) (Scheer et al., 2002).

1.4.4.1. Transgenesis methods for zebrafish

Another limiting factor for generating transgenic Gal4-UAS zebrafish was originally the lack of techniques for efficient integration of transgenes into the germ-line. The standard procedure, injection of linearized constructs at the one-cell stage, only yielded low integration rates (Linney et al., 2004).

Sagasti et al. (2005) succeeded in creating a stable transgenic line harbouring both Gal4-VP16 under control of the zebrafish *islet-1* enhancer and UAS:GFP using the meganuclease (*I-SceI*) mediated transgenesis method (Sagasti et al., 2005; Thermes et al., 2002).

In this method, transgenes of interest are flanked by *I-SceI* meganuclease recognition sites and co-injected together with the *I-SceI* meganuclease enzyme. It is believed that upon generating DNA double-strand breaks in the co-injected expression plasmid, this meganuclease remains linked to the cleaved recognition sites. Thus, *I-SceI* may protect the DNA double-strand breaks from strong internal ligase activity present in the fish egg cytoplasm as well as linear monomers from degradation. Instead of the *I-SceI* meganuclease enzyme *in vitro* synthesized mRNA encoding for *I-SceI* meganuclease can also be co-injected with *I-SceI* recognition site flanked transgenes (Babaryka et al., 2009).

A breakthrough in generating transgenic zebrafish was achieved by using transposable elements for germ-line integration of transgenes, including Tol2 (Kawakami et al., 1998; Kawakami and Shima, 1999), Sleeping Beauty (Davidson et al., 2003; Hermanson et al., 2004), PiggyBAC (Lobo et al., 2006) and Tol1 (Koga et al., 2008).

For example, Inbal et al. (2006) took advantage of the Sleeping Beauty system to create a transgenic zebrafish line with Gal4-VP16 under control of the gooseoid promoter driving expression at early embryonic stages (*gsc:Gal4-VP16*) (Inbal et al., 2006).

1.4.4.2. Tol2

The establishment of the Tol2 transgenesis system by members of the Koichi Kawakami laboratory has especially facilitated the generation of transgenic zebrafish by dramatically increasing the frequency of chromosomal integration and germ-line transmission of exogenous DNA (Kawakami, 2004). Importantly these insertions represent single copy integrations.

The Tol2 element was identified from the genome of the medaka fish (*Oryzias latipes*) and belongs to the class II DNA transposons. Class II DNA transposable elements are discrete segments of DNA that are capable of moving from one locus to another in the host genome or between different genomes. They are distributed across the living world and play a fundamental role as motors of genome plasticity. These DNA transposons contain inverted repeats at either end flanking a central region encoding a transposase, which catalyzes transposition. Transposase-deficient elements can be mobilized, if the transposase is provided *in trans* by means of an inducible transposase source or by co-injection of transposon and transposase mRNA (Grabher and Wittbrodt, 2007).

The autonomous Tol2 element (4.7kb) moves in a nonreplicative manner via excision and integration (cut and paste). For transposition, the transposase (649AA) binds to the inverted

repeats and cleaves the DNA, thereby precisely excising the transposon. Additionally, the transposase binds to the target DNA, introducing a staggered cut that leads to protruding single strands. The DNA repair machinery accomplishes integration into the host genome, resulting in target site duplications of 8bp directly adjacent to the transposon ends.

Short regions within the Tol2 terminal inverted repeats have been identified (150-200bp), which are capable of mediating integration of DNA inserts up to 11kb in size into the genome via Tol2 (Kawakami, 2007).

To generate transgenic zebrafish using the Tol2 system, the transgene of interest is cloned between the Tol2 recognition sites. This construct is co-injected with mRNA coding for the Tol2 transposase into one-cell stage zebrafish embryos. The Tol2 transposase mediates the integration of the construct into the genome but degrades overtime (Fig.17). Due to the described integration mechanism, no concatemers of the inserted transgenes, as often observed with linearized DNA injection transgenesis approaches, are formed. Carriers of germ-line integrations need to be identified by screening and as multiple integrations occur often, carriers need to be outcrossed until a single-copy integration carrier is obtained (Fig.17). Importantly Tol2 is not present in the zebrafish genome, ensuring that transgenes flanked by Tol2 recognition sites are not being remobilized.

1.4.4.3. Gal4 enhancer trapping and further Gal4 modifications for zebrafish

With the advent of Tol2 mediated transgenesis it was possible to perform Gal4 enhancer or gene traps in zebrafish similar to screens in *Drosophila* to obtain tissue specific Gal4 activator strains. However, what was still missing was a thorough characterization of the Gal4-UAS system in zebrafish to identify Gal4 activator variants in conjunction with numbers of UAS repeats, which are well adapted for their application in zebrafish.

Aside from the optimization strategy presented in my work several other groups have contributed to optimize Gal4 for its use in zebrafish and have increased the pool of Gal4 activator strains. A comparison of the different optimization approaches and Gal4 enhancer traps will be presented in the discussion under 4.1.1.

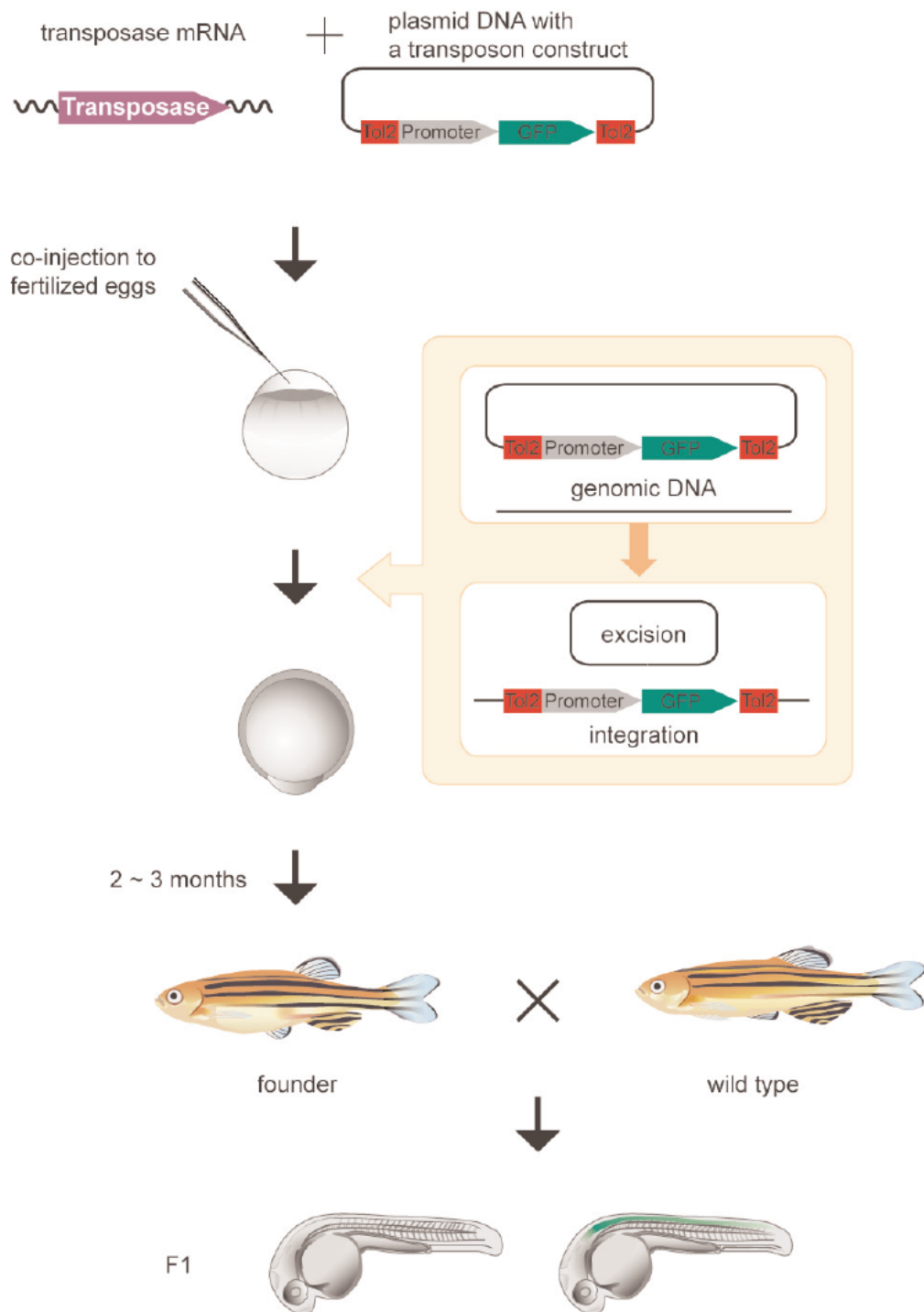


Fig. 17: Tol2 mediated transgenesis in zebrafish

The Tol2 donor plasmid carrying the gene of interest (here *gfp*) flanked by Tol2 recognition sites and the mRNA encoding the Tol2 transposase are co-injected into zebrafish embryos at the one cell-stage. The Tol2 construct is excised from the donor vector and randomly integrated into the genome. Tol2 insertions created in germ cells are transmitted to the F₁ generation. Germ cells of the injected fish are mosaic, and by crossing the injected founder fish with wild-type fish, non-transgenic and transgenic fish (depicted in the figure as fish with a green notochord) heterozygous for the Tol2 insertion are obtained. From (Kawakami, 2007)

1.5. In vivo time-lapse microscopy

To gain insight into dynamic processes like the migration or axonogenesis of THN precursors the method of investigation is of great importance. Commonly biological processes are analysed by static methods i.e. deducing cell and tissue behaviour from changes in sets of images recorded at different time points. As informative as such studies have been they carry the intrinsic danger of missing crucial events of dynamic processes (Lichtman and Fraser, 2001).

In vivo time-lapse microscopy is a powerful analytical method allowing for the continuous observation of a biological process. Embedding methods for zebrafish embryos allowing for time-lapse recording using conventional stereomicroscopes or confocal microscopes are established (Distel and Koester, 2007) (for details see **Appendix 7**). Using cost effective conventional fluorescence stereomicroscopes processes like axonogenesis can be studied on a cellular level (Distel et al., 2006) (**Appendix 6**). However, to study the interplay of subcellular structures like the centrosome, nucleus and microtubules high resolution confocal microscopes are required. As many processes such as INM or mitotic cleavages occur rather fast, *in vivo* cell biological investigations often require high speed image acquisition confocal microscopes. Such systems, like resonance point scanners, spinning disc scanners or widened laser beam slit scanners have recently been made commercially available promising that the two fields of developmental biology and cell biology might soon merge into the field of *in vivo* cell biology.

Methods for *in vivo* cell biology and advantages and disadvantages of different setups for high-speed and high-resolution time-lapse microscopy are described in greater detail in the bookchapter of **Appendix 8** (Distel et al., 2009a) .

However there is also a limitation of this approach. Since it is an optical approach it is restricted to optically accessible zebrafish embryos. To overcome this limitation and to be able to perform *in vivo* imaging of fluorescent markers in opaque animals such as the adult zebrafish obtained from my enhancer trap screen, we applied a new method called multispectral opto-acoustic tomography (MSOT) to fluorescent adult zebrafish (**Appendix 4**) (Razansky et al., 2009).

1.6. Photoacoustic tomography

High-resolution optical microscopy faces two fundamental challenges: diffraction and diffusion. Diffraction limits the spatial resolution, whereas diffusion limits the penetration depth. Recently, the resolution of optical microscopy has been improved beyond the diffraction limit by using sophisticated microscopy techniques like stimulated emission depletion (STED), stochastic optical reconstruction (STORM) or photoactivated localization (PALM) microscopy (Betzig et al., 2006; Bretschneider et al., 2007; Heintzmann and Ficz, 2006; Hell and Wichmann, 1994; Hofmann et al., 2005; Kaksonen and Drubin, 2006; Klar et al., 2001; Rust et al., 2006; Willig et al., 2006).

Most model organism, such as mouse, *Xenopus*, chick and also zebrafish at adult stages are highly diffuse, and can therefore not be studied using optical microscopy approaches. Haemoglobin, the primary chromophore in biological tissue absorbs light strongly in the green and blue spectral regions, allowing only red light to propagate further. In addition strong scattering of light by tissue components such as cell nuclei and mitochondria blurs any shadows of internal structure. In fact, a red photon may experience hundreds or thousands of scattering events before being absorbed. The reciprocal of the mean distance between equivalent isotropic scattering events -the transport mean free path- is approximately 1 mm for visible and near-infrared light. Below this depth, the description of photon propagation changes from the ballistic regime to the diffusive regime. Because optical focusing is ineffective in the diffusive regime, the transport mean free path is referred to as “the soft-depth limit for high-resolution optical imaging”. Beyond this limit, no purely optical imaging technologies have been able to achieve high spatial resolution (Wang, 2009).

In 1880, Alexander Graham Bell discovered that pulsed light striking a solid substrate can produce a sound wave (Bell, 1880). This phenomenon is called photoacoustic effect and it is the principle underlying photoacoustic tomography (PAT).

In PAT a short pulsed laser is used to generate a local heating in a sample (Fig.18). The absorption of the pulsed laser light causes thermoelastic expansion and hereby generates broadband elastic pressure waves (ultrasound), which can be detected outside the sample, e.g. by a piezoelectric device.

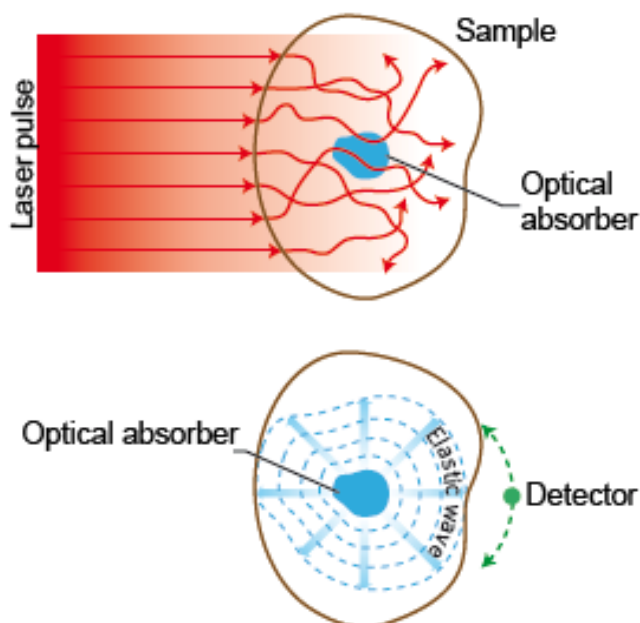


Fig. 18: Photoacoustic imaging

A) Propagation of light in tissue. Optical imaging methods suffer from scattering in biological tissues (red arrows). B) Propagation of ultrasound in tissue. Using laser pulses to generate elastic pressure waves (ultrasound – blue wave) allows high-resolution optical information to be obtained. Ultrasonic scattering is two to three orders of magnitude weaker than optical scattering. From (Burgholzer et al., 2009).

An image of the photogenerated pressure distribution in the sample can be generated by collecting ultrasound at many different locations, e.g. by rotating the sample, followed by data-processing using specific algorithms. The strength of the photoacoustic pressure depends on the optical energy deposition as well as the thermal and mechanical properties of the tissue. All photons, scattered and unscattered ones, can produce photoacoustic signals. In addition, ultrasonic scattering in biological tissues is two to three orders of magnitude less than optical scattering (Xu and Wang, 2006) allowing PAT to function in the optically diffuse regime.

PAT is extremely sensitive to optical absorption. The photoacoustic excitation converts a small change in optical absorption coefficient to a fractionally equal change in the ultrasound signal. Using the reporter enzyme β -galactosidase (encoded by *lacZ*), which converts the transparent substrate X-Gal into a dark blue product, which serves as an optical absorption contrast, PAT could be successfully applied to visualize *lacZ* expressing gliosarcoma tumor cells within a living rat (Li et al., 2007). Besides *lacZ*, fluorescent proteins are widely used as a reporter in a variety of organisms and a multitude of transgenic animals has been generated, which express fluorescent proteins of different colours.

As fluorescent proteins show strong absorbance at their respective wavelengths, they promise to also be visualizable by PAT. Having a technique that allows for detection of fluorescent markers deep within a highly scattering tissue such as in a mouse or adult zebrafish, would

offer the possibility to study processes like tumorigenesis and regeneration or to follow the development of a distinct tissue from embryonic until adult stages in a fate-mapping approach directly in the living organism. Furthermore, such a technique would also have medical impact as fluorescent markers to specifically label tumors are readily available and PAT promises to also be applicable to humans.

1.7. Aims and achievements

Although zebrafish is a well established model organism, until recently a reliable system for combinatorial and conditional genetics was not available for zebrafish. The Gal4-UAS system has proven a valuable tool in *Drosophila* research. However, its adaptation for zebrafish was delayed by the need for optimized transcription and translation of the components for the use in vertebrates.

The main aim of my PhD work was to establish a Gal4-UAS system that would be active and well tolerated in zebrafish. The zebrafish optimized Gal4-UAS system could then be applied to study aspects of hindbrain development on a cellular and subcellular level.

1.7.1. Adaptation of the Gal4-UAS system for zebrafish

To adapt the Gal4-UAS system for zebrafish I first quantified the activity of several combinations of Gal4 activator variants and different numbers of UAS repeats by luciferase assays in zebrafish cells. Promising combinations were further optimized for translation and tested for their tolerance in zebrafish. By this means viable and functional transgenic Gal4-UAS zebrafish strains could be established.

This part of my work is described in 3.1 and **Appendix 1** (Distel et al., 2009c).

1.7.2. Generation of hindbrain specific Gal4 activator strains by enhancer trapping

The combinatorial nature of the Gal4-UAS system allows one to express any transgene of interest under UAS control in a tissue specific manner. To study different aspects of hindbrain development, hindbrain specific Gal4 activator strains would be of great benefit. As the number of available specific regulatory elements is very limited in zebrafish, not many hindbrain Gal4 activator strains can be generated by directly cloning Gal4 under control of such a hindbrain specific regulatory element. In order to generate tissue specific Gal4 activator strains, I performed a Tol2 based pilot Gal4 enhancer trap screen. The screen yielded 60 different Gal4 activator strains, of which 18 showed expression of Gal4 in the hindbrain.

The results of the Gal4 enhancer trap screen are described in 3.2 and in **Appendix 1**. To make the isolated Gal4 strains available to the zebrafish community a database was created, which allows one to search for strains with expression of Gal4 in any desired tissue (see enclosed CD).

Gal4 strains obtained from the enhancer trap were further used in collaborative efforts to determine the role of Lunatic Fringe in lateral inhibition of neurogenesis as described in 3.4.1 and **Appendix 2** (Nikolaou et al., 2009) and to establish tumor models in zebrafish as described in 3.4.2 and **Appendix 3** (Anelli et al., 2009).

1.7.3. Investigation of rhombomere fate

The early vertebrate hindbrain is transiently organized in compartments, the so called rhombomeres by morphological criteria. These rhombomeres are also characterized by the expression of distinct genes (e.g. *hox* genes, *krox20*). The expression of these genes is not maintained until adulthood and rhombomeres cannot be found in the adult hindbrain.

To elucidate whether the rhombomeric organization is maintained until adult stages in zebrafish and to investigate, which adult structures are derived from rhombomeres 3 and 5, I created a transgenic “Kaloop” strain for Gal4 mediated permanent tissue specific labelling.

Mating this “Kaloop” strain to a Gal4 enhancer trap strain transiently expressing Gal4 in rhombomeres 3 and 5, I could show that a rhombomeric organization of the hindbrain persists until adult stages. Furthermore, I found that the secondary octaval nucleus, an important nucleus of the auditory system, is derived from rhombomere 5 from cells expressing *krox20* within a few hours of embryonic day 2. This part of my work is described in **3.3** and **Appendix 1**.

1.7.4. Opto-acoustic tomography of adult zebrafish

Imaging of fluorescently labelled cells has become a powerful tool to investigate biological processes directly in the living zebrafish embryo. However, only early developmental stages are accessible using conventional imaging methods such as fluorescence confocal microscopy, as zebrafish lose their embryonic transparency over time. Having established a zebrafish tumor model and a method to prolong reporter gene expression until adult stages, an *in vivo* imaging technique, capable of visualizing fluorescent reporters within the adult zebrafish, would be highly beneficial to follow tumor progression or the development of an organ from embryonic to adult stages in the living animal.

A novel technique promising to visualize fluorescent reporters within a highly scattering living organism is multispectral opto-acoustic tomography (MSOT). In a collaborative effort with Daniel Razansky, who developed the MSOT, we succeeded in visualizing tissues expressing fluorescent reporters in different zebrafish strains obtained from my Gal4 enhancer trap screen (Razansky et al., 2009). The results of this part of my work are described in **3.5** and **Appendix 4**.

1.7.5. In vivo cell biology of tegmental hindbrain nuclei (THN) neurons

During the development of the zebrafish hindbrain tegmental hindbrain nuclei precursors migrate from the upper rhombic lip in the cerebellar anlage to their final destinations to form functional networks. The behaviour of these cells has already been characterized *in vivo* on a cellular level. Nevertheless the fundamental subcellular mechanisms underlying processes like interkinetic nuclear movements, migration or axonogenesis, namely the interactions of cellular components still need to be elucidated *in vivo*.

Towards this goal I used my Gal4-UAS system to establish a tissue specific multicistronic labelling system to study the behaviour of rhombic lip derived precursors in detail on a subcellular level in the living zebrafish embryo.

I established a collection of fusion proteins labelling different cellular components in zebrafish cells. To cause expression of these labels simultaneously in a tissue specific manner I created modular bidirectional UAS cassettes. Upon binding of Gal4 two fusion proteins are expressed simultaneously from each UAS cassette. Such bidirectional cassettes were successfully used to establish a zebrafish Tauopathy model in a collaborative effort (**Appendix 5**) (Paquet et al., 2009).

Using vectors, which label the nucleus, the membrane, the centrosome and the emerging axon of tegmental hindbrain nuclei precursors, I studied early interkinetic movements and later migration and differentiation phases of these neurons on a subcellular level by fluorescence confocal time-lapse microscopy. My time-lapse experiments resolved the dynamics of organelles and their coordination in relation to each other during precursor proliferation, neuronal migration and axonogenesis. Hereby, I could show that in contrast to what has been shown *in vitro* in hippocampal neurons in culture, the centrosome does not determine the site of axon outgrowth *in vivo*.

The established Gal4 based subcellular labelling system can also be used to co-express any functional gene variant of interest to address molecular mechanisms of cell biological processes. This part of my work is described in **3.6**.

2. Materials & Methods

2.1. Materials

2.1.1. Bacteria

2.1.1.1. *E. coli* K12-strains

E. coli-strains of the following genotypes were used:

XL1-Blue *endA1, hsdR17*(rk⁻, mk⁺), *supE44, thi-1, λ⁻, recA1, gyrA96, relA1, (lacZYA-argF)U169* [F⁺: *proAB, lacIqZ.M15, Tn10(Tetr)*] (Bullock *et al.*, 1987)

2.1.2. Cell lines

zebrafish Pac2 embryonic fibroblasts (Chenn *et al.*, 1998) kindly provided by Christoph Leucht, IDG, GSF Neuherberg

HeLa mito-dsRedT4 a kind gift of Ravi Jagasia

2.1.3. Chemicals

Agarose, for routine use	Sigma Chemie GmbH, Deisenhofen
Agarose, low-melting	Sigma Chemie GmbH, Deisenhofen
Ampicillin-sodium salt	Sigma Chemie GmbH, Deisenhofen
BCIP (50mg/ml in DMF)	Sigma Chemie GmbH, Deisenhofen
Bodipy Ceramid	Molecular Probes
BSA (bovine serum albumine)	Sigma Chemie GmbH, Deisenhofen
10x Digoxigenin RNA labeling Mix	Roche Diagnostics GmbH, Mannheim
DMSO	Sigma Chemie GmbH, Deisenhofen
dNTPs	Fermentas
EtBr	Sigma Chemie GmbH, Deisenhofen
EtOH	E. Merck KGaA, Darmstadt
formamide	Fluka
6x Gel-loading buffer for RNA	Ambion
glascapillaries with filament	Harvard Apparatus
glycerol	Sigma Chemie GmbH, Deisenhofen
glycine	Sigma Chemie GmbH, Deisenhofen

heparine	Sigma Chemie GmbH, Deisenhofen
HEPES	Sigma Chemie GmbH, Deisenhofen
IPTG	Sigma Chemie GmbH, Deisenhofen
isopropanol	E. Merck KGaA, Darmstadt
kanamycin	Sigma Chemie GmbH, Deisenhofen
Lichrosolv H ₂ O	E. Merck KGaA, Darmstadt
MeOH	E. Merck KGaA, Darmstadt
MgCl ₂	Sigma Chemie GmbH, Deisenhofen
NaCl	Sigma Chemie GmbH, Deisenhofen
NaOAc	Sigma Chemie GmbH, Deisenhofen
NBT (100mg/ml in 70% DMF)	Sigma Chemie GmbH, Deisenhofen
NGS	Sigma Chemie GmbH, Deisenhofen
PFA (paraformaldehyde)	Sigma Chemie GmbH, Deisenhofen
PTU (phenylthiourea)	Sigma Chemie GmbH, Deisenhofen
Torula-RNA	Sigma Chemie GmbH, Deisenhofen
TrisHCl	Sigma Chemie GmbH, Deisenhofen
Tween [®] 20	Sigma Chemie GmbH, Deisenhofen
X-Gal	Sigma Chemie GmbH, Deisenhofen

2.1.4. Devices

4 well plate	Nunc
6 well plate	Nunc
96 well plate	Nunc
96 well plate for luciferase assays	Nunc
10cm petri dish	Nunc
6cm petri dish	Nunc
Nylon membrane, Hybond-N	Amersham Buchler
Sterile syringe filter (0.22µm)	Qualilab

2.1.5. Equipment

Microplate Luminometer Orion	Berthold Detection systems GmbH
Readout software: simplicity 2.0R1	Berthold Detection systems GmbH

Incubators:

BK-600 (28°C)	Heraeus GmbH, Karlsruhe
B15 (32°C)	Heraeus GmbH, Karlsruhe

Gel chamber QS-710	IBI, Shelton Scientific
Cold light source	KL 1500 LCD, Zeiss
Fluorescence light source	LEJ GmbH, Jena
Photometer	BioPhotometer, Eppendorf
Direct current device	EC105, Thermo, Electron Corporation

Centrifuges:

Tabletop Centrifuge 5415D	Eppendorf, Hamburg
Evolution	Kendro Laboratory Products GmbH, München
Rotors:	
F45-24-11	Eppendorf, Hamburg
SS-34, GSA, GS3	Kendro Laboratory Products GmbH, München

Microinjection:

micromanipulator	Narishige
microinjector Transjector 5246	Eppendorf, Hamburg
needle puller model 750	David Kopf Instruments, California
glas capillaries, with filament	Harvard Apparatus
binocular Stemi SV11	Zeiss, Oberkochen

Microscopes & equipment

Confocal Laser-Scanning	Zeiss, Jena
Microscope:	
Zeiss LSM 510 on Axiovert 200M	
with Meta unit	
software: Zeiss LSM 510 Software-Package	
objectives: 10x, 20x, 40x, 40x water, 40x oil,	
63x oil, 100x oil	
laser lines: 458nm, 488nm, 543nm	

Stereomicroscopes:

motorized fluorescence stereo-
microscope MZ 16 FA
objectives: 1x & 5x

Leica Microsystems, Bensheim

Filtersets:

GFP3

(exc. 450-490nm) (em. BP 500-550)

Rhodamine

(exc. 530-560nm) (em. BP 572-648)

Texas Red

(exc. 532-588nm) (em. BP 607-683)

DAPI

(exc. 340-380nm) (em. LP 420)

YFP

(exc. 500-520nm) (em. BP 540-580)

monochromatic camera DFC
350 FX R2

Leica Microsystems, Bensheim

Software:

FW4000 Version 1.1

Leica Microsystems, Bensheim

Deblur

Leica Microsystems, Bensheim

Zeiss Axioplan 2 Microscope
“R”

Zeiss, Jena

GNU project (<http://www.gnu.org/>)

Text- and Graphicssoftware:

Adobe Photoshop CS2

Adobe

ImageJ

Freeware

Word 2000

Microsoft

Quick Time Pro

Apple

Hardware:

McIntosh Apple G5, PC, Laptop Medion

2.1.6. Solutions

If not described differently all solutions were made using MilliQ water according to recipes in Mansatis et al.,(1982).

Ampicillin- stock solution

100mg/ml Ampicillin-sodium salt

The solution was sterilized by filtration (0.22µm), aliquoted and stored at -20°C

Kanamycin- stock solution

30mg/ml Kanamycin A

The solution was sterilized by filtration (0.22µm), aliquoted and stored at -20°C

LB-medium

10g/l Bacto-Trypton

5g/l yeast extract

10g/l NaCl

The pH value is set to 7.4. The solution is autoclaved and stored at 4°C.

If necessary Ampicillin respectively Kanamycin is added for selection purposes to a final concentration of 100µg/ml or 30µg/ml respectively.

LB-agar (-Amp./-Kan.)

10g/l BactoTrypton

5g/l yeast extract

10g/l NaCl

15g/l agar

The solution is boiled and subsequently cooled to 60°C. Ampicillin (100µg/ml) or kanamycin (30µg/ml) are added and the agar is casted into Petri-dishes.

10x PBS

100mM	NaCl
19.5mM	KCl
59mM	Na ₂ HPO ₄
11mM	KH ₂ PO ₄

The pH value is set to 7,3 and the solution is autoclaved.

16% PFA

16% PFA (w/v) in H₂O

The solution is heated to 60°C. To initiate depolymerization a few drops of 1M NaOH are added. After cooling to room temperature the pH is set to 7.5 and the adjusted solution is stored at 4°C.

300% Danieau-solution

NaCl (58mM)	60ml
KCl (0.7mM)	30ml
MgSO ₄ x 7H ₂ O (0.4mM)	30ml
Ca(NO ₃) ₂ (0.6mM)	30ml
HEPES (5.0mM, pH 7.2)	30ml
H ₂ O	820ml

PTW

0.1% Tween in PBS

All additional buffers or used solutions are stated together with the respective method.

2.1.7. Antibodies

sheep anti-Digoxygenin alkaline phosphatase coupled	Roche Diagnostics GmbH, Mannheim
goat anti- ChAT (1:100)	Chemicon
chicken anti-GFP (1:500)	Jackson ImmunoReserach
mouse anti-acetylated Tubulin (1:500)	Chemicon
anti-goat Alexa546 (1:100)	Invitrogen
anti-chicken FITC (1:100)	Jackson ImmunoReserach
anti-mouse Cy5 (1:1000)	Dianova

2.1.8. Enzymes and Kits

Alkaline Phosphatase (1U/ μ l)	Roche Diagnostics GmbH, Mannheim
DNaseI (RNase-free, 1U/ μ l)	Roche Diagnostics GmbH, Mannheim
Klenow-Fragment (10U/ μ l)	MBI Fermentas, New England Biolabs
Proteinase K	
Restriction endonucleases	MBI Fermentas, New England Biolabs, Roche Diagnostics GmbH, Mannheim
RNase Inhibitor (40U/ μ l)	Promega
SP6 RNA-Polymerase (20U/ μ l)	MBI Fermentas, New England Biolabs
T4 DNA-Ligase (5U/ μ l)	MBI Fermentas, New England Biolabs
Taq DNA-Polymerase (5U/ μ l)	MBI Fermentas, New England Biolabs
Dual Luciferase Assay	Promega
Effectene Transfection kit	Qiagen
Nanofectin Transfection kit	PAA
GENECLEAN <i>Turbo</i> Kit	QBIogene
Message mMachine SP6 Kit	Ambion
NucleoBond Kit	BD Biosciences
Quiaquick Nucleotide Removal Kit	Qiagen
RNeasy Mini Kit	Qiagen
TOPO TA Cloning	Invitrogen

2.1.9. DNA

Molecular weight marker

GeneRuler™ 1kb DNA Ladder: Invitrogen

2.1.10. Vectors:

Cloning strategies

801 pCS GFPDCX

The ORF encoding GFP-DCX was isolated from the pEGFP-C2DCX vector (a kind gift of Fiona Francis) by Eco47III/SalI digest and cloned into StuI/XhoI digested pCS2+.

U15: #699 pSK14xUASH2BmRFP

The ORF encoding H2BmRFP was isolated from the pCS-H2BmRFP (a kind gift of Sean Megason) by Asp718 (Klenow blunted)/Nsi digest and cloned behind the E1b promoter of the XhoI (Klenow blunted)/Nsi digested pSK14xUASE1b vector (Köster and Fraser, 2001b).

U16: #709 pSKH2BmRFP5xUASE1b

The E1b minimal promoter and the ORF encoding H2BmRFP were isolated from U15 by XbaI/NotI (Klenow blunted) digest and inserted into the SmaI site of the pSK5xUASE1b vector (Köster and Fraser, 2001b).

J1: #828 pSK-H2BRFP5xUASGFPDCX

The ORF encoding GFPDCX was isolated from pCSGFP-DCX by ClaI/Asp718 digest and cloned into ClaI/Asp718 digested U16.

U17: #627 pSK14xUASH2BGFP

H2BGFP was isolated from pCSH2BGFP (#95ref?) SalI (Klenow blunted) /ApaI digest and cloned behind the E1b promoter of the XhoI (Klenow blunted)/ApaI digested pSK14xUASE1b vector (Köster and Fraser, 2001b).

U18: #665 pSKH2BGFP5xUASE1b

The E1b minimal promoter and the ORF encoding H2BmGFP were isolated from U17 by XbaI/NotI (Klenow blunted) digest and inserted into the SmaI site of the pSK5xUASE1b vector (Distel et al., 2009c).

J11: #700 pSKH2BGFP5xUASmemmRFP

The ORF encoding memmRFP was isolated from pCSmemmRFP (a kind gift of Sean Megason) by XhoI(Klenow blunted)/Nsi digest and inserted into EcoRV/Nsi digested U18.

U2: #860 memmRFP5xUAS

The E1b minimal promoter and the ORF encoding memmRFP were isolated from J11 by XbaI/NotI (Klenow blunted) digest and inserted into the SmaI site of the pSK5xUASE1b vector (Distel et al., 2009c).

878 pH2BCFP map

The ORF encoding H2B was isolated from pCSH2BmRFP (a kind gift of Sean Megason) by XhoI/AgeI digest and inserted into XhoI/AgeI digested pECFP-C1 (Clontech).

895 pCSH2BCFP

The ORF encoding H2BCFP was isolated from pH2BCFP by NotI(Klenow blunted)/XhoI digest and cloned into XbaI(Klenow blunted)/XhoI digested pCS2+.

J2: #939 pSKmemmRFP5xUASH2BCFP

The ORF encoding H2BCFP was isolated from pCSH2BCFP by XhoI/NotI (Klenow blunted) digest and inserted into Asp718(Klenow blunted) U2.

#766 pCRIICentrin2

The open reading frame of zebrafish centrin2 (acc. nr.: EU183505) was cloned by RT-PCR to generate C-terminal fusions using total RNA from adult brain and the following primers: centrin-up: TTG GAT CCA TGG CGT CCG GCT TCA GGA A, centrin-low: TTT CTA GAT CAG TAC AGA TTG GTT TTC TTC. The fragment was subcloned into the pCRII-Topo-vector (Invitrogen, San Diego, CA) and sequenced.

#769 pCentrin2YFP

the ORF encoding Centrin2 was isolated by BamHI/HindIII digest and cloned into BamHI/HindIII digested pEYFP-N1 (Clontech).

#848 pCSCentrin2YFP

The ORF encoding Centrin2YFP was isolated from pCentrin2YFP by NotI(Klenow blunted)/XhoI digest and inserted into SnaBI/XhoI digested pCS2+.

U5: #996 pSK5xUAScentrin2YFP

The ORF encoding Centrin2YFP was isolated from pCScentrin2YFP by EcoRI/ApaI digest and inserted into EcoRI/ApaI digested pSK5xUAS (Distel et al., 2009c).

M1: #1595 pSKmemmRFP5xUASH2BCFP-5xUASCentrin2YFP

The 5xUASCentrin2YFP cassette was isolated from U5 by SpeI/Asp718(Klenow blunted) and inserted into SpeI(Klenow blunted) J2.

#938 pCSmemCFP

mRFP of pCSmemmRFP (a kind gift of Sean Megason) was removed by SnaBI/AgeI digest and replaced with CFP from NotI(klenow blunted)/AgeI digested pECFP-1 (Clontech).

U6: #997 pSK5xUASmemCFP

The ORF encoding memCFP was isolated from pCSmemCFP by ClaI/ApaI digest and inserted into ClaI/ApaI digested pSK5xUAS.

M2: #998 pSKH2BmRFP5xUASGFPDCX-5xUASmemCFP

The 5xUASmemCFP cassette was isolated from U6 by NotI(Klenow blunted) and inserted into Asp718(Klenow blunted) J1.

pCSEB3GFP

The ORF encoding EB3GFP was isolated from pEB3GFP (a kind gift of Anna Akhmanova) by NotI(Klenow blunted)/SalI digest and inserted into XbaI(Klenow blunted)/XhoI digested pCS2+.

J4: #780 pSKH2BmRFP5xUASEB3GFP

The ORF encoding EB3GFP was isolated from pCSEB3GFP by StuI/Asp718 digest and inserted into EcoRV/Asp718 digested U16.

M3: #999 pSKH2BmRFP5xUASEB3GFP-5xUASmemCFP

The 5xUASmemCFP cassette was isolated from U6 by NotI(Klenow blunted) and inserted into Asp718(Klenow blunted) J4.

#868 pCStdTomato

The ORF encoding tdTomato was isolated from pRSETtdTomato (a kind gift of Roger Tsien) by BamHI/EcoRI digest and inserted into BamHI/EcoRI digested pCS2+.

#879 Centrin2tdtomato

The ORF encoding Centrin2 was isolated from pCRIICentrin2 by BamHI/HindIII digest and inserted into BamHI/HindIII digested pCStdTomato.

#1532 pSKE1B5xUASE1b

The E1b5xUASE1b cassette was isolated from U2 by EcoRI digest and inserted into EcoRI digested pSK-.

U9: #2022 pSKH2BCFP5xUASE1b

The ORF encoding H2BCFP was isolated from pCSH2BCFP by Asp718 digest and inserted into SmaI digested pSKE1b5xUASE1b.

J8: #2146 pSKH2BCFP5xUASCentrin2tdTomato

The ORF encoding Centrin2tdTomato was isolated from pCSCentrin2tdTomato by HindIII/Asp718 digest and inserted into HindIII/Asp718 digested U9.

pSC-BKif5xYFP

Kif5cYFP was PCR amplified from Kif5cYFP (a kind gift of Gary Banker) and a Kozak sequence was added using primers Kif5cEcoHinfoKo: AAAGAATTCAAGCTTCCACCATGGCAGATCCAGCCGAATGCAGCATC and Venus4: TACTCGAGTTACTTGTACAGCTCGTCCAT and subcloned into pSC-B (Stratagene).

2328pCSKif5cYFP

The ORF encoding Kif5cYFP was isolated from pSC-BKif5cYFP by EcoRI(Klenow blunted)/HindIII digest and inserted into HindIII/SnaBI digested pCS2+.

U14: #2329 pSK5xUASKif5cYFP

The ORF encoding Kif5cYFP was isolated from pCSKif5cYFP by HindIII/Asp718 digest and inserted into HindIII/Asp718 digested pSK5xUAS (Distel et al., 2009c).

All other Vectors and cloning strategies can be found in the Materials and Methods sections of the respective **Appendices**

2.1.11. Zebrafish strains

AB-strain	inbred strain at the Helmholtz Center Munich
Brass	inbred strain of pigmentation mutant that is deficient in melanine synthesis at the Helmholtz Center Munich

2.2. Methods

2.3. Molecular biological methods

2.3.1. Restriction digest of plasmid-DNA

Plasmid-DNA is digested with restriction enzymes for analysis and for cloning. The endonucleases used, recognize specific base patterns and cut the DNA-doublestrand at these sites by catalysing the hydrolysis of phosphodiesterbonds. Typical amounts of restriction enzymes used are in the range between 2 and 12U and are incubated using the respective restriction buffer up to 12h at 37°C if not differently recommended by the manufacturer. For analytical digests up to 1µg of DNA, for preparative digests 5-10µg of DNA are used. One should take care that the amount of glycerol added with the respective enzyme does not exceed 10% of the total volume as it may disturb the enzyme's activity and possibly specificity. Gel-loading dye is added (1/10 of the reaction volume) and the DNA fragments are subsequently separated in an agarose gel (see 2.3.10) for analysis or excision respectively.

2.3.2. Blunting 5'-DNA overhangs

In order to blunt overhanging 5'-DNA-ends after preparative digests, the restriction digest is first incubated for 20min at 65°C. This step inactivates the restriction endonucleases to avoid any further unwanted digest after blunting. Afterwards both dNTP's (2mM) and Klenow polymerase at a final amount of 200µM or 2U respectively are added to the reaction, containing approximately 5-10µg DNA. The reaction is incubated at 37°C for 45-60min. The Klenow polymerase shows activity in nearly all restriction buffers. Subsequently the DNA is purified either by ethanol precipitation or by using the "Nucleotide Removal Kit" according to the manufacturer's (Qiagen) instructions. The principle of this kit is that DNA in contrast to enzymes or salts binds to a silica-gel membrane. Impurities such as salts, agarose, ethidium bromide, nucleotides, mineral oil or enzymes can be removed by washing the membrane with an ethanol containing high salt buffer. DNA can be eluted with H₂O afterwards, typically in a volume of 30µl H₂O.

2.3.3. Dephosphorylation of DNA

In order to avoid unwanted religation of vectors with blunted ends or matching overhangs after preparative digest, 5'-terminal phosphate residues of the DNA fragments have to be removed. For this purpose 2U of alkaline phosphatase and 1/10 of the volume of

the reaction of dephosphorylation buffer are added. The reaction is incubated for 20-60min at 37°C.

2.3.4. DNA-Ligation

To ligate DNA fragments with compatible overhanging ends (sticky ends) or blunt ends 7.5U of T4-DNA-Ligase and 1.5µl of ligase buffer are added to a reaction batch of a total volume of 15µl. This reaction batch is either incubated 30min at room temperature or over night at 16°C. Depending on their size, vector backbone DNA and insert are applied from euqimolar ratios up to 5fold excess of insert DNA with the molar ratio of insert to vector backbone being estimated by agarosegel electrophoresis. 2-5µl of the respective ligation batch are used for bacterial transformation.

2.3.5. Production of CaCl₂ competent cells

The classical CaCl₂ method (Cohen, 1972) was used to produce competent cells for DNA transformation. Here, positively charged Ca-ions bind to the negatively charged membranes of the bacteria and therefore facilitate the uptake of negatively charged DNA.

To produce such CaCl₂ competent cells 50ml LB-medium are inoculated with 4ml of a stationary overnight culture of the respective *E. coli* strain and incubated at 37°C until the culture reaches an OD₅₅₀ = 0.5. The culture is then transferred into 50ml centrifuge tubes and sedimented at 5000rpm (4416g) at 4°C for 10min. The cell pellet is resuspended in 40ml of a cold 100mM MgCl₂-solution and incubated on ice for 30min. This suspension is again centrifuged as described above, the obtained cell pellet is resuspended in 20ml of a cold 50mM CaCl₂-solution and subsequently incubated on ice for 30min. After another round of centrifugation at 5000rpm and 4°C for 10min the cells are resuspended in 2ml 50mM CaCl₂, 15% v/v glycerol and stored as aliquots of 200µl at -80°C.

All mentioned solutions were sterilized and cooled down before application.

2.3.6. Transformation of bacteria

To obtain bacterial colonies, which carry a cloned plasmid, 5 µl of a ligation reaction are transformed in 100µl CaCl₂-competent *E. coli* cells. Competent cells are slowly thawn on ice for 15-30min, then an aliquot of the ligation reaction is added and the mixture is incubated on ice for 20-30min. Afterwards the suspension is heated to 42°C for 45-60s to enable the

uptake of DNA, so far attached to the bacterial membranes, into the cytoplasm of the bacteria. Subsequently the transformation reaction is incubated on ice for 2min before 500ml of LB-medium are added. Now the cells are incubated at 37°C on a shaker to allow them to grow and develop the antibiotic's resistance encoded on the received plasmid. 100µl respectively 400µl are subsequently plated with sterile glass pearls on LB-plates supplemented with the respective antibiotic fitting to the resistance encoded on the plasmid. The plates are incubated at 37°C overnight up to 24h until the antibiotic resistant and thus vector carrying colonies show the desired size. Colonies can then be picked to inoculate liquid cultures for DNA preparations or the plates can be stored at 4°C for at least four weeks.

2.3.7. TA-Cloning

The TA-cloning strategy is used to ligate PCR-products in a vector to facilitate further subcloning. This cloning strategy is based on the sequence-independent addition of adenosine residues by the Taq DNA polymerase at the 3'-end of the synthesized DNA-strand. These residues allow ligation with a linearized vector containing a 5'-end tyrosine overhang.

TA-cloning was performed using the „TOPO TA-Cloning Kit“ with the PCR[®]II-TOPO[®]-vector according to the manufacturer's (Invitrogen) specifications. The PCR[®]II-TOPO[®]-vector is linearized and coupled to a gyrase, which mediates the fast ligation between PCR-fragment and vector.

For identification of bacteria containing a vector with insert blue-white selection was used. This can be done because the integration of an insert into the PCR[®]II-TOPO[®]-vector leads to disruption of the *β-galactosidase* gene. *E. coli* bacteria transformed with PCR[®]II-TOPO[®]-vector were plated on LB-Amp plates supplemented with the chromogen dye X-Gal (40µl) (40mg/ml in 70% DMF) and the inducer IPTG (40µl) (200mM). Addition of the inducer is necessary as the transformed bacteria express a repressor, which inhibits *β-galactosidase* expression. IPTG inhibits the repressor, therefore allowing transcription of the *β-galactosidase* gene. *β-galactosidase* catalyzes the conversion of X-Gal in a blue derivative of indigo. Bacteria containing a plasmid without insert therefore harbouring a functional *β-galactosidase* gene appear in blue because of the X-Gal reaction. In contrast to bacteria containing a plasmid with insert and thus disrupted *β-galactosidase* gene are colourless.

2.3.8. DNA-preparations

2.3.8.1. Mini-preparation

buffers:

S1

50mM TrisHCl

10mM EDTA

100µg/ml RNase A

buffer is stored at 4°C

S2

200mM NaOH

1% SDS

S3

2.8M KOAc

Bacterial colonies grown on LB-plates supplemented with antibiotics can either contain a religated vector providing the antibiotics resistance or different variants of vectors with inserts. To isolate a bacterial colony containing the desired vector, usually a couple of colonies are cultured separately in small amounts of LB-medium. After lysis of these bacteria, their plasmids are isolated and characterized by restriction digest.

5ml LB-medium are supplemented with the antibiotic corresponding to the resistance provided by the plasmid and are inoculated with a transformed bacterial colony. These cultures are incubated at 37°C overnight on a shaker (200rpm).

The bacterial cultures are sedimented in 1.5ml reaction tubes by centrifugation for 5min at 13200rpm (Centrifuge 5415D, Eppendorf). The supernatant is discarded and the pellet resuspended in 200µl cold S1 buffer. S1 contains RnaseA, which digests bacterial RNA. Afterwards 200µl alkaline S2 buffer are added to partially disintegrate the bacterial lipid membrane to set the plasmids free. After incubation for 2-5min 200µl neutralisation buffer S3 are added. After gentle mixing denatured proteins are visible as white flocks. To separate denatured proteins and bacterial debris from free-floating plasmids the solution is centrifuged for 10min at 13200rpm (Centrifuge 5415D, Eppendorf). The plasmid containing supernatant is transferred to another 1.5ml reaction tube. To sediment the plasmid DNA the supernatant is

supplemented with 400µl isopropanol and centrifuged for 30min at 4°C at 13200rpm (Centrifuge 5415D, Eppendorf). Subsequently the supernatant is discarded and the DNA-pellet is washed with 500µl 70% EtOH by centrifugation at 4°C, 13200rpm for 15min. The supernatant is again discarded and the DNA-pellet dried to let residual EtOH evaporate, which would influence the enzyme activity. The DNA is resuspended in 30-50µl H₂O and subsequently characterized by restriction digest to identify colonies carrying the desired vector.

This method has a yield of approximately 5-10µg of plasmid DNA.

2.3.8.2. Maxi-preparation

buffers:

N2

100mM Tris
15% EtOH
900mM KCl
0.15% TritonX-100

N3

100mM Tris
15% EtOH
1.15 M KCl

N5

100mM Tris
15% EtOH
1M KCl

Maxi-preparations are performed to obtain larger quantities of plasmid DNA for plasmid stocks and further cloning.

The maxi preparation was performed using the „NucleoBond Kit“ (BD Biosciences). The used buffers S1, S2 and S3 are stated in 2.3.8.1.

An individual *E. coli* colony containing the desired plasmid is cultured in 200ml LB-medium supplemented with the respective antibiotic according to the resistance encoded on the

plasmid on a shaker (200rpm) at 37°C overnight. The bacteria are sedimented by centrifugation at 5000rpm at 4°C for 20min (*Evolution* Sorvall, GSA-rotor). Afterwards the bacterial pellet is resuspended in 10ml buffer S1 and the suspension is transferred to SS34 tubes. To partially lyse the bacterial suspension 10ml of alkaline buffer S2 are added followed by 5 min of incubation at room temperature. Due to the perforation of the bacterial membranes plasmid DNA is set free into the medium. Afterwards 10ml S3 neutralization buffer are added and denatured proteins coagulate. After 10min of incubation on ice the solution is centrifuged for 20min at 10000rpm and 4°C (Sorvall *Evolution*, GSA-rotor). To remove remaining traces of denatured proteins and bacterial debris the supernatant is transferred to a new SS34 tube and centrifuged for 20min at 10000rpm and 4°C (Sorvall *Evolution*, GSA-rotor) again. The supernatant is now transferred to a chromatography column, which has been equilibrated with 6ml N6 buffer in advance. Plasmid DNA binds to the stationary phase of the column and is subsequently washed with 30ml of N3 buffer to remove residual nucleotides and proteins. By applying 15ml of N5 low salt buffer the DNA is eluted from the column.

To precipitate the DNA 11ml isopropanol are added. The plasmid DNA is now either purified using the “Finalizer Kit“ (BD Biosciences) or by classical centrifugation steps. Using the “Finalizer Kit“ the plasmid DNA solution is transferred to a syringe with a polypropylene filter containing a silica membrane, which binds the DNA. The plasmid DNA is purified by washing with 70% EtOH according to the manufacturer’s specifications and typically eluted with 250 µl H₂O.

For purifying the plasmid DNA via centrifugation steps, the solution is transferred into SS34 tubes and centrifuged for 20min at 10000rpm and 4°C (Sorvall *Evolution*, SS34-rotor). The supernatant is discarded, the DNA pellet is washed with 70% EtOH and repelleted by centrifugation for 20min at 10000rpm and 4°C. Before resuspending the DNA pellet in 200µl H₂O, the pellet is dried. Usual yields are in the range between 500µg and 1mg.

The DNA concentration is measured (see 2.3.9) and set to the desired concentration.

To verify that the correct plasmid has been isolated, analytical restriction digests are performed.

Such purified DNA can be stored at –20°C for several years.

2.3.9. Determination of nucleic acid concentration

Aromates of the different nucleic acids of DNA absorb UV-light in the range of 220 to 320nm proportional to their concentration as described by Lambert-Beer's Law. Photometric measurements can thus be used to determine nucleic acid concentrations. This method also allows to distinguish between DNA, RNA or double and single stranded DNA. The maximum absorbance occurs at 260nm. 50µg of double stranded DNA or 40µg of RNA in 1 ml solution have an OD value of 1 measuring absorbance at 260nm. As the absorption maximum of aromatic amino acids occurs around 280nm, it is possible to determine the grade of protein contamination of a DNA sample by measuring the OD at 260nm to OD at 280nm ratio. A sufficient purity of DNA or RNA is given at an OD_{260}/OD_{280} ratio greater than 1.8.

2.3.10. Separation of DNA in an agarose gel

10x TAE-buffer:

5M Tris-Acetate

50mM EDTA

gel-loading buffer:

30% (v/v) Glycerol

0.25% (v/v) EDTA

0.25% (w/v) Xylenecyanol FF

Using a polymerized agarose gel DNA and RNA fragments can be separated according to their molecular mass.

As DNA-molecules carry a negative charge due to their phosphate backbone they will migrate to the anode if a steady electrical field is applied.

Larger fragments will migrate more slowly than smaller fragments in the electrical field as they are held back in the polymerized agarose.

According to the presumed length of the DNA fragments between 0,6 and 1,5% (w/v) agarose/1x TAE-gels are used. Agarose is solved in 1x TAE-buffer by heating in a microwave oven and casted into a gel chamber fitted with a removable comb to obtain slots for the DNA samples after gel polymerization.

After solidifying the gel is covered with 1x TAE buffer. DNA loading buffer is added to the samples which are then pipetted into the slots. Subsequently the gel is run at 80-120V. Afterwards the gel is immersed in an EtBr/1xTAE solution (200µg/ml EtBr in 1x TAE-Puffer) and incubated for 15min. Fluorescence emission of EtBr increases manifold with its

intercalation into DNA-strands, which is used to visualize DNA under short wavelength UV of 320nm. A standard of DNA fragments of known size is used to determine the molecular weight of the DNA fragments.

2.3.11. Amplification of DNA sequences via PCR (polymerase chain reaction) (Saiki et al., 1988)

To amplify DNA-fragments with known end - or flanking sequences the polymerase chain reaction (PCR) is the method of choice.

Oligonucleotides between 18-30bp, which are homologous to the 5'-end of the sense and the 5'-end of the antisense strand are synthesized.

PCR is a three step reaction. During the first step template-DNA and Oligonucleotides are denatured for 1min at 95°C. This step separates sense and antisense strand of the template-DNA.

During the second step the PCR reaction is cooled down to a temperature which allows annealing of the oligonucleotides to the target sequence, because they are present in excess compared to template DNA. The annealing temperature is dependent on the composition of the oligonucleotides and is usually in the range of 50°C to 60°C. In the third step, the elongation step, the oligonucleotides serve as primers for the Taq-polymerase (a thermostable polymerase), which elongates the oligonucleotides according to the template.

Iterations (30-40cycles) of this three-step reaction lead to exponential enrichment of the DNA-region of interest framed by the oligonucleotides.

When performing a so called hot start PCR the first cycle of this three step reaction is preceded by incubation at 95°C for 5min to ensure a complete denaturation of the DNA. During this time Taq-Polymerase is added to the reaction batch together with its buffer.

After completion of all PCR-cycles the reaction batch is kept at 72°C for 10min to fill up uncomplete DNA-ends. After that the reaction is cooled down to 4°C to stop the PCR reaction.

An aliquot of the reaction is characterized by gel electrophoreses afterwards.

If PCR-reactions were ineffective one can try to optimize conditions by successively increasing or decreasing the annealing temperature, by varying the reaction buffer or throughout additives such as DMSO.

For cloning of amplified PCR-fragments, they are separated from remaining oligonucleotides via gel-electrophoreses, the respective DNA fragment is isolated and inserted into the TOPO vector via TA-cloning.

PCR-reaction batch:

Template -DNA	1-10ng
dNTPs	200-300 μ M
Oligonucleotide 1	50-200pmol
Oligonucleotide 2	50-200pmol
10x Taq-buffer	5 μ l
Taq DNA-Polymerase	2-5U = 1 μ l
H ₂ O	add. 50 μ l

Temperature profile of PCR reactions:

First complete denaturation:	95°C for 5min
Denaturation:	95°C for 30s
Annealing:	50°C-60°C for 30s
Extension:	72°C for 45s/kb
Cycles:	30-40
Complete extension:	72°C for 10min
Holding temperature:	4°C

2.3.12. DNA Extraction and Inverse Nested PCR

See Materials and Methods section of Appendix 1

2.3.13. Synthesis of mRNA

For the synthesis of capped mRNA 15 μ g of an expression vector coding for a gene of interest, carrying a phagepromoter at the 5'-end and a polyA sequence at the 3'-end, are linearized by digestion (see 2.3.1) with an appropriate restriction enzyme. This template is then purified using the QiaQuick reactionsystem "Nucleotide Removal Kit". To ensure that the restriction digest and the purification procedure were successful an aliquot is analysed by gel electrophoresis.

For the *in vitro* transcription the Ambion „mMessage mMachine SP6 Kit“ was used. The reaction was performed according to the manufacturers specifications for 2-3h at 37°C with the following volumes:

linearized template-DNA	6µl
2x NTP/CAP	10µl
10x SP6-polymerase reaction buffer	2µl
enzyme-mix (SP6)	2µl

Afterwards 1.5µl RNase-free DNaseI (1U/µl) is added to the reaction and the sample is incubated for 20 min at 37°C. The synthesized mRNA is purified using the Qiagen „RNeasy Mini Kit“ according to the specifications of Qiagen. The RNA is eluted in 50 µl water.

For further purification and concentration 1/10 of the reaction volume of 3M NaOAc and 3 times the reaction volume of EtOH is added and the sample is incubated for 20min at –20°C. To precipitate the mRNA the sample is centrifuged at maximum speed (Centrifuge 5415D, Eppendorf, 13200rpm) for 30min. The supernatant is discarded and the RNA pellet washed in 70% EtOH and centrifuged at maximum speed for 15min at 4°C (Centrifuge 5415D, Eppendorf, 13200rpm). The supernatant is discarded again and the pellet is dried and resuspended in 20µl water.

The yield as well as the integrity of the synthesized mRNA is controlled by gel electrophoresis and the concentration of the obtained mRNA solution is determined by measuring the OD₂₆₀.

The mRNA can be stored at –20°C for several months.

2.3.14. Separation of RNA in an agarose gel

To avoid all RNases, gel chamber and combs were washed with soap and MilliQ water in advance and the gel was run for half an hour at 80V before applying the samples to the slots. RNA-samples of 1µl are mixed with 4µl formamide containing RNA-loading buffer and are denatured for 10 min at 90°C to break up secondary structures of the mRNA before applying it to the gel slots.

2.3.15. RNA-cytoplasmic injection (Ekker et al., 1995)

For cytoplasmic injections one cell stage zebrafish eggs are lined up in petri dishes filled with agarose (1.5% agarose/ 30% Danieau`s solution) in which a mold was embedded to obtain grooves.

In vitro synthesized mRNA is diluted in water to the desired injection concentration with water (typically 100-250 ng/ μ l). To facilitate the injection phenol red can be added, usually 10% of an injection mix volume of 10-15 μ l.

A glass capillary needle is filled with the injection mix and positioned into a micromanipulator. With the help of a binocular the chorion and the cellular membrane of the embryo are penetrated with the needle and mRNA (500pg to 2ng) is injected into the cytoplasm. After the injection the embryos are separated spatially to allow an even oxygen supply which is necessary for synchronous development. The embryos are incubated at 28°C until they reach the desired development stage.

2.3.16. DNA-cytoplasmic injection

The injection of DNA is performed in analogy to the injection of mRNA. DNA plasmids are purified with the QBIoGene „GENECLEAN[®]Turbo Kit“ in advance according to the specifications of the manufacturer.

The DNA is eluted in 30 μ l water. The concentration of the injected DNA solution is determined by photometric measurements. Injection concentrations between 20-50ng/ μ l of total DNA were used.

2.3.17. Whole-mount in-situ-hybridisation (ISH)

Whole-mount in-situ- hybridisation is a method to specifically detect cells and tissues within a whole organism, which express a certain gene at a selected developmental stage.

For this technique a synthetic antisense RNA-probe is hybridized to its complementary mRNA. Due to an incorporated digoxigenin-tag the hybridized RNA can subsequently be detected by immuno-histochemistry.

Synthesis of the RNA-hybridisation-probe

To synthesize RNA-probes it is necessary to work with Rnase free material.

For in vitro transcription of an antisense RNA probe the respective gene has to be flanked by a phage promoter at its 3`-end. 10µg of such a plasmid are linearized at the 5`-end of the gene by restriction digest (see 2.3.1). The plasmid DNA is cleaned after restriction digest using the „Qiaquick Nucleotide Removal Kit“ and eluted in 50µl H₂O. Afterwards an aliquot of the purified digestion reaction is analysed by agarose gel-electrophoresis (see 2.3.10) to ensure that the digestion reaction is complete..

This template DNA can now be used to synthesize RNA with a RNA-polymerase. In the presence of ATP, GTP, CTP, UTP and a uridine triphosphate derivative, which is conjugated to digoxigenin at its 2`-Hydroxy-group RNA is synthesized, which can be detected by an anti-digoxigenin antibody.

All components for in vitro transcription are stated in the following:

linearized template –DNA (200ng/µl)	8µl
5x transcription buffer	4µl
10x Dig RNA labeling mix	2µl
RNase Inhibitor (40U/µl)	1µl
H ₂ O	3µl
RNA-Polymerase (20U/µl)	2µl

This reaction is incubated at 37°C for 2h.

Subsequently the template DNA is removed by incubating the reaction with 1.5µl Rnase-free DNase1(1U/µl) for 20min at 37°C.

The antisense digoxigenin-labelled-RNA-probe is then cleaned using the „RNeasy Mini Kit“ according to the manufacturer’s instructions. The RNA-probe is analysed by gel-electrophoresis (see 2.3.10) for the expected integrity.

Immunological analysis of digoxigenin-labelled RNA

buffer PI:

TrisHCl, pH7.5	100mM
NaCl	150mM

buffer PII

0.1% TritonX-100 in 1x PBS

buffer PIII

TrisHCl, pH9,5	100mM
NaCl	100mM
MgCl ₂	50mM

All solutions PI-PIII are sterilized.

Digoxigenin-labelled RNA bound to nylon membranes can be detected by anti-digoxigenin antibodies. These antibodies are coupled to alkaline phosphatase, which catalyze a colour reaction, leading to the precipitation of a water insoluble blue dye. This is a mean to control for successful incorporation of digoxigenin-UTPs in the antisense-RNA probe.

1µl of the antisense RNA probe, a 10-, 50-, 100- and 500-fold dilution of the RNA probe are applied on a nucleic acid-binding nylon membrane in a petri-dish. After the probe has dried, the membrane is coated with 15ml PI buffer. Unspecific binding sites for anti-digoxigenin antibodies are blocked by replacing buffer PI with buffer PII and gentle shaking for 30min. Buffer PII is discarded and the membrane is incubated in a 1:2000 dilution of antidigoxigenin antibody in 15ml buffer PII for 30min. Excessive, non bound antibody is removed by washing the membrane with buffer PI twice for 15min. To activate the alkaline phosphatase the membran is incubated with alkaline buffer PIII for 2min. Subsequently the membrane is covered with fresh colour solution containing 4,5µl/ml NBT and 3,5µl/ml BCIP in buffer III without shaking. The speed of the colour reaction can be compared with known probes to estimate the amount of incorporated digoxigenin incorporation and thus the quality of the probe.

As a rule of thumb if the colour reaction of 1µl of a 500fold diluted probe appears after 20s digoxigenin-UTP has been sufficiently incorporated into the probe. The colour reaction is stopped after 5min by washing with buffer PIII for 1-2min.

Fixation and storage of fish embryos (Hauptmann and Gerster, 1994)

Zebrafish embryos are fixed over night in 4% PFA at 4°C on a shaker. This way the tissue is conserved, without degradation of RNA by endogenous RNases.

Afterwards the embryos are dechorionated, washed in PTW for four times at room temperature for 5min each and subsequently dehydrated in a dilution series from 25%, 50%, 75% to 100% MeOH. After 5min the MeOH is replaced by fresh MeOH. The embryos are now stored at -20°C for up to half a year.

The longer the embryos stay in MeOH, the more permeable they get for the RNA probe and antibodies. Therefore freshly fixated embryos should stay in MeOH for at least 1 day to improve the quality of the in situ hybridisation.

Proteinase K-digest und postfixation of embryos (Hauptmann and Gerster, 1994)

For further experiments the dehydrated embryos have to be rehydrated. Embryos are transferred into 6 well plates and washed 5 min with 5ml MeOH/PTW (75%, 50%, 25%) each series and washed with PTW twice each for 5min at room temperature on a shaker.

Tab. 1: Recommend times for proteinase K digest

To obtain a better permeability of the tissue for RNA probes and antibodies, fish embryos are partly digested by proteinase K. The following table shows recommended times for this digest for different stages of embryonal development. Embryos younger than 24h are not treated with proteinase K.

developmental stage	proteinase K digest
24hpf	12min
36hpf	20min
48hpf	25min
3dpf	30min

Afterwards the embryos are incubated with proteinase K solution (10µg/ml in PTW) according to Tab.1. Proteinase K digest is stopped by washing with 2mg/ml Glycin/PTW (ProteinaseK-inhibitor) and refixation in 4% PFA for 20min. To remove the PFA, embryos are subsequently washed with PTW 5 times for 5min each. Embryos are sensitive after proteinase K digest, and are treated with care.

Hybridisation (Hauptmann and Gerster, 1994)

Hybridisation buffer

Formamide (100%)	25ml
20x SSC	12,5ml
Heparine (50mg/ml)	150µl

Torula-RNA 250mg

Tween[®]20 50µl

add H₂O to 50ml; the solution can be stored at –20°C.

20x SSC

3M Tris-Acetate

300mM NaCitrate

The pH-value is set to 7,0 and the solution is autoclaved.

Colour solution (NTMT)

NaCl 150mM

TrisHCl (pH 9.5) 100mM

MgCl₂ 50mM

Tween[®]20 0,1%

To investigate the expression pattern of a gene, the digoxigenin labelled RNA probe is applied to the PFA postfixed embryos.

The embryos are transferred to 2ml eppendorf tubes and are prehybridized with 1ml hybridisation buffer for at least 1h at 57°C. Afterwards the buffer is removed.

4µl of the hybridisation probe are denatured in 200µl hybridisation buffer for 10min at 90°C, before replacing the prehybridization mix.

Subsequent hybridisation occurs over night at 57°C. The following day the embryos are washed with 2ml of the following solutions each for 45min at 57°C: 2x 50% Formamide/2x SSCT, 1x 2x SSCT and 2x 0,2x SSCT.

Detection of the digoxigenin labelled hybridisation probe (Hauptmann and Gerster, 1994)

The hybridisation probe can be detected by anti digoxigenin-antibodies as it contains digoxigenin conjugated UTPs. The antibody is coupled to alkaline phosphatase, which catalyses the precipitation of a dark blue indigo-derivative from the watersoluble substrates

BCIP and NBT in cells that express the gene of interest.

First unspecific binding sites are blocked by incubation of the embryos with 2ml of 5% goat serum/PTW (filtered 0,22µm) for 1h on a rotater at room temperature. Then embryos are incubated in a 1:2000 solution of the anti digoxigenin antibody in 5% goat serum/PTW (filtered 0,22µm) at 4°C over night while rotating.

The following day embryos are transferred to 6 well plates and rinsed with PTW six times for 15min each at room temperature on a shaker to remove unbound antibodies.

The fish embryos are equilibrated in alkaline staining NTMT solution two times for 5min each. Then the embryos are incubated with 5ml of fresh NBT/BCIP solution containing 5µl/ml NBT and 3,75µl/ml BCIP in NTMT until the staining reveals the desired intensity. Because of the light sensitivity of the NBT/BCIP solution the colour reaction was performed in the dark (without shaking) and monitored every 30min.

To stop the colour reaction, embryos are rinsed 3 times 15min in PTW at room temperature and are stored over night in PTW at 4°C in the dark. The embryos are transferred to 90% glycerol / 10% PTW at 4°C for long term storage with glycerol partly dehydrating the embryos and thus condensing the staining.

To capture images of the expression pattern, embryos are removed from their yolk. They are embedded on a drop of 90%glycerol on a microscope slide and sealed with a cover slip.

2.3.18. Immunohistochemistry

see Materials and Methods section of Appendix 1

2.3.19. Rhodamine Dextran Retrograde Labelling

see Materials and Methods section of Appendix 1

2.3.20. Cell culture

Media and solutions used for cell culture:

Leibovitz L15 Medium 500ml (Gibco) supplemented with

FBS (fetal bovine serum) 75ml

Penicillin/Streptavidin 6ml

Non-essential aminoacids 6ml

Trypsin/EDTA (0.05%/0.53M) (Gibco)

Dulbecco's (D)-PBS (Gibco)

2.3.21. Culturing zebrafish pac2 embryonic fibroblasts

Zebrafish pac2 embryonic fibroblasts (Chenn et al., 1998) were kindly provided by Christoph Leucht, Institute of Developmental Genetics, Helmholtz Center Munich.

The obtained 1ml glycerol stock of pac2 fibroblasts is supplemented with 9ml Leibovitz medium and centrifuged at 1100rpm for 1min (Universal 32R, Hettich centrifuges). The supernatant is discarded, the cell pellet is resuspended in 5ml Leibovitz medium and transferred into a sterile 6cm petri dish. Then the cells are incubated at 30°C until they are grown to confluence. The cells are detached from the petri dish after the medium has been removed by addition of 1ml of Trypsin/EDTA (0.05%/0.53M). The Trypsin digests proteins, which attach the cells to the dish. After incubation at 37°C for 5min 4ml Leibovitz medium are added and the cell suspension is transferred to a 10cm petri dish. Leibovitz medium is added to a total volume of 10ml.

For stable culturing of cells Leibovitz medium is exchanged every two to three days. After approximately two weeks the cells are passaged. This is done by removing the medium and adding 2ml Trypsin/EDTA. After incubation at 37°C for 5min 8ml Leibovitz medium are added and typically 2ml of this cell suspension are transferred to a new 10cm petri dish already containing 8ml Leibovitz medium. Cells are cultured this way for up to 15 passages.

2.3.22. Determining cell numbers

To determine cell numbers of pac2 fibroblasts a Neubauer counting chamber was used. 25 squares of the counting chamber, which have a volume of 0,1µl were counted. The number of cells per µl can be calculated from this data, which is required to adjust the optimal cell number for subsequent transformation reactions. Typical numbers of cells in a cell suspension after Trypsin digest of a 10cm petri dish are 1 - 6*10⁵ cells/µl.

2.3.23. Transfection

For transfection of zebrafish fibroblasts the "Effectene®" transfection or the "Nanofectin®" kit were used according to the manufacturer's (Qiagen and PAA) specifications, respectively. Effectene® transfection reagent is a lipid formulation, which

forms complexes with DNA. In a first step DNA is condensed by interaction with the enhancer reagent. Upon subsequent addition of Effectene® transfection reagent DNA containing micelles are formed, which fuse with cell membranes and therefore transfer the encapsulated DNA into the zebrafish cells.

Transfections for evaluation of vectors encoding fusion proteins are done in 6cm petri dishes, transfections for luciferase assays are done in 96well plates using the recommended cell numbers and DNA volumes. Cells are transfected 24h after seeding.

2.3.24. Quantitation of the Gal4 – mediated expression system

To quantify expression levels of different combinations of Gal4 derived activators and Gal4 dependent effectors carrying different multiple iterations of Gal4 binding sites (UAS), luciferase assays (see 2.3.25) are performed.

The expression vectors used for this quantitation carry the gene for firefly (*Photinus pyralis*) luciferase under the control of 1x,2x,3x,4x,5x and 14x Gal4 binding sites and the E1b basal promoter (Argenton et al., 1996).

As control for transfection efficacy a vector encoding the Renilla (*Renilla reniformis*) luciferase under control of a SVTK promoter is used.

Zebrafish pac2 fibroblasts are first counted (see 2.3.22) and then seeded at the cell density recommended by the manufacturer in 96 well plates. After 24h the cells are co-transfected with 0.3µg of each: Gal4-activator, Gal4-effector and transfection control vector.

As control for background signal derived from the cell some wells are left non-transfected. As control for a potential leaky basal promoter pac2 cells are transfected with a firefly luciferase containing vector without UAS sites upstream of the firefly luciferase gene and with the renilla vector but without an activator vector. The transfection medium is replaced approximately 12h after transfection. The Luciferase assays (see 2.3.25) are performed 24h post transfection.

2.3.25. Luciferase assays

Luciferases catalyse photochemical reactions generating bioluminescence. When an excess of substrate is provided the light intensity is proportional to the amount of luciferase protein present. Therefore measuring bioluminescence produced by a Luciferase gene is a reliable way to quantify the efficacy of an expression vector system.

I used the “Dual-Luciferase[®] Reporter Assay System” (Promega) to quantify Gal4 mediated gene expression in cultured zebrafish pac2 fibroblasts. The “Dual-Luciferase[®] Reporter Assay System” is based on measuring the bioluminescence of two different luciferases. The firefly (*Photinus pyralis*) luciferase, which is used as the reporter under control of the Gal4 system and the Renilla (*Renilla reniformis*) luciferase under control of an SVTk promoter, which is used to correct for varying transfection efficacy. Bioluminescence of these luciferases can be measured independently as they have different substrates (see Fig.19).

To control for the reliability of the luciferase kit, some wells are transfected only with an activator vector and an expression vector but without a renilla vector. This can show that the firefly luciferase signal is stopped by adding the substrate.

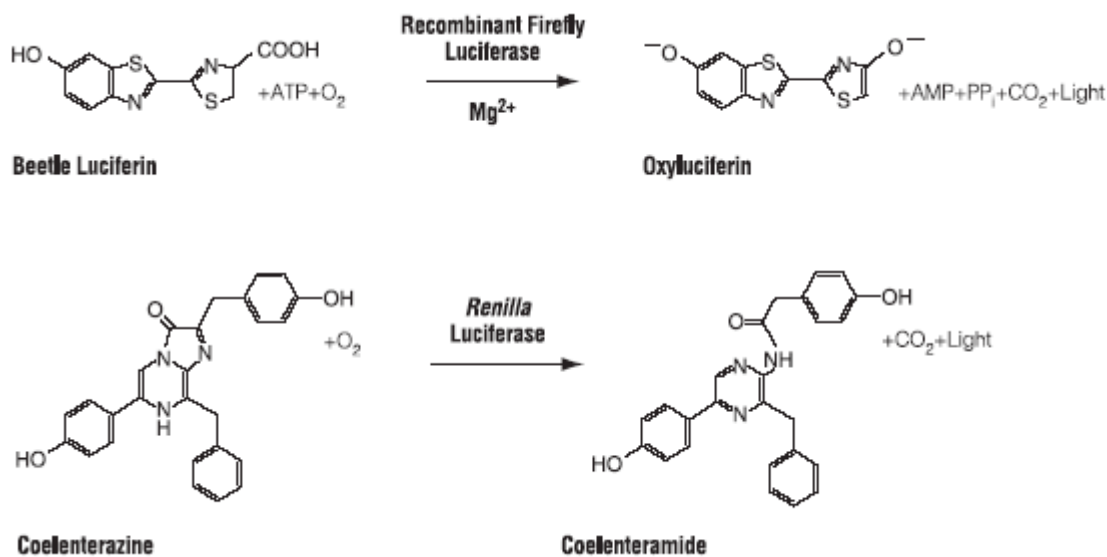


Fig. 19: Bioluminescent reactions catalyzed by firefly and Renilla luciferases.

Luciferase assays are performed in 96well plates and read out by the Orion Luminometer using the software “simplicity”.

First transfected cells are lysed by a combination of passive and active lysis. Passive lysis buffer from the luciferase kit (Promega) is added according to the manufacturer’s specifications and the 96well plate is gently mixed for 10min on a shaker. Afterwards it is stored at –80°C for 20min, followed by 20min at room temperature. This active lysis step is repeated once before the actual luciferase assay is performed.

First the firefly substrate is added to the lysed protein extract. After quantifying the emitted luminescence in a luminometer, the firefly luciferase mediated luminescence is quenched by a stop solution upon which the second substrate specific for the renilla luciferase generated

bioluminescence is quantified. The ratio of generated luminescence from firefly and renilla luciferase is an indicator for the amount of expressed firefly luciferase corrected for varying transfection efficacies.

Obtained light intensities from firefly luciferase are therefore corrected for background and for transfection efficacies in the following way:

$$(V_{\text{firefly}} - MV_{\text{Luciferase untransfected cells}}) / (V_{\text{Renilla}} - MV_{\text{Renilla untransfected cells}}) = V_{\text{firefly E corrected}}$$

$$V_{\text{firefly E corrected}} - MV_{\text{pCS + XxUAS}} = V_{\text{firefly B/E corrected}}$$

V_{firefly} = measured firefly signal

V_{Renilla} = measured Renilla signal

$MV_{\text{Renilla untransfected cells}}$ = mean value of measured Renilla signal of untransfected cells

$MV_{\text{Luciferase untransfected cells}}$ = mean value of measured Renilla signal of untransfected cells

$MV_{\text{pCS + XxUAS}}$ = mean of transfection efficacy corrected signal of cells transfected with pCS without Gal4 activator and respective 1-5xUAS or 14xUAS vector

The resultant value is standardized by division over the pCS $V_{\text{firefly corrected}}$ value.

$$V_{\text{firefly corrected}} / \text{pCS } V_{\text{firefly corrected}}$$

Statistics are calculated using the freeware statistics programm "R". (download: <http://www.gnu.org/>)

2.3.26. Bodipy Ceramide staining

In order to visualize cell membranes or the extracellular matrix by fluorescence, living or fixated zebrafish embryos are incubated in 0,001% Bodipy Ceramide/30%Danieau respectively PTW at room temperature for at least 6h. Before image acquisition, the stained embryos are rinsed twice in 30%Danieau for living embryos and in PTW for fixated embryos.

2.3.27. Embedding Embryos for microscopic investigations

Embryos were dechorionated and embedded in 1,2% ultra low melting agarose/30% Danieau before image recording. This prohibits unwanted movements of the embryo but ensures sufficient oxygen supply.

A 30%Danieau/0.01%Tricaine solution was added to sedate the embryo and therefore avoid muscle contractions. A detailed description of the embedding procedure can be found in **Appendix 7**.

3. Results

3.1. Adaptation of the Gal4-UAS system for zebrafish

The Gal4-UAS system has proven a versatile tool in *Drosophila* research (see 1.4.3). One of the possibilities offered by the system is the spatial and also, using modified Gal4 variants, temporal control over transgene expression (see 1.4.3.1 and 1.4.3.2). Further, established Gal4 activator strains and effector strains harbouring different transgenes can be crossed in any possible combination, so that for example one can perform a multitude of overexpression experiments using a limited number of Gal4 and UAS strains. In addition, the separation of activator and effector strains allows for the investigation of embryonic lethal phenotypes as both strains are viable and both can be raised to adult stages. Moreover, mutants can be rescued in a tissue specific manner, which allows one to study the role of specific genes in distinct tissues.

To take advantage of the many possibilities offered by the Gal4-UAS system I devoted the first part of my PhD project to adapt the Gal4-UAS system for its use in zebrafish.

Published Article (Distel et al., 2009b) see Appendix 1

3.1.1. Generation of transgenic Gal4 zebrafish

Initial approaches to generate transgenic zebrafish using the strong transcriptional activator Gal4VP16 and GFP as a reporter under control of 14 repeats of UAS sites failed, as embryos of the F1 generation were not viable (Fig.20A). Likely, this was due to toxic effects of Gal4VP16 causing “squenching” or deleterious expression levels of GFP. VP16 associates with many cellular transcription factors like TFIIB, TFIID or TFIIF (Baron et al., 1997). Therefore it is likely that overexpression of VP16 fused to Gal4 is not tolerated well by cells, as strong recruitment of transcription factors might lead to inhibition of transcription of essential house-keeping genes.

In order to overcome deleterious effects, the VP16 transactivation domain was replaced by different repeats of the 13-amino acid core sequence of the VP16 transactivation domain (TA2, TA3 and TA4), which are better tolerated by cells (Baron et al., 1997). In luciferase assays (n =3) using a 5xUAS:luciferase reporter construct the activation potential of GalTA2-TA4 was quantified in zebrafish Pac2 fibroblasts. The order of activation strength was determined to be TA2>TA3>TA4.

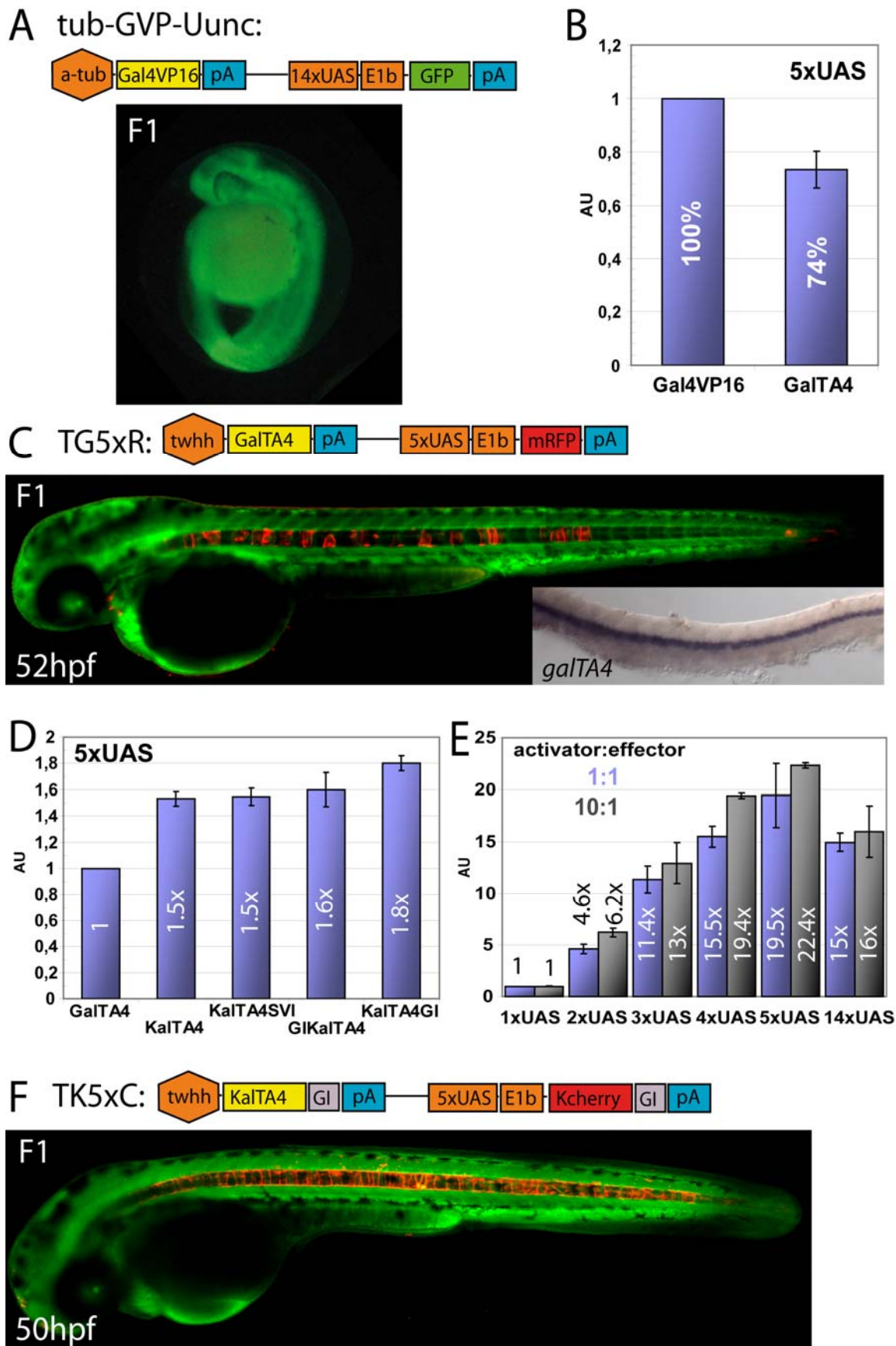


Fig. 20: Optimizing the Gal4-UAS system for zebrafish

(A) Schematic representation of the tub-GVP-Uunc construct and transgenic F1 zebrafish embryos. (B) Comparison of Gal4VP16 (set as 100%) and GalTA4 activity in luciferase assays (n=3, Pac2 fibroblasts) using a 5xUAS:luciferase construct. (C) Schematic representation of the TG5xR construct and transgenic F1 embryo. Inset: mRNA in situ hybridization of GalTA4 expression throughout the notochord. (D) Activation

potentials of differently modified Gal4 activators as determined by luciferase assays (n=3). The activity of GalTA4 was set as 1. (E) Effects of different numbers of Gal4 DNA binding sites using pCSKGalTA4GI and UAS-luciferase constructs (ratio 1:1 blue columns or 10:1 black columns) in luciferase assays (n=3, 1xUAS:luciferase set as 1). (F) Schematic representation of the TK5xC construct and transgenic F₁ embryo. Data are presented as mean \pm SEM. Embryos in C and F are counterstained with green Bodipy Ceramide.

To overcome potential “squenching” the least active variant, GalTA4, showing 74% activity compared to Gal4VP16 (Fig.20B), was consequently used to establish transgenic Gal4 fish. A construct (TG5xR) carrying GalTA4 under control of the notochord specific *tiggy winkle hedgehog* (*twhh*) regulatory element (Du et al., 1997) and mRFP under control of 5xUAS as an internal reporter cassette was generated. Stable transgenic embryos derived from injections of this linearized construct (TG5xR) were viable and fertile. Although they displayed notochord specific reporter expression, this expression was highly mosaic. In contrast, RNA in situ hybridizations revealed ubiquitous transcription of GalTA4 throughout the notochord suggesting a translation problem of either GalTA4 or mRFP (Fig.20C).

To generate an activator (KalTA4) and a reporter protein (mCherry) optimized for translation, their codon usage was adjusted to the preferred codon use in zebrafish and a Kozak sequence (GCCGCCACC) was added for efficient ribosome binding, which led to a 1.5fold increase in activity of KalTA4 compared to GalTA4 as determined by luciferase assays (n=3) (Fig.20D). In addition, an intron was added (KalTA4GI), which increases gene expression as splicing targets the mRNA for nuclear export (Amsterdam et al., 1995; Perz-Edwards et al., 2001). Luciferase assays (n=3) revealed that a rabbit β -Globin intron placed at the 3' end of KalTA4, now termed KalTA4GI further increased transactivation activity to 1.8fold compared to GalTA4 (Fig.20D). In addition, the effect of different numbers of UAS repeats was quantified by luciferase assays (n=3). A roughly linear increase in activity was found from a single up to five repeats of UAS sites (Fig.20E). Surprisingly, 14 repeats showed an activity comparable to 4 repeats, even with a ten fold excess of transfected activator (Fig.20E black columns), suggesting a threshold for the optimal number of UAS sites.

In a next step, the optimized activator KalTA4GI under control of the *twhh* regulatory element together with translation optimized mCherry (KCherryGI) under control of 5xUAS was used in a self-reporting construct (TK5xC) to establish transgenic Gal4 zebrafish. TK5xC carries Tol2 recognition sites so that integration into the genome was mediated by the Tol2 transposase (Kawakami, 2004). TK5xC transgenic zebrafish of the F₁ generation were viable and showed red fluorescence throughout the entire notochord, indicating a successful optimization strategy (Fig.20F).

Conclusion

The successful optimization of the Gal4-UAS system for zebrafish (by switching the transactivation domain of the Gal4 activator from VP16 to TA4, adding a Kozak sequence, adopting the codon usage for zebrafish and adding an intron, respectively to both, the activator and reporter protein) yielded a system, which is well tolerated and is capable of reliably expressing transgenes in a tissue specific manner. The quantification of expression levels from different numbers of UAS sites provides a quantitative basis for varying the dose of transgene expression in zebrafish

3.2. Generation of hindbrain specific Gal4 activator strains

In order to study the development of the hindbrain, activator strains expressing Gal4 specifically in the hindbrain would be of great value. As only very few regulatory elements are characterized in zebrafish, we decided to perform a pilot Gal4 enhancer trap screen using my zebrafish optimized Gal4-UAS system (see 3.1.1) in order to generate hindbrain specific Gal4 activator strains.

The trapping construct (TK1xC) (Fig.21) was based on the TK5xC vector as generation of TK5xC transgenic fish revealed that the *twhh* regulatory element is sensitive to positional effects, but does not show any background expression other than in the notochord.

To bias our enhancer trap screen toward detecting only strong positional effects a single UAS site was used.



Fig. 21: Gal4 self-reporting enhancer trap construct

The self-reporting trapping construct TK1xC carries the zebrafish optimized Gal4 (KaTA4GI) under control of the *twhh* regulatory element, which was found to be prone to position effects. The reporter cassette contains zebrafish optimized mCherry (KcherryGI) under control of a single UAS site to report trapping events of strong enhancers. The construct is flanked by Tol2 recognition sites (Tol2) for transposase mediated integration into the genome.

The trapping vector (Fig.21) was co-injected with mRNA encoding Tol2 transposase to mediate the integration into the genome (25ng/μl each). Fluorescent embryos were raised to adult stages and crossed to wildtype fish to identify transgenic fish. Screening for expression of mCherry in the F₁ generation was mainly performed between 2dpf and 3dpf. 40% of injected P₀ embryos (38/94) transmitted the TK1xC construct to the next generation, showing

tissue specific expression of mCherry, but no signs of malformation, retarded development or reduced viability.

A number of P₀ and F₁ transgenic fish gave rise to offspring displaying different tissue specific expression patterns, suggesting multiple independent integrations and enhancer trap events of the TK1xC construct, which could also be confirmed by Southern blot analysis. For example transgenic strains displayed in Fig.23B, F and J are derived from the same P₀ or F₁ parents.

In the F₃ generation 60 stable transgenic strains displaying different tissue specific expression patterns of mCherry (Fig.23) with a bias for expression in the CNS (Fig.22A) were established. Among these, 18 showed expression in the hindbrain (Fig.22B).

To make all strains available to the zebrafish community, a searchable database showing images and movies of enhancer trap strains was created (http://www.helmholtz-muenchen.de/en/id/groups/neuroimaging/lines_distel/) (also see website on enclosed CD).

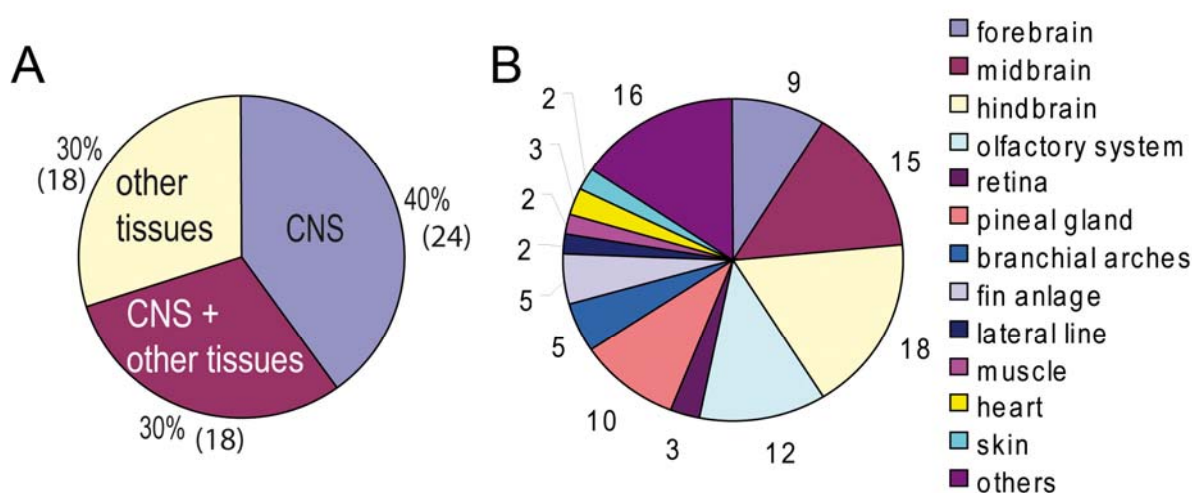


Fig. 22: Distribution of expression patterns of F₂ Gal4 enhancer trap strains

(A) Distribution of expression patterns in the isolated KalTA4 enhancer trap strains of the F₂ generation (numbers in brackets are the numbers of strains showing the indicated expression). (B) Distribution of all observed expression patterns throughout the isolated KalTA4 strains of the F₂ generation. Note that many strains show mCherry expression in several tissues.

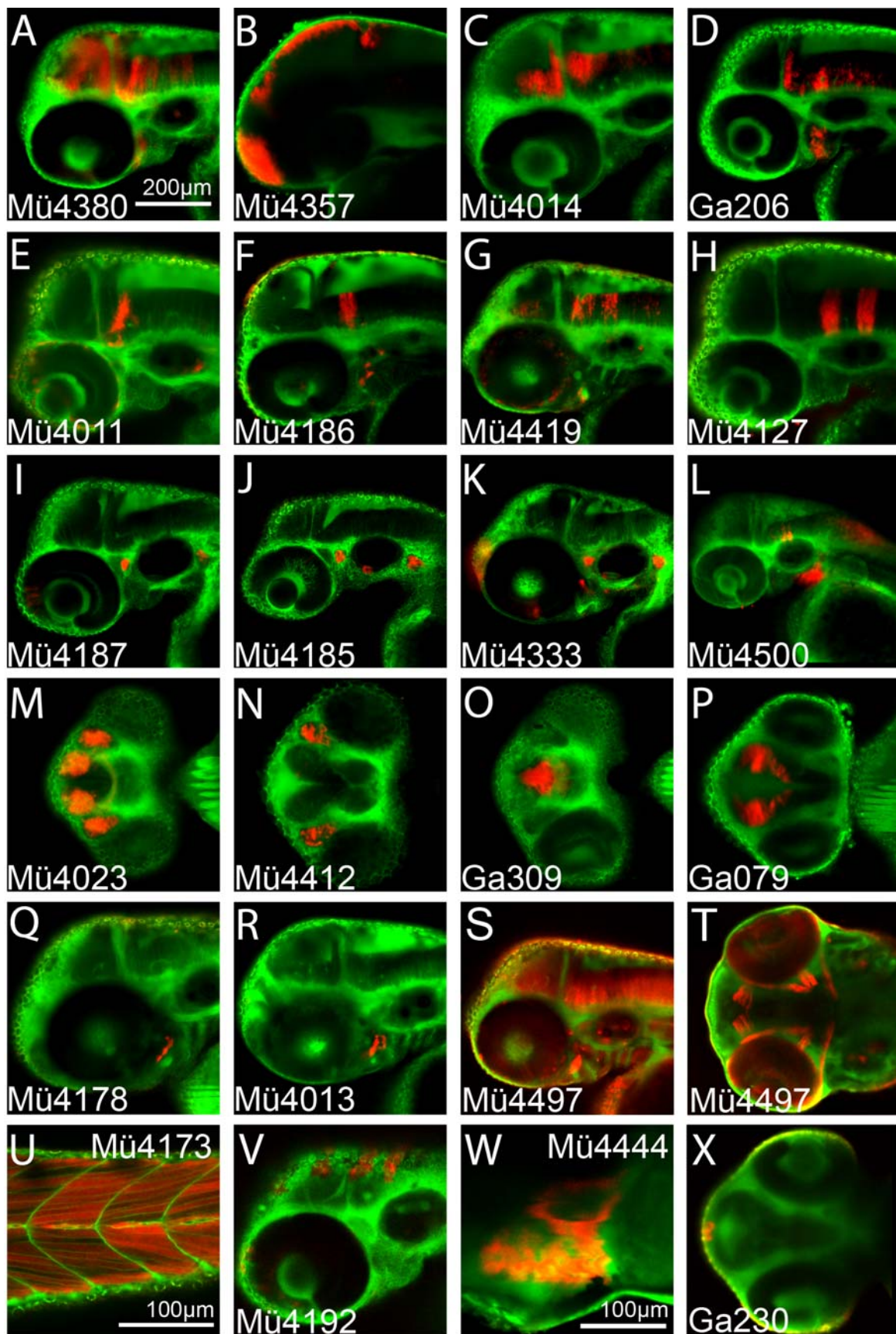


Fig. 23: Gal4 enhancer trap strains

Selective Gal4 strains obtained from the enhancer trap screen. Embryos were screened for mCherry expression (red) between 24hpf and 60hpf, Bodipy ceramide (green) counterstained and images were recorded approximately 50hpf-65hpf with a Zeiss LSM510 using a 20x objective. Lateral view in A-L, Q-S and U-W, ventral view in M-P and dorsal view in T and X. The heart of a 6 day old embryo is shown in W).

Next, I investigated if the Gal4 enhancer trap strains were capable of transactivation. Using strain Mü4023 (*olf:KalTA4*), which shows expression of mCherry in the olfactory system (Fig.24A), I first confirmed the expression of KalTA4 in this domain by in situ hybridisation (Fig.24B). Injection of the Ulyn construct (Köster and Fraser, 2001b) carrying a membrane tagged GFP under control of 14xUAS led to a mosaic expression of GFP restricted to the olfactory system (Fig.24C). Furthermore, I generated an effector strain (4xKGFPGI), carrying GFP under control of 4xUAS. The *olf:KalTA4* strain and other selected enhancer trap strains (n=15) were mated to this 4xKGFPGI strain and offspring of all matings showed expression of GFP confined to mCherry expression domains (Fig.24D). This indicated a robust KalTA4 activated and dependent expression in trans in transient injection experiments as well as in experiments with stable transgenic zebrafish.

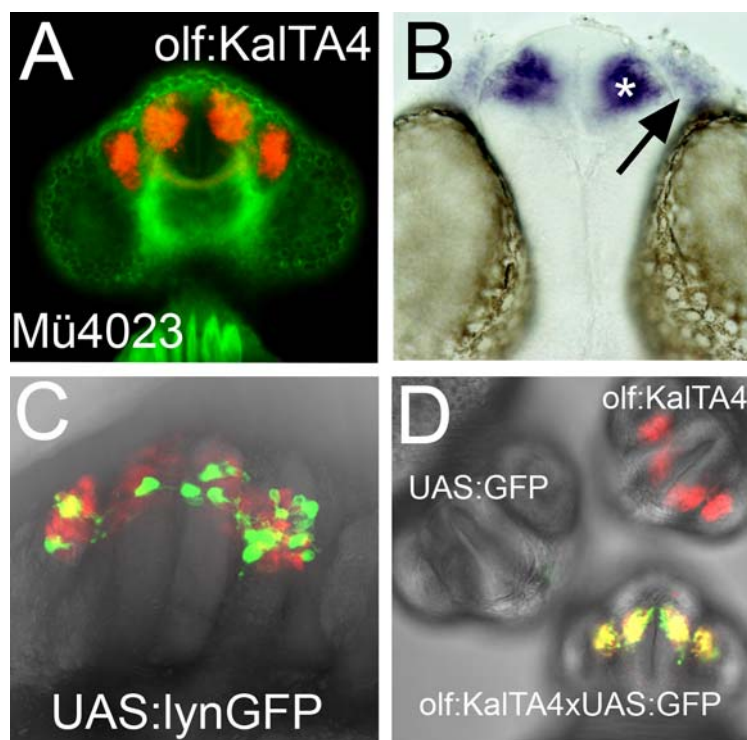


Fig. 24: Transactivation

(A) Expression of mCherry in the olfactory system of enhancer trap strain Mü4023 (*olf:KalTA4*). Cell membranes are counterstained with Bodipy ceramide (green).

(B) KalTA4 mRNA expression (asterisk: olfactory bulb, arrow olfactory epithelium) in strain *olf:KalTA4*.

(C) Transactivation of UAS:lynGFP in injected *olf:KalTA4* embryo at 26hpf. (D) KalTA4-mediated transactivation of GFP expression in offspring (26 hpf) from crosses of heterozygous *olf:KalTA4* and 4xUAS-KGFPGI carriers.

Furthermore, Gal4 enhancer trap strains can be crossed with each other, for example *r1:KalTA4GI* and *r3/5:KalTA4GI*. By this means, Gal4 expression domains can be expanded

in a combinatorical manner, so that e.g. effects of transgene expression can be studied in r1, r3/5 and r1/3/5 (Fig.25).



Fig. 25: Expanding Gal4 expression domains

Mating of enhancer trap strain Mü4011(r1:KalTA4) with expression in r1 and an additional cell cluster in r2 to strain Mü4127 (r3/5:KalTA4) with expression of Gal4 in r3/5 leads to offspring with combined expression domains in r1/3/5.

Notably, homozygous carriers could be established for several of the enhancer trap strains, which reliably passed on mCherry expression to 100% of their progeny. This will be useful for future studies, where large numbers of transgenic fish are required without prior laborious screening for positive fish.

Since the enhancer trap construct was inserted randomly into the genome, there was the potential to disrupt gene function and create mutant fish. Among the 17 strains tested, one strain (Mü4497_18 shown in Fig.23S) displayed a mutant phenotype when bred to homozygosity. At 5 dpf homozygous fish displayed a severe reduction in size of the retina and the brain and a failure in inflation of the swimbladder (Fig.26). Mutant fish could not be raised to adulthood as they died at around 10 dpf.

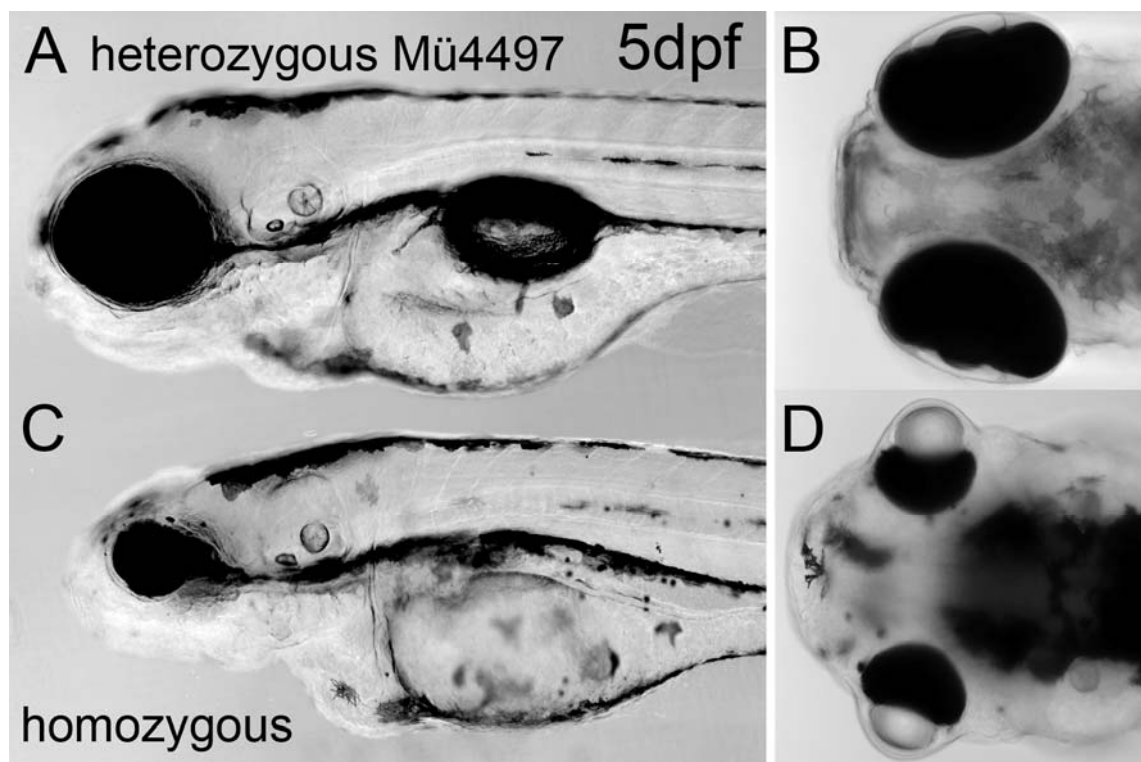


Fig. 26: Thymidylate synthetase mutant

A) Lateral and B) dorsal view of a heterozygous transgenic zebrafish (Mü4497) at 5 dpf. C) lateral and D) dorsal view of a homozygous transgenic zebrafish (Mü4497) at 5 dpf. Note the reduction in size of the retina and the brain and the absence of an inflated swimbladder in the homozygous transgenic fish.

Based on the known flanking regions of the trapping construct inverse nested PCR was performed to determine the genomic integration site of the construct and the gene affected by the integration. The integration could be mapped to chromosome 7, likely disrupting the first exon of the ORF encoding Thymidylate Synthetase (*tms*).

The integration sites of other selected strains were also determined in the same manner (Table1).

Among them I identified an inserted trap cassette about 1.5 kb downstream of the zebrafish *egr2b* gene known as *krox20* in other vertebrates. Its prominent expression in rhombomeres 3 and 5 (r3/5) during developmental stages of the hindbrain was reflected by mCherry fluorescence (Fig.23H). I subsequently used this insertion to investigate the dynamic regulation of *kalTA4* expression and of UAS:transgenes as direct KalTA4 downstream genes by mRNA in situ analysis. Like endogenous *egr2b* (Fig.27A-C), *kalTA4* expression was initiated first in rhombomere 3 and subsequently about 30 min later in rhombomere 5 (Fig.27D-F). Similarly, expression of both *egr2b* (Oxtoby and Jowett, 1993) and *kalTA4*

ceased during embryogenesis first in rhombomere 3 and about 2 h later in rhombomere 5 (Fig.27J-L) and was never detected again in these rhombomeres until adulthood (60, 84, 132 hpf, 4 months). Thus *kalTA4* expression in this strain closely reflects the endogenous expression dynamics of *egr2b*. Interestingly, I observed that *kalTA4* expression is initiated about 90 min after endogenous *egr2b* (compare Fig.27A and D) and turns off approximately 4–6h earlier compared to *egr2b* (Oxtoby and Jowett, 1993). This is probably due to the different distance of the inserted TK1C cassette to key regulatory elements. When heterozygous carriers of the r3/5:KalTA4 and the 4xUAS-KGFPGI transgenic strains were crossed, first transactivated *gfp* mRNA expression could be observed about 30–60 min after the onset of *kalTA4* expression, closely reflecting *kalTA4* expression (Fig.27G-I, note first visible *gfp* mRNA expression at 12 hpf). Thus, transactivation of a direct transcriptional target in zebrafish takes approximately 30–60min. Termination of *kalTA4* mRNA expression between 21 and 23hpf (Fig.27J-L) resulted in a decrease of transactivated *gfp* mRNA transcription at about 27 to 29 hpf (Fig.27M-O), reflecting the time needed for the degradation of the KalTA4 protein. This knowledge is important for planning transactivation experiments in which the lifetime of the transactivated protein (several days in the case of GFP) affects the full duration of ectopic expression.

Conclusion

In an enhancer trap approach using the zebrafish optimized Gal4-UAS system (3.1) 60 transgenic strains displaying tissue specific Gal4 expression in a variety of tissues could be established. The respective integration sites of the trapping construct were determined in 15 of the established strains. As all strains tested were capable of activating transgenes in a Gal4 dependent and tissue specific manner, these strains promise to be of great value in addressing a multitude of biological questions in zebrafish (see 3.3 and 3.4).

Table 1: Insertion sites of trapping construct

Line	Expression pattern	Insertion locus	Nearest gene	Insertion position	Reported gene expression pattern	Shown in
Mü4380_64	midbrain hindbrain	Chr.21 11852731/11852738	<i>efna5a</i>	intron	midbrain hindbrain	Fig.24 A
Mü4466_13	ventral CNS	Chr.16 near 13747710	<i>sp8l</i>	2.4kb downstream of <i>sp8l</i>	ventral CNS	Fig.24 C
Mü4357_9	telencephalon tectum, cerebellum, hindbrain	Chr.24 4310366/4310372	<i>zic1/zic4</i>	400bp upstream of <i>zic4</i>	telencephalon, tectum, cerebellum, hindbrain	Fig.24 B
Mü4572_46	r3/r5	Chr.12 6373073/6373076	<i>egr2b (krox20)</i>	1.5kb downstream of <i>egr2b</i>	r3/r5	Fig.24 H
Mü4410_30	melanocytes	Chr.20 20623777/20623784	<i>kit a</i>	140bp upstream of <i>kit a</i>	pigment cells	Fig.24 V
Mü4497_18	ubiquitous	Chr.7 near 69747338 - 69747444	<i>tms (thymidylate synthetase)</i>	exon1	ubiquitous	Fig.24 S
Mü4573_19	olfactory system	Chr.17 16748712	<i>A2CE94 DANRE</i>	22kb downstream of A2CE94 240bp upstream of marker z30232	not reported	Fig.24 M
Ga206_19	telencephalon cerebellum, r 3/5 lateral line ganglion	Chr.17 50466304/50466361	<i>zgc:154061</i>	intron	not reported	Fig.24 D
Ga286_86	telencephalon lateral line ganglion, retina	Chr.6 13479159/13479165	<i>pou23</i>	1.5MB upstream of <i>pou23</i>	cerebellum, r 3/5	Fig.24 K

Table 1 continued: Insertion sites of trapping construct

Line	Expression pattern	Insertion locus	Nearest gene	Insertion position	Reported gene expression pattern	Shown in
Mü4356_8	retina, hindbrain (day4)	Chr.17 28072728/28072734	<i>kif11b</i>	23kb downstream of <i>kif11b</i>	not reported	not shown
Ga234_65	telencephalon	Chr.7 23649835/23649908	ENSDARESTG000000130 70 <i>Imo1</i>	exon of ENSDARESTG000000130 70 22kb upstream of <i>Imo1</i>	telencephalon, hindbrain	Fig.24 O
Mü4435_64	muscle	Chr.15 8561461/8561468	ENSDARG00000058274	21kb downstream of ENSDARG00000058274	not reported	Fig.24 U
Mü4354_50	CNS	Chr.5 58511708/58511710	<i>notch1b</i>	Intron of <i>notch1b</i>	CNS	not shown
Ga079_8	diencephalon	Chr.6 near 15292344 - 15292395	<i>barh-like2</i>	82kb downstream of <i>barh-like2</i>	telencephalon, diencephalon, pretectum, lateral hindbrain	Fig.24 P
Mü4497_18	muscles around eye	Chr.9 29069994/29070000	peptide similar to JAM-2	500bp upstream of gene	muscles around eye	Fig.24 T

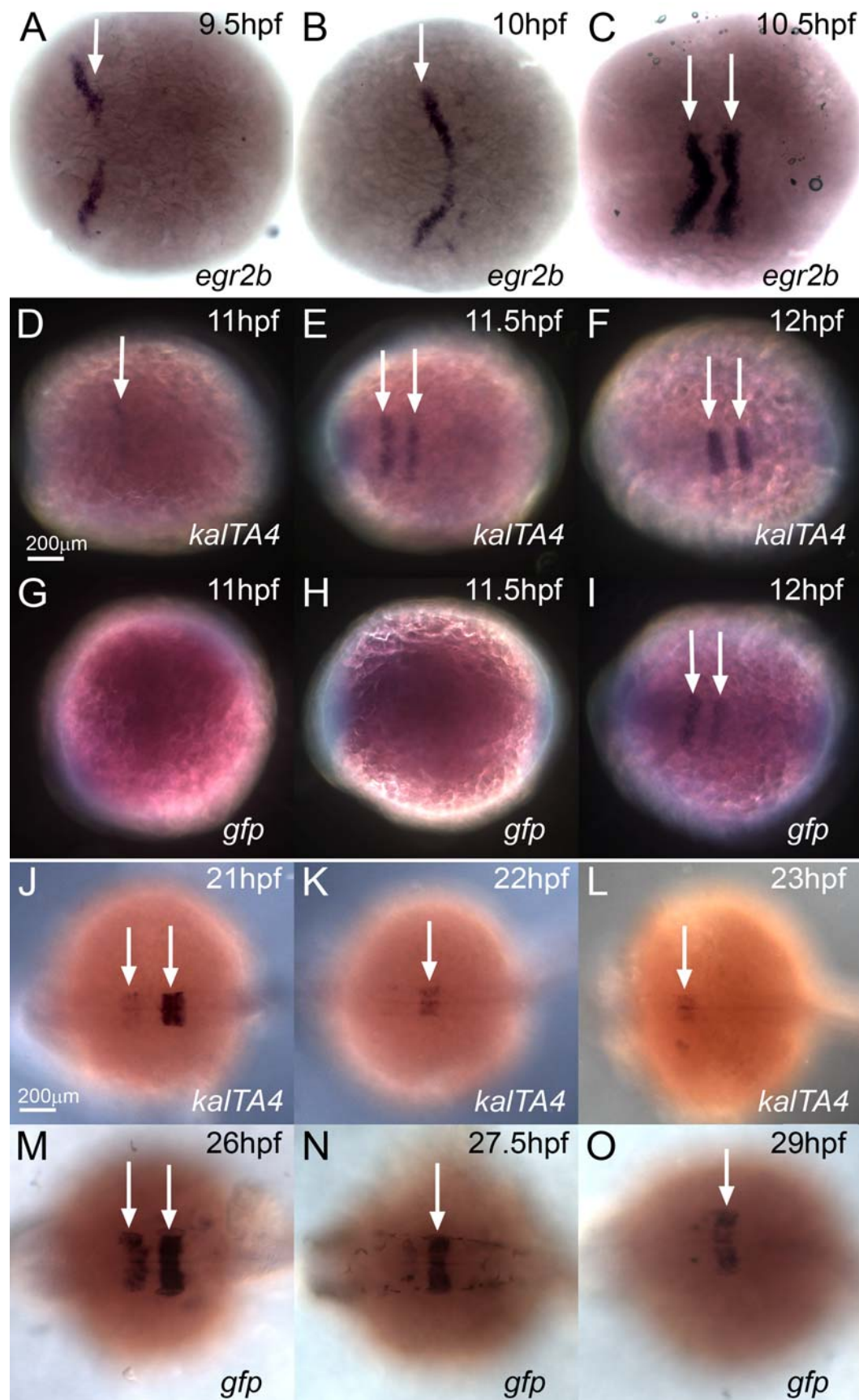


Fig. 27: Comparative mRNA *in situ* hybridization analysis

A-C) *egr2b* in WT embryos, D-F) *kalTA4* and (G-I) *gfp* in offspring of r3/5:KalTA4 x 4xKGFP cross. J-L) mRNA *in situ* hybridization analysis of downregulation of *kalTA4* and M-O) *gfp* in r3/5 of r3/5:KalTA4 x 4xKGFP embryos. Arrows indicate expression domains of the respective genes.

3.3. Investigating rhombomere fate

Rhombomeres are compartments of the hindbrain, which are only transiently visible around 18hpf as distinct bulges (Fig.4) (Kimmel et al., 1995). Molecularly the expression of rhombomere specific genes like *egr2b/krox20* is also only transient (Fig.27 and (Oxtoby and Jowett, 1993). The r3/5:KalTA4 strain offered the opportunity to follow the fate of r3/5 and to elucidate r3/5 derived structures by prolonging reporter gene expression in a Gal4 dependent manner. For this, I generated a stable transgenic effector strain, 4xKaloop, which carries a bicistronic 4xUAS effector construct driving GFP expression as reporter followed by a peptide backbone breaking T2A sequence, which mediates stoichiometric expression of KalTA4 (Provost et al., 2007). Once activated, this effector should continuously maintain its own expression by constantly providing KalTA4 activator in a feedback loop (Fig.28).

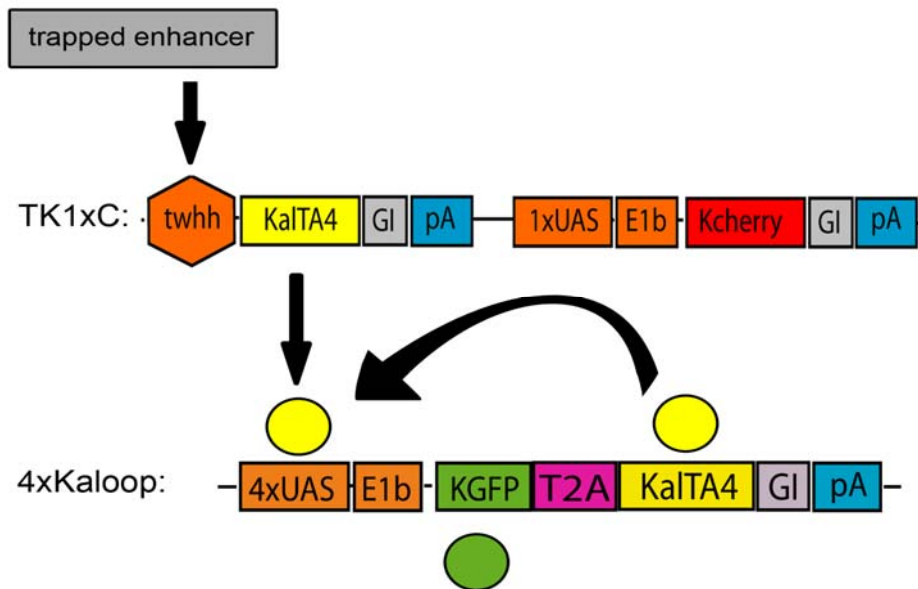


Fig. 28: Gal4 feedback loop mechanism to prolong reporter gene expression

In a cross between an enhancer trap strain and the 4xKaloop strain KalTA4 expression is initially activated from the TK1xC construct by the trapped regulatory element. KalTA4 binds to the 4xUAS sites of the 4xKaloop construct and activates stoichiometric expression of GFP and KalTA4. KalTA4 from the 4xKaloop construct binds back on its own regulatory UAS sites hereby creating a feedback loop, which prolongs expression of GFP and KalTA4.

To study the fate of r3/5, r3/5:KalTA4 transgenic fish were mated to 4xKaloop and as a control to 4xKGFP transgenic fish. At 26hpf, r3/5 specific transactivation of GFP expression was visible in double transgenic offspring of both crosses (Fig.29A-C; F-H). In r3/5:KalTA4 x 4xKaloop double transgenic offspring at adult stages, GFP was still detectable in the dorsal region of the hindbrain in a mosaic but spatially restricted manner consisting of two distinct stripes resembling the embryonic organisation of r3/5 ventral to the r1 derived cerebellum (Fig.29I,J). In contrast, GFP in the r3/5:KalTA4 x 4xKGFP control cross ceased in r3/5 at

around 11dpf and was absent at adult stages (5months) (Fig.29D,E). This indicates that the Gal4 mediated feedback loop is capable of prolonging GFP expression until adult stages. In addition, this shows that the rhombomeric organization persists until adulthood in zebrafish.

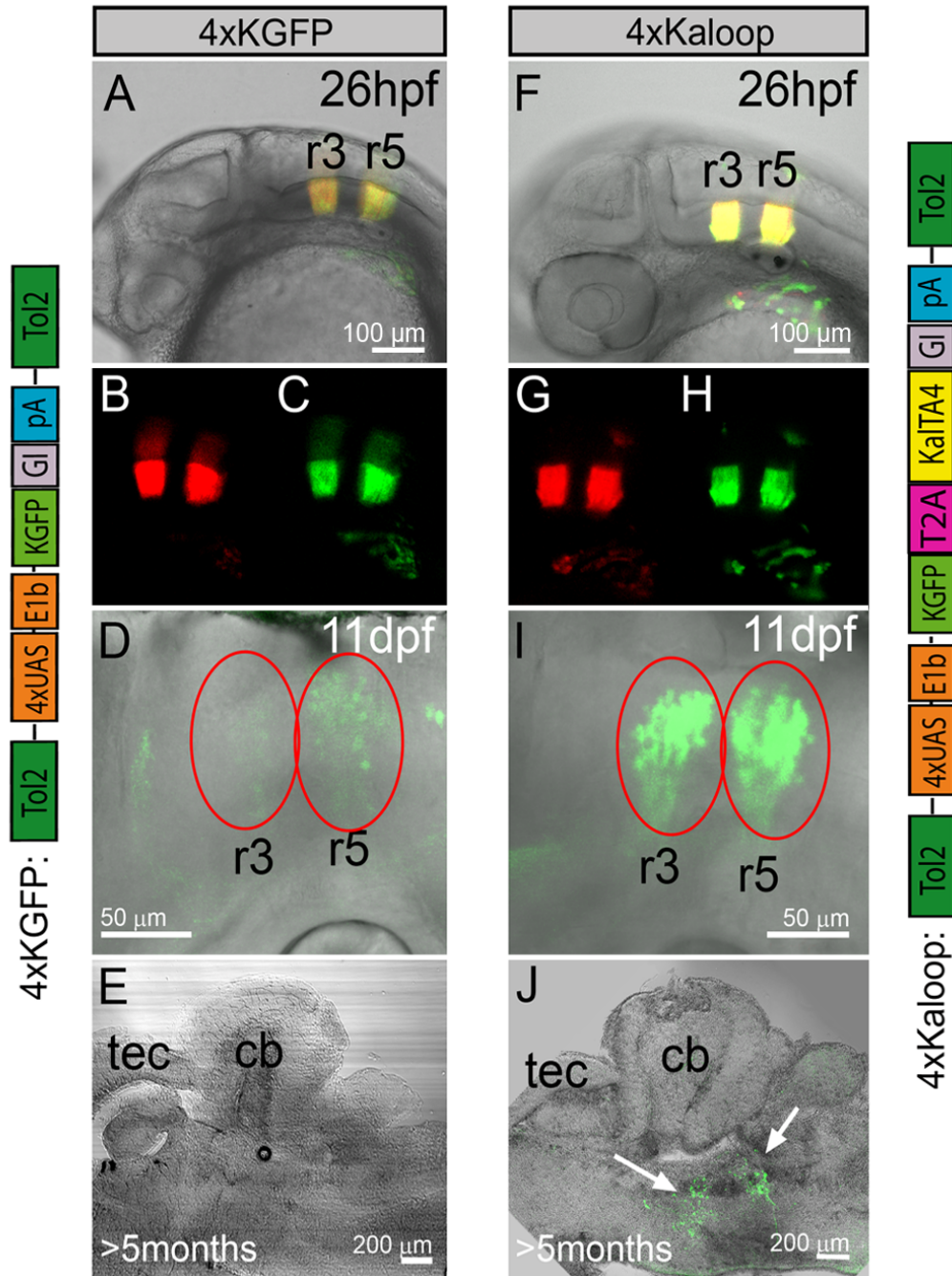


Fig. 29: Fate-mapping rhombomeres 3/5

A-E) Expression in r3/5 in offspring from a cross between r3/5:KalTA4 and 4xUAS-KGFPGI (schematic representation of the effector construct shown on the left). F-J) r3/5:KalTA4 crossed to 4xKaloop (schematic representation of the effector construct shown on the right). A-C, F-H) Expression of mCherry and transactivated GFP at 26hpf. D) At 11hpf, GFP fluorescence (red ovals) is diminished in r3/5 and E) lost in the adult brain of r3/5:KalTA4 x 4xUASKGFPGI carriers, while in r3/5:KalTA4 x 4xKaloop carriers GFP expression is maintained in two domains in the hindbrain until adulthood (I, J)

To identify adult structures derived from r3/5, I visualized GFP expressing cells and cholinergic cells by immunohistochemistry on vibratome sections of brains of r3/5:KalTA4 x 4xKaloop crosses. GFP positive cells of the r5 derived domain were localized dorso-medially to the cholinergic nucleus abducens (Fig.30A), suggesting an identity as neurons of the secondary octaval nucleus (SON). Neurons of the SON send dendrites into the crista cerebellaris and participate in transmitting directional acoustic information into the torus semicircularis of the midbrain, where this information converges at least in some species with sensory input from the second-order projections of the lateral line (Fame et al., 2006; McCormick and Hernandez, 1996). Indeed, GFP containing dendrites in the crista cerebellaris (Fig.30B) and axons innervating the torus semicircularis (TS) (Fig.30C) could be detected in the vibratome sections by anti-GFP immunohistochemistry.

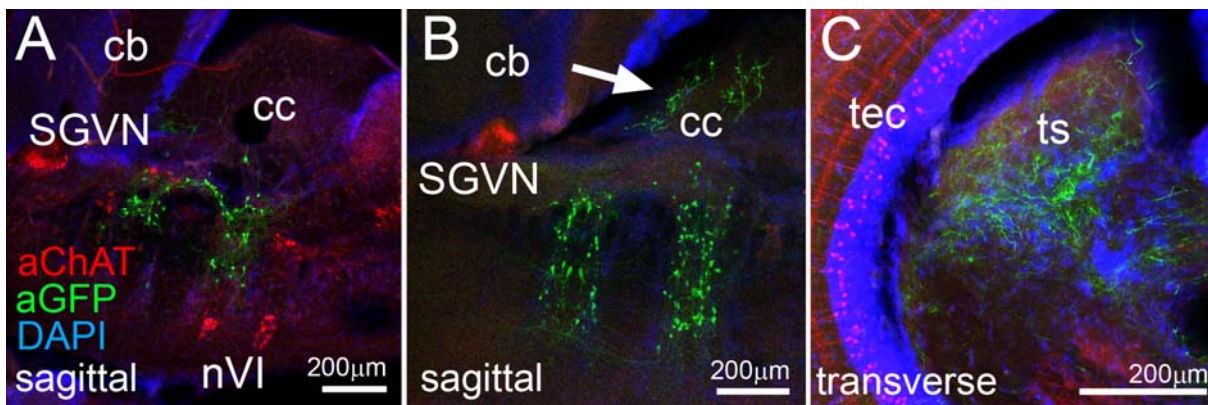


Fig. 30: Neurons of the SON are derived from rhombomere 5

Immunohistochemistry for GFP (green) and Cholinacetyltransferase (ChAT;red) on brain vibratome sections of adult zebrafish derived from a cross of r3/5:KalTA4 x 4xKaloop. All nuclei were counterstained with DAPI (blue). A) Sagittal section of the hindbrain (rostral is left) shows r5 derived GFP positive cells dorsal to the cholinergic abducens nuclei (nVI). B) Sagittal section (rostral is left) reveals GFP positive dendrites in the crista cerebellaris (cc) and in a transverse section in C) GFP positive axons innervating the torus semicircularis (ts), as described for neurons of the secondary octaval nucleus.

Abbr.: cb: cerebellum; cc:crista cerebellaris; SGVN secondary gustatory/viscerosensory nucleus; tec: tectum; ts: torus semicircularis; nVI: rostral and caudal abducens nuclei

To independently confirm, that GFP expressing cells in r5 innervate the torus semicircularis I performed retrograde labelling by focal administration of rhodamine dextran into the torus semicircularis (Fig.31A). Rhodamine dextran was transported retrogradely into the r5 region (Fig.31B) and colocalized with a subpopulation of GFP expressing neurons (Fig.31C-F), strongly suggesting an identity as neurons of the SON.

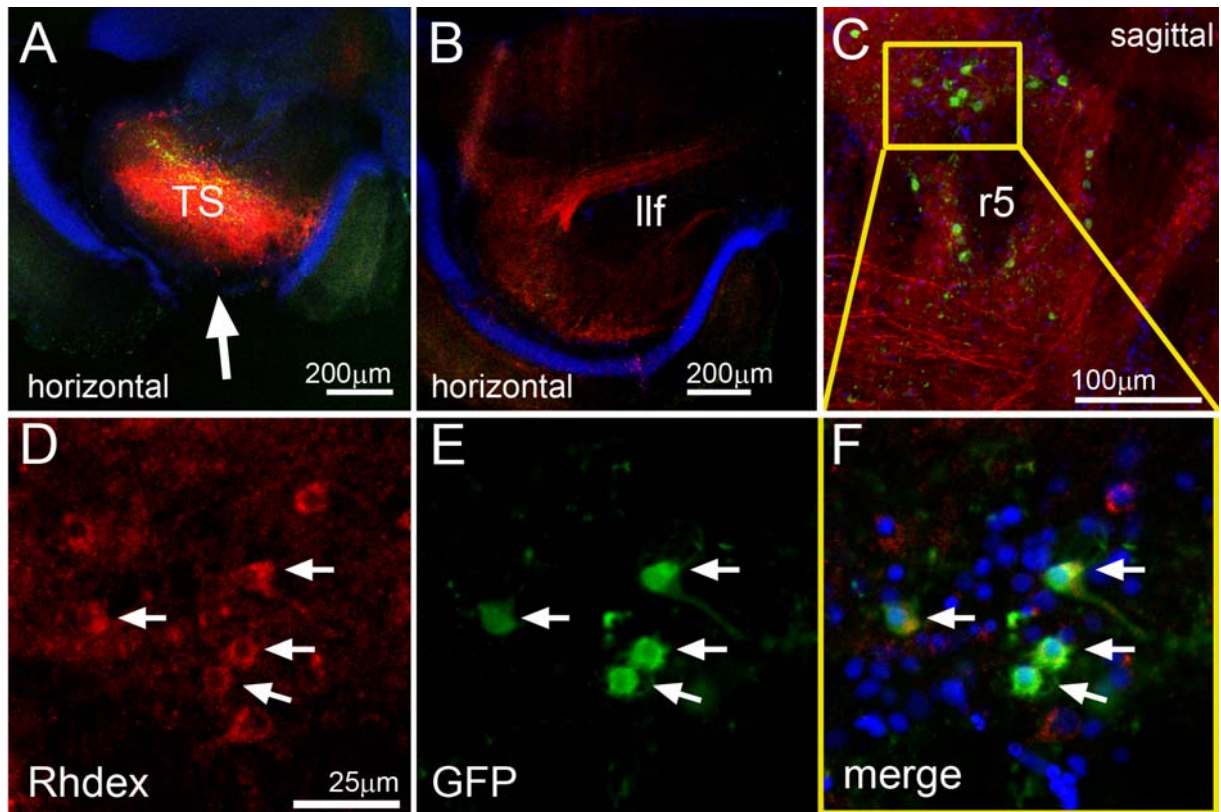


Fig. 31: Retrograde labelling of neurons of the SON

Adult brain cryostat sections (100 μ m) of rhodamine dextran injected adult r3/5:KalTA4 x 4xKaloop fish. A) Rhodamine dextran (red) injection site in the central nucleus of the torus semicircularis (TS). The arrow demarcates the site where the tectum was removed to inject the rhodamine dextran. B) Rhodamine dextran (red) positive axons of the lateral longitudinal fascicle (llf) that innervate the torus semicircularis originate from caudal projection nuclei in the hindbrain. C) Some of the r5 derived GFP positive neurons were labelled retrogradely with rhodamine dextran (Rhdx) (D-F) confirming their identity as r5 derived neurons of the secondary octaval nucleus.

Conclusion

The established 4xKaloop effector strain can be used to prolong gene expression until adult stages via a Gal4 mediated feedback loop. Using this technique, I could show that the embryonic organization of r3/5 as two distinct domains is maintained in the zebrafish hindbrain until adult stages. Furthermore it could be shown that neurons of the secondary octaval nucleus (SON) are derived from r5. The 4xKaloop strain thus promises to be a useful tool to investigate relationships between various embryonic and adult structures.

3.4. Further applications of Gal4 enhancer trap strains

3.4.1. Elucidating the role of Lunatic Fringe in hindbrain development

Published Article (Nikolaou et al., 2009). See Appendix 2

Notch signalling diversifies adjacent cells by lateral inhibition or induction. During the lateral inhibition of neurogenesis in the vertebrate nervous system, proneural transcription factors that drive the initial steps of neuronal differentiation upregulate expression of the Notch ligands, Delta or Serrate/Jagged. These ligands activate Notch in adjacent cells by promoting a proteolytic cleavage that releases the intracellular domain of Notch (Mumm et al., 2000), which then binds to the transcription factor CSL, causing it to switch from a repressor to an activator (Fryer et al., 2002). The activated CSL complex upregulates expression of members of the Hes/Her transcriptional repressor family, which in turn inhibit neurogenesis (Kageyama et al., 2007). Consequently, a pool of undifferentiated cells is maintained adjacent to differentiating neurons, and only once lateral inhibition is relieved e.g. as the forming neuron migrates away from the neural epithelium can neurogenesis be initiated.

Fringe glycosylates specific sites of the Notch extracellular domain during its intracellular processing, and this glycosylation alters the affinity of Notch binding to its ligands: Delta binds more strongly to Fringe-modified Notch, whereas the binding of Serrate is decreased (Moloney et al., 2000; Panin et al., 1997). At early stages, *lunatic fringe* (*lfng*) expression occurs at high levels in alternating segments in the hindbrain (Leve et al., 2001; Prince et al., 2001; Qiu et al., 2004), which by analogy with roles in other tissues could underlie boundary formation. In addition, *lfng* is expressed in dorsoventrally restricted domains in the neural tube (Prince et al., 2001) that could be associated with zones of neurogenesis.

In collaboration with us and using my enhancer trap derived *egr2b:KalTA4* strain, David Wilkinson's group at UCL investigated the role of Lunatic Fringe in the zebrafish hindbrain. We used Morpholino knockdown and target rescue experiments to show that Lunatic Fringe functions to maintain hindbrain cells in a progenitor state. First, Morpholino based knockdown of *lunatic fringe* led to increased expression of proneural and Delta genes, including *neurogenin1*, *delta*, *deltaB* and *neurod4* at 18hpf, 24hpf and 36hpf, but did not affect segmentation or boundary formation in the hindbrain.

Consistent with an enhancement of neurogenesis, *lfng* knockdown led to a 1.7-fold increase in the number of differentiated neurons, labelled my HuC/D, at 18 hpf and 30 hpf in the mantle zone (Fig.32E-H) compared to control MO injected animals (Fig.32A-D).

To assess the specificity of the phenotypic effect of the *lfng* MO, a rescue experiment was performed using the *egr2b:KalTA4GI* strain, which specifically expresses Gal4 in r3/5 (Fig.23H) (see 3.2).

A construct harbouring *lfng* and the reporter H2B-Citrine, each under the control of UAS sites, was generated and either injected alone or co-injected with *lfng* MO into zebrafish embryos. As a control, a construct containing UAS:H2B-Citrine was injected alone or together with *lfng* MO. Both constructs were transactivated in r3/5 and derivatives (Fig.32J). Transgenic overexpression of *lfng* alone decreased the amount of neurogenesis in r3/5. Co-injected with *lfng* MO, the *lfng* overexpression construct partly suppressed the MO-induced increase in neurogenesis (Fig.32K), whereas overexpression of the control H2B-Citrine did not alter the phenotype. Importantly, the effects of *lfng* overexpression occurred specifically in r3/5, where *lfng* was ectopically expressed, and not in r4.

A potential explanation for these findings is that *lfng* knockdown leads to a deficiency in the lateral inhibition of neurogenesis. In agreement with this hypothesis expression of *her4* and *her12* was found to be decreased at 40hpf following *lfng* knockdown. Analysis of neural progenitor markers *sox3* and *sox19a* further showed a decrease in neural progenitors. Taken together, knockdown of *lfng* eventually leads to a depletion of progenitor cells, consistent with a role in Notch-mediated lateral inhibition of neurogenesis.

Conclusion

Zebrafish embryos deficient in *lfng* showed increased neurogenesis in the hindbrain. By transient overexpression of *lfng* in r3/5 by injection of a UAS:*lfng* construct into the *egr2b:KalTA4* strain, the mutant phenotype could be partially rescued in these rhombomeres. In contrast, the enhanced neurogenesis was still observed in r4. This suggests that *lfng* is required to maintain neural progenitors. This study demonstrates that the tissue-specific expression of Gal4 in my enhancer trap strains provides a powerful tool to elucidate the function of a gene in distinct tissues.

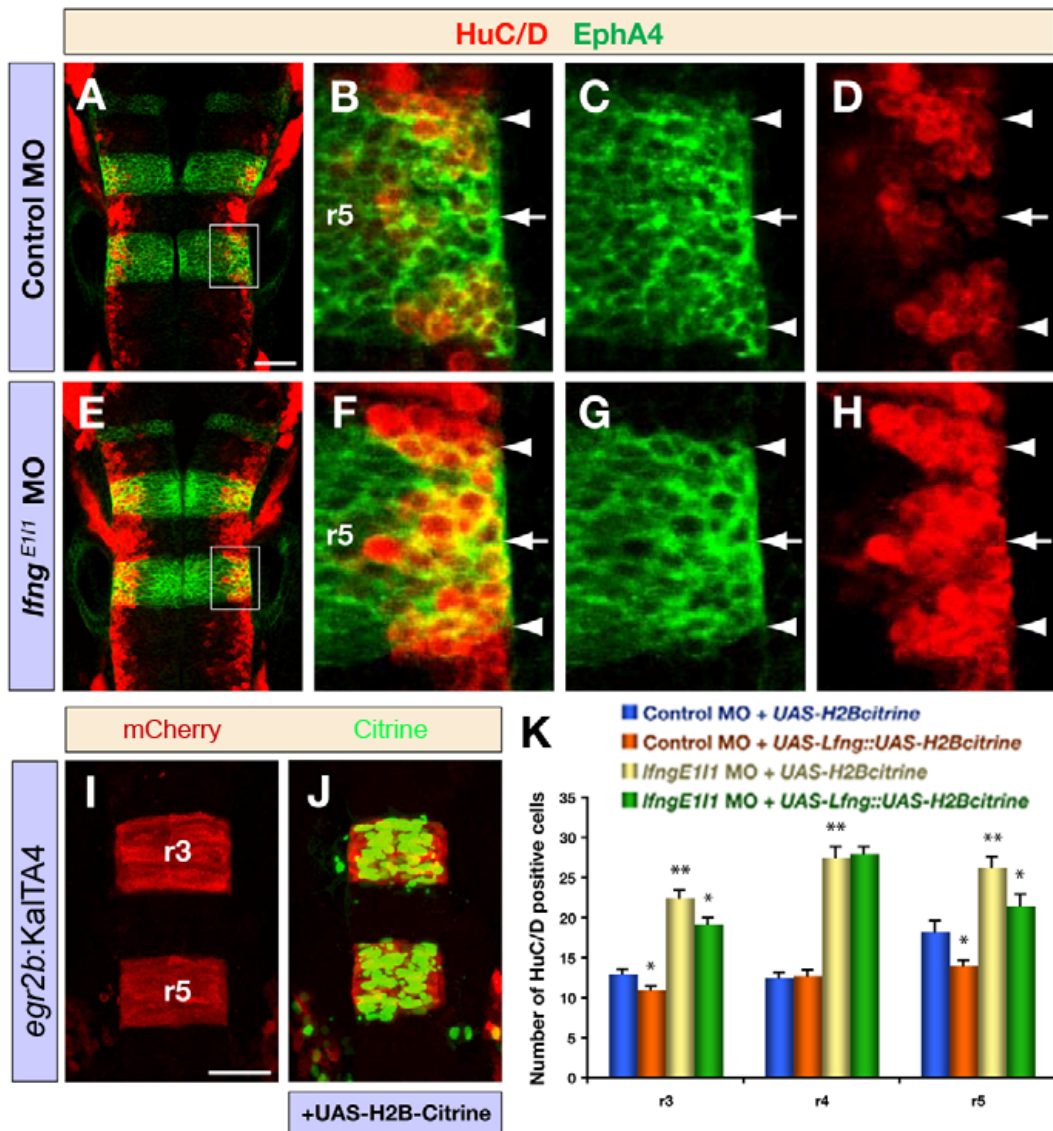


Fig. 32: Knockdown of *lunatic fringe* produces a neurogenic phenotype

A-H) Confocal images showing dorsal views of control MO (A-D) and *lfn* MO (E-H) injected embryos (30hpf), immunostained for HuC/D (red) and EphA4 (green) to mark postmitotic neurons and r3/5, respectively. B-D and F-H are higher magnifications of the areas indicated in A and E, respectively. Arrowheads and arrows indicate rhombomere boundaries and centres, respectively. I, J) Confocal images of the expression of mCherry (red) and H2B-Citrine (green) in r3/5 in the *egr2b:KalTA4* strain at 18hpf, either noninjected (I) or injected with UAS-H2B-Citrine. K) Quantification of the number of differentiating neurons (HuC/D expression) in *egr2b:KalTA4* injected with control MO or *lfn* MO together with either UAS-H2B-Citrine or UAS-*lfn*::UAS-H2B-Citrine. Transgenic overexpression of *lfn* in r3/5 leads to a decreased number of differentiated neurons, partly rescuing the effect of *lfn* knock down, whereas neurogenesis in r4 is not affected. Values are mean \pm standard error, neurons in four embryos were counted for each experimental group; *, $P < 0.05$, **, $P < 0.01$. Scale bars: 50 μ m in A for A-H and I for I, J.

3.4.2. Gal4 mediated tumor models

Accepted Article (Anelli et al., 2009) Appendix 3 and Santoriello et al. (2009) manuscript in preparation

Zebrafish develops an array of benign and malignant tumors resembling human malignancies (Amatruda et al., 2002; Beckwith et al., 2000; Langenau et al., 2003). Further, it is amenable to large-scale forward genetic screens that can be biased for conserved cancer pathways (Driever et al., 1996; Haffter et al., 1996). In addition, large screens for compounds effective against cancer can be easily performed in zebrafish (North et al., 2007). Zebrafish is thus a valuable vertebrate system in which to elucidate molecular pathways of oncogenesis.

The combinatorial nature of the Gal4-UAS system offers the opportunity to model a variety of human cancers in zebrafish by crossing tissue specific Gal4 activator strains with a UAS-effector strain containing an oncogene of interest.

An effector strain (UAS:EGFP-HRAS-G12V) harbouring a constitutively active variant of the human oncogene *H-RAS* (*H-RAS-G12V*) under control of 5xUAS was established in the lab of Marina Mione (IFOM, Milano) (Anelli et al., 2009). To visualize *H-RAS* expression, H-RAS was tagged with an N-terminal EGFP.

To study the effects of overexpression of the *H-RAS* oncogene in different tissues, the UAS:EGFP-HRAS-G12V (UAS:RAS) fish was mated to several tissue specific KalTA4 activator strains obtained from my enhancer trap screen.

Crossing transgenic UAS:RAS fish with *zic1/4*:KalTA4 transgenic fish resulted in GFP and H-RAS expression restricted to the KalTA4/mCherry expression domains in the telencephalon, tectum and cerebellum. At 5 dpf approximately 80% of double transgenic zebrafish embryos displayed tumors and edema in the forebrain and the tectum (Fig.33A).

At 12 dpf all embryos displaying tumors died. Tumor cells were identified in hematoxylin/eosin stains (Fig.33.C,D) and were found to express GFAP as revealed by anti-GFAP immunostainings on sections of 7 day old double transgenic embryos (Fig.33E,F).

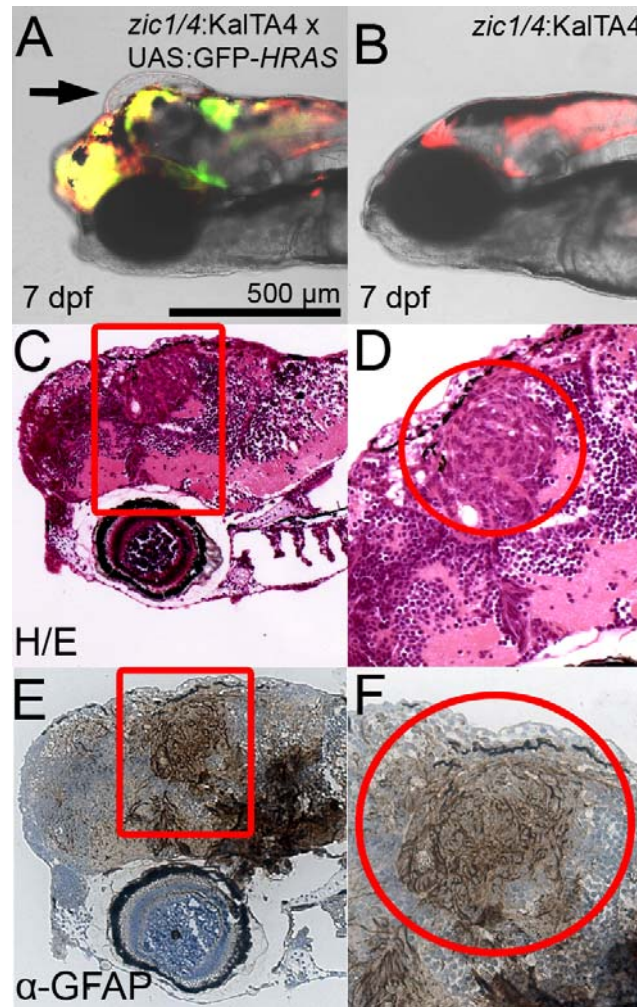


Fig. 33: Tissue specific expression of *H-RASG12V* using the Gal4-UAS system

Lateral views on living (A,B) and sectioned (C-F) zebrafish embryos at 7 dpf. A) Mating the *zic1/4:KalTA4* activator strain to a *UAS:GFP-HRAS* effector strain led to the development of tumors and edema (black arrow) in the *KalTA4* expression domain in the telencephalon and tectum of double transgenic embryos. B) Tumors or edema were never observed in *zic1/4:KalTA4* control fish. C,D) Hematoxylin/Eosin staining on a paraffin section of a double transgenic fish identified tumor cells (red circle in D). Boxed area in C) is enlarged in D). E,F) Tumor cells are expressing GFAP as revealed by anti-GFAP immunostainings (brown color, red circle in F). Boxed area in E) is enlarged in F).

In contrast to the high penetrance, early onset and fast progression of the disease in this glioma model, mating the *UAS:RAS* strain to the *kita:KalTA4* strain showed a different phenotype. In the *kita:KalTA4* strain, *KalTA4* is expressed like the endogenous *kit-a* in the melanocytic lineage (Hultman et al., 2007). Starting at 4 weeks, around 20% of double transgenic offspring developed pigmented tumors often at the level of the caudal fin (Fig.34). Strongly resembling human melanoma, tumors were found to be metastatic, infiltrating neighboring tissues like muscle, gills and brain.



Fig. 34: Zebrafish melanoma model

4 month old *kita:KalTA4* / *UAS:GFP-HRAS* double transgenic fish. Mating the *UAS:GFP-HRAS* effector strain to *kita:KalTA4* activator strain, which shows melanocytic lineage specific *KalTA4* expression, leads to tumor (black arrow) formation mainly in the caudal fin region and starting at around 4 weeks.

One possible use for these zebrafish cancer models is to study the importance of epigenetic processes during cancer progression. Recent studies have led to the realization that genetic and epigenetic mechanisms cooperate during all stages of cancer development. Surprisingly, expression studies have shown a general repressive state of the human cancer genome.

To investigate if this holds true for the established melanoma model, quantitative expression analysis of several putative cancer genes from known and predicted cancer gene lists was performed. Real-time PCR revealed that, like in human melanoma, the expression of many cancer genes is downregulated in zebrafish melanomas, whereas cell-cycle genes are upregulated. To understand if this trend is due to epigenetic alterations, histone methylation was investigated in the melanoma model by immunostainings. Substantial differences, similar to human melanoma, were found in the histone methylation state of tumor cells as compared to non-melanoma tissue. Such changes are likely to be responsible for the global repression of gene expression through epigenetic regulation observed in cancer.

Conclusion

The combinatorial Gal4-UAS system provides a powerful tool to model various types of cancer in zebrafish. By expressing the oncogene *H-RAS* in the CNS using the *zic1/4:KalTA4* transgenic strain, tumors resembling gliomas could be generated. Given the early onset of the disease, this model is suitable for large-scale screens for compounds effective against cancer. In addition, the developed melanoma model showed many of the molecular, genetic and epigenetic properties of human melanoma and therefore promises to be suitable for mechanistic studies of tumorigenesis *in vivo*.

3.5. Photoacoustic imaging of fluorescent proteins in adult zebrafish

Published Article (Razansky et al., 2009) Appendix 4

Due to its external development and transparency during embryonic stages, zebrafish is an ideal model organism for optical microscopy approaches, offering the opportunity to observe developmental processes at high-resolution in the living organism (see 3.6).

Commonly used zebrafish strains lose their transparency starting at approximately 14dpf and are thus not accessible for optical imaging approaches. However, in order to study processes like tumorigenesis (see 3.4.2) and regeneration or to use fate-mapping approaches to investigate how embryonic structures relate to adult structures (see 3.3), a means of visualizing fluorescent reporter proteins in the adult zebrafish would be extremely valuable.

Photoacoustic imaging (see 1.6) is a technique, which is capable of visualizing structures deep within highly scattering opaque tissue, like tumors.

Based on the photoacoustic effect, which relies on the conversion of absorbed photons into ultrasound, a variation of photoacoustic imaging (multispectral opto-acoustic tomography (MSOT)) should theoretically also allow one to detect fluorescent proteins. However, this technique has not previously been used to visualize fluorescent proteins.

In collaboration with the group of Daniel Razansky who established the MSOT technique at the Institute of Biological and Medical Imaging (IBMI) at the Helmholtz Center Munich, we tested whether the technique is applicable to the visualization of fluorescent proteins in the adult zebrafish.

To confirm the basic ability of the method to detect fluorescent proteins over background absorption and to quantify its performance, we generated a cylindrical agarose phantom, containing India ink and Intralipid to mimic absorption and scattering characteristics of animal tissue (optical absorption coefficient: 0.3cm^{-1} , scattering: 10cm^{-1}). Two 4-mm-diameter insertions were incorporated into the phantom. The first insertion contained stable transgenic HeLa cells ($4 \times 10^6 \text{mL}^{-1}$) expressing a mitochondrial targeted DsRedT4 fluorescent protein.

The second insertion served as a control and contained a higher concentration of India ink but no fluorescent cells. The principle of detection is based on differentiation of the absorption spectral signature of the protein over background tissue absorption by the analysis of

multiwavelength data. Fluorescent proteins are excellent molecules for this role compared to other chromophoric substances, because they exhibit a steep declining absorption slope at lower energies, which can easily be detected spectroscopically, as shown in Fig.35G, by recording absorption at multiple wavelengths. Although single-wavelength images only revealed the highly absorbing control insertion and some phantom heterogeneities (Fig.35D), the non-specific contrast from the insertion containing DsRed-expressing cells was barely visible. Nevertheless, multiwavelength processing of the images on a perpixel basis rendered high contrast from the FP-expressing cells (Fig.35E). The results showed excellent agreement with the epifluorescence image shown in Fig.35F, obtained after phantom sectioning to validate the tomographic images of the intact phantom.

Next we assessed the capacity of the method to image fluorescent proteins in intact adult zebrafish. The vertebral column represents a structure deep within the highly scattering trunk of the fish. To challenge the MSOT method, we thus decided to image adult zebrafish (TK1xC) obtained from the enhancer trap (see 3.2), which express mCherry in the vertebral column at adult stages.

Zebrafish were sacrificed and embedded in an agarose phantom for image recording at multiple wavelengths targeted to the steep declining slope of the mCherry extinction spectra (Fig.36C). A two dimensional plane (as indicated in Fig.36A) was imaged from different angles, while the fish was rotating. Spectral decomposition of the datasets generated an image that corresponded well with the transverse histological section (Fig.36G), which was made subsequent to optoacoustic imaging of the fish. In both cases mCherry expression could be visualized in a ring like domain in the vertebral column (Fig.36E,F). The MSOT image (Fig.36E) provided an in plane spatial resolution of approximately 40 μ m.

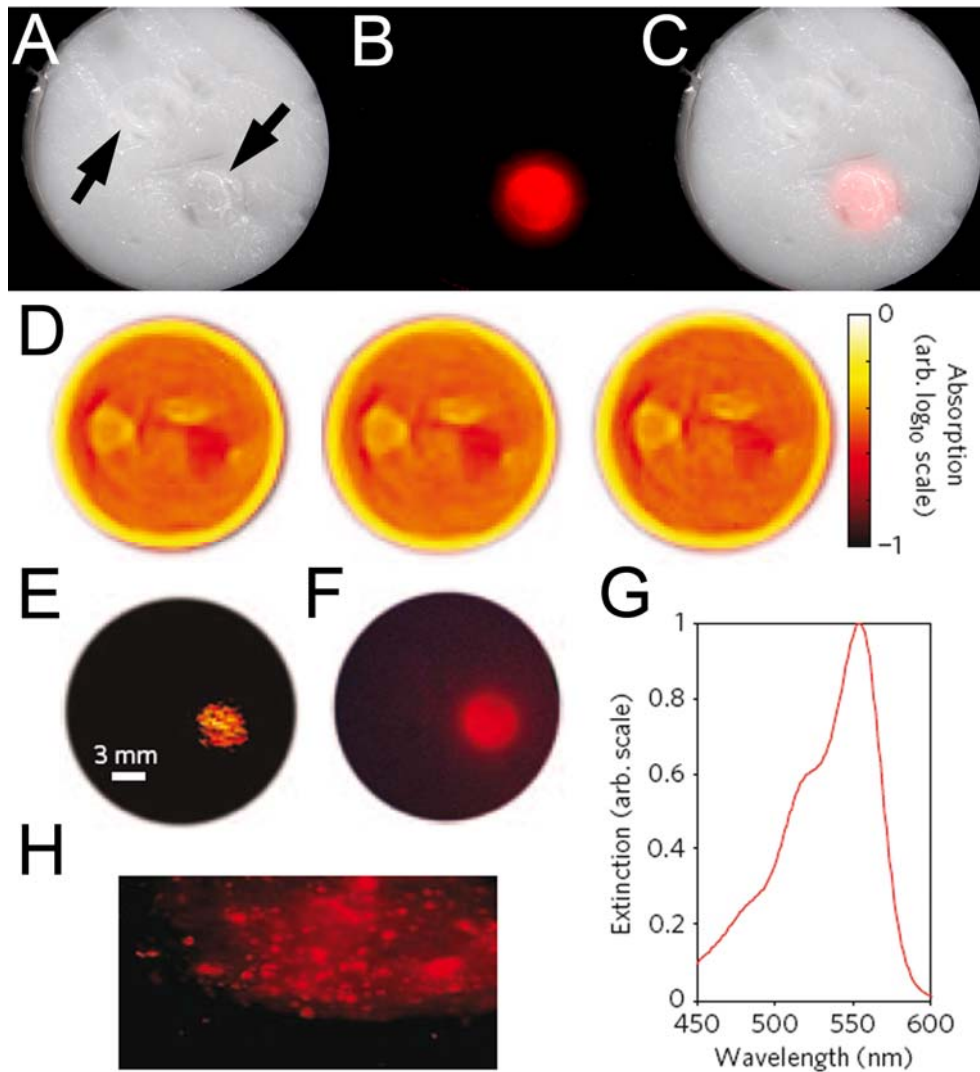


Fig. 35: MSOT imaging of DsRed expressing HeLa-cells

A) Brightfield image of the agarose phantom (1.9cm in diameter) containing Intralipid and India ink to mimic scattering and absorption characteristics of animal tissue (optical absorption coefficient: 0.3cm^{-1} ; scattering: 10cm^{-1}). The phantom contains two insertions (diameter: 4mm). A highly scattering control insertion (left arrow) and an insertion with $4 \times 10^6 \text{ mL}^{-1}$ stable transgenic HeLa cells expressing mitochondrial targeted DsRedT4 (right arrow). B) Fluorescence image of the phantom. The insertion with HeLa cells expressing mito-DsRedT4 is visible using the filter sets for Texas Red. C) Overlay of A) and B). Images in A-C were recorded using a Leica MZ16FA fluorescence stereomicroscope. D) Single wavelength opto-acoustic images of the phantom at three different wavelengths (550nm, 560nm and 570nm from left to right). E) Spectrally resolved MSOT image of DsRed expressing cells (red) in the phantom. F) Fluorescence stereomicroscope image of the dissected phantom at approximately the same imaging plane as for MSOT imaging. G) Extinction spectrum of DsRedT4. H) Magnified fluorescence stereomicroscopic image of a section of the phantom at the boundary of the area containing DsRed expressing cells.

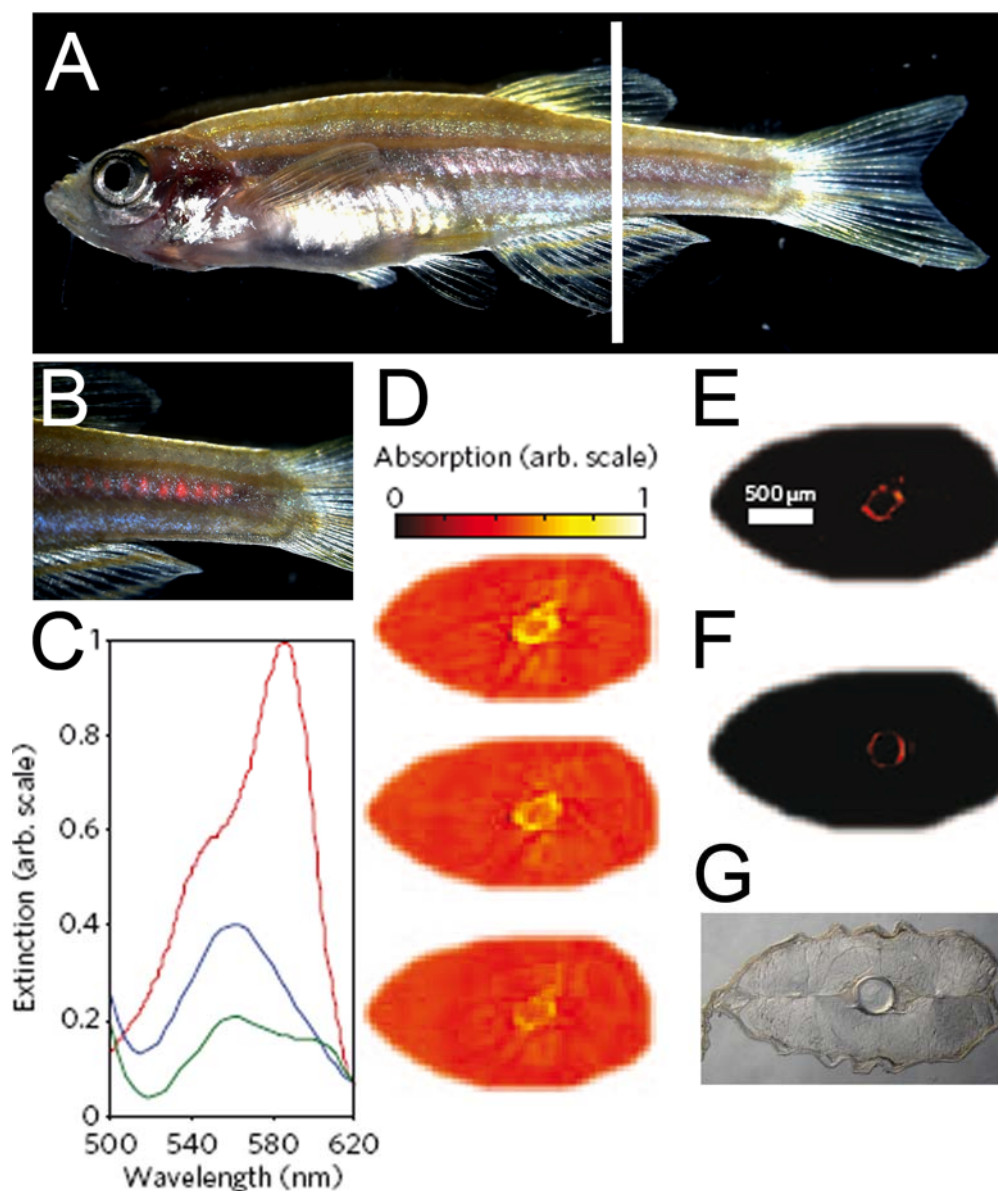


Fig. 36: MSOT imaging of mCherry distribution in the vertebral column of adult transgenic zebrafish

A) Brightfield image of TK1xC transgenic zebrafish. Location of MSOT imaging plane is indicated by white line. B) Overlay of fluorescence and brightfield image showing the expression of mCherry in the vertebral column. C) Extinction spectra of mCherry (red) and the intrinsic background (vertebral column: blue; muscles: green) D) Opto-acoustic images acquired at 587nm, 597nm and 607nm (from top to bottom). E) Spectrally resolved MSOT image of mCherry distribution in the intact animal. F) Fluorescence stereomicroscopic image of the histological section (shown in G) at approximately the same imaging plane as the opto-acoustic image. The vertebral column is expressing mCherry (red).

Having proven the method's capability to resolve fluorescent proteins in adult zebrafish, we next established *in vivo* opto-acoustic imaging parameters, as many biological applications, such as following tumor growth or metastases, ideally require continuous image acquisition.

We partially embedded an adult fish from the enhancer trap with expression of mCherry in the CNS (6months old) in model clay, so that the gills and the head were exposed to the anaesthetic solution in the imaging tank. Images of different planes in the hindbrain area were

recorded with a z-spacing of 0.5mm (Fig.37A). Multispectral reconstructions accurately resolved mCherry expression in the hindbrain, likely in the crista cerebellaris (Fig.36A) as revealed by comparison with histological sections (Fig.37B). The fish fully recovered after image acquisition.

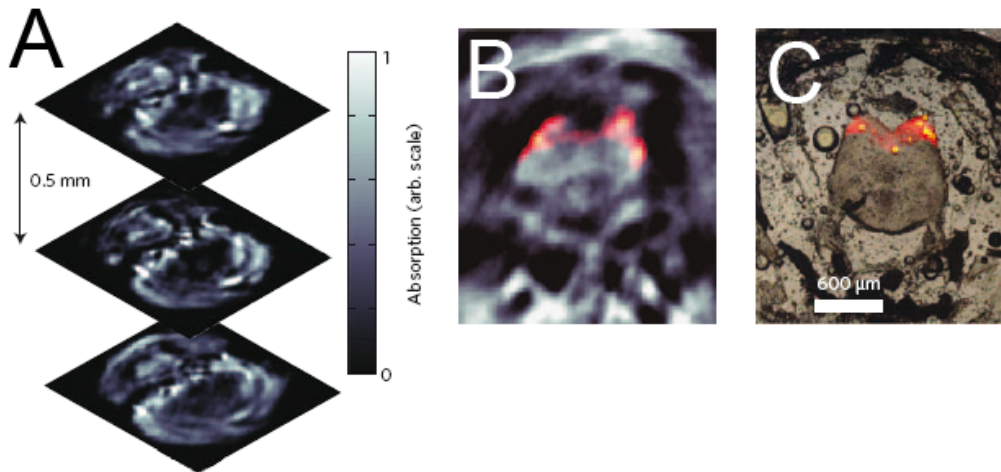


Fig. 37: Three-dimensional MSOT imaging of adult transgenic zebrafish *in vivo*

A) Transverse opto-acoustic images through the hindbrain area (from anterior to posterior) near the crista cerebellaris of a living transgenic adult zebrafish taken at 585nm. B) Spectrally resolved MSOT image of the hindbrain showing mCherry expression in red. C) Overlay of brightfield and fluorescent stereomicroscopic images of the corresponding histological section of the dissected zebrafish after MSOT imaging. mCherry expressing domains are shown in red.

Conclusion

MSOT displays a new generation of biological imaging offering to detect reporter molecules deep within the tissue of mature organisms. Here we could show that MSOT is capable of visualizing fluorescent reporter proteins at a depth of approximately 1.25mm in adult zebrafish with an in-plane spatial resolution of approximately 40μm. Phantom measurements showed that MSOT offers an imaging platform that is not limited by light diffusion and can achieve a penetration from several millimetres up to centimetres with spatial resolution ranging from 20μm-100μm.

Existing optical microscopy methods have higher spatial resolutions, but are not capable of penetrating highly scattering tissue like mouse or adult zebrafish beyond a depth of about 500μm. Furthermore, *in vivo* imaging parameters could be established, promising that processes like growth of a fluorescently labelled tumor or regeneration of a labelled organ could be followed over time using MSOT.

3.6. In vivo cell biology of tegmental hindbrain nuclei

During development of the CNS, neuronal precursors within a neuroepithelium perform interkinetic nuclear movements (INM) during their proliferative phase. Following cell cycle exit, a cell will often lose its connection to the apical surface, migrate, generate an axon and differentiate to become part of a functional neuronal circuit. The orchestration of all these events, whether inherent properties of the cell or directed by external cues, occurs at a subcellular level.

The cell architecture, which must change rapidly during cell migration and differentiation events, is mainly determined by the actin and the microtubule cytoskeletons. Also important is that neuronal precursors have a polarized structure, such as for example the distinct basal and apical processes extended by a neuroepithelial cell. The centrosome, also known as the microtubule organizing center (MTOC), is considered to be a key determinant for, and marker of cell polarity. The position of the centrosome is precisely regulated, leading to efficient neuronal migration and directed neurite outgrowth (Higginbotham and Gleeson, 2007).

To fully understand the development of the CNS it is thus necessary to study neuronal precursors on a subcellular level, ideally *in vivo*.

Time-lapse experiments on cerebellar granule cells co-cultured with glia cells have shown that neuronal migration occurs as a stepwise process termed nucleokinesis (see 1.3.2.2) (Solecki et al., 2004; Tsai and Gleeson, 2005). However, if this holds true for different cell types in the *in vivo* situation still needs to be addressed.

In addition, *in vitro* data from explanted hippocampal neurons suggested that the centrosome induces axon outgrowth and determines its formation from the nearest neurite (de Anda et al., 2005). However, controversial data for the influence of the positioning of the centrosome being essential for proper axonogenesis have accumulated (see 1.3.3.1), and these argue for differences between the *in vitro* and *in vivo* situation of neuronal differentiation or for different cell type specific mechanisms of axonogenesis. Therefore further *in vivo* data on the relationship between centrosome dynamics and the emerging axon is needed and requires cell type specific multiple organelle labelling techniques.

Zebrafish embryos are well suited for *in vivo* investigations and intravital microscopy techniques for zebrafish have already been established (Distel and Koester, 2007; Köster and Fraser, 2001a). Furthermore, transgenic Gal4 zebrafish strains allow for tissue specific expression of any transgenes (see 3.2). Together with advances in confocal microscopy and

the generation of multispectral fluorescent proteins, *in vivo* subcellular imaging in zebrafish should be feasible (also see Appendix 9).

Thus, in this part of my PhD project I developed a Gal4 based technique to investigate the position of the centrosome during migration and axonogenesis in tegmental hindbrain nuclei precursors in living zebrafish embryos by four dimensional fluorescence confocal microscopy.

3.6.1. Subcellular intravital labelling in zebrafish cells using fluorescent fusion proteins

To fluorescently label subcellular structures in zebrafish I first tested available fusion proteins generated from cDNA from different species for labelling the microtubule cytoskeleton in zebrafish Pac2 fibroblasts.

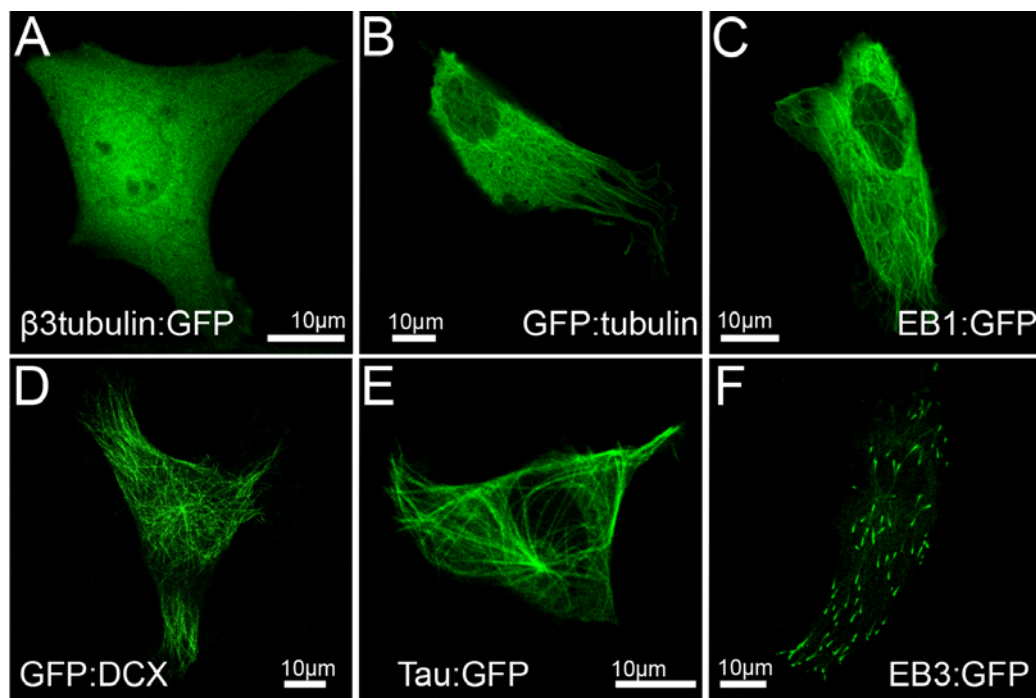


Fig. 38: Identification of microtubule markers for *in vivo* imaging of zebrafish cells

Zebrafish Pac2 fibroblasts transfected with A) β -3 Tubulin:GFP, B) GFP:Tubulin, C) EB1:GFP, D) GFP:DCX, E) Tau:GFP and F) EB3:GFP. All images were recorded approximately 24h after transfection using a 63x oil objective and a Zeiss LSM 510 confocal microscope.

Whereas some of the fusion proteins localized to the cytoplasm (mouse β 3Tubulin:GFP Fig.38A), or were very dose-sensitive (GFP:Tubulin (mouse, Fig.38B) and EB1:GFP (mouse, Fig.38C)) expression of GFP:DCX (mouse, Fig.38D) and Tau-GFP (mouse, Fig.38E) resulted in robust microtubule labelling, while EB3:GFP (mouse, Fig.38F) successfully marked microtubule plus ends. These data indicate that subcellular labelling constructs cannot be easily transferred from one species to another but require careful testing.

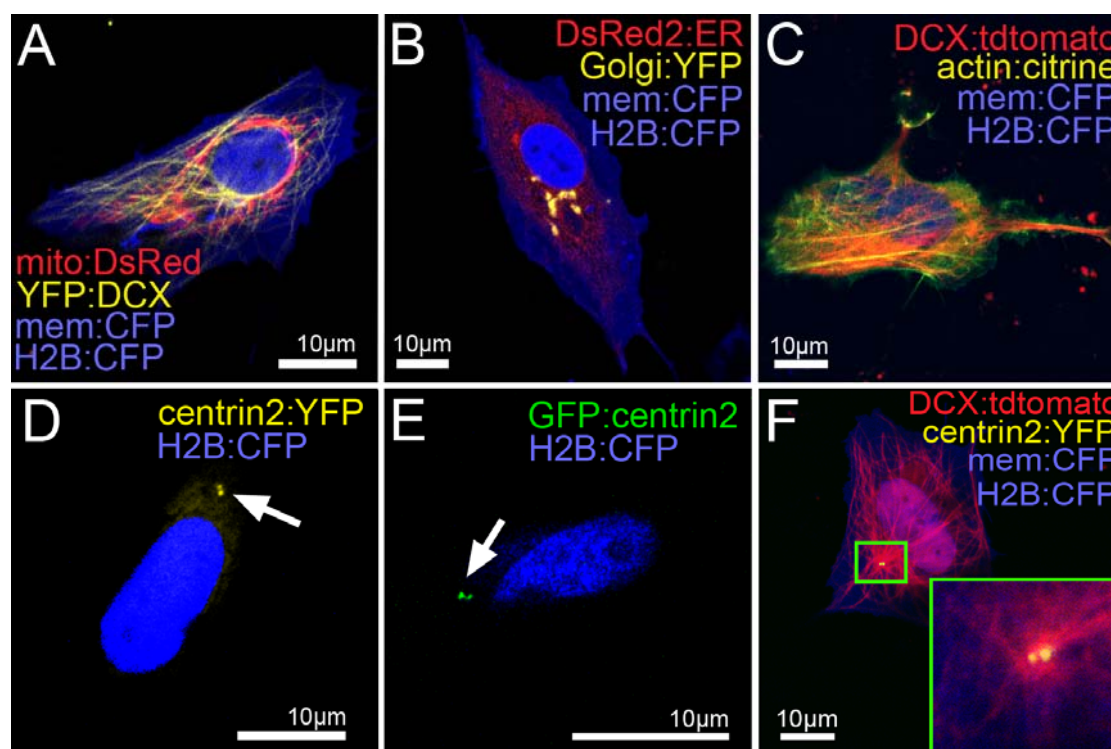


Fig. 39: Identification of subcellular markers for *in vivo* imaging of zebrafish cells

Zebrafish Pac2 fibroblasts co-transfected with A) mito:DsRed to label mitochondria in red, YFP:DCX to label microtubules in yellow, mem:CFP to label the cytoplasmic membrane in blue and H2B:CFP to label the nucleus in blue, B) DsRed2:ER to label the endoplasmatic reticulum in red, Golgi:YFP to label the Golgi Apparatus in yellow, mem:CFP and H2B:CFP, C) DCX:tdTomato to label microtubules in red, actin:citrine to label the actin cytoskeleton in yellow, mem:CFP, H2B:CFP, D) Centrin2:YFP to label the centrosome in yellow (arrow is indicating the two centrioles of the centrosome) and H2B:CFP, E) GFP:Centrin2 to label the centrosome in green (arrow is indicating the two centrioles of the centrosome) and F) DCX:tdTomato, Centrin2:YFP, mem:CFP and H2B:CFP. The inset shows the centrosome at the hub of the microtubule network at higher magnification. All images were recorded approximately 24h after transfection using a 63x oil objective and a Zeiss LSM 510 confocal microscope.

In a similar approach I generated fusion proteins, which successfully label the nucleus, the cytoplasmic membrane, mitochondria (Fig.39A), the endoplasmic reticulum, the Golgi Apparatus (ER, Golgi; Fig.39B), the actin cytoskeleton (Fig.39C) and the centrioles of the centrosome (Fig.39D-F). To eventually allow for multiple combinations in co-expression experiments, I generated a number of fusion proteins with spectrally different fluorescent proteins for most of these subcellular markers.

3.6.2. Simultaneous multicolour labelling

To mediate the simultaneous expression of two subcellular-localized fluorescent proteins by Gal4 transcriptional activators I generated bidirectional Gal4-dependent effector constructs. These so called Janus vectors carry UAS sites flanked on both sides by E1b minimal promoters (Fig. 40A). Recently, we showed in a similar approach that pathogenic

transgenes could be co-expressed with fluorescent reporters to generate a Tauopathy disease model in zebrafish accessible for bio-imaging analysis (Paquet et al., 2009) (**Appendix 5**).

Analysed Janus vectors (J1 and J2) reliably co-expressed the respective two fluorescent proteins *in vitro* and *in vivo* (co-expression ranging from 97-99%) indicating that UAS-bound KalTA4 is able to activate gene expression upstream and downstream, even when only a single UAS-site is used (vector J5).

Western blot analysis (n=3) of a 5xUAS Janus construct revealed a preference for the downstream position of the UAS sites as slightly higher amounts of protein could be detected from this position. This information is valuable in cases when the dose of expressed transgenes is of importance.

As KalTA4 is a freely diffusible activator molecule and can bind simultaneously to several independent UAS-sites (Köster and Fraser, 2001b), I next established so-called Medusa vectors containing additional UAS-sites or Janus-units for triple or quadruple transgene expression (Fig.40B). This for example allows the nucleus, the cytoplasmic membrane and the centrosome to be labelled simultaneously from a single Medusa UAS expression construct (Fig.40B-M1). In addition, Medusa vectors labelling microtubules (M2) or microtubule plus-ends (M3) together with the nucleus and the cell membrane were successfully expressed in zebrafish embryos and allow one to observe microtubule dynamics during cell divisions in great detail in living zebrafish embryos (see **Movie 10** and **Movie 11**).

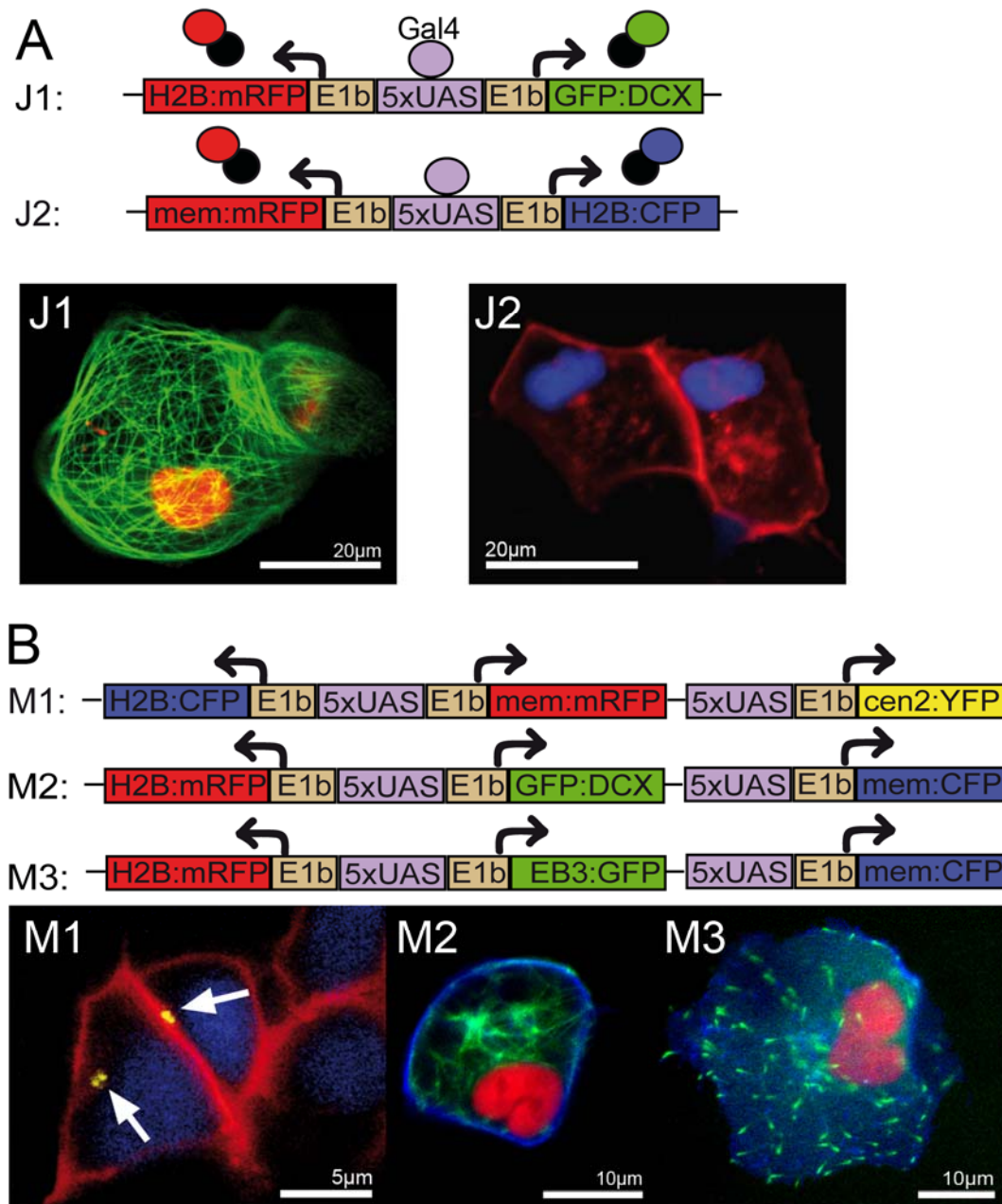


Fig. 40: Janus and Medusa Gal4 effector constructs for simultaneous expression of multiple subcellular labels

A) Schematic representation of bidirectional Janus vectors J1 and J2. Upon binding of Gal4 two subcellular markers (J1: H2B:mFRP labelling the nucleus in red and GFP:DCX labelling the microtubules in green. J2: mem:RFP labelling the nucleus in red and H2B:CFP labelling the nucleus in blue) are expressed simultaneously.

B) Schematic representation of Medusa vectors M1, M2 and M3. Upon binding of Gal4 H2B:CFP to label the nucleus in blue, mem:RFP to label the membrane in red and Centrin2:YFP to label the centrioles of the centrosome in yellow are being co-expressed from the M1 Medusa construct. From M2, H2B:mFRP to label the nucleus in red and GFP:DCX to label microtubules in green and memCFP to label the membrane in blue. M3 also codes for the same nuclear and membrane markers as M2 but contains EB3:GFP to label the plus ends of microtubules.

Images were obtained from living zebrafish embryos co-injected with the respective Janus or Medusa vectors and a vector coding for Gal4. Images were recorded using a Zeiss LSM 510 confocal microscope and 40x water (J1, J2, M1) or 63x oil objective (M2, M3).

3.6.3. Generation of a rhombic lip specific KalTA4 activator strain

The behaviour of neuronal precursors derived from the *atonalla* expressing zebrafish upper rhombic lip, which give rise tegmental hindbrain nuclei (THN) has recently been addressed in detail on a cellular level (Rieger et al., 2008) (Volkman et al. submitted). These cells are accessible for *in vivo* studies, and *in vivo* time-lapse movies suggested a two-phase migration of THN precursors (Köster and Fraser, 2001a). Cells first migrated anteriorly towards the MHB and then turn ventrally in a second migratory period. Having reached the MHB THN precursors were furthermore found to establish a presumptive axon. Thus, these cells are well suited to study the role of the centrosome in migration and axonogenesis *in vivo*. To express subcellular markers specifically in cells derived from the rhombic lip interspecies sequence alignments were performed to identify zebrafish *atonalla* regulatory elements. The analysis revealed a conserved 3kb fragment upstream and 6kb fragment downstream of the *atonalla* open reading frame. A KalTA4 expression cassette (Distel et al., 2009b) was cloned between these fragments and transgenic fish were generated using I-SceI-meganuclease mRNA co-injection (Babaryka et al., 2009) (generated by K.Volkman). *Atonalla:KalTA4* transgenic carriers showed the expected GFP-expression throughout the rhombic lip when crossed to a 4xUAS:GFP effector strain (Fig.41).

Furthermore, confocal time-lapse recording of mRFP expressing THN precursors in embryos from crosses of *atoh1a:KalTA4* x TG5xR (Distel et al., 2009b) strains revealed a behavior characteristic for URL derivatives. THN precursors were found to undergo INM (Fig.42B) and divided exclusively at the apical side (Fig.42C). Starting at about 24hpf these cells moved radially to the MHB while staying connected to the URL by a trailing process (Fig. 42D). Subsequently, these cells retracted their trailing process from the URL and migrated ventrally in a tangential manner along the MHB (Fig. 42E). Intriguingly, as has been described before (Köster and Fraser, 2001a) these THN neurons began to project axons along the MHB and into the midbrain already during ventral migration (Fig. 42F, **Movie 2**).

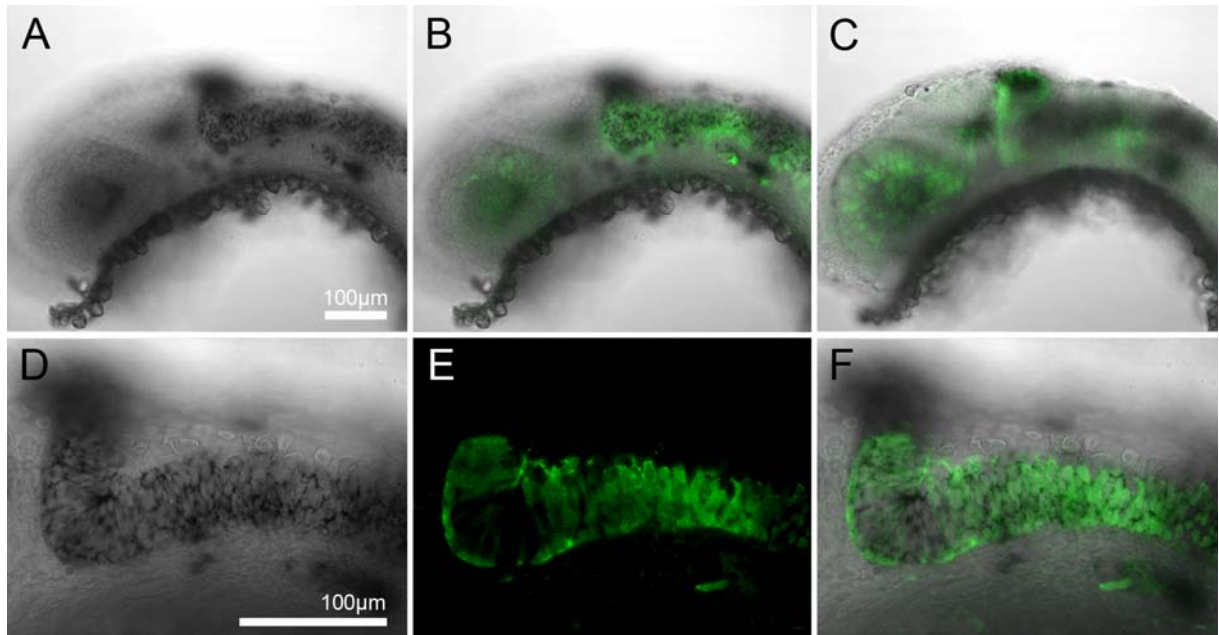


Fig. 41: Characterization of *atoh1a*:KalTA4Gi transgenic zebrafish

Lateral view on offspring of *atoh1a*:KalTA4GI x 4xUASKGFPPI transgenic fish at 24hpf.

A) Endogenous *atonalla* expression in the rhombic lip as revealed by in situ hybridisation.

B) Immunostaining for GFP and in situ hybridisation for *atonalla* on *atoh1a*:KalTA4GI/ 4xUASKGFPPI double transgenic fish show expression of GFP (green) in the rhombic lip in *atonalla* expressing cells. C) In addition some GFP expressing cells can be found in the retina, the tegmentum and the tectum of *atoh1a*:KalTA4/UAS:GFP double transgenic fish. D) Enlargement of boxed area in A) In situ hybridisation for *atonalla* in the hindbrain. E) Immunostaining for GFP. F) Overlay of D) and E).

Images were recorded using a 20x (A-C) and a 40x (D-F) objective on a Zeiss LSM510 confocal microscope.

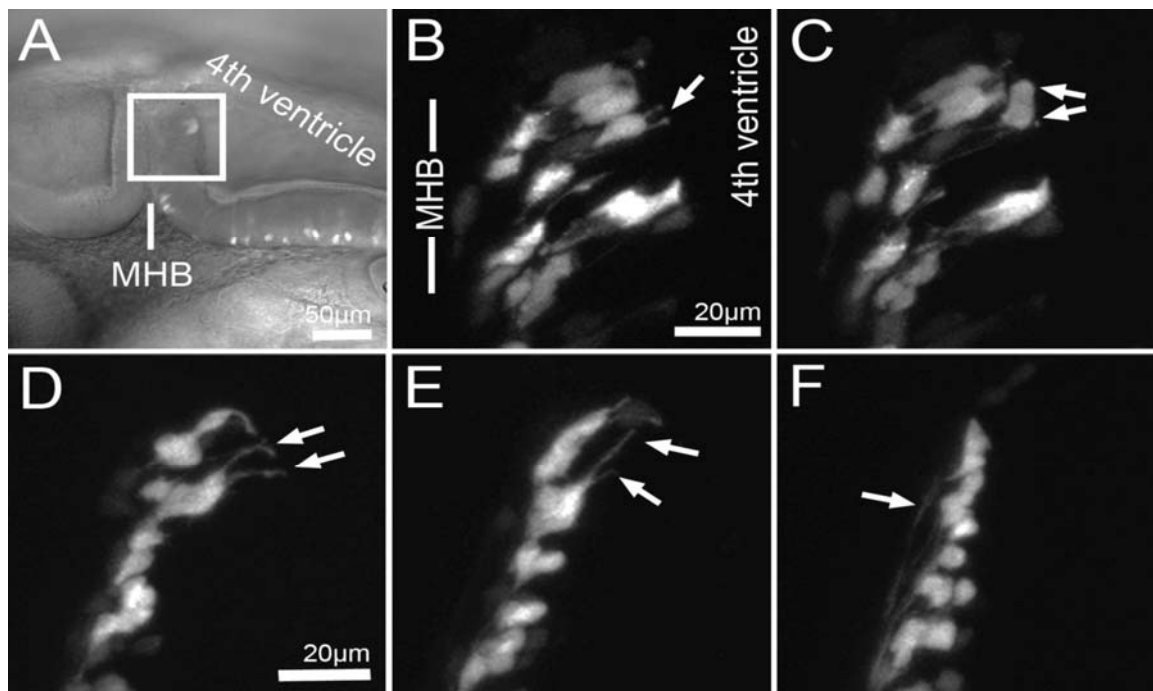


Fig. 42: Time-lapse analysis of THN precursor behaviour

A) Lateral view on the MHB region of an *atoh1a*:KalTA4 x TG5xR embryo at 24hpf. URL-derived THN precursors are labelled by mRFP expression. The boxed area is enlarged in B-F. B) mRFP expressing THN precursors are connected to the apical surface by thin processes (arrow) and undergo interkinetic nuclear movements. C) THN precursors divide at the apical side (arrows indicate dividing cell). D) During radial

migration these cells maintain apical processes (arrows), which are retracted (E) once nuclei reach the MHB. F) Around the same time axon-like processes become visible (arrow). Images are a maximum projection of a z-stack taken with 20x objective using a Zeiss LSM 510 confocal microscope.

3.6.4. Subcellular analysis of THN neuronal progenitor behaviour

For analysis of the subcellular organization of tegmental hindbrain nuclei precursors by fluorescence confocal time-lapse imaging, a Medusa vector (M1) was used to label the nucleus, the cell membrane and the centrosome (Fig.40B-M1).

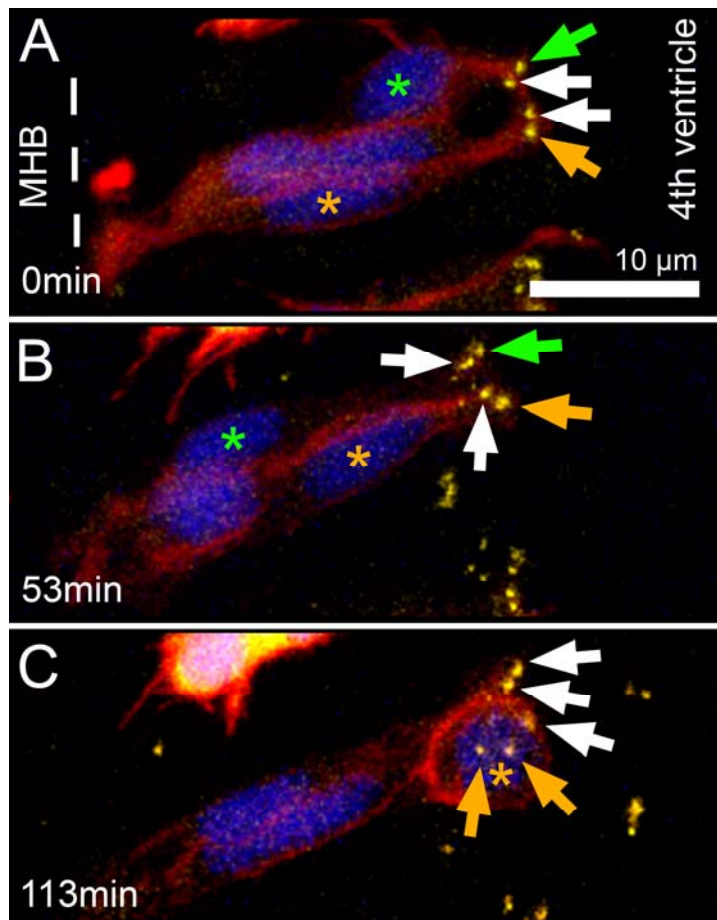


Fig. 43: *In vivo* subcellular imaging of INM and mitotic cleavages of THN precursors

Lateral views of a portion of the cerebellar anlage of an *atonal1a:KalTA4* transgenic zebrafish embryo injected with Medusa vector M1 at approximately 24hpf. Centrosomes are shown in yellow, cell nuclei in blue and cell membranes in red. A) Centrosomes (arrows) were found to line the 4th ventricle at the apical side of the four THN precursors undergoing INM between the mid-hindbrain boundary (MHB) and the 4th ventricle. Throughout INM centrosomes did not change their positions. Green asterisk demarcates a nucleus moving from apical to basal (A,B), while the corresponding centrosome (green arrow) stays at the apical side. The orange asterisk demarcates a nucleus, which moves from basal to apical (A-C) to undergo a mitotic cleavage at the apical side (C). The corresponding centrosome (orange arrow) stays at the apical side, replicating to build the two spindle poles of the spindle apparatus (orange arrows in C).

Images are a maximum projection of a z-stack recorded with a 40x water objective using a Zeiss LSM 510. The time between the images in B or C and A is indicated at the left bottom of each panel.

Atoh1a:KalTA4 embryos injected at the one cell stage with M1 showed expression of the subcellular markers in THN neuron progenitors from 24hpf onwards. Starting at this stage time-lapse recordings were performed over several hours in order to analyse the relation of the dynamics and the position of the centrosome and the nucleus during THN neuron development. THN progenitors were observed to span the entire cerebellar primordium being, connected by processes to the apically positioned URL and the basally located MHB. THN precursors underwent interkinetic nuclear movements (INM) and mainly divided at or close to the apical side along the ventricle (Fig. 43C, orange asterisk, n=31, 8 embryos). In addition, this apical position of proliferation was confirmed by immunostainings against the M-phase marker phosphohistone 3. During INM phases the centrosomes neither preceded nor followed the movement of the nuclei, but remained stationary and always localized at the apical membrane (green asterisk demarcates a nucleus moving from apical to basal while the corresponding centrosome (green arrow) stays at the apical side; orange arrow indicates a nucleus, which is moving from basal to apical to undergo a mitotic cleavage, while the centrosome (orange arrow(s)) replicates at the apical side in Fig. 43A-C, **Movie 3**). This has also been reported previously for mitotically active neuronal progenitors in polarized dividing neuroepithelia (Chenn et al., 1998; Hinds and Ruffett, 1971) (Xie et al., 2007).

After several mitotic events, nuclei were found to translocate towards the MHB, corresponding to the first phase of migration described in (Köster and Fraser, 2001a), leaving behind a long trailing process that remains connected to the apical side. The centrosome was still found at the ventricle (Fig.44A,B). However, within approximately 1.5h of the initiation of the ventrally directed second phase of migration, the neuronal progenitor retracted the trailing process with the centrosome still located at its most apical part (Fig.44C-I, **Movie 4** and **Movie 5**) (n=27, 7 embryos).

THN precursors were often found to initiate ventral migration before the centrosome reached the soma (Fig.44, compare C and F, **Movie 5**) (n=9, 6 embryos). In subsequent ventral migration steps, the centrosome translocated in front of the nucleus. This centrosomal movement was followed by a saltatory movement of the nucleus, so that the nucleus rapidly overtook the centrosome, which then was positioned behind the nucleus (n=16, 6 embryos). The centrosome was then translocated in front of the nucleus again followed by a second saltatory nuclear movement (Fig.45, **Movie 6** and **Movie 7**). Although THN neurons showed

saltatory nuclear movements during ventral migration, this migration mode differs from classic nucleokineses as the centrosome was not positioned in front of the nucleus all the time.

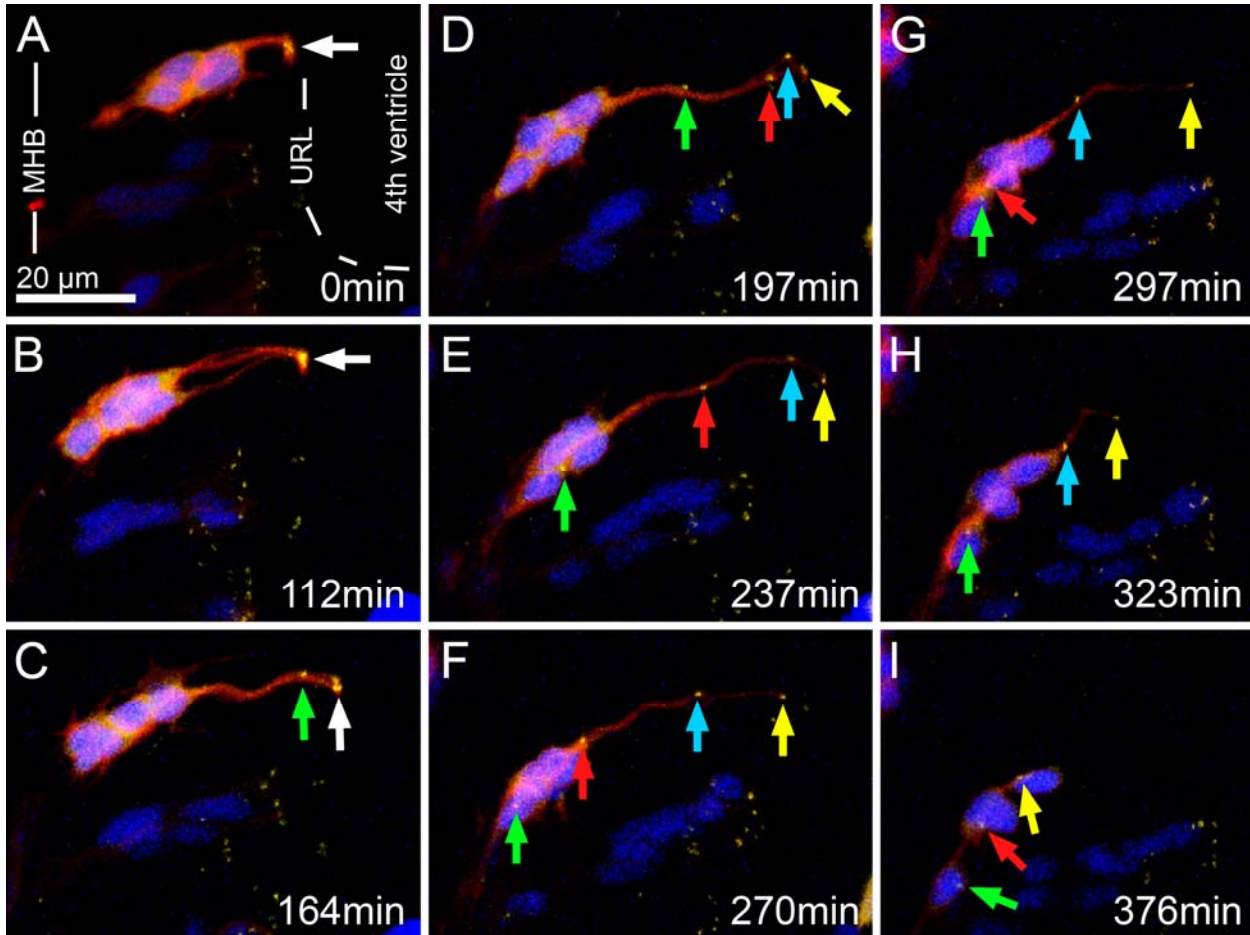


Fig. 44: *In vivo* subcellular imaging of centrosome retraction of THN precursors

Lateral view on a portion of the cerebellar anlage of an 36 hpf *atnall1a:KalTA4* transgenic zebrafish embryo previously injected with Medusa vector M1. Centrosomes (green arrow first centrosome, red arrow second, turquoise third and yellow fourth centrosome; white arrows are shown when centrosomes are indistinguishable) are shown in yellow, cell nuclei in blue and cell membranes in red. A) Centrosomes (arrow) of the four THN precursors were found to line the 4th ventricle. B) Nuclei translocate basally towards the MHB, leaving a long trailing process containing the centrosome at its most apical part behind. C-I) When nuclei reach the MHB trailing processes containing the centrosomes at the most apical position are retracted.

Images are maximum projections of z-stacks taken with a 40x water objective using a Zeiss LSM 510. The time between the images and image A is indicated in the right bottom of each panel.

Abbreviations: MHB: midbrain-hindbrain boundary; URL: upper rhombic lip

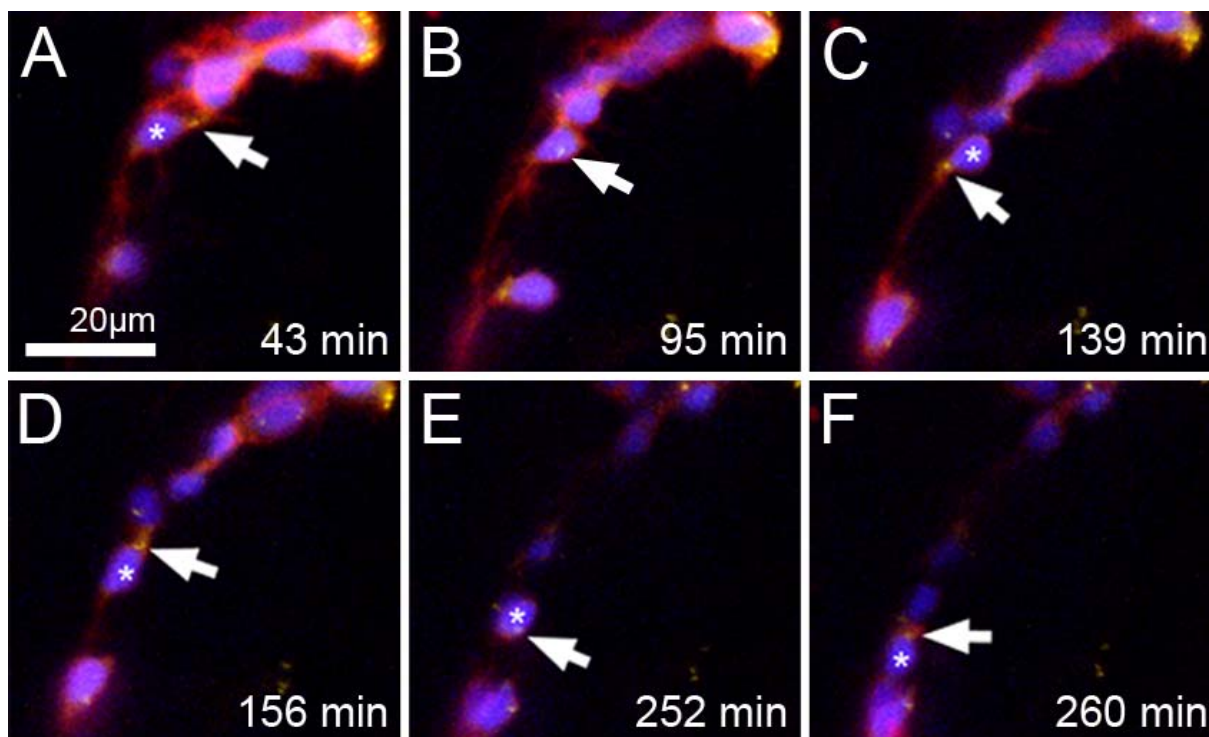


Fig. 45: *In vivo* subcellular imaging of nuclear saltatory movements of THN precursors

Lateral view on a portion of the cerebellar anlage of an approximately 36 hpf *atonalla:KalTA4* transgenic zebrafish embryo injected with Medusa vector M1. A-C) The centrosome (arrow) translocates in front of the nucleus (asterisk). C-D) The nucleus overtakes the centrosome in a rapid saltatory movement in the direction of migration so that the centrosome is located posterior to the nucleus afterwards (D). Later on the centrosome translocates in front of the nucleus again (E). In a second saltatory movement the nucleus overtakes the centrosome again (F).

Images are maximum projections of a z-stack and were taken with a 40x water objective using a Zeiss LSM 510. The time between images taken from **Movie 6** is indicated in the bottom right of each panel.

3.6.5. Axonogenesis in THN neurons is not induced by proximity of the centrosome

THN neurons begin to extend a long cellular process from their leading edge (Fig.46A white asterisk) that was previously identified as the arising axon based on the growth cone-like tip structure and the subsequent projection into midbrain areas (Köster and Fraser, 2001a) (for axon projection into the midbrain see also final image sequence of **Movie 2**). Interestingly though, subcellular Medusa labelling revealed that during the appearance of this axon-like protrusion, THN neurons were still in the process of retracting their trailing processes with the centrosome localized at the most apical position inside the trailing process (Fig.46A, **Movie 8**) (n=9, 8 embryos). This suggested that axonogenesis in THN neurons occurs in parallel or shortly after proliferative INM movements are terminated.

Stabilization of microtubules by acetylation of lysine40 of the α -Tubulin subunit is a key characteristic of the proximal axon region important for axon outgrowth (Hammond et al., 2008) (Conde and Caceres, 2009) (Witte and Bradke, 2008). To verify the axonal identity of the emerging leading process structures of THN neurons at the MHB on the molecular level, I performed immunohistochemistry against acetylated Tubulin. Double transgenic *atoh1a:KalTA4* x *4xKGFP* embryos were raised until 40-42hpf when GFP-expressing THN neurons had reached the MHB (Fig.46B).

Subsequent fluorescent immunohistochemistry against GFP and acetylated α -Tubulin showed that GFP expressing THN neurons at the MHB indeed already possessed acetylated α -Tubulin positive processes (Fig.46C white arrows), which likely emerged from the leading processes found in Medusa-labelled cells. This data indicates that THN neurons initiate axon formation at the beginning of their ventral migration phase.

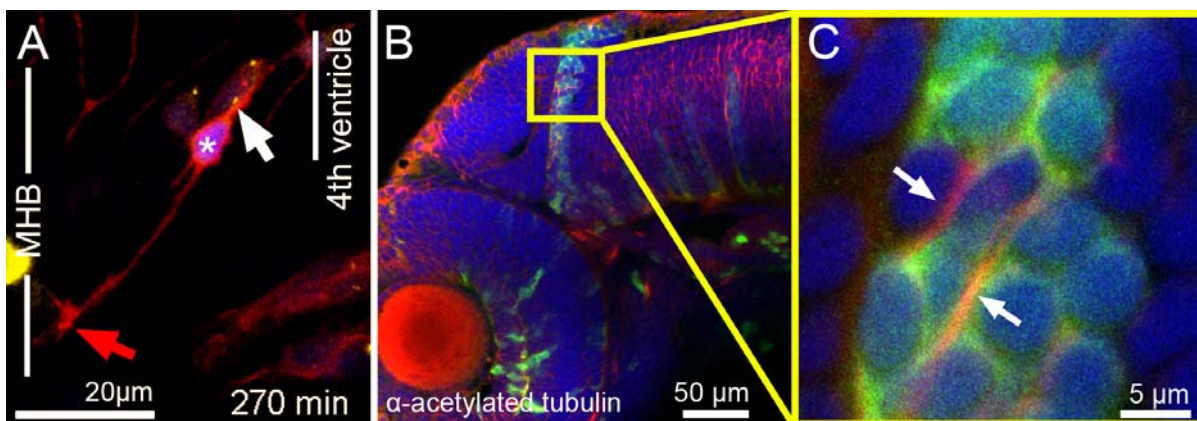


Fig. 46: Centrosome localization does not coincide with axon-like processes in THN precursors

A) Lateral view on the cerebellar anlage of an *atoh1a:KalTA4* transgenic zebrafish embryo injected with Medusa vector M1 at approximately 42hpf. An axon like protrusion (white asterisk) has formed, while the centrosome (white arrow) is still homing towards the soma. B) lateral view on *atoh1a:KalTA4* x *4xGFP* transgenic zebrafish embryo at 42hpf. GFP expressing cells are visualized by anti GFP immunostaining (green) and acetylated microtubules by anti acetylated α -Tubulin immunostaining (red). C) Enlargement of boxed area in (B). Arrows demarcate acetylated microtubules, deriving from GFP expressing THN precursors, indicating the presence of axons at 42hpf.

Images were taken with a 40x water objective using a Zeiss LSM 510.

My subcellular *in vivo* time-lapse studies of centrosome dynamics together with the immunohistochemical analysis of axon formation argued that axonogenesis of zebrafish THN neurons is initiated by a membrane protrusion that is far away from the microtubule organizing centrosome. This observation clearly contradicted *in vitro* findings from

hippocampal neurons showing that axon outgrowth is dependent on the proximity to centrosome and that the centrosome specifies the nearest neurite as the axon (de Anda et al., 2005). To directly resolve the temporal sequence of axonogenesis and centrosome dynamics in THN neurons *in vivo*, I made use of a reporter Kif5C⁵⁶⁰:YFP that accumulates selectively in the nascent axon (Reed et al., 2006) (Jacobson et al., 2006). When this axon reporter (U14) is expressed under UAS-control in *atoh1a:KalTA4* embryos together with a Janus construct (J8) demarcating the nucleus by blue and the centrosome by red fluorescence, the emergence of the THN axons in relation to the position and movement of the centrosome can be visualized in real time.

Time-lapse recordings starting at 36hpf were performed on THN neurons that had reached the MHB but showed a cytoplasmic distribution of Kif5C⁵⁶⁰:YFP (green arrow). Their centrosomes (red arrows) were still positioned in the apical URL (Fig.47A) indicating that these THN neurons had not initiated axonogenesis yet. Strikingly, Kif5C⁵⁶⁰:YFP fluorescence soon accumulated in front of the nucleus and close to the MHB (Fig.47B,C green arrow), while the centrosome remained stationary in the URL far away from the emerging axon (Fig.47B red arrows). Only when axonogenesis was well under way and the outgrowing axon extended ventrally along the MHB, did the centrosome begin to detach from the proliferation zone and moved towards the nucleus (Fig.47D-F, see also **Movie 9**). This temporal sequence of axonogenesis occurring significantly prior to centrosome movements towards the leading edge demonstrates that in THN neurons *in vivo* the proximity to the centrosome is not relevant for axon determination from the leading edge. Interestingly, also reorientation of the THN neuron from a caudo-rostral to a dorso-ventral orientation, which could be revealed by the relative position of the axon with respect to the oval-shaped nucleus, preceded the arrival of the centrosome in the cell soma (Fig.47C-F). This strongly suggests that also repolarization during turning behavior of THN neurons is not mediated by repositioning of the centrosome.

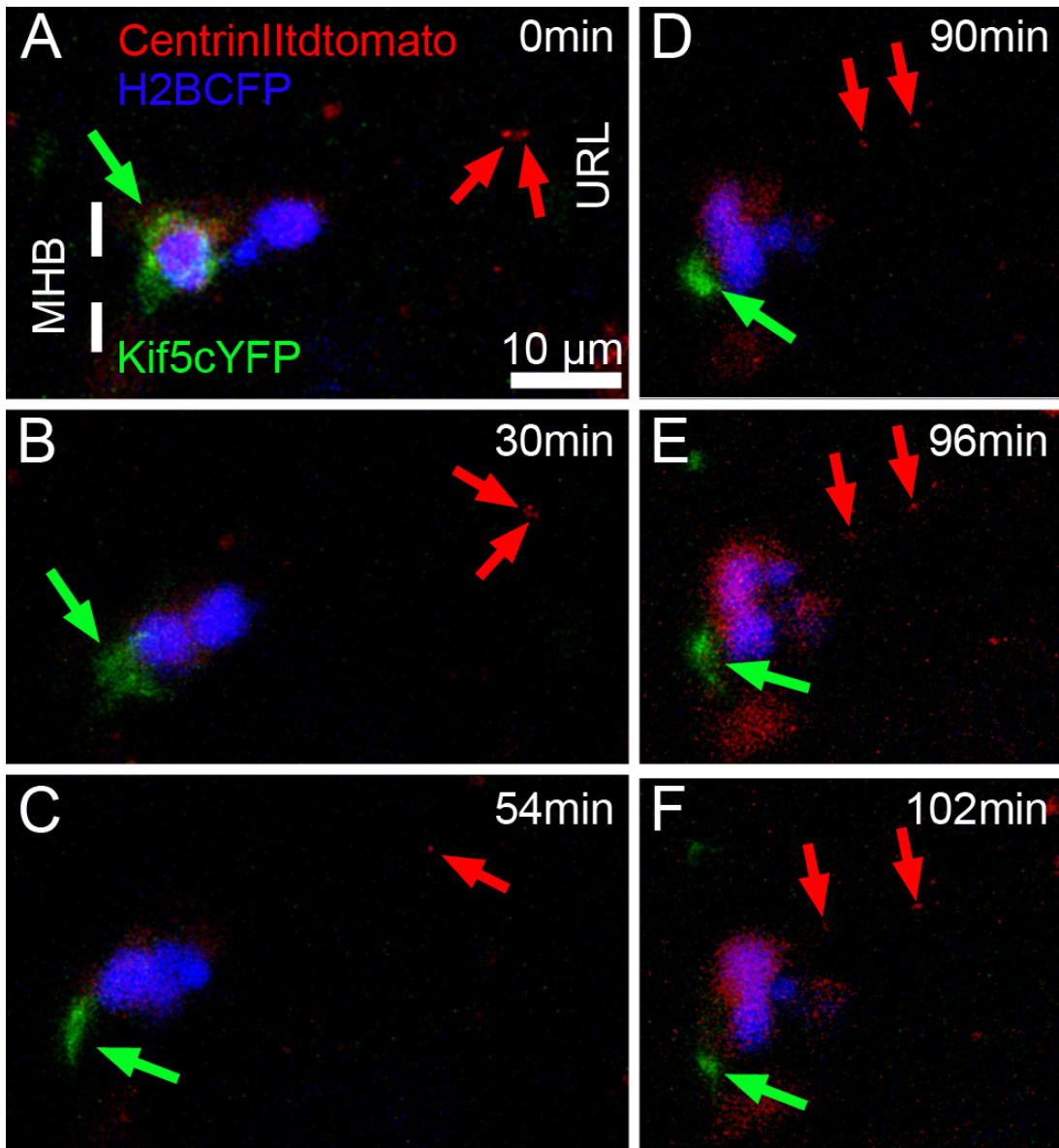


Fig. 47: *In vivo* imaging of axonogenesis

Lateral view on the cerebellar anlage of an *aton11a:KalTA4* transgenic zebrafish embryo co-injected with Janus vector J8 to demarcate the nucleus by blue and the centrosome by red fluorescence (red arrows) and 5xUAS:Kif5c-YFP (U14) to demarcate the emerging axons by yellow fluorescence (here shown in green) at approximately 36hpf. A) Due to co-injection only the more anterior located cell expresses the Kif5cYFP fusion protein labelling the arising axon. Kif5c-YFP is distributed throughout the soma of the cell (green arrow), while the centrosomes of both cells are localized at the apical side (red arrows). B-D) Kif5c-YFP localizes to a protrusion, the later axon, in the front of the cell, while the centrosome is homing towards the soma. E-F) Kif5c-YFP localizes to a growth cone like structure of the emerging axons, while the centrosome has not reached the soma.

Images are a maximum projection of a z-stack taken with a 40x water objective using a Zeiss LSM 510. The time between the images and image A is indicated at the right bottom of each panel.

Abbreviations: MHB: midbrain-hindbrain boundary; URL: upper rhombic lip

Conclusion

My detailed *in vivo* characterization of INM, migration and axonogenesis of THN precursors on a subcellular level resulted in novel findings, which are partially contradictory to common mechanistic models of the respective processes.

1) Anterior migration of THN precursors is likely the final interkinetic nuclear movement

My *in vivo* data suggests that the first phase of MHB directed movement of THN progenitors does not represent true neuronal migration with the centrosome moving ahead of the nucleus. Rather this cell movement displays an extended final interkinetic nuclear movement over long distances with the trailing process and apical centrosome maintaining contact to the 4th ventricle.

2) Ventral migration of THN neurons seems not to be performed via nucleokinesis

During early ventral migration phases the centrosome was found to be positioned in the trailing process. In subsequent ventral migration steps the centrosome translocated in front of the nucleus in direction of migration and the nucleus subsequently overtook the centrosome in a saltatory movement. Although the centrosome seemed to initiate a saltatory nuclear movement, my findings still differ from the classic model of neuronal migration via nucleokinesis, where the centrosome is positioned in front of the nucleus at any time. This suggests that THN neurons might migrate ventrally by a migration mode differing from classic nucleokinesis.

3) The site of axon outgrowth is not determined by the position of the centrosome in THN neurons *in vivo*

My dynamic *in vivo* investigations into the relationship between the relative positions of centrosome and the emerging axon showed that a proximal centrosome does not determine the site of axon outgrowth *in vivo* as previously postulated from *in vitro* data (de Anda et al., 2005). Whether this discrepancy is due to differences in the *in vivo* and *in vitro* situation needs further investigation.

In summary, my established tissue specific subcellular labelling system has proven useful to the study of subcellular processes in the living animal. Using the established Gal4 based subcellular labelling approach for time-lapse recordings of biological processes in living transgenic Gal4 zebrafish embryos promises to merge the fields of developmental genetics and cell biology into a new field of *in vivo* cell biology.

4. Discussion

4.1. Adaptation of the Gal4-UAS System for zebrafish

In the first part of my PhD project I aimed to systematically optimize the Gal4-UAS system for stable transgenic combinatorial genetics in zebrafish.

Previously used Gal4 components Gal4VP16 and 14xUAS had shown deleterious effects on the viability of zebrafish embryos, likely caused by promiscuous interaction of Gal4VP16 with transcription factors leading to “squenching” (Gill and Ptashne, 1988) or high deleterious levels of GFP. By replacing the VP16 transactivation domain by the VP16 derived minimal core activation domain TA4 (Baron et al., 1997) many transcription factor interaction sites were deleted and hereby potential “squenching” was decreased. This Gal4 activator (GalTA4) was further optimized for efficient translation in zebrafish by adapting the codon usage, adding a Kozak sequence and adding a globin intron. By this means a potent and well tolerated Gal4 activator variant (KalTA4GI) could be generated for use in zebrafish.

As the established KalTA4-UAS vectors were adapted for a vertebrate model organism, they promise to be applicable for other vertebrate model organisms, where Gal4-genetics have not yet received much attention (Ray et al., 2002).

One of the most exciting aspects of the Gal4 UAS system is the ability to quantitatively control gene expression by varying the number of UAS repeats. There is now a guideline on how to do this based on my quantification of the activity of one up to five UAS repeats by luciferase assays in zebrafish cells, which showed that expression levels can be varied from minute (1xUAS) to intense (5xUAS) overexpression concentrations. This finding offers the chance to adjust transgene expression to physiological levels and to avoid highly deleterious transgene levels as seen with 14xUAS-GFP. On the other hand, sufficient overexpression for example of dominant-negative protein variants to quantitatively titrate out the function of endogenous proteins can be achieved. Furthermore using different numbers of UAS sites can be employed to study dose-dependent effects of transgene expression. For example, it should be possible to tailor disease models for either slow or fast progressing phenotype development.

4.1.1. Self-reporting Gal4 enhancer trapping

In an enhancer trap approach, using the zebrafish optimized KalTA4-UAS system I generated a collection of tissue specific self-reporting Gal4 expressing strains. As the strains

report KalTA4 expression by a red fluorescent protein (mCherry) in distinct cell populations, they can be used to characterize the dynamics of the respective tissue. Furthermore, these strains can be readily combined with the many existing GFP expressing transgenic zebrafish strains to study the development of a tissue in relation to another tissue.

Coinciding with my screen, other laboratories performed similar Gal4 enhancer trap screens (Asakawa et al., 2008; Davison et al., 2007; Ogura et al., 2009; Scott et al., 2007). In two of the screens, a *hsp70* basal promoter was used in the trapping construct. This basal promoter showed background expression in skeletal muscle and in the heart (Asakawa et al., 2008; Scott et al., 2007). Such background expression e.g. in the heart might exacerbate the interpretation of functional studies of genes, which also influence the heart development. Of the basal promoters tested so far, only the *thymidine kinase* (TK) promoter of the human herpes simplex virus (Perz-Edwards et al., 2001) and the zebrafish *gata2* promoter (Meng et al., 1997) seem to be sufficiently weak to avoid background expression, while being at the same time responsive to genomic enhancers in the proximity to the insertion site, as Ogura et al. (2009) could show in their promoter analysis (Ogura et al., 2009). These promoters did not bias the performed pilot Gal4 enhancer trap screens towards expression of Gal4 in a distinct tissue (Ogura et al., 2009). In contrast, the *twhh* regulatory element, which showed no background expression beside the intrinsic notochord expression, provided a CNS bias for my Gal4 enhancer trap (70% of strains show expression in the CNS). This useful bias might be attributed to the many binding sites (40% of all predicted sites by MatInspector analysis) for transcription factors, expressed in neural tissue. However, the reason for the observed CNS bias needs further investigation. Future Gal4 enhancer trap screens in zebrafish might benefit from the discovery or engineering of regulatory elements, which provide a tissue specific bias, but show no background expression. A comparison of constructs used for Gal4 enhancer trapping in zebrafish is shown in Fig.48.

The first two Gal4 enhancer trap screens used Gal4VP16 as transcriptional activator (Davison et al., 2007; Scott et al., 2007). 5% of the recovered strains were not viable in the screen of Scott et al. 2007, likely due to deleterious effects of Gal4VP16 (Ogura et al., 2009). To avoid such deleterious effects Gal4 activators with minimal transactivation domains from VP16 or from transcription factors such as NFκB (GalTA3, GalTA2 and GalNFκB) were used in subsequent screens and displayed better tolerance in zebrafish cells (Asakawa et al., 2008; Ogura et al., 2009). However, in contrast to the Gal4 activator (KalTA4GI) used for my screen, none of these activators is optimized for translation in zebrafish to overcome the observed mosaic transactivation of UAS controlled transgenes.

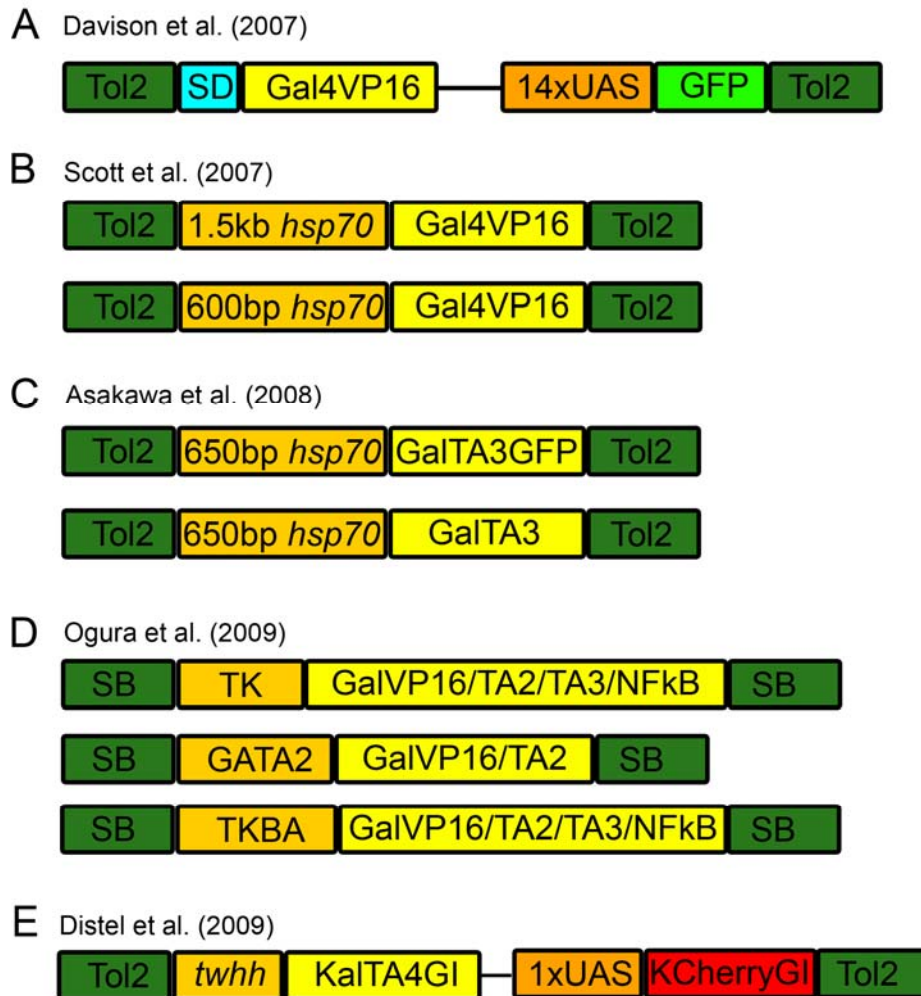


Fig. 48: Constructs used for Gal4 enhancer trap screens in zebrafish

Comparison of constructs A) (Davison et al., 2007), B) (Scott et al., 2007), C) (Asakawa et al., 2008), D) (Ogura et al., 2009) and E) (Distel et al., 2009b) used in Gal4 enhancer trap screens in zebrafish. Abbreviations: SD: splice donor, Tol2: Tol2 transposase recognition sites, SB: Sleeping Beauty transposase recognition sites, *twhh*: tiggy-winkle hedgehog regulatory element, *hsp70*: regulatory element of the 70kD heat shock protein, TK: human *herpes simplex virus thymidine kinase* regulatory element, GATA2: zebrafish *gata2* regulatory element, TKBA: fusion of the human *herpes simplex virus thymidine kinase* and carp β -actin regulatory elements, UAS: upstream activating sequence, GalVP16/TA2/TA3/TA4/NFkB: Gal4 fused to the VP16/TA2/TA3/TA4/NFkB transactivation domains, respectively, KalTA4GI: zebrafish optimized GalTA4, KCherryGI: zebrafish optimized mCherry.

As all of my tissue specific KalTA4 strains tested provided robust transactivation when injected with UAS constructs or when crossed to transgenic UAS effector fish, they represent a valuable resource to elucidate the function of specific genes by overexpression studies.

In addition, KalT4 activator strains could be bred to homozygosity. When these activator fish are crossed with homozygous UAS-effector strains, all of the offspring express the transgene of interest. This makes KalTA4-UAS genetics suitable for high-throughput *in vivo* approaches such as small compound screening in neurodegenerative disease models (Paquet et al., 2009).

In addition, my thorough characterization of KalTA4-mediated transactivation kinetics will allow for better planning of combinatorial genetic experiments.

4.1.2. Prolonging reporter gene expression until adulthood by a Gal4 dependent feedback loop

Relating embryonic structures to adult tissues is a challenge in developmental biology. I took advantage of my optimized Gal4 system to generate the 4xKaloop effector strain, which provides a self maintaining Gal4 activated feedback expression loop to propagate reporter fluorescence until adulthood. When combined with the available Gal4 activator strains, this single effector strain could serve to map the expression activity of many genetic loci to adult tissues.

I have demonstrated this reporting ability of the Kaloop strain for the *krox20/egr2b* locus. *KalTA4* expression controlled by the *egr2b* regulatory element is expressed in rhombomeres 3/5 at early embryonic stages for only a short period of time (approximately 11 hpf – 24 hpf). In adult brains of *egr2b:KalTA4* x 4xKaloop double transgenic fish, two stripes of GFP expressing cells were found, strongly resembling the organization of the *egr2b* expression in the embryonic brain (Oxtoby and Jowett, 1993). This suggests a preservation of segmental hindbrain organization similar to frog or chick brain.

In addition, using histological analysis and retrograde tracing of axons derived from neurons of the posterior GFP-expressing hindbrain stripe, I could show that neurons of the secondary ocatval nucleus are derived from cells of r5, which are expressing *egr2b* during the second day of development. This nucleus is part of the ascending acoustic neuronal network in teleosts, but its developmental origin was previously unclear (McCormick and Hernandez, 1996).

Although initial expression of GFP was observed throughout the r3/5 domains at 26 hpf, GFP-expression in both hindbrain stripes appeared to be mosaic at adult stages. This suggested an inactivation of the KalTA4 feedback loop in some cells derived from *egr2b* expressing progenitors.

The cause of the mosaic inactivation is unclear at the moment. Possibly the amount of KalTA4 produced by the Kaloop cassette is in some cells below what is needed to achieve a steady state level of KalTA4 activator concentration and maintain the feedback loop. Alternatively, epigenetic silencing might inactivate the oligomeric UAS repeats (5'-CGG-N₁₁-CCG- 3') as CpG dinucleotides in vertebrates and tandem repeats are frequent targets of DNA

methylation (Garrick et al., 1998). In fact, transgenic zebrafish derived from a Gal4VP16 gene/enhancer trap screen and expressing GFP under control of 14xUAS (Davison et al., 2007) showed such transcriptional silencing of GFP. Although recovered transgenic strains initially exhibited robust tissue specific GFP expression, variegated expression was observed in subsequent generations. Within two generations GFP expression vanished completely due to inactivation of *gfp* transcription by DNA methylation of the 14xUAS sites (Goll et al., 2009). However, such reporter silencing was not observed in my enhancer trap strains, which might be due to the single UAS site controlling mCherry expression. The Kaloop strain contains four repeats of UAS sites controlling the KalTA4 feedback loop and could thus be subject to methylation in some cells. However, my quantification of the effect of UAS numbers and different activators (KalTA2-4) will help to provide solutions to either of the possible explanations for mosaic inactivation of reporter expression. To achieve the steady state level of Gal4 activator concentration needed for the feedback loop, KalTA4 could be replaced by an activator with higher transcriptional activity like KalTA3 or KalTA2. In order to overcome epigenetic silencing the four repeats of UAS sites used in the Kaloop cassette could be replaced by fewer UAS sites. Stronger activators (KalTA3, KalTA2) could be used to counterbalance reduced expression levels of fewer UAS sites. Alternatively, different variants of UAS sites in different orientations might be used to overcome the organization of the same Gal4 binding sequence in tandem repeats. Bidirectional Janus vectors harbouring a single UAS site are capable of expressing two transgenes, therefore orientation of UAS sites appears not to be critical for initiation of transcription.

To further exploit continuous expression mediated by Gal4 and to allow for spatiotemporal fate mapping of KalTA4-expressing cells, temporal control over fate-mapping activation should be developed as a next step. This might be achieved by combining the Gal4-UAS system with an inducible recombinase based system (either Cre or Flp), similar to the G-TRACE system in *Drosophila* (Evans et al., 2009). Recent progress in establishing inducible Gal4 or recombinase activity in zebrafish (Hans et al., 2009) promises that spatiotemporal fate-mapping could be established in a straight forward manner, which will provide a powerful system for precise genetic control for functional *in vivo* analysis in zebrafish.

4.1.3. Further applications of Gal4 enhancer trap strains

The tissue specific Gal4 strains derived from my screen were capable of transactivating transgenes under UAS control in transient injection experiments as well as in stable transgenic UAS effector strains. Therefore, the established strains will be valuable tools for reverse genetic approaches to elucidate the function of a gene in a distinct tissue or cell type. Gain of function experiments can be performed by Gal4 mediated overexpression of the gene of interest as well as loss of function experiments by Gal4 mediated expression of dominant-negative variants of a gene of interest or by RNAi approaches. In either experiment expression can be adjusted from physiological to strong overexpression levels by using different numbers of repeats of UAS sites.

In addition, the Gal4 strains allow for tissue specific rescue experiments in zebrafish mutants or morphants. As several transgenes can be expressed simultaneously by the Gal4-UAS system, modifiers can be co-expressed together with a gene of interest e.g. a tumor suppressor together with an oncogene to study the effects on cell transformation. By this means protein networks can be directly investigated *in vivo*.

4.1.3.1. Elucidating the function of Lunatic Fringe in hindbrain development

In a collaborative effort with David Wilkinson's lab at UCL the *egr2b:KalTA4* strain was used to elucidate the function of the Notch modifier Lunatic Fringe in hindbrain development. KalT4 mediated overexpression of *lunatic fringe (lfng)* in rhombomeres 3/5 rescued the *lfng* knockdown phenotype. The data obtained from this Gal4 mediated rescue experiment helped to elucidate the role of *lfng* in neurogenesis and supports the hypothesis that *lfng* is required to maintain cells in a progenitor state in the hindbrain. This experiment demonstrated that my Gal4 strains can be applied for tissue specific overexpression or rescue experiments. Thus, they allow one to study the function of a gene in a distinct tissue or cell type *in vivo*. In addition to spatial control over gene expression, which is readily provided by my Gal4 strains, temporal control would be valuable to discriminate between the functions of a gene at different developmental stages. For example, *krox20* is involved in establishing rhombomeres 3/5 of the hindbrain at early stages of development. Later on, it is expressed in Schwann cells, myelinating axons of the lateral line. For the next generation of Gal4 strains such temporal control could be added by e.g using a hormone inducible Gal4 variant optimized for its use in zebrafish or by combination of the Gal4 system with inducible recombinase systems like the inducible CreER(T2) recombinase (Hans et al., 2009).

4.1.3.2. Establishing Gal4 mediated tumor models

In collaboration with Marina Mione we used several of the generated Gal4 enhancer trap strains to model types of hyperplasia in zebrafish. An effector strain harbouring a constitutively active form of the human oncogene *HRAS-G12V* under UAS control was established in the Mione lab. By crossing this effector strain to different KalTA4 enhancer trap strains, tumors could be induced in various tissues. Penetrance, onset of tumorigenesis and progression differed, depending on the respective activator strain. Some of the activator strains like *olf:KalTA4* did not show any effect when *HRAS* was overexpressed suggesting that some tissues are more prone than others to develop *HRAS*-dependent tumors, offering the opportunity to discover co-factors involved in *HRAS*-dependent tumorigenesis.

The expression of *HRAS* in the *zic1/4:KalTA4* activator strain led to tumors by 5 dpf. These tumors were found to be of glial origin. Such early onset tumor models promise to be a valuable model for large-scale screens to identify compounds effective against cancer.

In contrast, expression of *HRAS* in the melanocytic lineage specific *kita:KalTA4* strain led to tumor formation starting at 4 weeks postfertilization. Tumors were found to be invasive infiltrating neighboring tissues. Like in human melanoma a global repression of gene expression was found in tumor cells and is likely caused by epigenetic silencing through histone methylation. We have established a melanoma model strongly resembling human melanoma concerning its molecular, genetic and epigenetic properties. As a next step this model will be used in the Zon lab at Harvard Medical School in a screen to identify compounds effective against melanoma formation.

The system furthermore promises to be suitable for mechanistic studies of tumorigenesis *in vivo*. Modifiers like tumorsuppressors could be co-expressed with *HRAS* using the Gal4-UAS system to study effects on tumorigenesis. With MSOT, a novel imaging technique is available, which allows one to observe any effects on tumorigenesis in the living animal.

4.2. Photoacoustic imaging of fluorescent proteins in adult zebrafish

In order to study processes like tumorigenesis, regeneration or how embryonic structures relate to adult structures using fate-mapping approaches (see 3.3), a means of visualizing fluorescent reporter proteins in the living adult zebrafish would be extremely valuable. Although a zebrafish mutant has been established (White et al., 2008), which stays transparent throughout its life, but requires laborious inbreeding to be maintained and is thus prone to developmental defects, all other commonly used zebrafish strains, including

available Gal4 strains lose their embryonic transparency starting at approximately 14 dpf. Thus, conventional optical imaging techniques cannot be applied for *in vivo* imaging of adult zebrafish. In collaboration with Daniel Razansky at the Institute for Biological and Medical Imaging at the Helmholtz Center Munich we have established multispectral opto-acoustic tomography (MSOT) to visualize fluorescent reporter proteins within the living adult zebrafish. Cells expressing fluorescent proteins like mCherry usually display a steep decline in absorption (see Fig.36C), compared to non-fluorescent tissue. Opto-acoustic imaging of a sample at different wavelengths should thus allow for the detection of the localization of fluorescent proteins. Some of the established Gal4 enhancer trap strains show expression of mCherry in different tissues at adult stages and were used to test the potential of MSOT. Indeed, we could detect mCherry expression in the vertebral column approximately 500 μ m within the intact zebrafish at a resolution of approximately 40 μ m. In addition, mCherry expression could be visualized in the hindbrain of a living transgenic Gal4 fish, which fully recovered after the imaging procedure. No photobleaching occurred in the two applications as the method operates with significantly less power per unit volume than conventional techniques such as confocal microscopy.

Selective plane MSOT offers an imaging platform that is not limited by light diffusion and can achieve a penetration from several millimetres to potentially centimetres with a resolution ranging from 20-100 μ m. In comparison, surface-limited fluorescence microscopy methods achieve higher resolution but offer penetration depths limited to less than 1mm. Although optical tomography can be performed through entire mice with high sensitivity the resolution is only in the range of 1mm. (Ntziachristos et al., 2005; Ntziachristos et al., 2002).

We have shown that MSOT is capable of visualizing fluorescently labelled tissues in the living adult zebrafish. Processes like tumorigenesis, adult neurogenesis in zebrafish (Chapouton et al., 2007) or regeneration (Köster and Fraser, 2006) can therefore now be studied at stages, which had previously been inaccessible for *in vivo* approaches. Clearly, studying tumor progression as it occurs within a living animal will help us to understand the behaviour of cancer cells.

4.3. In vivo cell biology

It is the interplay of cellular components that determines the overall behaviour of a cell. To understand processes like cell migration or axonogenesis, they are therefore best studied on a subcellular level in a living organism. Zebrafish embryos are a model, which

allow for *in vivo* investigation, however a subcellular labelling system, which can be applied to visualize cellular components in a variety of tissues in a cell type specific manner was not previously available.

4.3.1. Gal4 mediated subcellular labelling

I initially verified a number of fusion proteins from different species, which successfully localized to distinct cell components like the nucleus, cytoplasmic membrane, microtubules or centrosome in zebrafish cells. For simultaneous expression, subcellular localized fusion proteins with different fluorescent spectra were cloned into bidirectional Janus cassettes, which are capable of expressing two transgenes upon the binding of Gal4. Janus cassettes could be combined in so called Medusa vectors to express three or even four transgenes simultaneously.

Expression levels are crucial for successfully labelling cellular components. For example, expression levels have to be tightly controlled to label the centrosome. Too low expression of the fusion protein will not label the centrosome enough for visualisation by fast image acquisition, while too high expression levels will lead to saturation of the centrosome and subsequent increasing cytoplasmic background making it hard to identify the centrosome due to a low signal to noise ratio. The Gal4 system allows one to adjust expression levels to the respective needs by either using different numbers of UAS repeats or a different Gal4 activator as described in 3.1. By this means optimal labelling results can be achieved for each targeted cellular component.

4.3.2. Investigating THN precursor behaviour on a subcellular level

By plasmid injection into a newly generated rhombic-lip specific KalTA4 activator strain (*atoh1a:KalTA4*) a Medusa vector was applied to investigate the localization of the centrosome in relation to the nucleus during interkinetic nuclear movements, radial (anterior) and tangential (ventral) migration and axonogenesis of tegmental hindbrain nuclei (THN) precursors.

In agreement with previous studies (Del Bene et al., 2008; Hinds and Ruffett, 1971; Zolessi et al., 2006), the centrosome was found to be localized at the apical side during interkinetic nuclear movements. During anterior migration phases, THN precursors were still connected to the ventricle by a long trailing process. Surprisingly, the centrosome was not observed to

translocate in front of the nucleus to initiate migration as predicted for neuronal migration via nucleokinesis (Tsai and Gleason, 2005). Instead, radial anterior migration began while the centrosome was still located at the ventricular surface. When nuclei reached close to the MHB, trailing processes of the respective THN cells were retracted, carrying the centrosome in their most apical part.

Based on the localization of the centrosome, these observations suggest, that this anterior migration phase might rather represent the final interkinetic nuclear movement, instead of true cell migration.

4.3.3. The centrosome does not precede nuclear movement during ventral migration

Centrosomes were found to travel towards the soma while THN neurons already started to migrate ventrally. During following ventral migration phases the centrosome reached the soma and translocated in front of the nucleus. Afterwards, the nucleus overtook the centrosome in a saltatory manner during each forward movement, so that the centrosome was positioned posterior to the nucleus after nuclear translocation. In contrast, previous time-lapse imaging studies (Bellion et al., 2005; Schaar and McConnell, 2005; Solecki et al., 2004; Tanaka et al., 2004) using several types of migrating neurons (cerebellar granule cells, subventricular zone neurons and neurons of the medial ganglionic eminence in the telencephalon) have demonstrated that the centrosome leads the nucleus and moves forward co-ordinately. This prompted the hypothesis that microtubule-dependent pulling forces on the nucleus converge at the centrosome. Contradicting this hypothesis, my imaging studies revealed nuclear migration past the centrosome, which makes a pulling effect of the centrosome as major driving force of nuclear translocation unlikely.

In support of my observations, Umeshima et al. (2007) suggested from time-lapse studies of migrating granule cells in mouse cerebellar slices that the movement of the nucleus and the centrosome occur independently of each other. The nucleus often migrated ahead of the centrosome during its saltatory movement, similar to my observations. In addition, the perinuclear cage was found not to converge at the centrosome. Both findings negate the supposed role of the centrosome in pulling the nucleus. However, as the centrosome moved ahead of the nucleus prior to each migration step of THN neurons, it is likely that the centrosome plays a role in the initiation of nuclear movement. Still, the question remains what is the underlying force that moves the nucleus forward, if it is not the force generated by centrosomal movement on the centrosome anchored microtubule network. The microtubule

network pulling the nucleus forward might be anchored on the Golgi apparatus instead of the centrosome, which has been reported to have microtubule organizing functions (Efimov et al., 2007). My established subcellular labelling system readily allows for investigating the dynamics of the Golgi apparatus with respect to the nucleus. Alternatively, pushing forces from behind the nucleus generated by the acto-myosin network as observed in migrating MGE cells, cerebellar granule cells, facial neurons and pontine neurons (Bellion et al., 2005; Ma et al., 2004) could also be responsible for the observed saltatory nuclear movement in THN neurons. A way to discriminate between microtubule versus acto-myosin mediated forces in nucleus translocation in THN neurons is to pharmacologically inhibit their respective functions by applying nocodazole (microtubules) respectively blebbistatin (myosinII). As a direct read-out, my subcellular labelling system could be used to observe the dynamics of the nucleus in pharmacologically treated THN neurons.

4.3.4. The centrosome position does not determine the site of axon outgrowth *in vivo*

THN neurons were found to establish axons, while they were migrating ventrally. Previous studies in cultured hippocampal neurons had shown that the position of the centrosome determines the site of axon outgrowth (de Anda et al., 2005).

To investigate, if this holds true for the *in vivo* situation I determined the position of the centrosome in relation to the arising axon *in vivo*, by using the Kif5cYFP fusion protein, which localizes to the emerging axon (Jacobson et al., 2006). Dynamic *in vivo* time-lapse recordings of THN neurons co-expressing fluorescent proteins to label the axon, nucleus and centrosome revealed that axons are emerging from the basal process while the centrosome is still positioned in the trailing process far away from the axon outgrowth site. This suggests, that proximity to the centrosome position does not determine the axon outgrowth site *in vivo*.

This finding is supported by zebrafish *in vivo* studies from Zolessi et al. (2007), who observed that the emerging axon in retinal ganglion cells as well forms from the basal process, while the centrosome is located at the opposite apical side (Zolessi et al., 2006).

The crucial differences between axonogenesis of cultured cells or cells within an intact organism may be explained on the basis of environmental influences. In contrast to RGCs or THN neurons within their natural context, cultured cells generate multiple neurites soon after their final mitosis. In the absence of external cues, neurons *in vitro* such as cultured zebrafish RGCs or mouse hippocampal neurons polarize by using intrinsic mechanisms to break the symmetry. Here, the position of the centrosome determines, which neurite becomes the later

axon. In contrast, in the *in vivo* situation, the polarity of the neuroepithelium seems to be a major determinant of the site of axon outgrowth (Zolessi et al., 2006). Axons of RGCs and THN neurons arise directly from the basal process of the cell in the absence of other emerging neurites and the centrosome is found opposite (apical) to the emerging axon.

To elucidate whether centrosome independent axon outgrowth is a common theme for various types of neurons *in vivo* needs further investigation. Due to the combinatorial nature of the Gal4-UAS system this question can be addressed by injection of the established Janus or Medusa vectors into different neuron-specific Gal4 activator strains. Zebrafish Gal4 enhancer and genetrapp screens have already generated many zebrafish Gal4 activator strains and more will follow. Therefore this Gal4 mediated labelling system will be of great value for future *in vivo* cell biological studies. Other aspects like the role of the Golgi apparatus in axonogenesis and migration could be studied, by injecting the respective Janus or Medusa vectors in the rhombic lip specific *atoh1a:KalTA4* strain.

To facilitate the so far laborious generation of vectors containing the combination of subcellular labels needed for the respective investigation, attempts are underway to generate a Gal4 mediated labelling system using the Gateway® System (Invitrogen) allowing for an easy exchange of subcellular labelling cassettes.

Preliminary results of co-electroporating Medusa vector M1 and a Gal4 encoding plasmid in chicken embryos further showed that this vector can be readily applied in chick. M1 expression in mouse embryonic stem cells resulted in a correct, but rather weak label of the respective subcellular structures, which might be overcome by using a mouse-specific basal promoter. My Gal4 mediated subcellular labelling system thus promises to be applicable to other vertebrate systems. However, it is of note that not all the subcellular markers from different species labelled the corresponding structures correctly in zebrafish cells. This might also be the case for our selected zebrafish markers in other species. Prior testing is therefore strongly recommended.

In summary, the established subcellular labelling system provides a powerful tool to study cell biological aspects of developmental processes in the living organism using 4D confocal microscopy. Processes like migration or axonogenesis can be observed with unprecedented detail, yielding novel mechanistic insights. Importantly, the Gal4 based system allows for simultaneous overexpression or loss of function experiments using dominant negative variants

of a protein co-expressed with the subcellular labels as a direct read out. Therefore, the role of distinct proteins in migration or axonogenesis can be studied *in vivo*.

Thus, 4D microscopy combined with subcellular labelling as provided by my Gal4 based labelling system promises to merge the fields of developmental biology and cell biology into a new field of *in vivo* cell biology.

5. **Movie legends**

Movie 1: Zebrafish Embryonic Development

Time-lapse movie of zebrafish embryonic development from the two-cell stage to 70 hpf. Images were recorded every 2-5min. using a Leica MZ16FA stereomicroscope and a 1x objective. Images were rendered using Adobe Photoshop CS2, ImageJ. The movie (6frames/sec) was animated using QuickTimePro.

Movie 2: THN precursor dynamics

Time-lapse movie of THN precursor dynamics starting at approximately 24 hpf. Lateral view on the cerebellar anlage of an *atoh1a:KalTA4* transgenic zebrafish embryo. Images are maximum projections of a z-stack (spacing = 2.5 μ m; 38 planes) recorded every 12min. using a 40x water objective and a Zeiss LSM 510 confocal microscope. Images were rendered using Adobe Photoshop CS2, ImageJ. The movie (6frames/sec) was animated using QuickTimePro.

Movie 3: Interkinetic Nuclear Movements and Mitotic Cleavages

Time-lapse movie of interkinetic nuclear movements and mitotic cleavages of THN progenitors starting at approximately 30 hpf. Lateral view on the cerebellar anlage of an *atoh1a:KalTA4* transgenic zebrafish embryo injected with vector M1 (15ng/ μ l–1.5nl) at the one-cell stage. Images are maximum projections of a z-stack (spacing = 1.8 μ m; 26 planes) recorded every 6min. using a 40x water objective and a Zeiss LSM 510 confocal microscope. Images were rendered using Adobe Photoshop CS2, ImageJ. The movie (2frames/sec) was animated using QuickTimePro.

Movie 4: Trailing Membrane Retraction and Centrosome Translocation I

Time-lapse movie of trailing membrane retraction and centrosome translocation of THN progenitors starting at approximately 36 hpf. Lateral view on the cerebellar anlage of an *atoh1a:KalTA4* transgenic zebrafish embryo injected with vector M1 (30ng/ μ l–1.5nl) at the one-cell stage. Images are maximum projections of a z-stack (spacing = 1.8 μ m; 18 planes) recorded every 5min. using a 40x water objective and a Zeiss LSM 510 confocal microscope. Images were rendered using Adobe Photoshop CS2, ImageJ. The movie (6frames/sec) was animated using QuickTimePro.

Movie 5: Trailing Membrane Retraction and Centrosome Translocation II

Time-lapse movie of trailing membrane retraction and centrosome translocation of THN progenitors starting at approximately 30 hpf. Lateral view on the cerebellar anlage of an *atoh1a:KalTA4* transgenic zebrafish embryo injected with vector M1 (15ng/μl–1.5nl) at the one-cell stage. Images are maximum projections of a z-stack (spacing = 1.8μm; 26 planes) recorded every 6min. using a 40x water objective and a Zeiss LSM 510 confocal microscope. Images were rendered using Adobe Photoshop CS2, ImageJ. The movie (6frames/sec) was animated using QuickTimePro.

Movie 6: Ventral Migration I

Time-lapse movie of ventral migration of THN neurons starting at approximately 36 hpf. Lateral view on the cerebellar anlage of an *atoh1a:KalTA4* transgenic zebrafish embryo injected with vector M1 (30ng/μl–1.5nl) at the one-cell stage. Images are maximum projections of a z-stack (spacing = 1.8μm; 6 planes) recorded every 8.7min. using a 40x water objective and a Zeiss LSM 510 confocal microscope. Images were rendered using Adobe Photoshop CS2, ImageJ. The movie (6frames/sec) was animated using QuickTimePro.

Movie 7: Ventral Migration II

Time-lapse movie of ventral migration of THN neurons starting at approximately 40 hpf. Lateral view on the cerebellar anlage of an *atoh1a:KalTA4* transgenic zebrafish embryo injected with vector M1 (30ng/μl–1.5nl) at the one-cell stage. Images are maximum projections of a z-stack (spacing = 2.48μm; 15 planes) recorded every 5min. using a 40x water objective and a Zeiss LSM 510 confocal microscope. Images were rendered using Adobe Photoshop CS2, ImageJ. The movie (6frames/sec) was animated using QuickTimePro.

Movie 8: Axonogenesis

Time-lapse movie of axonogenesis in THN neurons starting at approximately 36 hpf. Lateral view on the cerebellar anlage of an *atoh1a:KalTA4* transgenic zebrafish embryo injected with vector M1 (30ng/μl–1.5nl) at the one-cell stage. Images are maximum projections of a z-stack (spacing = 1.78μm; 23 planes) recorded every 6min. using a 40x water objective and a Zeiss LSM 510 confocal microscope. Images were rendered using Adobe Photoshop CS2, ImageJ. The movie (6frames/sec) was animated using QuickTimePro.

Movie 9: In Vivo Visualization of the Emerging Axon Using Kif5xYFP

Time-lapse movie of axonogenesis in THN neurons starting at approximately 36 hpf. Lateral view on the cerebellar anlage of an *atoh1a:KalTA4* transgenic zebrafish embryo injected with vectors J8 (20ng/ μ l–1.5nl) and U14 (25ng/ μ l–1.5nl) at the one-cell stage. Images are maximum projections of a z-stack (spacing = 3 μ m; 11 planes) recorded every 6min. using a 40x water objective and a Zeiss LSM 510 confocal microscope. Images were rendered using Adobe Photoshop CS2, ImageJ. The movie (6frames/sec) was animated using QuickTimePro.

Movie 10: Mitosis

Time-lapse movie of mitosis in keratinocytes of a zebrafish embryo co-injected with M2 and KalTA4 (each 25ng/ μ l–1.5nl) at the one-cell stage. Images are single planes recorded every 20sec. using a 63x oil objective and a Zeiss LSM 510 confocal microscope. Images were rendered using Adobe Photoshop CS2, ImageJ. The movie was animated at 6frames/sec using QuickTimePro.

Movie 11: Microtubule Dynamics

Time-lapse movie of microtubule dynamics in keratinocytes of a zebrafish embryo co-injected with M3 and KalTA4 (each 25ng/ μ l–1.5nl) at the one-cell stage. Images are single planes recorded every 2sec. using a 63x oil objective and a Zeiss LSM 510 confocal microscope. Images were rendered using Adobe Photoshop CS2, ImageJ. The movie (6frames/sec) was animated using QuickTimePro.

6. Abbreviations

AD	activation domain
atoh1a	zebrafish atonal homolog 1a
ATP	adenosine triphosphate
BCIP	5-bromo-4-chloro-3'-indolyphosphate p-toluidine salt
bp	base pair
BSA	bovine serum albumine
CFP	cyan fluorescent protein
ChAT	choline acetyltransferase
CNS	central nervous system
DBD	DNA binding domain
DCX	doublecortin
DMSO	dimethylsulfoxid
DNA	deoxyribonucleic Acid
DNase	desoxyribonuclease
dNTP	deoxynucleotide triphosphate
dox	doxycycline
dpf	days past fertilization
<i>E.coli</i>	<i>Escherichia coli</i>
EB1	microtubule end binding protein 1
EB3	microtubule end binding protein 3
EGL	external granular layer
EtBr	ethidium bromide
EtOH	ethanol
Fig	figure
GFP	green fluorescent protein
h	hour
H2B	histone 2B
hpf	hours past fertilization
HSV	<i>herpes simplex</i> virus
IGL	inner granular layer
IPTG	isopropyl- β -D-thiogalactopyranosid

Kan.	Kanamycin
LB	Luria-Bertani medium
μ	micro-
MeOH	methanol
MGE	medial ganglionic eminence of the basal telencephalon
MHB	mid-hindbrain boundary
min	minutes
mRFP	monomeric red fluorescent protein
mRNA	messenger RNA
MSOT	multispectral opto-acoustic tomography
n	nano-
NBT	nitro-blue tetrazolium chloride
NGS	Normal Goat Serum
OD	optical density
PBS	phosphate-buffered saline
PCR	polymerase chain reaction
PFA	paraformaldehyd
PTU	phenylthiourea
PTW	PBS with Tween
r	rhombomere
RGC	retinal ganglion cell
RNA	ribonucleic Acid
RNAse	ribonuclease
rpm	rounds per minute
RT	room temperature
RT-PCR	reverse transcription-polymerase chain reaction
sec	seconds
Tab	table
tet	tetracycline
TetO	tetracycline operator sequence
Tris	2-Amino-2-(hydroxymethyl)-1,3-propanediol
TS	temperature sensitive
Tween®20	poly(oxyethylen) _n -sorbitan-monolaurate

Abbreviations

twhh	<i>tiggy winkle hedgehog</i>
U	units
UAS	upstream activating sequence
URL	upper rhombic lip
UTP	Uridine Triphosphate
UV	ultra violette
V	volt
YFP	yellow fluorescent protein
zic1/4	zinc finger protein of cerebellum 1/4

7. Literature

- Amatruda, J. F., Shepard, J. L., Stern, H. M., and Zon, L. I. (2002). Zebrafish as a cancer model system. *Cancer Cell* **1**, 229-31.
- Amsterdam, A., Lin, S., and Hopkins, N. (1995). The *Aequorea victoria* green fluorescent protein can be used as a reporter in live zebrafish embryos. *Dev Biol* **171**, 123-9.
- Anelli, V., Santoriello, C., Distel, M., Köster, R. W., Ciccarelli, F. D., and Mione, M. (2009). Global repression of cancer gene expression in a zebrafish model of melanoma is linked to epigenetic regulation. *Zebrafish* **accepted**.
- Argenton, F., Arava, Y., Aronheim, A., and Walker, M. D. (1996). An activation domain of the helix-loop-helix transcription factor E2A shows cell type preference in vivo in microinjected zebra fish embryos. *Mol Cell Biol* **16**, 1714-21.
- Asakawa, K., and Kawakami, K. (2008). Targeted gene expression by the Gal4-UAS system in zebrafish. *Dev Growth Differ* **50**, 391-9.
- Asakawa, K., Suster, M. L., Mizusawa, K., Nagayoshi, S., Kotani, T., Urasaki, A., Kishimoto, Y., Hibi, M., and Kawakami, K. (2008). Genetic dissection of neural circuits by Tol2 transposon-mediated Gal4 gene and enhancer trapping in zebrafish. *Proc Natl Acad Sci U S A* **105**, 1255-60.
- Babaryka, A., Kuhn, E., and Koster, R. W. (2009). In vivo synthesis of meganuclease for generating transgenic zebrafish *Danio rerio*. *Journal of Fish Biology* **74**, 452-457.
- Bae, Y. K., Kani, S., Shimizu, T., Tanabe, K., Nojima, H., Kimura, Y., Higashijima, S., and Hibi, M. (2009). Anatomy of zebrafish cerebellum and screen for mutations affecting its development. *Dev Biol* **330**, 406-26.
- Baker, J. C., Beddington, R. S., and Harland, R. M. (1999). Wnt signaling in *Xenopus* embryos inhibits *bmp4* expression and activates neural development. *Genes Dev* **13**, 3149-59.
- Baron, U., Gossen, M., and Bujard, H. (1997). Tetracycline-controlled transcription in eukaryotes: novel transactivators with graded transactivation potential. *Nucleic Acids Res* **25**, 2723-9.
- Basto, R., Lau, J., Vinogradova, T., Gardiol, A., Woods, C. G., Khodjakov, A., and Raff, J. W. (2006). Flies without centrioles. *Cell* **125**, 1375-86.
- Baye, L. M., and Link, B. A. (2007). Interkinetic nuclear migration and the selection of neurogenic cell divisions during vertebrate retinogenesis. *J Neurosci* **27**, 10143-52.
- Baye, L. M., and Link, B. A. (2008). Nuclear migration during retinal development. *Brain Res* **1192**, 29-36.
- Beckwith, L. G., Moore, J. L., Tsao-Wu, G. S., Harshbarger, J. C., and Cheng, K. C. (2000). Ethylnitrosourea induces neoplasia in zebrafish (*Danio rerio*). *Lab Invest* **80**, 379-85.
- Beddington, R. S. (1994). Induction of a second neural axis by the mouse node. *Development* **120**, 613-20.
- Begemann, G., Schilling, T. F., Rauch, G. J., Geisler, R., and Ingham, P. W. (2001). The zebrafish neckless mutation reveals a requirement for *raldh2* in mesodermal signals that pattern the hindbrain. *Development* **128**, 3081-94.
- Bell, A. G. (1880). On the production and reproduction of sound by light. *Am. J. Sci.* **20**, 305-324.
- Bell, E., Wingate, R. J., and Lumsden, A. (1999). Homeotic transformation of rhombomere identity after localized *Hoxb1* misexpression. *Science* **284**, 2168-71.
- Bellion, A., Baudoin, J. P., Alvarez, C., Bornens, M., and Metin, C. (2005). Nucleokinesis in tangentially migrating neurons comprises two alternating phases: forward migration of the Golgi/centrosome associated with centrosome splitting and myosin contraction at the rear. *J Neurosci* **25**, 5691-9.

- Bertrand, N., Castro, D. S., and Guillemot, F. (2002). Proneural genes and the specification of neural cell types. *Nat Rev Neurosci* **3**, 517-30.
- Betzig, E., Patterson, G. H., Sougrat, R., Lindwasser, O. W., Olenych, S., Bonifacino, J. S., Davidson, M. W., Lippincott-Schwartz, J., and Hess, H. F. (2006). Imaging intracellular fluorescent proteins at nanometer resolution. *Science* **313**, 1642-5.
- Bhaumik, S. R., Raha, T., Aiello, D. P., and Green, M. R. (2004). In vivo target of a transcriptional activator revealed by fluorescence resonance energy transfer. *Genes Dev* **18**, 333-43.
- Born, J., Janeczek, J., Schwarz, W., Tiedemann, H., and Tiedemann, H. (1989). Activation of masked neural determinants in amphibian eggs and embryos and their release from the inducing tissue. *Cell Differ Dev* **27**, 1-7.
- Brand, A. H., and Perrimon, N. (1993). Targeted gene expression as a means of altering cell fates and generating dominant phenotypes. *Development* **118**, 401-15.
- Bretschneider, S., Eggeling, C., and Hell, S. W. (2007). Breaking the diffraction barrier in fluorescence microscopy by optical shelving. *Phys Rev Lett* **98**, 218103.
- Burcin, M. M., O'Malley, B. W., and Tsai, S. Y. (1998). A regulatory system for target gene expression. *Front Biosci* **3**, c1-7.
- Burgholzer, P., Grün, H., and Sonnleitner, A. (2009). Sounding out fluorescent proteins. *Nature Photonics* **3**, 378-379.
- Chakshumathi, G., Mondal, K., Lakshmi, G. S., Singh, G., Roy, A., Ch, R. B., Madhusudhanan, S., and Varadarajan, R. (2004). Design of temperature-sensitive mutants solely from amino acid sequence. *Proc Natl Acad Sci U S A* **101**, 7925-30.
- Chapouton, P., Jagasia, R., and Bally-Cuif, L. (2007). Adult neurogenesis in non-mammalian vertebrates. *Bioessays* **29**, 745-57.
- Chenn, A., Zhang, Y. A., Chang, B. T., and McConnell, S. K. (1998). Intrinsic polarity of mammalian neuroepithelial cells. *Mol Cell Neurosci* **11**, 183-93.
- Chitnis, A. B. (1995). The role of Notch in lateral inhibition and cell fate specification. *Mol Cell Neurosci* **6**, 311-21.
- Cohen, S. N., Chang, A.C.Y., Hsu, L. (1972). A rapid and convenient method for the preparing and storage of competent bacterial cells. *Nucleic Acids Res.* **16**, 3580.
- Conde, C., and Caceres, A. (2009). Microtubule assembly, organization and dynamics in axons and dendrites. *Nat Rev Neurosci* **10**, 319-32.
- Cooke, J. E., Kemp, H. A., and Moens, C. B. (2005). EphA4 is required for cell adhesion and rhombomere-boundary formation in the zebrafish. *Curr Biol* **15**, 536-42.
- Cui, S., Otten, C., Rohr, S., Abdelilah-Seyfried, S., and Link, B. A. (2007). Analysis of aPKClambda and aPKCzeta reveals multiple and redundant functions during vertebrate retinogenesis. *Mol Cell Neurosci* **34**, 431-44.
- Davidson, A. E., Balciunas, D., Mohn, D., Shaffer, J., Hermanson, S., Sivasubbu, S., Cliff, M. P., Hackett, P. B., and Ekker, S. C. (2003). Efficient gene delivery and gene expression in zebrafish using the Sleeping Beauty transposon. *Dev Biol* **263**, 191-202.
- Davison, J. M., Akitake, C. M., Goll, M. G., Rhee, J. M., Gosse, N., Baier, H., Halpern, M. E., Leach, S. D., and Parsons, M. J. (2007). Transactivation from Gal4-VP16 transgenic insertions for tissue-specific cell labeling and ablation in zebrafish. *Dev Biol* **304**, 811-24.
- de Anda, F. C., Pollarolo, G., Da Silva, J. S., Camoletto, P. G., Feiguin, F., and Dotti, C. G. (2005). Centrosome localization determines neuronal polarity. *Nature* **436**, 704-8.
- Del Bene, F., Wehman, A. M., Link, B. A., and Baier, H. (2008). Regulation of neurogenesis by interkinetic nuclear migration through an apical-basal notch gradient. *Cell* **134**, 1055-65.

- Distel, M., Babaryka, A., and Koster, R. W. (2006). Multicolor in vivo time-lapse imaging at cellular resolution by stereomicroscopy. *Dev Dyn* **235**, 1100-06.
- Distel, M., Hocking, J., and Koester, R. W. (2009a). "Imaging the cell biology of neuronal migration in zebrafish. ." World Scientific Publishing, Singapore,
- Distel, M., and Koester, R. W. (2007). In vivo time-lapse imaging of zebrafish embryonic development. *CSH Protocols* doi:10.1101/pdb.prot4816.
- Distel, M., Wullimann, M. F., and Koster, R. W. (2009b). Optimized Gal4 genetics for permanent gene expression mapping in zebrafish. *Proc Natl Acad Sci U S A*.
- Distel, M., Wullimann, M. F., and Koster, R. W. (2009c). Optimized Gal4 genetics for permanent gene expression mapping in zebrafish. *Proc Natl Acad Sci U S A* **106**, 13365-70.
- Driever, W., Solnica-Krezel, L., Schier, A. F., Neuhauss, S. C., Malicki, J., Stemple, D. L., Stainier, D. Y., Zwartkuis, F., Abdelilah, S., Rangini, Z., Belak, J., and Boggs, C. (1996). A genetic screen for mutations affecting embryogenesis in zebrafish. *Development* **123**, 37-46.
- Du, S. J., Devoto, S. H., Westerfield, M., and Moon, R. T. (1997). Positive and negative regulation of muscle cell identity by members of the hedgehog and TGF-beta gene families. *J Cell Biol* **139**, 145-56.
- Efimov, A., Kharitonov, A., Efimova, N., Loncarek, J., Miller, P. M., Andreyeva, N., Gleeson, P., Galjart, N., Maia, A. R., McLeod, I. X., Yates, J. R., 3rd, Maiato, H., Khodjakov, A., Akhmanova, A., and Kaverina, I. (2007). Asymmetric CLASP-dependent nucleation of noncentrosomal microtubules at the trans-Golgi network. *Dev Cell* **12**, 917-30.
- Ekker, S. C., Ungar, A. R., Greenstein, P., von Kessler, D. P., Porter, J. A., Moon, R. T., and Beachy, P. A. (1995). Patterning activities of vertebrate hedgehog proteins in the developing eye and brain. *Curr Biol* **5**, 944-55.
- Engineer, C. B., Fitzsimmons, K. C., Schmuke, J. J., Dotson, S. B., and Kranz, R. G. (2005). Development and evaluation of a Gal4-mediated LUC/GFP/GUS enhancer trap system in Arabidopsis. *BMC Plant Biol* **5**, 9.
- Erter, C. E., Wilm, T. P., Basler, N., Wright, C. V., and Solnica-Krezel, L. (2001). Wnt8 is required in lateral mesendodermal precursors for neural posteriorization in vivo. *Development* **128**, 3571-83.
- Etienne-Manneville, S., and Hall, A. (2001). Integrin-mediated activation of Cdc42 controls cell polarity in migrating astrocytes through PKCzeta. *Cell* **106**, 489-98.
- Evans, C. J., Olson, J. M., Ngo, K. T., Kim, E., Lee, N. E., Kuoy, E., Patananan, A. N., Sitz, D., Tran, P., Do, M. T., Yackle, K., Cespedes, A., Hartenstein, V., Call, G. B., and Banerjee, U. (2009). G-TRACE: rapid Gal4-based cell lineage analysis in Drosophila. *Nat Methods* **6**, 603-5.
- Fame, R. M., Brajon, C., and Ghysen, A. (2006). Second-order projection from the posterior lateral line in the early zebrafish brain. *Neural Dev* **1**, 4.
- Fan, S. S., and Ready, D. F. (1997). Glued participates in distinct microtubule-based activities in Drosophila eye development. *Development* **124**, 1497-507.
- Fields, S., and Song, O. (1989). A novel genetic system to detect protein-protein interactions. *Nature* **340**, 245-6.
- Fischer, J. A., Giniger, E., Maniatis, T., and Ptashne, M. (1988). GAL4 activates transcription in Drosophila. *Nature* **332**, 853-6.
- Flanagan, J. G., and Vanderhaeghen, P. (1998). The ephrins and Eph receptors in neural development. *Annu Rev Neurosci* **21**, 309-45.
- Furthauer, M., Thisse, C., and Thisse, B. (1997). A role for FGF-8 in the dorsoventral patterning of the zebrafish gastrula. *Development* **124**, 4253-64.

- Furthauer, M., Van Celst, J., Thisse, C., and Thisse, B. (2004). Fgf signalling controls the dorsoventral patterning of the zebrafish embryo. *Development* **131**, 2853-64.
- Gale, N. W., Holland, S. J., Valenzuela, D. M., Flenniken, A., Pan, L., Ryan, T. E., Henkemeyer, M., Strebhardt, K., Hirai, H., Wilkinson, D. G., Pawson, T., Davis, S., and Yancopoulos, G. D. (1996). Eph receptors and ligands comprise two major specificity subclasses and are reciprocally compartmentalized during embryogenesis. *Neuron* **17**, 9-19.
- Garrick, D., Fiering, S., Martin, D. I., and Whitelaw, E. (1998). Repeat-induced gene silencing in mammals. *Nat Genet* **18**, 56-9.
- Gavalas, A. (2002). ArRAnging the hindbrain. *Trends Neurosci* **25**, 61-4.
- Gavalas, A., and Krumlauf, R. (2000). Retinoid signalling and hindbrain patterning. *Curr Opin Genet Dev* **10**, 380-6.
- Geldmacher-Voss, B., Reugels, A. M., Pauls, S., and Campos-Ortega, J. A. (2003). A 90-degree rotation of the mitotic spindle changes the orientation of mitoses of zebrafish neuroepithelial cells. *Development* **130**, 3767-80.
- Gilbert, D. M., Heery, D. M., Losson, R., Chambon, P., and Lemoine, Y. (1993). Estradiol-inducible squelching and cell growth arrest by a chimeric VP16-estrogen receptor expressed in *Saccharomyces cerevisiae*: suppression by an allele of PDR1. *Mol Cell Biol* **13**, 462-72.
- Gill, G., and Ptashne, M. (1988). Negative effect of the transcriptional activator GAL4. *Nature* **334**, 721-4.
- Giniger, E., and Ptashne, M. (1987). Transcription in yeast activated by a putative amphipathic alpha helix linked to a DNA binding unit. *Nature* **330**, 670-2.
- Giniger, E., and Ptashne, M. (1988). Cooperative DNA binding of the yeast transcriptional activator GAL4. *Proc Natl Acad Sci U S A* **85**, 382-6.
- Giniger, E., Varnum, S. M., and Ptashne, M. (1985). Specific DNA binding of GAL4, a positive regulatory protein of yeast. *Cell* **40**, 767-74.
- Godsave, S. F., and Slack, J. M. (1989). Clonal analysis of mesoderm induction in *Xenopus laevis*. *Dev Biol* **134**, 486-90.
- Goll, M. G., Anderson, R., Stainier, D. Y., Spradling, A. C., and Halpern, M. E. (2009). Transcriptional silencing and reactivation in transgenic zebrafish. *Genetics* **182**, 747-55.
- Grabher, C., and Wittbrodt, J. (2004). Efficient activation of gene expression using a heat-shock inducible Gal4/Vp16-UAS system in medaka. *BMC Biotechnol* **4**, 26.
- Grabher, C., and Wittbrodt, J. (2007). Meganuclease and transposon mediated transgenesis in medaka. *Genome Biol* **8 Suppl 1**, S10.
- Gregory, W. A., Edmondson, J. C., Hatten, M. E., and Mason, C. A. (1988). Cytology and neuron-glia apposition of migrating cerebellar granule cells in vitro. *J Neurosci* **8**, 1728-38.
- Grunz, H., and Tacke, L. (1989). Neural differentiation of *Xenopus laevis* ectoderm takes place after disaggregation and delayed reaggregation without inducer. *Cell Differ Dev* **28**, 211-7.
- Guarente, L., Yocum, R. R., and Gifford, P. (1982). A GAL10-CYC1 hybrid yeast promoter identifies the GAL4 regulatory region as an upstream site. *Proc Natl Acad Sci U S A* **79**, 7410-4.
- Haffter, P., Granato, M., Brand, M., Mullins, M. C., Hammerschmidt, M., Kane, D. A., Odenthal, J., van Eeden, F. J., Jiang, Y. J., Heisenberg, C. P., Kelsh, R. N., Furutani-Seiki, M., Vogelsang, E., Beuchle, D., Schach, U., Fabian, C., and Nusslein-Volhard, C. (1996). The identification of genes with unique and essential functions in the development of the zebrafish, *Danio rerio*. *Development* **123**, 1-36.

- Hammond, J. W., Cai, D., and Verhey, K. J. (2008). Tubulin modifications and their cellular functions. *Curr Opin Cell Biol* **20**, 71-6.
- Han, D. D., Stein, D., and Stevens, L. M. (2000). Investigating the function of follicular subpopulations during *Drosophila* oogenesis through hormone-dependent enhancer-targeted cell ablation. *Development* **127**, 573-83.
- Hans, S., Kaslin, J., Freudenreich, D., and Brand, M. (2009). Temporally-controlled site-specific recombination in zebrafish. *PLoS ONE* **4**, e4640.
- Hauptmann, G., and Gerster, T. (1994). Two-color whole-mount in situ hybridization to vertebrate and *Drosophila* embryos. *Trends Genet* **10**, 266.
- Heintzmann, R., and Ficz, G. (2006). Breaking the resolution limit in light microscopy. *Brief Funct Genomic Proteomic* **5**, 289-301.
- Heisenberg, C. P., Houart, C., Take-Uchi, M., Rauch, G. J., Young, N., Coutinho, P., Masai, I., Caneparo, L., Concha, M. L., Geisler, R., Dale, T. C., Wilson, S. W., and Stemple, D. L. (2001). A mutation in the Gsk3-binding domain of zebrafish Masterblind/Axin1 leads to a fate transformation of telencephalon and eyes to diencephalon. *Genes Dev* **15**, 1427-34.
- Hell, S. W., and Wichmann, J. (1994). Breaking the diffraction resolution limit by stimulated emission-stimulated-emission-depletion fluorescence microscopy. *Opt Lett* **19**, 780-782.
- Hemmati-Brivanlou, A., Kelly, O. G., and Melton, D. A. (1994). Follistatin, an antagonist of activin, is expressed in the Spemann organizer and displays direct neuralizing activity. *Cell* **77**, 283-95.
- Hermanson, S., Davidson, A. E., Sivasubbu, S., Balciunas, D., and Ekker, S. C. (2004). Sleeping Beauty transposon for efficient gene delivery. *Methods Cell Biol* **77**, 349-62.
- Higginbotham, H., Tanaka, T., Brinkman, B. C., and Gleeson, J. G. (2006). GSK3beta and PKCzeta function in centrosome localization and process stabilization during Slit-mediated neuronal repolarization. *Mol Cell Neurosci* **32**, 118-32.
- Higginbotham, H. R., and Gleeson, J. G. (2007). The centrosome in neuronal development. *Trends Neurosci* **30**, 276-83.
- Hinds, J. W., and Ruffett, T. L. (1971). Cell proliferation in the neural tube: an electron microscopic and golgi analysis in the mouse cerebral vesicle. *Z Zellforsch Mikrosk Anat* **115**, 226-64.
- Hofmann, M., Eggeling, C., Jakobs, S., and Hell, S. W. (2005). Breaking the diffraction barrier in fluorescence microscopy at low light intensities by using reversibly photoswitchable proteins. *Proc Natl Acad Sci U S A* **102**, 17565-9.
- Holder, N., and Klein, R. (1999). Eph receptors and ephrins: effectors of morphogenesis. *Development* **126**, 2033-44.
- Horne-Badovinac, S., Lin, D., Waldron, S., Schwarz, M., Mbamalu, G., Pawson, T., Jan, Y., Stainier, D. Y., and Abdelilah-Seyfried, S. (2001). Positional cloning of heart and soul reveals multiple roles for PKC lambda in zebrafish organogenesis. *Curr Biol* **11**, 1492-502.
- Hultman, K. A., Bahary, N., Zon, L. I., and Johnson, S. L. (2007). Gene Duplication of the zebrafish kit ligand and partitioning of melanocyte development functions to kit ligand a. *PLoS Genet* **3**, e17.
- Inazawa, H., and Kitakaze, K. (1998). A locally inhibited lateral neural network: on the fundamental features of a network consisting of neurons with a restricted range of interaction. *Biol Cybern* **78**, 207-15.
- Inbal, A., Topczewski, J., and Solnica-Krezel, L. (2006). Targeted gene expression in the zebrafish prechordal plate. *Genesis* **44**, 584-8.

- Ito, K., Awano, W., Suzuki, K., Hiromi, Y., and Yamamoto, D. (1997). The *Drosophila* mushroom body is a quadruple structure of clonal units each of which contains a virtually identical set of neurones and glial cells. *Development* **124**, 761-71.
- Jackman, W. R., Langeland, J. A., and Kimmel, C. B. (2000). islet reveals segmentation in the *Amphioxus* hindbrain homolog. *Dev Biol* **220**, 16-26.
- Jacobson, C., Schnapp, B., and Banker, G. A. (2006). A change in the selective translocation of the Kinesin-1 motor domain marks the initial specification of the axon. *Neuron* **49**, 797-804.
- Jadhav, A. P., Cho, S. H., and Cepko, C. L. (2006). Notch activity permits retinal cells to progress through multiple progenitor states and acquire a stem cell property. *Proc Natl Acad Sci U S A* **103**, 18998-9003.
- Johnston, M. (1987). A model fungal gene regulatory mechanism: the GAL genes of *Saccharomyces cerevisiae*. *Microbiol Rev* **51**, 458-76.
- Johnston, S. A., Salmeron, J. M., Jr., and Dincher, S. S. (1987). Interaction of positive and negative regulatory proteins in the galactose regulon of yeast. *Cell* **50**, 143-6.
- Kaksonen, M., and Drubin, D. G. (2006). PALM reading: Seeing the future of cell biology at higher resolution. *Dev Cell* **11**, 438-9.
- Kandel, E. R., Schwartz, J. H., and T.M., J. (2000). "Principles of Neural Sciences." McGraw-Hill,
- Kang, T., Martins, T., and Sadowski, I. (1993). Wild type GAL4 binds cooperatively to the GAL1-10 UASG in vitro. *J Biol Chem* **268**, 9629-35.
- Kawakami, K. (2004). Transgenesis and gene trap methods in zebrafish by using the Tol2 transposable element. *Methods Cell Biol* **77**, 201-22.
- Kawakami, K. (2007). Tol2: a versatile gene transfer vector in vertebrates. *Genome Biol* **8 Suppl 1**, S7.
- Kawakami, K., Koga, A., Hori, H., and Shima, A. (1998). Excision of the tol2 transposable element of the medaka fish, *Oryzias latipes*, in zebrafish, *Danio rerio*. *Gene* **225**, 17-22.
- Kawakami, K., and Shima, A. (1999). Identification of the Tol2 transposase of the medaka fish *Oryzias latipes* that catalyzes excision of a nonautonomous Tol2 element in zebrafish *Danio rerio*. *Gene* **240**, 239-44.
- Kiecker, C., and Lumsden, A. (2005). Compartments and their boundaries in vertebrate brain development. *Nat Rev Neurosci* **6**, 553-64.
- Kimmel, C. B., Ballard, W. W., Kimmel, S. R., Ullmann, B., and Schilling, T. F. (1995). Stages of embryonic development of the zebrafish. *Dev Dyn* **203**, 253-310.
- Klar, T. A., Engel, E., and Hell, S. W. (2001). Breaking Abbe's diffraction resolution limit in fluorescence microscopy with stimulated emission depletion beams of various shapes. *Phys Rev E Stat Nonlin Soft Matter Phys* **64**, 066613.
- Koga, A., Cheah, F. S., Hamaguchi, S., Yeo, G. H., and Chong, S. S. (2008). Germline transgenesis of zebrafish using the medaka Tol1 transposon system. *Dev Dyn* **237**, 2466-74.
- Kopan, R., and Ilagan, M. X. (2009). The canonical Notch signaling pathway: unfolding the activation mechanism. *Cell* **137**, 216-33.
- Köster, R. W., and Fraser, S. E. (2001a). Direct imaging of in vivo neuronal migration in the developing cerebellum. *Curr Biol* **11**, 1858-63.
- Köster, R. W., and Fraser, S. E. (2001b). Tracing transgene expression in living zebrafish embryos. *Dev Biol* **233**, 329-46.
- Köster, R. W., and Fraser, S. E. (2006). FGF signaling mediates regeneration of the differentiating cerebellum through repatterning of the anterior hindbrain and reinitiation of neuronal migration. *J Neurosci* **26**, 7293-304.

- Kudoh, T., Concha, M. L., Houart, C., Dawid, I. B., and Wilson, S. W. (2004). Combinatorial Fgf and Bmp signalling patterns the gastrula ectoderm into prospective neural and epidermal domains. *Development* **131**, 3581-92.
- Langenau, D. M., Traver, D., Ferrando, A. A., Kutok, J. L., Aster, J. C., Kanki, J. P., Lin, S., Prochownik, E., Trede, N. S., Zon, L. I., and Look, A. T. (2003). Myc-induced T cell leukemia in transgenic zebrafish. *Science* **299**, 887-90.
- Lefcort, F., and Bentley, D. (1989). Organization of cytoskeletal elements and organelles preceding growth cone emergence from an identified neuron in situ. *J Cell Biol* **108**, 1737-49.
- Li, J. J., and Herskowitz, I. (1993). Isolation of ORC6, a component of the yeast origin recognition complex by a one-hybrid system. *Science* **262**, 1870-4.
- Li, L., Zemp, R. J., Lungu, G., Stoica, G., and Wang, L. V. (2007). Photoacoustic imaging of lacZ gene expression in vivo. *J Biomed Opt* **12**, 020504.
- Liang, S. D., Marmorstein, R., Harrison, S. C., and Ptashne, M. (1996). DNA sequence preferences of GAL4 and PPR1: how a subset of Zn² Cys₆ binuclear cluster proteins recognizes DNA. *Mol Cell Biol* **16**, 3773-80.
- Lichtman, J. W., and Fraser, S. E. (2001). The neuronal naturalist: watching neurons in their native habitat. *Nat Neurosci* **4 Suppl**, 1215-20.
- Linney, E., Upchurch, L., and Donerly, S. (2004). Zebrafish as a neurotoxicological model. *Neurotoxicol Teratol* **26**, 709-18.
- Lobo, N. F., Fraser, T. S., Adams, J. A., and Fraser, M. J., Jr. (2006). Interplasmid transposition demonstrates piggyBac mobility in vertebrate species. *Genetica* **128**, 347-57.
- Lohr, D., Venkov, P., and Zlatanova, J. (1995). Transcriptional regulation in the yeast GAL gene family: a complex genetic network. *Faseb J* **9**, 777-87.
- Luan, H., and White, B. H. (2007). Combinatorial methods for refined neuronal gene targeting. *Curr Opin Neurobiol* **17**, 572-80.
- Lumsden, A., and Krumlauf, R. (1996). Patterning the vertebrate neuraxis. *Science* **274**, 1109-15.
- Lumsden, A., Sprawson, N., and Graham, A. (1991). Segmental origin and migration of neural crest cells in the hindbrain region of the chick embryo. *Development* **113**, 1281-91.
- Ma, J., and Ptashne, M. (1987). The carboxy-terminal 30 amino acids of GAL4 are recognized by GAL80. *Cell* **50**, 137-42.
- Ma, X., Kawamoto, S., Hara, Y., and Adelstein, R. S. (2004). A point mutation in the motor domain of nonmuscle myosin II-B impairs migration of distinct groups of neurons. *Mol Biol Cell* **15**, 2568-79.
- Machold, R., and Fishell, G. (2005). Math1 is expressed in temporally discrete pools of cerebellar rhombic-lip neural progenitors. *Neuron* **48**, 17-24.
- Manzanares, M., Cordes, S., Kwan, C. T., Sham, M. H., Barsh, G. S., and Krumlauf, R. (1997). Segmental regulation of Hoxb-3 by kreisler. *Nature* **387**, 191-5.
- Marmorstein, R., Carey, M., Ptashne, M., and Harrison, S. C. (1992). DNA recognition by GAL4: structure of a protein-DNA complex. *Nature* **356**, 408-14.
- McClintock, J. M., Carlson, R., Mann, D. M., and Prince, V. E. (2001). Consequences of Hox gene duplication in the vertebrates: an investigation of the zebrafish Hox paralogue group 1 genes. *Development* **128**, 2471-84.
- McClintock, J. M., Kheirbek, M. A., and Prince, V. E. (2002). Knockdown of duplicated zebrafish hoxb1 genes reveals distinct roles in hindbrain patterning and a novel mechanism of duplicate gene retention. *Development* **129**, 2339-54.

- McCormick, C. A., and Hernandez, D. V. (1996). Connections of octaval and lateral line nuclei of the medulla in the goldfish, including the cytoarchitecture of the secondary octaval population in goldfish and catfish. *Brain Behav Evol* **47**, 113-37.
- Melcher, K., and Johnston, S. A. (1995). GAL4 interacts with TATA-binding protein and coactivators. *Mol Cell Biol* **15**, 2839-48.
- Meng, A., Tang, H., Ong, B. A., Farrell, M. J., and Lin, S. (1997). Promoter analysis in living zebrafish embryos identifies a cis-acting motif required for neuronal expression of GATA-2. *Proc Natl Acad Sci U S A* **94**, 6267-72.
- Moens, C. B., Cordes, S. P., Giorgianni, M. W., Barsh, G. S., and Kimmel, C. B. (1998). Equivalence in the genetic control of hindbrain segmentation in fish and mouse. *Development* **125**, 381-91.
- Moens, C. B., and Prince, V. E. (2002). Constructing the hindbrain: insights from the zebrafish. *Dev Dyn* **224**, 1-17.
- Moens, C. B., Yan, Y. L., Appel, B., Force, A. G., and Kimmel, C. B. (1996). valentino: a zebrafish gene required for normal hindbrain segmentation. *Development* **122**, 3981-90.
- Mondal, K., Dastidar, A. G., Singh, G., Madhusudhanan, S., Gande, S. L., VijayRaghavan, K., and Varadarajan, R. (2007). Design and isolation of temperature-sensitive mutants of Gal4 in yeast and Drosophila. *J Mol Biol* **370**, 939-50.
- Moores, C. A., Perderiset, M., Kappeler, C., Kain, S., Drummond, D., Perkins, S. J., Chelly, J., Cross, R., Houdusse, A., and Francis, F. (2006). Distinct roles of doublecortin modulating the microtubule cytoskeleton. *Embo J* **25**, 4448-57.
- Nellen, D., Burke, R., Struhl, G., and Basler, K. (1996). Direct and long-range action of a DPP morphogen gradient. *Cell* **85**, 357-68.
- Nelson, B. R., Gumuscu, B., Hartman, B. H., and Reh, T. A. (2006). Notch activity is downregulated just prior to retinal ganglion cell differentiation. *Dev Neurosci* **28**, 128-41.
- Nieuwkoop, P. D. (1952). Activation and organization of the central nervous system in amphibians. Part 1. induction and activation. Part II. Differentiation and organization. *J.Exp Zool* **120**, 1-81.
- Nikolaou, N., Watanabe-Asaka, T., Gerety, S., Distel, M., Koster, R. W., and Wilkinson, D. G. (2009). Lunatic fringe promotes the lateral inhibition of neurogenesis. *Development* **136**, 2523-33.
- Nilsson, L., and Hamberger, L. (1990). "Ein Kind entsteht." Mosaik Verlag, München.
- North, T. E., Goessling, W., Walkley, C. R., Lengerke, C., Kopani, K. R., Lord, A. M., Weber, G. J., Bowman, T. V., Jang, I. H., Grosser, T., Fitzgerald, G. A., Daley, G. Q., Orkin, S. H., and Zon, L. I. (2007). Prostaglandin E2 regulates vertebrate haematopoietic stem cell homeostasis. *Nature* **447**, 1007-11.
- Ntziachristos, V., Ripoll, J., Wang, L. V., and Weissleder, R. (2005). Looking and listening to light: the evolution of whole-body photonic imaging. *Nat Biotechnol* **23**, 313-20.
- Ntziachristos, V., Tung, C. H., Bremer, C., and Weissleder, R. (2002). Fluorescence molecular tomography resolves protease activity in vivo. *Nat Med* **8**, 757-60.
- O'Kane, C. J., and Gehring, W. J. (1987). Detection in situ of genomic regulatory elements in Drosophila. *Proc Natl Acad Sci U S A* **84**, 9123-7.
- Ogura, E., Okuda, Y., Kondoh, H., and Kamachi, Y. (2009). Adaptation of GAL4 activators for GAL4 enhancer trapping in zebrafish. *Dev Dyn* **238**, 641-55.
- Osterwalder, T., Yoon, K. S., White, B. H., and Keshishian, H. (2001). A conditional tissue-specific transgene expression system using inducible GAL4. *Proc Natl Acad Sci U S A* **98**, 12596-601.

- Oxtoby, E., and Jowett, T. (1993). Cloning of the zebrafish krox-20 gene (krx-20) and its expression during hindbrain development. *Nucleic Acids Res* **21**, 1087-95.
- Palazzo, A. F., Joseph, H. L., Chen, Y. J., Dujardin, D. L., Alberts, A. S., Pfister, K. K., Vallee, R. B., and Gundersen, G. G. (2001). Cdc42, dynein, and dynactin regulate MTOC reorientation independent of Rho-regulated microtubule stabilization. *Curr Biol* **11**, 1536-41.
- Paquet, D., Bhat, R., Sydow, A., Mandelkow, E. M., Berg, S., Hellberg, S., Falting, J., Distel, M., Koster, R. W., Schmid, B., and Haass, C. (2009). A zebrafish model of tauopathy allows in vivo imaging of neuronal cell death and drug evaluation. *J Clin Invest* **119**, 1382-95.
- Pera, E. M., Ikeda, A., Eivers, E., and De Robertis, E. M. (2003). Integration of IGF, FGF, and anti-BMP signals via Smad1 phosphorylation in neural induction. *Genes Dev* **17**, 3023-8.
- Pera, E. M., Wessely, O., Li, S. Y., and De Robertis, E. M. (2001). Neural and head induction by insulin-like growth factor signals. *Dev Cell* **1**, 655-65.
- Perron, M., and Harris, W. A. (2000). Determination of vertebrate retinal progenitor cell fate by the Notch pathway and basic helix-loop-helix transcription factors. *Cell Mol Life Sci* **57**, 215-23.
- Perz-Edwards, A., Hardison, N. L., and Linney, E. (2001). Retinoic acid-mediated gene expression in transgenic reporter zebrafish. *Dev Biol* **229**, 89-101.
- Pignoni, F., and Zipursky, S. L. (1997). Induction of Drosophila eye development by decapentaplegic. *Development* **124**, 271-8.
- Poliakov, A., Cotrina, M., and Wilkinson, D. G. (2004). Diverse roles of eph receptors and ephrins in the regulation of cell migration and tissue assembly. *Dev Cell* **7**, 465-80.
- Prince, V. E., Moens, C. B., Kimmel, C. B., and Ho, R. K. (1998). Zebrafish hox genes: expression in the hindbrain region of wild-type and mutants of the segmentation gene, valentino. *Development* **125**, 393-406.
- Provost, E., Rhee, J., and Leach, S. D. (2007). Viral 2A peptides allow expression of multiple proteins from a single ORF in transgenic zebrafish embryos. *Genesis* **45**, 625-9.
- Raftopoulou, M., and Hall, A. (2004). Cell migration: Rho GTPases lead the way. *Dev Biol* **265**, 23-32.
- Rakic, P. (1972). Mode of cell migration to the superficial layers of fetal monkey neocortex. *J Comp Neurol* **145**, 61-83.
- Ray, P., Pimenta, H., Paulmurugan, R., Berger, F., Phelps, M. E., Iyer, M., and Gambhir, S. S. (2002). Noninvasive quantitative imaging of protein-protein interactions in living subjects. *Proc Natl Acad Sci U S A* **99**, 3105-10.
- Razansky, D., Distel, M., Vinegoni, C., Ma, R., Perrimon, N., Koster, R. W., and Ntziachristos, V. (2009). Multispectral opto-acoustic tomography of deep-seated fluorescent proteins in vivo. *Nature Photonics* **3**, 412-417.
- Reece, R. J., and Ptashne, M. (1993). Determinants of binding-site specificity among yeast C6 zinc cluster proteins. *Science* **261**, 909-11.
- Reed, N. A., Cai, D., Blasius, T. L., Jih, G. T., Meyhofer, E., Gaertig, J., and Verhey, K. J. (2006). Microtubule acetylation promotes kinesin-1 binding and transport. *Curr Biol* **16**, 2166-72.
- Rieger, S., Volkmann, K., and Koster, R. W. (2008). Polysialyltransferase expression is linked to neuronal migration in the developing and adult zebrafish. *Dev Dyn* **237**, 276-85.
- Roman, G., Endo, K., Zong, L., and Davis, R. L. (2001). P[Switch], a system for spatial and temporal control of gene expression in Drosophila melanogaster. *Proc Natl Acad Sci U S A* **98**, 12602-7.

- Rorth, P. (1996). A modular misexpression screen in *Drosophila* detecting tissue-specific phenotypes. *Proc Natl Acad Sci U S A* **93**, 12418-22.
- Rust, M. J., Bates, M., and Zhuang, X. (2006). Sub-diffraction-limit imaging by stochastic optical reconstruction microscopy (STORM). *Nat Methods* **3**, 793-5.
- Sadowski, I., Ma, J., Triezenberg, S., and Ptashne, M. (1988). GAL4-VP16 is an unusually potent transcriptional activator. *Nature* **335**, 563-4.
- Sagasti, A., Guido, M. R., Raible, D. W., and Schier, A. F. (2005). Repulsive interactions shape the morphologies and functional arrangement of zebrafish peripheral sensory arbors. *Curr Biol* **15**, 804-14.
- Saiki, R. K., Gelfand, D. H., Stoffel, S., Scharf, S. J., Higuchi, R., Horn, G. T., Mullis, K. B., and Erlich, H. A. (1988). Primer-directed enzymatic amplification of DNA with a thermostable DNA polymerase. *Science* **239**, 487-91.
- Sasai, Y., and De Robertis, E. M. (1997). Ectodermal patterning in vertebrate embryos. *Dev Biol* **182**, 5-20.
- Sasai, Y., Lu, B., Steinbeisser, H., Geissert, D., Gont, L. K., and De Robertis, E. M. (1994). Xenopus chordin: a novel dorsalizing factor activated by organizer-specific homeobox genes. *Cell* **79**, 779-90.
- Schaar, B. T., and McConnell, S. K. (2005). Cytoskeletal coordination during neuronal migration. *Proc Natl Acad Sci U S A* **102**, 13652-7.
- Scheer, N., and Campos-Ortega, J. A. (1999). Use of the Gal4-UAS technique for targeted gene expression in the zebrafish. *Mech Dev* **80**, 153-8.
- Scheer, N., Riedl, I., Warren, J. T., Kuwada, J. Y., and Campos-Ortega, J. A. (2002). A quantitative analysis of the kinetics of Gal4 activator and effector gene expression in the zebrafish. *Mech Dev* **112**, 9-14.
- Schilling, T. F., and Kimmel, C. B. (1994). Segment and cell type lineage restrictions during pharyngeal arch development in the zebrafish embryo. *Development* **120**, 483-94.
- Scott, E. K., Mason, L., Arrenberg, A. B., Ziv, L., Gosse, N. J., Xiao, T., Chi, N. C., Asakawa, K., Kawakami, K., and Baier, H. (2007). Targeting neural circuitry in zebrafish using GAL4 enhancer trapping. *Nat Methods* **4**, 323-6.
- SenGupta, D. J., Zhang, B., Kraemer, B., Pochart, P., Fields, S., and Wickens, M. (1996). A three-hybrid system to detect RNA-protein interactions in vivo. *Proc Natl Acad Sci U S A* **93**, 8496-501.
- Shih, J., and Fraser, S. E. (1996). Characterizing the zebrafish organizer: microsurgical analysis at the early-shield stage. *Development* **122**, 1313-22.
- Sidow, A. (1996). Gen(om)e duplications in the evolution of early vertebrates. *Curr Opin Genet Dev* **6**, 715-22.
- Smith, W. C., and Harland, R. M. (1992). Expression cloning of noggin, a new dorsalizing factor localized to the Spemann organizer in *Xenopus* embryos. *Cell* **70**, 829-40.
- Solecki, D. J., Model, L., Gaetz, J., Kapoor, T. M., and Hatten, M. E. (2004). Par6alpha signaling controls glial-guided neuronal migration. *Nat Neurosci* **7**, 1195-203.
- Spemann, H., and Mangold, H. (1924). Über Induktion von Embryonalanlagen durch Implantation artfremder Organisatoren. *Roux's Arch. EntwMech. Org* **100**, 599-638.
- Stebbins, M. J., Urlinger, S., Byrne, G., Bello, B., Hillen, W., and Yin, J. C. (2001). Tetracycline-inducible systems for *Drosophila*. *Proc Natl Acad Sci U S A* **98**, 10775-80.
- Stebbins, M. J., and Yin, J. C. (2001). Adaptable doxycycline-regulated gene expression systems for *Drosophila*. *Gene* **270**, 103-11.
- Stern, C. D. (2005). Neural induction: old problem, new findings, yet more questions. *Development* **132**, 2007-21.

- Studer, M., Lumsden, A., Ariza-McNaughton, L., Bradley, A., and Krumlauf, R. (1996). Altered segmental identity and abnormal migration of motor neurons in mice lacking Hoxb-1. *Nature* **384**, 630-4.
- Tanaka, T., Serneo, F. F., Higgins, C., Gambello, M. J., Wynshaw-Boris, A., and Gleeson, J. G. (2004). Lis1 and doublecortin function with dynein to mediate coupling of the nucleus to the centrosome in neuronal migration. *J Cell Biol* **165**, 709-21.
- Thermes, V., Grabher, C., Ristoratore, F., Bourrat, F., Choulika, A., Wittbrodt, J., and Joly, J. S. (2002). I-SceI meganuclease mediates highly efficient transgenesis in fish. *Mech Dev* **118**, 91-8.
- Traven, A., Jelacic, B., and Sopta, M. (2006). Yeast Gal4: a transcriptional paradigm revisited. *EMBO Rep* **7**, 496-9.
- Tsai, J. W., Bremner, K. H., and Vallee, R. B. (2007). Dual subcellular roles for LIS1 and dynein in radial neuronal migration in live brain tissue. *Nat Neurosci* **10**, 970-9.
- Tsai, L. H., and Gleeson, J. G. (2005). Nucleokinesis in neuronal migration. *Neuron* **46**, 383-8.
- Umeshima, H., Hirano, T., and Kengaku, M. (2007). Microtubule-based nuclear movement occurs independently of centrosome positioning in migrating neurons. *Proc Natl Acad Sci U S A* **104**, 16182-7.
- Volkman, K., Rieger, S., Babaryka, A., and Koster, R. W. (2008). The zebrafish cerebellar rhombic lip is spatially patterned in producing granule cell populations of different functional compartments. *Dev Biol* **313**, 167-80.
- Waddington, C. H. (1932). Experiments on the development of chick and duck embryos, cultivated in vitro. *Phil.Trans.R.Soc.Lond.B Biol.Sci.* **221**, 179-230.
- Wang, L. V. (2009). Multiscale photoacoustic microscopy and computed tomography. *Nature Photonics* **3**, 503-509.
- Wang, V. Y., Rose, M. F., and Zoghbi, H. Y. (2005). Math1 expression redefines the rhombic lip derivatives and reveals novel lineages within the brainstem and cerebellum. *Neuron* **48**, 31-43.
- Webster, N. J., Green, S., Jin, J. R., and Chambon, P. (1988). The hormone-binding domains of the estrogen and glucocorticoid receptors contain an inducible transcription activation function. *Cell* **54**, 199-207.
- White, R. M., Sessa, A., Burke, C., Bowman, T., LeBlanc, J., Ceol, C., Bourque, C., Dovey, M., Goessling, W., Burns, C. E., and Zon, L. I. (2008). Transparent adult zebrafish as a tool for in vivo transplantation analysis. *Cell Stem Cell* **2**, 183-9.
- Whited, J. L., Cassell, A., Brouillette, M., and Garrity, P. A. (2004). Dynactin is required to maintain nuclear position within postmitotic Drosophila photoreceptor neurons. *Development* **131**, 4677-86.
- Wilkinson, D. G., Bhatt, S., Cook, M., Boncinelli, E., and Krumlauf, R. (1989). Segmental expression of Hox-2 homoeobox-containing genes in the developing mouse hindbrain. *Nature* **341**, 405-9.
- Willig, K. I., Rizzoli, S. O., Westphal, V., Jahn, R., and Hell, S. W. (2006). STED microscopy reveals that synaptotagmin remains clustered after synaptic vesicle exocytosis. *Nature* **440**, 935-9.
- Wilson, S. I., and Edlund, T. (2001). Neural induction: toward a unifying mechanism. *Nat Neurosci* **4 Suppl**, 1161-8.
- Wingate, R. J., and Lumsden, A. (1996). Persistence of rhombomeric organisation in the postsegmental hindbrain. *Development* **122**, 2143-52.
- Witte, H., and Bradke, F. (2008). The role of the cytoskeleton during neuronal polarization. *Curr Opin Neurobiol* **18**, 479-87.

- Woo, K., and Fraser, S. E. (1997). Specification of the zebrafish nervous system by nonaxial signals. *Science* **277**, 254-7.
- Woo, K., Shih, J., and Fraser, S. E. (1995). Fate maps of the zebrafish embryo. *Curr Opin Genet Dev* **5**, 439-43.
- Wu, Y., Reece, R. J., and Ptashne, M. (1996). Quantitation of putative activator-target affinities predicts transcriptional activating potentials. *Embo J* **15**, 3951-63.
- Wullmann, M. F., Reichert, H., and Rupp, B. (1996). "Neuroanatomy of the Zebrafish Brain: A Topological Atlas." Birkhauser Verlag,
- Wurst, W., and Bally-Cuif, L. (2001). Neural plate patterning: upstream and downstream of the isthmus organizer. *Nat Rev Neurosci* **2**, 99-108.
- Xie, Z., Moy, L. Y., Sanada, K., Zhou, Y., Buchman, J. J., and Tsai, L. H. (2007). Cep120 and TACCs control interkinetic nuclear migration and the neural progenitor pool. *Neuron* **56**, 79-93.
- Xu, L., Schaffner, W., and Rungger, D. (1993). Transcriptional activation by recombinant GAL4-VP16 in the *Xenopus* oocyte. *Nucleic Acids Res* **21**, 2775.
- Xu, M. H., and Wang, L. V. (2006). Photoacoustic Imaging in biomedicine. *Rev. Sci. Instrum.* **77**.
- Zecca, M., Basler, K., and Struhl, G. (1996). Direct and long-range action of a wingless morphogen gradient. *Cell* **87**, 833-44.
- Zenke, F. T., Engles, R., Vollenbroich, V., Meyer, J., Hollenberg, C. P., and Breunig, K. D. (1996). Activation of Gal4p by galactose-dependent interaction of galactokinase and Gal80p. *Science* **272**, 1662-5.
- Zhou, L., Schnitzler, A., Agapite, J., Schwartz, L. M., Steller, H., and Nambu, J. R. (1997). Cooperative functions of the reaper and head involution defective genes in the programmed cell death of *Drosophila* central nervous system midline cells. *Proc Natl Acad Sci U S A* **94**, 5131-6.
- Zmuda, J. F., and Rivas, R. J. (1998). The Golgi apparatus and the centrosome are localized to the sites of newly emerging axons in cerebellar granule neurons in vitro. *Cell Motil Cytoskeleton* **41**, 18-38.
- Zolessi, F. R., Poggi, L., Wilkinson, C. J., Chien, C. B., and Harris, W. A. (2006). Polarization and orientation of retinal ganglion cells in vivo. *Neural Dev* **1**, 2.
- Zumbrunn, J., Kinoshita, K., Hyman, A. A., and Nathke, I. S. (2001). Binding of the adenomatous polyposis coli protein to microtubules increases microtubule stability and is regulated by GSK3 beta phosphorylation. *Curr Biol* **11**, 44-9.

8. **Appendices**

The following pages contain published and accepted articles, protocols and bookchapters, which I contributed to.

Appendix 1

published Article in *PNAS*

Optimized Gal4 genetics for permanent gene expression mapping in zebrafish

Martin Distel, Mario F. Wullmann and Reinhard W. Köster

Proc Natl Acad Sci U S A. (2009), Aug 11;106(32):13365-70.

Contribution:

For this article, I conducted the majority of experimental research. I characterized all of the Gal4 enhancer trap lines, performed the quantification assays, generated effector lines and performed the immunohistology, in situ hybridisation and retrograde labelling experiments. Data analysis was performed by all three authors. I generated all of the figures of the article. The manuscript was written by all three authors. The website was mainly designed by Olga Lositsky.

Optimized Gal4 genetics for permanent gene expression mapping in zebrafish

Martin Distel^a, Mario F. Wullimann^b, and Reinhard W. Köster^{a,1}

^aHelmholtz Zentrum München, Institute of Developmental Genetics, Ingolstädter Landstrasse 1, 85764 Neuherberg, Germany; and ^bLudwig-Maximilians-University Munich, Department of Biology II, Graduate School of Systemic Neurosciences, Grosshadernerstrasse 2, 82152 Planegg-Martinsried, Germany

Edited by Igor B. Dawid, National Institute of Child Health and Human Development, Bethesda, MD, and approved June 15, 2009 (received for review March 24, 2009)

Combinatorial genetics for conditional transgene activation allows studying gene function with temporal and tissue specific control like the Gal4-UAS system, which has enabled sophisticated genetic studies in *Drosophila*. Recently this system was adapted for zebrafish and promising applications have been introduced. Here, we report a systematic optimization of zebrafish Gal4-UAS genetics by establishing an optimized Gal4-activator (KalTA4). We provide quantitative data for KalTA4-mediated transgene activation in dependence of UAS copy numbers to allow for studying dosage effects of transgene expression. Employing a *Tol2* transposon-mediated KalTA4 enhancer trap screen biased for central nervous system expression, we present a collection of self-reporting red fluorescent KalTA4 activator strains. These strains reliably transactivate UAS-dependent transgenes and can be rendered homozygous. Furthermore, we have characterized the transactivation kinetics of tissue-specific KalTA4 activation, which led to the development of a self-maintaining effector strain “Kaloop.” This strain relates transient KalTA4 expression during embryogenesis via a KalTA4-mediated autoregulatory mechanism to live adult structures. We demonstrate its use by showing that the secondary octaval nucleus in the adult hindbrain is likely derived from *egr2b*-expressing cells in rhombomere 5 during stages of early embryogenesis. These data demonstrate prolonged and maintained expression by Kaloop-ing, a technique that can be used for permanent spatiotemporal genetic fate mapping and targeted transgene expression in zebrafish.

enhancer trap | fate mapping | Gal4-UAS | secondary octaval nucleus

Zebrafish has received increasing attention as a model organism in the fields of developmental biology, cell biology, and behavioral analysis, and thus in recent years, combinatorial genetics has been established for this model organism as well. So far the adaptation of the Gal4 system used in *Drosophila* has received the most attention (1, 2). Here, variants of the yeast transcriptional activator Gal4 are expressed to drive the expression of effector transgenes under the control of Gal4-specific binding sites called upstream activating sequences (UAS). When the Gal4 activator and UAS effector are expressed by different stable transgenic strains, the offspring of activator/effector crosses express a Gal4-dependent transgene in a tissue-specific manner. As activator and effector strains can be freely combined, a multitude of targeted transgene expression studies can be performed from a limited number of transgenic strains. Such transgenic zebrafish strains have already proven their usefulness in cell type-specific ablation studies, the mapping of neuronal circuits and the inhibition of neuronal activity in distinct neuronal populations (3–5).

To fully exploit the potential of Gal4 genetics in zebrafish we have tested a series of activator and effector combinations and have successively optimized their transactivation potential in zebrafish. Subsequently, a *Tol2* transposon mediated self-reporting Gal4 enhancer trap screen was performed to establish a collection of cell type-specific activator lines with characterized transactivation kinetics that will provide a useful resource for targeted transgene activation in zebrafish.

Recently, a combinatorial genetic fate mapping system was established in mouse to permanently label cells with reporter gene

expression under inducible temporal and cell type-specific control (6). The use of this technique changed long-standing views about cerebellar and hindbrain development (7–9). Such a genetic fate mapping system is not yet available in zebrafish, but a first crucial step toward it is the possibility to continuously express transgenes in specific cell types by combinatorial genetics, thereby reporting the transient activity of an enhancer within the subsequently formed adult structures. We thus generated a stable transgenic UAS effector strain, 4xKaloop, which continuously self-maintains a period of transient embryonic Gal4 expression to adulthood via an autoregulatory Gal4-mediated expression loop. By such “Kaloop-ing” we demonstrate that the secondary octaval nucleus in the adult zebrafish hindbrain is likely derived from rhombomere 5 during early embryogenesis. Thus, by establishing a combinatorial genetic system for continuously reporting transient gene activity, we have laid the foundation for non-invasive spatiotemporal fate mapping and life-long continuous transgene expression in zebrafish.

Results

Optimizing the Gal4 System for Zebrafish. To establish transgenic zebrafish with neuronal-specific expression of the transcriptional activator Gal4VP16 we injected linearized, previously established tub-GVP-Uunc vector (10) into 1-cell stage embryos. Transgenic F₁-founders showed strong ubiquitous expression (Fig. 1A) and failed to survive beyond embryonic day 10. Previously, attenuated repeats of the 13-amino acid core sequence of the VP16 transactivation domain have been shown to be similarly potent in transgene activation but displaying fewer promiscuous and likely toxic protein-protein interactions and are thus better tolerated by cells (11). In luciferase assays ($n = 3$) using a 5xUAS:luciferase construct as reporter GalTA2, TA3, and TA4 fusion proteins, produced the same order of activation potential (TA2>TA3>TA4) in zebrafish Pac2 fibroblasts than reported for human cells (11). As the reduction of the activation potential was less severe than in these human cells, we continued to work with the least active GalTA4 fusion protein (74% activity of full VP16 domain, Fig. 1B), reasoning that zebrafish would better tolerate further attenuations of this milder Gal4 activator.

To establish stable transgenic fish, a construct was designed carrying the notochord specific regulatory element of the *tiggy winkle hedgehog* (*twhh*) promoter to drive expression of GalTA4 (12). As an internal reporter cassette, 5 Gal4-binding sites (5xUAS) followed by the E1b basal promoter and the red fluorescent protein mRFP1 were used (1, 13). Stable transgenic embryos derived from injections of this linearized expression construct, TG5xR, were

Author contributions: M.D. and R.W.K. designed research; M.D. and R.W.K. performed research; M.D., M.F.W., and R.W.K. analyzed data; and M.D., M.F.W., and R.W.K. wrote the paper.

The authors declare no conflict of interest.

This article is a PNAS Direct Submission.

¹To whom correspondence should be addressed. E-mail: reinhard.koester@helmholtz-muenchen.de.

This article contains supporting information online at www.pnas.org/cgi/content/full/0903060106/DCSupplemental.

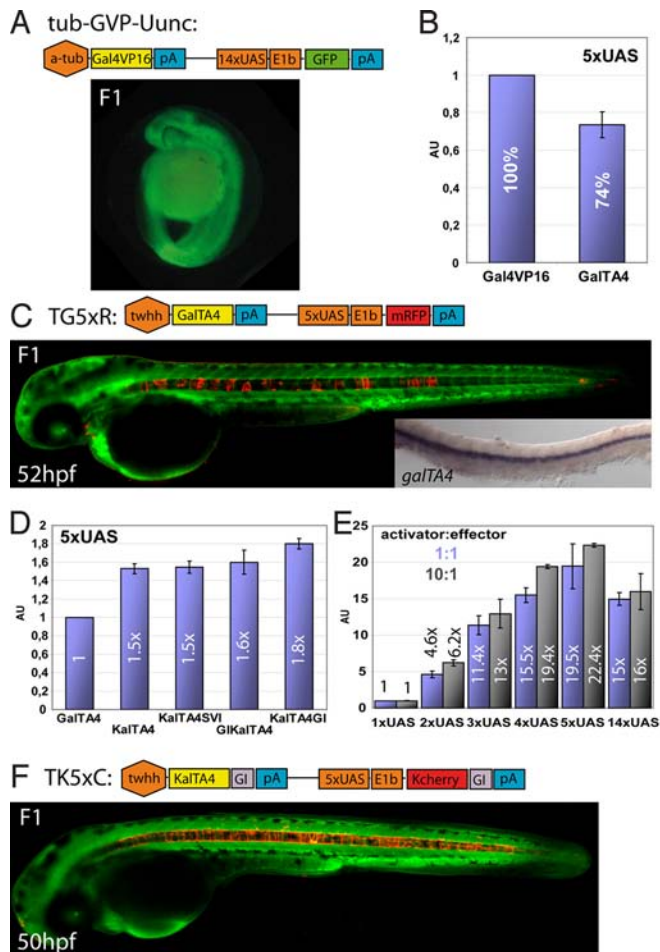


Fig. 1. Optimization of the Gal4 system in zebrafish. (A) Schematic representation of construct tub-GVP-Uunc (10) and transgenic F1 zebrafish embryos. (B) Comparison of Gal4VP16 (set as 100%) and GalTA4 activity in luciferase assays ($n = 3$, Pac2 fibroblasts) using a 5xUAS:luciferase construct. (C) Schematic representation of the TG5xR construct and transgenic F1 embryo. Inset: mRNA in situ hybridization of GalTA4 expression throughout the notochord. (D) Activation potentials of differently modified Gal4 activators as determined by luciferase assays ($n = 3$). The activity of GalTA4 was set as 1. (E) Effects of different numbers of Gal4 DNA binding sites using pCSKAlTA4GI and UAS-luciferase constructs (ratio 1:1 blue columns or 10:1 black columns) in luciferase assays ($n = 3$, 1xUAS:luciferase set as 1). (F) Schematic representation of the TK5xC construct and transgenic F1 embryo. Data are presented as mean \pm SEM. Embryos in C and F are counterstained with green Bodipy Ceramide.

viable, showed no malformations and could be raised to sexual maturity. Although they displayed notochord specific mRFP1 fluorescence, this expression was highly mosaic (Fig. 1C). Surprisingly, RNA in situ hybridizations revealed ubiquitous transcription of GalTA4 within the notochord (Fig. 1C, inset) suggesting a problem with GalTA4 translation. We thus altered the codon usage of GalTA4 ORF for efficient translation in zebrafish and added 5' the Kozak sequence GCCGCCACC (KalTA4). In addition, we tested intron sequences either from SV40 placed 3' to the ORF of KalTA4 (KalTA4SVI), or the rabbit β -globin intron used either in 5' or 3' position (GIKalTA4, KalTA4GI) (14, 15). Luciferase assays ($n = 3$ each) in zebrafish Pac2 fibroblasts revealed KalTA4GI as the most active variant, providing 1.8-fold luciferase activity compared to GalTA4 (Fig. 1D). Next, the effect of the number of Gal4-binding site repeats on KalTA4GI-mediated transgene activation was evaluated by luciferase assays. We found 2xUAS to be 4.6 \times stronger, 3xUAS 11.4 \times , 4xUAS 15.5 \times , and 5xUAS 19.5 \times stronger in

transgene activation than the minimal 1xUAS effector cassette (Fig. 1E). Intriguingly, 14xUAS did not show the maximal activation level, but was comparable to 4xUAS (similar results were found with a 10-fold excess of transfected activator constructs, black columns). These findings show that adding Gal4-binding sites in effector constructs increases transgene expression in a roughly linear manner, but suggest a threshold for the optimal number of Gal4-binding repeats. In addition, our data provide a quantitative basis for dose-varying transgene expression in zebrafish.

Next, we cloned an expression construct, TK5xC, in which translation-optimized KalTA4GI activated by the *twhh*-enhancer was followed by 5xUAS sites controlling the expression of KCherryGI (Kozak sequence 5' and rabbit β -globin intron 3' of ORF encoding the red fluorescent protein mCherry). In addition, this construct was flanked by inverted repeats of the *Tol2* transposon. Co-injection of TK5xC with *Tol2* transposase mRNA into 1-cell stage embryos resulted in the generation of transgenic strains, of which F2 founder embryos displayed bright red fluorescence throughout the notochord (Fig. 1F, 3 independent lines). This demonstrates that optimization of translation can efficiently counteract mosaic Gal4-dependent transgene expression (compare Fig. 1C with F) (16). Thus, for optimizing Gal4-dependent tissue-specific expression in zebrafish we have successfully balanced cellular concentrations of the activator (optimized translation) with its non-promiscuous activation strength (TA4 domain).

KalTA4 Enhancer Trapping. The *twhh* enhancer drives expression in notochord cells. The construction of TK5xC transgenic fish strains although revealed that this enhancer is sensitive to positional effects and does not result in any background expression (see database in *SI Text*). Based on this experimental observation we used this construct for systematic *Tol2* transposon-based KalTA4 enhancer trapping. To bias our screen toward detecting only strong positional effects only 1 instead of 5 Gal4-binding sites was used (construct: TK1xC, Fig. 2A). Screening of the F1 generation was performed between 24 and 36 hpf.

Out of 94 injected P₀ embryos that were raised to adulthood, 38 (40%) transmitted the transgene cassette to the next generation and gave stable transgenic strains with tissue specific mCherry fluorescence. These isolated enhancer trap strains showed no signs of malformation, retarded development or reduced viability.

For example, fish were recovered with expression in the midbrain and anterior hindbrain (Mü4380), specific rhombomeres (Mü4127), the diencephalon (Ga079), or the olfactory system (Mü4023, Fig. 2B). The latter (olf:KalTA4) was used for in situ hybridization, which showed that *kalTA4* mRNA was expressed bilaterally in both the olfactory epithelia and olfactory bulbs (Fig. 2C, black arrows and white asterisks). When the 14xUAS:lynGFP reporter construct (10) was injected into 1-cell stage embryos of this strain, mosaic membrane-targeted GFP expression confined only to KalTA4/mCherry expressing cells was observed (Fig. 2D). To further confirm that the isolated enhancer trap lines are capable of transactivating tissue specific transgene expression by combinatorial genetics, a 4xUAS-KGFPGI (Kozak-GFP-globin intron) transgenic strain was established and F1 heterozygous carriers were crossed with heterozygous KalTA4 enhancer trap carriers. All strains tested so far ($n = 15$) reliably activated GFP expression in a Mendelian ratio, but strictly confined to mCherry expressing cells (Fig. 2E), indicating that the isolated KalTA4 enhancer trap strains activate robust UAS-dependent expression in trans. Comparison of carrier crosses of 4xUAS-KGFPGI with either TK1xC (KalTA4, almost non-mosaic GFP) or TG5xR (GalTA4, highly mosaic GFP) fish revealed that the effects of KalTA4 optimization are also effective in trans. Moreover, homozygous carriers were established for several strains, which reliably passed on mCherry expression to 100% of the progeny when crossed to wild-type fish (Fig. 2G). This will be very useful for future studies where large numbers of

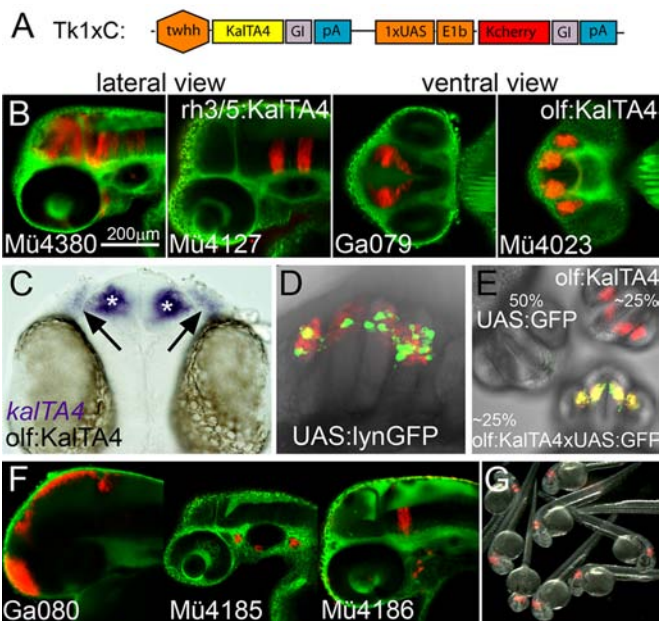


Fig. 2. KalTA4GI enhancer trapping. (A) Schematic representation of the TK1xC enhancer trapping construct. (B) Examples of transgenic Gal4 enhancer trap lines at 50 hpf (C) *kalTA4* mRNA expression (asterisk: olfactory bulb, arrow olfactory epithelium) in line olf:KalTA4. (D) Transactivation of lynGFP in Uly1 (10) injected olf:KalTA4 embryo. (E) KalTA4-mediated transactivation of GFP expression in offspring (26 hpf) from crosses of heterozygous olf:KalTA4 and 4xUAS-KGFPGI carriers. (F) Different expression patterns in F₁ embryos (50 hpf, lateral view) derived from the same P₀ founder fish. (G) Offspring of a rh3/5:KalTA4 homozygous carrier crossed to a wild-type fish. Note that all embryos display the characteristic mCherry fluorescence in rhombomeres 3 and 5. Embryos in B and F are counterstained with green Bodipy Ceramide.

transgene expressing offspring can be recovered without laborious screening for positive fish.

A number of P₀ or F₁ founders gave rise to fluorescent F₁ or F₂ offspring (F₂ at high non-Mendelian ratios) displaying different tissue specific expression patterns (for example, all 3 patterns in Fig. 2F were derived from the same P₀ founder), suggesting multiple independent transposon integrations and enhancer trap events in the germline of a single P₀ founder, as revealed by Southern blot analysis of F₁ offspring. In total, we have established 60 independent stable KalTA4 activator lines with tissue specific expression that remained stable over several generations (Figs. S1 and S2A). Most of their fluorescent expression patterns were recorded by laser scanning confocal microscopy and incorporated into a searchable database (Fig. S2B), providing a valuable resource for future studies by the zebrafish community. This systematic analysis indicated a bias of our enhancer trap approach for isolating central nervous system activator lines as 70% (42/60) of the identified transgenic strains showed expression in this tissue (Fig. S2C). In addition, when all analyzed fluorescent expression patterns were classified, 66% of these patterns could be clearly attributed to a neuroanatomically or neurodevelopmentally distinct cellular entity of the CNS (67/102, Fig. S2D). Currently the molecular reason for this bias is unclear and requires a detailed dissection of the regulatory *twhh* fragment. Intriguingly although a first bioinformatic analysis of all predicted transcription factor binding sites (MatInspector, Genomatix Software) in the *twhh* regulatory element revealed that more than 40% of these sites can be attributed to transcription factors that are expressed in neural tissue. Most expression patterns in the isolated enhancer trap lines were restricted to defined cell populations rather than being broadly distributed (Figs. S1 and S2D). This suggests that using a larger promoter element instead of a basal promoter to drive the Gal4

activator in the trapping construct allows one to suppress unwanted background expression and to restrict isolated trap lines to certain tissues of interest.

Based on the known flanking sequence of the *Tol2* transposon, we established nested inverse PCR for mapping integration sites (17). For several enhancer trap lines, the inserted KalTA4 expression cassette could be located near a zebrafish gene for which KalTA4 and mCherry expression closely reflected the endogenous expression (Table S1). Among them we identified an inserted trap cassette about 1.5 kb downstream of the zebrafish *egr2b* gene known as *krox20* in other vertebrates. Its prominent expression in rhombomere 3 and 5 during developmental stages of the hindbrain was reflected by mCherry fluorescence. We subsequently used this insertion to investigate the dynamic regulation of *kalTA4* expression and of UAS:transgenes as direct KalTA4 downstream genes by mRNA in situ analysis.

Like endogenous *egr2b* (Fig. S3A–C), *kalTA4* expression was initiated first in rhombomere 3 and next turned on in rhombomere 5 about 30 min later (Fig. S3D–F). Similarly, expression of both *egr2b* and *kalTA4* ceased during embryogenesis first in rhombomere 3 and about 2 h later in rhombomere 5 (18) (Fig. S3J–L) and was never detected again in these rhombomeres until adulthood (60, 84, 132 hpf, 4 months). Thus *kalTA4* expression in this strain closely reflects the endogenous expression dynamics of *egr2b*. Interestingly, we observed that *kalTA4* expression is initiated about 90 min after *egr2b* (compare Fig. S3A and D) and turns off approximately 4–6 h earlier compared to *egr2b* (18). This is probably due to the different distance of the inserted TK1C cassette to key regulatory elements. When heterozygous carriers of the rh3/5:KalTA4 and the 4xUAS-KGFPGI transgenic strains were crossed, the first transactivated *gfp* mRNA expression could be observed about 30–60 min later, closely reflecting *kalTA4* expression (Fig. S3G–I, note first visible *gfp* mRNA expression at 12 hpf). Thus, transactivation of a direct transcriptional target in zebrafish takes approximately 30–60 min. Termination of *kalTA4* mRNA expression between 21 and 23 hpf (Fig. S3J–L) resulted in a decrease of transactivated *gfp* mRNA transcription at about 27 to 29 hpf (Fig. S3M–O), reflecting the time needed for the degradation of the KalTA4 protein. This knowledge is important for planning transactivation experiments in which the lifetime of the transactivated protein (several days in the case of GFP) affects the full duration of ectopic expression.

KalTA4-Mediated Self-Maintenance of Cell Labeling. The detailed characterization of *kalTA4* expression and its restriction to rhombomere 3 and 5 during a short time window of embryonic development in the rh3/5:KalTA4 strain offered the chance for developing a self-maintaining KalTA4-mediated cell labeling technique that reports the spatiotemporal expression of KalTA4 to adult stages. For this, we generated a stable transgenic effector strain, 4xKaloop, that carries a bicistronic 4xUAS effector construct driving GFP expression as a reporter followed by a peptide backbone breaking T2A sequence, which mediates stoichiometric expression of KalTA4 (Fig. 3) (19). Once activated, this effector should continuously maintain its own expression by constantly providing the KalTA4 activator in a feedback loop. When heterozygous rh3/5:KalTA4 activator fish were crossed to carriers of the 4xUAS-KGFPGI and 4xKaloop effectors respectively, embryos displayed red and green fluorescence (*cis*- and *trans*-activation) strictly localized to rhombomeres 3 and 5 at 26 hpf (Fig. 3A–C and F–H). Fluorescence was maintained in both embryos by 3 dpf due to the stability of the fluorescent proteins. After 11 days, fluorescence in 4xUAS-KGFPGI control fish was significantly decreased and later vanished completely (Fig. 3D and E, *n* = 7). Strikingly, in the 4xKaloop carriers GFP continued to be expressed in 2 characteristic spatially separated stripes in the hindbrain through to adulthood (Fig. 3I and J, *n* = 10). This indicates that fluorescent protein expression in 4xKaloop fish is continuously maintained.

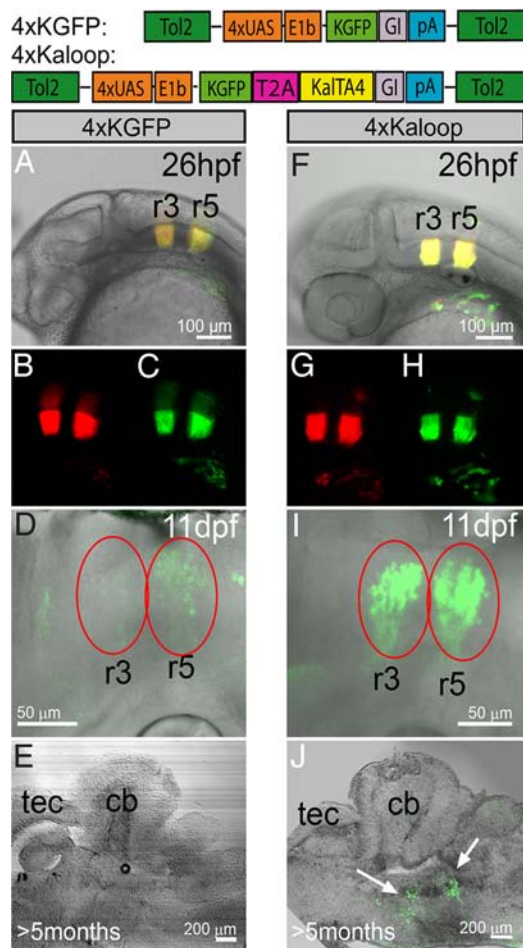


Fig. 3. Maintenance of rhombomeres 3/5 labeling in Kaloop fish. (A–E) Expression of GFP in rhombomeres 3/5 in offspring from a cross between rh3/5:KalTA4 and 4xUAS-KGFPGI or (F–J) rh3/5:KalTA4 and 4xKaloop carriers (schematic representation of effector constructs shown). (A–C, F–H) Expression of mCherry and transactivated GFP at 26 hpf. (D) At 11 hpf, GFP fluorescence (red ovals) is diminished in 4xUAS-KGFPGI carriers and (E) lost in the adult brain, while in 4xKaloop carriers (I, J) it is maintained in 2 clusters in the hindbrain until adulthood (white arrows). (E, J) Sagittal sections at 100 μ m, abbr.: see Fig. 4.

The Secondary Octaval Nucleus Is Likely Derived from Rhombomere 5.

Vibratome sections of adult rh3/5:KalTA4 \times 4xKaloop fish revealed that the stripes of GFP-expressing cell clusters in the hindbrain were not continuous, but displayed a mosaic arrangement of fluorescent cells (Figs. 3J and 4B, $n = 10$). Each time although the fluorescent cells labeled the same structures in the hindbrain but to a different extent. While this may be due to an inactivation of the 4xKaloop cassette in some cells of the total marked cell population, it serves to better reveal the detailed axonal projections of individual GFP-expressing neurons. However, it has to be kept in mind that a number of adults have to be analyzed to judge the extent of the cell population derived from the initial embryonic KalTA4-expression domain. First, to address the localization of the GFP-expressing cell clusters, we performed immunohistochemistry against GFP and choline acetyltransferase (ChAT) on sagittal sections through the hindbrain. These sections showed that GFP-expressing neurons in the anterior cluster were positioned caudally to the cholinergic secondary gustatory/viscerosensory nucleus (SGVN), which is derived from the embryonic cerebellar upper rhombic lip and positioned in the tegmental area of rhombomere 1 underneath the cerebellum. The posterior cluster of GFP-expressing neurons

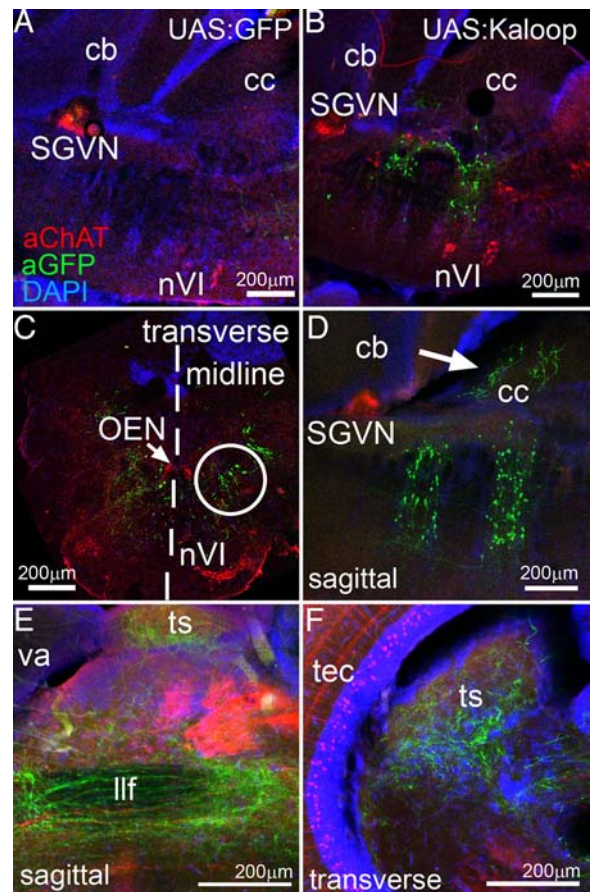


Fig. 4. Rh3/5-Kalooping identifies the secondary octaval nucleus (SON) as rhombomere 5-derived. Immunohistochemistry for GFP (green) and Cholinacetyltransferase (ChAT; red) on brain vibratome sections of adult zebrafish derived from crosses of (A) rh3/5:KalTA4 \times 4xKGFPGI and (B–F) rh3/5:KalTA4 \times 4xKaloop. All nuclei were counterstained with DAPI (blue). (A and B) Sagittal sections of the hindbrain. (C) Transverse section through the caudal GFP-expressing hindbrain region (r5) in B. (midline marked by dashed line). (D) Sagittal section (rostral is left) showing GFP-positive dendrites in the crista cerebellaris (white arrow). (E) Axons of GFP-positive neurons project through the midbrain into the (F) torus semicircularis. Note typical periventricular cholinergic cells in optic tectum. Abbr.: cb: corpus cerebelli, cc: crista cerebellaris, llf: lateral longitudinal fascicle, nVI: rostral and caudal abducens nuclei, OEN: octavolateralis efferent neurons, r: rhombomere, SGVN: secondary gustatory/viscerosensory nucleus, ts: torus semicircularis, tec: optic tectum, va: valvula cerebelli.

was positioned dorsally to the cholinergic abducens nuclei (Fig. 4B, nVI), which are localized in the ventral area of rhombomere 5-derived hindbrain tissue (20). Thus, the spatial arrangement of the GFP-expressing neurons in the adult hindbrain corresponds well to the embryonic expression pattern of *egr2b*. Transverse hindbrain sections revealed that the GFP-expressing neurons from rhombomere 5 were localized in a dorso-medial position with respect to the abducens nucleus (Fig. 4C, white circle) suggesting an identity as neurons of the secondary octaval nucleus [SON, (21)]. Neurons of this nucleus send dendrites into the crista cerebellaris and participate in transmitting directional acoustic information into the torus semicircularis of the midbrain, where this information converges at least in some species with sensory input from second-order projections of the lateral line (22, 23). Indeed, confocal sectioning revealed GFP-containing dendrites in the crista cerebellaris (Fig. 4D, white arrow) and axons leaving GFP-expressing neurons of the caudal GFP cell cluster in ventral directions and turning rostrally. These axonal projections passed ventrally to the tectum (Fig. 4E) into

the midbrain, where they turned dorsally to terminate in the central nucleus of the torus semicircularis just underneath the optic tectum (Fig. 4F).

To independently confirm the torus semicircularis as a target for axons of GFP-expressing neurons we performed retrograde tracing studies in adult rh3/5:KalTA4 × 4xKaloop fish. When axon terminals in the central nucleus of the torus semicircularis were labeled by focal rhodamine dextrane injections (Fig. S4A), the visualized afferents (Fig. S4B) were derived from the lateral longitudinal fascicle (llf), which descends caudally into the tegmentum and co-localized there with GFP-fluorescent axons (Fig. S4C, white arrow). At the level of both neuronal GFP clusters these retrogradely labeled axons traveled through ventral hindbrain regions (Fig. S4D), crossed the midline (Fig. S4E) and then turned dorsally (Fig. S4F) to eventually connect to their GFP-expressing somata (Fig. S4G–I) in the caudal cluster of rh3/5:KalTA4 × 4xKaloop fish.

The position and characteristic projection of GFP-expressing neurons in the caudal hindbrain cluster in each of the analyzed adult rh3/5:KalTA4 × 4xKaloop fish confirm their identity as neurons of the SON. Furthermore, these findings suggest that SON neurons in the adult hindbrain are derived from *egr2b*-expressing progenitors in rhombomere 5 during early stages of embryonic hindbrain development (before 29 hpf). Thus, genetic approaches based on the 4xKaloop effector fish may serve to permanently mark a period of transient transgene expression and provide a promising entry point for the development of genetic fate mapping technology with precise tissue specific and temporal control based on combinatorial KalTA4-UAS genetics.

Discussion

Systematic Optimization of Gal4-UAS Genetics in Zebrafish. Based on our previous experience with Gal4 expression in zebrafish (10) we have aimed to systematically optimize this system for stable transgenic combinatorial genetics. By choosing the minimal but potent TA4 core region from the herpes simplex virus VP16 transactivation domain, optimizing the codon usage of the Gal4 DNA-binding domain for use in zebrafish, adding a Kozak sequence and identifying the 3 prime region of the KalTA4 coding sequence as the best position for a globin intron, we optimized the expression and function of a Gal4-derived transactivator. KalTA4GI produced robust non-variegated and non-deleterious transactivation, which could be further enhanced by using the more active TA3 or TA2 transactivation domains (11). As the established KalTA4-UAS vectors were adapted for a vertebrate model organism, they should provide similar results in other vertebrates including mammals, where Gal4-genetics have not gained much attention so far (24). In addition, we showed that the expression levels of transactivated transgenes could be varied stepwise from minute (1xUAS) to intense overexpression concentrations (5xUAS) by increasing the numbers of UAS sites. This finding offers the chance for studying dose-dependent effects of transgene expression and for adjusting transgene expression to physiological levels. For example, it should be possible to tailor disease models for either slow or fast progressing phenotype development.

Enhancer Trapping with Self-Reporting Optimized KalTA4 Activator. We have used the optimized KalTA4-UAS genetic system to provide a collection of cell type-specific self-reporting KalTA4 activator lines with the help of a *Tol2* transposon enhancer trap screen. These lines themselves provide a valuable resource for characterizing the dynamics of the respective fluorescent tissues. Moreover, these red fluorescent strains can be readily combined with the numerous existing GFP-expressing zebrafish lines. Further, the red fluorescent cell population simultaneously expresses KalTA4, and so can be genetically manipulated either through crossing to fish stably expressing transgenes under UAS

control or through the injection of embryos with UAS constructs for mosaic analysis within a few days (10, 19).

All tissue-specific KalTA4 activator lines tested provided reliable robust transactivation when crossed to a 4xUAS-KGFPGI reporter strain and showed no expression in other tissues beside the intrinsic notochord activity of the *twhh* promoter. This notochord expression was weak and often appeared only at 2–3 dpf. As we have used only a single UAS site for reporting an enhancer trap event and as the trapped expression was usually much stronger than the weak notochord expression in these strains, we likely selected for strong position effects that provide sufficient levels of KalTA4 expression for robust transactivation.

Our thorough characterization of KalTA4-mediated transactivation kinetics will allow for better planning of combinatorial genetic experiments. We demonstrated that *kalTA4* mRNA expression was initiated with a lag time as compared to the endogenous expression of a gene nearby the insertion site. Of note however is our observation that the positional effect of the trapped enhancer acts not only on KalTA4 expression, but it also directly activates basal promoter driven *mcherry* transcription. Due to this additive effect of the positional effect and KalTA4-activation, mCherry expression is higher when activated in *cis* from the self-reporting cassette as compared to activation in *trans*. Thus fluorescence from 1xUAS-mCherry (*cis*) and GFP (4xUAS-KGFPGI reporter strain, *trans*) becomes visible about the same time. First mCherry fluorescence in our transgenic strains can therefore serve as a rough indicator for the onset of activity from a 4xUAS-transgene cassette activated by KalTA4 in *trans*. The collection of KalTA4 activator strains annotated in an image database searchable for tissue-specific mCherry expression patterns should provide a helpful resource for targeted gene expression studies in zebrafish.

We demonstrated that our KalTA4 activator strains could be bred to homozygosity. When these activator fish are crossed with homozygous UAS-effector strains, all of the offspring express the transgene of interest. This makes KalTA4-UAS genetics suitable for high-throughput *in vivo* approaches such as small compound screening in neurodegenerative disease models (25).

Self-Maintenance of Transgene Expression by a KalTA4-Dependent Feedback Loop. A challenge in developmental biology is to relate embryonic gene expression to adult functional structures. We have developed the 4xKaloop effector strain, which provides a self-maintaining KalTA4-mediated feedback expression loop for propagating activator activity and reporter fluorescence until adulthood. When combined with the collection of available activator strains, this single effector line could serve to map the expression activity of many genetic loci to adult tissues and organs. We have demonstrated this reporting ability of the Kaloop strain for the *krox20/egr2b* locus, which in zebrafish shows highly conserved expression restricted to rhombomeres 3 and 5 during early embryogenesis (18). The 2 stripes of GFP-expressing cells in adult rh3/5:KalTA4 × 4xKaloop fish, spatially distant from one another and to the rhombomere 1 derived SGVN, resemble the organization of the *egr2b* expression in the embryonic brain. This suggests a preservation of segmental hindbrain organization in sequential rostro-caudal neuromeres in zebrafish, similar to the frog and chick brain (26, 27). In addition, histological analysis, tracking of axonal projections and retrograde tracing of axons derived from neurons of the posterior GFP-expressing hindbrain stripe revealed that neurons of the secondary octaval nucleus are likely derived from cells of rhombomere 5 expressing *egr2b* during the first day of embryonic development. This nucleus is part of the ascending acoustic neuronal network in teleosts (22), but its developmental origin has remained unclear so far.

Expression of GFP in both adult hindbrain stripes was found

to be mosaic although during the first 2 weeks of development GFP expression was continuous and hindbrain organization is rather manifest by this time. This makes a migration of cells into or out of the expression stripes resulting in a dilution of the GFP expression pattern unlikely. As the degree of mosaic labeling of SON neurons varied in each analyzed specimen we do not think that only a specific subset of SON neurons is derived from the embryonic *egr2b* expression domain. We rather favor the explanation that GFP expression is prolonged but not maintained to the same degree in all cells derived from rhombomeres 3 and 5. In many cases, such a prolongation of reporter expression up to at least 4 weeks may be sufficient to identify the final fate of cells in the juvenile brain. It is important although to analyze several adult double transgenic carriers to fate map all adult structures that are derived from a transient tissue-specific embryonic KalTA4 expression domain in the activator strain.

At the moment, the cause for the mosaic inactivation of the 4xKaloop cassette is unclear, but it has been suggested that epigenetic events could inactivate oligomeric UAS repeats of multiple UAS sites (16). Alternatively, fewer amounts of KalTA4 from the Kaloop cassette may be produced than are needed to achieve a steady state level of KalTA4 activator concentration. Solutions to either explanation could potentially be achieved by further optimization of the Kaloop effector through the substitution of the 4xUAS with fewer UAS-sites (to reduce potential epigenetic inactivation) and of the KalTA4 with the stronger KalTA3 or KalTA2 activators (to counterbalance reduced expression from fewer UAS-sites). Our quantification of the effect of UAS numbers and different activation domains on KalTA-dependent transactivation will help to guide this optimization process. Given that GFP expression in the secondary octaval nucleus lasted for more than half a year although the initial enhancer-driven KalTA4 in the rh3/5:KalTA4 line is only active until 29 hpf (Fig. S3L and O), such further optimization promises to be feasible.

To further exploit continuous expression mediated by Kalooping and to allow for spatiotemporal fate mapping of KalTA4-expressing cells into adulthood, temporal control over KalTA4 feedback loop activation should be developed as a next step. Recent progress in establishing inducible Gal4 or recombinase activity in zebrafish (28,

29) promises that spatiotemporal Kalooping could be established in a straight-forward manner, which will provide a powerful system for precise genetic control for functional in vivo analysis in zebrafish.

Materials and Methods

Microscopy. Counterstaining of cellular membranes in living zebrafish embryos was performed using 0,001% BODIPY FL C₅ceramide (Invitrogen)/30% Danieau over night before image acquisition. For image recording embryos were dechlorinated and embedded in 1.2% ultra low melting agarose/30% Danieau (30). Images of living embryos were recorded using a Zeiss LSM510 confocal microscope. Images of in situ hybridizations were recorded using an Axioplan2 microscope equipped with an AxioCam HRC and Axiovision 4.5 software (all Zeiss).

Microinjection and Generation of Transgenic Zebrafish Lines. Zebrafish embryos were injected with Tol2 mRNA and the respective Tol2 based construct (25 ng/ μ L each, 1.5 nL) at 1-cell stage. Fluorescent embryos were raised to adulthood and crossed for analyzing germline transmission by screening the offspring for tissue-specific expression.

Immunohistochemistry. For immunohistochemistry brains were dissected from 3 month or older adult zebrafish and fixed in 4% PFA over night. After washing with PBS, brains were embedded in 2% agarose/PBS for vibratome sectioning. One hundred-micrometer brain slices were cut and fixed on slides for immunohistochemical analysis. After blocking in 5%BSA in PBS/0.2% Triton X-100 for 1 h at room temperature slides were incubated with the primary chicken α -GFP (1:500) (Jackson ImmunoResearch) and goat α -ChAT (1:100) (Chemicon) antibodies in 5% BSA in PBS/0.2% Triton X-100 at 4 °C over night. After several washes in PBS/0.2% Triton X-100 slides were incubated with the secondary α -goat Alexa546 (1:100, Invitrogen) and α -chicken FITC (1:100, Jackson ImmunoResearch) antibodies in 5% BSA in PBS/0.2% Triton X-100 at 4 °C over night. Nuclei were stained using DAPI (10236276001, 1 μ g/ μ L, Roche) and slides were mounted in Aqua Polymount (Polysciences Inc.).

ACKNOWLEDGMENTS. We thank Olga Lositsky, Vanessa Bednarz, Benjamin Wolf, Yuan Yuan Chu, Mark Schibler, Nina Dedic, Enrico Kühn, and Petra Hammerl for excellent technical assistance and animal care. We are grateful for obtaining vectors from Elwood Linney, Christoph Winkler, Adam Amsterdam, Atsushi Miyawaki, and Roger Tsien. We thank Ralf Kühn, Jan Deussing, and Jennifer Hocking for carefully commenting on the manuscript. We acknowledge the financial support of this study by a BioFuture Award Grant (R.W.K.) of the German Ministry of Education and Research (BMBF 0311889), and a Fellowship of the Studienstiftung des deutschen Volkes (M.D.), and the Graduate School for Systemic Neurosciences (L.M.U.-Munich).

- Scheer N, Campos-Ortega JA (1999) Use of the Gal4-UAS technique for targeted gene expression in the zebrafish. *Mech Dev* 80:153–158.
- Deiters A, Yoder JA (2006) Conditional transgene and gene targeting methodologies in zebrafish. *Zebrafish* 3:415–429.
- Davison JM, et al. (2007) Transactivation from Gal4-VP16 transgenic insertions for tissue-specific cell labeling and ablation in zebrafish. *Dev Biol* 304:811–824.
- Scott EK, et al. (2007) Targeting neural circuitry in zebrafish using GAL4 enhancer trapping. *Nat Methods* 4:323–326.
- Asakawa K, et al. (2008) Genetic dissection of neural circuits by Tol2 transposon-mediated Gal4 gene and enhancer trapping in zebrafish. *Proc Natl Acad Sci USA* 105:1255–1260.
- Joyner AL, Zervas M (2006) Genetic inducible fate mapping in mouse: Establishing genetic lineages and defining genetic neuroanatomy in the nervous system. *Dev Dyn* 235:2376–2385.
- Rodriguez CI, Dymecki SM (2000) Origin of the precerebellar system. *Neuron* 27:475–486.
- Landsberg RL, et al. (2005) Hindbrain rhombic lip is comprised of discrete progenitor cell populations allocated by Pax6. *Neuron* 48:933–947.
- Machold R, Fishell G (2005) Math1 is expressed in temporally discrete pools of cerebellar rhombic-lip neural progenitors. *Neuron* 48:17–24.
- Köster RW, Fraser SE (2001) Tracing transgene expression in living zebrafish embryos. *Dev Biol* 233:329–346.
- Baron U, Gossen M, Bujard H (1997) Tetracycline-controlled transcription in eukaryotes: Novel transactivators with graded transactivation potential. *Nucleic Acids Res* 25:2723–2729.
- Du SJ, Devoto SH, Westerfield M, Moon RT (1997) Positive and negative regulation of muscle cell identity by members of the hedgehog and TGF- β gene families. *J Cell Biol* 139:145–156.
- Campbell RE, et al. (2002) A monomeric red fluorescent protein. *Proc Natl Acad Sci USA* 99:377–382.
- Amsterdam A, Lin S, Hopkins N (1995) The Aequorea victoria green fluorescent protein can be used as a reporter in live zebrafish embryos. *Dev Biol* 171:123–129.
- Perz-Edwards A, Hardison NL, Linney E (2001) Retinoic acid-mediated gene expression in transgenic reporter zebrafish. *Dev Biol* 229:89–101.
- Halpern ME, et al. (2008) Gal4/UAS transgenic tools and their application to zebrafish. *Zebrafish* 5:97–110.
- Kawakami K, et al. (2004) A transposon-mediated gene trap approach identifies developmentally regulated genes in zebrafish. *Dev Cell* 7:133–144.
- Oxtoby E, Jowett T (1993) Cloning of the zebrafish *krox-20* gene (*krox-20*) and its expression during hindbrain development. *Nucleic Acids Res* 21:1087–1095.
- Provost E, Rhee J, Leach SD (2007) Viral 2A peptides allow expression of multiple proteins from a single ORF in transgenic zebrafish embryos. *Genesis* 45:625–629.
- Mueller T, Vernier P, Wullmann MF (2004) The adult central nervous cholinergic system of a neurogenetic model animal, the zebrafish *Danio rerio*. *Brain Res* 1011:156–169.
- Wullmann MF, Rupp B, Reichert H (1996) in *Neuroanatomy of the Zebrafish Brain: A Topological Atlas*. (Birkhäuser, Basel).
- McCormick CA, Hernandez CV (1996) Connections of the octaval and lateral line nuclei of the medulla in the goldfish, including the cytoarchitecture of the secondary octaval population in goldfish and catfish. *Brain Behav Evol* 47:113–138.
- Fame RM, Brajon C, Ghysen (2006) A second-order projection from the posterior lateral line in the early zebrafish brain. *Neural Dev* 1:4.
- Ray P, et al. (2002) Noninvasive quantitative imaging of protein-protein interactions in living subjects. *Proc Natl Acad Sci USA* 99:3105–3110.
- Paquet D, et al. (2009) A novel Tau transgenic zebrafish model for in-vivo research and drug discovery. *J Clin Invest*
- Wingate RJ, Lumsden A (1996) Persistence of rhombomeric organization in the post-segmental hindbrain. *Development* 122:2143–2152.
- Straka H, Baker R, Gilland E (2006) Preservation of segmental hindbrain organization in the adult frogs. *J Comp Neurol* 494:228–245.
- Esengil H, Chang V, Mich JK, Chen JK (2007) Small-molecule regulation of zebrafish gene expression. *Nat Chem Biol* 3:154–155.
- Hans S, Kaslin J, Freudenreich D, Brand M (2009) Temporally-controlled site-specific recombination in zebrafish. *PLoS ONE* 4:e4640.
- Distel M, Köster RW (2007) In vivo time-lapse imaging of zebrafish embryonic development. *CSH Protocols* 2:doi:10.1101/pdb.prot4816.

Supplementary Materials and Methods

Distel et al. 10.1073/pnas.0903060106

SI Text

Maintenance of Fish. Raising, spawning, and maintaining of zebrafish were performed as described (1, 2). All experiments were conducted according to the guidelines reviewed by the Ethics Committee of the Helmholtz Zentrum München.

Construction of Vectors. *pCR2xUAS*, *pCR3xUAS*, *pCR4xUAS*. Two, 3, and 4 repeats of the Gal4-binding site (CGGAGTACTGTCCTC-CGAG) containing 5' 1 *Pst*I and 3' 1 *Xba*I restriction site were synthesized by Entelchon GmbH and were provided in the pCR-Script Amp vector (Stratagene).

pSK5xUASE1b. pBSUASE1bNotch:intra (3) was *Eco*RI-digested and religated. The 5xUASE1bTATA fragment from this vector was isolated by a *Pst*I/*Eco*RI digest and cloned into a *Pst*I/*Eco*RI-digested pBluescript SK- (pBSK, Stratagene).

pSK1xUASE1b. pSK5xUASE1b was digested with *Not*I/*Xba*I to replace the 5 UAS repeats with a single UAS site using the annealed oligos GGCCGAGATCTCTGCAGCGGAGTACT-GTCTCCGAGT and CTAGACTCGGAGGACAGTACTC-CGCTGCAGAGATCTGC.

pSK1xUASFFL, **pSK5xUASFFL.** To clone firefly (*Photinus Pyralis*) luciferase under control of 1x or 5xUASE1b respectively the ORF of the firefly luciferase gene was isolated from pPLLUCII (kind gift of J. Graw) by a *Xho*I/*Hind*III digest and cloned into *Xho*I/*Hind*III-digested pSK1xUASE1b or pSK5xUASE1b respectively.

pSK2xUASFFL, **pSK3xUASFFL**, and **pSK4xUASFFL.** pCR2xUAS, pCR3xUAS, and pCR4xUAS were digested with *Xba*I/*Apa*I. A fragment containing the basal promoter E1b (3) was isolated from pSK5xUASlzkmRPF by a *Xba*I/*Apa*I digest and cloned behind the 2x, 3x, and 4xUAS sites respectively. Subsequently, the 5xUASE1b-fragment of vector pSK5xUASE1bFFL was replaced by 2x, 3x, and 4xUASE1b-fragments, which were isolated by a *Pst*I/*Hind*III digest from the respective 2x, 3x, and 4xUASE1b vectors.

14xUASE1bFFL. The ORF coding for firefly (*Photinus Pyralis*) luciferase was isolated from pPLLUCII (kind gift of J. Graw) by a *Xho*I/*Sal*I digest and cloned downstream of the 14xUASE1b sites of the pBSK- vector used to generate the UG vector (4).

SVTkRenilla. The SV40 enhancer/promoter fragment in front of the ORF coding for Renilla (*Renilla Reniformis*) luciferase of the pRL-SV40 vector (Promega) was removed by a *Bgl*III (Klenow blunted)/*Hind*III digest and replaced by the SVTk enhancer/promoter element from the *Xba*I (Klenow blunted)/*Hind*III-digested pSVtklacZ vector (kind gift of Christoph Winkler).

pCSGalTA2, **3**, and **4.** Gal4 activator plasmids with minimal VP16 transactivation domains were generated by removing the VP16 domain from the CMV-GVP vector (4) by a *Xba*I (Klenow blunted)/*Eco*RI digest and inserting the TA2, TA3, and TA4 transactivation domains from the ptTA2, 3, and 4 vectors (Clontech catalog K6243–1) as a *Sma*I/*Ppu*MI (Klenow-blunted) fragment.

pCSKalTA4. The Gal4 DNA binding domain from yeast was resynthesized as a *Eco*RI/*Sal*I fragment to remove potential methylation sites, inhibitory secondary mRNA structures and to optimize the codon usage for expression in zebrafish by Entelchon GmbH, Regensburg, Germany starting with a GCCGC-CACC Kozak sequence for efficient ribosome binding. The resulting *Eco*RI/*Sal*I Kal fragment was inserted into *Eco*RI/*Sal*I-digested pCSGalTA2, 3, and 4 plasmids to replace the yeast Gal4 DNA-binding domain.

pCSGIKalTA4. The rabbit β -globin intron was isolated from the pXIG vector (kind gift of Adam Amsterdam) by a *Bam*HI/*Sal*I digest and inserted as Klenow-blunted fragment into the *Eco*RI (Klenow blunted)-digested pCSKalTA4 vector.

pCSKalTA4GI. The rabbit β -globin intron from the pXIG vector was subcloned as a *Sal*I/*Xba*I fragment into the pBluescript SK-vector (Stratagene). From here the intron was isolated by a *Bam*HI (Klenow blunted)/*Sal*I digest and inserted into the *Xho*I/*Sna*BI-digested pCSKalTA4 downstream of KalTA4.

pCSKalTA4SVI. The SV40 intron was isolated by a *Spe*I (Klenow blunted)/*Not*I digest from pWI x/b (kind gift of Ava Udvadia and Elwood Linney) and cloned downstream of KalTA4 into the *Xho*I (Klenow blunted)/*Not*I-digested pCSKalTA4 vector.

TG5xR (pBScel-twvhGalTA45xUASmRFP). A *Not*I-expression cassette of 5xUAS-EIb driving the expression of the mRFP fluorescent protein was cloned behind a *Not*I-digested expression cassette of the notochord-specific *twhh* promoter element (5) driving the expression of GalTA4 in pBSK-2xSce [see also Tg(*twhh*:G-UmRFP) (6)].

TK1xC (pTol2Sce-twvhKalTA4GI1xUASKcherryGI). The MCS of the pBluescript SK- vector (Stratagene) with 2 flanking I-*Sce*I sites was inserted into the *Nde*I (Klenow blunted)-digested pTol2000 vector (7) to result in the plasmid pTol2000Sce. A *Not*I-expression cassette of 1xUAS-EIb driving the expression of the mCherry fluorescent protein flanked 5' by the Kozak sequence GCCGCCACC and 3' by the rabbit β -globin intron was cloned behind a *Not*I-digested expression cassette of the notochord-specific *twhh* promoter element (5) driving the expression of KAITA4GI in pBSK-2xSce. This entire cassette could be released by a I-*Sce*I restriction digest and was inserted into pTol2000-Sce.

TK5xC (pTol2Sce-twvhKalTA4GI5xUASKcherryGI). A *Not*I-expression cassette of 5xUAS-EIb driving the expression of the mCherry fluorescent protein flanked 5' by the Kozak sequence GCCGC-CACC and 3' by the rabbit β -globin intron was cloned behind a *Not*I-digested expression cassette of the notochord-specific *twhh* promoter element (5) driving the expression of KalTA4GI in pBSK-2xSce. This entire cassette was released by a I-*Sce*I restriction digest and was inserted into pTol2000-Sce.

pCSGI. A *Bam*HI/*Sal*I Klenow-blunted fragment containing the rabbit β -globin intron was inserted into the *Sna*BI site of the pCS2+ vector (8).

pTolmini. This plasmid was generated by inserting minimized inverted repeats recognized by the *Tol2* transposase amplified from vector pTol2000 (9) using primers:

473: ATTGGTACCCAGAGGTGTAAAGTACTTGAGTA-ATTTTAC and

474: ATACTCGAGCCGGCCCAAGTGATCTCCAA and

475: ATTCTCGAGATTAGATCTAATACTCAAGTACA-ATTTTAATGGAG and

476: ATTCGCGGCAGAGGTGTAAAAAGTACTCAA-AAAT

into *Asp*-718/*Sac*II-digested pBluescript SK- (Stratagene). A MCS from the pBluescript SK- vector flanked by 2 I-*Sce*I sites was inserted in the *Xho*I (Klenow blunted) site between the *Tol2* inverted repeats to allow for the I-*Sce*I-mediated insertion of fragments of interest.

4xKGFp (pTolmini-4xUASKGFPGI). GFP was amplified from pEGFP-N3 (Clontech) using primers

204: TACTCGAGTTACTTGTACAGCTCGTCCAT and
620: TATGAATTCCGCCACCATTGGTGAGCAAGGGC-GAGGAGCTGTTTAC and inserted in the *Eco*RI/*Xho*I site in

front of the rabbit β -globin intron of pCSGI. The KGFPpA fragment was isolated from this vector by a *EcoRI/Asp-718* digest and cloned into *EcoRI/Asp-718* digested pSK4xUASFFL to replace the luciferase. The resulting 4xUASKGFPpA-fragment was isolated as a *NotI* fragment and cloned into *NotI*-digested pTolmini.

4xKaloop (pTolmini-4xUASKGFP-T2A-KalTA4GI): A bicistronic T2A-peptide linked expression cassette (10) of GFP-T2A-KalTA4 flanked 5' by the Kozak sequence GCCGCCACC in the pCS-GI vector was cloned as a *EcoRI/Asp-718* fragment behind 4xUASEIb in pBSK. Subsequently, the entire 4xUASEIb-KGFP-T2A-KalTA4-GI was inserted into pTolminiSce as a *NotI* fragment.

Further details of cloning procedures are available on request.

Luciferase Assays. Zebrafish Pac2 embryonic fibroblasts (11, 12) were transfected using the "Nanofectin" transfection kit (PAA) according to the manufacturers' specifications. Concentrations for determining optimized activator activities were 8 ng/ μ L activator plasmids and 80 ng/ μ L effector plasmids. Concentrations used to determine the activity of different numbers of UAS repeats were either both 80 ng/ μ L or 80 ng/ μ L for activator and 8 ng/ μ L for effector plasmids. Luciferase assays were performed using the "Dual Luciferase Reporter Assay System" (Promega). As reporter firefly (*Photinus Pyralis*) luciferase was cloned downstream of the respective 1, 2, 3, 4, 5, or 14xUAS:E1b sequences. Renilla (*Renilla Reniformis*) luciferase under control of the SVTk promoter was used as control for transfection efficacy. Luciferase assays were performed in 96-well plates with 3 replicates per experiment and analyzed by a "Microplate Luminometer Orion" using the simplicity 2.0R1 software (both Berthold Detection Systems). Obtained light intensities from firefly luciferase were corrected for transfection efficacies and background in the following way:

$$\begin{aligned} V_{\text{firefly}} - MV_{\text{Luciferase untransfected cells}} / (V_{\text{Renilla}} - \\ MV_{\text{Renilla untransfected cells}}) &= V_{\text{firefly E corrected}} \\ V_{\text{firefly E corrected}} - MV_{\text{pCS+XxUAS}} &= V_{\text{firefly B/E corrected}} \\ V_{\text{firefly}} &= \text{measured firefly signal} \\ V_{\text{Renilla}} &= \text{measured Renilla signal} \\ MV_{\text{Renilla untransfected cells}} &= \text{mean value of measured Renilla} \\ &\text{signal of non-transfected cells} \\ MV_{\text{Luciferase untransfected cells}} &= \text{mean value of measured firefly} \\ &\text{signal of non-transfected cells.} \\ MV_{\text{pCS} + \text{XxUAS}} &= \text{Mean of transfection efficacy corrected} \end{aligned}$$

signal of cells transfected with pCS without Gal4 activator and respective 1, 2, 3, 4, 5, or 14xUAS vector

DNA Extraction and Inverse Nested PCR. To determine the integration sites in the transgenic zebrafish KalTA4 enhancer trap strains genomic DNA (gDNA) was purified from a single transgenic zebrafish embryo (around 5 dpf) using the gDNA wizard kit (Promega) according to the manufacturer's instructions. gDNA was digested using the restriction enzymes *AluI*, *HaeI* (both Fermentas) and *MboI* (NEB) respectively and self-ligated after heat-inactivation of the restriction enzymes by adding T4 DNA ligase (Fermentas). After ligation gDNA was ethanol precipitated and resuspended in water. Inverse nested PCR was performed for 5' and 3' ends of the enhancer trap construct using the primer pairs Tol2-5F1/Tol2-5R1 and Tol2-3F1/Tol2-3R1 for the first round of PCR

Tol2-5F1: AGTACTTTTTACTCCTTACA

Tol2-5R1: GTATTGATTTTTAATTGTACTCAAG

Tol2-3F1: TTTACTCAAGTAAGATTCTAG

Tol2-3R1: CTCCATTAATAATTGTACTTGA

and Tol2-5F2/Tol2-5R2 respectively Tol2-3F2/Tol2-3R2 as primers for the second round of the nested PCR.

Tol2-5F2: CTCCTTACAATTTTTATTACAGTC

Tol2-5R2: CTCAAGTAAAGTAAAAATCCCG

Tol2-3F2: ACTTGACTTTTCACTTGAGTA

Tol2-3R2: GCAAGAAAGAAAATAGAGA

Both cycles were carried out with Taq Polymerase (Fermentas) and gDNA from the respective line. PCR cycles were both: 94 °C 2', 35 \times (94 °C 30," 52 °C 45," 72 °C 1.5'), 72 °C 10', 4 °C Hold). PCR products were either subcloned or sent directly for sequencing. Sequences were blasted against the zebrafish genome using the Ensembl database (http://www.ensembl.org/Danio_rerio/Info/Index).

Rhodamine Dextran Retrograde Labeling. Adult zebrafish brains were dissected in PBS and fixed onto sylgard plates (World Precision Instruments) in DMEM (Invitrogen) using insect pins. After dissection, the tectum was removed to inject dextran tetramethylrhodamine (MW: 3000 kDa, Invitrogen) into the central nucleus of the torus semicircularis. After injection brains were perfused with CO₂ for 5 h to allow for retrograde transport of the rhodamine dextran. Afterward, brains were fixed in 4% PFA over night and vibratome sectioned at 100- μ m thickness.

1. Kimmel CB, Ballard WW, Kimmel SR, Ullmann B, Schilling TF (1995) Stages of embryonic development of the zebrafish. *Dev Dyn* 203:253–310.
2. Westerfield M (1995) in *The Zebrafish Book* (University of Oregon Press, Eugene, OR).
3. Scheer N, Campos-Ortega JA (1999) Use of the Gal4-UAS technique for targeted gene expression in the zebrafish. *Mech Dev* 80:153–158.
4. Köster RW, Fraser SE (2001) Tracing transgene expression in living zebrafish embryos. *Dev Biol* 233:329–346.
5. Du SJ, Devoto SH, Westerfield M, Moon RT (1997) Positive and negative regulation of muscle cell identity by members of the hedgehog and TGF- β gene families. *J Cell Biol* 139:145–156.
6. Babaryka A, Kühn E, Köster RW (2009) In vivo synthesis of meganuclease for generating transgenic zebrafish. *J Fish Biol* 74:452–457.
7. Kawakami K, et al. (2004) A transposon-mediated gene trap approach identifies developmentally regulated genes in zebrafish. *Dev Cell* 7:133–144.
8. Rupp RAW, Snyder L, Weintraub H (1994) Xenopus embryos regulate the nuclear localization of Xmyod. *Genes Dev* 8:1311–1323.
9. Urasaki A, Morvan G, Kawakami K (2006) Functional dissection of the Tol2 transposable element identified the minimal cis-sequence and a highly repetitive sequence in the subterminal region essential for transposition. *Genetics* 174:639–649.
10. Provost E, Rhee J, Leach SD (2007) Viral 2A peptides allow expression of multiple proteins from a single ORF in transgenic zebrafish embryos. *Genesis* 45:625–629.
11. Amsterdam A, et al. (1999) A large-scale insertional mutagenesis screen in zebrafish. *Genes Dev* 13:2713–2724.
12. Chen W, Burgess S, Golling G, Amsterdam A, Hopkins N (2002) High-throughput selection of retrovirus producer cell lines leads to markedly improved efficiency of germ line-transmissible insertions in zebra fish. *J Virol* 76:2192–2198.

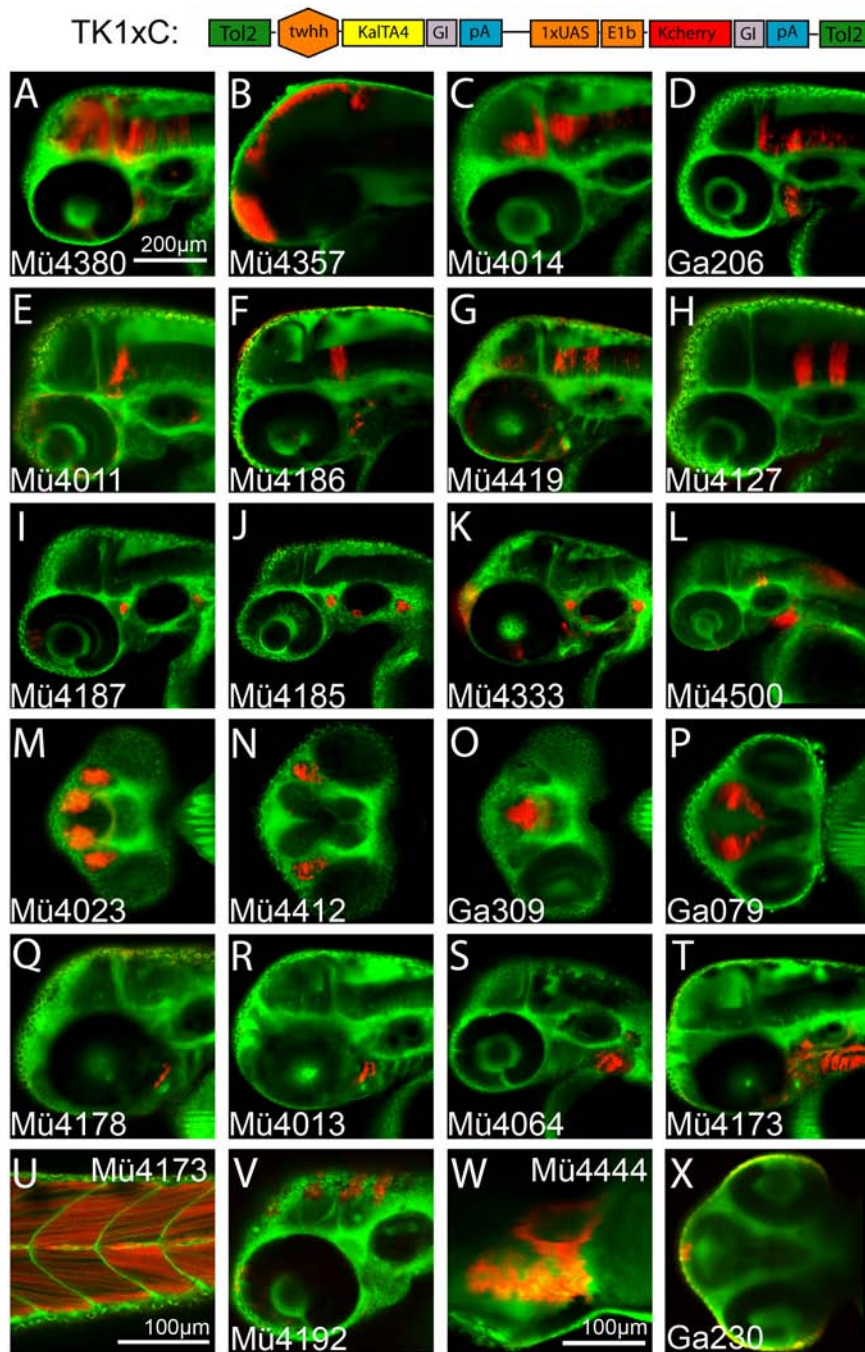


Fig. S1. Transgenic zebrafish KalTA4 enhancer trap strains. A schematic representation of the trapping construct TK1xC is shown at the top of the figure. (A–X) Confocal microscopy images of Bodipy ceramide-counterstained (green) embryos from isolated KalTA4 enhancer trap lines. Embryos were screened for tissue-specific mCherry fluorescence (red) between 24 and 36 hpf; images were recorded at approximately 50 hpf using a Zeiss LSM510 and a 20 \times objective. (A–L, Q–T, and U–W) lateral views (W 6dpf heart), (M–P) ventral views and (X) dorsal view. For detailed description of expression patterns see the database at: http://www.helmholtz-muenchen.de/en/idg/groups/neuroimaging/lines_distel/.

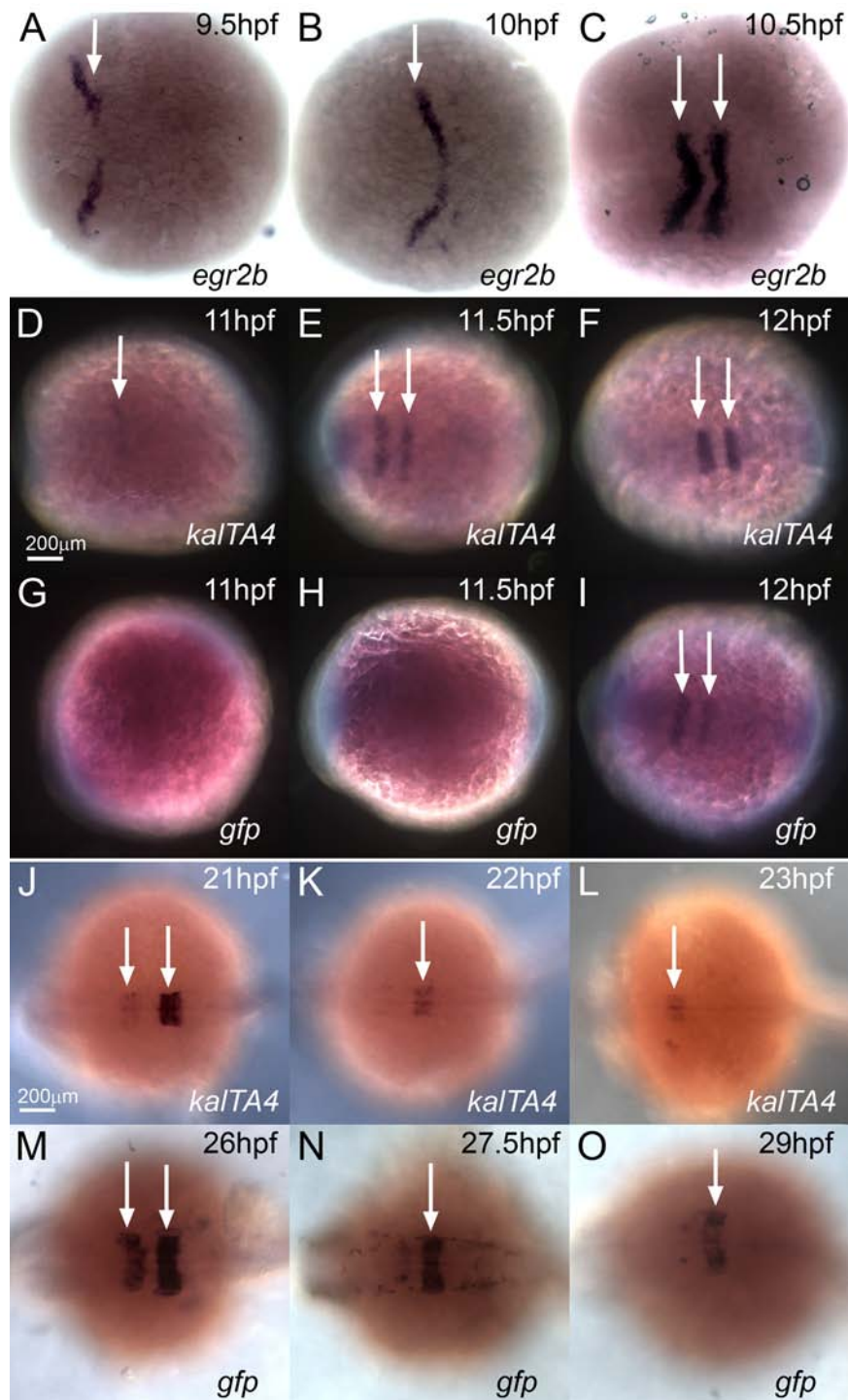


Fig. S3. Comparative mRNA in situ hybridization analysis to determine the onset of expression in rhombomeres 3 and 5 of (A–C) *egr2b* in WT embryos, (D–F) *kalTA4* and (G–I) *gfp* in offspring of rh3/5:KalTA4 × 4xKGFP cross. (J–L) mRNA in situ hybridization analysis of downregulation of expression of *kalTA4* and (M–O) *gfp* in rhombomeres 3 and 5 of rh3/5:KalTA4 × 4xKGFP embryos. Arrows indicate expression domains of the respective genes.

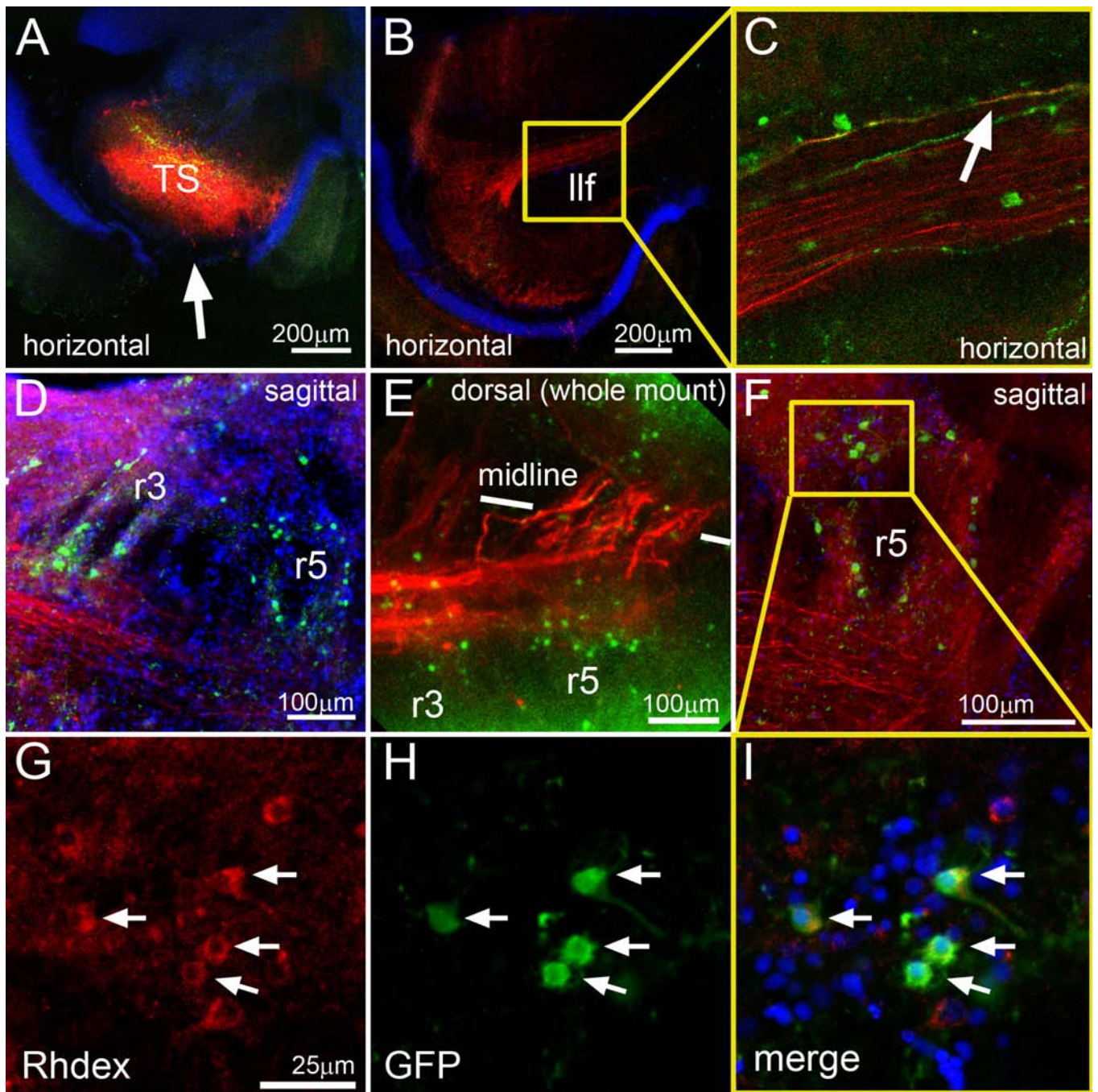


Fig. 54. Retrograde labeling of secondary octaval nucleus (SON) neurons. Adult brain cryostat sections ($100\ \mu\text{m}$) of rhodamine dextran injected adult $\text{rh3/5:KalTA4} \times 4\text{xKaloop}$ fish. (A) Rhodamine dextran (red) injection site in the central nucleus of the torus semicircularis (TS). The arrow demarcates the site where the tectum was removed. (B) Rhodamine dextran (red) positive axons innervate the TS coming from caudal projection nuclei and (C, enlarged area of B marked with yellow square) some are positive for GFP expression (white arrow). (D) Rhodamine dextran-positive axons are derived from hindbrain neurons, (E) they cross the midline at the level of r3 and r5 and (F) turn dorsally (G–I, enlarged area of F marked with yellow square) revealing their origin from GFP-expressing somata of $\text{rh3/5:KalTA4} \times 4\text{xKaloop}$ labeled neurons. Abbr.: llf: lateral longitudinal fascicle, r: rhombomere, TS: torus semicircularis.

Table 1. Analysis of insertion sites of KallTA4 enhancer trap cassette. Insertion analysis by nested inverse PCR of selected KallTA4 enhancer trap lines

Line	Expression pattern	Insertion locus	Nearest gene	Insertion position	Reported gene expression pattern	Shown in
Mü4380_64	Midbrain, hindbrain	Chr.21, 11852731/11852738	<i>efna5a</i>	Intron	Midbrain, hindbrain	Fig. S1A
Mü4466_13	Ventral CNS	Chr.16, near 13747710	<i>sp8l</i>	2.4 kb downstream of <i>sp8l</i>	Ventral CNS	Fig. S1C
Mü4357_9	Telencephalon, tectum, cerebellum, hindbrain	Chr.24, 4310366/4310372	<i>zic1/zic4</i>	400 bp upstream of <i>zic4</i>	Telencephalon, tectum, cerebellum, hindbrain	Fig. S1B
Mü4572_46	Rhombomeres 3/5	Chr.12, 6373073/6373076	<i>egr2b (krox20)</i>	1.5 kb downstream of <i>egr2b</i>	Rhombomeres 3/5	Fig. S1H
Mü4410_30	Melanocytes	Chr.20, 20623777/20623784	<i>kit a</i>	140 bp upstream of <i>kit a</i>	Pigment cells	Fig. S1V
Mü4497_18	Ubiquitous	Chr.7, 69747338 - 69747444	<i>tms (thymidylate synthetase)</i>	Exon1	Ubiquitous	Not shown
Mü4573_19	Olfactory system	Chr.17, 16748712	<i>A2CE94 DANRE</i>	22 kb downstream of <i>A2CE94</i> ; 240 bp upstream of marker z30232	Not reported	Fig. S1M
Ga206_19	Telencephalon, cerebellum, rhombomeres 3/5, lateral line ganglion	Chr.17, 50466304/50466361	<i>zgc:154061</i>	Intron	Not reported	Fig. S1D
Mü4356_8	Retina, hindbrain (day4)	Chr.17, 28072728/28072734	<i>kif11b</i>	23 kb downstream of <i>kif11b</i>	Not reported	Not shown
Ga234_65	Telencephalon	Chr.7, 23649835/23649908	ENSDARESTG00000013070; <i>lmo1</i>	Exon of ENSDARESTG00000013070; 22 kb upstream of <i>lmo1</i>	Telencephalon, hindbrain	Fig. S1O
Mü4435_64	Muscle	Chr.15, 8561461/8561468	ENSDARG00000058274	21 kb downstream of ENSDARG00000058274	Not reported	Fig. S1U
Mü4354_50	CNS	Chr.5, 58511708/58511710	<i>notch1b</i>	Intron of <i>notch1b</i>	CNS	Not shown
Ga079_8	Diencephalon	Chr.6, near 15292344 - 15292395	<i>barh-like2</i>	82 kb downstream of <i>barh-like2</i>	Telencephalon, diencephalon, preteectum, lateral hindbrain	Fig. S1P

The insertion loci are given together with the nearest gene and a comparison of its reported expression pattern with the mCherry fluorescence in the respective isolated KallTA4 enhancer trap strain.

Appendix 2

published Article in *Development*

Lunatic fringe promotes the lateral inhibition of neurogenesis.

Nikolaou, N., Watanabe-Asaka, T., Gerety, S., Distel, M., Köster, R.W. and Wilkinson, D.G.

Development (2009), **136**, 2523-2533.

Contribution:

This project was mainly conducted in David Wilkinson's lab. I discovered and isolated the rh3/5:KalTA4 enhancer trap strain used for the rescue experiment depicted in Fig.3. Furthermore, I performed inverse nested PCR and in situ hybridisation experiments to characterize the rh3/5:KalTA4 strain.

Lunatic fringe promotes the lateral inhibition of neurogenesis

Nikolas Nikolaou¹, Tomomi Watanabe-Asaka¹, Sebastian Gerety¹, Martin Distel², Reinhard W. Köster² and David G. Wilkinson^{1,*}

Previous studies have identified roles of the modulation of Notch activation by Fringe homologues in boundary formation and in regulating the differentiation of vertebrate thymocytes and *Drosophila* glial cells. We have investigated the role of Lunatic fringe (Lfng) expression during neurogenesis in the vertebrate neural tube. We find that in the zebrafish hindbrain, Lfng is expressed by progenitors in neurogenic regions and downregulated in cells that have initiated neuronal differentiation. Lfng is required cell autonomously in neural epithelial cells to limit the amount of neurogenesis and to maintain progenitors. By contrast, Lfng is not required for the role of Notch in interneuronal fate choice, which we show is mediated by Notch1a. The expression of Lfng does not require Notch activity, but rather is regulated downstream of proneural genes that are widely expressed by neural progenitors. These findings suggest that Lfng acts in a feedback loop downstream of proneural genes, which, by promoting Notch activation, maintains the sensitivity of progenitors to lateral inhibition and thus limits further proneural upregulation.

KEY WORDS: Lateral inhibition, Neurogenesis, Neural progenitors, Notch, Fringe, Zebrafish

INTRODUCTION

Intercellular signalling mediated by the Notch receptor has diverse roles in the regulation of cell differentiation, proliferation and migration during development (Louvi and Artavanis-Tsakonas, 2006). The response of cells to Notch activation is context dependent and can change within a tissue at different stages of development. This is illustrated by roles of Notch in cell differentiation in the vertebrate central nervous system, in which it mediates the lateral inhibition of neurogenesis (Lewis, 1998), promotes the formation of radial glial cells (Gaiano et al., 2000), which can act as neural progenitors (Malatesta et al., 2000; Malatesta et al., 2003), and regulates the choice to differentiate into specific neuronal cell types (Peng et al., 2007). A general feature of these functions is that Notch signalling diversifies adjacent cells by lateral inhibition or induction, in which cells expressing Notch ligands change the differentiation of their neighbours.

During the lateral inhibition of neurogenesis in the vertebrate nervous system, proneural transcription factors that drive the initial steps of neuronal differentiation upregulate expression of the Notch ligands, Delta or Serrate/Jagged. These ligands activate Notch in adjacent cells by promoting a proteolytic cleavage that releases the intracellular domain of Notch (Mumm et al., 2000), which, upon binding to the transcription factor CSL, switches it from a repressor to an activator (Fryer et al., 2002). The activated CSL complex upregulates expression of members of the Hes/Her transcriptional repressor family that inhibit neurogenesis (Kageyama et al., 2007). Consequently, a pool of undifferentiated cells is maintained adjacent

to differentiating neurons, within which neurogenesis can be initiated once lateral inhibition is relieved as the forming neuron migrates away from the neural epithelium.

In addition to roles in controlling cell differentiation, in some tissues Notch activation contributes to the inhibition of cell intermingling across boundaries (Dominguez and de Celis, 1998; Micchelli and Blair, 1999; Papayannopoulos et al., 1998). An example is the dorsoventral boundary in the *Drosophila* wing imaginal disc, in which the role of Notch depends upon the glycosyltransferase Fringe (Kim et al., 1995; Rauskolb et al., 1999). Fringe glycosylates specific sites of the Notch extracellular domain during its intracellular processing, and this glycosylation alters the affinity of Notch binding to its ligands: Delta binds more strongly to Fringe-modified Notch, whereas the binding of Serrate is decreased (Moloney et al., 2000; Panin et al., 1997). Consequently, the dorsal expression of Fringe and Serrate and the ventral expression of Delta leads to a stripe of Notch activation at the dorsoventral interface, which is required to form the compartment boundary (de Celis et al., 1996). Studies of vertebrate homologues of Fringe have suggested analogous roles in boundary formation for lunatic fringe (Lfng) in the chick forebrain (Zeltser et al., 2001), and for radical fringe in the chick limb (Laufer et al., 1997; Rodriguez-Esteban et al., 1997). Similarly, the expression of Radical fringe by zebrafish hindbrain boundary cells may modulate Notch activation that then regulates cell segregation (Cheng et al., 2004).

Some contexts have been found in which Fringe homologues are involved in the regulation of cell differentiation. During lymphopoiesis, Lfng expression in thymocyte progenitors promotes their differentiation by increasing the activation of Notch by limiting amounts of Delta expressed in thymic epithelial cells (Visan et al., 2006). Similarly, in the *Drosophila* CNS, Fringe is upregulated in specific glial cells and promotes Notch activation required for subtype-specific gene expression (Thomas and van Meyel, 2007). It is therefore intriguing that specific Fringe homologues are expressed in the vertebrate CNS; for example, Lfng expression occurs in dorsoventral stripes in the chick and mouse neural tube (Johnston et al., 1997; Laufer et al., 1997) that could correlate with neurogenesis, and Fringe homologues are expressed in progenitors and

¹Division of Developmental Neurobiology, MRC National Institute for Medical Research, The Ridgeway, Mill Hill, London NW7 1AA, UK. ²Helmholtz Zentrum München, German Research Center for Environmental Health, Institute of Developmental Genetics, Ingolstädter Landstrasse 1, 85764 Neuherberg-Munich, Germany.

* Author for correspondence (e-mail: dwilkin@nimr.mrc.ac.uk)

differentiating cells in the cerebral cortex in mouse (Ishii et al., 2000). Furthermore, overexpression of *Lfng* in the chick neural tube was found to increase the number of neurons (de Bellard et al., 2007). These findings raise the possibility that modulation of Notch activity by Fringe homologues regulates neurogenesis in vertebrates.

We set out to investigate the role of *Lfng* in the zebrafish nervous system, in which gene expression studies have suggested potential roles in boundary formation and/or neurogenesis. At early stages, *lfng* expression occurs at high levels in alternating segments in the hindbrain (Leve et al., 2001; Prince et al., 2001; Qiu et al., 2004), which by analogy with roles in other tissues could underlie boundary formation. In addition, *lfng* is expressed in dorsoventrally restricted domains in the neural tube (Prince et al., 2001) that could be associated with zones of neurogenesis. We show that *Lfng* limits neuronal differentiation and is required to maintain progenitor cells. *Lfng* acts cell autonomously in progenitors to inhibit their differentiation but, surprisingly, is upregulated downstream of proneural genes. We propose that *Lfng* acts in a feedback loop that maintains the competence of progenitor cells to receive lateral inhibition from differentiating neurons.

MATERIALS AND METHODS

Zebrafish lines

Wild-type, *mib^{ta52b}* (Jiang et al., 1996; Schier et al., 1996), *notch1a^{tp37}* (Gray et al., 2001; Holley et al., 2002; van Eeden et al., 1996) and *Tg(r3/r5-Gal4::UAS-RFP)* embryos were produced and staged according to hours post fertilisation (hpf) and morphological criteria (Kimmel et al., 1995).

Microinjection

Blastomeres (1- to 4-cell) were microinjected with 0.45–1.8 pmol morpholino oligonucleotide (MO; Gene Tools). The *lfng* splice-blocking MO (ACCGTGTATACCTGTCGCATGTTTC) corresponds to the boundary between exon 1 and intron 1, and a 5 bp mismatch MO (ACCCTCTATAGCTGTGGCATCTTTC) was used as control. To test the effect on splicing, RT-PCR was performed with ~20 24 hpf embryos using the primers P1, 5'-GGTTTCTGTTGTTTCTCTCGAG-3'; P2, 5'-CTCGCCGTCTGTGAAGATGTA-3'; and P3, 5'-CTTTAATGGGTTTGTGGTACAGC-3'. For proneural knockdown, *ascl1a*, *ascl1b* and *ngn1* MOs (Amoyel et al., 2005) were used. When used, 0.45 pmol of *p53* MO (Robu et al., 2007) was coinjected. Capped RNA encoding *ngn1-myc*, dominant-negative CSL [*dn-CSL*; *DBM* in Wettstein et al. (Wettstein et al., 1997)], *H2B-Citrine* (gift from S. Megason and S. Fraser, Caltech, Pasadena, CA, USA) and *Tol2* transposase (Balciunas et al., 2006; Kawakami et al., 2000) was prepared and 25–200 pg was injected at the 1-cell stage.

To generate *UAS-Lfng::UAS-H2B-Citrine*, a plasmid containing two UAS activator sequences followed by the *E1b* minimal promoter and flanked by miniTol2 sequences (Balciunas et al., 2006) was used to subclone *H2B-Citrine* downstream of the first UAS and the *lfng* coding region downstream of the second UAS. The plasmid was injected at 20 ng/μl with 25 pg *Tol2* transposase RNA.

In situ hybridisation and immunohistochemistry

RNA probes used are as follows: *lfng* (Leve et al., 2001; Prince et al., 2001); *deltaA*, *deltaB* (Haddon et al., 1998); *ngn1* (Blader et al., 1997; Kim et al., 1997; Korzh et al., 1998); *ascl1a*, *ascl1b* (Allende and Weinberg, 1994); *neurod4* (Wang et al., 2003); *isll* (Chandrasekhar et al., 1997); *tbx20* (Ahn et al., 2000); *pax2.1* (*pax2a* – ZFIN) (Mikkola et al., 1992); *gad67* (*gad1* – ZFIN) (Martin et al., 1998); *evx1* (Thaeron et al., 2000); *lhx2*, *lhx9* (Ando et al., 2005; Seth et al., 2006); *her4* (Takke et al., 1999); *her12* (Bae et al., 2005; Sieger et al., 2004); *sox3*, *sox19a* (Okuda et al., 2006); *rftng* (Cheng et al., 2004; Qiu et al., 2004); *foxb1.2* (Moens et al., 1996); *krox20* (*egr2a* – ZFIN) (Oxtoby and Jowett, 1993); *ephrin B3* (Chan et al., 2001); *notch1a* (Bierkamp and Campos-Ortega, 1993); *notch1b*, *notch3* (Westin and Lardelli, 1997); *vsx1* (Passini et al., 1998); *gata3* (Neave et al., 1995). Digoxigenin- or fluorescein-labelled probes were synthesized and in situ hybridisation performed as described (Thisse et al., 1993). Fluorescent in

situ hybridisation was performed as described (Julich et al., 2005), except that detection was with Alexa Fluor 488- or 594-labelled tyramide (Molecular Probes).

For immunohistochemistry, we used: rabbit anti-N-Cadherin [1:400 (Liu et al., 2001)], rabbit anti-EphA4 [1:450 (Irving et al., 1996)], mouse anti-HuC/D (1:100, Molecular Probes), rabbit anti-RFP (1:500, Chemicon International), sheep anti-GFP (1:500, AbD Serotec), mouse anti-neurofilament (RMO-44, 1:25, Zymed) and mouse anti-Zn-5 [1:200 (Trevarrow et al., 1990)]. Detection of primary antibodies was carried out using Alexa Fluor 488, 594 or 647 goat anti-rabbit or anti-mouse, or donkey anti-sheep, conjugates (1:500, Molecular Probes).

Mosaic analysis

Embryos were injected with control MO, *lfng^{E111}* MO or *dn-CSL* RNA together with 50 pg *H2B-Citrine* RNA at the 1-cell stage. Cells (20–30) were transplanted into uninjected or *lfng^{E111}* MO-injected embryos at 4 hpf, and embryos were allowed to develop until 24 hpf. Embryos were fixed and processed to detect GFP and HuC/D.

DAPT treatment

DAPT treatment was performed as described (Geling et al., 2002). DAPT (46 mM), dissolved in dimethyl sulphoxide (DMSO), was diluted to 0.2 mM in Danieau solution (Shih and Fraser, 1995) and applied to dechorionated embryos from 4 to 16 hpf. Control embryos were treated with Danieau solution containing the same concentration of DMSO.

Data analysis

To quantify neuronal differentiation, HuC/D-labelled cells were counted in stacked images of r3, r4 and r5, visualised by *r3/r5-Gal4::UAS-RFP* expression. For mosaic analysis, 1 μm optical sections were acquired every 10 μm by confocal microscopy, and the number of transplanted cells that had differentiated into HuC/D-expressing neurons was counted. The significance of results was analysed using Student's *t*-test.

RESULTS

The expression of *lfng* is associated with segmentation and neurogenesis

Previous studies have reported that at 12.5–14 hpf, *lfng* is expressed at higher levels in rhombomeres (r) 2 and 4 in the hindbrain, and by 20 hpf has been upregulated in other segments (Leve et al., 2001; Prince et al., 2001; Qiu et al., 2004). In a more extensive analysis, we observed that *lfng* expression is at higher levels in r2 and r4 at 14–18 hpf (Fig. 1A,B), by 24 hpf occurs in a punctate pattern (Fig. 1C), and then becomes restricted to zones adjacent to hindbrain boundaries (Fig. 1D,E). This later phase of expression is reminiscent of the pattern of neurogenesis in the zebrafish hindbrain (Amoyel et al., 2005). We therefore investigated whether *Lfng* has roles in hindbrain boundary formation and/or in neurogenesis.

Knockdown of *lfng* does not affect segmentation or boundary formation

We carried out loss-of-function experiments by using a morpholino oligonucleotide (MO) complementary to the splice donor site of intron 1 of *lfng* (*lfng^{E111}* MO) (Fig. S1A in the supplementary material); this is predicted to block splicing of intron 1 and terminate the open reading frame upstream of the region conserved between Fringe proteins (Johnston et al., 1997; Leve et al., 2001; Prince et al., 2001; Qiu et al., 2004). Microinjection of *lfng^{E111}* MO completely blocked splicing of intron 1, whereas a control MO with five changes in nucleotide sequence was ineffective at blocking intron 1 splicing (Fig. S1B in the supplementary material). We first assessed whether *Lfng* is involved in boundary formation or segmentation in the hindbrain. We detected no change in the expression of hindbrain boundary cell markers or in the formation

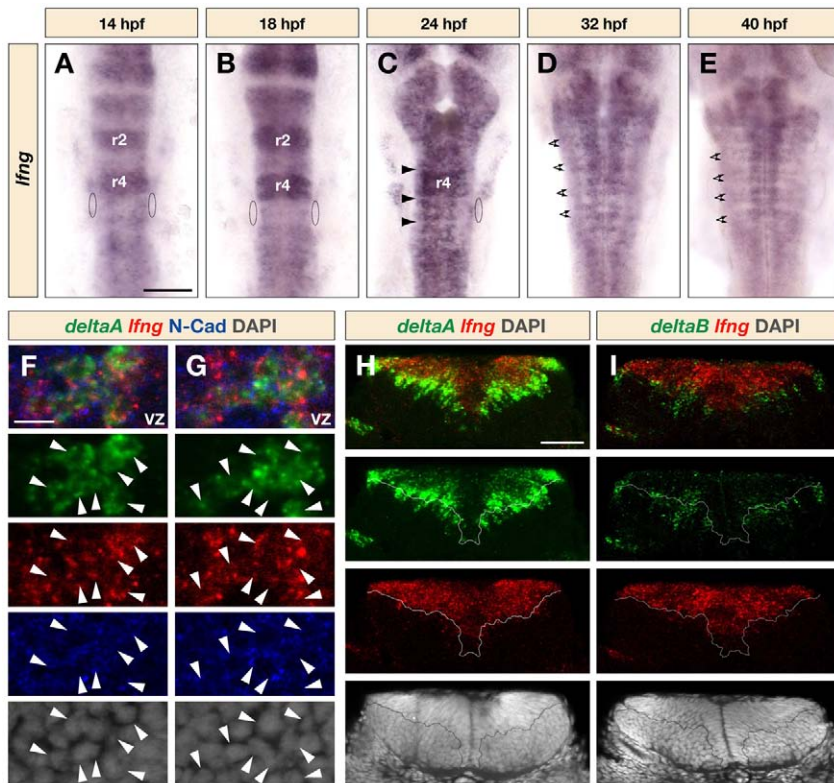


Fig. 1. Expression pattern of *lfng* in the zebrafish hindbrain. (A-E) Dorsal views of wild-type embryos following in situ hybridisation to detect *lfng* transcripts in the hindbrain between 14 and 40 hpf. Ovals indicate the otocyst, arrowheads in C indicate the location of hindbrain boundaries and double arrows in D and E indicate the neurogenic zones that form adjacent to boundaries. (F,G) Confocal images within the plane of the ventricular zone showing dorsal views of a 40 hpf embryo following detection of *lfng* (red) and *deltaA* (green) mRNA combined with anti-N-Cadherin (blue) and DAPI (grey) staining to reveal the cell surface and nucleus, respectively. Arrowheads indicate cells in which *lfng* and *deltaA* are coexpressed. VZ, ventricular zone. (H,I) Transverse sections of 40 hpf embryos following fluorescent in situ hybridisation to detect expression of *lfng* (red) in comparison to *deltaA* (H, green) and *deltaB* (I, green) combined with DAPI staining (grey). Dotted line indicates the boundary between the ventricular and mantle zones. Scale bars: 100 μ m in A for A-E; 10 μ m in F for F,G; 50 μ m in H for H,I.

of sharp borders of segmental markers following *lfng* knockdown (see Fig. S2 in the supplementary material). *Lfng* therefore does not appear to be required for these processes.

Lfng limits the amount of neurogenesis

To address whether *Lfng* has a role in the regulation of neurogenesis, we analysed the effect of *lfng* knockdown on the expression of proneural and Delta genes that are upregulated at the onset of neuronal differentiation (Allende and Weinberg, 1994; Haddon et al., 1998; Korzh et al., 1998), on *neurod4*, which is upregulated downstream of proneural genes (Park et al., 2003; Wang et al., 2003), and on HuC/D, which marks differentiating neurons in the mantle

zone (Park et al., 2000). We found that *lfng* knockdown leads to increased expression of proneural and Delta genes, including *ngn1* (*neurog1* – ZFIN), *ascl1a*, *ascl1b*, *deltaA* and *deltaB*, and of *neurod4* at all stages analysed, for example at 18 and 28 hpf (see Fig. S3 in the supplementary material) and 36 hpf (Fig. 2A-L). This increase appeared to be due in part to a higher level of gene expression per cell, as more intense signals are observed at single cell resolution following *lfng* knockdown (see, for example, Fig. 2A'-L'). In addition, there was an increased number of cells expressing high levels of proneural and Delta genes, seen for example at 36 hpf, when neurogenesis is confined to narrow neurogenic zones: in control embryos there is a mixture of low- and high-expressing cells within

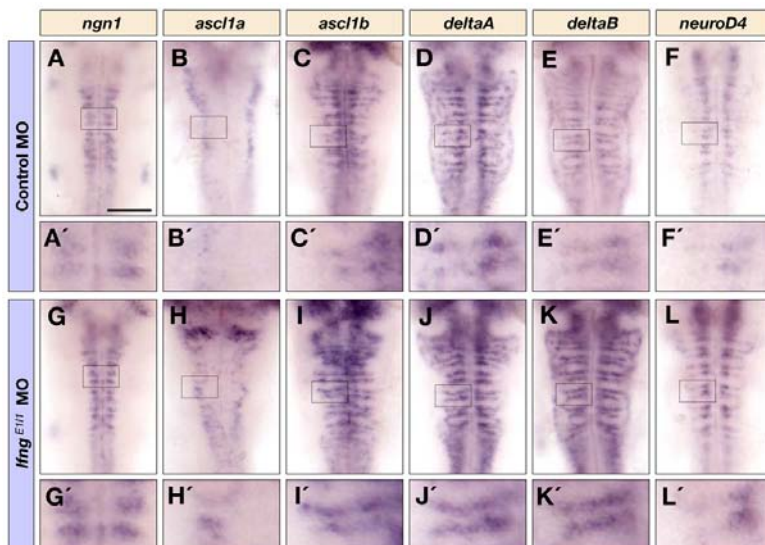


Fig. 2. Knockdown of *lfng* increases the initiation of neuronal differentiation. Dorsal views of control MO (A-F') and *lfng*^{E111} MO (G-L') injected embryos at 36 hpf showing *ngn1* (A,A',G,G'), *ascl1a* (B,B',H,H'), *ascl1b* (C,C',I,I'), *deltaA* (D,D',J,J'), *deltaB* (E,E',K,K'), and *neurod4* (F,F',L,L') expression in the hindbrain. A'-L' are higher magnifications of the indicated areas in A-L. Scale bar: 100 μ m.

these zones, whereas following *lfng* knockdown there are more cells with high level expression (Fig. 2B'-D',H'-J'). Consistent with an increased number of cells initiating neurogenesis, we observed more differentiating neurons in the mantle zone marked by HuC/D (Fig. 3A-H). In order to quantify the effect on neuronal differentiation, we compared the number of HuC/D-positive cells in control and *lfng* MO embryos. We found that *lfng* knockdown leads to a 1.7-fold increase in the number of differentiating neurons, both at 18 and 30 hpf (Fig. 3K and data not shown).

These findings raised the question of whether Lfng limits the production of all types of neurons in the hindbrain, or acts in a specific subset. To examine this, we analysed markers of different neuronal types, including interneurons, and reticulospinal, branchiomotor, somatic motor and commissural neurons. We found that there was an increase in the number of all neuronal types examined, apart from reticulospinal neurons (see Fig. S4 in the supplementary material). These findings reveal that Lfng has a widespread role in limiting neurogenesis, with the exception of reticulospinal neurons.

A potential difficulty with MOs is that they can have off-target effects leading to p53-mediated cell death, although this can be suppressed by coinjection with *p53* MO (Robu et al., 2007). Since such apoptosis leads to the loss of cells, it seemed unlikely that this underlies the observed increase in neurogenesis. Nevertheless, we tested the effect of coinjecting *p53* MO and found that this does not alter the increase in neurogenesis following injection of *lfng* MO (data not shown). In addition, we assessed the specificity of the phenotypic effect of *lfng* MO in a rescue experiment in which Lfng is transgenically overexpressed in r3/r5 using a Gal4 enhancer-trap line (Fig. 3I,J). We found that transgenic overexpression of Lfng decreased the amount of neurogenesis in control embryos and partly suppressed the *lfng* MO-induced increase in neurogenesis (Fig. 3K); both of these effects specifically occurred in r3/r5, where Lfng is ectopically expressed, and not in r4.

Lfng is required to maintain progenitors

A potential explanation for our findings is that *lfng* knockdown leads to a deficiency in the lateral inhibition of neurogenesis. We therefore analysed expression of Hes/Her family genes that are targets of the Notch pathway during lateral inhibition. We observed no change in the expression of *her4* (*her4.1* – ZFIN) at 28 hpf (see Fig. S3 in the supplementary material), whereas by 40 hpf the expression of *her4* and *her12* was decreased following *lfng* knockdown (Fig. 4A,B,E,F). This appeared to be due to a decrease in the levels of expression, as well as in the number of cells expressing the Notch effectors (Fig. 4A',B',E',F'). However, *her4* expression may not provide a sensitive read-out of Notch modulation since, as occurs for the homologous genes in *Drosophila* (Castro et al., 2005), its expression may also be upregulated by proneural genes (Yeo et al., 2007); the upregulation of proneural genes following *lfng* knockdown could thus mask any decrease in Notch activation. A potential explanation for the late decrease in *her4* and *her12* gene expression is that the reduced lateral inhibition of neurogenesis led to a depletion of progenitors, so we analysed the expression of *sox3* and *sox19a*, which mark neural progenitor cells. We found that, although no change was detected at 28 hpf (see Fig. S3 in the supplementary material), by 40 hpf there was lower expression of these markers, which is suggestive of fewer neural progenitors in the neural tube (Fig. 4C',D',G',H'). Taken together, these results suggest that knockdown of *lfng* eventually leads to a depletion of progenitor cells, consistent with a role in Notch-mediated lateral inhibition of neurogenesis.

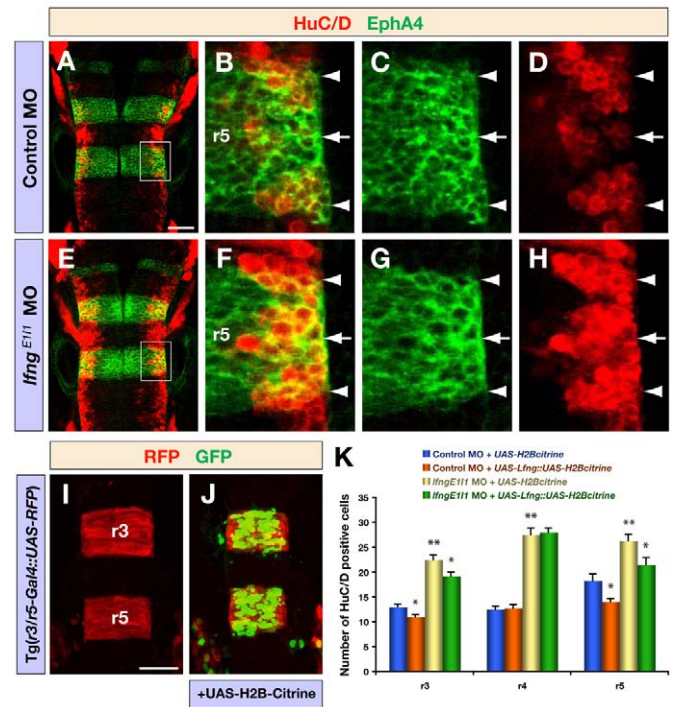


Fig. 3. Knockdown of *lfng* produces a neurogenic phenotype.

(A-H) Confocal images showing dorsal views of control MO (A-D) and *lfng*^{E111} MO (E-H) injected embryos at 30 hpf, immunostained for HuC/D (red) and EphA4 (green) to mark postmitotic neurons and r3/r5, respectively. B-D and F-H are higher magnifications of the areas indicated in A and E, respectively. Arrowheads and arrows indicate rhombomere boundaries and centres, respectively. (I,J) Confocal images of the expression of RFP (red) and H2B-Citrine (green) in r3 and r5 in Tg(r3/r5-Gal4::UAS-RFP) embryos at 18 hpf, either noninjected (I) or injected with UAS-H2B-Citrine plasmid (J). Tg(r3/r5-Gal4::UAS-RFP) is an enhancer trap that drives Gal4 and mCherry expression in r3/r5; the expression of UAS-citrine in r3/r5 illustrates the targeting of transgene expression to these rhombomeres. (K) Quantification of the number of differentiating neurons (HuC/D expression) in Tg(r3/r5-Gal4::UAS-RFP) 18 hpf embryos injected with control MO or *lfng*^{E111} MO together with either a control vector (UAS-H2B-Citrine) or a vector to overexpress Lfng (UAS-Lfng::UAS-H2B-Citrine). Transgenic expression of Lfng in r3/r5 leads to a decreased number of differentiated neurons and partly rescues the effect of *lfng* knockdown, whereas neurogenesis in r4 is not affected. Values are mean \pm standard error, neurons in four embryos were counted for each experimental group; *, $P < 0.05$, **, $P < 0.01$. Scale bars: 50 μ m in A for A-H; 50 μ m in I for I,J.

Lfng is not required for neuronal subtype specification

Recent work has shown that, in addition to being required in progenitors during the lateral inhibition of differentiation, Notch1 activation regulates the choice to form V2b rather than V2a interneurons in the spinal cord (Batista et al., 2008; Del Barrio et al., 2007; Peng et al., 2007). This raises the possibility that, in addition to a role in the inhibition of neurogenesis, Lfng enables the activation of Notch required for this fate choice. We therefore analysed whether Notch1 is required for interneuron fate choice in the zebrafish hindbrain. We found that, whereas *notch1b* and *notch3* are widely expressed in the nervous system, *notch1a* expression occurs initially at higher levels in r2 and r4 and subsequently in neurogenic zones (see Fig. S5 in the supplementary material).

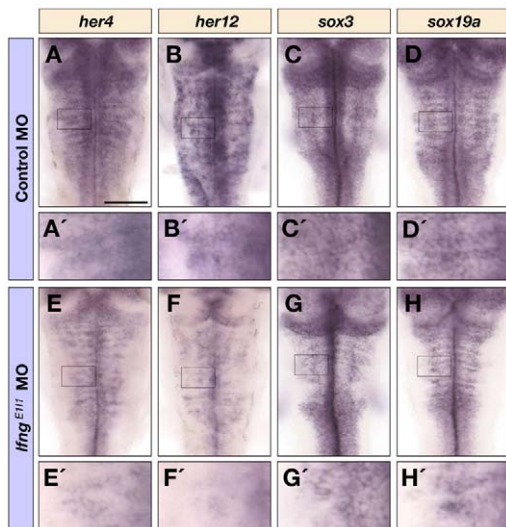


Fig. 4. Notch target gene and progenitor marker expression following *lfng* knockdown. Dorsal views of control MO (A-D') and *lfng*^{E111} MO (E-H') injected embryos at 40 hpf following detection of *her4* (A,A',E,E'), *her12* (B,B',F,F'), *sox3* (C,C',G,G') and *sox19a* (D,D',H,H') mRNA in the hindbrain. A'-H' are higher magnifications of the indicated areas in A-H. Scale bar: 100 μ m.

Furthermore, unlike other Notch receptors (data not shown), *notch1a* is coexpressed with Delta genes (see Fig. S6 in the supplementary material) and upregulated in neurogenic *mib* mutants (Fig. 5A-D). We therefore analysed whether interneuron subtype choice regulated by Notch signalling is altered in the *notch1a*^{tp37} mutant. Indeed, we found that there is a loss of V2b and an increase in V2a interneurons in this mutant (Fig. 5E,F,I,J), as occurs following global Notch inhibition (Batista et al., 2008; Peng et al., 2007).

If Lfng is required for Notch1a function in differentiating neurons, knockdown of *lfng* would have a similar effect on neuronal subtype specification as occurs in the *notch1a*^{tp37} mutant. However, we found that *lfng* knockdown does not lead to a switch in the fate of interneuron subtypes, but rather increases the numbers of both interneuron populations (Fig. 5G,H,K,L). We therefore conclude that Lfng is required to promote the lateral inhibition of neurogenesis but not for interneuron subtype specification.

The expression of *lfng* is regulated by proneural genes

In order to understand how Lfng contributes to the inhibition of neurogenesis, it is essential to determine in which cells *lfng* is expressed and how its expression is regulated. For example, *lfng* could be upregulated by Notch activation in progenitors and/or by proneural genes that are widely expressed at low levels and upregulated in differentiating neurons. We therefore compared neuronal marker and *lfng* expression at single cell resolution. *deltaA* is widely expressed at low levels in progenitors, and upregulated in cells selected to differentiate during lateral inhibition, whereas *deltaB* is only expressed in cells that have initiated differentiation (Haddon et al., 1998). In confocal sections in a superficial plane of the neural epithelium we found that *lfng* overlaps with *deltaA* expression (Fig. 1F,G). To visualise how *lfng* expression relates to the transition from progenitors to differentiating neurons, we analysed transverse hindbrain sections and found that *lfng*

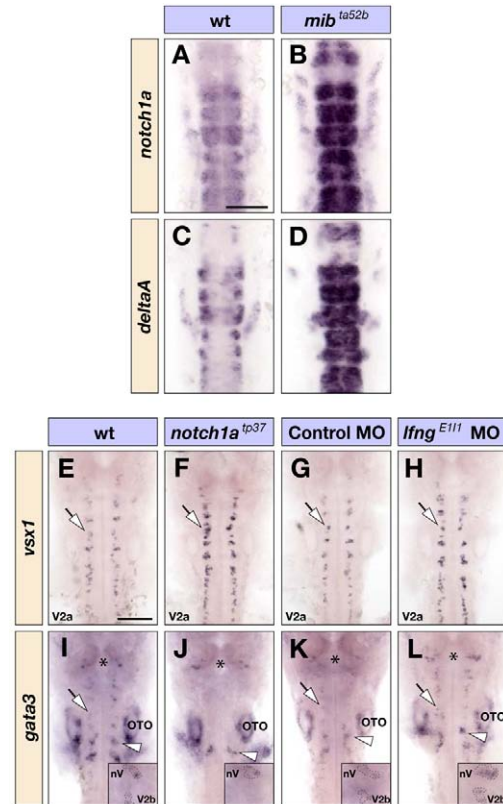


Fig. 5. *lfng* and Notch1a in neuronal subtype choice. (A-D) Dorsal views of wild-type (A,C) and *mib*^{ta52b} homozygous mutant (B,D) embryos at 18 hpf showing *notch1a* (A,B) and *deltaA* (C,D) expression in the hindbrain. (E-L) Dorsal views of wild-type (E,I), *notch1a*^{tp37} homozygous mutant (F,J) embryos, or control MO (G,K) and *lfng*^{E111} MO (H,L) injected embryos at 26 hpf showing *vsx1* (E-H) and *gata3* (I-L) expression in the hindbrain that mark V2a and V2b interneurons (indicated by arrows), respectively. Expression of *gata3* in nV and nVII branchiomotor neurons, indicated by the asterisks and arrowheads (I-L), respectively, is not affected in *notch1a*^{tp37} embryos but increased following knockdown of *lfng* (insets in I-L). OTO, otocyst. Scale bars: 100 μ m

expression is confined to the ventricular zone, where it overlaps with the low- and high-level expression of *deltaA* (Fig. 1H). By contrast, *lfng* expression occurs complementary to the expression of *deltaB* in differentiating neurons migrating to the mantle zone (Fig. 1I). We conclude that *lfng* is coexpressed with Delta genes in neural progenitors and is downregulated in cells that have embarked upon neurogenesis.

To test whether *lfng* is regulated by proneural genes and/or by Notch activation, we first carried out knockdown and gain-of-function experiments with proneural genes. Knockdown of *ngn1* or *ascl1b* alone had only a moderate effect on *lfng* expression, as was also seen for *deltaA* expression (see Fig. S6 in the supplementary material). By contrast, triple knockdown of *ngn1*, *ascl1b* and *ascl1a* led to a major decrease in *lfng* expression (Fig. 6A,E and see Fig. S6 in the supplementary material). In gain-of-function experiments, we found that misexpression of *ngn1* (Fig. 6G,I,K,M), but not of *ascl1b* (data not shown), led to upregulation of *lfng* expression. Taken together, these observations suggest that *lfng* is a downstream target of multiple proneural genes that can compensate for each other following knockdown, but there are differences between proneural genes in their ability to upregulate *lfng*.

An alternative explanation for the effects of proneural knockdown or misexpression on *lfng* expression is that they are secondary to the regulation of Delta/Serrate genes that activate Notch. If proneural genes (or downstream transcription factors) regulate *lfng* directly, blocking Notch activation will lead to more cells expressing *lfng* due to the consequent loss of lateral inhibition and increase in neurogenesis. By contrast, if Notch activation regulates *lfng*, blocking Notch activation will decrease *lfng* expression. We therefore tested the effect of inhibiting Notch activation with DAPT (Geling et al., 2002), and found that this leads to increased *lfng* expression (Fig. 6A,C), concurrent with more neurogenesis marked by strong *deltaA* expression (Fig. 6B,D). A further possibility is that proneural genes and Notch activation synergise to upregulate *lfng*. However, we found no further change in *lfng* expression by combining triple proneural gene knockdown with the blocking of Notch activation with DAPT, or with the overexpression of *ngn1* together with dominant active Su(H) to activate the Notch pathway (data not shown). These data suggest that *lfng* is upregulated downstream of proneural genes, and not indirectly via Notch activation by Delta ligands.

Lfng acts cell autonomously to inhibit neurogenesis

The finding that *lfng* expression is upregulated downstream of proneural genes raises the question, which cells is Lfng required in? Lfng could act cell autonomously in progenitors to promote Notch activation and thus inhibit their differentiation. Alternatively, *lfng* expression in cells selected to differentiate could act non-autonomously to increase Notch activation in adjacent progenitors, as Lfng promotes the translocation of Delta to the cell surface (Sakamoto et al., 2002). These possibilities lead to different predictions for the

effect of mosaic knockdown. In the former model, *lfng* knockdown cells will have increased differentiation, similar to the effect of inhibiting Notch pathway activation with dominant-negative CSL [DBM in Wettstein et al. (Wettstein et al., 1997)]. In the latter model, there would be no increase in the differentiation of *lfng* knockdown cells, as the increase in neurogenesis occurs in adjacent cells.

To test these models, we carried out transplantations to generate embryos mosaic for *lfng* MO plus GFP expression, and determined the relative number of Lfng-deficient cells that had differentiated or remained as progenitors in comparison with mosaic GFP expression alone. We found that there was increased differentiation of *lfng* MO cells transplanted into a noninjected host, as also occurred for cells overexpressing *dn-CSL* (Fig. 7A). Furthermore, in the reciprocal experiment there was decreased neuronal differentiation of wild-type cells that had been transplanted into a *lfng* MO-injected host (Fig. 7A). We observed that, when a large number of transplanted *lfng* MO cells were present, a lower proportion of these cells differentiated compared with embryos in which there were a low number of Lfng-deficient cells (Fig. 7B). These data are consistent with competition whereby *lfng* MO cells preferentially undergo neurogenesis at the expense of cells in which Lfng function is not inhibited. In mosaics with a low number of Lfng-deficient cells (Fig. 7D), most are competing with cells expressing *lfng*, and thus a high proportion of Lfng-deficient cells differentiate. By contrast, in mosaics with a large number of Lfng-deficient cells (Fig. 7E), many will be competing with each other and not be biased to differentiate preferentially at the expense of their neighbours.

DISCUSSION

The expression of Lfng initially in a segmental pattern and subsequently in neurogenic regions raised the possibility that this Notch modulator may have roles in the regulation of segmentation and/or neurogenesis. We find that *lfng* is expressed in neurogenic domains of the zebrafish hindbrain, where its expression occurs in progenitors and is rapidly downregulated in differentiating neurons. The results of loss-of-function studies reveal that Lfng is required to limit the amount of neurogenesis in the hindbrain and to maintain neural progenitors at late stages. Analysis of mosaic embryos reveals that Lfng acts cell autonomously in progenitors to inhibit their differentiation. Furthermore, the bias of *lfng* knockdown cells to preferentially differentiate depends upon the degree of mosaicism, consistent with the competition of cells that occurs during the lateral inhibition of neurogenesis. Taken together, these findings suggest that Lfng acts within progenitor cells to promote the lateral inhibition of neurogenesis.

Significance of segmental expression of Lfng

In some tissues, Fringe homologues regulate boundary formation by modulating Notch activity at the interface of expressing and nonexpressing cells (Dominguez and de Celis, 1998; Laufer et al., 1997; Panin et al., 1997; Rodriguez-Esteban et al., 1997). It was therefore possible that the elevated expression of *lfng* in r2 and r4 reflected a role in hindbrain boundary formation. However, we found no effect of *lfng* knockdown on segmentation or boundary marker expression. Furthermore, hindbrain boundary cells initially form in *mib* mutants in which there is a major decrease in Notch activation, but are not maintained, as decreased lateral inhibition of neurogenesis leads to the loss of neural epithelial cells (Cheng et al., 2004). There is thus no evidence to support a role for Notch in hindbrain boundary formation. An alternative explanation for segmental *lfng* expression is suggested by the observation that the proneural gene *ascl1b* is initially expressed at higher levels

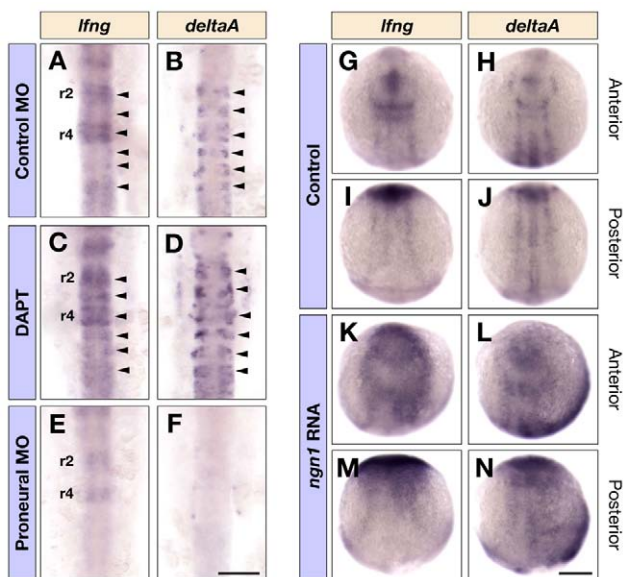


Fig. 6. Regulation of *lfng* expression. (A-F) Dorsal views of control MO (A,B) and triple *ascl1a*, *ascl1b* and *ngn1* MO (E,F) injected embryos, or DAPT (C,D) treated embryos at 16 hpf showing *lfng* (A,C,E) and *deltaA* (B,D,F) expression in the hindbrain. Arrowheads in A-D indicate the expression of *lfng* and *deltaA* in the middle of each rhombomere. (G-N) Dorsal views of control (G-J) and *ngn1* RNA (K-N) injected embryos at ~3-somite stage showing *lfng* (G,I,K,M) and *deltaA* (H,J,L,N) expression in the anterior and posterior neural plate. Scale bars: 100 μ m in F for A-F; 200 μ m in N for G-N.

throughout r2 and r4 (Amoyel et al., 2005), correlating with neurogenesis occurring in even- before odd-numbered segments (Bally-Cuif et al., 1998; Maves et al., 2002). The early segmental phase of *lfng* expression may therefore reflect the fact that neurogenesis is segmentally regulated, rather than suggest a role in segmentation.

Notch in the lateral inhibition of neurogenesis

There are similarities and differences between the effect of *lfng* knockdown and the major deficiency of Notch activation in *mib* mutants (Itoh et al., 2003; Jiang et al., 1996). In *mib* mutants, there is a 2- to 4-fold increase in early differentiating neurons, such as reticulospinal neurons, and the consequent depletion of progenitors leads to a decrease or loss of later-generated branchiomotor and commissural neurons, with neurogenesis almost absent by 24 hpf (Bingham et al., 2003; Jiang et al., 1996). *lfng* knockdown leads to a 1.7-fold increase in overall neurogenesis and increased production of many neuronal cell types, including branchiomotor neurons, somatic motor neurons, interneurons and commissural neurons. This is a milder neurogenic phenotype than *mib* mutants, consistent with Lfng

increasing, rather than being essential for, Notch activation. As would be anticipated, *lfng* knockdown leads to later depletion of neural progenitors than in *mib* mutants, with normal expression of progenitor markers at 24 hpf and a decrease by 40 hpf. However, there is a distinct effect of the *mib* mutation compared with *lfng* knockdown on reticulospinal neurons, which are born during gastrulation and are the first to differentiate in the hindbrain (Hanneman et al., 1988; Mendelson, 1986). Whereas in *mib* mutants the single Mauthner reticulospinal neuron increases to 3-4 neurons (Jiang et al., 1996), there is no increase following *lfng* knockdown. One possibility is that the milder neurogenic effect of *lfng* knockdown cannot be detected for reticulospinal neurons due to their low number, or there may be differences in the regulation of their differentiation compared with subsequent neurogenesis.

Our findings appear contrary to a study in which retroviral-mediated overexpression of Lfng in the chick neural tube increases the number of neurons (de Bellard et al., 2007), as we found that transgenic expression of Lfng in r3/r5 decreases neurogenesis. One contributory factor is suggested by our observation that widespread knockdown of *lfng* has less of an effect on neurogenesis than occurs cell autonomously for mosaic knockdown, consistent with the competition to differentiate during the lateral inhibition of neurogenesis. This can explain our finding that widespread transgenic overexpression of Lfng within r3/r5 inhibits neurogenesis only to a modest extent. A potential explanation for increased neurogenesis in the chick neural tube is suggested by the major increase in cell proliferation that occurs following Lfng expression (de Bellard et al., 2007). Since effects on neuronal differentiation were analysed 24-48 hours after retroviral infection, expansion of the progenitor pool may underlie the increased number of neurons and outweigh a modest inhibition of differentiation by widespread Lfng expression. There would be less of an impact of such effects in our study, in which the number of neurons was analysed 6 hours after the onset of Gal4 driver expression.

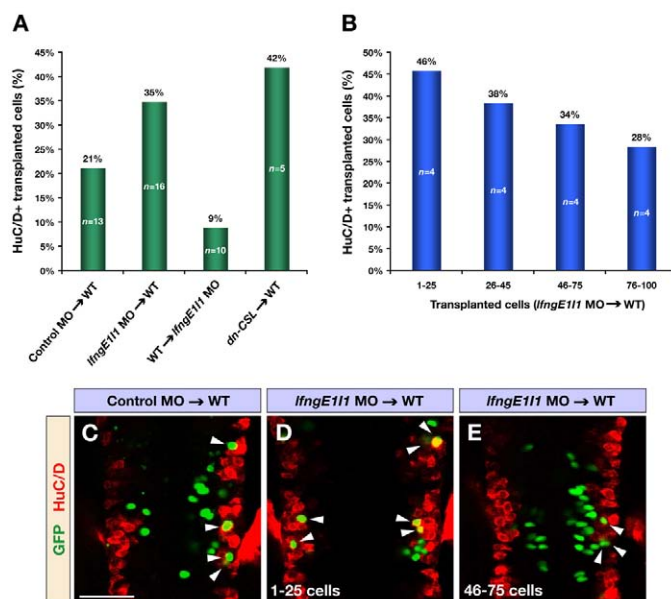


Fig. 7. Mosaic analysis of Lfng function. (A) Transplantations of cells from control or *lfngE111* MO- and *dn-CSL* RNA-injected donor embryos into wild-type or *lfngE111* MO-injected hosts. The bar graph shows the percentage of transplanted cells that have differentiated into neurons marked by HuC/D. For *lfngE111* MO and *dn-CSL* cells transplanted into wild-type hosts, only embryos with <100 transplanted cells are included. All changes were significant compared with control MO transplantations ($P < 0.03$). (B) Analysis of *lfngE111* MO cells transplanted into wild-type embryos. The bar graph shows the percentage of Lfng-deficient cells that have differentiated into neurons marked by HuC/D. Note the linear relationship between the increasing number of transplanted cells and decreasing number of transplanted cells differentiating into neurons. (C-E) Confocal images of dorsal views of wild-type embryos transplanted with control MO (C) and *lfngE111* MO (D, E) injected cells at 24 hpf immunostained for GFP (green) and HuC/D (red) to mark transplanted cells and postmitotic neurons, respectively. The embryo in E contains a higher number of transplanted cells compared with the one in D. Arrowheads indicate transplanted cells that have differentiated into neurons. Scale bar: 50 μ m.

Notch1a and neuronal specification

In addition to its role in mediating the lateral inhibition of neurogenesis, Notch mediates inhibitory or inductive signalling required for the specification of interneuronal subtype (Batista et al., 2008; Del Barrio et al., 2007; Peng et al., 2007). We find that in zebrafish, Notch1a is upregulated in differentiating neurons, suggesting that it is expressed downstream of proneural genes, whereas other Notch genes, including *notch1b*, are expressed predominantly in progenitors. These data suggest that there has been subfunctionalisation, as found for other genes duplicated in the zebrafish genome (Postlethwait et al., 2004), with expression of Notch1 divided between orthologues expressed in progenitors and neurons. We show Notch1a is required for interneuron subtype fate choice, but *lfng* knockdown leads to an increase of both interneuron subtypes, rather than a decrease in the population that requires Notch1a. We therefore conclude that Lfng acts to limit the amount of neuronal differentiation, but is not required for subtype specification regulated by Notch1a.

Regulation of *lfng* expression during neurogenesis

We find that *lfng* expression is decreased following knockdown of proneural genes, and increased following DAPT treatment that inhibits Notch activation, leading to increased proneural gene expression. Furthermore, the effect of proneural knockdown or overexpression on *lfng* expression was not exacerbated by the

alteration of Notch activation, arguing against a synergistic input of proneural and Notch activity. These findings suggest that, like Delta genes, *lfng* is a target of proneural proteins or downstream transcription factors and does not require Notch activity. This is consistent with studies in mouse suggesting that *Lfng* is a direct target of proneural transcription factors (Castro et al., 2006), and furthermore, the proneural factor binding motif is present in the zebrafish *lfng* gene (D. S. Castro, personal communication). However, whereas *lfng* expression overlaps with *deltaA* that is widely expressed in progenitors, it is not coexpressed with *deltaB* in cells committed to neuronal differentiation and initiating migration from the neural epithelial layer. The rapid downregulation of *lfng* upon the onset of neuronal differentiation suggests that there are regulatory inputs in addition to proneural genes, such as a transcription factor(s) restricted to progenitors.

Analysis of the effects of knockdown or overexpression of single proneural genes suggests that they have overlapping and specific roles in the regulation of *lfng*. The finding that *lfng* is upregulated by *ngn1* overexpression but little affected by *ngn1* knockdown suggests that other proneural genes also regulate *lfng*. However, *ascl1b* overexpression did not upregulate *lfng*, and *ascl1a* expression overlaps with *lfng* only in dorsal regions. Further work is required to determine whether this complexity is due, for example, to other factors required for specific proneural genes to regulate *lfng*.

Lfng in the regulatory logic of the lateral inhibition of neurogenesis

The initiation of neuronal differentiation requires an increase in proneural gene expression from the low level that occurs widely in the neural epithelium. This increase is enabled by positive feedback

on proneural expression within cells (Bae et al., 2000; Culi and Modolell, 1998; Dubois et al., 1998; Koyano-Nakagawa et al., 2000), which is countered by inhibitory loops that occur within and between cells (Bai et al., 2007; Heitzler et al., 1996; Kunisch et al., 1994; Ohtsuka et al., 1999). The process of lateral inhibition requires that there is sufficient Notch activation in progenitors to inhibit proneural expression and thus prevent differentiation.

Our findings that *lfng* is upregulated by proneural genes raises the question of where *Lfng* acts in the regulatory logic of lateral inhibition. A potential clue is the observation that the level of proneural and Delta gene expression per cell appears to be higher following *lfng* knockdown. This finding suggests that *Lfng* acts in a feedback loop downstream of proneural genes, in which the promotion of Notch activation by *Lfng* limits further upregulation of proneural and Delta genes in progenitors (Fig. 8). As found in other tissues, *Lfng* may increase the binding of Notch to Delta expressed on adjacent cells, but it is not obvious in this model why *lfng* would be upregulated in progenitors downstream of proneural genes rather than by Notch activation. Previous studies have found another functional relationship between *Lfng* and Delta genes that provides a potential explanation for this. Studies in the *Drosophila* wing margin (Glittenberg et al., 2006; Micchelli et al., 1997) and peripheral nervous system (Jacobsen et al., 1998) have shown that, whereas Delta proteins activate Notch on adjacent cells, Delta also has cis-interactions with Notch that cell autonomously inhibits its activation. Similarly, in vertebrate cell culture, cis-interactions with Delta decrease the level of cell surface Notch, thus decreasing its availability for activation by Delta presented by adjacent cells (Sakamoto et al., 2002). *Lfng* blocks such cis-interactions, and could thus lead to increased Notch at the cell surface (Sakamoto et al., 2002). Recent work showing that cis-interactions with Notch promote the endocytosis of DeltaD in the zebrafish hindbrain suggests that inhibition occurs by removal of the Notch-Delta complex from the cell surface (Matsuda and Chitnis, 2009).

Based upon these findings, we propose the following model (Fig. 8). Progenitor cells have widespread expression of proneural and downstream Delta genes, and compete to further upregulate proneural genes and laterally inhibit their neighbours. Due to cis-inhibition, there will inevitably be decreased activation of Notch in Delta-expressing cells. If cis-inhibition is too strong in progenitor cells, it will decrease their sensitivity to lateral inhibition, leading to positive feedback in which increased expression of proneural and Delta genes inhibits Notch activation that would normally inhibit further upregulation of proneural genes (Fig. 8). The coexpression of *lfng* with Delta downstream of proneural genes prevents this loop by blocking cis-inhibition, thus preventing the inappropriate upregulation of proneural genes that would lead to neurogenesis. By contrast, in cells that have initiated differentiation, *lfng* is downregulated and no longer coupled to Delta expression. Consequently, cis-inhibition of Notch by Delta will facilitate the further upregulation of proneural genes. This proposed change in cis-inhibition is consistent with recent work showing that in some progenitors DeltaD endocytosis is mainly due to trans-interactions, whereas in others cis-interactions are more important (Matsuda and Chitnis, 2009).

An alternative view of how *Lfng* may regulate neurogenesis is suggested by evidence that oscillations of proneural gene expression maintain progenitor cells and sustained high levels of expression promote neurogenesis (Kageyama et al., 2008). Such oscillations require Notch activation in order to downregulate proneural expression from its peak level (Shimojo et al., 2008). A

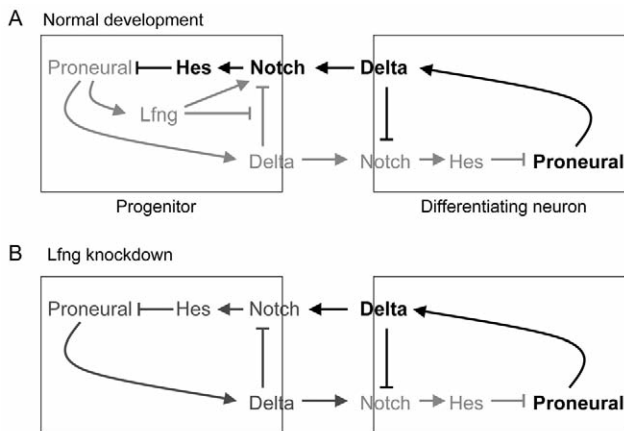


Fig. 8. Model of role and regulation of Lfng in the lateral inhibition of neurogenesis.

Depiction of regulatory relationships between *Lfng* and components of the lateral inhibition network. Strongly expressed or activated components are in black and less strongly expressed or activated components in grey. (A) In progenitor cells, expression of proneural genes upregulates *lfng*, which by increasing Notch activation ensures that progenitors are sensitive to lateral inhibition of their differentiation. *Lfng* may inhibit further upregulation of proneural genes by promoting trans-activation of Notch and/or by blocking cis-inhibition of Notch that would otherwise occur due to the expression of Delta downstream of proneural genes. *Lfng* is downregulated in differentiating neurons. (B) Following knockdown of *lfng*, proneural gene expression that drives neuronal differentiation is elevated in progenitors due to decreased lateral inhibition, possibly as a consequence of cis-inhibition of Notch by Delta that leads to positive feedback on proneural upregulation.

desensitisation of Notch due to cis-inhibition by Delta would lead to decreased signalling, such that there is sustained proneural gene expression and consequently neurogenesis. Further insights into the role of Lfng may therefore be obtained by real-time visualisation of its expression, and by analysing whether *lfng* knockdown affects oscillations of proneural gene expression.

Acknowledgements

We thank Francois Guillemot, Qiling Xu and Diogo Castro for discussions; and Julian Lewis, Scott Fraser, Sean Megason, Kamal Sharma and Caroline Erter Burns for constructs and reagents. This work was supported by the Medical Research Council (N.N., T.W.-A., S.G. and D.G.W.), by a BioFuture Grant (BMBF 0311889) of the German Ministry of Education and Research (R.W.K.) and by the Studienstiftung des deutschen Volkes (M.D.). Deposited in PMC for release after 6 months.

Supplementary material

Supplementary material for this article is available at <http://dev.biologists.org/cgi/content/full/136/15/2523/DC1>

References

- Ahn, D. G., Ruvinsky, I., Oates, A. C., Silver, L. M. and Ho, R. K. (2000). *tbx20*, a new vertebrate T-box gene expressed in the cranial motor neurons and developing cardiovascular structures in zebrafish. *Mech. Dev.* **95**, 253-258.
- Allende, M. L. and Weinberg, E. S. (1994). The expression pattern of two zebrafish achaete-scute homolog (*ash*) genes is altered in the embryonic brain of the cyclops mutant. *Dev. Biol.* **166**, 509-530.
- Amoyel, M., Cheng, Y. C., Jiang, Y. J. and Wilkinson, D. G. (2005). Wnt1 regulates neurogenesis and mediates lateral inhibition of boundary cell specification in the zebrafish hindbrain. *Development* **132**, 775-785.
- Ando, H., Kobayashi, M., Tsubokawa, T., Uyemura, K., Furuta, T. and Okamoto, H. (2005). Lhx2 mediates the activity of Six3 in zebrafish forebrain growth. *Dev. Biol.* **287**, 456-468.
- Bae, S., Bessho, Y., Hojo, M. and Kageyama, R. (2000). The bHLH gene *Hes6*, an inhibitor of *Hes1*, promotes neuronal differentiation. *Development* **127**, 2933-2943.
- Bae, Y. K., Shimizu, T. and Hibi, M. (2005). Patterning of proneuronal and inter-proneuronal domains by hairy- and enhancer of split-related genes in zebrafish neuroectoderm. *Development* **132**, 1375-1385.
- Bai, G., Sheng, N., Xie, Z., Bian, W., Yokota, Y., Benezra, R., Kageyama, R., Guillemot, F. and Jing, N. (2007). *Id* sustains *Hes1* expression to inhibit precocious neurogenesis by releasing negative autoregulation of *Hes1*. *Dev. Cell* **13**, 283-297.
- Balciunas, D., Wangensteen, K. J., Wilber, A., Bell, J., Geurts, A., Sivasubbu, S., Wang, X., Hackett, P. B., Largaespada, D. A., Mclvor, R. S. et al. (2006). Harnessing a high cargo-capacity transposon for genetic applications in vertebrates. *PLoS Genet.* **2**, e169.
- Bally-Cuif, L., Dubois, L. and Vincent, A. (1998). Molecular cloning of *Zco2*, the zebrafish homolog of *Xenopus Xco2* and mouse *EBF-2*, and its expression during primary neurogenesis. *Mech. Dev.* **77**, 85-90.
- Batista, M. F., Jacobstein, J. and Lewis, K. E. (2008). Zebrafish V2 cells develop into excitatory CiD and Notch signalling dependent inhibitory VeLD interneurons. *Dev. Biol.* **322**, 263-275.
- Bierkamp, C. and Campos-Ortega, J. A. (1993). A zebrafish homologue of the *Drosophila* neurogenic gene *Notch* and its pattern of transcription during early embryogenesis. *Mech. Dev.* **43**, 87-100.
- Bingham, S., Chaudhari, S., Vanderlaan, G., Itoh, M., Chitnis, A. and Chandrasekhar, A. (2003). Neurogenic phenotype of mind bomb mutants leads to severe patterning defects in the zebrafish hindbrain. *Dev. Dyn.* **228**, 451-463.
- Blader, P., Fischer, N., Gradwohl, G., Guillemot, F. and Strahle, U. (1997). The activity of neurogenin1 is controlled by local cues in the zebrafish embryo. *Development* **124**, 4557-4569.
- Castro, B., Barolo, S., Bailey, A. M. and Posakony, J. W. (2005). Lateral inhibition in proneural clusters: cis-regulatory logic and default repression by Suppressor of Hairless. *Development* **132**, 3333-3344.
- Castro, D. S., Skowronska-Krawczyk, D., Arman, O., Donaldson, I. J., Parras, C., Hunt, C., Critchley, J. A., Nguyen, L., Gossler, A., Gottgens, B. et al. (2006). Proneural bHLH and Brn proteins coregulate a neurogenic program through cooperative binding to a conserved DNA motif. *Dev. Cell* **11**, 831-844.
- Chan, J., Mably, J. D., Serluca, F. C., Chen, J. N., Goldstein, N. B., Thomas, M. C., Cleary, J. A., Brennan, C., Fishman, M. C. and Roberts, T. M. (2001). Morphogenesis of prechordal plate and notochord requires intact Eph/ephrin B signalling. *Dev. Biol.* **234**, 470-482.
- Chandrasekhar, A., Moens, C. B., Warren, J. T., Jr, Kimmel, C. B. and Kuwada, J. Y. (1997). Development of branchiomotor neurons in zebrafish. *Development* **124**, 2633-2644.
- Cheng, Y. C., Amoyel, M., Qiu, X., Jiang, Y. J., Xu, Q. and Wilkinson, D. G. (2004). Notch activation regulates the segregation and differentiation of rhombomere boundary cells in the zebrafish hindbrain. *Dev. Cell* **6**, 539-550.
- Culi, J. and Modolell, J. (1998). Proneural gene self-stimulation in neural precursors: an essential mechanism for sense organ development that is regulated by Notch signaling. *Genes Dev.* **12**, 2036-2047.
- de Bellard, M., Barembaum, M., Arman, O. and Bronner-Fraser, M. (2007). Lunatic fringe causes expansion and increased neurogenesis of trunk neural tube and neural crest populations. *Neuron Glia Biol.* **3**, 93-103.
- de Celis, J. F., Garcia-Bellido, A. and Bray, S. J. (1996). Activation and function of Notch at the dorsal-ventral boundary of the wing imaginal disc. *Development* **122**, 359-369.
- Del Barrio, M. G., Taveira-Marques, R., Muroyama, Y., Yuk, D. I., Li, S., Wines-Samuelson, M., Shen, J., Smith, H. K., Xiang, M., Rowitch, D. et al. (2007). A regulatory network involving *Foxn4*, *Mash1* and delta-like 4/Notch1 generates V2a and V2b spinal interneurons from a common progenitor pool. *Development* **134**, 3427-3436.
- Dominguez, M. and de Celis, J. F. (1998). A dorsal/ventral boundary established by Notch controls growth and polarity in the *Drosophila* eye. *Nature* **396**, 276-278.
- Dubois, L., Bally-Cuif, L., Crozatier, M., Moreau, J., Paquereau, L. and Vincent, A. (1998). *XCoe2*, a transcription factor of the *Col/Olf-1/EBF* family involved in the specification of primary neurons in *Xenopus*. *Curr. Biol.* **8**, 199-209.
- Fryer, C. J., Lamar, E., Turbachova, I., Kintner, C. and Jones, K. A. (2002). Mastermind mediates chromatin-specific transcription and turnover of the Notch enhancer complex. *Genes Dev.* **16**, 1397-1411.
- Gaiano, N., Nye, J. S. and Fishell, G. (2000). Radial glial identity is promoted by Notch1 signaling in the murine forebrain. *Neuron* **26**, 395-404.
- Geling, A., Steiner, H., Willem, M., Bally-Cuif, L. and Haass, C. (2002). A gamma-secretase inhibitor blocks Notch signaling in vivo and causes a severe neurogenic phenotype in zebrafish. *EMBO Rep.* **3**, 688-694.
- Glittenberg, M., Pitsouli, C., Garvey, C., Delidakis, C. and Bray, S. (2006). Role of conserved intracellular motifs in Serrate signalling, cis-inhibition and endocytosis. *EMBO J.* **25**, 4697-4706.
- Gray, M., Moens, C. B., Amacher, S. L., Eisen, J. S. and Beattie, C. E. (2001). Zebrafish *deadly seven* functions in neurogenesis. *Dev. Biol.* **237**, 306-323.
- Haddon, C., Smithers, L., Schneider-Maunoury, S., Coche, T., Henrich, D. and Lewis, J. (1998). Multiple delta genes and lateral inhibition in zebrafish primary neurogenesis. *Development* **125**, 359-370.
- Hanneman, E., Trevarrow, B., Metcalfe, W. K., Kimmel, C. B. and Westerfield, M. (1988). Segmental pattern of development of the hindbrain and spinal cord of the zebrafish embryo. *Development* **103**, 49-58.
- Heitzler, P., Bourouis, M., Ruel, L., Carteret, C. and Simpson, P. (1996). Genes of the Enhancer of split and achaete-scute complexes are required for a regulatory loop between Notch and Delta during lateral signalling in *Drosophila*. *Development* **122**, 161-171.
- Holley, S. A., Julich, D., Rauch, G. J., Geisler, R. and Nusslein-Volhard, C. (2002). *her1* and the notch pathway function within the oscillator mechanism that regulates zebrafish somitogenesis. *Development* **129**, 1175-1183.
- Irving, C., Nieto, M. A., DasGupta, R., Charnay, P. and Wilkinson, D. G. (1996). Progressive spatial restriction of *Sek-1* and *Krox-20* gene expression during hindbrain segmentation. *Dev. Biol.* **173**, 26-38.
- Ishii, Y., Nakamura, S. and Osumi, N. (2000). Demarcation of early mammalian cortical development by differential expression of fringe genes. *Brain Res. Dev. Brain Res.* **119**, 307-320.
- Itoh, M., Kim, C. H., Palardy, G., Oda, T., Jiang, Y. J., Maust, D., Yoo, S. Y., Lorick, K., Wright, G. J., Ariza-McNaughton, L. et al. (2003). Mind bomb is a ubiquitin ligase that is essential for efficient activation of Notch signaling by Delta. *Dev. Cell* **4**, 67-82.
- Jacobsen, T. L., Brennan, K., Arias, A. M. and Muskavitch, M. A. (1998). Cis-interactions between Delta and Notch modulate neurogenic signalling in *Drosophila*. *Development* **125**, 4531-4540.
- Jiang, Y. J., Brand, M., Heisenberg, C. P., Beuchle, D., Furutani-Seiki, M., Kelsch, R. N., Warga, R. M., Granato, M., Haffter, P., Hammerschmidt, M. et al. (1996). Mutations affecting neurogenesis and brain morphology in the zebrafish, *Danio rerio*. *Development* **123**, 205-216.
- Johnston, S. H., Rauskolb, C., Wilson, R., Prabhakaran, B., Irvine, K. D. and Vogt, T. F. (1997). A family of mammalian Fringe genes implicated in boundary determination and the Notch pathway. *Development* **124**, 2245-2254.
- Julich, D., Hwee Lim, C., Round, J., Nicolaije, C., Schroeder, J., Davies, A., Geisler, R., Lewis, J., Jiang, Y. J. and Holley, L. A. (2005). *beamter/deltaC* and the role of Notch ligands in the zebrafish somite segmentation, hindbrain neurogenesis and hypochord differentiation. *Dev. Biol.* **286**, 391-404.
- Kageyama, R., Ohtsuka, T. and Kobayashi, T. (2007). The *Hes* gene family: repressors and oscillators that orchestrate embryogenesis. *Development* **134**, 1243-1251.

- Kageyama, R., Ohtsuka, T., Shimojo, H. and Imayoshi, I. (2008). Dynamic Notch signaling in neural progenitor cells and a revised view of lateral inhibition. *Nat. Neurosci.* **11**, 1247-1251.
- Kawakami, K., Shima, A. and Kawakami, N. (2000). Identification of a functional transposase of the Tol2 element, an Ac-like element from the Japanese medaka fish, and its transposition in the zebrafish germ lineage. *Proc. Natl. Acad. Sci. USA* **97**, 11403-11408.
- Kim, C. H., Bae, Y. K., Yamanaka, Y., Yamashita, S., Shimizu, T., Fujii, R., Park, H. C., Yeo, S. Y., Huh, T. L., Hibi, M. et al. (1997). Overexpression of neurogenin induces ectopic expression of HuC in zebrafish. *Neurosci. Lett.* **239**, 113-116.
- Kim, J., Irvine, K. D. and Carroll, S. B. (1995). Cell recognition, signal induction, and symmetrical gene activation at the dorsal-ventral boundary of the developing *Drosophila* wing. *Cell* **82**, 795-802.
- Kimmel, C. B., Ballard, W. W., Kimmel, S. R., Ullmann, B. and Schilling, T. F. (1995). Stages of embryonic development of the zebrafish. *Dev. Dyn.* **203**, 253-310.
- Korz, V., Sleptsova, I., Liao, J., He, J. and Gong, Z. (1998). Expression of zebrafish bHLH genes *ngn1* and *nrd* defines distinct stages of neural differentiation. *Dev. Dyn.* **213**, 92-104.
- Koyano-Nakagawa, N., Kim, J., Anderson, D. and Kintner, C. (2000). *Hes6* acts in a positive feedback loop with the neurogenins to promote neuronal differentiation. *Development* **127**, 4203-4216.
- Kunisch, M., Haenlin, M. and Campos-Ortega, J. A. (1994). Lateral inhibition mediated by the *Drosophila* neurogenic gene *delta* is enhanced by proneural proteins. *Proc. Natl. Acad. Sci. USA* **91**, 10139-10143.
- Laufer, E., Dahn, R., Orozco, O. E., Yeo, C. Y., Pisenti, J., Henrique, D., Abbott, U. K., Fallon, J. F. and Tabin, C. (1997). Expression of *Radical fringe* in limb-bud ectoderm regulates apical ectodermal ridge formation. *Nature* **386**, 366-373.
- Leve, C., Gajewski, M., Rohr, K. B. and Tautz, D. (2001). Homologues of *c-hairy1* (*her9*) and *lunatic fringe* in zebrafish are expressed in the developing central nervous system, but not in the presomitic mesoderm. *Dev. Genes Evol.* **211**, 493-500.
- Lewis, J. (1998). Notch signalling and the control of cell fate choices in vertebrates. *Semin. Cell Dev. Biol.* **9**, 583-589.
- Liu, Q., Babb, S. G., Novince, Z. M., Doedens, A. L., Marrs, J. and Raymond, P. A. (2001). Differential expression of *cadherin-2* and *cadherin-4* in the developing and adult zebrafish visual system. *Vis. Neurosci.* **18**, 923-933.
- Louvi, A. and Artavanis-Tsakonas, S. (2006). Notch signalling in vertebrate neural development. *Nat. Rev. Neurosci.* **7**, 93-102.
- Malatesta, P., Hartfuss, E. and Gotz, M. (2000). Isolation of radial glial cells by fluorescently-activated cell sorting reveals a neuronal lineage. *Development* **127**, 5253-5263.
- Malatesta, P., Hack, M. A., Hartfuss, E., Kettenmann, H., Klinkert, W., Kirchhoff, F. and Gotz, M. (2003). Neuronal or glial progeny: regional differences in radial glia fate. *Neuron* **37**, 751-764.
- Martin, S. C., Heinrich, G. and Sandell, J. H. (1998). Sequence and expression of glutamic acid decarboxylase isoforms in the developing zebrafish. *J. Comp. Neurol.* **396**, 253-266.
- Matsuda, M. and Chitnis, A. B. (2009). Interaction with Notch determines endocytosis of specific *Delta* ligands in zebrafish neural tissue. *Development* **136**, 197-206.
- Maves, L., Jackman, W. and Kimmel, C. B. (2002). *FGF3* and *FGF8* mediate a rhombomere 4 signaling activity in the zebrafish hindbrain. *Development* **129**, 3825-3837.
- Mendelson, B. (1986). Development of reticulospinal neurons of the zebrafish. I. Time of origin. *J. Comp. Neurol.* **251**, 160-171.
- Micchelli, C. A. and Blair, S. S. (1999). Dorsal-ventral lineage restriction in wing imaginal discs requires Notch. *Nature* **401**, 473-476.
- Micchelli, C. A., Rulifson, E. J. and Blair, S. S. (1997). The function and regulation of cut expression on the wing margin of *Drosophila*: Notch, *Wingless* and a dominant negative role for *Delta* and *Serrate*. *Development* **124**, 1485-1495.
- Mikkola, I., Fjose, A., Kuwada, J. Y., Wilson, S., Guddal, P. H. and Krauss, S. (1992). The paired domain-containing nuclear factor *pax[b]* is expressed in specific commissural interneurons in zebrafish embryos. *J. Neurobiol.* **23**, 933-946.
- Moens, C. B., Yan, Y. L., Appel, B., Force, A. G. and Kimmel, C. B. (1996). *valentino*: a zebrafish gene required for normal hindbrain segmentation. *Development* **122**, 3981-3990.
- Moloney, D. J., Panin, V. M., Johnston, S. H., Chen, J., Shao, L., Wilson, R., Wang, Y., Stanley, P., Irvine, K. D., Haltiwanger, R. S. et al. (2000). *Fringe* is a glycosyltransferase that modifies Notch. *Nature* **406**, 369-375.
- Mumm, J. S., Schroeter, E. H., Saxena, M. T., Griesemer, A., Tian, X., Pan, D. J., Ray, W. J. and Kopan, R. (2000). A ligand-induced extracellular cleavage regulates gamma-secretase-like proteolytic activation of Notch1. *Mol. Cell* **5**, 197-206.
- Neave, B., Rodaway, A., Wilson, S. W., Patient, R. and Holder, N. (1995). Expression of zebrafish *GATA 3* (*gta3*) during gastrulation and neurogenesis suggests a role in the specification of cell fate. *Mech. Dev.* **51**, 169-182.
- Ohtsuka, T., Ishibashi, M., Gradwohl, G., Nakanishi, S., Guillemot, F. and Kageyama, R. (1999). *Hes1* and *Hes5* as notch effectors in mammalian neuronal differentiation. *EMBO J.* **18**, 2196-2207.
- Okuda, Y., Yoda, H., Uchikawa, M., Furutani-Seiki, M., Takeda, H., Kondoh, H. and Kamachi, Y. (2006). Comparative genomic and expression analysis of group B1 *sox* genes in zebrafish indicates their diversification during vertebrate evolution. *Dev. Dyn.* **235**, 811-825.
- Oxtoby, E. and Jowett, T. (1993). Cloning of the zebrafish *krox-20* gene (*krx-20*) and its expression during hindbrain development. *Nucleic Acids Res.* **21**, 1087-1095.
- Panin, V. M., Papayannopoulos, V., Wilson, R. and Irvine, K. D. (1997). *Fringe* modulates Notch-ligand interactions. *Nature* **387**, 908-912.
- Papayannopoulos, V., Tomlinson, A., Panin, V. M., Rauskolb, C. and Irvine, K. D. (1998). Dorsal-ventral signaling in the *Drosophila* eye. *Science* **281**, 2031-2034.
- Park, H. C., Hong, S. K., Kim, H. S., Kim, S. H., Yoon, E. J., Kim, C. H., Miki, N. and Huh, T. L. (2000). Structural comparison of zebrafish *Elav/Hu* and their differential expressions during neurogenesis. *Neurosci. Lett.* **279**, 81-84.
- Park, S. H., Yeo, S. Y., Yoo, K. W., Hong, S. K., Lee, S., Rhee, M., Chitnis, A. B. and Kim, C. H. (2003). *Zath3*, a neural basic helix-loop-helix gene, regulates early neurogenesis in the zebrafish. *Biochem. Biophys. Res. Commun.* **308**, 184-190.
- Passini, M. A., Kurtzman, A. L., Canger, A. K., Asch, W. S., Wray, G. A., Raymond, P. A. and Schechter, N. (1998). Cloning of zebrafish *vsx1*: expression of a paired-like homeobox gene during CNS development. *Dev. Genet.* **23**, 128-141.
- Peng, C. Y., Yajima, H., Burns, C. E., Zon, L. I., Sisodia, S. S., Pfaff, S. L. and Sharma, K. (2007). Notch and MAML signaling drives *Scf*-dependent interneuron diversity in the spinal cord. *Neuron* **53**, 813-827.
- Postlethwait, J., Amores, A., Cresko, W., Singer, A. and Yan, Y. L. (2004). Subfunction partitioning, the teleost radiation and the annotation of the human genome. *Trends Genet.* **20**, 481-490.
- Prince, V. E., Holley, S. A., Bally-Cuif, L., Prabhakaran, B., Oates, A. C., Ho, R. K. and Vogt, T. F. (2001). Zebrafish *lunatic fringe* demarcates segmental boundaries. *Mech. Dev.* **105**, 175-180.
- Qiu, X., Xu, H., Haddon, C., Lewis, J. and Jiang, Y. J. (2004). Sequence and embryonic expression of three zebrafish *fringe* genes: *lunatic fringe*, *radical fringe*, and *manic fringe*. *Dev. Dyn.* **231**, 621-630.
- Rauskolb, C., Correia, T. and Irvine, K. D. (1999). *Fringe*-dependent separation of dorsal and ventral cells in the *Drosophila* wing. *Nature* **401**, 476-480.
- Robu, M. E., Larson, J. D., Nasevicius, A., Beiraghi, S., Brenner, C., Farber, S. A. and Ekker, S. C. (2007). *p53* activation by knockdown technologies. *PLoS Genet.* **3**, e78.
- Rodriguez-Esteban, C., Schwabe, J. W., De La Pena, J., Foy, B., Eshelman, B. and Belmonte, J. C. (1997). *Radical fringe* positions the apical ectodermal ridge at the dorsoventral boundary of the vertebrate limb. *Nature* **386**, 360-366.
- Sakamoto, K., Ohara, O., Takagi, M., Takeda, S. and Katsube, K. (2002). Intracellular cell-autonomous association of Notch and its ligands: a novel mechanism of Notch signal modification. *Dev. Biol.* **241**, 313-326.
- Schier, A. F., Neuhauss, S. C., Harvey, M., Malicki, J., Solnica-Krezel, L., Stainier, D. Y., Zwartkruis, F., Abdellah, S., Stemple, D. L., Rangini, Z. et al. (1996). Mutations affecting the development of the embryonic zebrafish brain. *Development* **123**, 165-178.
- Seth, A., Culverwell, J., Walkowicz, M., Toro, S., Rick, J. M., Neuhauss, S. C., Varga, Z. M. and Karlstrom, R. O. (2006). *belladonna/lhx2* is required for neural patterning and midline axon guidance in the zebrafish forebrain. *Development* **133**, 725-735.
- Shih, J. and Fraser, S. E. (1995). Distribution of tissue progenitors within the shield region of the zebrafish gastrula. *Development* **121**, 2755-2765.
- Shimojo, H., Ohtsuka, T. and Kageyama, R. (2008). Oscillations in notch signaling regulate maintenance of neural progenitors. *Neuron* **58**, 52-64.
- Sieger, D., Tautz, D. and Gajewski, M. (2004). *her11* is involved in the somitogenesis clock in zebrafish. *Dev. Genes Evol.* **214**, 393-406.
- Takke, C., Dornseifer, P. v., Weizsacker, E. and Campos-Ortega, J. A. (1999). *her4*, a zebrafish homologue of the *Drosophila* neurogenic gene *E(spl)*, is a target of NOTCH signalling. *Development* **126**, 1811-1821.
- Thaeron, C., Avaron, F., Casane, D., Borday, V., Thisse, B., Thisse, C., Boulekbache, H. and Laurenti, P. (2000). Zebrafish *evx1* is dynamically expressed during embryogenesis in subsets of interneurons, posterior gut and urogenital system. *Mech. Dev.* **99**, 167-172.
- Thisse, C., Thisse, B., Schilling, T. F. and Postlethwait, J. H. (1993). Structure of the zebrafish *snail1* gene and its expression in wild-type, spadetail and no tail mutant embryos. *Development* **119**, 1203-1215.
- Thomas, G. B. and van Meyel, D. J. (2007). The glycosyltransferase *Fringe* promotes *Delta*-Notch signaling between neurons and glia, and is required for subtype-specific glial gene expression. *Development* **134**, 591-600.

- Trevarrow, B., Marks, D. L. and Kimmel, C. B.** (1990). Organization of hindbrain segments in the zebrafish embryo. *Neuron* **4**, 669-679.
- van Eeden, F. J., Granato, M., Schach, U., Brand, M., Furutani-Seiki, M., Haffter, P., Hammerschmidt, M., Heisenberg, C. P., Jiang, Y. J., Kane, D. A. et al.** (1996). Mutations affecting somite formation and patterning in the zebrafish, *Danio rerio*. *Development* **123**, 153-164.
- Visan, I., Tan, J. B., Yuan, J. S., Harper, J. A., Koch, U. and Guidos, C. J.** (2006). Regulation of T lymphopoiesis by Notch1 and Lunatic fringe-mediated competition for intrathymic niches. *Nat. Immunol.* **7**, 634-643.
- Wang, X., Emelyanov, A., Korzh, V. and Gong, Z.** (2003). Zebrafish atonal homologue *zath3* is expressed during neurogenesis in embryonic development. *Dev. Dyn.* **227**, 587-592.
- Westin, L. and Lardelli, M.** (1997). Three novel *Notch* genes in zebrafish: implications for vertebrate *Notch* gene evolution and function. *Dev. Genes Evol.* **207**, 51-63.
- Wettstein, D. A., Turner, D. L. and Kintner, C.** (1997). The *Xenopus* homolog of *Drosophila* Suppressor of Hairless mediates Notch signaling during primary neurogenesis. *Development* **124**, 693-702.
- Yeo, S. Y., Kim, M., Kim, H. S., Huh, T. L. and Chitnis, A. B.** (2007). Fluorescent protein expression driven by *her4* regulatory elements reveals the spatiotemporal pattern of Notch signaling in the nervous system of zebrafish embryos. *Dev. Biol.* **301**, 555-567.
- Zeltser, L. M., Larsen, C. W. and Lumsden, A.** (2001). A new developmental compartment in the forebrain regulated by Lunatic fringe. *Nat. Neurosci.* **4**, 683-684.

Appendix 3

accepted Article in *Zebrafish*

Global repression of cancer gene expression in a zebrafish model of melanoma is linked to epigenetic regulation

Viviana Anelli, Cristina Santoriello, Martin Distel, Reinhard W. Köster, Francesca Ciccarelli and Marina Mione

Accepted in *Zebrafish* 2009

Contribution:

This project was mainly conducted in Marina Mione's lab. I discovered, isolated and characterized the *kita:KalTA4* enhancer trap strain, used in this melanoma model as depicted in Fig.1. I also contributed to writing the parts of the manuscript concerning the *kita:KalTA4* strain.

Zebrafish

Journal Name: <http://mc.manuscriptcentral.com/zebrafish>

Global repression of cancer gene expression in a zebrafish model of melanoma is linked to epigenetic regulation.

Journal:	<i>Zebrafish</i>
Manuscript ID:	ZEB-2009-0612.R1
Manuscript Type:	Special Issue on Cancer Biology
Date Submitted by the Author:	
Complete List of Authors:	Anelli, Viviana; IFOM, The FIRC Institute of Molecular Oncology Santoriello, Cristina; IFOM, The FIRC Institute of Molecular Oncology Distel, Martin; Helmholtz Center Munich, Institute of Developmental Genetics Koester, Reinhard; Helmholtz Zentrum München, Institute of Developmental Genetics Cicarelli, Francesca; IEO, Institute of European Oncology Mione, Marina; IFOM, the FIRC Institute of Molecular Oncology
Keyword:	Cell biology, Molecular Biology, Zebrafish, Pigment Biology, Disease Model



1
2
3 **Global repression of cancer gene expression in a zebrafish model of melanoma is**
4 **linked to epigenetic regulation.**
5
6
7

8 Viviana Anelli¹, Cristina Santoriello¹, Martin Distel³, Reinhard W. Köster³, Francesca
9 D. Ciccarelli², Marina Mione¹
10
11

12
13 ¹IFOM, The Firc Institute of Molecular Biology, ²IEO, Institute of European Oncology, via Adamello
14 16, 20139 Milan, ITALY; ³Helmholtz Center Munich - Institute of Developmental Genetics. Munich,
15 Germany
16
17

18
19 We have established a model of melanoma progression in zebrafish through the
20 generation of transgenic lines specifically expressing oncogenic human HRAS in the
21 melanocytic lineage.
22
23

24
25 In these tumors we have carried out quantitative expression analysis of several
26 putative cancer genes, from known¹ and predicted cancer gene lists. In particular we
27 analysed 39 out of 101 putative cancer genes identified with a bioinformatics
28 approach² and selected for the low frequency of duplication and the high connectivity
29 in protein networks. Data obtained by real-time PCR analysis from zebrafish
30 melanoma tissue shows that the expression of many cancer genes is down-regulated
31 in zebrafish melanomas, whereas only cell cycle genes are up-regulated. In order to
32 understand whether this trend is due to global repression of gene expression
33 associated to a repressive chromatin state, we investigated whether changes of histone
34 methylation were detectable in our melanoma model. We found substantial
35 differences in the levels of H3K9me3, H4K20me2, H3K27me3, H3K4me3 and
36 H3R2me2a immunostaining in melanoma tissue as compared with normal skin. Thus
37 our analysis suggests that in our model, like in human melanoma, important changes
38 occur to the methylation status of histones. Although the outcome of these changes is
39 still unknown, they could be responsible for the global repression of gene expression
40 through epigenetic regulation shown in this study.
41
42
43
44
45
46
47
48
49
50
51
52
53
54
55
56

57 **Introduction**

58 For decades, scientists have been engaged in dissecting the origins of human cancer,
59 and the relative roles of genetic versus epigenetic abnormalities. An explosion of data
60

1
2
3 indicating the importance of epigenetic processes, especially those resulting in the
4 silencing of key regulatory genes, has led to the realization that genetics and
5 epigenetic mechanisms cooperate during all stages of cancer development. Epigenetic
6 is defined as mitotically and meiotically heritable changes in gene expression that are
7 not accompanied by changes in DNA sequence. These epigenetic alterations may
8 involve changes in the methylation status of cytosine bases in the context of CpG
9 dinucleotides within the DNA itself and covalent modifications of amino acid
10 residues in the histones around which the DNA is wrapped. Like most biological
11 processes, silencing can become deregulated, resulting in the development of a
12 disease status. Somewhat surprisingly, expression studies have shown a general
13 repressive state of the cancer genome³ This seems to be due to an abnormally high
14 concentration of methyltransferases⁴. The consequences of these generalized changes
15 on the progression of the disease are currently unknown.

16 Zebrafish is now emerging as an effective system for the study of the fundamental
17 aspects of tumorigenesis. In fact, it develops a wide spectrum of cancers resembling
18 human malignancies. A comparative analysis of microarray data from zebrafish
19 tumors revealed molecular conservation of expression profiles between fish and
20 human tumors, highlighting the potential of zebrafish for modeling human cancers⁵.
21 Most remarkably, zebrafish cancer models allow large-scale genetic and
22 pharmacological approaches, including modifier screens, drug screens and
23 modulation of tumor suppressors. One of the approaches for which zebrafish cancer
24 models could be particularly useful is the study of the mechanisms of action of
25 oncogenes and oncosuppressors. For many of these genes the definition of
26 “oncogenes/oncosuppressor” is based on their ability to transform or prevent
27 transformation *in vitro*⁶.

28 The link between “cancer genes” and the disease is based on the detection of genetic
29 alterations – that is number of copies in the genome, expression levels, single base
30 substitutions and rearrangements - of these genes in human cancer samples. These
31 data are collected in the Cancer Gene Census project developed by the Sanger
32 Institute (<http://www.sanger.ac.uk/genetics/CGP/census/>). From the very beginning
33 the Cancer Gene Census project faced the difficult task to distinguish between
34 “passengers and drivers”⁷. Often this distinction will only be possible on an
35 experimental basis: i.e. do mutations of that gene induce cancer?
36
37
38
39
40
41
42
43
44
45
46
47
48
49
50
51
52
53
54
55
56
57
58
59
60

1
2
3 To provide an in vivo genetic model of cancer progression, for the study of cancer
4 gene function and other mechanistic studies, we develop a transgenic reporter line
5 *tg(UAS:eGFP-HRAS_GV12)*, that when crossed with fish expressing a modified
6 version of the yeast transactivator GAL4 in the melanocytic lineage, develops
7 malignant melanomas with high frequency. Furthermore, as a first step towards in
8 depth mechanistic studies and genetic manipulation, we have used this model to
9 quantify the expression of a number of oncogenes and oncosuppressors in the tumors.
10
11
12
13
14
15
16

17 **Material and Methods**

20 **Fish maintenance and generation of the transgenic lines**

21 Zebrafish were maintained and crossed according to standard methods⁸.

22 The *tg(UAS:eGFP-HRAS_G12V)io6* line was generated using a T2MUAMCS
23 plasmid⁹ in which we subcloned the fusion cassette *eGFP-HRAS_G12V*. This cassette
24 encodes for a chimaeric protein composed of eGFP at the N-terminus and the oncogenic
25 version of the human HRAS gene, carrying the mutation G12V¹⁰. Fertilized eggs were
26 injected with 2nl of a mixture containing 25ng/ml of circular plasmid and 25ng/ml of
27 T2 transposase mRNA. Injected embryos were raised to adulthood and crossed with
28 the *Et(kita:GalTA4,UAS:mCherry)hzm1*. Fish from this cross were raised; the
29 occurrence and frequency of fish displaying tumor or black fins at the age of 4 months
30 was recorded.
31
32
33
34
35
36
37
38
39

40 The *Et(kita:GalTA4,UAS:mCherry)hzm1;Tg(UAS:eGFP-H-RASV12)io6* was also
41 crossed and raised in *tp53*^{-/-} background. The genotyping was performed on fin clips
42 as previously described¹¹.
43
44
45
46
47
48
49

50 **RNA extraction and Quantitative PCR**

51 Caudal fins sectioned from 5 months old WT and
52 *Et(kita:GalTA4,UAS:mCherry)hzm;Tg(UAS:eGFP-H-RASV12)io6* (with tumor) were
53 homogenized in RLT buffer and total RNA was extracted with RNeasy mini kit
54 (Quiagen). After treatment with turbo DNase (Ambion), RNA quantity was
55 determined by spectrophotometer. cDNA was synthesized from total RNA (100 ng)
56 with oligo(dT)₂₀ primers using Superscript III reverse transcriptase (Invitrogen)
57 according to the manufacturer's instructions.
58
59
60

1
2
3
4
5
6
7
8
9
10
11
12
13
14
15
16
17
18
19
20
21
22
23
24
25
26
27
28
29
30
31
32
33
34
35
36
37
38
39
40
41
42
43
44
45
46
47
48
49
50
51
52
53
54
55
56
57
58
59
60

Quantitative Real-time PCR was performed with an ABI PRISM 7900HT thermocycler using the SYBR Green Supermix kit (Applied Biosystem). cDNA was amplified in triplicate in a reaction volume of 25 μ l. Primers were designed using Primer 3 software and are shown in the supplementary Table I. The conditions for the reactions were the following: 10 min at 95 $^{\circ}$ C, followed by 40 cycles of 15 s at 95 $^{\circ}$ C and 60 s at 60 $^{\circ}$ C. For any sample the expression level was analyzed using Q-Gene[®] software¹², which expresses data as mean normalized expression. This software calculates means and standard errors for the reference gene (β -actin) as well as for the targets and determines a Mean Normalized Expression (MNE) (Supplementary Table II). Data in Figure 2 are presented as % of MNE of target genes in the tumor tissue compared to MNE of the target genes in the control tissue. The number and genotype of the analysed tumor samples is as follows: 3 melanoma, *tp53*^{+/+}, 5 melanoma *tp53*^{+/-}, 3 melanomas *tp53*^{-/-}

Database

We used Oncomine¹³ cancer Microarray database (<http://www.oncomine.org>) to study gene expression of our candidate cancer genes in human melanoma tumors (versus their normal tissue). Gene expression analysis derived from two studies were used: 1) Telantov melanoma¹⁴, which analyzes 45 primary melanoma versus 7 normal skin tissue); 2) Hoek melanoma¹⁵ which analyzes 18 cutaneous melanoma lines versus 3 normal melanocyte lines.

Immunofluorescence and antisera

Adult fish were sacrificed by anaesthetic overdose and tumors or corresponding areas from wild type fish were excised and embedded unfixed in OCT. Cryostat sections, 14 μ m thick were fixed in 2% paraformaldehyde for 2'. We used the following antisera: anti H3K9me3 (Upstate, 07-442), H3K4me3 (Abcam, ab1012), H3R2mea (Abcam, ab8046) H3K27me3 (Upstate, 07-449), H4K20me2 (Upstate, 07-367), mouse anti HP1 (Millipore, clone 42s2). Secondary antibodies conjugated with Alexa 633 were from Molecular Probes. Dapi counterstain was carried out on all sections. The expression of HRASGV12-GFP was still visible as green fluorescence in fixed sections.

Results

Generation of the melanoma zebrafish line.

In order to generate a transgenic line developing melanoma we took advantage of the binary GAL4-UAS system¹⁶. This system has been extensively used in *Drosophila* and it is becoming very popular also in zebrafish⁹.

The system is based on the cross between a driver (expressing the transactivator GAL4) and a reporter line (expressing any reporter gene under the control of the UAS elements). For our purpose we used a melanocytic specific driver line, which was crossed with an oncogenic reporter line.

The driver line was generated through an enhancer trap approach using a modified Gal4-activator optimized for expression in zebrafish¹⁷. One of the lines “trapped” the *kita* enhancer. This driver line was named *Et(kita:GalTA4,UAS:mCherry)hzm1* and the construct used to generate it is depicted in Figure 1A. *Kita* is expressed in the melanocytic lineage¹⁸ and the expression of the internal reporter mCherry recapitulates the expression of the endogenous *kita* gene.

For the reporter line we decided to use the human *H-RAS* gene and in particular a constitutively active form carrying the mutation G12V.

We previously generated a chimaeric H-RASV12 protein tagged with GFP at the N-terminus¹⁰. We inserted this cassette in the pT2MUAMCS⁹ as shown in Figure 1A. The reporter line so generated has been named *Tg(UAS:eGFP-H-RAS_GV12)io6*. A full description of the single and double lines will be reported elsewhere (Santoriello et al., in preparation).

We raised fish from the crosses between *Et(kita:GalTA4,UAS:mCherry)hzm1* and *Tg(5XUAS:eGFP-H-RASV12)io6* and we observed that starting from 4 weeks of age these fish developed pigmented tumors more often at the level of the caudal fin (Figure 1B). We evaluated the number of the fish bearing visible tumor masses at 2-3 months of age, and this accounted for around 20% of the double transgenic fish, as shown in Figure 1C. The development of melanoma in the line will be described in more details elsewhere (Santoriello et al., in preparation).

1
2
3
4
5
6
7
8
9
10
11
12
13
14
15
16
17
18
19
20
21
22
23
24
25
26
27
28
29
30
31
32
33
34
35
36
37
38
39
40
41
42
43
44
45
46
47
48
49
50
51
52
53
54
55
56
57
58
59
60

As the GAL4-UAS system allows to express or re-express tumor suppressors and modifiers specifically in the melanoma cells using UAS-mediated expression constructs, we decided to screen hyperplastic melanoma tissue for the best candidate tumor suppressor for a re-expression approach using quantitative RT-PCR analysis. Indeed, one of the requisites of an ideal tumor suppressor candidate would be its downregulation in melanoma tissue. From a list of 101 potential cancer genes² we started with 39 genes and evaluated their expression levels. We chose this list as opposed to the list of the Cancer Gene Census because the evaluation of their expression levels is a first step towards the validation of these genes as novel cancer genes.

Expression level of new candidate cancer genes in zebrafish melanoma tumor.

Using the genetic melanoma model described above we carried out quantitative analysis of expression of several candidate cancer genes, which have been identified as such because they share the same systems-level properties of known cancer genes. In particular, these genes tend not to retain duplications² but unlike most human singletons, they encode central hubs of highly interconnected modules within the protein-protein interaction network (PIN) derived from the Human Protein Reference Database, which consist of manually curated collections of in vivo, in vitro and high-throughput data¹⁹. Of the 101 identified putative cancer genes² we chose 39 genes that belongs to different categories (see below).

To this purpose we extracted mRNA from caudal fin tumors of 5 months old *Et(kita:GalTA4,UAS:mCherry)hzm1; Tg(5XUAS:eGFP-H-RASV12)io6* double transgenic fish and compared the expressions of 39 candidate cancer genes in several melanoma samples with that in the fins of age-matched wild type zebrafish. All the genes were normalized to the expression of β -actin as an endogenous control using the Q-gene¹² software, which calculate means and standard errors for the reference gene as well as for the targets and determines a Mean Normalized Expression (MNE) (Supplementary Table II). Data in Figure 2 are presented as % of MNE of target genes in the tumor tissue on the MNE of the target genes in the control tissue. The MNE are shown in the Supplementary Table II.

As shown in Figure 2, approximately 40% of the putative cancer genes (16/39) were

1
2
3 found to be down-regulated, whereas approximately 12% (5/39) were up-regulated,
4 and the remaining 19 genes showed no statistically significant changes in expression.
5 (shown in Supplementary Table II).
6
7

8 Downregulated genes included both oncogenes and tumor suppressors as classified in
9 OMIM (Online Mendelian Inheritance in Man) database
10 (<http://www.ncbi.nlm.nih.gov/sites/entrez?db=OMIM>). The downregulated genes
11 belong to different categories: 7 (*cd247*, *igf1R*, *il2Rb*, *epor*, *ghra*, *ghrb* and *cxcr4a*)
12 encode for membrane receptors/ligands; 3 (*cebpb*, *ets1*, *runx2*) are transcription factor
13 genes, 3 (*crkl*, *erbb3*, *grin2*) encode for intracellular adaptors/signal transducers; one
14 (*dlg3*) is an apico-basal polarity gene; one (*apex*) is a DNA mismatch repair gene and
15 one (*ahr*) is a nuclear hormone receptor. By contrast the upregulated genes are *ccna2*
16 (cyclin A2), *tie2* and *kdr* (vascular specific receptor/ligands), *rad51* (DNA double
17 strand break repair gene) and *pard3* (apical cell-polarity gene). The levels of
18 repression or induction varied between different tumors (n=11), but the trend was the
19 same for all the analyzed samples.
20
21

22 We also grew the double transgenic line in a *tp53*^{+/-} and *tp53*^{-/-} background¹¹ ; this was
23 done because the absence of functional *tp53* has been shown to accelerate the
24 development of melanoma in zebrafish²⁰ and is therefore likely to exacerbate the
25 cancer-related changes in transcriptome. To distinguish between heterozygous and
26 homozygous *tp53* mutants, we evaluated the *tp53* genomic status of the fish bearing
27 tumors and used them in the QPCR screen. We found that the changes in gene
28 expression for the 39 studied predicted cancer genes were independent of the *tp53*
29 genotype. In fact as shown in the two examples of Figure 2B, the gene expression
30 profile (i.e. repression or induction) was nearly the same in all tumors analyzed,
31 independently of the presence of an inactivating mutation of *tp53* in either
32 heterozygosity or homozygosity.
33
34
35
36
37
38
39
40
41
42
43
44
45
46
47
48
49
50
51
52

53 **Human/zebrafish melanoma comparison**

54 To make sure that this “repressive” trend was not specific to the zebrafish cancer
55 model we use, we searched for the levels of expression of these genes in a number of
56 human cancers by screening the Oncomine database, which integrates cancer profile
57 data from a large number of human cancer samples. In brief, Oncomine is a public
58 cancer microarray platform incorporating 264 independent microarray dataset, totaling
59
60

1
2
3 more than 18,000 microarray experiments, which span 35 cancer types
4 (<http://www.oncomine.org>).
5

6
7 Interestingly, we observed that the trend for repression or increase in gene expression
8 for the genes studied here is very similar also in human melanoma samples. Of the 39
9 genes studied here only 16 were found in the melanoma samples reported in
10 Oncomine. These observations are summarized in Table I, which reports a summary
11 of the observations from 11 zebrafish melanoma samples and 2 sets of microarray
12 data obtained from human melanoma (see M&M for a list of the melanoma samples
13 taken from Oncomine).
14
15
16
17
18

19 20 21 **Increase in repressive histone marks in melanoma tissue**

22
23 To address whether epigenetic differences exist between melanoma cells and normal
24 tissues in the zebrafish model that could be responsible for the changes in gene
25 expression described above, we evaluated the levels of immunofluorescence
26 following staining with a panel of antibodies that recognize different histone
27 modification. We evaluated 5 markers of histone modifications and one of
28 heterochromatin (heterochromatin protein 1, HP1) in 4 different tumor samples
29 (including 1 from *tp53*^{-/-} genotype) and compared them with levels of
30 immunofluorescence in normal skin adjacent to the tumor, or in skin from 2 wild
31 type, age matched, controls. Again, we did not observe any difference between the
32 tumors with different *tp53* genotype (data not shown).
33
34

35
36 We found that the levels of immunofluorescence associated with the repressive mark
37 Histone 3 Lysine 9 trimethyl (H3K9me3) are higher in the tumors than in the
38 surrounding skin (Figure 3A, B) or in untransformed melanocytes, and that the
39 nuclear localization of HP1 immunofluorescence was also high in melanoma cells
40 (Figure 3E, F). In addition, the levels of immunofluorescence associated with the
41 active marks H3K4me3 (Figure 3C, D) and H4K20me2 (Figure 4E, F) were reduced
42 in the tumors compared to normal skin (Figure 4E, F). At odd with these observations
43 that suggest a general increase of a repressive chromatin state, we found that the
44 repressive mark H3K27me3 is expressed at higher levels in normal skin (Figure 4A)
45 than in zebrafish melanoma (Figure 4B) and the immunofluorescence for H3-
46 asymmetric dimethyl Arg2 (H3R2me2a, often associated with active transcription)
47 was instead higher in the tumor cells than in normal skin (Figure 4C, D). Although
48 these observations were from whole nuclei of melanoma cells, and did not provide
49
50
51
52
53
54
55
56
57
58
59
60

1
2
3 any information on the state (activation or repression) of a specific gene (which will
4 require chromatin IP) they are indicative of a profound misregulation of epigenetic
5 control of gene expression in the zebrafish model of melanoma presented here.
6
7 Significantly we found that melanoma cells are homogeneous in displaying either an
8 increase or decrease in expression of these epigenetic marks, suggesting that the
9 alterations in gene expression, or the cell composition of the tumors, are equally
10 homogeneous.
11
12
13
14
15
16

17 DISCUSSION

18 Here we report the use of a novel zebrafish model of melanoma to investigate the
19 expression of a number of genes potentially involved in cancer (as a first step towards
20 their validation as “cancer genes”) and the findings that in this melanoma model many
21 of these genes are downregulated in comparison with normal skin. This generalized
22 repression of several genes of different ontology classes prompted us to evaluate the
23 epigenetic status of melanoma cells. On a broad basis, we compared the levels of
24 immunofluorescence for different histone modifications between tumor cells and
25 adjacent normal skin. The results of the immunofluorescence screen shows: a) that 2
26 out of 3 histone repressive marks are increased, and 2 out of 3 histone marks of
27 transcriptionally active chromatin are decreased; b) that melanoma cells (and
28 adjacent normal skin cells) are remarkably homogeneous in their pattern of
29 immunofluorescence, both intra- and inter-samples.
30
31
32
33
34
35
36
37
38
39

40 In the following paragraphs we will discuss briefly the most interesting findings of
41 this study.
42
43
44
45

46 **The GAL4-UAS system as a flexible tool for re-expression of tumor suppressors**

47 The GAL4-UAS system has been developed and optimized for the zebrafish through
48 the effort of several laboratories^{9, 21-23}. We have adopted the system for the
49 development of cancer models with UAS-mediated expression of oncogenes. The
50 availability of a large number of GAL4 driver lines through the generosity of the
51 zebrafish community renders this system extremely appealing both for the variety of
52 cancer models that can be generated with a single oncogene reporter line and for the
53 flexibility of the system. Indeed, the GAL4-UAS binary system used for the
54 generation of the melanoma model reported here allows precise and specific
55 expression of any modifier gene exclusively in the transformed cells, both in transient
56
57
58
59
60

1
2
3 (insertion in somatic cell) and in stable transgenics (insertion in germ line). While it is
4 beyond the scope of this report to give a full description of the melanoma transgenic
5 line and how it differs from previously reported zebrafish melanoma models (which
6 will be described in details elsewhere), it is important to highlight that: a) the
7 frequency of melanoma development in heterozygous double transgenics is relatively
8 high (20% of transgenic fish at 3 months); b) that these cancer lesions develop
9 predominantly at the level of the tail fin; c) the H-RAS_GV12 is a powerful oncogene
10 when expressed in the melanocytic lineage of the zebrafish (as already reported²⁴);
11 and d) different stages of melanoma progression can be reliably classified in these
12 cancer lesions. The beauty of the system lies in the possibility of driving the
13 expression of modifiers and/or oncosuppressors in the same cells that are transformed
14 by HRAS_GV12. We have addressed the efficiency of this approach in transient
15 transgenic experiments, and found it to be very reliable (Santoriello et al., in
16 preparation).

30 **An in vivo experimental model to validate novel cancer genes.**

31 Cancer genes are genes for which mutations have been causally implicated in cancer.
32 The Cancer Gene Census is an ongoing effort to catalogue all these genes and is
33 carried out by the Sanger Centre. The original census and analysis was published in
34 Nature Reviews Cancer¹. As stated in the Census website: "Currently, more than 1%
35 of all human genes are implicated via mutation in cancer. Of these, approximately
36 80% have somatic mutations in cancer, 20% bear germline mutations that predispose
37 to cancer with 10% showing both somatic and germline mutations. The census is not
38 static but rather is updated regularly/as needed". The majority of mutations in cancer
39 genes have been identified through their sequencing from cancer genomes. The
40 choice of the genes to sequence is therefore restricted to a limited number of
41 candidates. Predictive methods are an alternative to whole cancer genome sequencing,
42 that is becoming feasible, but yield too many data for analysis. Predicted cancer
43 genes need to be validated for their causal role in cancer. The possibility of validating
44 cancer genes in a live organism (as opposed to a simple in vitro transformation assay
45 i.e. soft agar colony assay) is extremely appealing. Moreover, there are no ways to
46 validate tumor suppressors in vitro. Oncosuppressors are particularly interesting from
47 a therapeutic point of view, as their inactivation is a necessary step towards oncogenic
48 transformation, thus making their re-expression in cancer a therapeutic goal. Among
49
50
51
52
53
54
55
56
57
58
59
60

1
2
3 the different approaches used to identify tumor suppressors, one is the evaluation of
4 their expression levels in cancer. This is one of the reasoning behind the QPCR screen
5 described here to evaluate the expression levels of a pool of genes suggested to act as
6 cancer genes on the basis of predictive methods.
7
8

9
10 To our surprise the QPCR investigation showed that genes with clear signatures as
11 oncogenes (i.e. *igf1R*, *kdr*) were downregulated in our melanoma model. We then
12 compared our results with the data on the expression of the ortholog genes in human
13 melanoma, to make sure that this repression was not associated with the particular
14 melanoma model that we were using, and found it to be similar. Only 6 genes behave
15 differently between zebrafish and human melanoma samples. An evaluation based on
16 gene function or the presence of paralogues in zebrafish suggests that these
17 differences could be due to stage-specific behaviour of each of the six genes in the
18 different sets of melanomas (zebrafish versus human). While increased expression of
19 *CXCR4* and *AHR* in human melanoma have been correlated with an advanced tumor
20 stage²⁵, the increase of expression of *cyclin A2*, *rad51* and *pard3* in zebrafish
21 melanoma suggests a “young” (i.e. still highly proliferative) tumor stage. Moreover,
22 the changes in gene expression were the same in the presence or absence of functional
23 *tp53*.
24
25

26 We realized that we were facing a generalized repression of gene expression similar
27 to that occurring in human melanoma and therefore hypothesized that an epigenetic
28 mechanism may be responsible for these changes. Our study further confirms that
29 gene repression is a hallmark of melanoma²⁶ and suggests that our model recapitulates
30 the human pathology also in these aspects.
31
32
33
34

35 **Changes in the epigenome of zebrafish melanoma can be visualized through** 36 **immunofluorescence.** 37

38 First we carried out a preliminary analysis, mainly aimed at establishing if the
39 commercially available antisera worked in zebrafish tissue. All the antisera that we
40 tried (listed in M&M section) worked well in cryostat sections. In addition they
41 allowed us to distinguish between melanoma tissue and normal skin containing
42 untransformed melanocytes because all the antisera labeled these two adjacent tissues
43 with a different pattern.
44
45

46 Although these observations are not informative about the epigenetic status of
47 individual genes, they nevertheless provide some information on the distribution of
48
49
50
51
52
53
54
55
56
57
58
59
60

1
2
3 specific histone marks in melanoma tissue. First, cells within melanoma are
4 remarkably homogeneous in terms of staining for given histone marks; second, levels
5 of immunofluorescence associated with 2 repressive marks²⁷ (H3K9me3 and HP1) are
6 increased, whereas levels of immunofluorescence associated with 2 active chromatin
7 marks²⁷ (H3K4me3 and H4K20me2) are decreased in the tumors compared to normal
8 skin. These observations fit well with our hypothesis of a general repression of
9 specialized genes related to a self-propagating epigenetic mechanism, perhaps
10 initiated during the earliest stages of melanoma development by the *ras* oncogene²⁸. If
11 so, identifying the first epigenetic event induced by Ras at the earliest stages of tumor
12 progression may provide valuable therapeutic targets, which can be validated in our
13 model.

14 At the moment we cannot explain why the repressive mark H3K27me3 in contrast to
15 H3K4me3 and H4K20me2 was found to be decreased in zebrafish melanoma (as
16 compared to normal skin). In addition, the meaning of the increase of
17 immunofluorescence for H3R2me2a (often associated with active transcription) in the
18 tumor cells compared to normal skin is currently unclear. Whether these changes
19 reflect a specific signature of the *ras* oncogene represents an important point that we
20 aim to address by exploiting our melanoma model. Anyhow the H3R2me2a mark is
21 often associated with a reduction of H3K4me3 at the same promoters²⁹, which
22 corresponds to what we observe in our model.

23 In the future, we plan to analyze the presence of a range of histone posttranslational
24 modifications and DNA methylation patterns at specific promoters and transcription
25 start sites²⁷ of the cancer genes in our melanoma model.

26 In conclusion, this study has shown that the zebrafish melanoma model developed in
27 our lab show many of the molecular, genetic and epigenetic properties of human
28 melanoma and is therefore suitable for mechanistic studies.

29 30 31 32 33 34 35 36 37 38 39 40 41 42 43 44 45 46 47 48 49 50 51 52 53 54 55 **Figure legends**

56 57 58 59 **Figure 1** 60

1
2
3 A) Schematic representation of the constructs used for the generation of the enhancer
4 trap line *Et(kita:GalTA4,UAS:mCherry)hzm1* and *Tg(UAS:eGFP-HRAS_G12V)io6*
5 line. B) Picture of a 5 month old transgenic fish displaying a large black tumor in the
6 stalk of the caudal fin. C) Quantification of the number of fish displaying a black fin
7 phenotype (BF) and tumor (TU) at 4 months (mean+SD, n=150).
8
9
10
11
12

13 14 **Figure 2**

15 A) mRNA expression of the candidate cancer genes extracted from 11
16 melanoma tumors from *Tg(UAS:eGFP-HRAS_G12V)io6*. B) Representative example
17 of down-regulated (*erbb3*) and up-regulated gene (*ccna2*) in 11 melanoma tumor
18 samples with different *tp53* genotypes. All the data are expressed as % of MNE of the
19 target gene in the tumor tissue from the fins compared to MNE of the target genes in
20 the control wild type fins (as reported in Materials and Methods). All the genes were
21 normalized to the expression levels of β -actin as an endogenous control.
22
23
24
25
26
27
28
29
30
31

32 **Figure 3**

33 A, C, E) Confocal images of single scans through sections stained for different
34 histone marks (as indicated on top right corner) in magenta. Inset in A shows the same
35 section imaged with Normaski optics for orientation. M=melanoma tissue
36 fluorescing in green because it expresses GFP:HRAS_G12V; S=normal skin. B, D,
37 F) Close up on the nuclei of melanoma cells, immunostained for the markers
38 indicated on the left panel and counterstained with DAPI. Calibration bars: 20 μ m
39
40
41
42
43
44
45

46 **Figure 4**

47 A) Confocal image of single scans through a sections of a wild type control fin
48 stained for H3K27me3 in magenta. B-F) Confocal images of single scans through
49 sections with tumors stained for different histone marks (as indicated on top right
50 corner) in magenta. Inset in C shows the same section imaged with Normaski optics
51 for orientation. M=melanoma tissue fluorescing in green because it expresses
52 GFP:HRAS_G12V; S=normal skin. Calibration bars: 20 μ m
53
54
55
56
57
58
59
60

Table I: Changes of expression levels of some of the candidate genes in zebrafish

1
2
3 melanoma (QPCR) and in samples from the oncomine database.

4
5 + means increase; - means decrease as compared with the respective controls.
6
7
8
9

10 **Acknowledgements:** We would like to thank Federica Pezzimenti for expert
11 technical support; Koichi Kawakami (Mishina, Japan) for the Tol2 and UAS vectors.
12 This work is supported by Cariplo foundation (grant no. 2007-5500 to Mione and
13 Ciccarelli). We are grateful for the financial support of this study by a BioFuture
14 Award Grant (RWK) of the German Ministry of Education and Research (BMBF
15 0311889) and a Fellowship of the Studienstiftung des deutschen Volkes (MD).
16
17
18
19
20
21
22
23

24 **References**

- 25 1. Futreal PA, Coin L, Marshall M, et al. A census of human cancer genes. *Nat*
26 *Rev Cancer* 2004;4:177-83.
- 27 2. Rambaldi D, Giorgi FM, Capuani F, Ciliberto A, Ciccarelli FD. Low
28 duplicability and network fragility of cancer genes. *Trends Genet* 2008;24:427-30.
- 29 3. Jones PA, Baylin SB. The epigenomics of cancer. *Cell* 2007;128:683-92.
- 30 4. Keshet I, Schlesinger Y, Farkash S, et al. Evidence for an instructive
31 mechanism of de novo methylation in cancer cells. *Nat Genet* 2006;38:149-53.
- 32 5. Lam SH, Wu YL, Vega VB, et al. Conservation of gene expression signatures
33 between zebrafish and human liver tumors and tumor progression. *Nat Biotechnol*
34 2006;24:73-5.
- 35 6. Knudson AG, Jr. Hereditary cancer, oncogenes, and antioncogenes. *Cancer*
36 *Res* 1985;45:1437-43.
- 37 7. Haber DA, Settleman J. Cancer: drivers and passengers. *Nature* 2007;446:145-
38 6.
- 39 8. Westerfield M. The zebrafish book a guide for the laboratory use of zebrafish
40 (Danio rerio). Eugene: Institute of Neuroscience University of Oregon; 2000.
- 41 9. Asakawa K, Suster ML, Mizusawa K, et al. Genetic dissection of neural
42 circuits by Tol2 transposon-mediated Gal4 gene and enhancer trapping in zebrafish.
43 *Proc Natl Acad Sci U S A* 2008;105:1255-60.
- 44 10. Santoriello C, Deflorian G, Pezzimenti F, et al. Expression of H-RASV12 in a
45 zebrafish model of Costello syndrome causes cellular senescence in adult
46 proliferating cells. *Dis Model Mech* 2009;2:56-67.
- 47 11. Berghmans S, Murphey RD, Wienholds E, et al. tp53 mutant zebrafish
48 develop malignant peripheral nerve sheath tumors. *Proc Natl Acad Sci U S A*
49 2005;102:407-12.
- 50 12. Simon P. Q-Gene: processing quantitative real-time RT-PCR data.
51 *Bioinformatics* 2003;19:1439-40.
- 52 13. Rhodes DR, Yu J, Shanker K, et al. ONCOMINE: a cancer microarray
53 database and integrated data-mining platform. *Neoplasia* 2004;6:1-6.
54
55
56
57
58
59
60

14. Talantov D, Mazumder A, Yu JX, et al. Novel genes associated with malignant melanoma but not benign melanocytic lesions. *Clin Cancer Res* 2005;11:7234-42.
15. Hoek KS, Schlegel NC, Brafford P, et al. Metastatic potential of melanomas defined by specific gene expression profiles with no BRAF signature. *Pigment Cell Res* 2006;19:290-302.
16. Brand AH, Perrimon N. Targeted gene expression as a means of altering cell fates and generating dominant phenotypes. *Development* 1993;118:401-15.
17. Distel M, Wullimann MF, Köster RW. Optimized Gal4 genetics for permanent gene expression mapping in zebrafish. *PNAS* 2009; 106:13365-70.
18. Hultman KA, Bahary N, Zon LI, Johnson SL. Gene Duplication of the zebrafish kit ligand and partitioning of melanocyte development functions to kit ligand a. *PLoS Genet* 2007;3:e17.
19. Peri S, Navarro JD, Amanchy R, et al. Development of human protein reference database as an initial platform for approaching systems biology in humans. *Genome Res* 2003;13:2363-71.
20. Patton EE, Widlund HR, Kutok JL, Kopani KR, Amatruda JF, Murphey RD, Berghmans S, Mayhall EA, Traver D, Fletcher CD, Aster JC, Granter SR, Look AT, Lee C, Fisher DE, Zon LI. BRAF mutations are sufficient to promote nevi formation and cooperate with p53 in the genesis of melanoma. *Current Biology* 2005;15:249-54.
21. Halpern ME, Rhee J, Goll MG, Akitake CM, Parsons M, Leach SD. Gal4/UAS transgenic tools and their application to zebrafish. *Zebrafish* 2008;5:97-110.
22. Koster RW, Fraser SE. Tracing transgene expression in living zebrafish embryos. *Dev Biol* 2001;233:329-46.
23. Scott EK, Mason L, Arrenberg AB, et al. Targeting neural circuitry in zebrafish using GAL4 enhancer trapping. *Nat Methods* 2007;4:323-6.
24. Michailidou C, Jones M, Walker P, Kamarashev J, Kelly A, Hurlstone AF. Dissecting the roles of Raf- and PI3K-signalling pathways in melanoma formation and progression in a zebrafish model. *Dis Model Mech* 2009;2:399-411.
25. Bartolome RA, Ferreira S, Miquilena-Colina ME, et al. The chemokine receptor CXCR4 and the metalloproteinase MT1-MMP are mutually required during melanoma metastasis to lungs. *Am J Pathol* 2009;174:602-12.
26. Dahl C, Guldborg P. The genome and epigenome of malignant melanoma. *APMIS* 2007;115:1161-76.
27. Barski A, Cuddapah S, Cui K, et al. High-resolution profiling of histone methylations in the human genome. *Cell* 2007;129:823-37.
28. Patra SK. Ras regulation of DNA-methylation and cancer. *Exp Cell Res* 2008;314:1193-201.
29. Guccione E, Bassi C, Casadio F, et al. Methylation of histone H3R2 by PRMT6 and H3K4 by an MLL complex are mutually exclusive. *Nature* 2007;449:933-7.

A



Et(kita:Gal4TA4, UAS:mCherry)

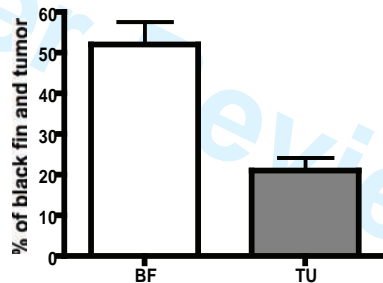


tg(5XUAS:eGFP-HRAS_GV12)

B



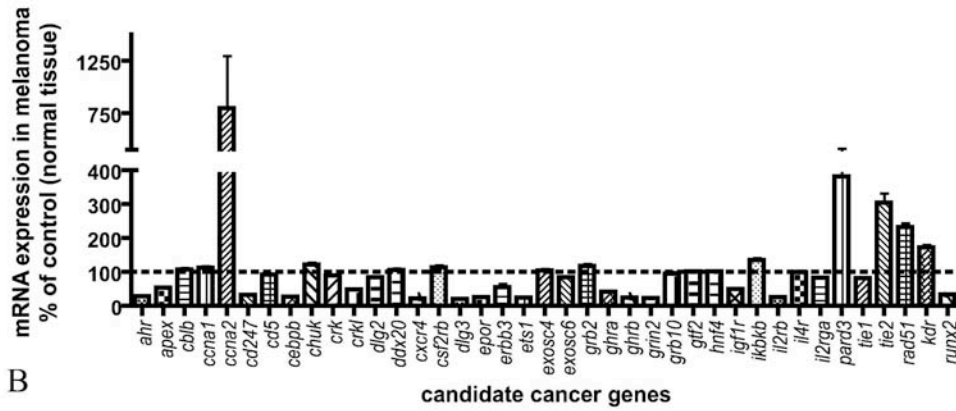
C



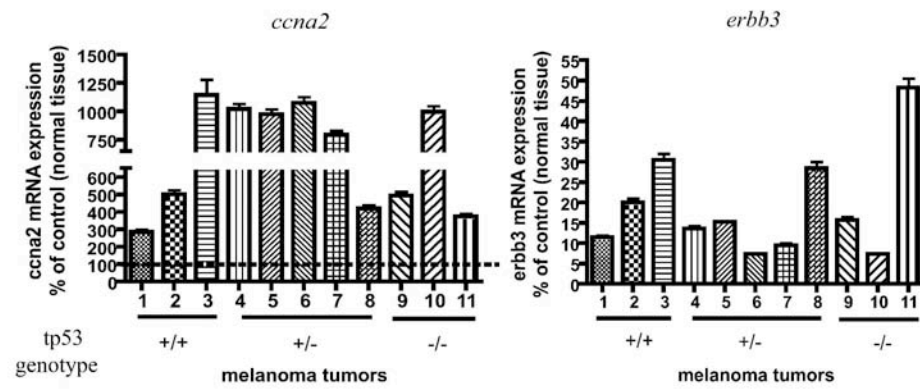
1
2
3
4
5
6
7
8
9
10
11
12
13
14
15
16
17
18
19
20
21
22
23

1
2
3
4
5
6
7
8
9
10
11
12
13
14
15
16
17
18
19
20
21
22
23
24
25
26
27
28
29
30
31
32
33
34
35
36
37
38
39
40
41
42
43
44
45
46
47
48
49
50
51
52
53
54
55
56
57
58
59
60

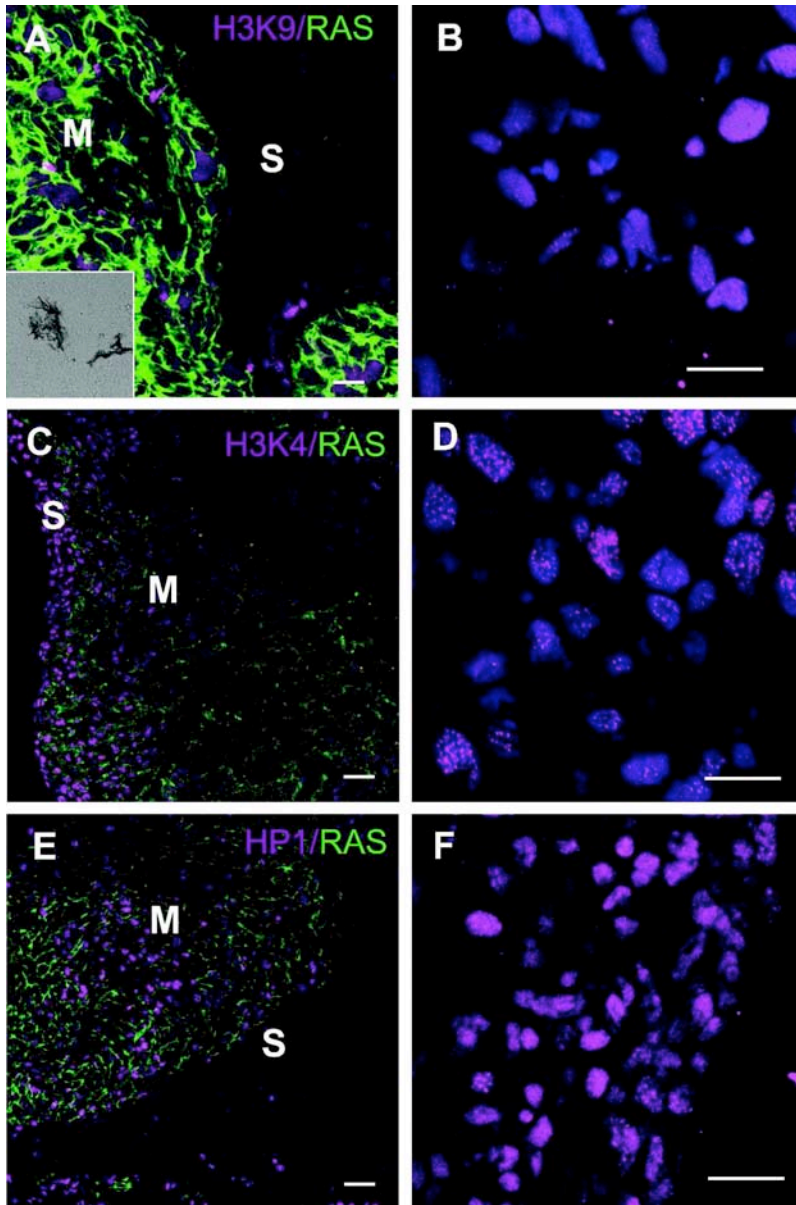
A



B

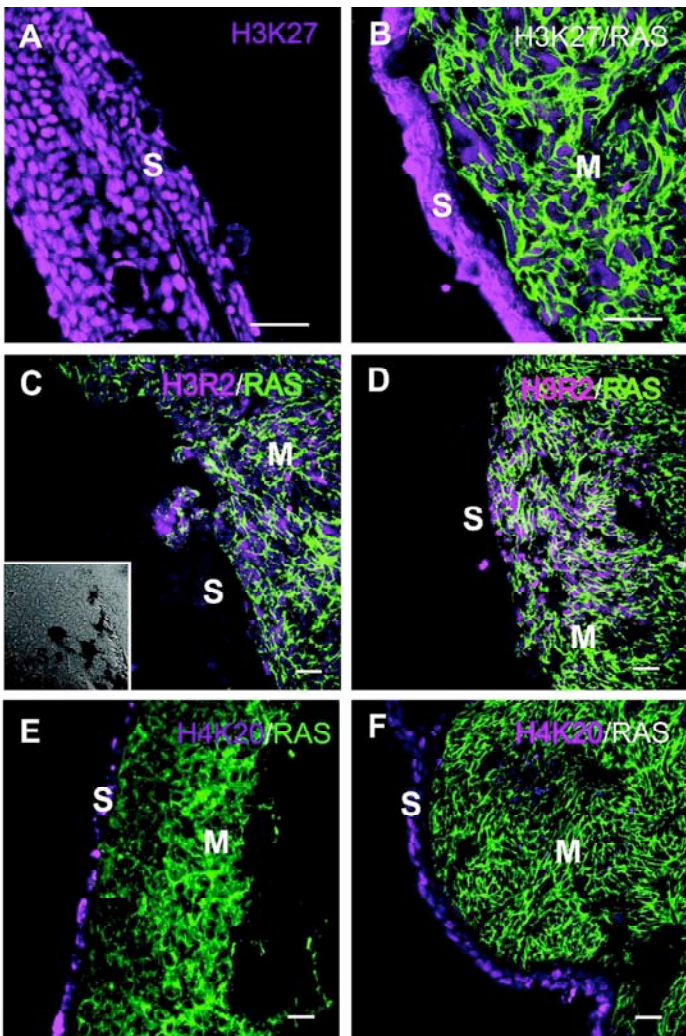


187x181mm (600 x 600 DPI)



176x265mm (600 x 600 DPI)

1
2
3
4
5
6
7
8
9
10
11
12
13
14
15
16
17
18
19
20
21
22
23
24
25
26
27
28
29
30
31
32
33
34
35
36
37
38
39
40
41
42
43
44
45
46
47
48
49
50
51
52
53
54
55
56
57
58
59
60



257x265mm (600 x 600 DPI)

Candidate genes	QPCR (zebrafish melanoma)	Oncomine database (human melanoma)
AHR	-	+
RUNX2	-	-
CEBPB	-	n.d.
CD247	-	-
IL2RB	-	-
GXCR4	-	+
IGF1R	-	-
DLG3	-	-
EPOR	-	-
HRBB3	-	-
GRIN2	-	-
GHR	-	-
CCNA2	+	-
APEX	-	-
PARD3	+	-
RAD51	+	=

1
2
3 **Legend to supplementary tables**
4
5

6
7 **Supplementary Table I: List of specific primers used in Real-time PCR**
8
9

10 **Supplementary Table II: Average Ct values and Mean Normalized Expression of**
11 **the target genes analyzed by Real-Time PCR.**

12 Ct means cycle threshold (defined as the number of cycles required for the fluorescent
13 signal to cross the threshold. Ct levels are inversely proportional to the amount of
14 target nucleic acid in the sample). The Mean Normalized Expression (MNE) of each
15 target gene is calculated using Q-gene, a software which processes quantitative real-
16 time PCR data through a mathematical calculation of means and applies Standard
17 Error (SE) for the reference gene as well for the targets.
18
19
20
21
22
23
24
25
26
27
28
29
30
31
32
33
34
35
36
37
38
39
40
41
42
43
44
45
46
47
48
49
50
51
52
53
54
55
56
57
58
59
60

Candidate genes	Primer Forward	Primer Reverse
<i>ahrla</i>	GTGACCTCCAGTGGGACAGT	GGGGTAAAGCCAGGGTAGAG
<i>apex1</i>	ACTGCCATGCCTGAGTATCC	AAACCACGACTGGCATTAGG
<i>aplb</i>	CCACGTTTCAGAGTGGGTTT	CCAGAAGCTAGTGGCTGGAC
<i>ccna1</i>	CTGCGCCAGAACTCTAAACC	CCCGAGATGGAGCTTATGAA
<i>ccna2</i>	AGTGGACTGGTTGGTGGAAG	AAACTTCGAAGCCAAAAGCA
<i>cd247</i>	CCGGTGGAGGAGTCTCATT	CCGAGCTCAGACCCTGATAG
<i>cd5</i>	TATACGGGGTCTCTGCTTTTG	GAATGCTGGGTGACGTTTTT
<i>cebpb</i>	GTATGCAAGCAGCCAGTCAA	CTTGCTCTTGTTCCCCTCAG
<i>chuk</i>	TGAAAATTGCTGTGGGTTGA	AGTCCCCACAAATGAAGTGC
<i>crk</i>	ACCTGGACACCACCACTCTC	CCAGCACTCGAAGAACATCA
<i>crkl</i>	CTATGCCCAGCCTCAGACTC	CCTTCCCACTGACCACTGAT
<i>ddx2</i>	GCTGAGAGGGGTAAGCACTG	GGCACGGTCGTATGTCTTTT
<i>ddx20</i>	ACGCAACTACACAGGTGCTG	CAGGGCTCCCATCTCAATTA
<i>ccr4a</i>	TGTACAGCAGCGTCCTCATC	ACCCAGGTGACAAACGAGTC
<i>csf2rb</i>	AGGACTCTGGAGCAACTGGA	CTCATCGTTGCTGGACTTCA
<i>ddx3</i>	ATCTGTACGGGACCAGCATC	CGAACTCCTGTTCCAGCTTC
<i>enpr</i>	CCGAGATGAAACCGAGGATA	GAAACCGCACAAATCCATCTT
<i>erb3</i>	CTGATGAGTGCAAAGCGTGT	GAATATGACGCTCAGCACGA
<i>esr1</i>	TCAGACAGCGGATCTTGTTG	TCAGCACACTCCAGATCGTC
<i>exosc4</i>	GCAGGGCAACACTAAAGCTC	GTCTCCGTGTGGACGTCTCT
<i>exosc6</i>	CGTGAATGTCATGGTTTTGG	TATGACGGGTCAACGAGACA
<i>gpb2</i>	GGACTCAACAGACACGCAGA	TAGTCAAGTGGAGGGCTGCT
<i>gtra</i>	CCAGAAATCCCAGATCCTGA	CAGTTGTCCAGGTGAGAGCA
<i>gtrb</i>	GTGAGTTCGTGCTGAGTCCA	CCAAGGGGATGTCTCTGTGT
<i>grn2a</i>	CCAAGGGGATGTCTCTGTGT	TCTCCATCTCACCATCTCC
<i>grp10</i>	GGCAGAACGACCTCTGTCTC	TGGTGGATGAGCGTTTATGA
<i>gtf2</i>	TCTCTTTCCTCCCGACTTCA	AGCCTGCAAACCTGCGTTTAT
<i>hnf4a</i>	GCCGACACTACAGAGCATCA	AGGTGTTCCCTGGACCAGATG
<i>igf1r</i>	CAGACCTCCAGACAGGAAGC	GCACCGGTGGACTTCATAGT
<i>ikbkb</i>	GGCACACTGTCAAAGCAGAA	GGTCATCATCTCCTCCTCCA
<i>ik2rb</i>	GATGAGCAGCATTGTGAGGA	TCTGCTGGCTCACAGAGAGA
<i>il4r</i>	GAAC TGGTCGTCTGGACGTT	GTCACAAAGTGCTTGGCAGA
<i>il2rga</i>	ATTATCTTGCGGCCCTTTTT	AGCAGATCCGGGTATTGTTG
<i>pard3</i>	GTTAAACCTGACGGCGATGT	GCCTTTTCACGCTGAAACTC
<i>tie1</i>	GCGATGGATGGCTATTGAGT	ATCACAGTTTCTGGGCTGCT
<i>tie2</i>	GCCACTTTCTCCACACAGGT	TGGAAGGTCCCTCAGTGTTCC
<i>Atf151</i>	GTGGCTGAACGGTATGGTCT	TCGTCCCAGTAATCTGTCC
<i>ldr</i>	GGTGATCTGGGATAGCAGGA	AGCCTCTCATGCTGTGGACT
<i>rxn2a</i>	ACCTGGGCGCTTTAAGGTTCT	CCCTATGGCTCTGGTAA
<i>beta-actin</i>	CGAGCAGGAGATGGGAACC	CAACGGAAACGCTCATTGC

Candidate genes	Average Ct values		Mean Normalized Expression	
	control	melanoma	control	melanoma
<i>B-actin</i>	18.68	19.12	reference gene	reference gene
<i>ahr</i>	24.93	26.61	4.07E -03±7.13E -04	1.09E -03±4.07E -04
<i>apex</i>	20.79	21.62	7.46E -02±2.40E -03	3.82E -02±2.65E -03
<i>cblb</i>	20.64	20.27	8.19E -02±2.28E -03	8.37E -02±7.53E -03
<i>ccna1</i>	27.46	27.77	7.48E -04±2.79E -04	7.98E -04±1.00E -04
<i>ccna2</i>	27.90	25.98	6.39E -04±6.29E -06	3.62E -03±1.70E -03
<i>cd247</i>	20.52	21.94	8.83E -02±2.37E -02	2.72E -02±8.59E -03
<i>cd5</i>	27.22	27.11	8.34E -04±1.39E -04	7.33E -04±1.58E -04
<i>cebpb</i>	28.51	30.88	4.39E -04±1.31E -04	1.15E -04±3.97E -05
<i>chuk</i>	23.72	23.27	5.61E -03±2.54E -03	6.51E -03±1.70E -03
<i>erk</i>	22.30	22.32	1.46E -02±2.45E -03	1.25E -02±2.60E -03
<i>crkl</i>	23.53	24.66	1.33E -02±4.52E -03	8.81E -03±4.31E -03
<i>dlg2</i>	24.41	24.50	3.36E -03±7.97E -04	2.73E -03±2.34E -06
<i>ddx20</i>	26.11	25.76	1.14E -03±7.47E -04	1.15E -03±2.52E -04
<i>cxcr4</i>	24.06	26.09	4.43E -03±1.98E -03	9.22E -04±2.05E -04
<i>csf2rb</i>	25.59	25.29	1.45E -03±7.80E -05	1.59E -03±1.24E -04
<i>dlg3</i>	23.86	25.47	7.38E -03±7.93E -04	1.44E -03±4.93E -04
<i>epor</i>	27.27	29.32	4.65E -04±1.52E -04	1.16E -04±3.09E -05
<i>erbb3</i>	27.66	29.68	7.59E -04±7.11E -05	1.27E -04±1.14E -04
<i>ets1</i>	23.27	25.29	7.38E -03±2.21E -03	1.71E -03±9.28E -04
<i>exosc4</i>	26.66	26.44	7.05E -04±2.11E -04	7.12E -04±3.42E -05
<i>exosc6</i>	23.05	23.07	9.19E -03±5.26E -04	7.40E -03±3.00E -04
<i>grb2</i>	25.21	24.85	1.90E -03±3.91E -04	2.15E -03±3.77E -04
<i>ghra</i>	25.25	26.37	1.89E -03±6.42E -04	7.53E -04±1.33E -04
<i>ghrb</i>	24.95	26.72	2.47E -03±1.42E -03	5.88E -04±8.07E -05
<i>grin2</i>	24.99	26.87	2.31E -03±1.04E -03	5.30E -04±7.30E -05
<i>grb10</i>	22.48	22.45	1.11E -03±9.20E -05	1.31E -03±1.76E -03
<i>gfi2</i>	24.37	24.20	3.43E -03±9.15E -04	3.36E -03±2.50E -04
<i>hnf4</i>	23.37	23.20	6.86E -03±1.83E -03	6.71E -03±5.00E -04
<i>igf1r</i>	25.13	26.23	1.62E -03±3.96E -05	7.84E -04±1.61E -05
<i>ikbbk</i>	24.95	24.64	1.85E -03±1.84E -05	2.37E -03±5.55E -05
<i>il2rb</i>	24.20	26.25	3.08E -03±9.33E -05	7.76E -04±4.42E -06
<i>il4r</i>	24.54	24.67	2.44E -03±1.90E -04	2.33E -03±1.33E -04
<i>il2rga</i>	23.93	24.32	3.74E -03±8.77E -05	2.96E -03±4.96E -06
<i>pard3</i>	26.94	25.93	1.25E -03±5.41E -05	4.33E -03±3.40E -03
<i>tie1</i>	27.92	28.75	6.37E -04±8.51E -05	4.99E -04±1.70E -04
<i>tie2</i>	31.91	30.88	4.16E -05±1.24E -05	1.15E -04±3.97E -05
<i>rad51</i>	26.54	26.00	1.66E -03±1.93E -04	3.69E -03±1.91E -03
<i>kdr</i>	30.75	30.51	9.44E -05±3.14E -05	1.55E -04±6.48E -05
<i>runx2</i>	28.30	30.59	4.86E -04±3.80E -05	1.54E -04±1.01E -05

Supplemental Table II: Average Ct values and Mean Normalized Expression of the gene analyzed by Real-Time PCR

163x263mm (600 x 600 DPI)

Appendix 4

published Article in *Nature Photonics*

Multispectral opto-acoustic tomography of deep-seated fluorescent proteins *in vivo*

**Daniel Razansky, Martin Distel, Claudio Vinegoni, Rui Ma, Norbert Perrimon,
Reinhard W. Köster and Vasilis Ntziachristos**

Nature Photonics (2009), **3**, 412-417.

Contribution:

This project was mainly conducted by Daniel Razansky, who developed the MSOT method. I contributed to all cell or zebrafish experiments in this article. I prepared phantoms with fluorescent cells for MSOT measurements shown in Fig.2, phantoms with transgenic zebrafish, histological sections of zebrafish and microscope images shown in Fig.4 and Fig.5. I contributed to data analysis and to writing the manuscript (zebrafish and cell sections).

Multispectral opto-acoustic tomography of deep-seated fluorescent proteins *in vivo*

Daniel Razansky^{1*}, Martin Distel², Claudio Vinegoni³, Rui Ma¹, Norbert Perrimon⁴, Reinhard W. Köster² and Vasilis Ntziachristos^{1*}

Fluorescent proteins have become essential reporter molecules for studying life at the cellular and sub-cellular level, re-defining the ways in which we investigate biology. However, because of intense light scattering, most organisms and tissues remain inaccessible to current fluorescence microscopy techniques at depths beyond several hundred micrometres. We describe a multispectral opto-acoustic tomography technique capable of high-resolution visualization of fluorescent proteins deep within highly light-scattering living organisms. The method uses multiwavelength illumination over multiple projections combined with selective-plane opto-acoustic detection for artifact-free data collection. Accurate image reconstruction is enabled by making use of wavelength-dependent light propagation models in tissue. By performing whole-body imaging of two biologically important and optically diffuse model organisms, *Drosophila melanogaster* pupae and adult zebrafish, we demonstrate the facility to resolve tissue-specific expression of eGFP and mCherry fluorescent proteins for precise morphological and functional observations *in vivo*.

Fluorescence protein (FP) imaging is increasingly being used as a key technology allowing the comprehension of complex and diverse mechanisms in many areas of biology and medical research¹. By allowing *in vivo* observation of multifactorial dynamic interactions, confocal and multiphoton tissue-sectioning microscopies have become the major means of FP visualization, radically changing biological understanding^{2–4}. Despite significant technological progress^{4–7}, high-resolution imaging is limited by the interaction of photons with cellular interfaces and organelles, which results in high levels of photon scattering. Consequently, state-of-the-art intravital (*in vivo*) microscopy operates only at depths that are less than one transport mean free path length (MFPL) in tissue⁸ (the distance it takes for light to become highly diffuse, typically between a few hundred micrometres and 1 mm). As a result, a significant amount of *in vivo* biological research revolves around the study of organisms that are virtually transparent, such as early-stage *Caenorhabditis elegans* or zebrafish (*Danio rerio*)⁹, or uses highly invasive techniques such as the implementation of biocompatible windows to study activity deeper in the body¹⁰. Optical projection tomography (OPT)¹¹, selective-plane illumination microscopy (SPIM)¹² and ultramicroscopy¹³ have been developed recently as alternative tomographic methods to confocal and nonlinear microscopy, but are also strongly limited by tissue scattering. They can be similarly applied to the imaging of naturally transparent live specimens, such as organisms at very early stages of development, or organisms and tissues chemically treated to remove scattering (when applied to dimensions of the order of one MFPL or larger), which applies therefore only to studies that can be performed post mortem.

The urgent need to improve *in vivo* visualization capacity in the post-genomic era has been recently outlined¹⁴. *In vivo* imaging beyond one transport MFPL can be used to follow cell motility and interaction or organ development and function within large tissue

volumes over long periods of time¹⁵. Non-invasive high-resolution tomographic imaging of FPs in adult organisms and mice could therefore offer an important visualization tool for functional genomics and proteomics at different system levels, that is, from the cell to the organ. Such a capacity will also shift the paradigm of biological observations and accelerate discovery by enabling *in vivo* longitudinal observation of dynamic phenomena on the same growing or developing organism, thus minimizing the need for laborious histological examinations and large cohorts to obtain meaningful statistics. From high-throughput whole-body phenotyping and time-lapse imaging in adult model organisms to understanding signalling and interactions of tissues with drugs and environmental factors, visualization beyond the penetration limit of modern microscopy will open new pathways for biological discovery.

In this work we report on the visualization of fluorescent proteins well beyond the penetration limits of optical microscopy while preserving high sensitivity and spatial resolution. To achieve this, we have developed and implemented a selective-plane multispectral opto-acoustic tomography (MSOT) method based on ultrasonic detection of pressure waves generated by the absorption of pulsed light in elastic media. The amplitude of the broadband ultrasound waves, generated by the absorption of pulsed light by tissue chromophores¹⁶, is processed tomographically to offer three-dimensional images of optical contrast reaching ultrasonic diffraction-limited resolution, not limited by the degree of light scattering. The ability to create images based on opto-acoustics has already been established in resolving vascular structures^{17,18} and functional imaging in mice¹⁹. Applied in reflectance scanning mode, high-resolution functional photoacoustic microscopy²⁰ has also demonstrated the ability to image subcutaneous tumour angiogenesis and blood oxygen saturation in rats and humans at a depth of ~600 μm . In recent years, attention has also been given to resolving molecular contrast using fluorescent contrast agents²¹, chromogenic assays²² and nanoparticles²³.

¹Institute for Biological and Medical Imaging, Technical University of Munich and Helmholtz Center Munich, Ingolstädter Landstraße 1, D-85764 Neuherberg, Germany, ²Institute of Developmental Genetics, Helmholtz Center Munich, Ingolstädter Landstraße 1, D-85764 Neuherberg, Germany, ³Center for Systems Biology, Massachusetts General Hospital and Harvard Medical School, Richard B. Simches Research Center, 185 Cambridge Street, Boston, Massachusetts 02114, USA, ⁴Department of Genetics, Harvard Medical School and Howard Hughes Medical Institute, 77 Avenue Louis Pasteur, Boston, Massachusetts 02115, USA. *e-mail: dr@tum.de; v.ntziachristos@tum.de

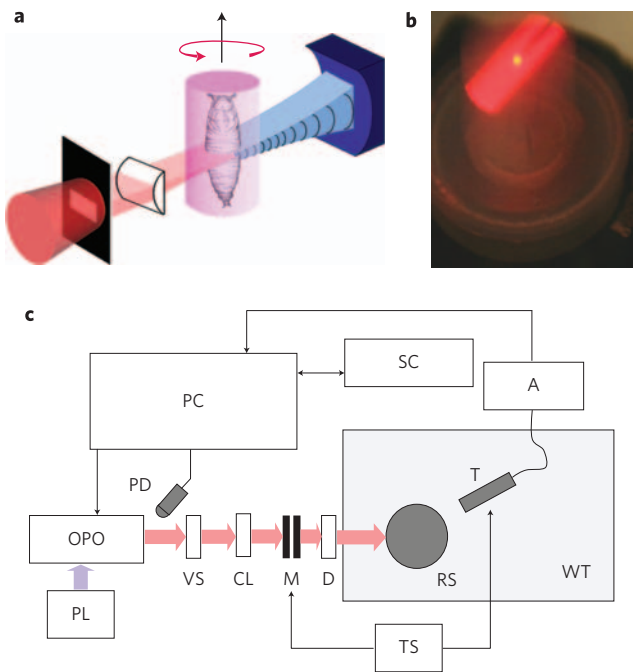


Figure 1 | Experimental setup of multispectral opto-acoustic tomography. **a**, Confocal illumination and detection scheme (red, illuminating light beam; blue, generated ultrasonic waves). **b**, Top-view photograph of the cylindrically focused beam passing through agar phantom with embedded *Drosophila* pupae. **c**, Schematic of the experimental setup. OPO, optical parametric oscillator; RS, rotation stage; SC, stage controller; VS, variable slit; CL, cylindrical lens; WT, water tank; D, engineered diffuser; T, ultrasonic transducer; M, mirror; TS, translation stage; PD, photodiode; PC, computer; A, amplifier; PL, pump laser.

In contrast to existing studies, we have established a multiprojection MSOT method that can volumetrically resolve FPs *in vivo* in small animals and tissues. By combining selective-plane illumination to minimize out-of-plane contributions and tomographic principles for image reconstruction, we demonstrate that it is possible to tune accurately the inversion process and detect specific FPs over non-specific background absorption with high sensitivity. In addition, the underlying anatomical images of the tissue are simultaneously provided. Applied to biological specimens, this technology extends fluorescence imaging to dimensions never visualized optically in the past, because it is capable of *in vivo* visualization of fluorescent proteins in intact model organisms at depth scales that are significantly larger than 1 mm, currently unattainable by other imaging techniques applied to living specimens, including confocal and multiphoton microscopies.

The experimental setup used nanosecond pulsed laser illumination at multiple wavelengths, which passed through a variable-slit aperture and focused, using a cylindrically focusing lens, onto the sample, creating a planar sheet of light (Fig. 1). The imaged objects were fixed on a rotation stage submerged into water to facilitate detection of acoustic signals. Opto-acoustic signals were recorded by a broadband ultrasonic transducer, cylindrically focused at the optical illumination plane (confocal arrangement). At each illumination wavelength and imaging height, the in-plane images were reconstructed using a filtered back-projection algorithm (see Methods for details on the experimental system and image reconstruction algorithms).

To confirm the basic ability of the method to detect fluorescent proteins over background absorption and quantify its performance, a cylindrical tissue-mimicking phantom (diameter, 1.9 cm; optical absorption coefficient, 0.3 cm^{-1} ; scattering, 10 cm^{-1}) was generated

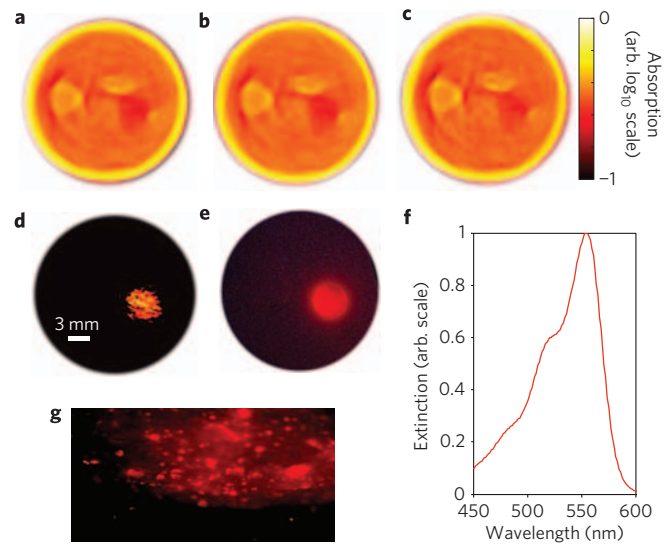


Figure 2 | Multispectral opto-acoustic imaging of tissue-mimicking phantom containing DsRed-expressing HeLa cells. **a–c**, Single-wavelength opto-acoustic images of the phantom acquired at 550 nm (**a**), 560 nm (**b**) and 570 nm (**c**). **d**, Spectrally resolved (MSOT) image of DsRed distribution in the phantom. **e**, Fluorescence image of dissected phantom at approximately the same imaging plane (red colour corresponds to the location of fluorescent cells). **f**, Extinction spectra of DsRed. **g**, Magnified image of phantom at the boundary of the area containing the DsRed cells.

by dissolving India ink and Intralipid in agar (see Supplementary information for a detailed description of phantom preparation). The phantom mimics the dimensions and average optical properties of mouse tissue at a wavelength of $\sim 630 \text{ nm}$. Two 4-mm-diameter insertions were incorporated into the phantom. The first insertion contained stable transgenic HeLa cells ($4 \times 10^6 \text{ ml}^{-1}$) expressing a mitochondrial targeted DsRedT4 fluorescent protein variant mixed with a solution of Intralipid and ink similar to background. The second insertion (absorption coefficient, 0.6 cm^{-1} ; scattering, 10 cm^{-1}) served as a control and contained a higher concentration of India ink but no fluorescent cells.

The principle of detection is based on differentiation of the absorption spectral signature of the protein over background tissue absorption by the analysis of multiwavelength data. Fluorescent proteins are excellent molecules for this role compared to other chromophoric substances such as India ink, because they exhibit a steep declining absorption slope at lower energies, which can easily be detected spectroscopically, as shown in Fig. 2f, by taking measurements at multiple wavelengths. Although single-wavelength images only reveal the highly absorbing control insertion and some phantom heterogeneities (Fig. 2a–c), the non-specific contrast from the insertion containing DsRed-expressing cells is barely visible. Nevertheless, multiwavelength processing of the images on a per-pixel basis (see Methods) renders high contrast from the FP-expressing cells with a contrast-to-noise ratio (CNR) of 32, while suppressing other non-specific contrast (Fig. 2d). The results show excellent agreement with the epifluorescence image shown in Fig. 2e, obtained after phantom sectioning to validate the tomographic images of the intact phantom.

To investigate the *in vivo* capacity of the method to image tissues beyond the limits of modern microscopy, the zebrafish and *Drosophila melanogaster* (fruit fly) were selected as the imaging targets, partly because these organisms are extensively used in various fields of genetics and other areas of modern biology. By extending non-invasive fluorescence imaging of optically transparent organisms in early development stages to imaging opaque

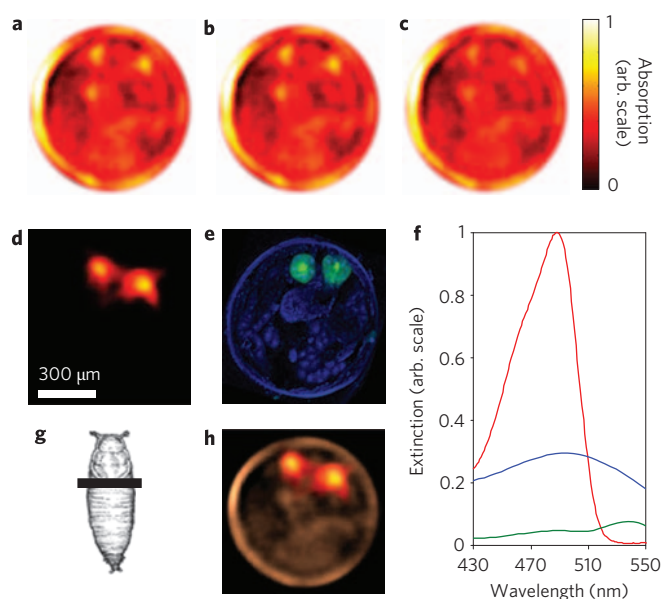


Figure 3 | Imaging of eGFP distribution in *Drosophila melanogaster* pupa. **a–c**, Opto-acoustic images acquired at 488 nm (**a**), 498 nm (**b**) and 508 nm (**c**). **d**, Spectrally resolved (MSOT) image of eGFP distribution in an intact pupa. **e**, Corresponding histology of DAPI-stained pupa at approximately the same imaging plane (green colour corresponds to GFP-expressing salivary glands). **f**, Extinction spectra of eGFP (red) along with measured absorption of pupa case (blue) and fat areas (green). **g**, Imaging plane. **h**, Overlay between the image at 508 nm (**c**) and the spectrally resolved image.

organisms through adulthood, several dynamic aspects of molecular and cellular mechanisms of disease aetiology and progression, aging and the effects of environmental factors may be studied *in vivo* in an intact specimen. Furthermore, the large number of FPs available have provided powerful tools for mechanistic and functional genetic research, and many transgenic models expressing these genetic fluorescent markers in a cell-type-specific manner have been established to investigate cellular and sub-cellular function.

Imaging results from a *Drosophila melanogaster* pupa are presented in Fig. 3. In this case, a Gal-4/UAS system was used to specifically express eGFP (enhanced green fluorescent protein) in the salivary glands of the fly pupae (see Supplementary information for details). The imaging plane was located in the posterior part of the salivary glands area, as shown in Fig. 3g. In this pupal stage, the *Drosophila* exhibits significant scattering²⁵ and is not accessible through its intact case by conventional fluorescent microscopy. The opto-acoustic images at three representative wavelengths are shown in Fig. 3a–c. The pupal case is readily identified in those images as having rather high optical absorption compared to internal structures. The various fatty structures are also clearly visualized. As in the previous imaging sessions, despite their strong eGFP expression, the salivary glands are not clearly distinguishable on single-wavelength images due to other non-specific background absorption. Figure 3f shows the spectral response of the pupal tissue as calculated by corresponding multiwavelength opto-acoustic measurements. After spectral processing, the salivary glands can be accurately visualized as shown in Fig. 3d,h. The corresponding histological section at approximately the same imaging plane is shown in Fig. 3e and is in good agreement with the reconstruction. The in-plane spatial resolution of opto-acoustic images is mainly determined by the effective bandwidth of the ultrasonic detector (20 MHz), leading to $\sim 38 \mu\text{m}$ diffraction limited (half-wavelength) resolution in water. The vertical resolution was limited by the focal width of the ultrasonic detector to $150 \mu\text{m}$.

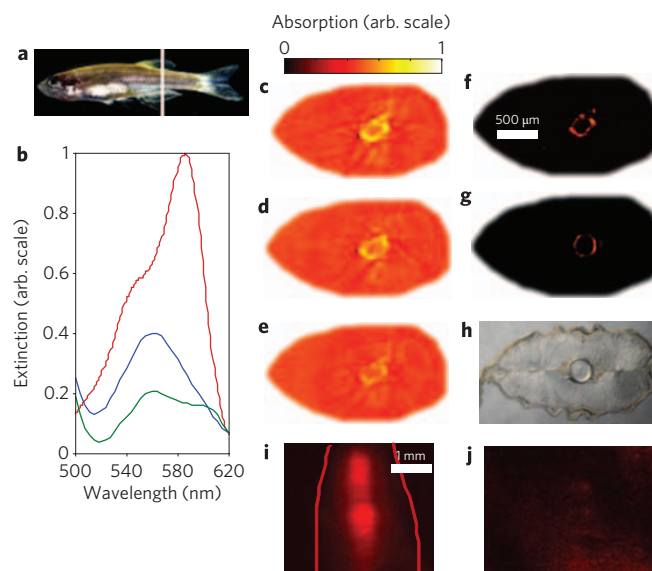


Figure 4 | Imaging of mCherry distribution in the vertebral column of an adult zebrafish. **a**, Location of the imaging plane. **b**, Extinction spectra of mCherry (red curve) and the intrinsic background (vertebral column, blue; muscles, green). **c–e**, Opto-acoustic images acquired at 587 nm (**c**), 597 nm (**d**) and 607 nm (**e**). **f**, Spectrally resolved image of mCherry distribution in an intact animal. **g**, Histological epifluorescence image of dissected tissue at approximately the same imaging plane (red colour corresponds to mCherry-expressing vertebral column). **h**, Regular histological section. **i**, Epifluorescence image of a living zebrafish. Red curves show the surface outline. **j**, Coronal confocal image at a depth of $\sim 500 \mu\text{m}$ from the surface. A juvenile two-month-old zebrafish was used in this case (short axis thickness of $\sim 1 \text{ mm}$ in the imaged area).

To demonstrate the ability of the system to image through larger dimensions, we imaged adult zebrafish. Figure 4 shows results from a transgenic three-month old zebrafish in which the Gal-4/UAS system was used to express the mCherry FP in the vertebral column (see Supplementary information for details). This transgenic strain was chosen because the vertebral column represents one of the deeper structures in the highly scattering adult trunk and thus provides a significant imaging challenge. The specimen, measuring $2.5 \times 4 \text{ mm}^2$ (see image cross-section in Fig. 4a), was held in the imaging setup by an agar phantom. Illumination was performed at multiple wavelengths, targeting the steep declining slope of the mCherry extinction spectra shown in Fig. 4b. Opto-acoustic images of the mCherry-expressing zebrafish at three representative wavelengths are shown in Fig. 4c–e and, as expected, exhibit strong contrast from varying tissue absorption in the vertebral column and surrounding structures. Similarly, spectral decomposition accurately resolves the location of mCherry expression in the intact animal (Fig. 4f). Subsequent histological sectioning (Fig. 4h) and epifluorescence image recording of tissue sections (Fig. 4g) demonstrated high congruence between *in vivo* and *ex vivo* images from the animal. The MSOT images provided an in-plane spatial resolution of less than $40 \mu\text{m}$, as can be elucidated from the thickness of the fluorescent ring-like structure of the vertebral column in Fig. 4f. This spatial resolution can be substantially improved by using ultrasonic detectors with larger bandwidth. There is no methodology currently available that allows visualization of reporter molecules at these resolutions and these dimensions. Existing microscopy methods are mostly limited by resolution and SNR degradation due to light diffusion beyond depths of $\sim 500 \mu\text{m}$ in scattering tissue. For comparison, we also provide an image of a juvenile (one-month-old) zebrafish using confocal

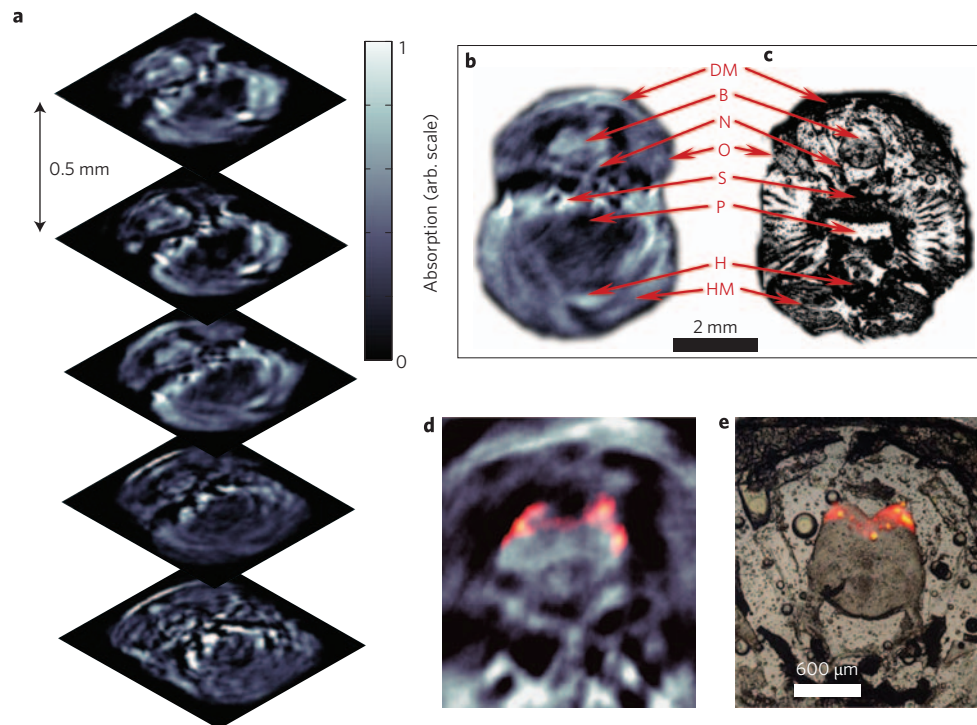


Figure 5 | Three-dimensional *in vivo* imaging through the brain of an adult (six-month-old) mCherry-expressing transgenic zebrafish. **a**, Five transverse opto-acoustic imaging slices through the hindbrain area at the level of crista cerebellaris of a living zebrafish taken at 585 nm. **b,c**, Example of an imaged slice (**b**) and its corresponding histological section in inverted colours (**c**). DM, dorsal fin musculature; B, hindbrain; N, lateral line nerve; O, operculum; S, skull bones; P, pharynx; H, heart; HM, hypobranchial musculature. **d**, MSOT image of the brain (enlarged) with mCherry expression shown in colour. **e**, Corresponding fluorescent histology of a dissected fish at the hindbrain level.

microscopy in Fig. 4j. Even though the cross-section here measures only ~ 1 –2 mm as compared to 2.5–4 mm as imaged by MSOT, the confocal microscopy cannot image through the highly scattering juvenile zebrafish while an additional epifluorescence image (Fig. 4i) shows that the fluorescent vertebral column exhibits a highly diffusive appearance through 1–2 mm of tissue. Although multiphoton microscopy could possibly penetrate slightly deeper, it would also be limited by this light diffusion at about one transport MFPL, that is, < 1 mm in scattering tissue.

To further showcase the MSOT capacity of performing three-dimensional *in vivo* scans we also imaged through the head of an adult (six-month-old) mCherry-expressing transgenic zebrafish (see Supplementary Information for details) with a cross-sectional diameter of ~ 6 mm. To guarantee survival, the fish was attached to the rotation stage by partially embedding it into modelling clay so that the upper parts including the head and gills were exposed to the anaesthetic solution (Tricaine) in the imaging tank. The fish fully recovered from the *in vivo* imaging sessions. The imaging results, shown in Fig. 5, demonstrate the ability of the process to reveal many morphological features, as is evident from Fig. 5a,b, supported by the corresponding histology (Fig. 5c). Moreover, multispectral reconstructions accurately resolved FP expression in the hindbrain of an intact living animal (Fig. 5d), in high congruence with the corresponding epifluorescence images of the dissected brain (Fig. 5e).

The ability to optically interrogate and visualize intact organisms beyond the limits of microscopy is of great importance in the post-genomic era for accelerating the study of genomics and proteomics. This work reports on the development of multiprojection multispectral opto-acoustic tomography (MSOT) for imaging biological organisms, and discusses its previously undocumented capacity for effectively detecting FPs in tissues, *in vivo*. The method was found to be capable of offering a new generation of

biological imaging by visualizing optical reporter molecules deep inside the body of mature organisms with high (mesoscopic) resolution, while simultaneously providing the necessary reference anatomical images. A particular strength of the technology is its ability to scale with different tissue sizes. Imaging of a zebrafish up to 6 mm thick was shown. However, as demonstrated in phantom experiments, several centimetres of penetration with nearly the same resolution can be achieved, particularly when using near-infrared light. Indeed, many relevant biological samples and model organisms (such as worms, developing and adult insects, and vertebrates including small mammals and their extremities) have sizes lying in this range and could therefore be visualized.

The phantom measurements of Fig. 2 allow for the calculation and prediction of the detection limits of the current system. To achieve this, we performed a theoretical analysis to translate the system noise and signals detected from known volumes and cell populations to predict signals from different volumes and cell numbers of interest. The method uses an analytical solution of optical and acoustic propagation as well as target size and depth and yields, as recently described in ref. 24, a nonlinear dependence of signal strength with target volume. According to the spatio-temporal characteristics of the ultrasonic detector, the model assumed that the effective volume in the phantom of Fig. 2, from which the individual opto-acoustic signals were detected, contained on average $\sim 10^4$ cells and assumed a minimum detection limit corresponding to a CNR of 5 (that is, $\text{CNR} < 5$ does not constitute detection). In this case, the minimal detectable number of cells was found to be $\sim 10^3$. It was further calculated that, for achieving single cell detection sensitivity, the SNR of the system would need to be improved by a factor of ~ 2500 , which corresponds to an equivalent increase of the signal or reduction of the noise floor by a factor of $\sqrt{2500} = 50$ (in rms voltage terms). Such an improvement is technically feasible and can be achieved by a combination of using

detectors of higher sensitivity, averaging over longer periods of time, or using larger arrays of detectors in parallel.

Multiwavelength imaging combined with selective-plane illumination offers the possibility of improving contrast, reducing out-of-plane and other imaging artifacts (see, for example, Fig. 3), as well as simultaneously resolving multiple FPs, dyes and other chromophores. In the applications shown, no photobleaching effects were observed, because the method operates with significantly less power per unit volume than that achieved with focused light, as in confocal microscopy. Although the spatial resolution in these studies was $\sim 38 \mu\text{m}$, broadband acoustic detectors constructed in arrays may lead to superior resolution and also offer real-time imaging capability, which is the goal of the next-generation setup. One important issue to be addressed regarding the accuracy of multispectral reconstruction is the wavelength dependence of the light distribution in tissue. As the MSOT method proposed herein capitalizes on the steep changes in absorption spectra of FPs in the vicinity of their excitation wavelength, it only needs very narrow spectral bands to operate efficiently (of the order of 30 nm). Within this spectral region the scattering properties of even very diffuse tissues are not expected to differ by more than 10% (assuming scattering is normally inversely proportional to the square of the wavelength), leading to corresponding fluence changes of less than 5%, as can be calculated by the light diffusion equation. However, if scattering variations in certain applications are higher, then correction on the data could be applied by corresponding adjustment of the photon diffusion model used to account for wavelength-dependent light propagation differences in the tissues due to scattering. In addition, because contrast is calculated in the spectral analysis on a relative per voxel basis, there is also low sensitivity to spatially varying scattering. Therefore, in contrast to conventional opto-acoustic imaging, MSOT is not affected significantly by possible scattering heterogeneity within the tissues or wavelengths used.

In comparison, surface-limited fluorescence microscopy methods or those applied to transparent or post mortem to chemically treated samples achieve better spatial resolution but offer penetration depths limited to less than one MFPL²⁵, that is, $\sim 1 \text{ mm}$ in the case of opaque living tissue. It is also possible to perform optical tomography through entire mice with high sensitivity, but low resolution^{8,26} ($\sim 1 \text{ mm}$ or worse). In contrast, selective-plane MSOT offers an imaging platform that is not limited by light diffusion and can achieve a penetration from several millimetres to potentially centimetres with a resolution that can vary practically in the range 20–100 μm . Importantly, the resolution achieved remains constant as a function of depth and depends only on the ultrasonic detector characteristics, that is, on bandwidth and sensitivity, as well as on the overall SNR achieved. MSOT therefore fills a significant area in biological imaging that goes well beyond the penetration limit of modern microscopy and could become the method of choice in studying signalling pathways and gene expression, morphogenesis, disease progression and many other targeted mechanisms through whole bodies of opaque living organisms and animals. It may not only significantly enhance the usefulness of currently existing transgenic FP lines, but may even call for the development of more reporters and probes that could tag, with higher flexibility, development, disease and aging-related processes.

Methods

Experimental setup and data acquisition. The schematic of the experimental setup is shown in Fig. 1c. It uses an optical parametric oscillator (OPO) based laser (MOPO series, Spectra Physics Inc.), tunable in the visible and near-infrared region (430–1,800 nm) and capable of producing 8-ns pulses with a repetition frequency of 30 Hz. The imaged objects were fixed on the rotation stage, controlled by a stage controller (ESP-3000, Newport Corp.). The laser beam was passed through a variable-slit aperture, and focused using a cylindrically focusing lens onto a sample submerged in water, thus creating a planar sheet of light. Before entering the water tank, the beam was further homogenized in the imaged (horizontal) plane using a diffuser to reduce the effects associated with hot spots and other beam instability

artifacts. Maximal light intensity at the surface of the imaged objects was $\sim 5 \text{ mW mm}^{-2}$. The geometric focal line was extended for $\sim 2\text{--}3 \text{ mm}$ into the scattering object to allow maximal possible confinement of a planar light sheet within the acoustic detection plane (image plane). This kind of selective-plane illumination strategy is especially useful in cases where the studied organism presents high absorption contrast between different structures. This is because, for the first one or two millimetres, the light is only partially diffused as it passes through the scattering object, thus, signals coming from ‘out-of-focus plane’ absorptive structures are minimized. Each imaged object was illuminated by up to seven wavelengths spaced by 10 nm and located near the peak excitation of the particular FP being imaged; however, a minimum of three wavelengths are normally required for efficient spectral decomposition. Broadband ultrasonic transducers (Models V382 and V319, Olympus-Panametrics, 100% bandwidth, central frequencies 3.5 and 15 MHz, respectively), cylindrically focused at the optical illumination plane (confocal arrangement), were used to detect the opto-acoustic signals. The V382 transducer was used for phantom measurements while the V319 model served in other high-resolution *in vivo* experiments. The samples were rotated 360° with 3° steps to enable in-plane two-dimensional image reconstruction. Three-dimensional data acquisition was enabled by means of vertical scanning of both illumination and detection planes by mounting the transducer and a 45° -angled mirror onto a vertical translational stage. The recorded time-resolved signals were amplified, digitized and averaged by an embedded oscilloscope PCI card at 100 Msps (NI PCI-5122, National Instruments Corp.) with 14-bit resolution. To further reduce beam instability artifacts and increase the accuracy of multispectral reconstructions, a photodiode was used to detect pulse energy and all recorded signals were normalized with the actual light energy on a per-pulse basis. Planar image data acquisition normally took $\sim 2 \text{ min}$ at each wavelength.

Image reconstruction. A filtered backprojection algorithm²⁷ was used to reconstruct the detected opto-acoustic responses. Two-dimensional single-wavelength image reconstruction was carried out on a dual-core Pentium IV 3.2 GHz processor with 2 GB RAM, and typically required $\sim 3 \text{ s}$ on a 200×200 mesh. Because the raw opto-acoustic signals represent a combined contribution of light fluence and optical absorption, to extract more accurate optical absorption data it might be necessary to normalize the images by the light distribution in the object. It was, however, found that for *Drosophila* and zebrafish, due to their relatively small size, normalization for light distribution was not critical for the quality of the reconstructed images. This is because, in the range considered, the signal drop of the light sheet is not significant (less than an order of magnitude) so it does not significantly affect image quality through SNR deterioration. Nevertheless, correction for light distribution is essential for the 1.9-cm-diameter phantom to obtain contrast from the deep structures²⁸. To facilitate the correction, we represent the initially reconstructed opto-acoustic image as a product between optical absorption distribution $\mu_a(\mathbf{r})$ and local light fluence $U(\mathbf{r})$. The latter is calculated using a finite-element method (FEM) solution to the light diffusion equation

$$\nabla^2 U(\mathbf{r}) - k^2 U(\mathbf{r}) = -q_0$$

where $k = \sqrt{3\mu_a(\mu_a + \mu'_a)}$. The light source term q_0 is assigned onto the phantom boundary, directly extracted from the opto-acoustic image. For first-order correction, we further assume that the phantom has homogeneous a priori known background optical properties. The average background properties of an object can in principle be approximately measured by comparing the magnitude of the surface opto-acoustic response to the one recorded from a calibrated object with known optical properties. Subsequently, the initial images at each wavelength are normalized by the calculated light distribution to obtain quantified optical absorption data on a per-pixel basis. In cases with a highly heterogeneous background with unknown optical properties, iterative normalization methods have been suggested for planar boundary two-dimensional configurations²⁹, and were recently extended to three dimensions by iteratively feeding data from a segmented opto-acoustic image into the FEM-based light diffusion model³⁰.

The correct location and concentration of FPs was resolved by spectral processing of opto-acoustic images^{21,31} obtained at n discrete wavelengths $\lambda_1, \dots, \lambda_n$. As mentioned, opto-acoustic measurements were taken in control animals containing no FPs to establish the spectral behaviour of the background absorption. It was subsequently assumed that every pixel k in the opto-acoustic image represents a combined contribution of the FP and the background. This can be written in the form of N linear equations:

$$\mu_a^k(\lambda_m) = \alpha_b(\lambda_m)c_b^k + \alpha_{FP}(\lambda_m)c_{FP}^k, \quad m = 1, \dots, N$$

where $\mu_a^k(\lambda)$ is the reconstructed wavelength-dependent absorption in pixel k , $\alpha_b(\lambda)$ and $\alpha_{FP}(\lambda)$ are the molar extinction spectra of the FP and the background, and c_b^k and c_{FP}^k are the corresponding concentrations. Using the measured total absorption values and the known spectra for the measured wavelengths, the concentrations c_{FP}^k of the FP and the background c_b^k are subsequently reconstructed from the above linear equations on a per-pixel basis using a linear regression method. It should be noted that, although $\alpha_{FP}(\lambda)$ and c_{FP}^k represent the actual molar extinction coefficient of the FP and its concentration, the measured background spectra $\alpha_b(\lambda)$ and the extracted

values of the concentration c_k^* have arbitrary scale values and only their product $\alpha_k(\lambda)c_k^*$ has a real physical interpretation. Additional spectral contributions can be introduced by simply adding new terms to the spectral equations.

Received 27 November 2008; accepted 20 May 2009;
published online 21 June 2009

References

- Giepmans, B. N. G., Adams, S. R., Ellisman, M. H. & Tsien, R. Y. The fluorescent toolbox for assessing protein location and function. *Science* **312**, 217–224 (2006).
- Lichtman, J. W. & Conchello, J. A. Fluorescence microscopy. *Nature Methods* **2**, 910–919 (2005).
- Conchello J. A. & Lichtman, J. W. Optical sectioning microscopy. *Nature Methods* **2**, 920–931 (2005).
- Bahlmann, K. *et al.* Multifocal multiphoton microscopy (MMM) at a frame rate beyond 600 Hz. *Opt. Express* **15**, 10991–10998 (2007).
- Minsky, M. Microscopy apparatus. US patent 3,013,467 (1961).
- Denk, W., Strickler, J. H. & Webb, W. W. 2-photon laser scanning fluorescence microscopy. *Science* **248**, 73–76 (1990).
- Helmchen, F. & Denk, W. Deep tissue two-photon microscopy. *Nature Methods* **2**, 932–940 (2005).
- Ntziachristos, V., Ripoll, J., Wang, L. H. V. & Weissleder, R. Looking and listening to light: the evolution of whole-body photonic imaging. *Nature Biotechnol.* **23**, 313–320 (2005).
- Hove, J. R. *et al.* Intracardiac hemodynamics are an essential epigenetic factor for embryonic cardiogenesis. *Nature* **421**, 172–177 (2003).
- Jain, R. K., Munn, L. L. & Fukumura, D. Dissecting tumor pathophysiology using intravital microscopy. *Nature Rev. Cancer* **2**, 266–276 (2002).
- Sharpe, J. *et al.* Optical projection tomography as a tool for 3D microscopy and gene expression studies. *Science* **296**, 541–545 (2002).
- Huisken, J. *et al.* Optical sectioning deep inside live embryos by selective plane illumination microscopy. *Science* **305**, 1007–1009 (2004).
- Doty, H. U. *et al.* Ultramicroscopy: three-dimensional visualization of neuronal networks in the whole mouse brain. *Nature Methods* **4**, 331–336 (2007).
- Editorial. Geneticist seeks engineer: must like flies and worms. *Nature Methods* **4**, 463 (2007).
- Schroeder, T. Imaging stem-cell-driven regeneration in mammals. *Nature* **453**, 345–351 (2008).
- Gusev, V. E. & Karabutov, A. A. *Laser Optoacoustics (American Institute of Physics, 1993)*.
- Zhang, E. Z., Laufer, J. G., Pedley, R. B. & Beard, P. C. *In vivo* high-resolution 3D photoacoustic imaging of superficial vascular anatomy. *Phys. Med. Biol.* **54**, 1035–1046 (2009).
- Lao, Y., Xing, D., Yang, S. & Xiang, L. Noninvasive photoacoustic imaging of the developing vasculature during early tumor growth. *Phys. Med. Biol.* **53**, 4203–4212 (2008).
- Wang, X. *et al.* Noninvasive laser-induced photoacoustic tomography for structural and functional *in vivo* imaging of the brain. *Nature Biotechnol.* **21**, 803–806 (2003).
- Zhang, H. F., Maslov, K., Stoica, G. & Wang, L. V. Functional photoacoustic microscopy for high-resolution and noninvasive *in vivo* imaging. *Nature Biotechnol.* **24**, 848–851 (2006).
- Razansky, D., Vinegoni, C. & Ntziachristos, V. Multispectral photoacoustic imaging of fluorochromes in small animals. *Opt. Lett.* **32**, 2891–2893 (2007).
- Li, L., Zemp, R. J., Lungu, G., Stoica, G. & Wang, L. V. Photoacoustic imaging of lacZ gene expression *in vivo*. *J. Biomed. Opt.* **12**, 020504 (2007).
- De La Zerda, A. *et al.* Carbon nanotubes as photoacoustic molecular imaging agents in living mice. *Nature Nanotechnol.* **3**, 557–562 (2008).
- Razansky, D., Baeten, J. & Ntziachristos, V. Sensitivity of molecular target detection by multispectral optoacoustic tomography (MSOT). *Med. Phys.* **36**, 2891–2893 (2009).
- Vinegoni, C., Pitsouli, C., Razansky, D., Perrimon, N. & Ntziachristos, V. *In vivo* imaging of *Drosophila melanogaster* pupae with mesoscopic fluorescence tomography. *Nature Methods* **5**, 45–47 (2008).
- Ntziachristos, V., Tung, C.-H., Bremer, C. & Weissleder, R. Fluorescence molecular tomography resolves protease activity *in vivo*. *Nature Med.* **8**, 757–760 (2002).
- Xu, M. & Wang, L. V. Universal back-projection algorithm for photoacoustic computed tomography. *Phys. Rev. E* **71**, 016706 (2005).
- Razansky, D. & Ntziachristos, V. Hybrid photoacoustic fluorescence molecular tomography using finite-element-based inversion. *Med. Phys.* **34**, 4293–4301 (2007).
- Cox, B. T., Arridge, S. R., Kostli, K. P. & Beard, P. C. 2D quantitative photoacoustic image reconstruction of absorption distributions in scattering media using a simple iterative method. *Appl. Opt.* **45**, 1866–1875 (2006).
- Jetzfellner, T. *et al.* Iterative optoacoustic image normalization in non-uniform illumination configurations. *Appl. Phys. Lett.* **95**, (2009) (in the press).
- Laufer, J. G., Delpy, D. T., Elwell, C. E. & Beard, P. C. Quantitative spatially resolved measurement of tissue chromophore concentrations using photoacoustic spectroscopy: application to the measurement of blood oxygenation and haemoglobin concentration. *Phys. Med. Biol.* **52**, 141–168 (2007).

Acknowledgements

D.R. acknowledges financial support by the Deutsche Forschungsgemeinschaft (DFG) research grant RA 1848/1-1. M.D. is a fellow of the Studienstiftung des deutschen Volkes. R.W.K. is supported by a BioFuture Award Grant (0311889) of the German Ministry for Education and Research (BMBF). We thank R. Jagasia for providing HeLa mitodsRed cells.

Additional information

Supplementary information accompanies this paper at www.nature.com/naturephotonics. Reprints and permission information is available online at <http://npg.nature.com/reprintsandpermissions/>. Correspondence and requests for materials should be addressed to D.R. and V.N.

Appendix 5

published Article in *The Journal of Clinical Investigations*

A zebrafish model of tauopathy allows in vivo imaging of neuronal cell death and drug evaluation

Dominik Paquet, Ratan Bhat, Astrid Sydow, Eva-Maria Mandelkow, Stefan Berg, Sven Hellberg, Johanna Fälting, Martin Distel, Reinhard W. Köster, Bettina Schmid and Christian Haass

J Clin Invest (2009), **119**, 1382-1395.

Contribution:

This project was mainly conducted by Dominik Paquet. I contributed bidirectional Gal4 effector vectors as depicted in Fig.1, used to generate the zebrafish tauopathy model.



A zebrafish model of tauopathy allows in vivo imaging of neuronal cell death and drug evaluation

Dominik Paquet,^{1,2} Ratan Bhat,³ Astrid Sydow,⁴ Eva-Maria Mandelkow,⁴ Stefan Berg,³ Sven Hellberg,³ Johanna Fälting,³ Martin Distel,⁵ Reinhard W. Köster,⁵ Bettina Schmid,^{1,2} and Christian Haass^{1,2}

¹Deutsches Zentrum für Neurodegenerative Erkrankungen (DZNE) and ²Adolf-Butenandt-Institute, Biochemistry, Ludwig-Maximilians-University, Munich, Germany.

³AstraZeneca Research & Development, Södertälje, Sweden. ⁴Max-Planck Unit for Structural Molecular Biology at DESY, Hamburg, Germany.

⁵Helmholtz Zentrum München, Institute of Developmental Genetics, Neuherberg, Germany.

Our aging society is confronted with a dramatic increase of patients suffering from tauopathies, which include Alzheimer disease and certain frontotemporal dementias. These disorders are characterized by typical neuropathological lesions including hyperphosphorylation and subsequent aggregation of TAU protein and neuronal cell death. Currently, no mechanism-based cures are available. We generated fluorescently labeled TAU transgenic zebrafish, which rapidly recapitulated key pathological features of tauopathies, including phosphorylation and conformational changes of human TAU protein, tangle formation, neuronal and behavioral disturbances, and cell death. Due to their optical transparency and small size, zebrafish larvae are well suited for both in vivo imaging and drug development. TAU-induced neuronal cell death was imaged by time-lapse microscopy in vivo. Furthermore, we used this zebrafish model to identify compounds targeting the TAU kinase glycogen synthase kinase 3 β (GSK3 β). We identified a newly developed highly active GSK3 β inhibitor, AR-534, by rational drug design. AR-534 reduced TAU phosphorylation in TAU transgenic zebrafish. This transgenic zebrafish model may become a valuable tool for further studies of the neuropathology of dementia.

Introduction

Neurodegenerative diseases are the most frequent cause of dementia in our aging society. For these disorders, which include Alzheimer disease (AD) and frontotemporal dementia (FTD), disease-modifying treatments represent a highly unmet medical need. AD and FTD are characterized by posttranslationally modified amyloidogenic proteins, which form neurotoxic oligomers and are finally deposited as insoluble aggregates (1). Examples of the proteinaceous building blocks of these deposits are amyloid β peptide in AD and TAU in AD and FTD (2, 3). The TAU protein is an important target for research and drug development, since its pathological alterations strongly correlate with disease progression in AD and FTD and other neurodegenerative diseases (4) and TAU suppression improves memory function (5). Furthermore, mutations in the TAU-encoding gene microtubule-associated protein TAU (*MAPT*) have been found in patients with FTD with Parkinsonism linked to chromosome 17 (FTDP-17) (6). One of the first characteristic modifications of TAU is its pathologic phosphorylation at multiple residues, which are dis-

tributed over the whole protein (3, 7). The initial steps, which lead to TAU phosphorylation and subsequent aggregation, were mainly studied in cell culture but are still poorly understood in vivo. These early stages are difficult to investigate in transgenic mice, since it is not feasible to image cells accurately over longer periods during early disease stages (8). Furthermore, vertebrate in vivo models for rapid high-throughput screening for inhibitors of TAU pathology are not available.

Here, we propose the zebrafish as a small vertebrate model of tauopathies and other neurodegenerative diseases. It offers genetic tractability in combination with a translucent embryo allowing imaging of disease progression at cellular and subcellular levels in the living animal. Furthermore, the potential of using small zebrafish embryos for large-scale drug screening has already been demonstrated (9). Large amounts of small fish, which can be analyzed in a 96-well format, can be rapidly produced. Fish are kept in water, which facilitates uptake of substances from the aqueous medium, allowing for automated compound application. In addition, simple readouts of characteristics such as altered mobility and fluorescence or changes in biochemical composition of proteins can be analyzed on a large scale. Moreover, the endothelial blood-brain barrier (BBB) begins to become functional 3 days after fertilization in zebrafish and has a structure similar to that in higher vertebrates, allowing one to test for bioavailability of drugs in the nervous system (10).

We have optimized the transgenic expression of the human protein TAU-P301L (a mutation genetically linked to FTD; ref. 6) in zebrafish neurons by a newly designed Gal4-upstream activating sequence-based (Gal4/UAS-based) vector system, which also great-

Conflict of interest: D. Paquet, A. Sydow, E.-M. Mandelkow, M. Distel, R.W. Köster, and B. Schmid declare no conflict of interest. R. Bhat, S. Berg, S. Hellberg, and J. Fälting are employees of AstraZeneca R&D. C. Haass is a consultant for Elan Pharmaceuticals and receives research support from Boehringer Ingelheim KG.

Nonstandard abbreviations used: AD, Alzheimer disease; BBB, blood-brain barrier; CDK2, cyclin-dependent kinase 2; dN-GSK3 β , dominant-negative *Xenopus* GSK3 β -K85R; FTD, frontotemporal dementia; GSK3 β , glycogen synthase kinase 3 β ; hpf, hours post fertilization; IF, immunofluorescence; IHC, immunohistochemistry; Ins, insert; MCS, multiple cloning site; UAS, upstream activating sequence; WB, Western blot.

Citation for this article: *J. Clin. Invest.* 119:1382–1395 (2009). doi:10.1172/JCI37537.



ly facilitates identification of the transgenic fish by a simultaneously expressed fluorescent reporter. We have further advanced the system to allow introduction of various other genes and promoters to facilitate the generation of different zebrafish disease models. In contrast to previous studies (11, 12), we were able to monitor early pathology, including disease-specific hyperphosphorylation and conformational changes of TAU, neuronal and behavioral abnormalities as well as increased neuronal cell death within the first days of embryonic development in stable transgenic zebrafish. The rapid appearance of a pathologic phenotype allows one not only to use the embryos to study disease progression in a transparent vertebrate but also to validate and even screen on a relatively large scale for compounds that modify early phenotypes, such as TAU hyperphosphorylation, *in vivo*.

Hyperphosphorylation of TAU is believed to be a key initiator of detachment of normal TAU from microtubules and subsequent oligomerization and aggregation. Several kinases, including glycogen synthase kinase 3 β (GSK3 β), cyclin-dependent kinase 5 (CDK5), ERK2, and microtubule affinity-regulating kinase (MARK), directly phosphorylate TAU and are therefore considered as key therapeutic targets (13). Inhibitors that selectively block these enzymes could therefore be used to slow the progression of disease pathology. Over the last years, selective inhibitors for kinases involved in TAU phosphorylation have been identified, and some of these compounds have even been tested in TAU transgenic mice, where they showed some effects on TAU phosphorylation. The activity of these inhibitors, however, has been hampered by poor water solubility and bioavailability and substantial side effects (13). In addition, large quantities of the compounds are needed, since long-term administration is usually required to observe potential efficacy. Therefore, there is a significant need for technologies that can rapidly and efficiently identify more active and specific compounds with optimized bioavailability in *in vivo* models that represent disease pathology. We have shown previously that novel substances can be developed by structure-based design, which uses crystal structures of proteins, to model small molecules into the active site of the targeted enzyme (14). This approach can deliver inhibitors with excellent potency and specificity. However, it requires validating the bioavailability and selective inhibition of the target molecule in an *in vivo* setting. We have now developed several highly specific inhibitors by structure-based design, which bind to the active site of GSK3 β and block the enzyme function with high potency *in vitro*. Two of the best inhibitors were then investigated for their potential efficacy in zebrafish. We demonstrate here for the first time, to our knowledge, that we could reduce the pathologic phosphorylation of the human disease-associated protein TAU *in vivo* in a transgenic zebrafish model by several published GSK3 β inhibitors. Furthermore, we tested 2 newly developed highly selective GSK3 β inhibitors with potent *in vitro* activity and could show with our model that one of them is also very potent in a whole organism *in vivo*.

Our study not only provides a small vertebrate model of tauopathies and other neurodegenerative diseases, which can be used to monitor progression of pathology *in vivo*, but also a powerful combination of *in silico* prediction of compounds with *in vivo* validation of their bioavailability in a small transgenic vertebrate disease model. Finally, our newly developed zebrafish transgenesis vectors will allow modeling of numerous human disorders that are based on protein misfolding and overexpression, 2 phenomena often connected to each other (15).

Results

A Gal4/UAS-based bidirectional expression system in zebrafish. The first goal of this study was to generate transgenic zebrafish stably expressing the FTD-associated human protein TAU-P301L (6). Inefficient transgenesis and low protein expression levels have in the past hampered the efficient generation of zebrafish disease models expressing human genes. To overcome these limitations, we have generated vectors that combine several features to increase transgenesis rates and protein levels, facilitate the expression of disease proteins of interest, and allow efficient identification of transgenic lines as well as simultaneous *in vivo* monitoring of pathology and phenotypes. We cloned 2 constructs, Driver and Responder, based on the medaka *Tol2* transposable element (16), which greatly increases the rate of transgenesis (see Methods for details), and integrated the Gal4/UAS expression system (17) into the 2 vectors (Figure 1A). Furthermore, we introduced Gateway recombination sites, which allow rapid introduction of other genes and promoters (18) (see Supplemental Figure 1 for details; supplemental material available online with this article; doi:10.1172/JCI37537DS1). The Driver construct contains the neuronal promoter HuC (19), controlling the expression of a Gal4-VP16 fusion protein, which in turn efficiently transactivates and amplifies protein expression from a UAS on the Responder construct. To achieve transgene expression in 2 orientations, we flanked the UAS sequence with 2 short minimal promoters. In our constructs, this cassette drives the expression of human TAU-P301L in one direction and the expression of the fluorescent reporter DsRed in the other (Figure 1A). This bidirectional expression allows the identification of TAU-expressing cells in live embryos by concomitant DsRed fluorescence.

Transgenic fish were generated by injecting circular Driver and Responder constructs together with *Tol2* transposase mRNA, which is translated into active transposase (a protein not encoded by the zebrafish genome) in embryonic cells to catalyze integration of both constructs into the zebrafish genome for a short period of time (16). Both constructs integrate randomly into a subset of embryonic cells leading to mosaic TAU- and DsRed-expressing embryos. DsRed-positive embryos are raised and outcrossed to wild-type fish. The offspring of founder fish with germ-line transmission can be easily identified, as the embryos express DsRed in mature neurons, making PCR screenings dispensable (Figure 1B). The expression of TAU and DsRed in the transgenic zebrafish fully overlaps, as shown by immunofluorescence (IF) staining using the pan-TAU antibody T46 (20) and DsRed antibodies (Figure 1C).

We raised 76 injected founder fish to sexual maturity and identified 15 (19.7%) with DsRed-positive offspring. We analyzed 3 generations descending from 1 of the founder fish for genetic inheritance by counting DsRed-negative and -positive embryos and always found about one-fourth of the offspring to be DsRed positive, implying that these embryos carry Driver and Responder constructs (Supplemental Figure 2A). This ratio indicates independent inheritance of both constructs, with single or multiple insertions at 2 different genomic loci. We verified this by analyzing 225 embryos of an F2 outcross by PCR for Driver and Responder genotypes (Supplemental Figure 2B). In addition, the embryos showed stable protein levels and expression domains over 3 generations (Supplemental Figure 2C), indicating stable inheritance and activity of the Gal4/UAS transgene. Finally, we did not observe any morphological alterations in the transgenic fish (data not shown) and also excluded alterations in the function of the zebrafish BBB (for details see Supplemental Figure 3).

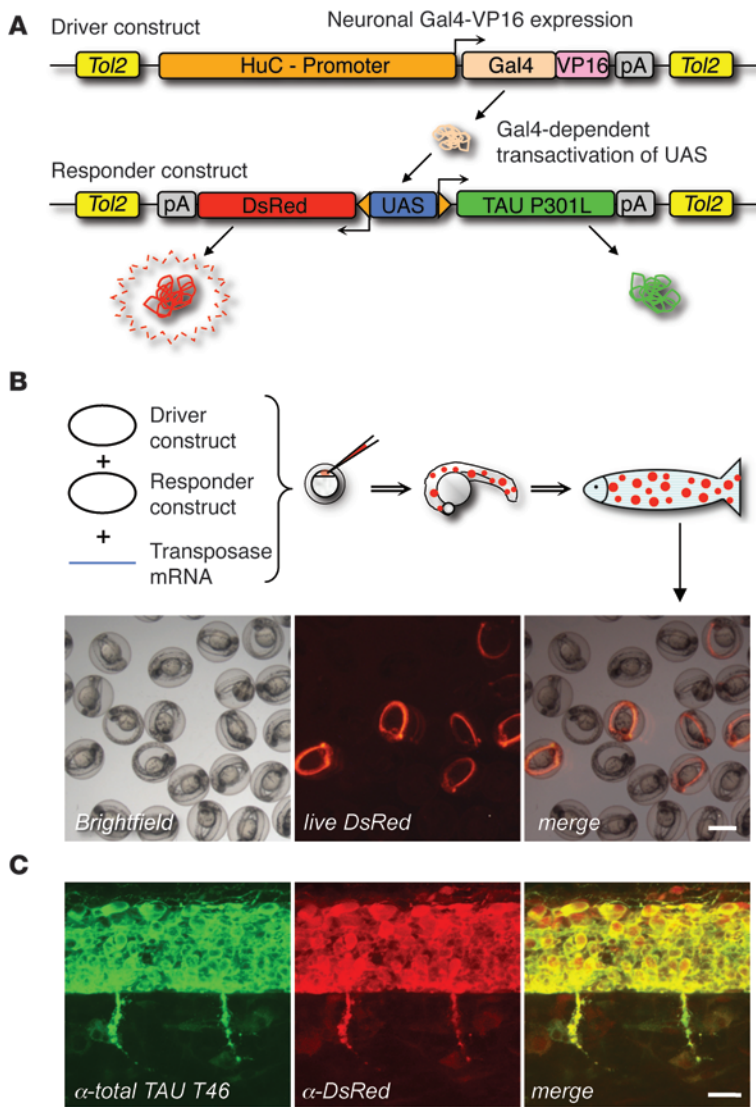


Figure 1

A Gal4/UAS-based bidirectional expression system in zebrafish. **(A)** The Driver construct contains the neuronal zebrafish promoter HuC driving the expression of Gal4-VP16, which binds to the UAS on the Responder construct. Here, it activates the bidirectional expression of hTAU-P301L and DsRed via the minimal promoters. UAS-dependent gene expression of TAU and DsRed is indicated in living fish by DsRed fluorescence. Driver and Responder constructs are flanked by *Tol2* transposon sites. **(B)** To generate transgenic fish, the Driver and Responder constructs were mixed and injected together with *Tol2* mRNA. The mRNA is translated to active transposase, which detects the flanking *Tol2* elements and catalyzes random integration into the zebrafish genome in a subset of embryonic cells for a short time period, generating mosaic founder embryos. Mosaic DsRed-positive larvae were raised and outcrossed with wild-type fish. A subset of the offspring will be transgenic and can be easily identified and sorted by DsRed-positive neurons. Scale bar: 1 mm. **(C)** Double immunostainings for total TAU (T46 antibody) and DsRed of 32-hpf transgenic zebrafish embryos expressing hTAU-P301L and DsRed. Transgenic embryos express both hTAU-P301L and DsRed in spinal cord neurons, showing effective bidirectional expression from the Responder construct. Lateral views of the trunk above the end of the yolk extension, anterior to the left. Scale bar: 20 μ m.

The transgenic zebrafish rapidly develop disease-specific alterations. Phosphorylation of TAU at certain serine and threonine residues serves as a biochemical marker for pathologic alterations in AD and FTD (3, 7). We therefore determined whether and when the TAU transgenic fish recapitulate this hallmark of disease progression. Strikingly, in embryos that were only 32 hours old, we could already detect positive immunoreactivity in spinal cord neurons with the antibodies AT180 (21), AT270 (21), 12E8 (22), PHF1 (23), 422 (24), and AT8 (25), which specifically detect abnormally phosphorylated residues T231/S235, T181, S262/S356, S396/S404, S422, and S202/T205, respectively (Figure 2A). These findings were corroborated by immunoblots of lysates from 48-hour-old transgenic and nontransgenic fish. The pan-TAU antibody T46 reveals a broad band around 64 kDa, which corresponds to the largest CNS TAU isoform in a mixed state of phosphorylation. Human TAU was also recognized by antibodies against phosphorylated epitopes that are typically elevated in AD (AT180, AT270, 12E8, PHF1, and 422) (Figure 2B).

In addition to pathologic hyperphosphorylation, TAU also changes its conformation during disease progression (26), which finally culminates in aggregation and formation of tangles. The early con-

formational changes can be monitored by immunostaining using antibody MC1, which is specific for a pathologic conformation of TAU (26). Strikingly, we already found MC1-positive TAU in neurons of 32-hour-old embryos, again demonstrating rapid occurrence of AD- and FTD-like pathology in our transgenic zebrafish model (Figure 2C). We also determined whether and when these changes to pathologic conformation led to the formation of tangles and therefore analyzed later stages. In 5-week-old fish, which are still quite transparent, we could not only observe the expression of the DsRed transgene in living fish (Figure 2D) but also depict TAU-expressing cells with the pathologic AT8 epitope in immunohistochemical stainings (Figure 2E) and Gallyas silver-positive tangles (Figure 2F) in paraffin sections of spinal cord tissue. To demonstrate specificity of the stainings, we also stained control transgenic lines, which express DsRed only, and nontransgenic siblings. No cross-reactivity in neurons was observed (Figure 2F and Supplemental Figure 4).

Rapid progression of AD/FTD-like late-stage pathology in TAU transgenic fish. We have observed remarkable differences in the amount of TAU-expressing cells, which are stained by early pathology-marking antibodies, such as AT180, AT270 and 12E8, versus late markers, such as

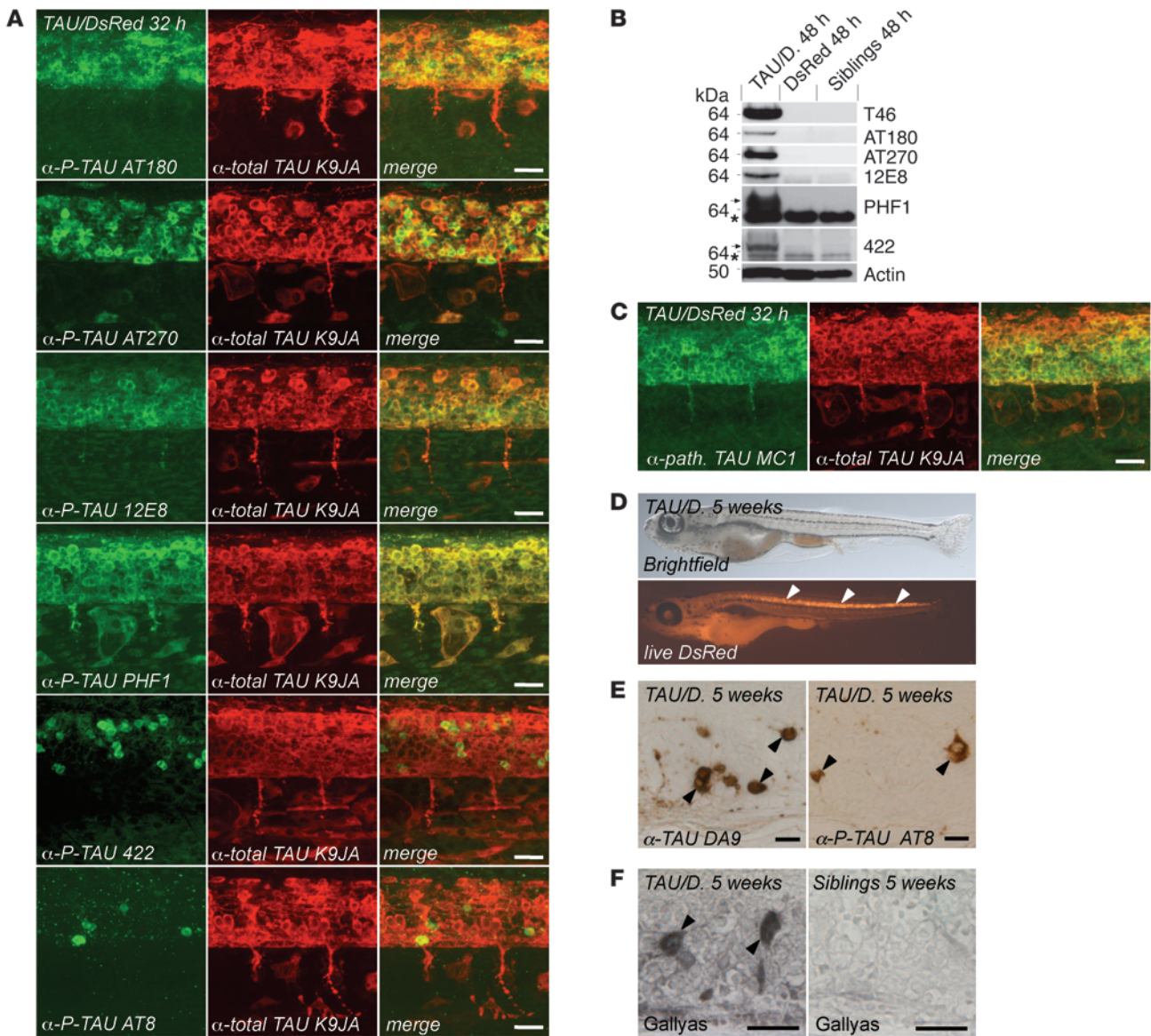


Figure 2

Expression of hTAU-P301L induces rapid pathological hyperphosphorylation, conformational changes, and aggregation of TAU in transgenic zebrafish. **(A)** Double whole-mount immunostainings for phosphorylated and total TAU of 32-hour-old transgenic zebrafish embryos expressing hTAU-P301L and DsRed. TAU is phosphorylated in spinal cord neurons at residues Thr231/Ser235 (AT180), Thr181 (AT270), Ser262/Ser356 (12E8), Ser396/Ser404 (PHF1), Ser422 (422), and Ser202/Thr205 (AT8). **(B)** WBs of total and phosphorylated TAU of 48-hour-old transgenic zebrafish embryos expressing hTAU-P301L and DsRed or DsRed alone or nontransgenic siblings. Phosphorylated TAU is only detected in TAU/DsRed transgenic embryos. No cross-reacting bands are detectable in controls at the same molecular weight. In addition to the specific band above 64 kDa (arrow) in TAU-positive embryos, antibodies PHF1 and 422 detect a nonspecific band at lower molecular weight in all embryos (asterisk). **(C)** TAU changes its conformation to a pathologic state, as shown in whole-mount immunostainings, by using the conformation-specific antibody MC1, in most neurons of 32-hour-old embryos expressing the TAU transgene. **(D)** Side views of 5-week-old living zebrafish in bright field and DsRed illumination. The fish are still rather translucent, and the transgene-expressing cells can be detected by their red fluorescence (arrowheads). **(E)** Immunohistochemical stainings of spinal cord paraffin sections of the same 5-week-old TAU transgenic zebrafish for total TAU (antibody DA9) and pathologically phosphorylated TAU (AT8) (arrowheads). **(F)** In addition, tangles are observed by Gallyas silver staining in sections of the same 5-week-old TAU transgenic zebrafish (arrowheads). Scale bars: 20 μ m.

422 and AT8, in 32-hour-old transgenic zebrafish. While the epitopes that are detected by early marker antibodies are present in most TAU-expressing cells, the signals of the late markers can only be found in a small subset of neuronal cells (Figure 2A). This observation raises the question of whether there is a progression to advanced pathology

that these immunopositive neurons have already reached in contrast to the surrounding neurons and whether other neurons will follow later. To monitor progression of the pathological AT8 immunoreactivity, we compared the number of positive neurons in 24-hour-old, 32-hour-old, 48-hour-old, and 7-day-old embryos from a single trans-

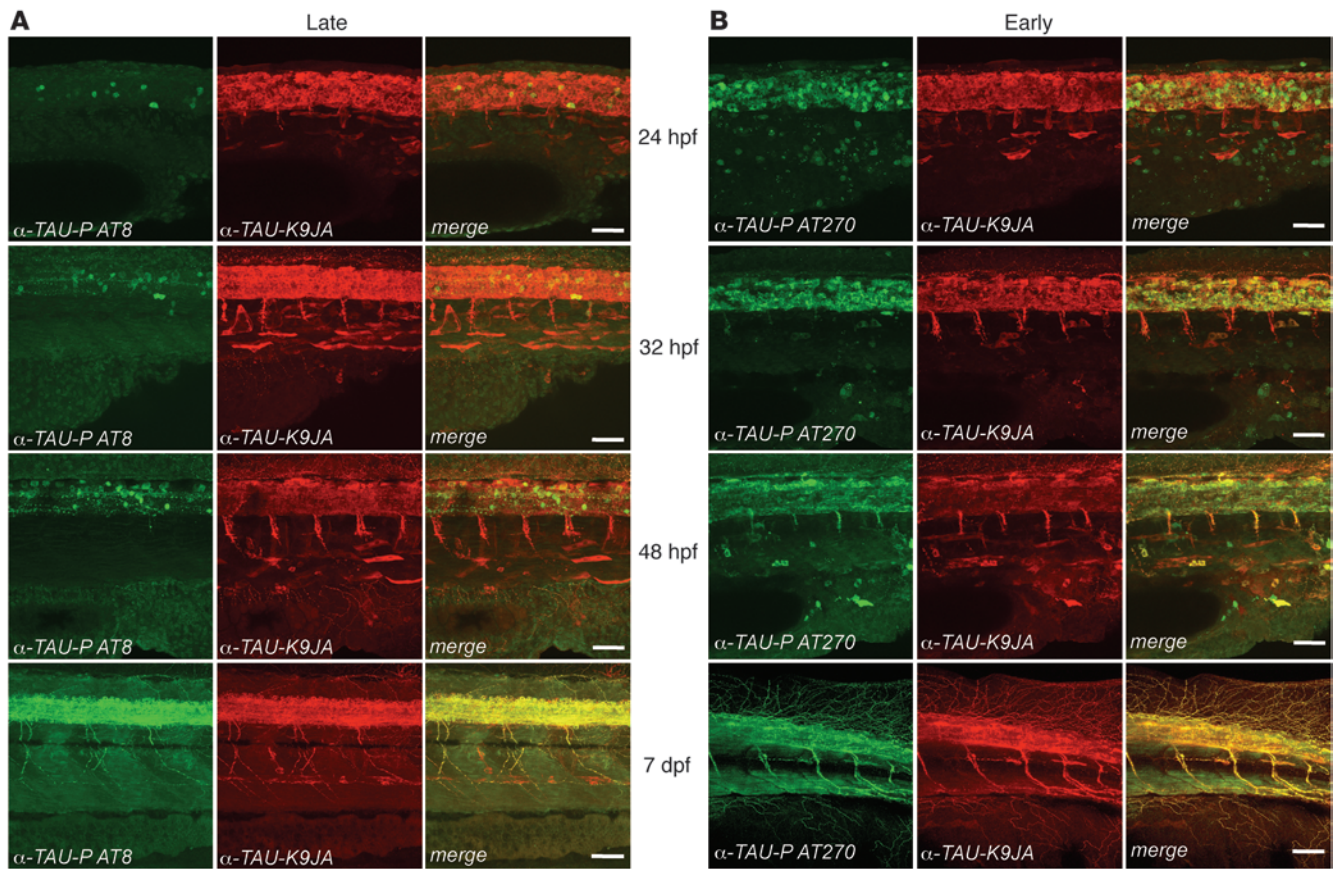


Figure 3

Rapid progression of AT8-positive late-stage FTD/AD-like pathology in transgenic embryos. **(A)** Double whole-mount immunostainings for TAU phosphorylated at the AT8 epitope (a late marker of pathology) and the AT270 epitope (an early marker) together with staining by antibody K9JA, which shows expression of total TAU in 24-, 32-, and 48-hpf and 7-day-old transgenic zebrafish embryos. There are very few AT8-positive neurons in the spinal cord of 24-hour-old embryos, while this number increased significantly in 32-hour-old embryos and rose even further in 48-hour-old embryos. Finally, all TAU-expressing neurons contained the AT8 epitope in 7-day-old larvae. **(B)** In contrast, immunoreactivity of the early marker AT270 was already strong in many TAU-expressing cells at 24 hpf and became only slightly stronger at older stages. The level of total TAU detected in the same embryos by double staining with the K9JA antibody was similar between 24 hpf and 32 hpf. After 48 hours, a substantial part of TAU was transferred to the neuronal projections. In contrast, AT8-positive TAU remained mainly in the cell bodies. The AT8-positive somata combined with a lack of strongly AT8-positive neuronal projections is consistent with the pathological accumulation of modified TAU in neuronal cell bodies of patients. Lateral views of the trunk above the end of the yolk extension, anterior to the left. Scale bars: 50 μ m.

genic line, with comparable levels of transgene expression. We could indeed observe a rapid and robust increase in AT8-positive neurons over this short period of time (Figure 3A). This was not the case for AT270-positive cells (Figure 3B).

Increased cell death in hTAU-expressing zebrafish neurons. Neuronal cell death is the ultimate reason for the neurological deficits of AD and FTD patients. We have therefore engaged in analysis to determine whether neurons indeed degenerate when TAU is expressed in transgenic zebrafish. Cell death can be monitored in living fish by incubation in acridine orange (27), a dye that stains nucleic acids in dying cells. We have compared 6-day-old fish expressing TAU/DsRed to DsRed only-expressing fish and nonexpressing siblings. Strikingly, we could detect a significant increase of cell death in the whole spinal cord of TAU-expressing fish, as compared with both controls (Figure 4, A–D).

To analyze neurodegeneration in more detail and to demonstrate the suitability of zebrafish larvae to study cellular processes in a whole living animal *in vivo*, we monitored the neurodegeneration in TAU

transgenic fish by confocal time-lapse imaging. We recorded neurons in the spinal cord that express DsRed over a period of 12 hours (typical examples of still images are shown in Figure 4E; see also Supplemental Video 1) and searched for dying cells by monitoring uptake of acridine orange. An intact neuron in the field of view first altered its shape and started to round up (54.0 to 58.1 hours post fertilization [hpf]). Subsequently, this cell fragmented and took up acridine orange, indicating a breakdown of the cellular membranes (58.1 to 60.3 hpf), and eventually began to disappear (60.3 to 65.7 hpf). To our knowledge, this is the first demonstration of *in vivo* cell death imaging in the field of neurodegeneration.

Expression of hTAU-P301L causes neuronal and behavioral abnormalities. It has been previously demonstrated that elevation of TAU leads to inhibition of intracellular transport with toxic consequences, which are particularly pronounced in long-projecting motoneurons (28, 29). This is accompanied by elevated pathologic phosphorylation. To investigate abnormalities in neuronal morphology, we stained TAU transgenic fish and control fish with antibody znp1, which labels

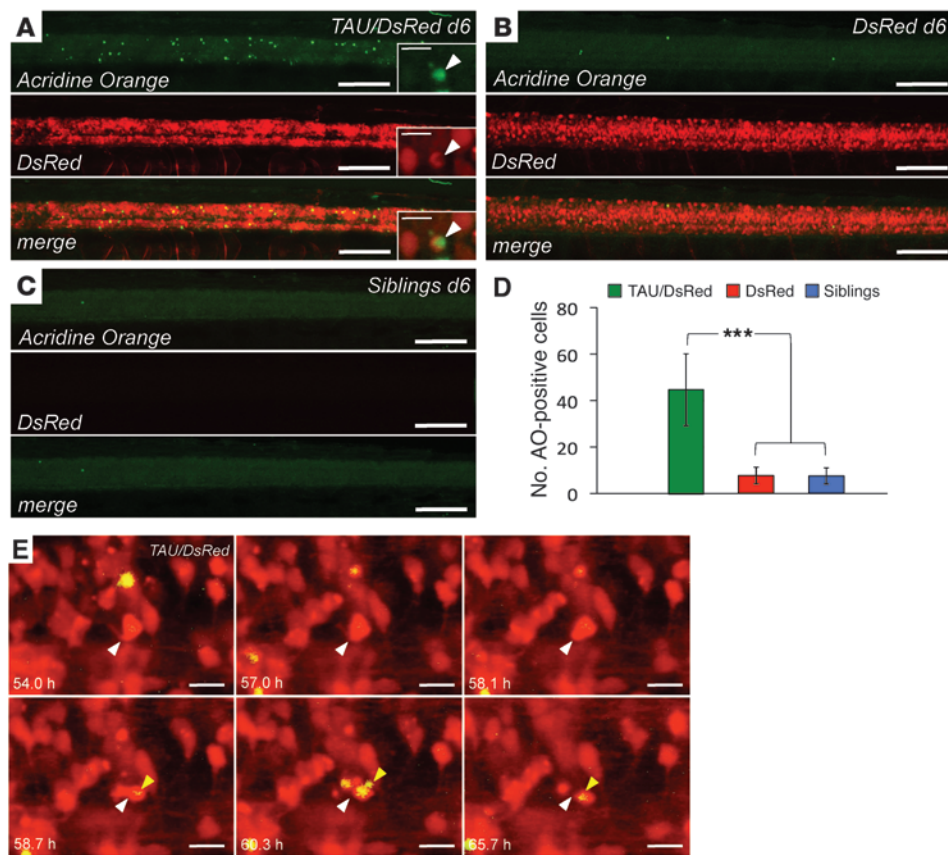


Figure 4
 In vivo imaging of neuronal cell death in TAU-expressing zebrafish. (A–D) Side views of 6-day-old living zebrafish larvae expressing TAU/DsRed (A, see single acridine orange–positive neuron in inset, depicted by arrowhead), only DsRed (B), or no transgene (siblings, C) stained with acridine orange. TAU-expressing fish show substantial cell death while DsRed-expressing and nontransgenic fish show only a low, basal amount of dying cells (quantified in D). AO, acridine orange. Data represent mean ± SD. ****P* < 0.01. Scale bars: 100 μm; 10 μm (insets). (E) Still images of several time points of a time-lapse video, showing a close-up of TAU-expressing neurons in the spinal cord of transgenic zebrafish, which were stained with acridine orange. An intact neuron (white arrowhead) with an axon first changes its shape and rounds up. Subsequently, fragmentation and uptake of acridine orange is observed (yellow arrowhead; see also Supplemental Video 1). Scale bars: 10 μm.

the synaptic protein synaptotagmin in extending axons of all primary motoneurons (30, 31). We measured the length of the first 4 outgrowing caudal primary (CaP) motoneurons anterior to the end of the yolk extension, which leave the spinal cord ventrally and grow around the muscle in a stereotypic, time-dependent manner as judged by synaptotagmin (*znp1*) staining (32). The length of the developing motoneurons, in which synaptotagmin is present, is substantially shorter at 28 hpf in TAU transgenic fish (Figure 5, A–C). In a later stage at 48 hpf, distribution of synaptotagmin is still altered (Figure 5, D and E), although the projections have grown further. Seven-day-old larvae are able to swim and catch food (data not shown). On the cellular level, the motoneurons in both control and TAU fish have grown around the muscle to the midline (Figure 5, F and G); however, the fine projections to the muscle are still reduced in the TAU transgenic fish in comparison with controls.

Consistent with the altered motoneuron morphology, we observed behavioral deficits, such as slow or absent movement in most of the larvae at 48 hpf, an age at which a stereotypic escape response behavior can be evoked by applying a touch stimulus to the animals. We have collected pools of transgenic fish expressing high levels of TAU/DsRed and quantified the escape response of 50 randomly picked individual larvae at 48 hpf. While most transgenic DsRed only–expressing fish with comparable expression levels or nontransgenic fish responded to a touch stimulus at the dorsal tip of the tail with a stereotypic escape response, most TAU-expressing fish show a significantly reduced or even absent response (Figure 5, H, I, and J; see also Supplemental Video 2). We hypothesize that the motoneuron defect is the reason for the observed movement deficits at this age.

Generation of potent GSK3β inhibitors by structure-based design. Our transgenic zebrafish rapidly recapitulated key disease markers for tauopathies, including hyperphosphorylation. We therefore determined whether our fish would be a useful tool for developing compounds that could delay or stop the pathology of tauopathies. To identify inhibitors of TAU kinases by structure-based design, we refined a previously described approach (14) and found approximately 2000 actives in a high-throughput screening campaign against the human GSK3β enzyme. The actives were confirmed for dose response and encompassed hits from multiple chemical series. Several compounds from the pyrazine chemical series were cocrystallized with the GSK3β protein. Data from x-ray analysis of the binding of the inhibitors within the ATP pocket of the GSK3β protein led to the optimization of potency and selectivity of the pyrazines. Since CDK2 is the closest homolog to GSK3β, we optimized for CDK2 selectivity aided by structure-based design. By optimizing against CDK2, pan-kinase selectivity (27 kinases) was also obtained. This understanding of structural activity relationships subsequently led to the design of potent and selective GSK3β inhibitors AR-164 and AR-534 (Figure 6, A–C). AR-164 and AR-534 inhibit recombinant human GSK3β with Ki values (the concentration of inhibitor that reduces the formation speed of the metabolite by 50% at low substrate concentration) of 8.9 nM and 2 nM respectively. In contrast, AR-164 and AR-534 do not significantly inhibit CDK2/cyclin E (Kis of 1440 nM and 100 nM, respectively), demonstrating at least a 50-fold selectivity versus CDK2. Both inhibitors were cell permeable. The permeability coefficients, which were determined in Caco2 cells and in an in vitro BBB assay, were 11 × 10⁻⁶ cm/s and 3.9 × 10⁻³ cm/min, respectively, for AR-164 and 20 × 10⁻⁶ cm/s and

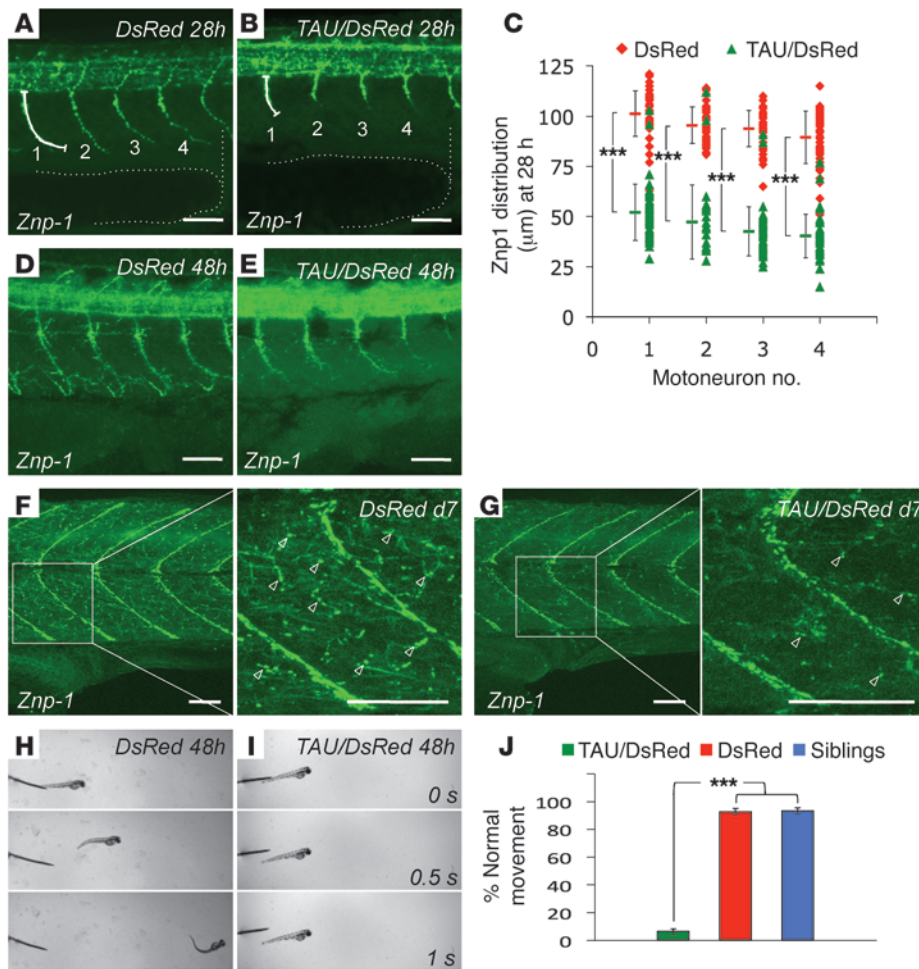
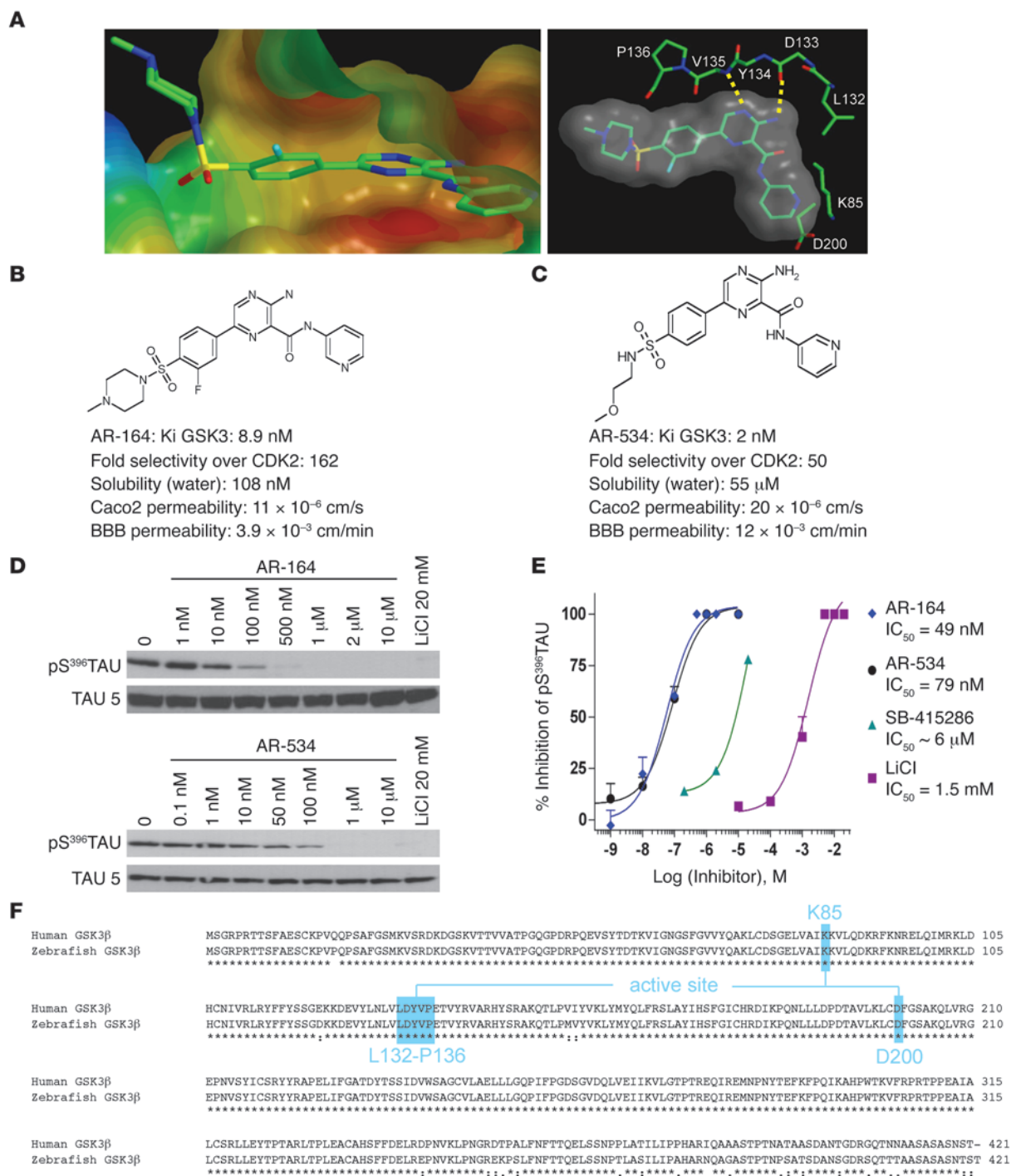


Figure 5

Expression of hTAU-P301L causes abnormalities in neuronal morphology and behavior. (A–G) Whole-mount immunostainings for *znp1*, which labels synaptotagmin in the extending axons of primary motoneurons. Expression of TAU causes a dramatically reduced extension of *znp1*-positive motoneurons already at 28 hpf (A and B). The difference in motoneuron length is quantified (C) by measuring the length of the first 4 *znp1*-stained motoneuron projections (marked 1, 2, 3, 4 in A and B) before the end of the yolk extension (marked by dotted line). Triangles and diamonds represent values from individual motoneurons; colored horizontal lines represent mean ± SD. ****P* < 0.01. In 48-hour-old embryos, the motoneurons have grown further in both TAU fish and controls, but the motoneuron extensions are still reduced (D and E). 5 days later, the motoneurons have grown around the muscle in both TAU fish and controls (F and G). The fine projections of motoneurons (see enlarged insets, arrowheads), are still highly reduced in TAU transgenic fish. Lateral views of the trunk above the end of the yolk extension, anterior to the left. Scale bars: 50 μm. (H–J) The stereotypic escape response, which is normal in DsRed-expressing (H) and nontransgenic larvae at 48 hpf (data not shown), is highly reduced or absent in TAU-expressing larvae (I; see also Supplemental Video 2). The phenotype was quantified in groups of 50 TAU/DsRed versus DsRed transgenic larvae, which were pooled from several clutches and selected for strong and comparable DsRed expression (J). Error bars represent mean ± SD; ****P* < 0.01.

12 × 10⁻³ cm/min respectively for AR-534 (Figure 6, B and C). These data suggest that the bioavailability of AR-534 in the brain is most likely higher than that of AR-164. Both AR-164 and AR-534 inhibit the phosphorylation of TAU at Ser396 in a dose-dependent fashion in 3T3 fibroblasts engineered to stably express 4-repeat TAU protein, exhibiting IC₅₀ values of 49 nM and 79 nM, respectively (Figure 6, D and E). Effects were compared with those of the previously published GSK3 inhibitors SB-415286 (33) and lithium chloride, which exhibited IC₅₀ values of 6 μM and 1.5 mM, respectively, in our assay. Although AR-164 and AR-534 potently block phosphorylation of human TAU expressed in cell culture and display a sufficiently good BBB permeability in our in vitro test, this does not necessarily predict that the compounds are also active in a whole organism. Vali-

dating the in vivo activity of the inhibitors in TAU transgenic mice, which were the only available vertebrate models of tauopathies so far, is an expensive and time-consuming process and not amenable to high-throughput screening for optimizing compounds for determining structural activity relationships. We have therefore studied the conservation of the targeted enzyme in zebrafish, in which drug screening would be more feasible, and found that GSK3β is highly conserved, with over 90% identity at the amino acid level (Figure 6F). Furthermore, the residues of the active site, which interact with our inhibitors, are completely identical. This high conservation to the human GSK3β kinase allows using the zebrafish as a model to validate the in vivo activity of GSK3β inhibitors and helps to further develop this lead structure.

**Figure 6**

Chemical structure, design, and characteristics of GSK3 inhibitors AR-164 and AR-534. **(A)** Left panel shows surface representation of the x-ray structure of GSK3 β with inhibitor AR-164 in the active site. Polar areas are colored blue and lipophilic areas red. The methylpiperazine sulfone amide extends out toward the solvent area. Right panel shows top view of the active site of GSK3 β . Dotted yellow lines represent hydrogen bonds between the protein backbone and AR-164. The 6-membered aromatic pyrazine moiety binds together with its anilino function to the backbone of the kinase. The pyridine ring binds to the conserved salt bridge formed by Lys85 and Asp200 (x-ray resolution: 2.47 Å). AR-534 binds in a similar way (not shown). **(B and C)** Chemical structure of AR-164 and AR-534 and compound characterization values including Ki (mean from 3 independent experiments performed in duplicate), selectivity over CDK2, solubility and permeability coefficient Pe (cm/min) over cell membranes (Caco2 cells), and BBB. **(D)** AR-164 and AR-534 inhibit pSer396 TAU phosphorylation in 3T3 fibroblasts harvested at 4 hours after treatment in comparison with total TAU, as analyzed by quantitative WB. **(E)** Graphical representation with IC₅₀ values of AR-164 and AR-534 effects on inhibition of TAU phosphorylation compared with SB-415286 and LiCl. **(F)** Alignment of protein sequences of human and zebrafish GSK3 β . Over 90% of the amino acids are identical; the residues in the active site of the enzyme, which interact with the inhibitors, are completely conserved.

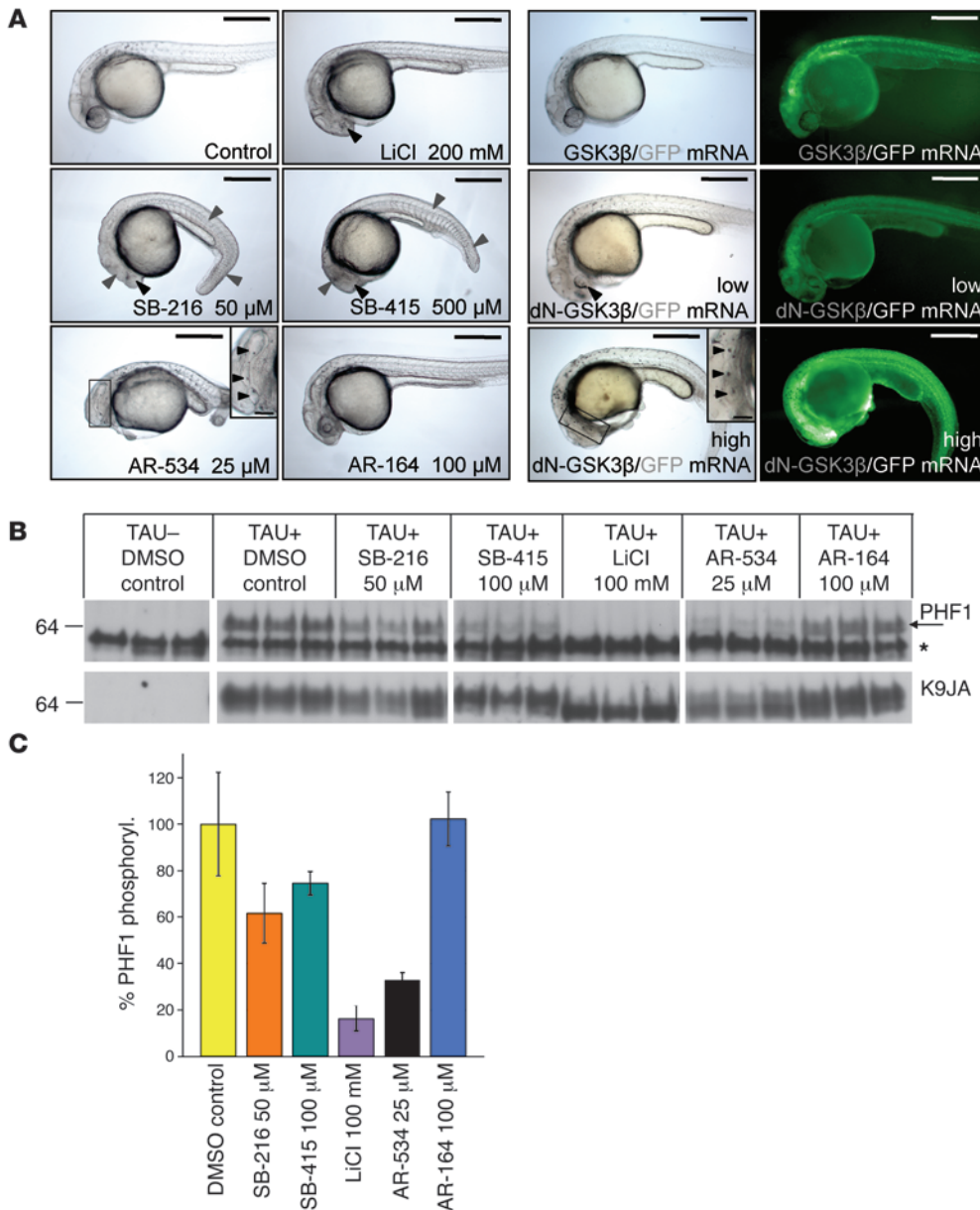


Figure 7

GSK3 inhibitors phenocopy a genetic loss of GSK3β and reduce pathologic hyperphosphorylation of TAU in vivo. **(A)** GSK3 inhibitors have specific effects on early wild-type zebrafish development when treatment occurs between 4 and 24 hpf. LiCl treatment caused strongly reduced eye formation (black arrowheads), while SB-216763 and SB-415286 also perturbed formation of brain, somites, and tail (gray arrowheads). In addition to these phenotypes, AR-534 also caused multiple ear formation (arrowheads in enlargement). In contrast, AR-164, which has in vitro activity comparable to that of AR-534, did not cause any detectable change in phenotype even at 4-fold concentration. Embryos injected with dN-GSK3β mRNA to suppress the function of endogenous GSK3β phenocopied alterations of compound-treated fish; however, only AR-534 was potent enough to phenocopy the ear multiplication seen in embryos expressing high levels of dN-GSK3β (arrowheads in enlargement). Embryos injected with wild-type GSK3β did not display a phenotype at comparable mRNA concentrations. Scale bars: 500 μm; 100 μm (insets). **(B)** GSK3 inhibitors reduce pathologic TAU phosphorylation in vivo when applied to TAU transgenic fish between 20 and 100 hpf. Phosphorylated TAU was detected by WB using antibody PHF1 and normalized to total TAU (K9JA). The band intensities were compared with a DMSO control on the same gel. The upper specific PHF1-band (arrow) was quantified. As already shown in Figure 2, the lower PHF1 band was unspecific (asterisk). **(C)** Quantification of WB band intensities of phospho-specific TAU as a percentage of the total amount of TAU detected by K9JA shown in **B**.

Potent in vivo effects of a newly developed GSK3β inhibitor. After demonstrating that the TAU transgenic zebrafish display a number of pathological symptoms that are diagnostic for tauopathies, we used the fish to investigate in vivo 2 known GSK3 inhibitors, SB-216763

and SB-415286 (33), as well as our 2 newly developed compounds, AR-534 and AR-164, which have a strong and selective inhibitory activity on GSK3β in vitro (see Figure 6). In addition, we treated transgenic fish with LiCl as described (34), as a positive control.



To evaluate whether the compounds affect zebrafish Gsk3 β activity, we first treated wild-type zebrafish embryos between 4 and 24 hpf and examined their developmental phenotype. GSK3 β is a component of the canonical Wnt pathway that is required for many early patterning events in the developing vertebrate embryo. Disturbances of this pathway therefore lead to characteristic developmental defects (35). LiCl treatment caused strongly reduced eye formation, as previously described (36), while SB-216763 and SB-415286 also perturbed the normal formation of brain, somites, and tail in addition to the eye phenotype (Figure 7A). The inhibitor AR-534 had an even more drastic effect on the fish, causing multiple ear formation in addition to the described phenotypes. In contrast, AR-164, which has a comparable *in vitro* activity to AR-534, did not cause any detectable phenotype even at 4-fold higher concentration (Figure 7A). To compare the efficiency of the inhibitors and the specificity of the evoked phenotypes with a genetic loss of the endogenous enzyme function, we injected mRNA encoding dominant-negative *Xenopus* GSK3 β -K85R (dN-GSK3 β), which is over 92% identical to zebrafish Gsk3 β , into zebrafish eggs. To monitor dose-dependent effects, we coinjected dN-GSK3 β mRNA and GFP mRNA and used GFP fluorescence to select embryos with lower or higher protein expression. Strikingly, embryos expressing lower amounts of dN-GSK3 β phenocopied the eye loss, which was also observed in embryos treated with SB-216763 and SB-415286 and LiCl, whereas only the embryos expressing higher amounts also phenocopied the multiple ear formation monitored in AR-534-treated embryos (Figure 7A). This result indicates that AR-534 has the highest specific *in vivo* efficacy of all compounds used in this study. Similar to γ -secretase inhibitors, which cause very profound defects in Notch signaling during early development of zebrafish (37), such inhibitors may only be used during late adulthood when FTD and AD develop, thus excluding their negative effects on embryonic development. To confirm that treatment of larvae at later stages does not cause deleterious developmental problems but reduces pathologic TAU phosphorylation *in vivo*, we now treated TAU transgenic fish for 3 days starting at 20 hpf, after early development was completed. Treatment starting at this time point did not cause any major morphological phenotype to the larvae (data not shown). After the treatment period, embryos were lysed and subjected to quantitative Western blot (WB) analysis, in which the levels of phosphorylated TAU were normalized to total TAU to exclude differences in expression levels or gel loading. SB-216763 and SB-415286 reduced phosphorylation of TAU at the disease-specific PHF1 epitope by 30% to 40%, a low activity in comparison with the nonspecific inhibitor LiCl, which reduces phosphorylation by nearly 90% when used at high concentration (Figure 7, B and C). AR-534 was more potent than the existing specific inhibitors SB-216763 and SB-415286 and reduced TAU phosphorylation by 70% (Figure 7, B and C). In contrast to the other inhibitors, AR-164 did not show any inhibitory activity on TAU phosphorylation *in vivo* (Figure 7B), which is consistent with both its lack of activity on early development and the lower penetrability in the *in vitro* BBB screen, as shown in Figure 6. We conclude that, consistent with its activity on early zebrafish development, AR-534 is also the most potent specific inhibitor of GSK3 β -mediated TAU phosphorylation.

Discussion

We provide a newly developed technology approach for the fast and efficient generation of transgenic zebrafish to study human diseases resulting from protein misfolding and/or overexpression

and to optimize promising drug candidates *in vivo*. The generation of transgenic zebrafish overexpressing high levels of human proteins has so far been rather difficult. We have overcome these limitations with the efficient *Tol2* transposon and Gal4/UAS-based expression of human TAU-P301L in transgenic zebrafish. In contrast to previous studies (11, 12), we could monitor early pathology, including disease-specific hyperphosphorylation and conformational changes of TAU as well as neuronal and behavioral abnormalities within the first 2 days of embryonic development in stable transgenic zebrafish. Furthermore, the larvae developed substantial neurodegeneration after a few days. These phenotypes appear much more rapidly in our fish model than in the existing mouse models, although zebrafish kept under laboratory conditions live as long as 3 to 5 years (38), which is comparable to laboratory mice (39). Importantly, this early pathology is crucial to fully exploit all advantages of the zebrafish system, such as optical clarity and ease of manipulation. The similarity of the evoked phenotypes to human disease is completed by the appearance of neurofibrillary tangles after 5 weeks, validating our fish as a well-suited model for tauopathies *in vivo*.

We expect the transgenic zebrafish to become a valuable model system for gaining further insights into the pathology of dementias by exploiting the unmatched potential for the analysis of cellular processes in the living organism, which the zebrafish offers in contrast with other vertebrate models. Although living cells can also be monitored in transgenic mice, experiments in the zebrafish can be performed in a noninvasive way in much higher spatial and temporal resolution. Whole-cell imaging of neurons comprising somata and projections can be done in embryos and larvae over several days without removing the specimen from the microscope (40). Since FTD-like pathology can be detected already after 1 to 2 days for early and late disease markers and this pathology progresses rapidly, we can monitor disease progression in a compressed timescale in young zebrafish embryos and larvae, which are perfectly suited for *in vivo* imaging of neurons due to their optical transparency. In fact, confocal imaging even allowed us to follow neuronal cell death *in vivo*. To our knowledge, this is the first demonstration of *in vivo* cell death imaging in the field of neurodegeneration. Moreover, neurons can be imaged in their natural environment together with neighboring cell types such as astroglia, oligodendrocytes, and microglia, which have been shown to participate in the pathology of several neurodegenerative diseases (1). These important environmental influences are not faithfully recapitulated in tissue explants or primary cell culture. The early phenotypes allow testing for possible genetic modifiers of pathology *in vivo* through transient overexpression of wild-type or dominant-negative forms of proteins by DNA or RNA injection or downregulation mediated by injection of antisense oligonucleotides.

The rapid appearance of pathologic phenotypes allows use of the transgenic zebrafish larvae not only to image and understand disease processes in a living animal but also to validate and even screen on a relatively large scale for compounds that modify the pathology *in vivo*. The hyperphosphorylation of TAU, which our fish model develops within 32 hours after fertilization, is believed to be a key initiator of detachment of normal TAU from microtubules and subsequent oligomerization and aggregation. Preventing this phosphorylation by blocking the involved kinases could potentially slow further progression of pathology and thus be an efficient treatment option for AD and FTD (13). We have developed compounds that bind to the active site of GSK3 β and effectively block enzyme activity. The identifica-



tion of potent cell-permeable kinase inhibitors with *in vivo* efficacy is a key component of the drug discovery process. With the use of rational drug design, optimization of the pyrazine chemical series led to the identification of several GSK3 inhibitors. We demonstrated by *in vitro* studies that 2 of these compounds have high selectivity for the target enzyme, good bioavailability, and high potency to block TAU phosphorylation in cell culture. However, it is frequently observed that such inhibitors may not be active *in vivo*, since they, for example, do not enter the cells, are transported out, or are rapidly metabolized when tested in whole organisms (13). This emphasizes the necessity of rapid, high volume *in vivo* drug testing in disease models, which is not feasible in transgenic mice on a large scale. Transgenic zebrafish offer advantages of both *in vitro* and *in vivo* systems and allow rapid screening for pathology-modifying drugs on a large scale, since embryos can be tested for rescue of the pathologic phenotypes after compound treatment in a 96-well-plate scale (9).

We show that GSK3 β inhibitors cause specific phenotypes when applied during early embryonic development and that the evoked phenotypes already indicate the *in vivo* potency of the inhibitor. Moreover, the GSK3 β inhibitors can effectively reduce the rapid disease-specific hyperphosphorylation of TAU in our transgenic zebrafish. Using our model, we have evaluated the activity of 2 newly developed GSK3 β inhibitors with comparable *in vitro* activity. One of the inhibitors, AR-534, was also very active *in vivo*, with a much higher effect than the previously described GSK3-specific inhibitors SB-216763 and SB-415286, which we used for comparison. In contrast, the inhibitor AR-164, which is equally potent in cell culture, was inactive *in vivo*. These data were consistent with the over 3-fold lower performance of AR-164 in our BBB test. As this is an *in vitro* test, which can only serve as a model of the *in vivo* situation, the bioavailability of AR-164 could be even lower in our transgenic zebrafish, explaining the lack of activity. It has been shown recently that zebrafish form a functional BBB that is similar to that of higher vertebrates. The BBB in zebrafish consists of endothelial cells, which can be characterized by the expression of the marker proteins claudin-5 and ZO1 and starts to become functional at 3 days after fertilization (10). The developing BBB might be less permeable to AR-164 versus AR-534 and could therefore be one reason for the absent *in vivo* activity of AR-164. Alternatively, degradation or metabolism of AR-164 could also account for the activity differences we observed. Taken together, the different activities of AR-534 and AR-164 in the *in vitro* versus the *in vivo* situation clearly illustrate the need for effective *in vivo*-screening tools, as this can help to identify promising compounds more quickly and directly, while at the same time allowing one to eliminate substances without reasonable *in vivo* activity early in the screening process. Taken together, our transgenic zebrafish model could be a promising tool for streamlining pharmacological screening for many neurodegenerative diseases. In fact, we have already successfully used this technology to generate transgenic zebrafish lines overexpressing a number of other amyloidogenic proteins, such as amyloid β peptide, TDP-43, and α -synuclein (data not shown).

Methods

Animal husbandry

All experiments were performed in accordance with animal protection standards and were approved by the government of Upper Bavaria (Regierung von Oberbayern, Munich, Germany). The zebrafish wild-type AB line was maintained, mated, and raised as described (41). Embryos were kept in E3 medium at 28.5°C and staged as described (42).

Constructs

Our transgenesis constructs are based on the pT2KXIGdeltaIN plasmid (a gift from K. Kawakami, National Institute of Genetics, Shizuoka, Japan), which is derived from the medaka *Tol2* transposable element (16). pT2KXIGdeltaIN was cleaved by BglII and XhoI to remove the insert between the *Tol2* sites, and a multiple cloning site (MCS) was introduced. The MCS was cut out by PvuII from pBS_I-SceI, which contains the pBluescript MCS flanked on both sides by I-SceI restriction sites. To assemble the final transgenesis constructs, fragments were first combined in pBS_I-SceI, as this vector contained more suitable restriction sites, and later transferred to pT2KXIGdeltaIN.

Driver construct. The SV40 late polyA signal was PCR amplified from pCS2⁺ using the primers pCS2⁺ poly(A)-F SacII (5'-AAAAAACCGCG-GAGTCGTATTACGTAGATCCAGACATGA-3') and pCS2⁺ poly(A)-R SacI (5'-AAAGAGCTCCACACCTCCCCCTGAAC-3'), cleaved by SacI/SacII, and ligated into pBS_I-SceI. The neuronal HuC promoter (19) was PCR amplified using the primers HuC-F XhoI/EcoRI (5'-GCTCGAGGAATTCATA-ATTGGAATTTAAATGC-3') and HuC-R2 EcoRI/ClaI (5'-GGAATTCATC-GATTCTTGACGTACAAAGATGATATTGATCTAGG-3'), cut by XhoI/ClaI, and ligated into pBS_I-SceI_pA. Gal4-VP16 (17) was cleaved by BamHI/SnaBI from pBS_HuC_Gal4-VP16, blunted, and ligated into pBS_I-SceI_HuC_pA cut by EcoRV/SnaBI. The HuC-Gal4-VP16-pA fragment was transferred to pT2KXIGdeltaIN by I-SceI digest and ligation.

Responder constructs. We generated transgenic control fish expressing DsRed but not TAU using a construct that contained E1b-UAS-E1b flanked by DsRed and TAU, but TAU was isolated from the minimal E1b promoter by an insert of 200 bp (Ins), which inhibits expression of TAU. DsRed.T4 (43) was cleaved from pCS2⁺_DsRed.T4 by NcoI/SnaBI digest to replace GFP in the vector pBS_E1b_UAS_E1b_GFP_pA. This vector contains UAS flanked by E1b minimal promoters (17) on both sides. Ins-hTAU-P301L was cleaved by BglII/BamHI from pNG2htau40/P301L and ligated at the BamHI site of pBS_I-SceI_pA. E1b-UAS-E1b-DsRed-pA was cleaved by HindIII/SmaI from pBS_E1b_UAS_E1b_DsRed.T4_pA, blunted and ligated into EcoRV-cleaved pBS_I-SceI_Ins_hTAU-P301L_pA. The full expression cassette was transferred to pT2KXIGdeltaIN by I-SceI digest and subsequent ligation. The final Responder construct was used together with the Driver construct to generate transgenic fish Tg(HuC:Gal4/UAS-DsRed).

To generate transgenic fish expressing DsRed and TAU, hTAU-P301L was amplified from pNG2htau40/P301L by PCR using primers hTAU ATG-F BamHI/NcoI (5'-GGGATCCCATGGCTGAGCCCCGCCAGGA-3') and hTAU TAG-R NcoI/EcoRI (5'-GGAATTCATGGTCACAAACCCT-GCTTGGCTA-3'), cleaved by NcoI and inserted into pBS_E1b_UAS_E1b_GFP_pA cleaved by NcoI/SnaBI to remove GFP. DsRed together with the SV40 late polyA signal were cleaved by ClaI/ApaI from pCS2⁺_DsRed.T4 and introduced into pBS_E1b_UAS_E1b_hTAU-P301L_pA. The insert in pT2KXIGdelta-hTAU-P301L-Ins-E1b-UAS-E1b-DsRed was removed by ApaI/NheI digest and replaced by the new cassette cleaved from pBS_pA_DsRed_E1b_UAS_E1b_hTAU40-P301L_pA. The distance of TAU from E1b is only 35 bp in this construct; therefore, TAU is efficiently expressed together with DsRed. The final Responder construct was used together with the Driver construct to generate transgenic fish Tg(HuC:Gal4/TAU-P301L-UAS-DsRed).

Gateway constructs. Gateway recombinations were performed according to the manufacturer's instructions (Invitrogen). Details about Gateway cloning can be found at www.invitrogen.com/site/us/en/home/Products-and-Services/Applications/Cloning/Gateway-Cloning.html.

To adapt our responder construct to Gateway cloning, hTAU-P301L was replaced by a Gateway destination site flanked by attR1/2, which was cleaved from pBS-DEST_attR1-2 (a gift from P. Lemaire, IBDMML, Marseille, France) by EcoRV. The resulting construct was termed Destination Responder vector.



To adapt our Driver construct to Gateway cloning, the HuC promoter was also replaced by a Gateway destination site flanked by attR1/2. The resulting construct was termed Destination Driver vector. To test the functionality of the vectors, the HuC and α Tub promoter and hTAU-P301L were amplified by PCR using the following primers: HuC-F XhoI/EcoRI (5'-GCTCGAGGAATTCACAAATTTGAATTTAAATGC-3') and HuC-R2 EcoRI/ClaI (5'-GGAATTCATCGATTCTTGACGTACAAAGATGATATTGATCTAGG-3') for HuC; M13-FP (5'-TGTAACACGACGCCAGT-3') and α Tub-R (5'-GGCAGCTGTGAAGAAAAAG-3') for α Tub; and hTAU ATG-F BamHI/NcoI (5'-GGGATCCCATGGCTGAGCCCCGCCAGGA-3') and hTAU TAG-R NcoI/EcoRI (5'-GGAATTCATGGTCAAAACCTGCTTGGCTA-3') for hTAU-P301L. PCR products were TOPO-cloned into entry vectors using the pCR8/TOPO/GW Kit from Invitrogen and sequenced. Promoters and TAU were then LR recombined into Destination Driver and Responder vectors, using LR Clonase II from Invitrogen according to the manufacturer's instructions.

Plasmid preparation, mRNA synthesis, and embryo injection

Plasmids were prepared by extraction with a MACHEREY-NAGEL Maxi Kit and further cleaned up by using the Qbiogene GENECLEAN Kit according to the manufacturer's instructions. The vectors pCS-TP (a gift from K. Kawakami, National Institute of Genetics, Shizuoka, Japan), pCS2⁺-GFP, pCS2⁺-dn-GSK3 β , and pCS2⁺-GSK3 β (both gifts from R. Rupp, Ludwig-Maximilians-University) were linearized by NotI and cleaned up by phenol/chloroform precipitation. mRNAs were synthesized from the linearized vectors with the Ambion mMESSAGE mMACHINE kit (Applied Biosystems) according to the manufacturer's instructions and stored in small aliquots at -80°C. Shortly before injection, circular Driver and Responder plasmids were mixed with *Tol2* transposase mRNA, all at a final concentration of 25 ng/ μ l, in dH₂O containing diethylenepyrocabonate-treated (DEPC-treated) 0.2 M KCl and 20% phenol red (44). GFP mRNA was used at a concentration of 100 ng/ μ l and GSK3 β mRNAs were used at a concentration of 50 ng/ μ l, all diluted in DEPC-treated dH₂O containing 20% phenol red.

One-cell-stage embryos were collected, oriented on agar plates, and injected with approximately 1 nl of the injection solution. Plasmid DNA and transposase mRNA were injected through the yolk into the cytoplasm of the first cell before the first cell division. GFP and GSK3 β mRNAs were mixed before use and injected into the yolk. At around 6 to 8 hpf, 2 random fertilized embryos from each dish were tested for transposition by PCR as described (44). At 30 hpf, embryos were selected for DsRed expression under a Leica fluorescent stereomicroscope and raised at 28.5°C to adulthood. Adult founder fish were identified by outcrossing them to AB wild-type fish and screening the F1 generation for DsRed-expressing embryos. These embryos were raised to establish transgenic lines.

Identification of transgenes by PCR

The offspring of 225 embryos of an F2 outcross were analyzed by PCR. Three independent PCRs were performed to show Gal4 on the Driver construct, TAU on the responder construct, and actin as a loading control. The following primers were used: Gal4: HuC 3'F 5'-TGGCGAAGACTGTCCTTTTT-3', Gal4-R 5'-GGTCTTCTCGAGGAAAAATCAG-3'; hTAU: TAU-OF 5'-AGGAGTTCGAAGTGATGGAAGAT-3', TAU-IR 5'-GTGGC-GATCTTCGTTTTACCAT-3'; and actin: actin-F 5'-TGTTTTCCCTC-CATTGTTGG-3', actin-R 5'-TTCTCCTTGATGTCACGGAC-3'. For the PCRs, the 4- to 24-hour-old eggs were fixed in methanol; then the DNA was extracted by digestion with proteinase K for 4 hours at 55°C followed by inactivation of the enzyme for 10 minutes at 95°C. The extracted DNA was used as a template for PCR. To analyze the results, the products of the 3 PCRs for each possible genotype from 2 different embryos were mixed together, loaded on a gel, counted, and imaged.

IF, immunohistochemical stainings, Gallyas silver stainings, and WBs

Whole-mount IF stainings were performed according to standard methods (45). For immunohistochemical and Gallyas silver stainings on paraffin sections, the 5-week-old fish were deeply anesthetized and killed in water with ice. Then the whole fish were fixed overnight in 4% PFA and transferred to PBS and the sections and stainings were performed as described for mouse tissue (46).

WBs were performed according to standard methods. Embryos or larvae were frozen in liquid nitrogen and 10 to 50 μ l of chilled Laemmli buffer were added per fish. Fish were homogenized by sonication and incubated at 95°C for 10 minutes. Embryo lysates were subjected to centrifugation at 13,000 g for 1 minute, and 10 to 20 μ l of the supernatant was loaded on an 8% or 10% polyacrylamide gel. The following antibodies were used for IF, immunohistochemistry (IHC), and WB: (a) TAU. T46 (20) (IF: 1:200, WB: 1:1000; Invitrogen), K9JA (IF: 1:500, WB: 1:5000; no. A0024; Dako), DA9 (IHC: 1:250; a gift from P. Davies, Albert Einstein College of Medicine, New York, New York, USA), AT8 (25) (IF: 1:200, IHC: 1:50, WB 1:1000; Pierce, Thermo Scientific), 422 (24) (IF: 1:200, WB 1:1000; a gift from C. Czech, Hoffmann La Roche, Basel, Switzerland), AT180 (21) (IF: 1:200, WB: 1:1000; Pierce, Thermo Scientific), AT270 (21) (IF: 1:200, WB: 1:1000; Pierce, Thermo Scientific), 12E8 (22) (IF: 1:200, WB: 1:1000; a gift from P. Seubert, Elan Pharmaceuticals, San Francisco, California, USA), MC1 (26) (IF: 1:50; a gift from P. Davies, Albert Einstein College of Medicine, New York, New York, USA), PHF1 (23) (IF: 1:100, WB 1:1000; a gift from P. Davies, Albert Einstein College of Medicine, New York, New York, USA); (b) Other. DsRed (IF: 1:200; Clontech), actin (WB: 1:1000; Sigma-Aldrich), znp1 (30) (IF: 1:100; Developmental Studies Hybridoma Bank), Alexa Fluor 488 goat anti-mouse IgG (1:500; Invitrogen), Alexa Fluor 546 goat anti-rabbit IgG (1:500; Invitrogen), Alexa Fluor 488 goat anti-rat IgG (1:500; Invitrogen).

Acridine orange stainings and time-lapse imaging

Living zebrafish larvae were anesthetized with Tricaine (Sigma-Aldrich), incubated in a solution of 3 μ g/ml acridine orange (Sigma-Aldrich) in E3 medium with Tricaine for 30 minutes (27), and washed twice in E3 with Tricaine. For imaging, fish were embedded in 1.6% low melting agarose in E3 and overlaid with E3/Tricaine. The green nuclei of the neurons were counted in the whole spinal cord of 44 fish for each genotype using a Zeiss compound microscope with a Zeiss Plan-Apochromat 10 \times /0.45 lens. For time-lapse imaging, a z-stack of a chosen region of the spinal cord of the transgenic fish with a thickness of 10 μ m was imaged every 3 minutes for 10 to 16 hours on a Zeiss LSM 510 META inverted confocal microscope (Zeiss, provided by the Hans and Ilse Breuer Foundation, Frankfurt am Main, Germany) in a heated chamber. The images of the z-stack were combined in a maximum projection, and the time series of image projections was exported to a time-lapse video with 8 frames per second using Zeiss LSM 510 Confocal software, version 4.2 SP1. The videos and still images taken from the videos were processed with ImageJ 1.41 (<http://rsb.info.nih.gov/ij/>) and iMovie 7 on Mac OSX 10.5.

Behavioral assays

48-hour-old living zebrafish larvae of several clutches were pooled together and sorted for visible DsRed expression. The selected fish were dechorionated manually at least 3 hours before the experiment. To evaluate the escape response, fish were touched with the tip of a fine needle for at least 2 times at the dorsal tip of the tail. An escape response in which the fish did not move a distance of at least 3 times its own body length was considered as reduced. A minimum of 3 groups of 50 fish were quantified for each genotype. At least one experiment was recorded and processed as a video.



Microscopy

Living zebrafish embryos, larvae, and 5-week-old juveniles were examined and imaged on a fluorescent stereomicroscope (Leica). For imaging fixed stainings, heads of zebrafish embryos were removed, and the tails were flat mounted in 1% low melting agarose in 50% glycerol/dH₂O on coverslips and visualized with an LSM 510 META inverted confocal microscope. Motoneuron length measurements of confocal pictures were done using the overlay function of the Zeiss LSM software with maximum projections of z-stacks with constant stack height containing the whole neuronal projection. Images comparing 2 groups of fish were always done at the same time using identical settings. Paraffin sections were imaged on a Zeiss compound microscope. Images were assembled in Adobe Photoshop 8.0.

Analysis of compound characteristics

The GSK3 β Kis were determined using a scintillation proximity assay with a biotinylated peptide sequence from eIF2B and [γ -³³P]ATP as substrates. The CDK2 Kis were determined using a scintillation proximity assay with a biotinylated peptide sequence from GST retinoblastoma and [γ -³³P]ATP as substrates. Scintillation proximity assays and kinetic analyses were performed as described earlier (14). IC₅₀ inhibition curves were analyzed by nonlinear regression using GraphPad Prism 5 (GraphPad Software).

BBB permeability *in vitro* was analyzed using an *in vitro* cell culture model for permeability across the BBB as described earlier (47).

Analysis of GSK3 β inhibition in TAU transfected cells

3T3 fibroblasts were engineered to stably express 4-repeat TAU protein. The cells were treated with vehicle or with increasing concentrations of inhibitors and harvested at 4 hours after treatment. Cultures were then washed twice with 5 mM MgCl₂ PBS. Extracts for WB analysis were prepared by homogenizing cells in ice-cold extraction buffer consisting of 20 mM HEPES, pH 7.4, 100 mM NaCl, 10 mM NaF, 1% Triton X-100, 1 mM sodium orthovanadate, 10 mM EDTA, and protease inhibitors (2 mM phenylmethylsulfonyl fluoride, 10 μ g/ml aprotinin, 10 μ g/ml leupeptin, and 10 μ g/ml pepstatin). The samples were homogenized at 4°C, and protein content was determined by the Bradford method. Total protein (25 μ g) was electrophoresed on 10% SDS-PAGE gel and transferred to a nitrocellulose membrane (Schleicher & Schuell Bioscience Inc.). The experiments were performed using the following primary antibodies: pS396, 1:1000, and Tau5, 1:1000. The filters were incubated with the antibody at 4°C overnight in 5% nonfat dried milk. A secondary horseradish peroxidase-linked sheep anti-mouse (1:1000; Amersham Biosciences) or horseradish peroxidase-linked donkey anti-rabbit (1:5000; Amersham Biosciences) followed by ECL detection reagents (Amersham Biosciences) was used for immunodetection. Quantitation of immunoreactivity was performed by densitometric scanning.

Compound treatments

Stock solutions were prepared by dissolving compounds in DMSO (SB-216763 and SB-415286, 20 mM), 50% DMSO/dH₂O (AR-534, 5 mM), or dH₂O (AR-164, 10 mM, and LiCl, 3 M). Stock solutions were diluted with embryo medium E3 containing 1% DMSO to final dilutions of 50 μ M for SB-216763, 100 μ M for SB-415286, 100 mM for LiCl, 25 μ M for AR-534, and 100 μ M for AR-164. The unpermeable chorions of fragile 4-hour-old embryos were only slightly opened to allow access to the compounds, while rather robust 24 hpf embryos were completely dechorionated. Embryos were incubated in 1 ml compound dilutions or control medium (E3 containing 1% DMSO) in 12-well plates; the solutions were changed daily. Embryos were either treated from 4 to 24 hpf or from 24 to 100 hpf.

Statistics

Mean values and SD were calculated with Microsoft Excel, version 12.1.3. Statistical analysis was performed using 2-tailed Student's *t* test in Microsoft Excel. Data are presented as mean \pm SD. *P* < 0.05 was considered significant.

Acknowledgments

This work was supported by grants from the Deutsche Forschungsgemeinschaft (SFB 596 to B. Schmid and C. Haass; the Center for Integrated Protein Science to C. Haass and B. Schmid; and the Leibniz Award to C. Haass); Elitenetzwerk Bayern and Universität Bayern (to D. Paquet); the Federal Ministry for Education and Research (BMBF, BioFuture-Award 0311889 to R.W. Köster); the Studienstiftung des deutschen Volkes (to M. Distel); and the European Community's Seventh Framework Programme (FP7/2007-2013) under grant agreement no. 200611 (MEMOSAD to C. Haass, B. Schmid, E.-M. Mandelkow, and D. Paquet). C. Haass is supported by a research professorship at Ludwig-Maximilians-University. We thank A. Hruscha, M. Teucke, S. Schätzle, H. Kaiser, D. Drexler, O. Petrova, Y. Xu, E. Jerning, J. Neelissen, and Y. Nilsson for technical help; K. Kawakami, R. Rupp, and P. Lemaire for providing constructs; and P. Seubert, P. Davies, and C. Czech for providing antibodies. We thank the Hans and Ilse Breuer Foundation for the confocal microscope and K. Winklhofer for critically reading this manuscript.

Received for publication September 23, 2008, and accepted in revised form February 25, 2009.

Address correspondence to: Christian Haass, Deutsches Zentrum für Neurodegenerative Erkrankungen (DZNE) and Adolf-Butenandt-Institut, Biochemistry, Ludwig-Maximilians-University, Schillerstr. 44, 80336 Munich, Germany. Phone: 49-89-2180-75472; Fax: 49-89-2180-75415; E-mail: chaass@med.uni-muenchen.de.

- Haass, C., and Selkoe, D.J. 2007. Soluble protein oligomers in neurodegeneration: lessons from the Alzheimer's amyloid beta-peptide. *Nat. Rev. Mol. Cell Biol.* **8**:101–112.
- Kosik, K.S., Joachim, C.L., and Selkoe, D.J. 1986. Microtubule-associated protein tau (tau) is a major antigenic component of paired helical filaments in Alzheimer disease. *Proc. Natl. Acad. Sci. U. S. A.* **83**:4044–4048.
- Grundke-Iqbal, I., et al. 1986. Abnormal phosphorylation of the microtubule-associated protein tau (tau) in Alzheimer cytoskeletal pathology. *Proc. Natl. Acad. Sci. U. S. A.* **83**:4913–4917.
- Braak, H., and Braak, E. 1991. Neuropathological staging of Alzheimer-related changes. *Acta Neuropathol.* **82**:239–259.
- Santacruz, K., et al. 2005. Tau suppression in a neurodegenerative mouse model improves memory function. *Science.* **309**:476–481.
- Hutton, M., et al. 1998. Association of missense and 5'-splice-site mutations in tau with the inherited dementia FTDP-17. *Nature.* **393**:702–705.
- Mandelkow, E.M., and Mandelkow, E. 1998. Tau in Alzheimer's disease. *Trends Cell Biol.* **8**:425–427.
- Gotz, J., and Ittner, L.M. 2008. Animal models of Alzheimer's disease and frontotemporal dementia. *Nat. Rev. Neurosci.* **9**:532–544.
- Zon, L.I., and Peterson, R.T. 2005. In vivo drug discovery in the zebrafish. *Nat. Rev. Drug Discov.* **4**:35–44.
- Jeong, J.Y., et al. 2008. Functional and developmental analysis of the blood-brain barrier in zebrafish. *Brain Res. Bull.* **75**:619–628.
- Tomasiewicz, H.G., Flaherty, D.B., Soria, J.P., and Wood, J.G. 2002. Transgenic zebrafish model of neurodegeneration. *J. Neurosci. Res.* **70**:734–745.
- Bai, Q., Garver, J.A., Hukriede, N.A., and Burton, E.A. 2007. Generation of a transgenic zebrafish model of tauopathy using a novel promoter element derived from the zebrafish *eno2* gene. *Nucleic Acids Res.* **35**:6501–6516.
- Mazanetz, M.P., and Fischer, P.M. 2007. Untangling tau hyperphosphorylation in drug design for neurodegenerative diseases. *Nat. Rev. Drug Discov.* **6**:464–479.
- Bhat, R., et al. 2003. Structural insights and biological effects of glycogen synthase kinase 3-specific inhibitor AR-A014418. *J. Biol. Chem.* **278**:45937–45945.
- Winklhofer, K.F., Tatzelt, J., and Haass, C. 2008. The two faces of protein misfolding: gain- and loss-of-function in neurodegenerative diseases. *EMBO J.* **27**:336–349.
- Urasaki, A., Morvan, G., and Kawakami, K. 2006.



- Functional dissection of the Tol2 transposable element identified the minimal cis-sequence and a highly repetitive sequence in the subterminal region essential for transposition. *Genetics*. **174**:639–649.
17. Koster, R.W., and Fraser, S.E. 2001. Tracing transgene expression in living zebrafish embryos. *Dev. Biol.* **233**:329–346.
18. Walhout, A.J., et al. 2000. GATEWAY recombinational cloning: application to the cloning of large numbers of open reading frames or ORFeomes. *Methods Enzymol.* **328**:575–592.
19. Park, H.C., et al. 2000. Analysis of upstream elements in the HuC promoter leads to the establishment of transgenic zebrafish with fluorescent neurons. *Dev. Biol.* **227**:279–293.
20. Kosik, K.S., et al. 1988. Epitopes that span the tau molecule are shared with paired helical filaments. *Neuron*. **1**:817–825.
21. Goedert, M., et al. 1994. Epitope mapping of monoclonal antibodies to the paired helical filaments of Alzheimer's disease: identification of phosphorylation sites in tau protein. *Biochem. J.* **301**:871–877.
22. Seubert, P., et al. 1995. Detection of phosphorylated Ser262 in fetal tau, adult tau, and paired helical filament tau. *J. Biol. Chem.* **270**:18917–18922.
23. Greenberg, S.G., Davies, P., Schein, J.D., and Binder, L.I. 1992. Hydrofluoric acid-treated tau PHF proteins display the same biochemical properties as normal tau. *J. Biol. Chem.* **267**:564–569.
24. Hasegawa, M., et al. 1996. Characterization of mAb AP422, a novel phosphorylation-dependent monoclonal antibody against tau protein. *FEBS Lett.* **384**:25–30.
25. Biernat, J., et al. 1992. The switch of tau protein to an Alzheimer-like state includes the phosphorylation of two serine-proline motifs upstream of the microtubule binding region. *EMBO J.* **11**:1593–1597.
26. Jicha, G.A., Berenfeld, B., and Davies, P. 1999. Sequence requirements for formation of conformational variants of tau similar to those found in Alzheimer's disease. *J. Neurosci. Res.* **55**:713–723.
27. Furutani-Seiki, M., et al. 1996. Neural degeneration mutants in the zebrafish, *Danio rerio*. *Development*. **123**:229–239.
28. Thies, E., and Mandelkow, E.M. 2007. Missorting of tau in neurons causes degeneration of synapses that can be rescued by the kinase MARK2/Par-1. *J. Neurosci.* **27**:2896–2907.
29. Terwel, D., et al. 2005. Changed conformation of mutant Tau-P301L underlies the moribund tauopathy, absent in progressive, nonlethal axonopathy of Tau-4R/2N transgenic mice. *J. Biol. Chem.* **280**:3963–3973.
30. Trevarrow, B., Marks, D.L., and Kimmel, C.B. 1990. Organization of hindbrain segments in the zebrafish embryo. *Neuron*. **4**:669–679.
31. Fox, M.A., and Sanes, J.R. 2007. Synaptotagmin I and II are present in distinct subsets of central synapses. *J. Comp. Neurol.* **503**:280–296.
32. Myers, P.Z., Eisen, J.S., and Westerfield, M. 1986. Development and axonal outgrowth of identified motoneurons in the zebrafish. *J. Neurosci.* **6**:2278–2289.
33. Smith, D.G., et al. 2001. 3-Anilino-4-arylmaleimides: potent and selective inhibitors of glycogen synthase kinase-3 (GSK-3). *Bioorg. Med. Chem. Lett.* **11**:635–639.
34. Hong, M., Chen, D.C., Klein, P.S., and Lee, V.M. 1997. Lithium reduces tau phosphorylation by inhibition of glycogen synthase kinase-3. *J. Biol. Chem.* **272**:25326–25332.
35. Doble, B.W., and Woodgett, J.R. 2003. GSK-3: tricks of the trade for a multi-tasking kinase. *J. Cell Sci.* **116**:1175–1186.
36. Stachel, S.E., Grunwald, D.J., and Myers, P.Z. 1993. Lithium perturbation and goosecoid expression identify a dorsal specification pathway in the pre-gastrula zebrafish. *Development*. **117**:1261–1274.
37. Geling, A., Steiner, H., Willem, M., Bally-Cuif, L., and Haass, C. 2002. A gamma-secretase inhibitor blocks Notch signaling in vivo and causes a severe neurogenic phenotype in zebrafish. *EMBO Rep.* **3**:688–694.
38. Gerhard, G.S., et al. 2002. Life spans and senescent phenotypes in two strains of Zebrafish (*Danio rerio*). *Exp. Gerontol.* **37**:1055–1068.
39. Roberts, R.C. 1961. The lifetime growth and reproduction of selected strains of mice. *Heredity*. **16**:369–381.
40. Koster, R.W., and Fraser, S.E. 2001. Direct imaging of in vivo neuronal migration in the developing cerebellum. *Curr. Biol.* **11**:1858–1863.
41. Mullins, M.C., Hammerschmidt, M., Haffter, P., and Nusslein-Volhard, C. 1994. Large-scale mutagenesis in the zebrafish: in search of genes controlling development in a vertebrate. *Curr. Biol.* **4**:189–202.
42. Kimmel, C.B., Ballard, W.W., Kimmel, S.R., Ullmann, B., and Schilling, T.F. 1995. Stages of embryonic development of the zebrafish. *Dev. Dyn.* **203**:253–310.
43. Bevis, B.J., and Glick, B.S. 2002. Rapidly maturing variants of the Discosoma red fluorescent protein (DsRed). *Nat. Biotechnol.* **20**:83–87.
44. Kawakami, K. 2005. Transposon tools and methods in zebrafish. *Dev. Dyn.* **234**:244–254.
45. Nüsslein-Volhard, C., and Dahm, R. 2002. *Zebrafish: a practical approach*. Oxford University Press, Oxford, United Kingdom. 303 pp.
46. Mocanu, M.M., et al. 2008. The potential for beta-structure in the repeat domain of tau protein determines aggregation, synaptic decay, neuronal loss, and coassembly with endogenous Tau in inducible mouse models of tauopathy. *J. Neurosci.* **28**:737–748.
47. Cecchelli, R., et al. 1999. In vitro model for evaluating drug transport across the blood-brain barrier. *Adv. Drug Deliv. Rev.* **36**:165–178.

Appendix 6

published Article in *Developmental Dynamics*

Multicolor in vivo time-lapse imaging at cellular resolution by stereomicroscopy

Martin Distel, Andreas Babaryka and Reinhard W. Köster

Developmental Dynamics (2006), **235**, 1100-1106

Contribution:

For this article, I conducted the majority of experimental research. I performed all stereomicroscope experiments, generated the time-lapse movies and analysed the data. Andreas Babaryka conducted the confocal microscope experiments. The article was written by Reinhard Köster.

Multicolor In Vivo Time-Lapse Imaging at Cellular Resolution by Stereomicroscopy

Martin Distel, Andreas Babaryka, and Reinhard W. Köster*

Intravital time-lapse imaging has altered significantly many long-standing rules of biological mechanisms, but being apparatus-intense and laborious, time-lapse imaging remained mostly restricted to specialized labs. We show that recently introduced fully automated fluorescence stereomicroscopes represent cost-effective but powerful means of imaging dynamic events ranging from observing embryogenesis over several days to detailed tissue rearrangements and fast blood cell rolling in vivo. When combined with deconvolution approaches, even subcellular resolution in several colors can be achieved. Using three-dimensional image recording, we show the spatial reconstruction of expression patterns. Furthermore, by combining three-dimensional image recording over time with subsequent deconvolution analysis, we demonstrate that subcellular dynamics such as axonal pathfinding in vivo can be resolved. These findings promise that time-lapse imaging using a stereomicroscope will become a hands-on standard method for phenotype analysis in many fields of biology. *Developmental Dynamics* 235:1100–1106, 2006.

© 2006 Wiley-Liss, Inc.

Key words: zebrafish; bio-imaging; time-lapse; stereomicroscopy; fluorescence

Accepted 22 December 2005

INTRODUCTION

Biological processes such as embryonic morphogenesis, cell migration, wound healing, axon and blood vessel pathfinding are of dynamic nature. Commonly, these processes are being analyzed by static methods with deducing cell and tissue behavior from changes in sets of images recorded at different time points. As informative as such studies have been, they carry the intrinsic danger of missing crucial events or misinterpreting the obtained data (Lichtman and Fraser, 2001). For example, retinal axons lacking the Robo2 receptor often misproject into the ipsilateral area of the

tectum, suggesting a role in controlling midline-crossing for this receptor (Fricke et al., 2001). As subsequent time-lapse imaging in zebrafish embryos revealed that wild-type axons occasionally show the same initial misrouting, it became evident that Robo2 confers to an axonal growth cone the ability to prevent or correct misprojections rather than unambiguously selecting its projection trajectory (Hutson and Chien, 2002). This underscores that dynamic cellular events require dynamic analytical methods to be fully understood.

Despite the wealth of data unraveled by time-lapse microscopy, this

technique has not become a standard analytical tool for intravital phenotype diagnosis. This finding may be due to the fact that time-lapse microscopy is a time-consuming, laborious, and expertise-demanding analysis requiring lengthy periods of image recording on costly equipment such as confocal microscopes. In contrast, stereomicroscopes can be found in nearly any laboratory and every biologist is familiar with their use. Due to their immense working distance, their high depth of field, and their dual light path generating a three-dimensional image, stereomicroscopes have been the favorite optical setup for the ob-

The Supplementary Material referred to in this article can be found at <http://www.interscience.wiley.com/jpages/1058-8388/suppmat>
 GSF – National Research Center for Environment and Health, Institute of Developmental Genetics, Ingolstädter, Neuherberg-Munich, Germany

Grant sponsor: the German Bundesministerium für Bildung und Forschung; Grant number: Biofuture-Award 0311889.

*Correspondence to: Reinhard W. Köster, GSF – National Research Center for Environment and Health, Institute of Developmental Genetics, Ingolstädter Landstrasse 1, 85764 Neuherberg-Munich, Germany. E-mail: reinhard.koester@gsf.de

DOI 10.1002/dvdy.20694

Published online 2 February 2006 in Wiley InterScience (www.interscience.wiley.com).

TABLE 1. Comparison of Stereomicroscope and Compound Microscope Objectives^a

Objective	Numerical aperture	Lateral resolution in μm	Axial-resolution in μm
MZ16FA – Planapo 1.0 zoom 0.71–11.5	0.021–0.141	13.4–2.0	1247.2–27.7
MZ16FA – Planapo 5.0 zoom 0.71–11.5	0.084–0.5	3.3–0.6	77.9–2.2
C Plan 4.0 (Leica)	0.1	2.8	55.0
Plan Neofluar 5.0 (Zeiss)	0.15	1.9	24.4

^aNumerical apertures (NA) of stereomicroscope objectives with zooming properties are in the similar range or can even surpass the NAs of low-magnification objectives from compound microscopes (data provided by Leica Microsystems). As the lateral resolution ($0.51 \times \lambda_{\text{em}}/\text{NA}$) and axial resolution ($n \times \lambda_{\text{em}}/\text{NA}^2$) only depend on the numerical aperture, similar resolutions are achieved with both objectives, making intravital time-lapse microscopy accessible for fully automated fluorescence stereomicroscopes. Examples given here have been calculated with refraction index $n = 1.0$, $\lambda_{\text{em}} = 550 \text{ nm}$.

servation of embryonic or adult laboratory model organisms as well as for specimen and tissue manipulations. Over several decades though, stereomicroscope construction and design has remained essentially unaltered; thus, they mainly remained a dissection tool but had no significant relevance for vital analytical time-lapse recording.

Probably triggered by the discovery and further engineering of increasing numbers of genetically encoded fluorescent proteins over the past years (Chalfie et al., 1994; Matz et al., 1999; Nagai et al., 2002; Shaner et al., 2004; Miyawaki, 2005), stereomicroscopes have experienced an impressive renaissance. Becoming successively equipped with fluorescence excitation, multi-color filter wheels, and even remote focusing controls, the first fully automated stereomicroscope and camera units have been introduced recently. This advancement motivated us to establish intravital three-dimensional long-term time-lapse recording techniques for stereomicroscopes, thereby converting the stereomicroscope from a mainly optical dissecting tool to a powerful but easy to use analytical instrument for observing *in vivo* dynamics at cellular resolution by still using the stereomicroscope-specific advantages such as the great working distance and high depth of field. This process should render intravital time-lapse imaging into a widely used standard technique for recording cell and tissue dynamics as well as phenotype analysis.

RESULTS AND DISCUSSION

Stereomicroscopes usually are equipped with objectives that provide a great depth of field at the cost of lateral resolution. This finding is due to the low numerical apertures of stereomicroscope objectives. With the development of extensive zooming properties for such objectives, numerical apertures at high magnifications have reached similar or even surpassing values of typical low magnification objectives of compound microscopes. For example, the objectives of the MZ16FA (Leica Microsystems) reach numerical apertures between 0.021 (Planapo 1.0, zoom: 0.71) and 0.5 (Planapo 5.0, zoom: 11.5), whereas numerical apertures of similar $\times 5$ objectives of compound microscopes range around 0.1 (Table 1). Thus, three-dimensional (3D) time-lapse imaging with such recently developed fully automated stereomicroscopes should provide sufficient resolution to follow tissue rearrangements and individual cells within living embryos. Reaching this goal would make time-lapse imaging more amenable to biologists in many fields due to the significantly lower costs of a stereomicroscopic setup compared with confocal microscopes (stereomicroscope setup with 3D deconvolution software ca. 60,000Euro, confocal microscope setup with image rendering software ca. 300,000Euro).

The zebrafish embryo is one of the preferred vertebrate model organisms for bio-imaging approaches due to its transparency, external development, and ease of manipulation. We first established culture conditions to allow long-term image recording. Mounting

of the embryos in 1.2% ultra-low gelling agarose was performed as described in detail (Köster and Fraser, 2004). A simple but effective evaporation protection was constructed from two snugly-fitting, nested but sliding cylinders of polymethylmethacrylate almost sealing the space between the moving objective and the microscope base. In addition, the stereomicroscope was insulated by a chamber fed with air from a low power heater (80Watts, TX7, Lyon Electric Company, Inc.) to provide zebrafish embryos with their physiological temperature of 28°C (Supplementary Fig. S1, which can be viewed at <http://www.interscience.wiley.com/jpages/1058-8388/suppmat>).

To test the feasibility of this setup, zebrafish embryogenesis was recorded starting right after fertilization with image capturing every 2 or 5 min for periods of up to 3 consecutive days. Not only cell behavior such as the cleavages of the first blastomeres could be followed in detail (Fig. 1a–c), but also cytoplasmic streams (Mae-gawa et al., 1999) from the yolk into the embryonic cells (Fig. 1b, arrowhead, see Supplementary Movie 1). At subsequent stages, gastrulation movements such as epiboly, axis formation, somitogenesis, and eye and ear development could be observed with the embryo eventually starting to contract somitic muscles and to form pigment (see Supplementary Movie 2).

To capture a distinct morphogenetic process, image recording was focused on the formation of the fourth brain ventricle. This analysis revealed that, between 17 and 19 hr postfertilization

(hpf), the neural rod of the zebrafish hindbrain cavitates along the neuraxis starting from anterior to posterior (Fig. 1d,e, white arrowhead) as has been shown recently with Texas Red dextran injections (Lowery and

Sive, 2005). Furthermore, melanocytes become visible at around 26 hpf due to melanin production (Fig. 1f, white arrowhead). Intriguingly, they migrate across the developing cerebellum lining the rhombic lip (Fig. 1g, see

Supplementary Movie 3). This finding demonstrates that time-lapse stereomicroscopy is able to reveal the dynamics of morphogenetic processes at cellular resolution.

To increase the resolution of the analysis of hindbrain morphogenetic rearrangements, we switched from a Planapo 1.0 to a Planapo 5.0 objective, resulting in an approximately fivefold increase of the numerical aperture. Instead of capturing a single plane, we recorded z-stacks of images of the hindbrain region over time. Capturing data from three-dimensions rather than from a single plane allows out-of-focus signal to be efficiently eliminated by deconvolution—an iterative mathematical approach based on Fourier-transformations using the point spread function of the microscopic setup (McNally et al., 1999). Starting at 18 hpf, the ventricle formation is clearly visible (Fig. 1h, white star). While the cells at the midbrain–hind-

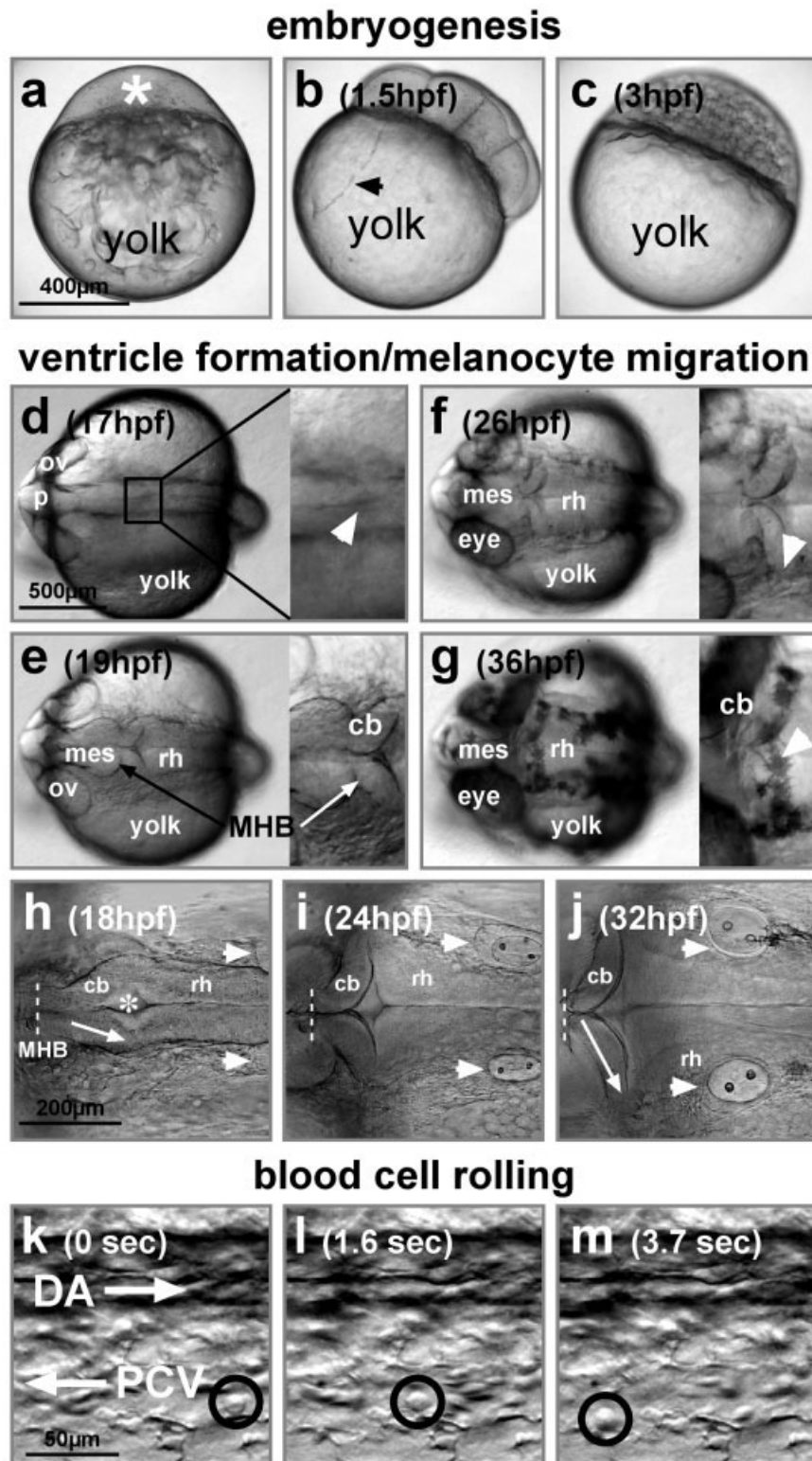


Fig. 1. Bright-field time-lapse stereomicroscopy of zebrafish embryos. **a–c:** Time-lapse analysis displaying morphogenetic changes during zebrafish embryogenesis. First cleavages of blastomeres beginning at the one-cell stage (a, white star) can be followed. Recording conditions: $\times 1$ objective, single plane, every 2 min. See also Supplementary Movie 1 and 2. **d–g:** Time-lapse analysis of fourth ventricle formation in the developing zebrafish hindbrain; digital zoom of cerebellar region is displayed on the right of each picture. Note explorative membrane protrusions of individual melanocytes (f, white arrowhead). Recording conditions: $\times 1$ objective, single plane, every 4 min. See also Supplementary Movie 3. **h–j:** Time-lapse analysis of the developing zebrafish cerebellum. Cells at the midbrain–hindbrain boundary (MHB; dashed line) remain together during fourth ventricle opening (white star), leading to a rotation of the cerebellar primordium (compare white arrows in h and j). Note compaction of the hindbrain by shortening of the distance between MHB and otic vesicles (white arrowheads). Recording conditions: $\times 5$ objective, 25 planes at $2 \mu\text{m}$ distance each, every 12 min for 14 hr, images of individual time points were deconvoluted (settings in Leica Deblur: image spacing 0.997, adaptive PSF, 10 iterations, low noise) and converted in a single sum projection. See also Supplementary Movie 4. **k–m:** Blood cell rolling along the endothelium of the posterior cardinal vein in 32 hours post-fertilization (hpf) old embryo; traced cell is marked by black circle. Recording conditions: $\times 5$ objective, single plane, nearly every 0.1 sec. See also Supplementary Movie 5. cb, cerebellum; DA, dorsal aorta; mes, mesencephalon; ov, otic vesicle; p, prosencephalon; PCV, posterior cardinal vein; rh, rhombencephalon.

brain boundary (MHB; dashed line) remain together, the hindbrain ventricle opens extensively (see Supplementary Movie 4). This change causes the primordium of the cerebellum just posterior to the MHB to rotate around its dorsoventral axis changing from a rostrocaudal to a mediolateral orientation (Fig. 1h,j, compare white arrows). Furthermore, the position of the MHB remains almost unaltered, whereas the otic vesicles (Fig. 1, h–j, white arrowheads) become positioned much closer to the MHB over time (at 18 hpf MHB–otic vesicle distance, 400 μm ; at 32 hpf MHB–otic vesicle distance, 250 μm), indicating that the hindbrain condenses significantly during differentiation. Thus, time-lapse stereomicroscopy is able to capture details of morphogenetic tissue rearrangements during embryonic development.

Using the streaming modus of the camera (maximal temporal resolution of 8 frames per second at 512×512 pixels), the possible resolution of moderate dynamic processes was tested by recording blood flow in the posterior cardinal vein (PCV) of a 32 hpf embryo. Although delineating erythrocyte movements require faster acquisition speeds (Hove et al., 2003), rolling of individual blood cells along the venous wall could be captured successfully (Fig. 1h–j, black circle; see Supplementary Movie 5). Such behavior is characteristic for blood cell types involved in inflammatory processes such as leukocytes and neutrophils (Kubes and Kerfoot, 2001; Ley, 2002). This finding promises that inflammatory response dynamics can be imaged at the individual cell level directly in vivo (Redd et al., 2004).

While brightfield microscopy resolves the dynamics of tissue compartments or of few individual cell types with intrinsic labeling (such as melanocytes), imaging at the cellular level usually requires specific labeling with fluorescent markers such as dyes or the genetically encoded green fluorescent protein (GFP). To prove the feasibility of automated fluorescence stereomicroscopy for capturing dynamic multicolor information over time, we made use of zebrafish embryos expressing the fluorescent protein Kaede, which can be converted from green to red fluorescence emission by

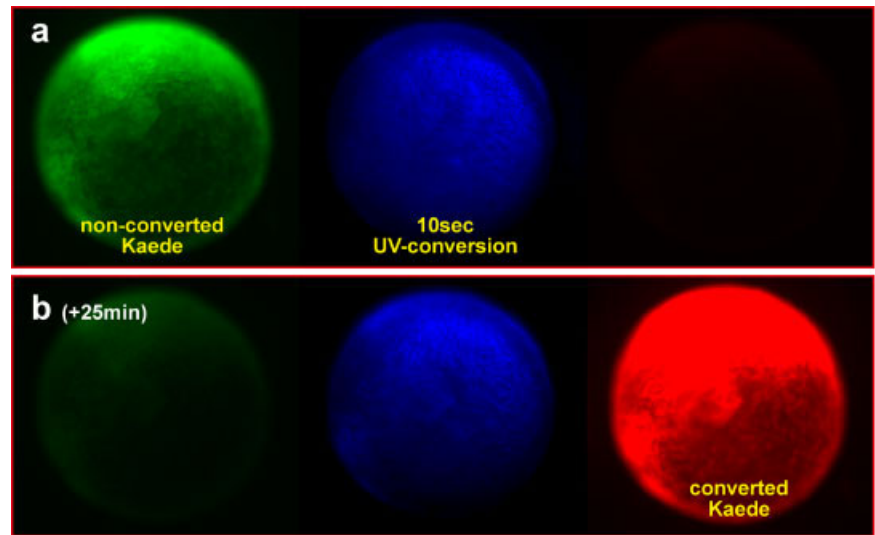


Fig. 2. Multicolor time-lapse recording of fluorescent zebrafish embryo. **a,b:** Time-lapse analysis displaying conversion dynamics of Kaede (MBL International) in zebrafish embryos. Recording conditions: $\times 1$ objective; single plane; filter routine: GFP (60 msec)/DAPI (1.5 sec)/Texas Red (60 msec) every 30 sec, respectively. See also Supplementary Movie 6.

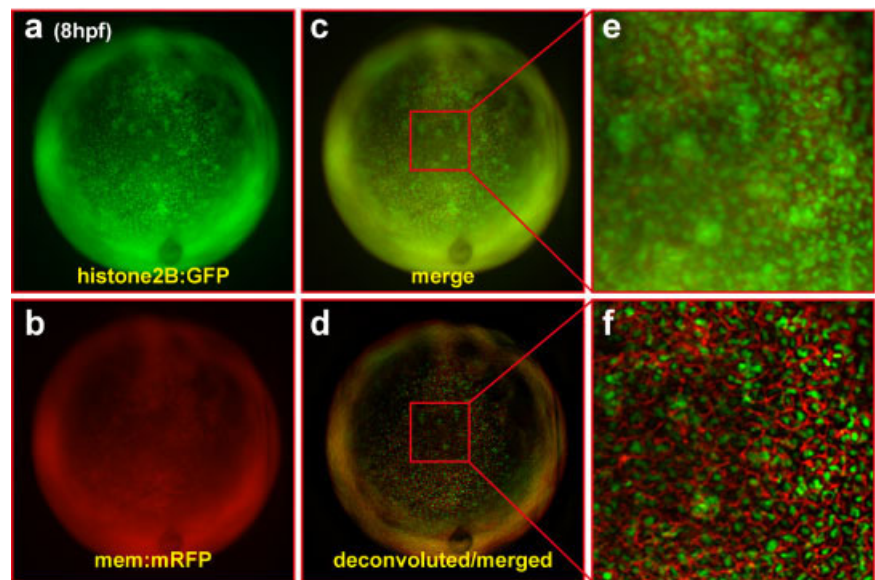


Fig. 3. Subcellular resolution by deconvolution approaches with z-stack recordings of a stereomicroscope. **a,b:** z-stack recording and deconvolution of 8 hours postfertilization (hpf) embryo coexpressing histone2B::GFP (a) and mem::mRFP (b). **c,d:** Merged picture of a single plane from both channels (c) before and (d) after deconvolution. **e,f:** Digital magnifications (ca. $4\times$) of the animal pole region of the embryos displayed in c and d, respectively. Recording conditions: $\times 5$ objective; z-stack, 128 μm with 2 μm spacing; deconvolution settings in Leica Deblur: image spacing 0.853, adaptive PSF, 10 iterations, low noise.

ultraviolet (UV) irradiation (Ando et al., 2002). Kaede-mRNA injection at the one-cell stage resulted in green fluorescent embryos at 10 hpf (Fig. 2a). To record the dynamics of Kaede-conversion, the embryos were exposed to blue (450–490 nm, 60 msec), UV (350–390 nm, 1.5 sec) and green (532–588 nm, 60 msec) light every 30 sec

(see Supplementary Movie 6). A rapid decrease in green and concomitant increase in red fluorescence could be observed with the fluorescent protein being almost completely converted after 50 cycles (Fig. 2b). This finding demonstrates the capability of automated fluorescence stereomicroscopes for intravital multicolor time-lapse analysis.

Nonconfocal fluorescence microscopy bears the difficulty of signal overlap from within and outside the focal plane. Thus, fluorescent emission from embryos coexpressing a nuclear targeted histone2b::GFP variant (Fig. 3a) and a cytoplasmic membrane targeted mem::mRFP variant (Fig. 3b) after mRNA injection appear to overlap (Fig. 3c, a merged image of 3a and 3b, 3e is a digital magnification of cells from the animal pole). To circumvent this problem, we used multicolor z-stack recording for subsequent deconvolution analysis. After image processing, individual cells with differently labeled nuclei and cytoplasmic membranes could be clearly resolved (Fig. 3d, 3f is digital magnification of cells from the animal pole).

When used on transgenic embryos expressing GFP under control of the olig2 enhancer (Shin et al., 2003), z-stack recording with subsequent deconvolution allows even individual axon tracts of motoneurons to be three-dimensionally reconstructed and animated (Fig. 4a,b; see Supplementary Movie 7 for 3D animation). Such detailed but technically simple 3D reconstruction of expression patterns will be very valuable for the analysis of the many GFP transgenic fish strains recently generated by various enhancer trap screens (Grabher et al., 2003; Parinov et al., 2004; Balciunas et al., 2004; Kawakami et al., 2004; Ellingsen et al., 2005).

The astonishing cellular resolution obtained with a stereomicroscope prompted us to ultimately challenge this setup with a dynamic biological problem at the subcellular level: the navigation of axons during embryogenesis. Transgenic olig2:GFP embryos initiate the outgrowth of GFP-expressing secondary motoneuron axons into the somites of the trunk at around 26 hpf. The lateral trunk region of these embryos was imaged under GFP-fluorescence conditions by recording z-stacks of images every 20 min for periods of up to 20 hr. Combining 3D fluorescence time-lapse recording, deconvolution, and image projection allowed individual axons to be followed as they navigated through the somitic tissue. For example, growth cones of axons were found to hold at the myoseptum (Fig. 4c,d, white arrowhead) for more than 3 hr.

Here, they project protrusions in several directions before progressing to project further ventrally (Fig. 4e–g), indicating a crucial pathfinding decision at this intermediate target. During later ventral projection, a saltatory progression mode for the growth cone rather than a continuous movement was observed (see Supplementary Movie 7). In addition, this intravital dynamic analysis indicates that axons of the secondary motoneurons unlike retinal axons project almost straight into their target tissue as deviations from their ventral route or corrections of initial misrouting were never observed ($n = 4$ movies, 24 axons). Although being able to navigate independently, this absence of initial misrouting may be due to the pioneering network laid down by axons of the earlier projecting primary motoneurons (Pike et al., 1992).

To compare the quality of our time-lapse stereomicroscopy to results obtained with a compound microscope, we repeated the same axon pathfinding analysis using a $\times 5$ Plan Neofluar objective at similar magnification, detector resolution, and deconvolution settings. Again, secondary motoneurons halted at the myoseptum for several hours before projecting ventrally in a saltatory manner (Fig. 4h–l; see Supplementary Movie 8). Whereas both approaches were able to record motor axon pathfinding, the images of the stereomicroscopy approach appear to be better resolved. This finding can be explained by the higher numerical aperture of the $\times 5$ stereomicroscope objective at high magnifications (see Table 1). Thus, the zooming optics of a stereomicroscope offer the advantage that they can be adjusted more dynamically to processes that are to be imaged.

We have demonstrated by this set of experiments that, with the newly introduced automated fluorescence stereomicroscopes, dynamic *in vivo* imaging in brightfield and multicolor mode can be achieved at the cellular and even subcellular level in three dimensions over time. Certain limitations of the used setup have to be kept in mind though. Due to the lack of monochromatic light sources, excitation of fluorophores with the mercury lamp of a stereomicroscope is less specific and efficient when compared with laser-

mediated excitation with a confocal microscope. Probably, more-powerful photodiodes may solve this issue in the near future (Martin et al., 2005). In addition, a stereomicroscope is usually equipped with a single camera. Thus, when several fluorescent fluorophores are detected simultaneously with dual excitation/emission filters, less-sensitive RGB cameras are required for picture recording. Alternatively, as in this study, more sensitive monochromatic cameras can be used, but they require successive recording of the emission of each fluorophore involving filter changes. As such mechanical changes are time-consuming, the temporal resolution of multicolor recordings with an automated stereomicroscope is low compared with confocal microscopes. Also, we showed that deconvolution approaches could resolve individual cells and larger subcellular structures with a stereomicroscope. Deconvolution requires lengthy periods of calculation; thus, the final imaging results will only be obtained considerably late after image recording and not instantly as with confocal microscopy. Finally, the low magnification and low resolution of stereomicroscope objectives will make recordings of small cellular structures such as microtubule fibers or secretory vesicles difficult.

Nevertheless, as demonstrated here, an automated stereomicroscope combined with 3D deconvolution software represents a cost-effective, easy to handle, intuitive means of intravital time-lapse recording at a convenient working distance. This approach will prove useful for understanding a wealth of biological processes as demonstrated for morphogenetic tissue rearrangements during embryogenesis, melanocyte migration, leukocyte rolling, 3D reconstruction of expression patterns, and axon pathfinding. In addition to the ones shown here, many more processes can likely be included such as lens or otic vesicle invagination, somite formation, fin and limb budding, 3D microangiography, angiogenesis, wound healing, and tumor cell invasion, in both wild-type and mutant animals. As almost every biologist is familiar with handling stereomicroscopes, we hope to have laid the ground for dynamic imaging, leaving its niche, and becoming a widely

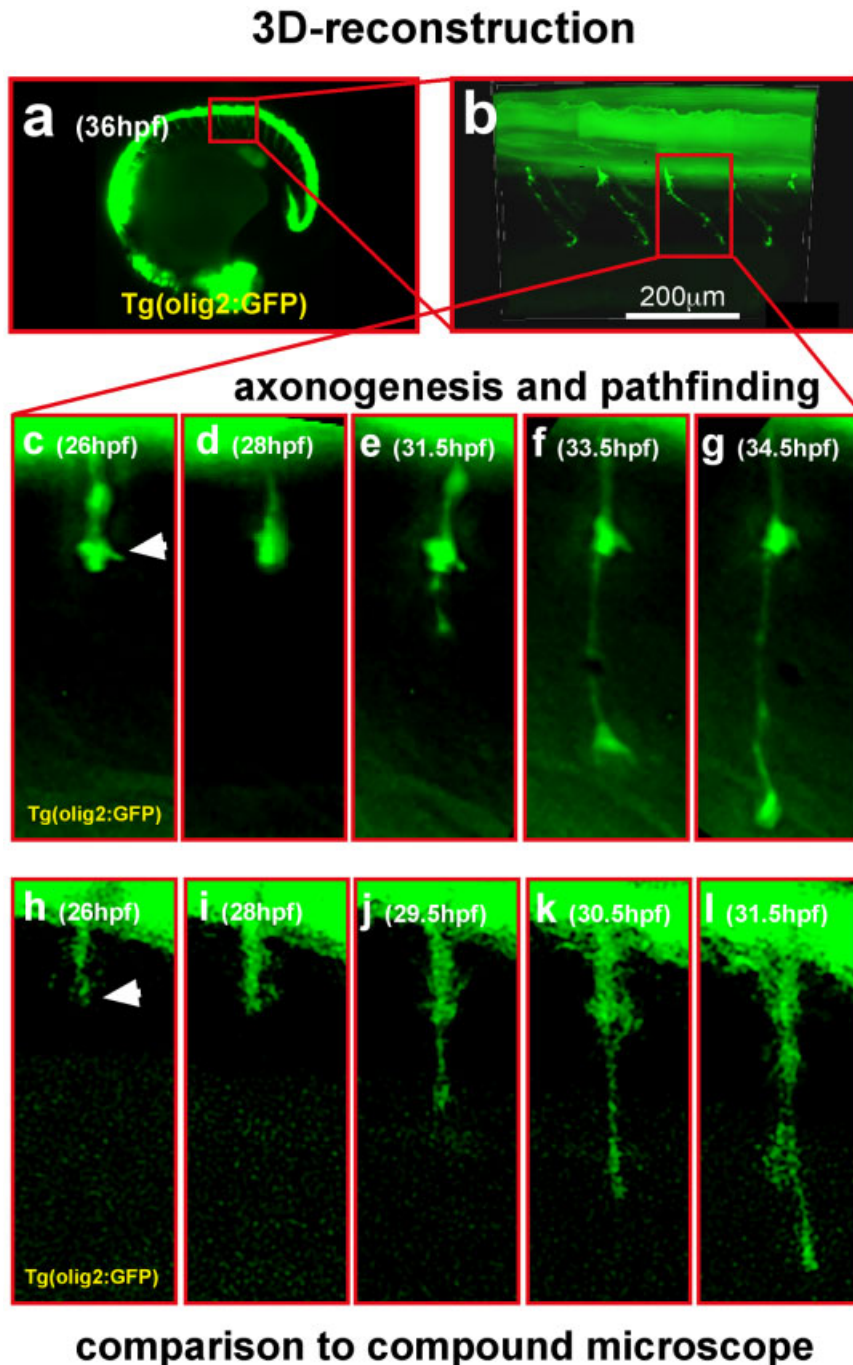


Fig. 4. Three-dimensional (3D) reconstruction of green fluorescent protein (GFP) expression pattern and fluorescence 3D time-lapse stereomicroscopy of motor axon pathfinding in zebrafish embryos. **a,b:** The 3D reconstruction of the trunk region with axons of secondary motoneurons after deconvolution (**b**) of 36 hours postfertilization (hpf) transgenic olig2:GFP embryo (**a**). Recording conditions: $\times 1$ objective (**a**); $\times 5$ objective (**b**); z-stack, $116\ \mu\text{m}$ with $2\ \mu\text{m}$ spacing; deconvolution settings in Leica Deblur: image spacing 0.226, adaptive PSF, 10 iterations, low noise. **c–g:** The 3D time-lapse recording of axon pathfinding of secondary motoneurons into trunk somites in transgenic olig2:GFP zebrafish embryo using a fluorescence stereomicroscope. Recording conditions: $\times 5$ objective; Planapo NA 0.5; total magnification, $\times 30$; z-stack, $20\ \mu\text{m}$ with $2\ \mu\text{m}$ spacing; deconvoluted images (for settings, see **a,b**) were subsequently projected into single plane, every 20 min. See also Supplementary Movie 7. **h–l:** The 3D time-lapse recording of axon pathfinding of secondary motoneurons into trunk somites in transgenic olig2:GFP zebrafish embryo using a compound microscope. Recording conditions: $\times 5$ objective; Plan Neofluar NA 0.15, total magnification: $\times 30$, z-stack: $20\ \mu\text{m}$ with $2\ \mu\text{m}$ spacing, deconvoluted images (for settings, see **a,b**) were subsequently projected into single plane, every 20 min. See also Supplementary Movie 8.

used standard tool for analyzing the dynamics of biological processes in a variety of model organisms, their embryos and adults, in wild-type, mutants, and disease models.

EXPERIMENTAL PROCEDURES

Zebrafish Maintenance

Raising, spawning, and maintaining of zebrafish lines were performed as described (Westerfield, 1995; Kimmel et al., 1995).

Injection

Capped mRNA for microinjection was synthesized from histone2B::EGFP (Kanda et al., 1998), mem::mRFP (Megason and Fraser, 2003), and Kaede (Ando et al., 2002) encoding cDNA cloned in the pCS2+ vector (Rupp et al., 1994) using the SP6 mMACHINE mMACHINE Kit (Ambion Inc., Austin, TX). Synthesized mRNA was purified with RNeasy spin columns (Qiagen) and subsequent EtOH precipitation. A total of 1.5 nl of $150\ \text{ng}/\mu\text{l}$ mRNA solution in 0.05% PhenolRed were injected into the cytoplasm of one-cell stage zebrafish embryos by means of glass capillary tubes.

Imaging

Before image recording, embryos were anesthetized in 0.01% tricaine in 30% Danieau medium containing 0.75 mM phenylthiourea (PTU) to prevent pigmentation. Mounting of embryos in 1.2% ultra-low gelling agarose to restrict embryonic movements was performed as described in detail previously (Köster and Fraser, 2004). As imaging setup, a motorized fluorescence stereomicroscope (MZ16FA, Leica) equipped with a digital camera (DFC350FX, Leica) was used with both being controlled by automating software (FW4000, Leica). For comparison with a compound microscope (Fig. 4), a confocal microscope (LSM510Meta, Zeiss) was used for automated z-stack recording with maximum opening of the pinhole. Deconvolution of the obtained images was performed with the Deblur module of the FW4000 software (Leica). Subsequent image processing, projections, and animations were performed using Photoshop 6.0 (Adobe), After Ef-

fects 6.5 (Adobe), LSM software (Zeiss), and QuickTime 6.5.1 (Apple), respectively.

ACKNOWLEDGMENTS

We thank Christian Leibold and Karl-Heinz Koertje for continuous support. We thank Chichung Lie and Peter Hutzler for critically reading and commenting on the manuscript. We also thank Atsushi Miyawaki for his advice and experimental suggestions. We thank Bruce Appel for providing us with the transgenic olig2:GFP zebrafish line. We thank all members of our laboratory as well as the Wurst, Bally-Cuif, Imai, Graw, and Lie laboratories at the Institute of Developmental Genetics for helpful discussions and suggestions.

REFERENCES

- Ando R, Hama H, Yamamoto-Hino M, Mizuno H, Miyawaki A. 2002. An optical marker based on the UV-induced green-to-red photoconversion of a fluorescent protein. *Proc Natl Acad Sci U S A* 99:12651–12656.
- Balciunas D, Davidson AE, Sivasubbu S, Hermanson SB, Welle Z, Ekker SC. 2004. Enhancer trapping in zebrafish using the Sleeping Beauty transposon. *BMC Genomics* 5:62.
- Chalfie M, Tu Y, Euskirchen G, Ward WW, Prasher DC. 1994. Green fluorescent protein as a marker for gene expression. *Science* 263:802–805.
- Ellingsen S, Laplante MA, König M, Kikuta H, Furmanek T, Hoivik EA, Becker TS. 2005. Large-scale enhancer detection in the zebrafish genome. *Development* 132:3799–3811.
- Fricke C, Lee JS, Geiger-Rudolph S, Bonhoeffer F, Chien CB. 2001. Astray, a zebrafish roundabout homolog required for retinal axon guidance. *Science* 292:507–510.
- Grabher C, Henrich T, Sasado T, Arenz A, Furutani-Seiki M, Wittbrodt J. 2003. Transposon-mediated enhancer trapping in medaka. *Gene* 322:57–66.
- Hove JR, Köster RW, Forouhar AS, Acevedo-Bolton G, Fraser SE, Gharib M. 2003. Intracardiac fluid forces are an essential epigenetic factor for embryonic cardiogenesis. *Nature* 421:172–177.
- Hutson LD, Chien CB. 2002. Pathfinding and error correction by retinal axons: the role of astray/robo2. *Neuron* 33:205–217.
- Kanda T, Sullivan KF, Wahl GM. 1998. Histone-GFP fusion enables sensitive analysis of chromosome dynamics in living mammalian cells. *Curr Biol* 8:377–385.
- Kawakami K, Takeda H, Kawakami N, Kobayashi M, Matsuda N, Mishina M. 2004. A transposon-mediated gene trap approach identifies developmentally regulated genes in zebrafish. *Dev Cell* 7:133–144.
- Kimmel CB, Ballard WW, Kimmel SR, Ullmann B, Schilling TF. 1995. Stages of embryonic development of the zebrafish. *Dev Dyn* 203:235–310.
- Köster RW, Fraser SE. 2004. Time-lapse microscopy of brain development. *Methods Cell Biol* 76:207–235.
- Kubes P, Kerfoot SM. 2001. Leukocyte recruitment in the microcirculation: the rolling paradigm revisited. *News Physiol Sci* 16:76–80.
- Ley K. 2002. Integration of inflammatory signals by rolling neutrophils. *Immunol Rev* 186:8–18.
- Lichtman JW, Fraser SE. 2001. The neuronal naturalist: watching neurons in their native habitat. *Nat Neurosci* 4:1215–1220.
- Lowery LA, Sive H. 2005. Initial formation of zebrafish brain ventricles occurs independently of circulation and requires *nagie oko* and *snakehead/atp1a1a.1* gene products. *Development* 132:2057–2067.
- Maegawa S, Yasuda K, Inoue K. 1999. Maternal mRNA localization of zebrafish DAZ-like gene. *Mech Dev* 81:223–226.
- Martin G, Agostini HT, Hansen LL. 2005. Light emitting diode microscope illumination for green fluorescent protein or fluorescein isothiocyanate epifluorescence. *Biotechniques* 38:204–206.
- Matz MV, Fradkov AF, Labas YA, Savitsky AP, Zaraisky AG, Markelov ML, Lukyanov SA. 1999. Fluorescent proteins from nonbioluminescent Anthozoa species. *Nat Biotechnol* 17:969–973.
- McNally JG, Karpova T, Cooper J, Conchello JA. 1999. Three-dimensional imaging by deconvolution microscopy. *Methods* 19:373–385.
- Megason SG, Fraser SE. 2003. Digitizing life at the level of the cell: high-performance laser-scanning microscopy and image analysis for in toto imaging of development. *Mech Dev* 120:1407–1420.
- Miyawaki A. 2005. Innovations in the imaging of brain functions using fluorescent proteins. *Neuron* 48:189–199.
- Nagai T, Ibata K, Park ES, Kubota M, Mikoshiba K, Miyawaki A. 2002. A variant of yellow fluorescent protein with fast and efficient maturation for cell-biological applications. *Nat Biotechnol* 20:87–90.
- Parinov S, Kondrichin I, Korzh V, Emelyanov A. 2004. Tol2 transposon-mediated enhancer trap to identify developmentally regulated zebrafish genes in vivo. *Dev Dyn* 231:449–459.
- Pike SH, Melancon EF, Eisen JS. 1992. Pathfinding by zebrafish motoneurons in the absence of normal pioneer axons. *Development* 114:825–831.
- Redd MJ, Cooper L, Wood W, Stramer B, Martin P. 2004. Wound healing and inflammation: embryos reveal the way to perfect repair. *Philos Trans R Soc Lond Series B Biol Sci* 359:777–784.
- Rupp RAW, Snider L, Weintraub H. 1994. *Xenopus* embryos regulate the nuclear-localization of Xmyod. *Genes Dev* 8:1311–1323.
- Shaner NC, Campbell RE, Steinbach PA, Giepmans BNG, Palmer AE, Tsien RY. 2004. Improved monomeric red, orange and yellow fluorescent proteins derived from *Discosoma* sp. red fluorescent protein. *Nat Biotechnol* 22:1567–1572.
- Shin J, Park H-C, Topczewska JM, Mawdsley DJ, Appel B. 2003. Neural cell fate analysis in zebrafish using olig2 BAC transgenics. *Methods Cell Sci* 25:7–14.
- Westerfield M. 1995. *The zebrafish book*. Eugene, OR: University of Oregon Press.

Appendix 7

published peer-reviewed Protocol in *Cold Spring Harbor Protocols*

In vivo time-lapse imaging of zebrafish embryonic development

Martin Distel and Reinhard W. Köster

CSH Protocols (2007), doi:10.1101/pdb.prot4816

Contribution:

I wrote this protocol and generated all figures and movies.

Please cite as: CSH Protocols; 2007; doi:10.1101/pdb.prot4816



Protocol

In Vivo Time-Lapse Imaging of Zebrafish Embryonic Development

Martin Distel and Reinhard W. Köster¹

GSF--National Research Center for Environment and Health, Institute of Developmental Genetics, 85764 Neuherberg-Munich, Germany

¹Corresponding author (reinhard.koester{at}gsf.de)

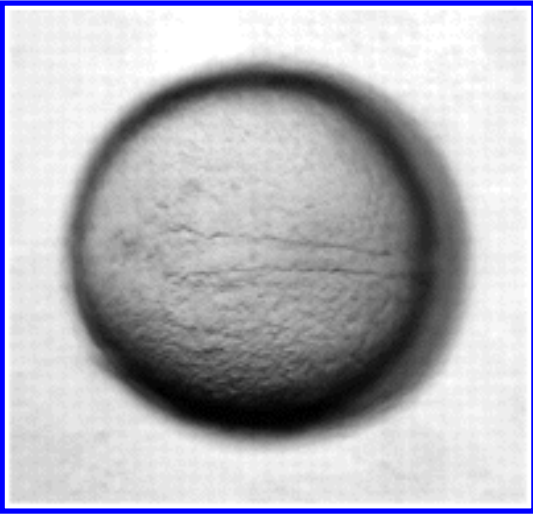
INTRODUCTION

Intravital time-lapse imaging is a powerful technique for investigating continuous developmental processes without missing crucial events. Because of the rapid embryogenesis, external development, and transparency of zebrafish embryos, their developmental processes can be visualized in time-lapse studies in the context of the living organism. The following protocol describes a method for performing intravital time-lapse imaging of zebrafish embryos over several days using confocal or compound stereomicroscopes.

RELATED INFORMATION

Time-lapse imaging of zebrafish embryos is also described by [Köster and Fraser \(2004\)](#) and [Distel et al. \(2006\)](#).

Somitogenesis in the zebrafish embryo is shown in [Movie 1](#) . Cytokinesis and cell migration in the zebrafish hindbrain is shown in [Movie 2](#) .



Movie 1. Somitogenesis in the zebrafish embryo. Recorded using the Leica MZ 16 FA compound microscope. Recording conditions were: brightfield, 1X objective, single plane, every 4 min. Adobe Photoshop rendering, QuickTimePro animation at 6 frames per second.

View as movie: (52K):

[\[in QuickTime\]](#)



Movie 2. Cytokinesis and cell migration in the zebrafish hindbrain. The nuclei of the cells are marked with RFP shown in red, the cell membranes are marked with CFP in blue, and the centrosomes are marked with GFP in green. Recorded using the Zeiss LSM 510 Meta confocal microscope. Recording conditions were: 40X/0.75 objective, z-stacks spacing 2 μ m, every 10 min. Images of individual time-lapse points were converted in a single maximum projection. Adobe Photoshop rendering, QuickTimePro animation at 6 frames per second.

View as movie: (126K):

[\[in QuickTime\]](#)

MATERIALS

Reagents

1.2% agarose, ultra-low melting temperature (Sigma-Aldrich), prepared in 30% Danieau solution

  Danieau solution

  Sedative solution

Zebrafish embryos, dechorionated

Equipment

Coverslips

High-vacuum silicon grease (Dow Corning)

Ice

Incubation chamber (see [Figs. 1](#) and [2](#))



Figure 1. A Zeiss LSM 510 confocal microscope with a custom-fit incubation chamber. Cardboard covered with insulating foil was used to construct a custom-fit chamber around the microscope stage.

View larger version (116K):

[\[in this window\]](#)

[\[in a new window\]](#)

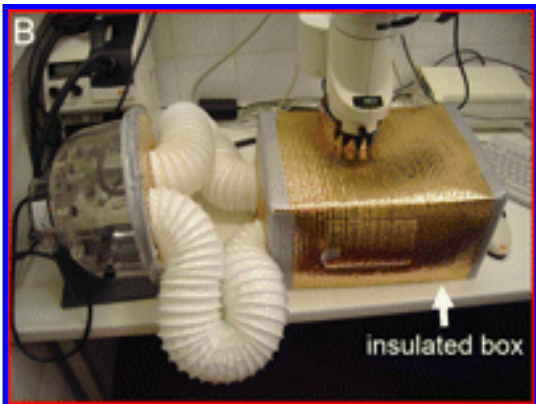


Figure 2. A Leica MZ16FA compound stereomicroscope with a custom-fit incubation chamber, which is fed with warm air by a heated fan. The fan is connected to the incubation chamber by two flexible plastic tubes that allow the warm air to circulate.

View larger version (117K):

[\[in this window\]](#)

[\[in a new window\]](#)

Use cardboard covered with insulating foil to design a custom-fit chamber around the microscope stage. Use a heater to feed the incubation chamber with warm air. The heater and incubation chamber can be

connected by flexible plastic tubes. The incubation chamber can be constructed as described in [Construction of a Heated Incubation Chamber around a Microscope Stage for Time-Lapse Imaging](#).

Microcentrifuge tubes

Microscopes (one of the following is needed):

- Confocal laser scanning microscope (Zeiss LSM 510 META on an Axiovert 200M, with the Zeiss LSM 510 software package; objectives of 10X, 20X, 40X, 40X water, 40X oil, 63X oil, and 100X; and laser lines of 458 nm, 488 nm, and 543 nm)
- Motorized fluorescence stereomicroscope (Leica Microsystems MZ16FA, with 1X and 5X objectives)

Needle or pipette tip to position the embryo (see Step 6)

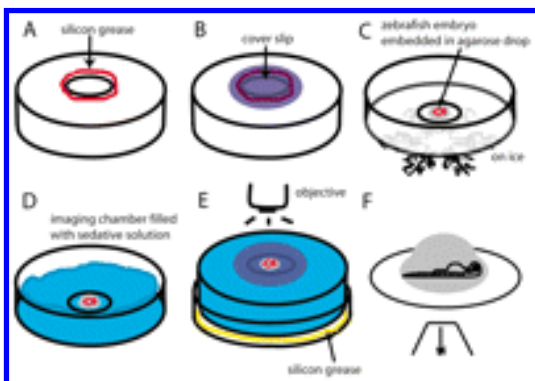
Petri dishes (6-cm; Nunc)

METHOD

Preparing the Imaging Chamber

Instead of building an imaging chamber from scratch, a ready-to-use imaging chamber may be purchased (MatTek; <http://www.glass-bottom-dishes.com>).

1. Create a 1-cm hole in the bottom of a 6-cm Petri dish. Apply silicon grease around the hole in the Petri dish as shown in [Figure 3A](#).



View larger version (32K):

[\[in this window\]](#)

[\[in a new window\]](#)

Figure 3. Embedding the zebrafish embryo. (A) An imaging chamber is coated with silicon grease (red). (B) A coverslip (purple) is fixed on the imaging chamber using silicon grease (red). (C) A zebrafish embryo is embedded in an agarose drop on the coverslip. To solidify the agarose and immobilize the embryo, the imaging chamber is put on ice. (D) The imaging chamber is filled with sedative solution and is ready for image recording using a confocal microscope. (E) For imaging with an upright compound microscope, the imaging chamber is sealed with a silicon-grease-coated lid and turned over. (F) A schematic drawing of a zebrafish

embryo in an imaging chamber.

2. Place a coverslip on top of the hole as shown in [Figure 3B](#). Apply a gentle force to the edges of the coverslip to seal the imaging chamber.

Embedding the Zebrafish Embryo

3. Transfer the dechorionated embryos into a Petri dish containing sedative solution. Keep the embryos in this sedative solution for at least 15 min.

4. Dissolve 1.2% ultra-low melting temperature agarose in 30% Danieau solution by boiling it and subsequently cooling the solution to 28°C.

A stock of agarose dissolved in 30% Danieau solution can be kept at 28°C.

5. Transfer the embryos into a microcentrifuge tube containing the 1.2% agarose/30% Danieau solution.

6. Embed the embryos in an agarose drop on the coverslip of the imaging chamber ([Fig. 3C,F](#)). Orient the embryos in the agarose according to imaging requirements using a pipette tip or needle.

7. Place the imaging chamber on ice ([Fig. 3C](#)) to cool the agarose and fix the embryo in position. *The orientation of the embryo should be checked during the cooling process and corrected for any movement.*

8. When the agarose has solidified, add sedative solution to the top of the agarose drop to sedate the embryo ([Fig. 3D](#)).

See Troubleshooting.

9. Fill the imaging chamber with sedative solution and seal it with a silicon-coated Petri dish lid ([Fig. 3E](#)). To image using an upright microscope, turn the imaging chamber over.

Time-Lapse Imaging

Because several embryos can be embedded in a single imaging chamber, simultaneous image recording of several embryos using a motorized microscopic stage should be possible.

10. To ensure that the embryo develops normally on the microscope stage, keep the lid on the Petri dish to prevent evaporation and use an incubation chamber around the microscope to maintain a temperature of 28°C-29°C (see [Figs. 1, 2](#)). To prevent the solution inside the imaging chamber from moving, do not allow warm air from the heated fan to blow directly on the imaging chamber. In order to avoid focus shifts, allow the setup to equilibrate until the temperature inside the

incubation chamber does not change (~1 h) before proceeding with image capturing.

11. Define a z-stack around the region of interest and record stacks over time.

TROUBLESHOOTING

Problem: The ultra-low melting agarose does not solidify.

[Step 8]

Solution: Use freshly prepared ultra-low melting temperature agarose, which solidifies within 1-2 min.

Problem: Embryo pigmentation interferes with imaging.

[Step 11]

Solution: The best stages for imaging are the early developmental stages, as pigmentation interferes with imaging in later-stage embryos. However, this problem can be solved by adding *N*-phenylthiourea (PTU) at a final concentration of 0.15 mM in the Danieau solution, which allows imaging of embryogenesis even later than 1 wk post-fertilization.

DISCUSSION

Although embedding a zebrafish embryo in ultra-low melting agarose prior to time-lapse imaging involves placement of the embryo on ice, this method has proven robust. Using freshly prepared agarose reduces the time on ice to 1 min, though incubation of embryos on ice for up to 15 min does not obviously affect development. Alternatively, 3%-5% methyl cellulose can be used to embed the embryo. Agarose is more reliable than methyl cellulose in keeping the embryo in the same spot because agarose is more rigid. In some cases, however, the rigidity of agarose can be a disadvantage. For example, an early embryo (about 14 h post-fertilization [hpf]) embedded in agarose cannot stretch out its tail.

To ensure that the zebrafish embryo develops normally, and to allow the comparison of results from the same time point (hpf) between embryos, the temperature of the embryo must be kept at 28°C-29°C. Time-lapse analysis as described in this protocol allows continuous imaging of zebrafish development for at least 3 d. A temperature equilibrium between the microscope setup and the specimen cannot be obtained in an open system that relies on a heated stage or heated objective. Such a setup is very sensitive to environmental changes, such as the entrance of researchers into the microscopy room. Also, because image recording is usually done in the micrometer range, it is critical to avoid focus drifts caused by

temperature shifts. A self-made heating chamber made from inexpensive cardboard (see [Fig. 1](#), [Fig. 2](#), and [Construction of a Heated Incubation Chamber around a Microscope Stage for Time-Lapse Imaging](#)) represents an easy but effective means to generate a closed system around the microscope. After reaching a temperature equilibrium, this setup is very stable with respect to focus drifts and can run overnight without focus adjustments. Commercially available incubation chambers are similarly useful, but are expensive because of the inclusion of features such as CO₂ control, which are not necessary for zebrafish time-lapse imaging.

ACKNOWLEDGMENTS

This work was supported by the Ministry for Education and Research through a Biofuture Award (0311889), by the Helmholtz Association, and by the Studienstiftung des deutschen Volkes.

REFERENCES

- Distel, M., Babaryka, A., and Köster, R.W. 2006. Multicolor in vivo time-lapse imaging at cellular resolution by stereomicroscopy. *Dev. Dyn.* **235**: 1100–1106. [\[Medline\]](#)
- Köster, R.W. and Fraser, S.E. 2004. Time-lapse microscopy of brain development. *Methods Cell Biol.* **76**: 207–235. [\[Medline\]](#)



Caution



General warning

This material contains hazardous components. Please see recipe for full details.



Recipe



Danieau solution (300%)

Reagent	Amount to add
2.9 M NaCl	60 mL
70 mM KCl	30 mL
 40 mM MgSO ₄ • 7H ₂ O	30 mL
 60 mM Ca(NO ₃) ₂	30 mL
0.5 M HEPES (pH 7.2)	30 mL
H ₂ O	to 1000 mL



Recipe

Sedative solution

  0.01% tricaine

  30% Danieau solution

Copyright © 2007 by Cold Spring Harbor Laboratory Press. Online ISSN: 1559-6095 [Terms of Service](#)

All rights reserved. Anyone using the procedures outlined in these protocols does so at their own risk. Cold Spring Harbor Laboratory makes no representations or warranties with respect to the material set forth in these protocols and has no liability in connection with their use. All materials used in these protocols, but not limited to those highlighted with the Warning icon, may be considered hazardous and should be used with caution. For a full listing of cautions, [click here](#).

All rights reserved. No part of these pages, either text or images, may be used for any reason other than personal use. Reproduction, modification, storage in a retrieval system or retransmission, in any form or by any means-electronic, mechanical, or otherwise-for reasons other than personal use is strictly prohibited without prior written permission.



This article has been cited by other articles: ([Search Google Scholar for Other Citing Articles](#))



[CSHL Protocols](#)

[▶ HOME](#)

K. Volkmann and R. W. Köster

In Vivo Retrograde Labeling of Neurons in the Zebrafish Embryo or Larva with Rhodamine Dextran

CSH Protocols, September 1, 2007; 2007(18): pdb.prot4832 - pdb.prot4832.

[\[Abstract\]](#) [\[Full Text\]](#)

Appendix 8

Bookchapter in: Live imaging in Zebrafish: Insights into Development and Disease

Imaging the cell biology of neuronal migration in zebrafish

Martin Distel, Jennifer Hocking and Reinhard W. Köster

Live imaging in Zebrafish: Insights into Development and Disease,
World Scientific Publishing, Singapore

Contribution:

This bookchapter was mainly written by Reinhard Köster. I contributed to some chapters, created the figures of the bookchapter and wrote the figure legends.

Title: **Imaging the cell biology of neuronal migration
In zebrafish**

Authors: Martin Distel, Jennifer Hocking, Reinhard W. Köster

Affiliation: Helmholtz Zentrum München
German Research Center for Environmental Health,
Institute of Developmental Genetics
Ingolstädter Landstrasse 1,
85764 Munich-Neuherberg
Germany

Correspondence: Reinhard W. Köster
Email: Reinhard.Koester@helmholtz-muenchen.de
Phone: +49-89-3187-3036, Fax: +49-89-3187-3192

Keywords: zebrafish, neuronal migration, branchiomotoneurons, cerebellum,
granule cells, bio-imaging, Gal4, cell biology, nucleokinesis,
centrosome

INTRODUCTION

Zebrafish embryos are ideal model organisms for the investigation of dynamic cell behaviors and their underlying molecular mechanisms in a vertebrate system. In particular, their external development, small size, fast embryogenesis and transparency mean that zebrafish can be used for continuous time-lapse imaging of *in vivo* cell movements. Combined with the steadily increasing repertoire of genetic methods, time-lapse studies have elucidated molecular processes regulating cell dynamics within the context of a living organism and such complexities as co-developing cell populations, simultaneously occurring tissue rearrangements or parallel acting signal transduction mechanisms. Thus imaging approaches in zebrafish help to verify and refine the models of cell behavior previously derived from *in vitro* studies of cultivated cells or explanted tissues.

Figure 1

The dynamic process of neuronal migration is particularly complicated to mimic under culture conditions because of both the difficulty in cultivating neuronal progenitors of specific populations and the multiple players and interactions that are involved on the cellular and molecular level. Although the migratory pathways of neuronal progenitors and some of the molecular guidance mechanisms have been elucidated *in vivo*, the underlying cell biological processes that translate signal transduction events into directed cellular motility are only now beginning to be addressed. In this chapter we will propose that with the current knowledge about neuronal migration mechanisms in zebrafish, the recent advances in bio-optics and

genetic technologies as well as the possibilities for high resolution bio-imaging on both the spatial and temporal level, zebrafish could serve to fuse the two large research areas of developmental genetics and cell biology into a single research field of in vivo cell biology. Moreover, such an approach can be used to address the molecular mechanisms of subcellular dynamics regulating neuronal migration, in the context of organ differentiation and brain function. Thus in zebrafish embryos, bio-imaging at multiple levels will be able to interconnect intracellular events with cell behavior, organogenesis, and eventually animal behavior in order to reveal a true development-structure-function relationship in a vertebrate model organism.

NEURONAL MIGRATION

Embryonic development is characterized by extensive movements of tissues and cells. In some cases, cellular positions change passively through morphogenetic rearrangements. Alternatively, many cells undergo active migration away from their birthplace, in order to settle in a final position where their function is required in the mature organism. Some cell types, such as leukocytes or macrophages, are even destined to travel their entire life to fulfill control and safeguarding functions.

The central nervous system is one area where well-ordered migration of both neuronal progenitors and the growth cones of their protruding axons is of essential importance. This directed motility establishes the highly ordered cellular composition of brain compartments and the correct wiring of the nervous system. In the vertebrate brain, migration of neuronal progenitors can be found in nearly every compartment. For example, **a)** the olfactory system in the anterior-most region of the forebrain shows pronounced neuronal migration from the subventricular zone, along the rostral migratory stream (RMS), and into the olfactory bulbs (1). The RMS is of

special importance as it is maintained throughout life, providing a potential source of undifferentiated neuronal progenitors for therapeutic purposes (2). **b)** In the cortex, neuronal migration occurs mainly radially in a characteristic inward-out sequence, but it is accompanied by tangentially migrating cells emanating from the medial and lateral ganglionic eminence (3). **c)** The development of the mesodiencephalic dopaminergic neurons requires extensive migration and it has been hypothesized that their positioning may contribute to differences in vulnerability to Parkinson's disease (4). **d)** In the cerebellum, granule neuron progenitors undergo a biphasic migration: tangential movement across the dorsal surface followed by a radial outward-in migration. Granule cell migration has been the focus of intense study to understand how neuronal migration is accomplished on the cellular and molecular level. However, other systems of interest in the posterior hindbrain include **e)** the caudal migration of branchio-motoneurons and, **f)** the circumferential migration of neurons forming the precerebellar system (5). **g)** Finally, radial migration occurs in the spinal cord along the entire length of the neural tube.

Imaging neuronal migration in zebrafish

Neuronal migration involves numerous and complex interactions among different cell populations and with the extracellular matrix, constraints from tissue boundaries, and coordination with concomitant tissue rearrangements. In addition, the migration of neuronal progenitors can occur over long distances and sometimes along complex routes (6). In consideration of this natural complexity, processes of neuronal migration are ideally observed in the living organism and in a continuous manner involving methods of *in vivo* time-lapse microscopy. For such an approach the zebrafish embryo is ideally suited. Foremost, it is nearly transparent and small in size, allowing for excitation light to penetrate easily, while resulting fluorescence

is not scattered extensively. In addition, the differentiation of the central nervous system occurs within two to three days; thus compared to other vertebrate model organisms the time-scale from neural proliferation, through migration, to terminal differentiation is condensed, allowing all of these events to be observed in a single time-lapse recording session.

The setup for time-lapse *in vivo* observations at cellular resolution is fairly simple as zebrafish can be mounted and anaesthetized without major effort, oxygenation is not required and simple incubation chambers maintaining an ambient temperature of about 28°C can be constructed easily. Numerous detailed protocols for *in vivo* imaging of cellular behavior in zebrafish embryos have been established (7-9). Due to their external development, zebrafish embryos can be easily manipulated to challenge migratory processes. Moreover, large collections of mutants are now available and many sophisticated genetic methods for tissue-specific and conditional genetics have been developed in recent years (10-12). Finally, the collection of fluorescent proteins in many different colors, targeted to almost all subcellular locations and even being able to report many functional events inside cells, is expanding continuously (13). Given the easy methods for generating transient and stable transgenics and the transparency of zebrafish embryos, this vertebrate model organism is ideal for investigating cellular and molecular processes of neuronal migration within a natural context.

Migration of branchiomotoneurons in the zebrafish hindbrain

In vivo time-lapse studies of neuronal migration have shown the migration of neuronal progenitors cells in many regions of the developing zebrafish brain. One population that has caught particular attention is the nVII branchiomotor neurons (bmns) of the facial cranial nerve in the ventral hindbrain. Expression of the green

fluorescent protein (GFP) inside the progenitors of these neurons under control of the *islet1*-enhancer in stable transgenic zebrafish embryos has allowed for directly monitoring of their migratory behavior and for the unraveling of molecular mechanisms controlling their migration. nVII bmns arise in ventral regions of rhombomere 4, where they begin to project axons that exit further dorsally from this rhombomere. At the same time, nVII bmns start to migrate caudally along a track running parallel to the ventral floor plate; the elongating axon is left behind and subsequently marks the migratory pathway. By this rostro-caudal tangential migration, nVII bmns cross the boundaries of rhombomere 5 to reach rhombomere 6 or 7, at which point nVII bmns turn to again migrate tangentially, but this time dorsally to eventually settle in dorsolateral regions of the respective rhombomere (14).

Figure 2

Homotypic xenografts of nVII bmns between mouse and chick embryos have suggested that nVII bmn migration is regulated largely in a non-cell-autonomous manner by environmental cues. With the combination of mutant analysis, transgenic fluorescent labeling and in vivo time-lapse imaging in zebrafish, such non-cell-autonomous regulation of neuronal migration could be shown and analyzed directly in vivo. Wild type nVII bmns fail to migrate caudally in homozygous mutants of a loss of function allele of the transmembrane protein Strabismus. In contrast, mutant nVII bmns are able to migrate in a wild type environment, although not to the full extent of wild type cells (15). In addition, Prickle 1 and Scribble 1 are required for nVII bmn migration and Prickle 1 interacts genetically with Strabismus (16, 17).

Both Strabismus and Prickle 1 can act as important components of the planar cell polarity (PCP) pathway of Wnt signal transduction; however neither the lack of Wnt ligands known to trigger non-canonical Wnt-signal transduction, nor the overexpression of Dishevelled variants that effectively block non-canonical Wnt signaling, impair nVII bmn migration (15, 18). Thus, the tangential migration of branchiomotor neurons in the caudal hindbrain is unlikely to be under control of the Wnt/PCP pathway, but under a new pathway involving some of the PCP components. Importantly, nVII bmn differentiation is unaffected in these mutants, underscoring the specific impact of the Strabismus/Prickle 1/Scribble 1 pathway on neuronal migration.

Neuronal migration in the zebrafish cerebellum

Work in recent years from our and other labs has demonstrated that in particular the development of the zebrafish cerebellum is characterized by long-distance migration of neuronal progenitors (6, 19). These migratory cells arise from a dorsally positioned proliferation zone called the upper rhombic lip (URL). In vivo time-lapse studies indicated that progenitors migrate in an apparent two-phase migration: initially in an anterior direction towards the midbrain-hindbrain boundary (MHB), which delineates the anterior border of the cerebellum, and secondly, the progenitor cells turn at the MHB and migrate to more ventral positions. Significant numbers of neuronal progenitors emanate from the URL for at least three days starting at about 28hpf, but individual URL-derived cells pass their entire migratory route in about 1.5 to 2 days. Thus, in vivo time-lapse imaging in zebrafish is able to capture the entire migratory phase of individual cells, starting with cell divisions in the URL and ending with their terminal differentiation in ventral cerebellar regions.

Figure 3

The URL does not give rise to the same cell type over the entire three or more days of generating migrating neuronal progenitors. First, during the second day of zebrafish embryogenesis until about 50hpf, neuronal progenitors are being generated for several brain stem nuclei positioned outside the cerebellum. These cells require for their motility the polysialylation of the neural adhesion molecule NCAM as enzymatic removal of polysialic acid in vivo largely impaired their migration (20). Subsequently, the URL begins to generate progenitors of the largest neuronal population in the vertebrate brain, the cerebellar granule neurons. Direct tracing of individual granule progenitor cells (GPCs), combined with retrograde axon labeling after terminal differentiation, indicated that a spatial pattern exists already inside the URL and reflects the different functional compartments of the mature cerebellum. While medial aspects of the URL generate GPCs that migrate in dorso-anterior directions and contribute to the non-vestibular cerebellar system, lateral URL regions provide GPCs that migrate along a latero-ventral route to generate granule neurons of the vestibular system of the cerebellum (21). Recent studies combining time-lapse imaging of GPC migration with mutant analysis and molecular manipulation revealed that a different adhesion system consisting of classical Cadherins is playing a key role in orchestrating directional GPC migration, in particular of the dorsally migrating non-vestibular granule neurons (Rieger & Köster, unpublished data). Thus the cerebellar URL in zebrafish, like in other vertebrates, generates different neuronal cell populations over time, which employ different molecular adhesion systems to regulate their migration over long distances. Intriguingly, cerebellar development in zebrafish is very plastic and can be

recapitulated during later stages. This has been demonstrated for early FGF-signaling events emanating from the MHB, which are involved in patterning of the cerebellum (22), but also for later stages of URL-derived GPC migration. Thus, when the entire primordium of the cerebellum is ablated during stages of prominent neuronal migration, FGF-signaling from the MHB re-patterns the anterior hindbrain to re-establish cerebellar tissue. Subsequently, neuronal migration of GPCs becomes re-initiated, occurs along the characteristic antero-ventral pathway, and is followed by proper parallel fiber projection from regenerated granule neurons (23). This amazing capacity of the teleost cerebellum, which appears to last into adulthood (24), provides a powerful system to study mechanisms of neuronal migration in the context of regenerating neuronal circuits in the vertebrate brain.

Challenges of imaging neuronal migration

The studies of motoneuron and GPC migration, in the zebrafish hindbrain and cerebellum respectively, are but two examples to demonstrate the power of combining embryonic manipulation, molecular genetics and intravital time-lapse imaging in the unraveling of cellular behavior and its underlying molecular mechanisms in a natural context. However, as zebrafish is a fairly young model organism in the field of developmental genetics, many open questions remain. For example, the events triggering or ceasing migration have remained elusive so far, the guidance factors steering these neuronal populations along their pathways are mainly unidentified and the co-ordination of the migration of one neuronal population with the developmental behavior of co-developing neuronal populations is simply unknown. Answers to these questions will similarly come from studies of mutants or gene knock down, as well as by analyzing double transgenic zebrafish expressing differently colored fluorescent proteins in co-developing neuronal

populations. For these investigations, the current technological level should be sufficient and technical advancements in the field of genetics or in vivo imaging are not necessarily required.

What needs to be addressed though to push the analysis of neuronal migration to the next level is to understand how molecular communication and signal transduction is translated into ordered subcellular and organelle behavior. Research over the past few decades in cell biology has contributed immense data sets addressing cellular motility and the regulation of subcellular dynamics. These data though are almost exclusively derived from cultured cells isolated from their natural environment and lacking the constraints and demands of brain compartment differentiation during embryogenesis. Thus models for neuronal migration derived from in vitro cell biology need to be transferred into and challenged in a novel field of in vivo cell biology. Given the fast embryogenesis, and genetic and imaging accessibility, the zebrafish is perfectly suited for merging the fields of developmental biology and cell biology in a vertebrate model organism. If intravital imaging can be pushed further in spatial and temporal resolution, then combined with advances in multi-transgene expression technologies using temporal and cell type specific control, the orchestration of neuronal migration will be understood in unprecedented detail. Thus, one day it may be possible by multi-level in vivo imaging in zebrafish to interconnect molecular processes with resulting organelle dynamics and cellular behaviors that in turn lead to proper organ differentiation and eventually control the behavior of the organism.

ADVANCES IN TECHNOLOGY

Confocal laser scanning microscopy at high speed

In vivo time-lapse imaging of neuronal migration at the cell biological level must be able to resolve the dynamics of subcellular components, which usually occur within the microsecond range. Thus, strong intrinsic contrast between cellular components and fast image recording technology at high sensitivity are each required. Recent advances in both biophysical optics and conditional zebrafish genetics mean that time-lapse in vivo cell biology of neuronal migration is now becoming possible.

Confocal microscopy is currently the method of choice for time-lapse imaging of living zebrafish at cellular resolution. However, the temporal resolution of image recording at full spatial resolution with conventional scan heads lies in the range of about 1 Hz. While this scan speed is more than sufficient to capture movements of entire cells, it is too slow to capture subcellular dynamics and behaviors such as fissions or fusions of mitochondria, cytoskeletal rearrangements or vesicle transport. Recently, various modifications to laser scanning confocal microscopy have increased the scan speed by one to two orders of a magnitude so that it now lies well within the range of cell biological events.

Spinning disk confocal microscopy

Spinning disk confocal microscopy uses a Nipkow disk for illumination and detection. This disk is equipped with a spiral pattern of holes and rotates through the excitation and emission light paths, thus converting the conventional single excitation beam into a parallelized multi-beam scanner. Because the spinning disk is placed in a conjugate position to the focal plane of the objective, emitted fluorescence from planes above or below the focal plane will not pass through the

center of the holes but will travel further sideways, eventually hitting the rim and reflecting away. This confocal effect allows one to image optical sections of a specimen, with the size of the holes in the Nipkow disk determining the thickness of the section. As the disk can rotate with up to several thousand rounds per minute, a raster scanning effect with low light exposure of the object is achieved, allowing for long-term time-lapse imaging of up to about 1000 frames per second at full frame size. Disadvantageous though, is that the pinhole cannot be variably adjusted in a continuous manner and that the system suffers from somewhat mediocre spatial resolution (25, 26).

Slit-scanning confocal microscopy

Instead of multiplexing, as performed by the spinning disk technology, slit scanners illuminate the entire line of a recorded image simultaneously by widening of the excitation laser beam. Thus only unidirectional scanning is required for obtaining a full frame image, thereby reducing the scan time significantly. A slit that is aligned in a confocal manner in front of the detector assures optical sectioning and can be changed stepwise to project emitted fluorescence onto a line array of CCDs. At full frame size, this setup can reach image acquisition rates of about 100 Hz and is thus well suited for monitoring intracellular dynamics. As it is not a true point scanner, a reduction in spatial resolution along the slit axis, lack of precise optical manipulation (e.g. of photo-convertible fluorescent proteins) and discontinuous “pin-slit” adjustments are the trade-offs (26).

Resonant-scanning confocal microscopy

Resonant scanners are a recent addition to the scan heads used in the field of confocal microscopy. Here, the principal of a traditional laser-scanning confocal microscopy system has remained almost the same. Point illumination with a pinhole

in confocal arrangement is used for optical sectioning and the focused excitation beam is moved across the sample using moving mirrors. If these mirrors are allowed to move at their 'Eigenfrequenz' or resonant frequency, control over scan speed is lost but a significant increase in scan speed is gained. This resonant scanning does not reach the temporal resolution of a slit-scanning or spinning-disk system, but it still lies in the range of about 25 Hz at full frame resolution, which should be enough to resolve most cell biological processes. As with the slit scanner, faster frame rates can be achieved when the frame size is reduced, allowing a resonant scanner to operate above 100 Hz at small frame sizes. Of advantage is that the system is still a true point scanner with accompanying superior spatial resolution, the size of the pinhole can be continuously adjusted to allow for freely-defined optical manipulation, and multi-photon excitation can be combined with the speed of resonant scanning. Thus, nowadays several confocal laser-scanning technologies are available with sufficient spatio-temporal resolution for in vivo cell biology in living zebrafish embryos.

Figure 4

Conditional genetic methods in zebrafish

Monitoring neuronal migration often requires marking of the observed cells by extrinsic contrast. Since the discovery of the Green Fluorescent Protein, a whole battery of differently colored and functionalized fluorescent proteins has been identified or engineered (13). Being genetically encoded, these vital dyes allow cell type-specific labeling to be achieved by using regulatory genetic elements.

Therefore, the identification of cell type-specific enhancers for use in generating

stable transgenic zebrafish strains with fluorescently-labeled cell populations has become one of the major areas of interest in the zebrafish research community. Such isolation of enhancers can be even more powerful when being used for combinatorial genetic approaches. Here, rather than simply labeling a cell population of interest, the cell type-specific enhancer is used to drive the expression of a transcription factor or recombinase. This activator line, when crossed into specific responder strains, can not only be used to activate the expression of fluorescent reporters but also to mediate the expression of different transgenes. Since different activator and responder strains can be crossed together, such combinatorial genetic systems are multifunctional, save laborious efforts, make transgene expression data more comparable and allow for the establishment of embryonic-lethal disease models that are accessible for bio-imaging approaches. Mainly two different systems are currently being used.

Cre-recombinase mediated expression

In the Cre system, a cell type-specific enhancer drives the expression of the bacteriophage P1-derived Cre-recombinase in the activator line. When crossed to a Cre-responder strain, this recombinase mediates the excision of DNA fragments that are flanked by sequence-specific recognition sites, called loxP sites. Commonly, such loxP-flanked spacer cassettes separate an enhancer from a transgene of interest, which only becomes expressed in the case of a tissue-specific recombination event. When expression in both the Cre-activator line and the Cre-responder line is under control of a cell-type specific enhancer, it is possible to even restrict transgene expression exclusively to the overlapping fraction of cells in which both enhancers are active. More sophisticated Cre-recombinase controlled genetic systems can be established if different sets of non-compatible loxP variants are used in combination

and are arranged in a way to mediate a temporal sequence of Cre-recombination events, as has been demonstrated for the Flex system in mouse (27). In zebrafish, a few reports show the usefulness of Cre-mediated transgene activation. For example, expression of the murine *myc* oncogene under control of the zebrafish *rag2* enhancer causes lethality prior to sexual maturity due to aggressive tumor formation. Thus transgene-expressing carriers can only be maintained by in vitro fertilization. Separation of the *myc* oncogene cassette from the *rag2* promoter by insertion of a loxP-flanked spacer cassette allows for propagation of transgenic carriers through subsequent generations, but tumor formation can be induced in a tissue specific manner by injection of Cre-recombinase expression vectors into single-cell stage embryos (28). Currently, the Cre-recombinase system is not widely used in zebrafish, probably because a large collection of tissue-specific Cre-activator lines is missing. However, with the recent advances in enhancer and gene trapping technologies in zebrafish, tissue-specific Cre-activator lines can be generated without major effort.

Gal4-UAS system

Compared to Cre-recombinase, the Gal4 system adopted from *Drosophila* has recently obtained far more attention in zebrafish research, probably because experimental requirements have already been worked out in more detail. In this combinatorial system, an activator line drives the expression of the transcriptional activator Gal4 or a modified version under control of a tissue-specific enhancer. Gal4-binding sites, called upstream activating sequences (UAS), mediate Gal4-dependent transgene expression in the effector line. When activator and effector strains are crossed together, tissue-specific transgene activation in the offspring is achieved by the tissue specificity of Gal4 expression. Recently, transposon-

mediated enhancer and gene trapping have been used to generate libraries of many different tissue-specific Gal4-activator lines; thus for virtually any tissue of interest a Gal4-activator line should now be available (11, 12, 29).

Figure 5

To even restrict transgene activation to a smaller cell population that shares the co-expression of two genes of interest, the split-Gal4 technique can be employed (30). Here, the DNA-binding domain of Gal4 and the transcriptional activation domain, both fused to heterodimerizing leucine zippers, are expressed by separate cell type specific enhancers. In cell types where both enhancers are active, overlapping expression is obtained and the DNA binding domain and the transactivation domain can reconstitute to form a functional Gal4 transcription factor. It requires though that two enhancers of interest are known and that triple-transgenic carriers are generated containing both Gal4 parts and a UAS-transgene cassette. Powerfully though, if one of the two Gal4 domains are expressed under control of a heat-shock inducible promoter, temporal as well as spatial control over transgene activation is achieved.

Recently, Gal4-combinatorial genetics and Cre-recombinase mediated transgene activation have been combined in an elegant study to generate single transgene-expressing neurons with tissue-specific control in transient transgenic zebrafish. Here, tectal neuron-specific Gal4-mediated activation (*brn3a*-promoter dependent) of a fluorescent reporter or transgene was restricted to a few cells by enabling Gal4 expression only in the case of a Cre-mediated activation event, which occurred at

low efficiency because three different plasmids needed to be incorporated by a targeted cell of interest (31).

In summary, these studies demonstrate that a number of genetic methods and their combinations are at hand or are currently being developed to achieve precise temporal and tissue-specific control of transgene expression in zebrafish. Thus the controlled activation of cell biological reporters, ideally in only a few cells to create optimal contrast, for use in time-lapse imaging approaches is within reach. Such precise spatio-temporal control of transgene expression is especially important for manipulating the cell biological events of neuronal migration in that the key players in cellular motility, polarity and adhesion are usually expressed ubiquitously and changes to their activity will cause severe and early phenotypes prior to nervous system development.

Multi-transgene expression systems

While combinatorial genetics allows control over the where and when of transgene activation in specific cells, additional tools are necessary to address the cell biological events of neuronal migration. In particular, in order to understand their interdependence, simultaneous labeling and observation of different subcellular structures through the co-expression of multi-colored fluorescent markers is required. Moreover, addressing cell biological and molecular mechanisms of neuronal migration requires specific mechanism-manipulating genetic variants. This can be achieved through spatio-temporal control of transgene expression combined with multi-cistron expression systems - indeed making cell biological imaging of neuronal migration the gold standard for high-speed high-resolution single cell in vivo imaging (leaving open a platinum-standard for single molecule imaging in vivo).

IRES expression vectors

Internal ribosomal entry sites (IRES) are probably the oldest method to achieve the co-expression of several transgenes from a single vector. Here the ribosome can bind and start translation in a cap-independent mechanism that relies on internal secondary structures in the mRNA. Such polycistronic IRES-containing vectors have found widespread use in higher vertebrate model organisms such as mouse and chick. On the downside though, IRES-containing mRNAs mediate non-stoichiometric expression of both cistrons, with the IRES-dependent cistron often being expressed at significantly reduced levels (32). Furthermore, IRES sequences are very context dependent; thus their functionality is difficult to predict and has to be confirmed for every constructed vector. In zebrafish, IRES sequences have so far not received much attention. This is likely due to the low level expression obtained with the IRES sequences conventionally used in mouse and chick (33, 34). Low level expression however could be attributed to the fact that mostly mammalian IRES sequences have been tested so far, and the isolation of a zebrafish-inherent IRES sequence could probably revive this method. The reduced expression from IRES-dependent cistrons compared to cap-dependent cistrons could even be of use when different expression levels need be obtained. For example, labeling of some organelles like the centrosome with targeted fluorescent proteins quickly reaches saturation levels. This has the consequence that conventional cap-dependent expression often leads to the accumulation of excessive fluorescent protein in the cytoplasm, thereby significantly reducing the signal to noise ratio of centrosome labeling. In summary, the use of IRES-dependent expression in zebrafish should not be neglected completely, but instead be attempted again with IRES sequences isolated from teleosts (or from a teleost-infecting virus).

2A-peptides

In contrast to IRES sequences, viral 2A-peptides mediate strictly stoichiometric expression. In these self-processing polypeptides, several cistrons are linked by small viral peptide sequences between 18-22 amino acids in length and usually ending with a PGP-sequence stretch. ‘Cleavage’ between the penultimate glycine and the terminal proline residues does not occur posttranslationally and does not involve additional co-factors. Rather peptide ‘cleavage’ has been attributed to a sequence-dependent skip by the ribosome in forming a peptide bond (35). Thus the production of proteins from two or more 2A-linked cistrons occurs at equimolar amounts and is highly efficient. Use of 2A-linked peptides was elegantly demonstrated in an approach to rescue CD3-deficient T-cells by expressing all four chains of the CD3-receptor complex in a 2A-peptide-linked arrangement in a single expression vector (36). Given the global features of 2A-peptide ‘cleavage’ characteristics, these peptides have been demonstrated to work in both animals and plants for obtaining reliable multi-transgene expression. Recently the technique has been successfully applied to zebrafish, in which virtually background-free 2A-peptide ‘cleavage’ and subsequent proper sorting of differently targeted fluorescent proteins was demonstrated (37) (own unpublished data). It has to be kept in mind though that proteins translated from two 2A-linked cistrons carry parts of the 2A-peptide with them. The C-terminal protein is usually marked with a single proline residue at its N-terminus. Although this single amino acid may not have a significant influence on the protein’s function, cDNAs of proteins with an N-terminal signal peptide should be positioned as the 5-prime cistron. Unlike the almost unmodified C-terminal protein of a 2A-linked protein pair, the N-terminal protein is “tagged” by roughly 20 amino acids at its C-terminus. Thus it has to be

verified that this C-terminal fusion does not interfere with the function of the protein. For example, peroxisome targeting, which is often mediated by the C-terminal-most amino acids of a protein, will be compromised if the peroxisomal protein is encoded by the 5-prime cistron of a bicistronic 2A-linked expression construct. On the other hand this sequence tag could be turned into an advantage as antibodies have been successfully established against the 2A-peptide (38), allowing for immunohistochemical detection, Western blot analysis and immunoprecipitation assays to be performed with the 5-prime cistron-encoded protein. Given the robust co-expression of 2A-linked proteins in zebrafish, combined with the easy cloning procedures of simply adding 2A-sequences to a protein of interest by a PCR reaction, one can foresee that this powerful co-expression approach will obtain a lot of attention throughout the zebrafish research community. For bioimaging approaches several differently targeted fluorescent proteins could be used for simultaneously labeling a number of subcellular structures with unique colors, while for molecular studies transgene-expressing cells could be marked by the simultaneous 2A-mediated co-expression of a fluorescent reporter.

Multicistronic Gal4 effectors

An alternative approach to obtain reliable co-expression of several transgenes, and one that completely avoids the generation of fusion proteins, is provided in conjunction with Gal4-activated transgene expression. As the transcriptional activator Gal4 is freely diffusible, it can bind to several independent UAS sequences and thereby activate a number of transgenes. Furthermore, several UAS-dependent expression cassettes can be placed in a linear arrangement onto a single expression vector, which ensures co-segregation of several transgenes of interest, thereby allowing for the reliable fluorescent labeling of transgene-expressing cells (31, 39).

Recent studies showed that two transgenes can also be activated from a single UAS sequence by flanking the UAS sites with two basal promoters in a mirror-image arrangement (M. Distel & R. W. Köster, unpublished data). This “Janus” orientation facilitates cloning as it reduces recombination events in bacteria when two highly similar sequences are used in the expression vector (e. g. CFP/YFP). Moreover, co-activation of two transgenes does not require two independent binding events of Gal4 at different UAS sites of the expression vector, but theoretically a single binding event of Gal4 should be sufficient to activate transgene expression in two directions. This is supported by the finding that co-activation of two transgenes in a Janus vector can be achieved by a single UAS site. However, we cannot exclude that transgene activation involves cycles of Gal4 binding and release, with each new binding event involving the choice of selectively activating only one transgene at a time. Nevertheless, co-activation of transgene expression occurs reliably, although not in equimolar amounts. Quantification of transgene expression showed that usually one transgene is expressed in slightly higher amounts up to about 30%. One advantage of this multi-cistronic UAS arrangement is that different expression modules can be prepared in advance allowing for very efficient cassette-like cloning procedures to generate new co-expression constructs. In addition, several of these expression cassettes can be combined on a single vector allowing four or more different transgenes to be co-expressed. Moreover, as pointed out above, strong transgene expression is not always of advantage as it can reduce signal to noise ratio in the case of saturating fluorescent reporter protein expression. Further, high expression levels can lead to significant overexpression phenotypes, such as those often observed with the expression of microtubule-binding fluorescent reporter proteins. Multi-cistronic UAS-cassette vectors allow one to account for

these problems as expression levels can be adjusted through varying the number of Gal4-binding sites in the UAS-sequence stretch. While strong expression can be reached with five UAS sites in tandem order, reducing the number of UAS sites in the sequence stretch successively reduces the expression level of the transgene. For example, strong nuclear and membrane labeling can be achieved with a 5x UAS Janus cassette, while moderate but sufficient expression levels can be obtained from the same vector from a 2x UAS centrosome/microtubule-labeling Janus unit (unpublished observations). This possibility to fine-tune expression levels of transgenes is particularly valuable for addressing cell biological questions of neuronal migration, and for monitoring and influencing migratory processes without interfering with other basic cellular processes such as cell proliferation.

Figure 6

In summary, several valuable methods for the efficient and reliable co-expression of numerous transgenes have been established in recent years. For more sophisticated approaches these methods can of course be combined, for example to drive 2A-peptide linked transgene expression from several UAS cassettes. In addition, cell type-specific combinatorial expression systems have been established for zebrafish and a number of cell type-specific enhancers or expression-activating transgenic strains are readily available. Further, the recent advances in bio-optics now allow for the observation of subcellular dynamics at sufficient spatial and temporal resolution without significant photo-bleaching or photo-toxicity. Thus the stage is set for true *in vivo* cell biology in zebrafish, a vertebrate model organism that will allow for challenging the many models for neuronal migration derived from

in vitro data of cultured cells or tissue explants. Hence zebrafish can serve to fuse the large fields of developmental genetics and cell biology in vertebrates. Given that currently significant progress is being made in the areas of single molecule imaging and in the automatic monitoring of zebrafish behavior, imaging at many organismic levels is coming into sight in zebrafish. In summary, tracing individual molecules, observing subcellular dynamics and monitoring cell behavior can be connected to the processes of organ differentiation and ultimately explain consequences for animal behavior, providing a truly dynamic structure-function relationship.

CELL BIOLOGY OF NEURONAL MIGRATION – MORE QUESTIONS THAN ANSWERS

Expression analysis, fate mapping approaches and time-lapse studies have revealed many migratory pathways of neuronal populations in the vertebrate brain. Moreover, pharmacological manipulations, conditional mutagenesis and analysis of genetically mosaic animals have provided insight into how cellular motility, directionality, coherence and pathfinding of neuronal migration are regulated at a molecular level. But how are these molecular signals translated into coordinated subcellular dynamics to achieve directional motility? What are the subcellular consequences of interactions between migratory and non-migratory cells and how do groups of cells jointly orchestrate their cellular migration machineries?

Coordination of nucleokinesis

First insights into these complex mechanisms were derived from analyzing the normal functions of molecules altered in neuronal migration diseases, collectively called lissencephalies. Lissencephaly-causing genes (when compromised in their function), such as *lis1*, *nde*, *ndel* and *dcx*, are highly conserved from slime molds to

humans. Interestingly, the proteins that they encode are usually associated with the microtubule cytoskeleton and/or the centrosome. When these cellular structures were analyzed in detail during neuronal migration, it became evident that many neuronal progenitors do not translocate as an entire body with all their cellular components (a migratory mechanism termed somal translocation), but rather that their organelles are transported forward in a well-choreographed sequential manner. Initially, the neuronal progenitor forms and extends a leading process, which is subsequently filled by microtubule fibers. Most characteristic for this migratory mode is that the centrosome travels in front of the nucleus, based on the direction of travel, and then translocates into the leading process. This centrosomal movement extends the centrosomal-nuclear distance and is believed to trigger subsequent nuclear forward movement towards the centrosome. Finally, the cytoplasm travels behind.

Figure 7

Forward movements of neuronal progenitors alternate with resting phases, giving the appearance of saltatory motion. The orchestration of this coordinated set of organelle movements is thought to be mediated by the microtubule skeleton, which is organized by the centrosome through its function as a microtubule organizing center (MTOC). Microtubules connect the leading process with the centrosome and from there surround the nucleus in a characteristic perinuclear microtubule cage that is believed to mediate the forward transport of the nucleus during nucleokinesis (40-42). The protein products of lissencephaly type I-causing genes are often involved in microtubule-nucleus coupling and so it is thought that the nucleus is affected

neurons of these patients is unable to follow the migration-initiating movements of the centrosome. As a consequence, neuronal progenitors stall close to or inside of proliferation zones and fail to reach their proper place of function (41).

The current understanding of nucleokinesis though is rudimentary and partially contradictory results have been published. In addition, data from isolated, cultured neuronal progenitors, cells grown in collagen, matrigel or similar assays, tissue explants and organotypic slice cultures are often compared to one another and using different neuronal populations. Furthermore, although both radially and tangentially migrating neuronal progenitors have been shown to migrate via nucleokinesis, homotypic and heterotypic migratory modes clearly involve different cell-cell interactions, suggesting that variations of a common theme of nucleokinesis have to be taken into account. This is a field where zebrafish can contribute significantly as an *in vivo* cell biology model without the need to extensively manipulate the cells that are to be observed.

One current open question in understanding nucleokinetic migration regards the driving force behind movement of the nucleus. Studies on the function of lissencephaly-causing genes suggest that the nucleus follows the centrosome in a Dynein-dependent manner along the microtubule fibers that interconnect the centrosome with the nucleus. Pharmacological inhibition of the actin-myosin network though suggested that instead of a microtubule-mediated ‘pulling’ force, non-muscle myosinII-mediated pushing from the rear of the cell is responsible for nuclear movements towards the centrosome (43). Which of these forces is active *in vivo* remains to be clarified and first requires a careful analysis of the coordination of the microtubule as well as the actomyosin system in relation to the different steps during neuronal progenitor forward movement. Specific *in vivo* perturbations of

both of these systems in several migrating neuronal populations need to be performed in order to reveal whether nuclear forward movement relies on one force and whether this machinery is reused in neuronal populations that migrate in different modes. URL-derived neuronal progenitors and branchiomotor neurons in the zebrafish cerebellum and hindbrain respectively, may represent interesting model cell types for answering these questions because the hindbrain is highly accessible for pharmacological treatments through injections of the IVth ventricle. Rather than acting in an either/or mechanism, both systems, microtubule-dependent nuclear ‘pulling’ and actomyosin-dependent nuclear ‘pushing’, may well act together. The question that arises then is how do both systems coordinate and synchronize their activity mechanistically and on the molecular level. Do they regulate different aspects of nuclear forward transport or do they cooperate as partners in the same process? Detailed in vivo time-lapse studies at high temporal resolution in zebrafish embryos could help to resolve these questions and thus provide further insights into the etiology of lissencephaly.

The centrosome as maître de danse?

Given its characteristic positioning and its prominent role in interconnecting the leading process with the nucleus through organizing the microtubule network, the centrosome has achieved major attention in the field of neuronal migration research. Yet its role remains undefined and evidence for its direct involvement in organizing nucleokinesis is largely circumstantial. In fact, in a recent time-lapse study it was demonstrated that in radially migrating cerebellar granule progenitor cells, the nucleus can overtake the centrosome during nucleokinetic forward movement and that perinuclear microtubules do not converge at the centrosome (44). Nevertheless, during resting periods of the cell, the centrosome was found in front of the nucleus

and interference with Lis1 demonstrated an uncoupling of centrosome dynamics with nuclear movements. Thus rather than serving as a permanent guide for the nucleus, the centrosome could play a preparatory role during cell resting and leading process elongation in setting up the next forward nuclear forward movement. Whether such a role for the centrosome holds true for tangentially migrating neurons, in which the centrosome has been reported to stay strictly in front of the nucleus, remains to be shown and probably requires a similar high-resolution in vivo study to unravel the temporal order of organelle dynamics.

Prior to neuronal migration, the centrosome plays an important role in neuroblast division and the maintenance of apico-basal polarity. Neural cell divisions usually occur with the mitotic spindle aligning parallel to, and the division axis orthogonal to, the ventricular zone. After such a symmetric division, the centrosome moves to the apical cell surface while the nucleus resumes so-called interkinetic nuclear movement until it returns to the ventricular zone for the next round of mitosis. Until now the molecular and cell biological mechanisms that ensure repositioning of the centrosome at the apical membrane, and thus re-establishment of apico-basal polarity in both daughter cells, remain largely elusive. Similarly, the driving forces of interkinetic nuclear movements, which are thought to occur to provide space at the ventricle for cell divisions, are mostly unknown. How is the centrosome transported and anchored to the apical ventricular side? Does the centrosome indeed re-establish apico-basal polarity de novo after every round of neuroblast mitosis or do other cues maintain polarity during cell divisions, with the centrosome simply following these cues in resuming its position?

Although there is still debate about the existence of clearly asymmetric neuroblast divisions responsible for the generation of the neuronal precursors that

emigrate from germinal zones, initiation of neuronal migration must involve significant rearrangements in the centrosome-nuclear relationship. Nucleokinesis would require that the centrosome leaves the apical membrane and repositions itself in front of the nucleus; furthermore centrosome-nucleus coupling needs to be established, as these organelles do not coordinate their movements during interkinetic nuclear migration. Thus, one could define the onset of migration by following the repositioning of the centrosome *in vivo*. Indeed, first results in the zebrafish cerebellum suggest that interkinetic nuclear movements can occur over significant spatial distances, thereby obscuring the onset of real neuronal migration and the interpretation of molecular guidance mechanisms (own unpublished results).

Another important question that arises with respect to centrosome function during neuronal migration is its role in initiating and determining axon formation. Elegant studies have shown that explanted neuronal progenitors rely on intrinsic mechanisms to establish neuronal polarity, with the centrosome selecting the nearest neurite to become the future axon (45). Interestingly, time-lapse imaging of neuronal migration has shown that *in vivo* axon formation and projection can occur simultaneously to neuronal migration with the leading process extending to become the forming axon (19). This is in good agreement with the centrosome traveling close to and moving into the leading process during nucleokinetic neuronal migration. However, elegant *in vivo* time-lapse studies demonstrated for retinal ganglion cells in the developing zebrafish eye that the position of the centrosome does not predict the site of axon formation *in vivo*; in fact, axon formation was found to occur basally after the cells have left the apical membrane, but prior to centrosome positioning close to the nucleus (46). Whether these findings are a

common scheme of axon formation by migrating neurons or are confined to specific migratory modes needs to be addressed.

Finally, centrosome amplification is often found in cancerous cells and may be responsible for the genetic instability of tumorigenic cells. Interestingly though, a recent study in *Drosophila* demonstrated that flies with extra centrosomes in about 60% of their cells develop normally and maintain a stable diploid genome over several generations (47). During most cell divisions, spindle formation is achieved by centrosome clustering; however the asymmetric division of neuroblasts, which usually precedes and initiates neuronal migration, is perturbed and results in symmetric divisions that give rise to more proliferating cells. In addition, transplanted brain cells with multiple centrosomes can induce metastatic tumors in host flies. This finding suggests that neuroblastoma formation could result from a failure in proper centrosome-mediated neuronal migration, keeping neural progenitors in contact with proliferation signals inside germinal zones for too long. Time-lapse imaging of the behavior of neuroblasts with induced extra centrosomes in tissues of pronounced neuronal migration in zebrafish would reveal if neuronal migration can be accomplished by centrosome clustering or whether migration is stalled but leaves the neuroblasts competent for proliferation.

Organelle dynamics during neuronal migration

Clearly the centrosome is not the only organelle that needs to contribute to neuronal migration. While it can be postulated that cellular organelles are simply dragged along, cell biological observations argue against such a passive role. For example, along with the centrosome, the Golgi apparatus and the endoplasmic reticulum (ER) are found in front of the nucleus with at least the Golgi preceding nuclear movement during nucleokinesis (43). Thus a first question that arises is

whether the centrosome precedes and controls Golgi movements or whether these organelles move independently from one another. Is there a temporal order in which specific organelles are moved inside migrating neuronal progenitors and do they use the same molecular mechanisms? Are *Lis1*-defective cells also impaired in Golgi or ER transport? What are the molecular and cellular mechanisms that trigger organelle forward movement? One could postulate that forward extension of the leading process shifts the cell centroid further to the front and thus organelles become readjusted in their position along microtubule fibers with respect to that centroid. In such a model, adhesion factors in connection with the cytoskeletal networks must play an important role in transmitting tension. Intriguingly, recent studies about molecular tracing revealed that adhesion factors are far more flexible than assumed and are transported inside cells and along the membrane (48, 49). They could thus play an active role in shifting tension forces inside migrating neuronal progenitors and relocating the cell centroid, which is then followed by organelle repositioning. To answer these types of questions *in vivo* would require even further improvement in the temporal and spatial resolution of bio-imaging techniques in zebrafish and the development of intelligent fluorescent reporter systems. Thus the next challenge for zebrafish imaging is already in sight.

CONCLUSIONS

Neuronal migration is a key step in nervous system development and in the integration of adult neural stem cells into functional circuits. Although migratory pathways have been delineated, the molecular and cell biological mechanisms underlying neuronal migration are just beginning to be understood. In recent years, research in zebrafish has primed this model organism to address the *in vivo* mechanisms of neuronal migration. Major pathways of migrating neurons have been characterized in several regions of the nervous system and significant advances in optical imaging, combinatorial genetics and multi-transgene expression systems have been achieved. Thus the stage is set in zebrafish to merge the large research fields of cell biology and developmental genetics to decipher the subcellular coordination of directed cellular motility and its molecular regulatory mechanisms. Many exciting open questions await this research field and due to its superb bio-imaging properties as well as genetic accessibility, zebrafish will allow us to watch how cells organize their internal machineries to accomplish one of the most difficult tasks in central nervous system differentiation. This *in vivo* cell biology will challenge many existing models of cellular and neuronal migration to verify, modify or redefine our knowledge of the events that occur within a moving cell in the context of a living and developing organism. Zebrafish researchers can look forward to a bright future.

ACKNOWLEDGMENT

We wish to apologize to all colleagues whose work we could not reference due to limited space. We thank all members of our research group for intense discussions. M. Distel is supported by the Studienstiftung des deutschen Volkes, J. Hocking is a fellow of the Natural Sciences and Engineering Research Council of Canada and R.W. Köster is financed by the German Research Foundation (DFG KO1949/3-1) and a BioFuture Grant Award (0311889) of the German Ministry of Education in Research (BMBF).

REFERENCES

1. Murase, S. and Horwitz, A.F. (2004) Directions in cell migration along the rostral migratory stream: the pathway for migration in the brain. *Current Topics in Developmental Biology*, **61**, 135-152.
2. Soares, S. and Sotelo, C. (2004) Adult neural stem cells from the mouse subventricular zone are limited in migratory ability compared to progenitor cells of similar origin. *Neuroscience*, **128**, 807-817.
3. Nadarajah, B. and Parnavelas, J.G. (2002) Modes of neuronal migration in the developing cerebral cortex. *Nature Reviews Neuroscience*, **3**, 423-432.
4. Jacobs, F.M., Smits, S.M., Hornmann, K.J., Burbach, J.P. and Smidt, M.P. (2006) Strategies to unravel molecular codes essential for the development of meso-diencephalic dopaminergic neurons. *Journal of Physiology*, **575**, 397-402.
5. Bloch-Gallego, E., Causeret, F., Ezan, F., Backer, S. and Hidalgo-Sanchez, M. (2005) Development of precerebellar nuclei: instructive factors and intracellular mediators in neuronal migration, survival and axon pathfinding. *Brain Research. Brain Research Reviews*, **49**, 253-266.
6. Mione, M., Baldessari, D., Deflorian, G., Nappo, G. and Santoriello, C. (2008) How neuronal migration contributes to the morphogenesis of the CNS: insights from the zebrafish. *Developmental Neuroscience*, **30**, 65-81.
7. Cooper, M.S., D'Amico, L.A. and Henry, C.A. (1999) Analyzing morphogenetic cell behaviors in vitally stained zebrafish embryos. *Methods in Molecular Biology*, **122**, 185-204.
8. Langenberg, T., Brand, M. and Cooper, M.S. (2003) Imaging brain development and organogenesis in zebrafish using immobilized embryonic explants. *Developmental Dynamics*, **228**, 464-474.
9. Distel, M. and Köster, R.W. (2007) In vivo time-lapse imaging of zebrafish embryonic development. *Cold Spring Harbor Protocols*, **2**, doi:10.1011/pdb.prot4816.
10. Hardy, M.E., Ross, L.V. and Chien, C.B. (2007) Focal gene misexpression in zebrafish embryos induced by local heat shock using a modified soldering iron. *Developmental Dynamics*, **236**, 3071-3076.
11. Scott, E.K., Mason, L., Arrenberg, A.B., Ziv, L., Grosse, N.J., Xiao, T., Chi, N.C., Asakawa, K., Kawakami, K. and Baier, H. (2007) Targeting neural circuitry in zebrafish using GAL4 enhancer trapping. *Nature Methods*, **4**, 323-326.
12. Asakawa, K., Suster, M.L., Mizusawa, K., Nagayoshi, S., Kotani, T., Urasaki, A., Kishimoto, Y., Hibi, M. and Kawakami, K. (2008) Genetic dissection of neural circuits by Tol2 transposon-mediated Gal4 gene and enhancer trapping in zebrafish. *Proceedings of the National Academy of Sciences USA*, **105**, 1255-1260.
13. Miyawaki, A. (2005) Innovations in the imaging of brain functions using fluorescent proteins. *Neuron*, **48**, 189-199.
14. Chandrasekhar, A. (2004) Turning heads: development of vertebrate branchiomotor neurons. *Developmental Dynamics*, **229**, 143-161.

15. Jessen, J.R., Topczewski, J., Bingham, S., Sepich, D.S., Marlow, F., Chandrasekhar, A. and Solnica-Krezel, L. (2002) Zebrafish trilobite identifies new roles for Strabismus in gastrulation and neuronal movements. *Nature Cell Biology*, **4**, 610-615.
16. Carreira-Barbosa, F., Concha, M.L., Takeuchi, M., Ueno, N. and Wilson, S.W. (2003) Prickle 1 regulates cell movements during gastrulation and neuronal migration in zebrafish. *Development*, **130**, 4037-4046.
17. Wada, H., Iwasaki, M., Sato, T., Masai, I., Nishiwaki, Y., Tanaka, H., Sato, A., Nojima, Y. and Okamoto, H. (2005) Dual roles of zygotic and maternal Scribble 1 in neural migration and convergent extension movements in zebrafish embryos. *Development*, **132**, 2273-2285.
18. Bingham, S., Higashijima, S., Okamoto, H. and Chandrasekhar, A. (2002) The zebrafish trilobite gene is essential for tangential migration of branchiomotor neurons. *Developmental Biology*, **242**, 149-160.
19. Köster, R.W. and Fraser, S.E. (2001) Direct imaging of in vivo neuronal migration in the developing cerebellum. *Current Biology*, **11**, 1858-1863.
20. Rieger, S., Volkmann, K. and Köster, R.W. (2008) Polysialyltransferase expression is linked to neuronal migration in the developing and adult zebrafish. *Developmental Dynamics*, **237**, 276-285.
21. Volkmann, K., Rieger, S., Babaryka, A. and Köster, R.W. (2008) The cerebellar rhombic lip is spatially subdivided in producing granule cell populations of different functional compartments. *Developmental Biology*, **313**, 167-180.
22. Jaszai, J., Reifers, F., Picker, A., Langenberg, T. and Brand, M. (2003) Isthmus-to-midbrain transformation in the absence of midbrain-hindbrain organizer activity. *Development*, **130**, 6611-6623.
23. Köster, R.W. and Fraser, S.E. (2006) FGF signaling mediates regeneration of the differentiating cerebellum through repatterning of the anterior hindbrain and reinitiation of neuronal migration. *Journal of Neuroscience*, **26**, 7293-7304.
24. Zupanc, G.K.H. (2001) Adult neurogenesis and neuronal regeneration in the central nervous system of teleost fish. *Brain Behavior and Evolution*, **58**, 250-275.
25. Nakano, A. (2002) Spinning-disk confocal microscopy - a cutting-edge tool for imaging of membrane traffic. *Cell Structure and Function*, **27**, 349-355.
26. Conchello, J.-A. and Lichtman, J.W. (2005) Optical sectioning microscopy. *Nature Methods*, **2**, 920-931.
27. Floss, T. and Schnütgen, F. (2008) Conditional gene trapping using the FLEx system. *Methods in Molecular Biology*, **435**, 127-138.
28. Langenau, D.M., Feng, H., Berghmans, S., Kanki, J.P., Kutok, J.L. and Look, A.T. (2005) Cre/lox-regulated transgenic zebrafish model with conditional myc-induced T cell acute lymphoblastic leukemia. *Proceedings of the National Academy of Sciences of the United States of America*, **102**, 6068-6073.
29. Davison, J.M., Akitake, C.M., Goll, M.G., Rhee, J.M., Gosse, N., Baier, H., Halpern, M.E., Leach, S.D. and Parsons, M.J. (2007) Transactivation from

- Gal4VP16 transgenic insertions for tissue-specific cell labeling and ablation in zebrafish. *Developmental Biology*, **304**, 811-824.
30. Luan, H., Peabody, N.C., Vinson, C.R. and White, B.H. (2006) Refined spatial manipulation of neuronal function by combinatorial restriction of transgene expression. *Neuron*, **52**, 425-436.
 31. Sato, T., Hamaoka, T., Aizawa, H., Hosoya, T. and Okamoto, H. (2007) Genetic single-cell mosaic analysis implicates ephrinB2 reverse signaling in projections from the posterior tectum to the hindbrain in zebrafish. *Journal of Neuroscience*, **27**, 5271-5279.
 32. Mizuguchi, H., Xu, Z., Ishii-Watabe, A., Uchida, E. and Hayakawa, T. (2000) IRES-dependent second gene expression is significantly lower than cap-dependent first gene expression in a bicistronic vector. *Molecular Therapy*, **1**, 376-382.
 33. Köster, R., Götz, R., Altschmied, J., Sendtner, R. and Scharf, M. (1996) Comparison of monocistronic and bicistronic constructs for neurotrophin transgene and reporter gene expression in fish cells. *Molecular Marine Biology and Biotechnology*, **5**, 1-8.
 34. Fahrenkrug, S.C., Clark, K.J., Dahlquist, M.O. and Hackett, P.B. (1999) Dicistronic gene expression in developing zebrafish. *Marine Biotechnology*, **1**, 552-561.
 35. Donnelly, M.L., Luke, G., Mehrotra, A., Li, X., Hughes, L.E., Gani, D. and Ryan, M.D. (2001) Analysis of the aphthovirus 2A/2B polyprotein 'cleavage' mechanism indicates not a proteolytic reaction, but a novel translational effect: A putative ribosomal 'skip'. *Journal of General Virology*, **82**, 1027-1041.
 36. Szymczak, A.L., Workman, C.J., Wang, Y., Vignali, K.M., Dilioglou, S., Vanin, E.F. and Vignali, D.A. (2004) Correction of multi-gene deficiency in vivo using a single 'self-cleaving' 2A peptide-based retroviral vector. *Nature Biotechnology*, **22**, 589-594.
 37. Provost, E., Rhee, J. and Leach, S.D. (2007) Viral 2A peptides allow expression of multiple proteins from a single ORF in transgenic zebrafish embryos. *Genesis*, **45**, 625-629.
 38. Ryan, M.D. and Drew, J. (1994) Foot-and-mouth disease virus 2A oligopeptide mediated cleavage of an artificial polyprotein. *Embo Journal*, **13**, 928-933.
 39. Köster, R.W. and Fraser, S.E. (2001) Tracing transgene expression in living zebrafish embryos. *Developmental Biology*, **233**, 329-346.
 40. Marin, O., Valdeolmillos, M. and Moya, F. (2006) Neurons in motion: same principles for different shapes? *Trends in Neuroscience*, **29**, 655-661.
 41. Kerjan, G. and Gleeson, J.G. (2007) Genetic mechanisms underlying abnormal neuronal migration in classical lissencephaly. *Trends in Genetics*, **23**, 623-630.
 42. Higginbotham, H.R. and Gleeson, J.G. (2007) The centrosome in neuronal development. *Trends in Neurosciences*, **30**, 276-283.
 43. Bellion, A., Baudoin, J.P., Alvarez, C., Bornens, M. and Metin, C. (2005) Nucleokinesis in tangentially migrating neurons comprise two alternating phases: forward migration of the Golgi/centrosome associated with

- centrosome splitting and myosin contraction at the rear. *Journal of Neuroscience*, **25**, 5691-5699.
44. Umeshima, H., Hirano, T. and Kengaku, M. (2007) Microtubule-based nuclear movement occurs independently of centrosome positioning in migrating neurons. *Proceedings of the National Academy of Sciences of the United States of America*, **104**, 16182-16187.
 45. de Anda, F.C., Pollarolo, G., Da Silva, J.S., Camoletto, P.G., Feiguin, F. and Dotti, C.G. (2005) Centrosome localization determines neuronal polarity. *Nature*, **436**, 704-708.
 46. Zolessi, F.R., Poggi, L., Wilkinson, C.J., Chien, C.B. and Harris, W.A. (2006) Polarization and orientation of retinal ganglion cells in vivo. *Neural Development*, **1**, 2.
 47. Basto, R., Brunk, K., Vinadogrova, T., Peel, N., Franz, A., Khodjakov, A. and Raff, J.W. (2008) Centrosome amplification can initiate tumorigenesis in flies. *Cell*, **133**, 1032-1042.
 48. Kametani, Y. and Takeichi, M. (2007) Basal-to-apical cadherin flow at cell junctions. *Nature Cell Biology*, **9**, 92-98.
 49. Ogata, S., Morokuma, J., Hayata, T., Kolle, G., Niehrs, C., Ueno, N. and Cho, K.W.Y. (2007) TGF-beta signaling-mediated morphogenesis: modulation of cell adhesion via cadherin endocytosis. *Genes & Development*, **21**, 1817-1831.

FIGURE LEGENDS

Figure 1: Zebrafish as a model organism for microscopic investigations.

Transparent zebrafish embryo 24 hours past fertilization (hpf) embedded in agarose.

The inset shows subcellular structures in the living embryo, such as the cell nucleus in red, the microtubule cytoskeleton in green and cellular membranes in blue recorded using confocal fluorescence laser scanning microscopy.

Figure 2: Migration of branchiomotoneurons in zebrafish.

In the *islet1:GFP* line (obtained from H. Okamoto) branchiomotoneurons are labelled with GFP. Rhombomere 3 and 5 are labelled with mCherry for better orientation.

A) nVII branchiomotoneurons are born in rhombomere 4 (asterisk) and migrate through rhombomere 5 (the arrow indicates the direction of migration) while leaving an axon behind. B) These branchiomotoneurons settle in rhombomere 6 and 7 and extend their axons further anterior to innervate their respective target areas.

Figure 3: Migration of cerebellar precursors.

A) Lateral view on the brain of a living zebrafish embryo 27hpf. The midbrain-hindbrain boundary (MHB, dotted line) separates the mesencephalon (mes) from the rhombencephalon (rh). The cerebellum (cb) evolves from rhombomere 1 of the rhombencephalon.

Cerebellar precursors (arrow) labelled with GFP arise from the proliferative upper rhombic lip (yellow line).

B) Cerebellar precursors start to migrate tangentially towards the MHB. C) Precursor cells reaching the MHB turn ventrally in a second migratory step and start to extend first axonal like processes. D) Cerebellar precursors settle in ventral regions of rhombomere 1. All Images are maximum projections of z-stacks taken from a time-lapse movie.

Figure 4: Confocal laser scanning at high speed.

Spinning disk:

Spinning disk confocal microscopes use a rotating Nipkow disk for image acquisition. The specimen is scanned with a multi beam in a raster pattern with a fast horizontal scan (line scan) in conjunction with a slower vertical scan (frame scan) achieved by the spiral arrangement of holes in the collector disk. In recent microscopes the holes in the collector disk contain microlenses, which focus the laser beam through the pinholes in the pinhole disk for higher excitation efficiency and a better signal to noise ratio. The pinhole disk is also rotating, allowing only in focus information to pass through and reach the detector.

Slit scanner:

In contrast to point scanner microscopes slit scanner microscopes gain speed as they record entire lines instead of individual points. This is achieved by widening the laser beam to a line. The so called Achromatic Gate executes the function of the dichroic mirror of a point scan system to allow the excitation wavelength to reach the specimen, but only the emission wavelength to reach the detector. In order to obtain confocal images the pinhole in front of the detector is replaced by a slit in a slit scanning system.

Resonant scanner:

The difference between a resonant scanning and a traditional confocal point scanning system is the scanning mirror, which is oscillating at the so-called “Eigenfrequenz” at up to 8000Hz. As a resonant scanning system uses regular pinholes, true confocal images can be obtained. The inset shows a resonant scanning system with two y-mirrors for precise illumination of the specimen and the x-mirror, which is oscillating at resonant frequency for fast scanning of a specimen.

Figure 5: Genetic techniques for manipulation of zebrafish.

- A) A heterozygous Gal4 activator line (*zic4:Gal4*) is crossed to a homozygous effector fish (*UAS:GFP*). Neither of the parent fish express GFP, but half of the offspring express GFP in a tissue specific manner. As the *zic4:Gal4* activator line carries Gal4 under control of the *zic4* enhancer, Gal4 is only expressed in distinct tissues and cell types such as cerebellar granule cells. Gal4 will transactivate GFP specifically in these cells so that cerebellar granule cells express GFP.
- B) Confocal image of a double transgenic embryo (*zic4:Gal4* and *UAS:GFP*) showing expression of GFP in the cerebellum (asterisks) and other *zic4* expression domains. Confocal image recorded at approximately 7 days past fertilization using a Zeiss LSM510 with a 20x objective.

Figure 6: Subcellular labelling using multicistronic vectors.

Using multicistronic vectors several cellular components can be labelled simultaneously. A) The nuclei of these cells of a living zebrafish embryo are labelled with RFP (red), microtubules are labelled with GFP (green) and the cellular membranes are labelled with CFP (blue). B) Keratinocyte of a living zebrafish embryo with the nucleus labelled with RFP (red) and microtubules labelled with GFP (green). Images were recorded with a Zeiss LSM510 using a 40x water objective.

Figure 7: Visualization of subcellular dynamics during cell migration.

Using a multicistron subcellular labelling technique several cellular components were labelled in migrating cells undergoing nucleokinesis in a living zebrafish embryo approximately 28hpf.

A-D) The nucleus of the cell (white circle in A) is labelled with RFP (red), the cell membrane with CFP (blue) and the microtubules with GFP (green). Images are taken from a time-lapse movie recorded with a Zeiss LSM510 using a 40 water objective.

A) The cell starts to establish a process (arrow) in the later direction of migration. A bundle of microtubules (green) is already visible in this process.

B) Microtubules extend more and more and the process elongates.

C) The nucleus (red) is translocated in the direction of migration (two arrows showing the translocation), leaving a cytoplasm filled membrane behind. The movement of the nucleus appears in a saltatory fashion.

D) The trailing membrane is retracted, hereby finishing the cycle of nucleokinesis.

E-G) The nucleus of this cell of interest (white circle in E) is labelled with CFP (blue), the membrane with RFP (red) and the centrosome with YFP (yellow). The migratory step is initiated by the movement of the centrosome. From E to F the

distance between nucleus and centrosome (arrow) increases, indicating the forward movement of the nucleus.

G) The nucleus is translocated in the direction of the centrosome movement. The centrosome disappears as it moves out of the focal plane. Images are taken from a time-lapse movie recorded with a Zeiss LSM510 using a 40 water objective.

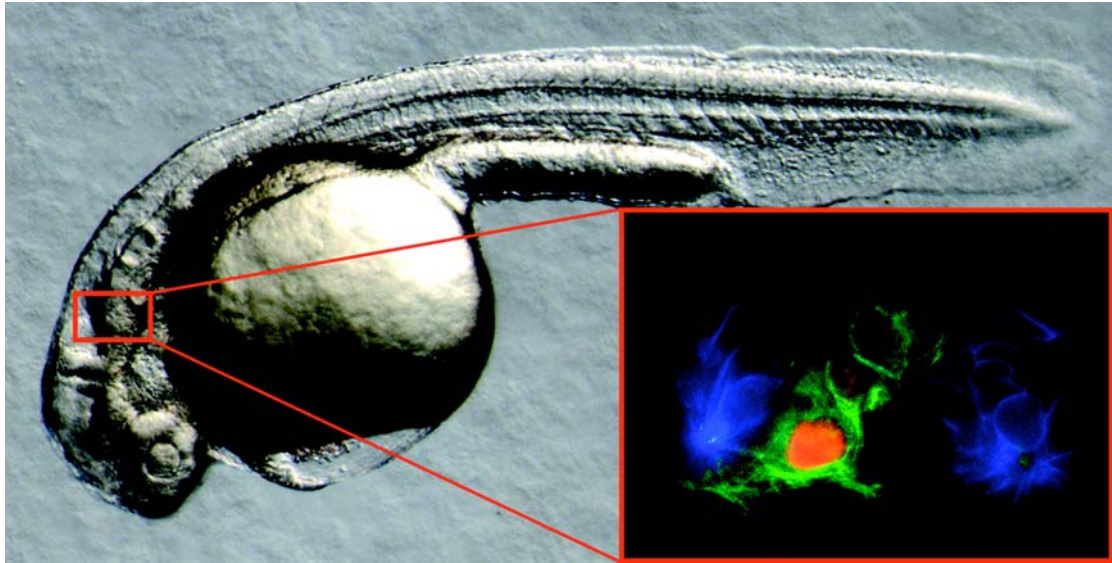


Figure 1

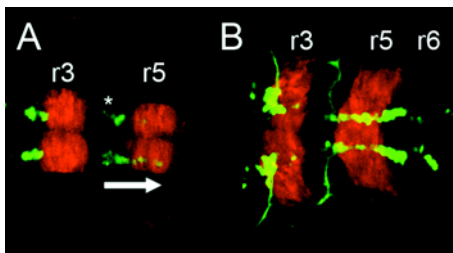


Figure 2

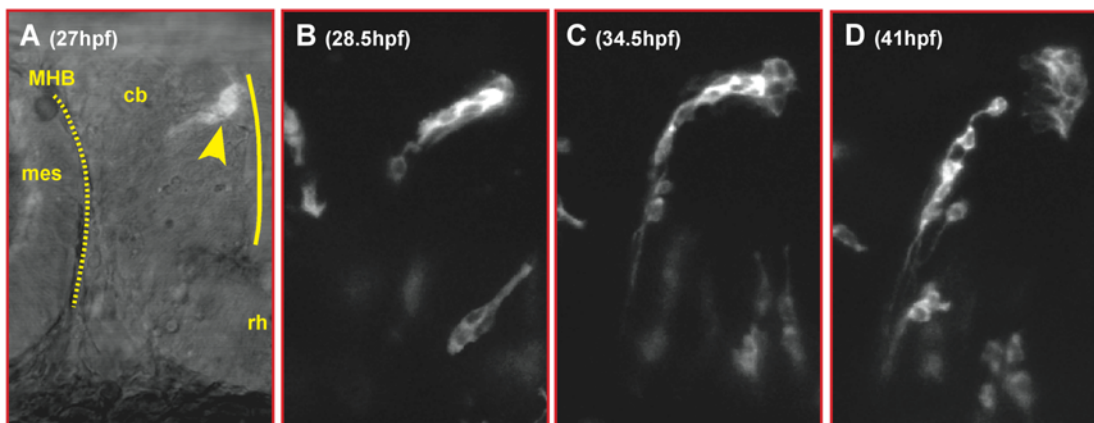


Figure 3

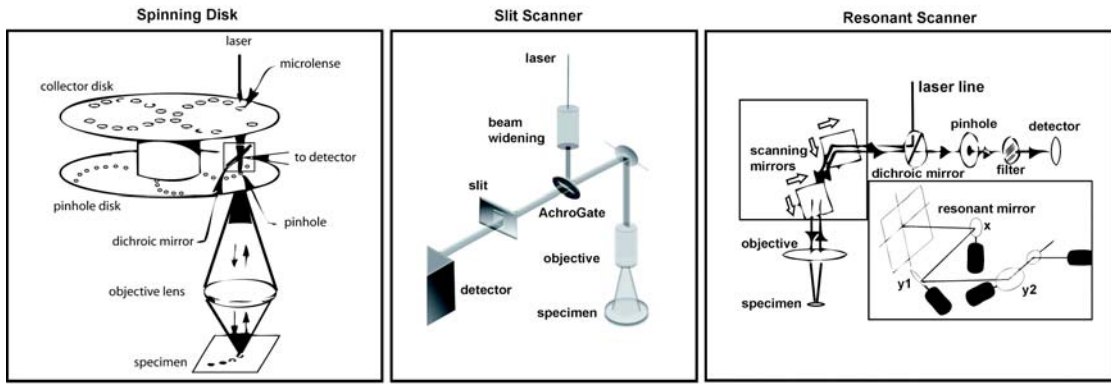


Figure 4

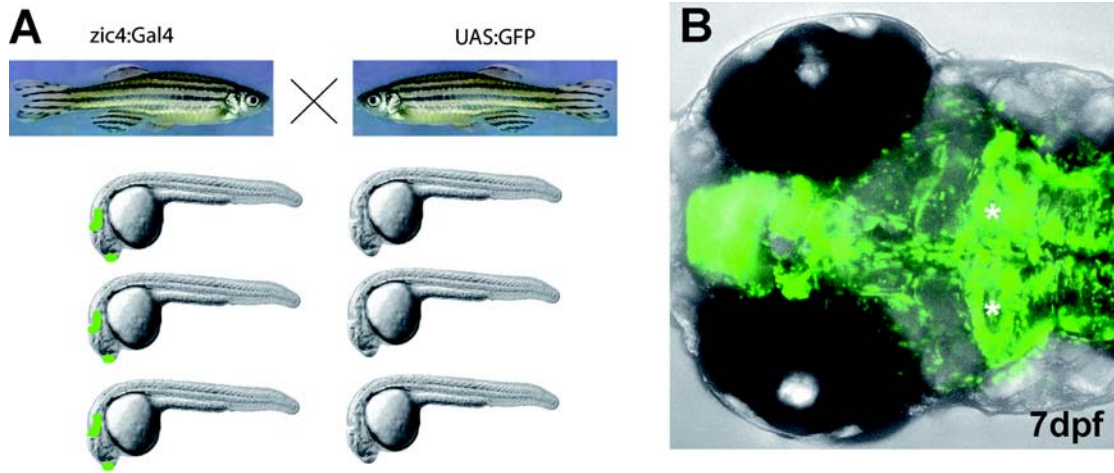


Figure 5

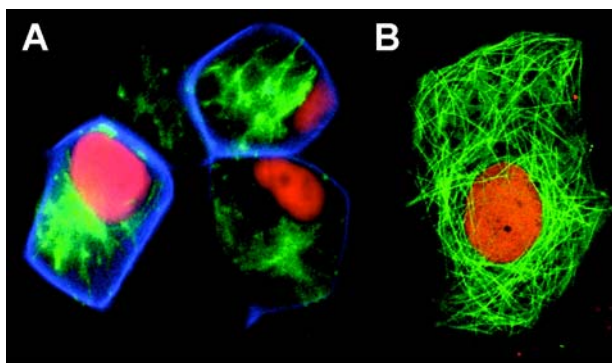


Figure 6

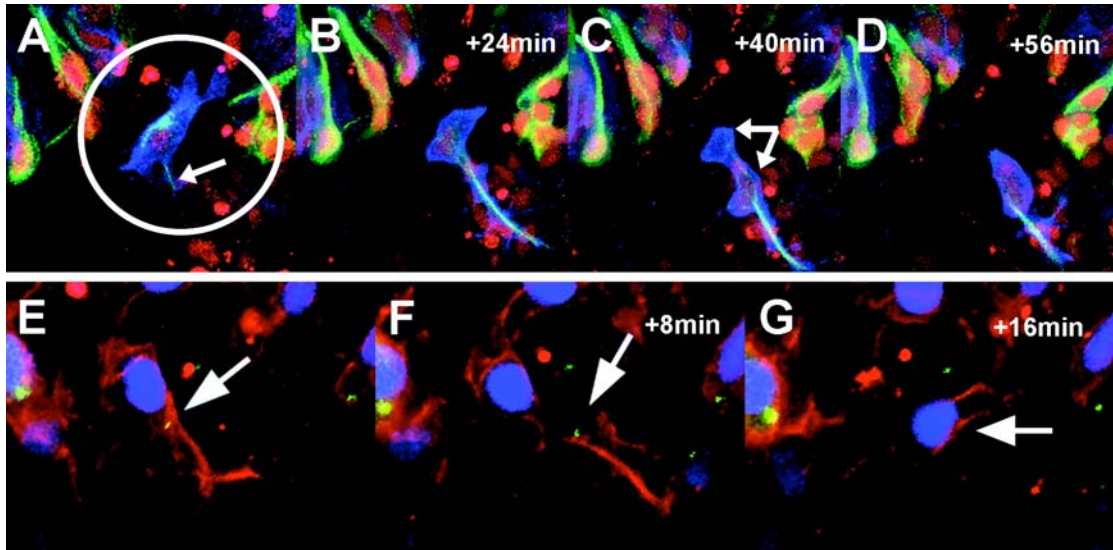


Figure 7

Acknowledgements

First of all, I want to thank my supervisor Dr. Reinhard Köster for being an outstanding mentor over the last years. Working in his lab was a great experience, as he provided a good mixture of guidance, but also freedom to develop my own ideas. I deeply appreciate that he always had time for discussions. He was also extremely supportive of all my different applications for courses, scholarships and my future position, which I am truly thankful for.

I want to thank my wife Nicole for her very selfless support throughout the last years and for taking care of our babies Marie and Lena so that I could get some sleep to write this thesis.

A special thank you goes to my parents and my sister for continuously giving me encouragement and exceptional support.

I am thankful to the new and old members of the Neuroimaging Group -Andreas Babaryka, Sandra Rieger, Katrin Volkmann, Veronika Zapilko, Petra Hammerl, Kazuhiko Namikawa, Jen Hocking, Enrico Kühn, Anna-Lena Kerner, Christiane Lach, Thomas Weber, Changsheng Liu, Niklas Senghaas and Rosi Söllner- for being good bench neighbours, being very helpful, for critical discussions and for ensuring that working in the lab was enjoyable.

In particular I want to thank

- Jen for reading and thoughtfully commenting on my thesis. I also always enjoyed discussing scientific and “baby problems” with her.
- Enrico for his great assistance in the lab, eating my sweets and for the fun activities outside the lab.
- my students Olga Lositsky, Mark Schibler, Nina Dedic, Vanessa Bednarz, Benjamin Wolf and Yuanyuan Chu for their hard work, excellent assistance and important contribution to my research projects.

I also want to thank Prof. Wolfgang Wurst for his support, advices and for giving me the opportunity to conduct my research project within the stimulating environment of the IDG.

I am indebted to all of the neighbouring groups at the IDG, IHG and ISF, for sharing materials, teaching methods and for general support. I want to thank Dr. Laure Bally-Cuif for her great support of my applications for scholarships and my future position and the members

of her group for many interesting discussions. Prisca, Anja, Steffi, Elisa, Corinna, Ruth, Annerose, Jordi and Saida for great experimental help and advices with vibratome sectioning, immunohistochemistry, southern blots and retrograde labelling. Furthermore, Theresa and Gerd for statistical analysis of data.

I also want to thank the members of my thesis committee, Dr. Timm Schröder and Dr. Christian Brösamle for their interest and advice.

Furthermore, I thank:

- the fish facility crew, who kept all my fish happy and alive.

- all my collaborators and in particular:
 - Marina Mione and Cristina Santoriello for a great ongoing collaboration and for being very generous in sharing ideas and tools.
 - Daniel Razansky and Rui Ma for the insight into photoacoustic imaging and for experimental help. Furthermore, Daniel for offering me a position and for being an understanding boss.
 - Mario Wullimann for his great help with zebrafish neuroanatomy.

- the staff of the Marine Biological Laboratory at Woods Hole for an unforgettable course and especially the course director Nipam Patel for his support for my application for my future position.

- the secretaries of the IDG for unbureaucratic and fast help

Fiona Francis, Anna Akhmanova, Roger Tsien, Gary Banker, Alexander Reugels, Jürgen Wehland, Sean Megason, Timm Schröder, Koichi Kawakami, Atsushi Miyawaki, Christoph Winkler, Adam Amsterdam, Elwood Linney and Marina Mione generously provided constructs, which I am grateful for.

I am also indebted to the Studienstiftung des deutschen Volkes, who supported my work by a PhD fellowship.

Publications

published:

Distel, M., Babaryka, A. and Köster, R.W. (2006) Multicolor in vivo time-lapse imaging at cellular resolution by stereomicroscopy. *Dev Dyn*, **235**, 1100-1106.

Distel, M., and Köster, R. W. (2007). In vivo time-lapse imaging of zebrafish embryonic development. *CSH Protocols* doi:10.1101/pdb.prot4816.

Paquet, D., Bhat, R., Sydow, A., Mandelkow, E.M., Berg, S., Hellberg, S., Falting, J., **Distel, M.**, Köster, R.W., Schmid, B. and Haass, C. (2009) A zebrafish model of tauopathy allows in vivo imaging of neuronal cell death and drug evaluation. *J Clin Invest*, **119**, 1382-1395.

Nikolaou, N., Watanabe-Asaka, T., Gerety, S., **Distel, M.**, Köster, R.W. and Wilkinson, D.G. (2009) Lunatic fringe promotes the lateral inhibition of neurogenesis. *Development*, **136**, 2523-2533.

Razansky, D., **Distel, M.**, Vinegoni, C., Ma, R., Perrimon, N., Köster, R.W. and Ntziachristos, V. (2009) Multispectral opto-acoustic tomography of deep-seated fluorescent proteins in vivo. *Nature Photonics*, **3**, 412-417.

Distel, M., Wullimann, M.F. and Köster, R.W. (2009) Optimized Gal4 genetics for permanent gene expression mapping in zebrafish. *Proc Natl Acad Sci U S A*. **106**, 3365-70.

Distel, M., Hocking, J., and Köster, R. W. (2009). "Imaging the cell biology of neuronal migration in zebrafish. ." World Scientific Publishing, Singapore,

in press:

Anelli, V., Santoriello, C., **Distel, M.**, Köster, R. W., Ciccarelli, F. D., and Mione, M. (2009). Global repression of cancer gene expression in a zebrafish model of melanoma is linked to epigenetic regulation. *Zebrafish*

manuscript:

Distel, M., Volkmann, K. and Köster, R.W. (2009). In vivo centrosome dynamics during neuronal migration and axonogenesis in the zebrafish cerebellum. *Journal of Cell Biology*